Cranfield University

SUNIL MISTRY

A NOVEL AIRFRAME DESIGN METHODOLOGY FOR SILENT AIRCRAFT

School of Engineering

Doctor of Philosophy (PhD) Thesis

[Page intentionally left blank]

Cranfield University

SCHOOL OF ENGINEERING

PhD THESIS

Academic Year 2004-2008

SUNIL MISTRY

A Novel Airframe Design Methodology For Silent Aircraft

Supervisor: Prof. J. P. Fielding

Academic Year 2007 to 2008

This thesis is submitted in partial fulfilment of the requirements for the degree of Doctor of Philosophy (PhD)

[Page intentionally left blank]

Abstract

The impact of noise on civil aviation is not just a localised airport problem, but a global concern, due to the ever-increasing demands for passenger travel. The challenge of designing a 'Silent Aircraft' lies within the development, integration, and optimisation of efficient airframe-engine technologies. This research study investigates the design of novel airframes with the aim of producing a methodology that incorporates airframe noise. Studies investigating the design of Broad Deltas (BD), Blended Wing Bodies (BWB), and Joined Wing airframe configurations are integrated with innovative propulsion systems designs to identify key parameters in order to design a Silent Aircraft.

The airframe configuration plays an important role in the total aircraft noise, where the novel airframes that are analysed, are compared to a datum 'baseline' aircraft. All novel configurations show significant improvements in airframe noise reduction, enhanced by the addition of ultra-efficient propulsion systems, for which integration studies are discussed. The research into novel airframes uses a developed design methodology which integrates design considerations such as aerodynamics, performance, and cost models to complement the noise analysis and identify the most silent airframe configuration.

The research goal was to identify a silent airframe solution for a future viable short-medium range airliner, where the final solutions described suggest proposals for the future development of aviation. The proposals suggested describe a short-term solution to the noise challenge, with a longer-term solution to aid the development of technologies, maturity in technology release levels (TRLs), and development of a future 2050 medium capacity civil airliner.

Acknowledgements

First and foremost I would like to express my sincere gratitude to my supervisor and mentor, Professor J. P. Fielding, for his continuous support throughout my time at Cranfield University and for the opportunities which he has presented me over the last four years.

This project would not have been a success without my knowledgeable colleague and friend Georgios Doulgeris, with whom many hours were spent burning the midnight oil to achieve our research targets, and it has been a great honour to work alongside him.

I would like to thank all those within the Silent Aircraft Initiative, both in Cambridge University (UK) and MIT in Boston, because of their welcoming attitudes and willingness to assist and integrate our parallel study with their own research. A special thanks goes to Prof Zolti Spakovszky, Dr Jim Hileman, Mr Tom Reynolds, and Mr Ryan Tam for their critical analysis and guidance throughout my research.

The opportunity to work within the Aircraft Design Centre was a great challenge and experience, for which I would like to thank Dr Howard Smith, along-with work on numerous MSc projects over the years, which has not only expanded my knowledge base, but also industrial contacts.

In my time at Cranfield, I have had the privilege to get to know and work with some interesting characters, where the support of my office colleagues in both social and academic needs has helped me through, along with academic staff who are more friends than colleagues.

Finally I would not have been able to complete my PhD research without the love, support, and guidance of my family, who have held together over these last two years through the loss of three family members, all of whom were a crucial part of my life and upbringing. Despite the arguments and usual sibling rivalry they have never held me back and have always urged me to fulfill my ambitions, so it is my family that deserve the most credit for my achievements to date, as without their support, drive, and enthusiasm for my success, I honestly do not know where I would be.

Contents Page

List of Figures

List of Tables

List of Symbols

a	Speed of sound
a_{cruise}	Speed of sound at cruise
A	Aspect ratio
Arm	Moment arm
Av/req	Ratio between the available and required thrust-to-weight ratios
A_f	Airfoil design factor
A_{Side}	Fuselage side view cross sectional area
A_t	Tail aspect ratio
A_{Top}	Fuselage plan view (top) cross sectional area
A_{vt}	Vertical tail / fin aspect ratio
A_{wl}	Winglet aspect ratio
b	Wing span
b_t	Tail wing span
b_{vt}	Vertical tail span
B_{max}	Maximum fuselage width
BPR	Engine bypass ratio
c	Specific fuel consumption
c'	Specific fuel consumption factor
c^{BAR}	Standard mean aerodynamic chord
c_{tip}	Tip chord length
c_{root}	Root chord length
c_{kink}	Kink chord length
$(c)_0$	Datum sea level static specific fuel consumption
$(c)_0'$	Static sea level specific fuel consumption factor
$(c)_1$	Specific fuel consumption in climb condition
$(c)_{des}$	Design specific fuel consumption
$(c)_{OD}$	Off-design specific fuel consumption
c_d	Airfoil drag coefficient
$(c_d)_0$	Airfoil zero lift drag coefficient
$(c_d)_{co}$	Airfoil zero lift drag coefficient at climb-out condition
$(c_d)_{wave}$	Airfoil wave drag coefficient
$(c_d)_{wl}$	Winglet drag reduction coefficient
$(c_{dz})_{ls}$	Equivalent zero lift drag term at low speed

$(c_{dz})_{cr}$	Equivalent zero lift drag coefficient at cruise
c_D	Wing drag coefficient
$(c_D)_0$	Wing zero lift drag coefficient
$(c_D)_{co}$	Wing zero lift drag coefficient at climb-out condition
$(c_D)_{wave}$	Wing wave drag coefficient
c_l	Airfoil lift coefficient
$(c_l)_{wl}$	Winglet lift coefficient
c_L	Wing lift coefficient
c_{La}	Wing approach lift coefficient
c_{Lmax}	Maximum lift Coefficient
$c_{L\,us}$	Un-stick lift Coefficient
$c_{L\,use}$	Useable lift coefficient
$(c_L)_{cr}$	Wing cruise lift coefficient
$(c_{L,a})_0$	Wing zero sweep approach lift coefficient
$(c_{L.\,us})_0$	Zero sweep un-stick lift Coefficient
$(c_{L.\,us})_{max}$	Maximum un-swept lift Coefficient
c_m	Moment coefficient
c.g.	Centre of gravity
C_1	Lifting surface mass factor
C_2	Fuselage mass coefficient factor
C_3	Propulsion system installation factor
C_4	Systems mass factor
C_5	Secondary lifting surfaces mass factor
C^{BAR}_1	Evaluation factor to determine the lifting surface mass
C_{1_EAS}	Constant equivalent air speed climb factor
D_{piston}	Piston diameter
d	The piston diameter denominator factor
D0	Equivalent diameter at the nose
D1	Diameter where the nose locally ends at ln
D2	Maximum equivalent diameter either at lp, or (L-lt)
D3	Diameter at lt
D4	Diameter at the tail.
D/t	Thickness ratio for the piston
D_i/D_o	Inside-to-outside piston diameter ratio
f_a	Airframe material
fw	Wing correction factor

$f(A)$	Wing aspect ratio function
$f(Thrust)$	Thrust correction factor
$f(Drag)$	Drag correction factor
$f(\lambda)$	Taper ratio function
F_F	Flap factor
F_{op}	Mass of operational items factor
F_{wave}	Wave drag factor
F_τ	Afterburning correction factor
g	gravitational acceleration
H_{ztail}	Horizontal tail
$IPS\ mass$	Is the sum of two key parameters
k_5	Fuselage design that merges into the tail-rudder region
k_6	Represents coefficient Class of a/c & incorporated design features
k_{12}	Factor for vertical location of the horizontal tail relative to the fin.
k_e	Engine thrust coefficient
k_{MO}	The ratio of all masses directly proportional to the total mass
K	Constants for a given propulsion system with a defined operating condition and Mach number range ($K1\tau$, $K2\tau$, $K3\tau$, $K4\tau$)
Kv	Speed induced drag
$(K_v)_0$	The low speed induced drag
$(Kv)cr$	Cruise induced drag
l	Length
l_n	Distance aft of the nose which effectively blends into a parallel section,
l_p	Distance aft of the nose where a cross sectional discontinuity occurs
l_t	Distance forward of the aft fuselage where the cross-section fairs down
l_{APEX}	Tail wing apex location
l_{Fus}	Fuselage mass
$l_{Op\ it}$	Operational items
l_{Pay}	payload
l_{sys}	the overall fuselage length, and so are the systems
l_T ,l_{Tail}	Tail length
$l_{T\text{-}arm}$	Tail moment arm
L	Overall fuselage length
L/D	The Lift-to-drag ratio
L_L	Landing field length
L_{Lcor}	Correct landing length

LL_{RT}	Reverse thrust landing length
m_C	1st term representing structural wing box including spanwise shear webs
m_r	Second term represents the ribs required to support the first webs.
M_0	Overall aircraft mass
(M_0)	The accurate estimate for the final mass
$(M_0)_{EST-1}$	The first estimate for the total mass
$(M_0)_{EST-2}$	The second estimate for total mass
$(M_0)_{est2}$	Second estimate of overall mass
$(M_0)_{calc}$	Calculation of the total mass.
$(M_0)_{\kappa M0}$	The mass of items proportional to the overall mass
$M_{aileron}$	Aileron mass
M_{AM}	Alternate materials mass allowing for departure from a structural ideal
$(M)_{Basline}$	Baseline Aircraft Mass
$(M_N)_{co}$	The climb Mach numbers
$(M_N)_{cr}$	Cruise Mach numbers / the climb Mach number
$(M_N)_{2\,cr}$	Second cruise Mach numbers
$(M_N)_{crit}$	Critical Mach numbers
M_{cr}/M_0	The ratio of initial cruise to take-off mass
M_{cr1}/M_0	The initial cruise mass ratio
M_{cr2}/M_0	The ratio of end of cruise mass to take-off mass ratio
M_{cr1}/M_{cr2}	The cruise fuel ratio
M_{cr2}/M_{cr1}	The inverse of the cruise fuel ratio
M_{disp}	The total disposable items mass for the BDSF is therefore
M_{DLW}	The design landing weight
M_{DTOW}	The design takeoff weight
M_{EOW}	Operational Empty mass
(M_f)	the fuel mass
M_{f_a}	The available internal fuel mass
$(M)_{fuel}$	The fuel to take-off mass ration
M_{fixed}	The ‘fixed’ mass
(M_f/M_0)	The ratio of fuel mass to take-off mass ratio
M_{fuel}/M_0	the ratio of fuel to take-off mass
$(M)_{lift\text{-}surf}$	The mass of the lifting surfaces
$M_{LEdroop}$	Drooped leading edge slat mass
M_{Tail}	The tail mass
M_{VCF}	Trailing edge variable camber flap mass

Mg/S	Wing loading
$(Mg/S)_0$	Static wing loading
$(Mg/S)_{0.ld}$	The take-off wing loading approach velocity
$(Mg/S)_{0.gt}$	Gust sensitivity at take-off wing loading
$(Mg/S)AV$	Wing loading weight ratio at take-off
(M_G)	The undercarriage mass
M_{IP}	Ideal primary structural mass
M_L/M_O	Landing mass to take off mass ratio
M_N	Mach numbers
$(M_N)_{TO}$	Take-off Mach number
$(M_{PAY.L})$	Payload mass
$M_{pay.L}$	The Mass total payload
$(M)_{Sys}$	The systems mass ratio
M_{SS}	Secondary structural mass allowance
M_T	Mass of Tail components + winglets
$M_{CompSurf}/M_0$	Composite moving surfaces
M_{Pen}/M_0	Weight penalty for a/c with an AUM of less than 140 tonnes
$M_{PP}/_{M0}$	Installed propulsion system mass
$M_{spoiler}/M_0$	spoilers/airbrakes
M_{SS}/M_0	Total SS mass for the BDSF
(M_{Sys}/M_0)	The Systems mass ratio
$M_{V\text{-}tail}$	Mass of the V-tail
(M_W)	Major mass wing component
M_{ZW}	The design zero fuel mass
N	Ultimate Normal manoeuvre / acceleration factor
N^{BAR}	The effective factored wing normal acceleration factor
N_e	Number of engines
$(N)_{pax}$	Number of passengers
N_S	Function of the area at the nose for a pointed nose region
N_W	Number of wheels
p_m	Main gear unit pressure
p_n	Nose gear pressure
p^{BAR}	Cabin differential pressure
P	Pressure
$P_{extended}$	The extended gas force is calculated using a shock absorber ratio
P_L	Load parameter

P_P	Power Plant
$PP_{FAC\text{-}S}$	Power Plant altitude dependence power factor
Q	Constant
Q_M	The Constant Mach number
$Q_M\ \sigma_{cr.1}$	Cruise to relative density thrust –to-weigh evaluation
Q_V	Constant for climb characteristics
r	Inertial relief factor
R	Gas Constant
$R_{Mdynamics}$	Main under carriage dynamic reaction load
$R_{MSteadybrake}$	Nose landing gear steady brake load
$R_{Mstatic}$	Main under carriage static reaction load
$R_{Ndynamics}$	Nose gear dynamic reaction load
$R_{Nstatic}$	Nose gear static reaction load
R_S	Shock absorber ratio
Rw	Wetted Area
Rw_FT	fin and tail configuration of wetted area
Rw_SF	Single fin contribution to wetted area
(S)	The Wing / The wing reference area
$S^{-0.1}$	The wing area parameters for zero lift drag
$S_{BD\_Estimate}$	Estimate of Broad Delta wing area
$(S)_{BD\_Estimate}$	The wing area estimate for both BD configurations
S_f	The structural surface area on the fuselage
S_g	The Ground run to reach lift-off speed
S_G	The horizontal distance covered whilst descending from cruise
S_G	Ground distance for descent
$(S_G)_{cr1}$	Ground distance during first phase of constant Mach number climb
$(S_G)_{cr2}$	Ground distance during second phase of constant Mach number climb
$(S_G)_{desc}$	Horizontal distance covered whilst descending from cruise
$S_{exposed}$	Exposed area
$(S_G)_{EAS}$	Ground distance covered during constant EAS climb phase
$(S_G)_{EAS}$	The ground distance covered during constant EAS climb phase
S_{HT}	Horizontal Tail Area
$(s)_{NET}$	The net range
$(S)_{s.range}$	Function of design range
S_{static}	Static closure is the vertical distance between static and
$S_{V\text{-}tail}$	Area is calculated as the effective area of tail outside the fuselage boundary

S_{VT}	Vertical Tail Area
S_{wet}	Wetted area
$(S_{wet})_{FUS}$	Fuselage wetted area
$(S_{wet})_{Hztail}$	Horizontal tail wetted area
$(S_{wet})_{nacelle}$	Wetted area of engine nacelles
$(S_{wet})_{nacelle}$	Wetted area of engine nacelles
$(S_{wet})_{Total}$	Total wetted area
$(S_{wet})_{Vztail}$	Vertical tail wetted area
$(S_{wet})_{winglets}$	Winglet wetted area
$(S_{wet})_{wing}$	Wing wetted area
S_{wet}/s	wing reference of wetted area
S_{wl}	Winglet aspect reference ratio
SP	Structural parameter
t/c	Thickness-to-chord
(T_0)	Static engine thrust
$(T/Mg)_0$	Static thrust-to-weight ratio
$(T/Mg)_{0.input}$	Thrust-to-weight ratio at take-off input
$(T/Mg)_{0.input.1}$	Initial input at thrust-to-weight ratio at take-off
$(T/Mg)_{0input2}$	Second input at thrust-to-weight ratio at take-off
T/T_{OD}	Off design specific fuel consumption
T_0/Mg_1	Thrust-to-weight ratio during the initial constant Mach number climb
$(T/Mg)_{av}$	The available cruise thrust to weight ratio
$(T/Mg)_{eng}$	The basic thrust-to-weight ratio of propulsion system
$(T/Mg)_{req}$	The required propulsion systems thrust-to-weight ratio
T_f	Type factor parameter
T_G	Landing gear track
ToL	Take-off length
T_P	Tyre inflation pressure
$T_{RRstatic}$	The tyre rolling radius calculations for static loading[mm]
TS	Function of truncated tail area
u/c	The undercarriage
V	Velocity, speed [m/s]
V_a	Approach Velocity [m/s]
$(V_a)_{3deg}$	Approach Velocity for 3 degree FPA
$(V_a)_{6deg}$	Approach Velocity for 6 degree FPA
$V_{a.calc}$	Calculation for approach velocity

$V_{a.max}$	Maximum approach velocity
V_D	Design Speed / The structural design speed
V_{LOF}	Lift coefficient climb-out at ground Speed lift-off
V_{stall}	Stall speed
V_{TO}	Take-off velocity
V^{BAR}	Horizontal tail coefficient
$(V^{BAR})_V$	Vertical tail coefficients
$V_{C1.EAS}$	Velocity at Constant equivalent air speed climb
V_V	The vertical velocity
$(Vv)c$	Vertical velocity at the climb ceiling.
$(Vv)_{MN1}$	Initial constant Mach number at Vertical velocity
$(Vv)_{MN2}$	Constant Mach number rate of climb at the second phase
VCF	Variable camber flaps
W	Tyre width
Wf	Fuel Mass function
$W_f/(Mg)_0$	The fuel mass ratio
'x'	Represents the wing span (b)n
X_{AS}	Axial Spacing
X_{LS}	Longitudinal Spacing
Z	Datum value
α, *alpha*	Angle of attack / incidence
α_{SS}	Second segment Climb-out factors
α_{wl}	Winglet aspect ratio
β	Orientation angle where β = 47 degrees
β^{BAR}	Drag term factor
$(\beta^{BAR})_{co}$	Climb-out drag factor
$(\beta^{BAR})_{cr}$	The start of cruise thrust-to-weight ratio
γ	decent Angle (set at 3 degree)
γ_G	The 'dry' polytropic gas index
γ_T	Tyre deflection under load
λ	Taper ratio
λ_G	The landing gear reaction factor
$\Lambda_{1/4}$	Wing quarter-chord sweep angle
$\Delta(cd)_{wl\_lower}$	Increment of drag for the lower winglet section
$\Delta(cd)_{wl\_upper}$	Increment of drag for the upper winglet section
Δ_L	Increment in lift

Δl_{fuel}	Incremental position of the fuel mass
ΔL_{BDSF}	Broad Delta single fin incremental lift
ΔL_{BL}	Baseline Aircraft increment lift
Δ_{LEL}	Increment in lift due to Leading Edge devices
Δl_{fuel}	Incremental position of the fuel mass
Δ_{TEL}	Increment in lift due to Trailing Edge devices
Δl_{pp}	The propulsion system mass
Δl_{w}	Incremental position of the wing mass
ρ	density
ρ_0	Sea level static density
σ	Relative density
σ_{C1_EAS}	Calculation for relative air density
σ_{cr}	Relative density at start of cruise
σ_{cr1}	The relative air density at start of cruise
σ_{cr2}	Second cruise altitude stage of relative density
$\sigma_{Fin\ cr}$	The maximum cruise relative density
σ	Relative atmospheric density ($\sigma = \rho/\rho 0$)
φ	Structural sweep parameter
η_o	Shock absorber efficiency
ηt	Tyre efficiency
μ_G	The Breaking coefficient
τ	Thrust factor
τ_{co}	Climb-out condition
τ^{BAR}	Thickness correction factor
$\tau_{C1\ EAS}$	The thrust factor at constant equivalent airspeed climb
τ_{cr1}	Initial cruise Thrust factor
τ_{cr2}	Second cruise Thrust factor
$\tau_{Mn.1}$	Thrust factor for constant Mach number climb
$\tau_{Mn.2}$	Second phase of the thrust factor for constant Mach number climb

Subscripts

0	Static conditions
a	Approach conditions
av	Available
calc	Calculated
cor	Corrected

cr1	Start of Cruise flight condition
cr2	Second cruise stage flight condition
Crit	Critical flight phase
cruise	Cruise flight condition
des	Design
Desc	Descent flight condition
des.range	Design range
eng	Engine reference parameter
error	calculated error
EST-1	1st Iterated design estimate
EST-2	2nd Iterated design estimate
Est	Estimate
exposed	Exposed
Fac-s	Altitude dependency factor
FIN	Final condition
Fin cr	Final cruise flight condition
Fuel	Fuel flight condition
FUS	Fuselage
G	Gear/undercarriage
H, h	Height
ht	Horizontal Tail
hw	The height of winglets
i	Incidence angle
input	Input
It	items
kink1	Inboard kink section of the main wing
kink2	Outboard kink section of the main wing
limit	Limit design condition
l_{Tail}	The tail mass of Fuselage length
lw	Lower winglet
max	Maximum design condition
min	Minimum design condition
nacelle	Engine nacelle
NET	Net
OD	Off design condition
Op.it	Operational items

Pay	payload
PAY.L	Payload
Q	Constant
req	Required
root	Root chord section
Side	Side - cross sectional view area
stall	Stall
surf	Surface(s)
sys	The Systems
T	Temperature
Tail	The tail mass
tip	Tip chord section
Top	top - cross sectional view area
Total	Total
TO	Take-off
ultimate	Ultimate design condition
us	Un-stick
use	useable
uw	Upper winglet
Vztail, VT	Vertical tail
W, wing	Wing
wave	Wave
wet	Wetted
wl, winglets	Winglet

Acronyms:

A/C	Aircraft
AE	All Electric
ATC	Air Traffic Control
AUM	All-up mass
AV	Avro Vulcan
AVL	Athena Vortex Lattice
BD	Broad Delta
BDFT	Broad Delta fin and tail configuration
BDSF	Broad Delta single fin
BDVT	Broad delta V-tail configuration

BL	Baseline Aircraft
BPR	By pass ratio
CFD	Computational fluid dynamics
CR	Compression ratio
DSF	Double-slotted flaps
EAR	Effective Aspect Ratio
EAS	Equivalent airspeed
EDA	Effective Dihedral Angle
FE	Finite element
FPA	Approach flight path angle
HBPR	high bypass ratio
LE	Leading Edge
LEX	Leading Edge device/extension
LHR	London Heathrow
MAC	The mean aerodynamic chord
MG	Mass of gear/undercarriage
MLG	Main landing gear
MPP	Mass of Propulsion Systems
MT	Mass of the tail
MW	Mass of the wing
NLG	Nose landing gear
OEM	Operational empty mass
OTW	Over-the-wing
SAI	Silent Aircraft Initiative
SL	Sea level
SP	Structural design parameter
TE	Trailing Edge
ToL	Take-off length
T/W	Thrust-to-weight ratio
UHBPR	Ultra-high-bypass ratios
VAT	Vertical axle travel
VCF	Variable camber flap
WB	Wheel-base

Chapter 1 Introduction & Objectives

1.1 Background

Jet powered commercial aircraft (aircraft) have been flying since the first de Havilland Comet which entered into service in 1952 and was followed by the Boeing 707 in 1958. The introduction of long-range aircraft opened up the skies to a global customer base resulting in growth of the aviation industry and the challenge now referred to as airport expansion. As airports developed, passenger number, flight frequency, and airport congestion increased, which in-turn resulted in environmental and political debates on local community health and aircraft noise. At present this is still a major concern because airport expansion projects, such as Heathrow Terminal 5, are expected to require an additional runway to meet the operator and passenger demands when up and running; resulting in more aircraft, flights, passengers, noise complaints and so-on, currently the situation is spiraling out of control [1].

In the past, noise from the engines were held responsible for community noise complaints and resulted in noise monitoring and policing around the major airports. The challenge remains to reduce commercial aircraft noise and is because of ever-changing legislation governing noise levels. The idea is to provide a capacity limit (or cap) for all airports and introduce quiet aircraft that are inaudible outside the airport perimeter; daily airport capacity could be increased by using 24-hour flight operations without expanding airport boundaries.

1.1.1 Introduction to the Silent Aircraft Design Challenge

The silent aircraft design challenge began in 2004 where The University of Cambridge and The Massachusetts Institute of Technology (*MIT*) combined resources to create a C-MIT three year study into the Silent Aircraft Initiative (SAI). The aim of the research project was to investigate the possibility of conceptually designing a virtually silent[1] aircraft, and the decision was taken to base the design on a Blended-Wing-Body (*BWB*) concept.

The integration of Cranfield University into the SAI project occurred one year after the initial project launch, where the aim of the Cranfield study was to investigate alternate configurations for a silent aircraft. The Cranfield approach was to take a step backward, assess alternate airframe geometries and propulsion systems, and to compare these relative to a conventional aircraft design.

[1] The term “silent” refers to noise of the vehicle being imperceptible to the human ear and not that there is no sound produced by the aircraft.

The main purpose of Cranfield's research was to identify novel airframe configurations and engine technologies, integrate the designs, and determine an ideal configuration solution for a silent aircraft. The integrated airframe-engine designs would then be compared to the *SAI* noise target of 60db(A) at the airport perimeter, and to a baseline design study. The expected outcome of the Cranfield study is to assess which novel aircraft design concept is a competitive solution to meet legislative and operator requirements, and is an economically viable solution for entry into service as discussed within [2]. The research was divided into two main areas of focus, the airframe design (author), and the engine design, which was analysed by Mr G. Doulgeris.

Prior to Cranfield's involvement, the airframe selection for the *SAI* was based on a Boeing BWB planform, for which a preliminary concept design was presented in February 2007 [3]. Silent airframe designs [4] and novel propulsion systems technologies [5] were investigated by Doctoral and Masters candidates from C-MIT. The research was supported with faculty support and advice from industry and this merger of academia and industry was referred to as the Knowledge Integration Community (*KIC*). The final design produced by the *SAI* was a functionally silent aircraft concept with a noise of 63 dB(A) at the airport perimeter. The design was presented as being virtually silent and boasted a substantial reduction in fuel consumption classifying the design as not just silent but also 'green'.

The challenge for the author was set to identify the most silent airframe and combine this with an equally silent propulsion system from Mr. Doulgeris, with the aim to create a viable silent aircraft concept and compare with the findings of the SAI research.

1.2 Research Objectives

The design of a fuel efficient and silent aircraft concept cannot be achieved without identifying a mission specification and a series of design objectives. The design mission for this PhD research study was based upon a Boeing 767 class of airliner, with a 3 class seating arrangement of 216 passengers for a 4,000 nautical mile range at a cruise of Mach 0.8. This aircraft specification was identical to that used by the SAI study, where the main emphasis was to identify the benefits of the unconventional configurations based on the same mission specification.

The research aims and objectives for the study are linked to the doctoral research 'intellectual contribution' to science, where the following objectives define how future research can benefit from the results of this dissertation.

- Develop an aircraft conceptual design methodology which is capable of analysing novel airframe configurations alongside current conventional aircraft.

- Integration of an airframe noise prediction tool to identify the key characteristics for the design of a silent airframe concept.

- Identify the most silent airframe concept given certain entry-into-service (EIS) technology and manufacturing assumptions for a range of innovative and more conventional designs.

- Investigate adaptable aircraft operations (*AAO*) to identify the impact of continuous descent approaches, displaced landing thresholds, and alternate operational considerations that may enhance efficiency and reduce aircraft noise.

- To provide a comparative study for the integration of novel propulsion systems with innovative airframes in-order to determine an ideal silent aircraft solution.

- To quantify the reduction in noise achievable through redesign of the current tube-and-wing airframe, and identify possible short and long-term solutions to the aviation noise challenge.

The main objectives of this research are defined above, where the process involves develop a design methodology for innovative silent aircraft configurations, with the capability of identifying key parameters to reduce airframe component noise and have minimal effect on performance and cost. The research contained within this dissertation focuses primarily on the design of airframes and considers the integration of propulsion systems cycles designed by Mr. Doulgeris [6].

Engine integration is a critical design challenge, where an incorrect installation with the airframe could be detrimental to the noise and performance of the aircraft. There is no logic in matching a noisy engine with a quiet airframe, because the higher noise source will always dominate and provide a noisy aircraft and vice-versa, so engine-airframe matching is essential. The ideal integration of airframe and engines would provide mutual benefits in reducing installed drag, increasing flight performance, and more importantly maximising noise shielding potential of both airframe and engine noise sources.

The target for both doctoral researchers is to investigate, design, and integrate silent airframes and engines to achieve a single goal, a silent, socially and economically viable aircraft for the future.

1.3 Thesis Structure

The development of a novel airframe design methodology for silent aircraft is a broad and challenging area of research, which is described within seven main chapters and concluded with a detailed discussion.

Chapter 2 identifies the major contributors of airframe and engine noise; providing a background on noise, legislation, operations, and new technology studies aimed at reducing aircraft noise. An extensive review of current literature enables projects conducted by large aerospace organisations to be investigated; with a view to integrating a handful of these technologies into the novel airframe designs. Additional studies by the author explored geometry variations for potentially low noise, low cost, and environmentally friendly (green) airframe configurations. Integration of novel technologies, combined with the investigation into innovative airframes, assisted with selecting seven airframe configurations to develop the design methodology for a silent aircraft.

Chapter 3 introduces the conceptual design methodology. The methodology was developed using a parametric analysis method and combined results from a detailed component analysis; which included detailed wing design, component sizing, performance, cost prediction, and a low fidelity airframe noise analysis. This chapter introduces the design specification and results of the datum baseline aircraft, where the results were used to validate the design methodology against published data and FAA noise certification results for an existing aircraft.

Chapter 4 provides a detailed design and review of the broad delta (BD) airframe concept, investigating the design of a tailed and tailless variant in-parallel with a new-technology variant of the baseline aircraft. Advancements in technologies were factored into the design of these three configurations and provided a similar technology level design comparison to try and identify any performance and noise benefits of the BD airframes.

Chapter 5 provides a design review of innovative concepts such as the Blended Wing Body (BWB) and Joint Wing (JW) airframe configurations. The preliminary design considerations for the BD airframes were used as a guide to determine the main challenges in designing the alternate airframe designs. The changes made to the design methodology are described alongside a discussion of the methods used to generate these alternate airframes. The analysis is combined with a preliminary design comparison to the more conventional tube and wing designs previously discussed in chapter 4.

Chapter 6 details the noise analysis procedure which was integrated into the design methodology. A description of the low fidelity noise prediction tool enabled design cases to be analysed for alternate configurations using current airworthiness legislation. The changes in noise perceived on the ground is corrected for altitude, ground reflection, and shielding, and is mainly dependent upon the type of airframe and the engine installation of that particular airframe. A description of the methods used is described so that once each configuration was optimised, alternate engine installations were considered (to further reduce vehicle noise). The calculated noise of each tube-and-wing airframe

was compared directly to the noise of the novel airframes, where the optimum low noise aircraft was identified.

Chapter 7 provides a detailed discussion into the design process and identifies the major conclusions of this research. The discussion provides a summary of the work completed within the preceding chapters, and identifies the major goals, challenges, and research concerns that complicate the airframe design process. It was considered essential to identify sources of error, so that future design methodologies may evolve to iron out some of the wrinkles, reducing future error margins. The dissertation concludes by answering the main questions raised at the beginning of chapter 1, and in identifying the main airframe design considered to be the most practical and silent solution for a more environmentally focussed aircraft design.

Results contained within this dissertation are followed by the accompanying appendices which contain the relevant analysis and formulae to complement the text within the chapters. The appendices are mainly focussed on detailed analysis for one airframe family, the BD, so that the design development was consistent throughout the evolution of the conceptual design methodology. The BD airframe design is used as the main focus of the appendices, where that knowledge captured during the design process was transferred to the alternate airframe configurations where applicable. Alternative design methods used for the novel airframe designs are noted within the relevant chapters, references are quoted where necessary, but analyses used are not discussed further within the appendices.

References

[1] DfT, [DfT, 2003], 'The future of air transport – white paper and the civil aviation bill', *Department for Transport*, CM-6046, www.dft.gov.uk/aviation/whitepaper, December 2003, UK Government.

[2] Smith C. P., [Smith, 2005], 'The environmental challenge – bringing technology to the market', *17th International Symposium on Air Breathing Engines*, ISABE-2005-1008, September 2005, Munich, Germany.

[3] SAI, [SAI, 2007], 'The 'silent aircraft initiative' (SAI) – a new approach', Cambridge and Massachusetts Institute of Technology (C-MIT) Official website, http://silentaircraft.org/, February 2007, Cambridge, UK, US.

[4] Hileman J. I., Spakovszky Z. S., Drela M., Sargeant M. A., [Hileman et al, 2007], 'Airframe design for 'silent aircraft'', *45th AIAA Aerospace Sciences Meeting and Exhibit*, AIAA 2007-453, January 2007, Reno, Nevada.

[5] de la Rosa Blanco E., Hall C. A., Crichton D., [de la Rosa Blanco et al, 2007], 'Challenges in the silent aircraft engine design', *45th AIAA Aerospace Sciences Meeting and Exhibit*, AIAA 2007-454, January 2007, Reno, Nevada.

[6] Doulgeris G., [Doulgeris, 2008], 'Modelling & integration of advanced propulsion systems', *PhD Research Thesis*, March 2008, Cranfield University, UK.

Chapter 2 Aircraft Design for Reduced Noise

In order to provide an aircraft (aircraft) design tailored towards silent flight, a review of current literature is required so that the main sources of, and contributors to aircraft noise can be identified. Investigating the fundamentals of how and why noise is generated is of primary importance so that solutions can be sought to significantly lower the dominant noise sources. A description of noise reduction technologies is discussed within this chapter, with the aim to integrate these technologies on several novel airframe concepts; identified to be the most promising in-terms of noise, low cost, and 'green' considerations. The following text represents literature relevant at the time of publication and has influenced the design path of the author in order to initiate the design methodology.

2.1 Noise Metrics

The target to meet noise legislation is an important feature, but the main question aircraft designers must face is, what is noise? How can it be measured? How can it be isolated? Smith, 1989 [1], best describes noise as being *"a common parlance for undesirable sound"*. Noise is generally quantified in decibels (dB), but due to the Committee on Aircraft Noise (CAN) legislation, airport perimeter measurements use the effective perceived noise scale EPNdB, which was created specifically in order to validate aircraft noise level certification. *"The decibel addresses a wide range of sound intensities by using a logarithmic ratio of the actual sound pressure level (SPL) to a nominal value, the threshold"*, where *"a doubling of sound intensity or noise level is reflected by a change of 3dB"* [1].

Noise frequencies between 50Hz and 10kHz describe the noise limits that provide the most annoyance to the human ear. The 'A'-weighted decibel dB(A) scale is used to determine the degree of irritation to the ear [1]. Alternate noise metrics are used for many applications and for aviation there are two main noise metrics, the first is the A weighted scale, which is used to implement noise restrictions at a number of airports and the second is EPNL. EPNL is the effective perceived noise level (EPNdB), which is a measure of the noise heard on the ground by an observer, corrected for aircraft broadband noise sources as well as the duration of the noise [2]. As mentioned above EPNL and dB(A) are both used for certification and can be measured at specific flight segments such as take off, flyover, or approach. The dB(A) scale was used for the present study to validate airframe and engine noise prediction tools, due to its simplicity and metrics obtained for the FAA noise comparison/validation data [3].

2.2 Aircraft Noise Regulations

The International Civil Aviation Organization (ICAO) is the governing body on aircraft noise, where the release of a technical document to the Convention on International Civil Aviation (Chicago,

1944), established the ICAO as the worldwide government civil aviation body [4]. The aviation industry was the first regulator of all transport industries to implement global noise regulations, for example, legislation has existed at London Heathrow airport since 1958. Volume 1 of Annex 16 was established in 1968 and contains standards and recommended practices for limiting aircraft noise, where the latest release in January 2006 of Chapter 4, Annex 16 – Environmental Protection, provides the current noise legislative standards [5]. The ICAO is the main authority for CAN, which provides essential updates to the certification standards, and are enforced by a Committee on Aviation Environmental Protection (CAEP).

In the UK and Europe, the legislative requirements of the ICAO fall into Joint Airworthiness Requirements (JAR), part 36, which supersede the old British Civil Airworthiness Requirements (BCAR). Noise limits are set at three points, two for take-off (one underneath the flight-path, and one to the side,) and one for approach (underneath), and new aircraft types have to demonstrate that they meet these limits to be allowed to operate. The European Aviation Safety Agency (EASA) is currently drafting certification specifications for both noise and emissions standards. These will come into force in the EU as CS-36 for noise after a transitional period.

Noise Certification Reference Points - Defined
In noise certification, aircraft noise levels are measured at three certification points:

1- **Fly-over**: 6.5 km from the brake release point, under the take-off flight path;

2- **Sideline**: the highest noise measurement recorded at any point 450 m from the runway axis during take-off;

3- **Approach**: 2 km from the runway threshold, under the approach flight path.

Cumulative levels are defined as the arithmetic sum of the certification levels at each of the three points.

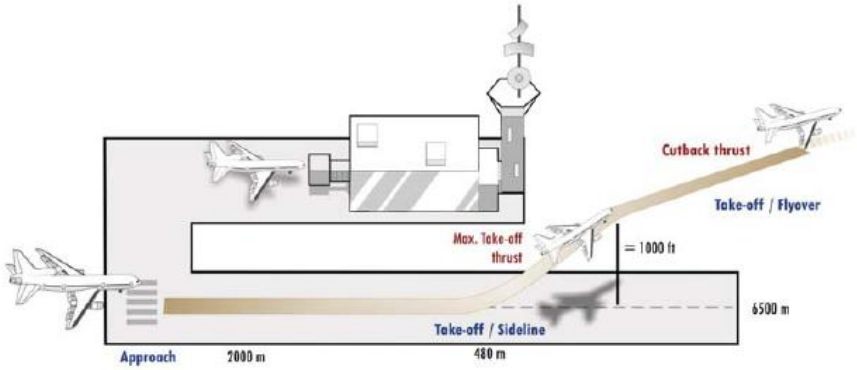

Fig 2-1: ICAO noise reference points [6]

The FAA introduced noise regulations in 1971 (Stage 1), which have been amended to this date with the current FAR Part 36, Stage 4 requirements released at the same time as Chapter 4, Annex 16. Similarly in the US, legislation for the ICAO fall into the Federal Aviation Requirements (FAR), part 36, which are the American equivalent noise certification standards. Fig 2-1 represents the ICAO noise reference points for the three major flight cases of take-off, sideline (lateral), and approach. The ICAO noise certification standards are similar to the FAA requirements and can be compared using FAR Part 36, Appendix A [7].

The ICAO Environmental report published in 2007 [6] clearly defines the evolution of the noise certification standards, and is one of the main sources of information available for those without access to the ICAO noise certification standards [5].

The environmental report addresses the reduction in noise achieved through the fact that "*aircraft manufacturers were continuously researching and developing technologies to reduce aircraft noise and striving for a better understanding of the sources of aircraft noise. Accordingly, the inclusion of the noise absorbing material in engines and engine nacelles, as well as overall nacelle design, and mechanical refinements on engines, together with airframe adjustments, have all contributed incrementally to further reducing the noise of jet powered aircraft. Although none of these improvements individually has matched the step forward that came from the increase in bypass ratio, together they have been significant*" [6]. Fig 2-2 is an extract from [6], which depicts the reduction in noise limits over time.

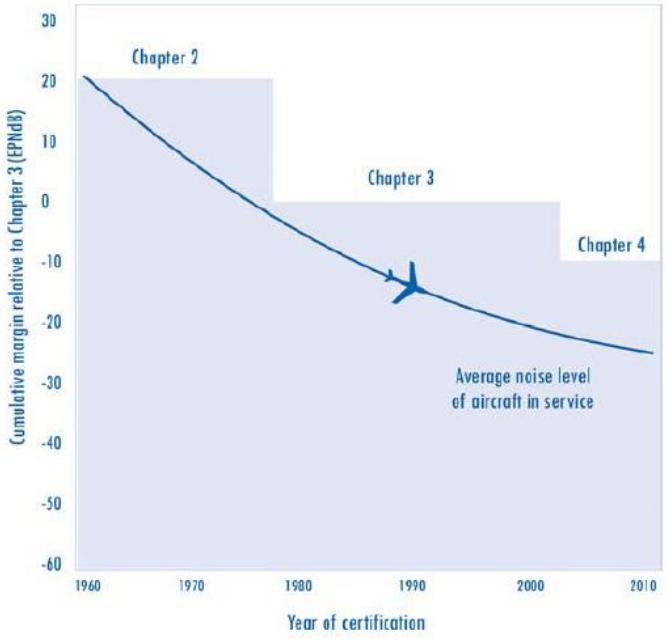

Fig 2-2: Progress made in noise reduction at the source since implementation of aircraft noise standards [6]

The CAEP "*concluded that although no increase in stringency of the noise limit at any one measuring point was possible, it was reasonable to introduce a limit on the sum of the noise indices at all three measuring points. It therefore decided that this sum of the measured noise levels would have to be lower (by 10dB) than the sum of the limits imposed by Chapter 3 of Annex 16. A further requirement was that the sum of the measured levels at any two measuring points would have to be below the sum of the corresponding Chapter 3 limits by at least 2dB. These requirements subsequently became applicable in March 2002. This change in approach to the method of applying*

noise limits, while ensuring an overall reduction in noise, still allowed manufacturers some freedom to take advantage of large improvements at some measuring points to offset smaller reduction, or no reductions, at others. Additional changes to Annex 16, Volume 1, are proposed for applicability in November 2008. That proposal includes: provisions related to atmospheric conditions in noise certification testing and measurements conditions (e.g. clarification of definitions relating to wings speeds), the measurement of aircraft noise perceived on the ground, the evaluation method for noise certification of helicopters, and an update to the guidelines for obtaining helicopter noise data for land-use planning purposes."

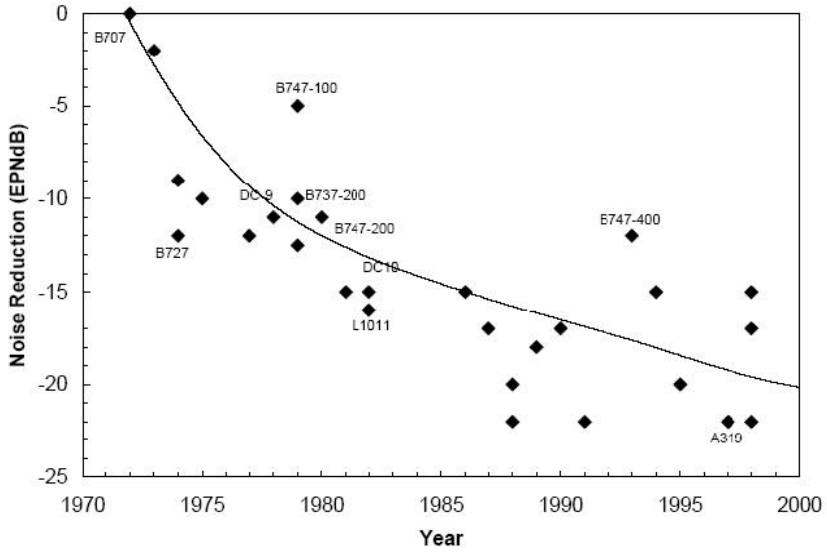

Fig 2-3: Noise abatement improvement in Civil Aviation [8].

The environmental report on noise limits concludes with the suggestion that "*While research and development in noise reduction technology continues, it appears likely that the future will be similar to the past, with steady incremental progress in a number of areas; but no dramatic improvement in any one area. We may therefore expect small advances which will only accumulate into significant changes over a longer period of time"*. This is trend described can be seen within Fig 2-3, where the design of new aircraft are following the trend of providing gradual noise reduction, without a drastic step change.

Prior to the release of Annex 16 certification standards in 2001, research was conducted to investigate the proposed noise cut-backs from independent aviation organisations, such as NASA. Fig 2-4 describes the targets set by NASA, suggesting limits to reduce aircraft noise by 20 EPN(dB) within the next twenty years, and an optimistic target of half of this, 10 EPN(dB), by 2007. The results of the Quiet Aircraft Technology (QAT) research [9], suggests that individual airframe and engine component noise has met targets, with plans to implement these technologies onto a fleet of aircraft in

2010. Another institution researched was ACARE, the Advisory Council for Aeronautics Research in Europe [10]. The ACARE targets suggested a reduction of perceived noise of 10 EPN(dB) by 2020, referring to a -10 EPN(dB) noise reduction for flight operations, where a limit of a 65 LDEN outside the airport boundaries was set for evening flights. LDEN is a noise metric defined as the equivalent continuous noise level (Leq) calculated for an annual period with variable weightings depending upon the time (5dB for evenings and 10dB at night) [11].

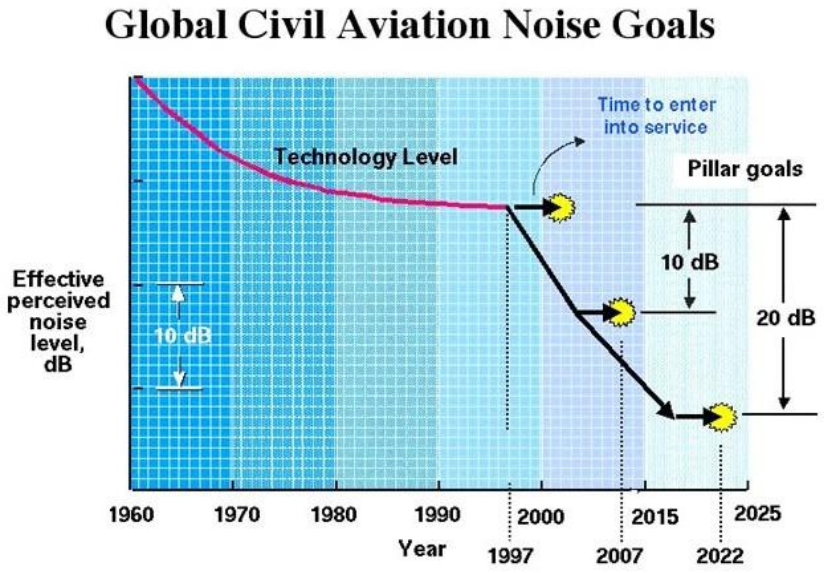

Fig 2-4: Aviation Noise Goals extracted from NASA future noise targets for QAT program [9]

The SAI team provided a maximum target noise of 60 EPNdB, which includes both airframe and engine noise. The main challenge was to reduce airframe and engine noise limits to approximately 55 EPNdB, so that if the combined noise of both components should fluctuate around the 58 EPNdB mark, there would be a 2dB margin of error available.

2.3 Aircraft Noise

Glancing through history, noise produced by an aircraft was regarded as the sound originating from the engines, where in effect no consideration was made for the airframe. As noise measurements progressed, it was found that airframe noise contributed to a larger amount of undesirable sound than initially expected, due to development of significant engine noise reduction methods. Tests such as those conducted by NASA [9] and ACARE [10] have been conducted on modifying conventional airframes to reduce noise in order to meet legislative requirements, but these minor changes resulted in a small reduction in decibels (dB), but nothing significant to drastically lower airframe noise.

Options are now running out for the current ‘tube and wing’ configuration and new radical designs are required to meet future noise targets.

Aircraft noise is described as undesirable sound emanating from two principal noise sources, being the airframe and engines, where both vary depending upon specified flight conditions. In the past, engine noise was the dominant source of noise but over the last 30 years, manufacturers have made modifications to such an extent, that during approach and take-off flight phases, airframe noise is now comparable, if not the greater of the two.

Fig 2-5: Conventional aircraft on approach for landing ‘dirty’ configuration, with flaps and slats deployed, undercarriage extended, and at close proximity to the ground [‘Science of Flight’].

2.3.1 Airframe Noise Sources

There are a number of noise producers on a conventional ‘tube and wing’ airframe, and these are due to surfaces or obstructions to the flow around the aircraft. If no surfaces were deflected the aircraft is considered to be in a clean flight configuration, where when all surfaces are deployed, for example on an approach, then this is considered as a ‘dirty’ flow configuration.

The main contributors to noise are the undercarriage, leading edge (LE) slats, trailing edge (TE) flaps, ailerons, elevators, and the empennage. Although these provide the majority of noise, additional smaller sources are present, for example the wing-fuselage interface, the wing-pylon, and pylon-nacelle joins. These are minor disruptions to the flow, but never-the-less they generate noise which is propagated towards the ground. Additional noise sources include hatches and doors that vibrate during flight, and even the vibrations felt through the airframe from engines.

The major airframe noise sources are identified above, where the key contributors are the landing gear and flaps on approach. The principal noise source from the use of flaps is the turbulent flow passing through the slot (or vein), where this noise source can be alleviated by using new technology variable camber flaps [12]. The idea of fairing flaps and the undercarriage to reduce the wake generated at the

edges is shown within Fig 2-7, Fig 2-8 and Fig 2-9. The possibility of reducing noise further is to use trailing edge brushes [13], which "*indicate a significant source noise reduction in excess of 10 dB, thereby revealing two relevant noise reduction mechanisms. In addition to broadband turbulent boundary layer trailing edge noise also narrow band contributions due to vortex shedding from the edge were alleviated*".

Present research into reducing the noise produced by undercarriage is generally focussed in the same direction, where researchers and industry have their sights set on producing miraculous fairings that will silence the gear noise without adding weight or maintenance complexities, which in the authors' opinion is highly unrealistic.

Fig 2-6: Honda Jet with engines mounted above the wing to enhance engine noise shielding on the ground, with passenger cabin directly in sight of engines (images courtesy of Honda website), [14].

Fig 2-7: Nose landing gear bare (left) compared to new SILENCE(R) fairing design (middle) [images courtesy of the SAI], and a main landing gear fairing design concept (right) ['Science of Flight'].

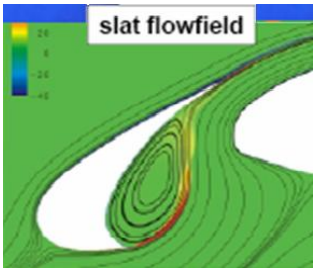

Fig 2-8: Flow-field around a conventional slat, identifying the noisy region of the slat cove ['Science of Flight'].

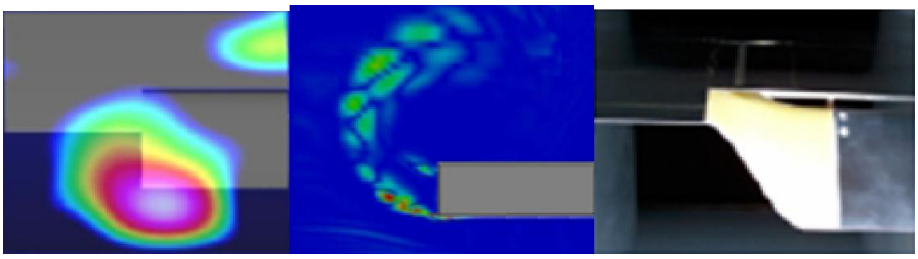

Fig 2-9: Flow-field and wake (left & middle images) around a conventional deployed flap, identifying the noisy region at the flap corner, compared to new faired ACARE concept (right) ['Science of Flight'].

In reality, this is not the only solution to combat noise, but there are numerous alternate and some might say radical solutions to the challenge. One such far-fetched idea would be to remove the undercarriage completely, and train the pilots to land on trolleys fixed by tracks to the runway. This would completely remove the undercarriage noise source, with the potential for great tragedy too, as piloting to land a 300 plus passenger aircraft is difficult enough as it is without having to also perform a pin-point landing. Alternatively, a safer option would be to relax current legislation regarding the deployment of undercarriage and allow the aircraft to approach into the airport perimeter before extending the gear. This would avoid most concerns regarding approaching noise from undercarriage, but in the event of a fault/failure where a gears-up landing is required, this would reduce the pilots response time and also there may not be enough time for the pilot to pull up for a go-around.

An additional option of drastic change would be to redesign the current mentality for airport designs and locations, and re-introduce amphibious aircraft (sea-planes). Since the earth is almost 70% water, why not take advantage of this and use old shipping ports and docks for water landings? Airframes are already designed to withstand the pressure loading from a ditching case, so why not tailor the aircraft to land on water. Despite the obvious disadvantages of corrosion due to salt water, this could solve many noise complaints, but introduces many more challenges to the aircraft manufacturers to try and create a 300 plus seat amphibian aircraft.

2.3.2 Engine Noise and Sources

The launch of the de Havilland Ghost MK I, in 1949 was the first jet engine and a milestone for civil aviation history of civil, boosting the air-travel industry [8], [15]. The one hindrance to the more efficient jet powered flight was the significant amount of noise produced by the aircraft, which has been a major concern since the beginning of the jet era [16]. The use of jet engine, in early '50s, allowed numerous innovations, such as a reduced thickness highly swept wing, leading to higher cruise speed, and resulted in lower operating costs.

The extensive research on gas turbine technology led to significant progress in the field of propulsion. As a result, turbofan engines such as the Rolls Royce (*RR*) Conway or GE CF700 were introduced,

followed by propulsion systems like the *RR* RB-211, GE CF6, or PW JT9D. These new engine were combined with new technology applications, such as lining in the intake, leading to a ~15-20dB reduction in noise by 1985, as shown by the step change in Fig 2-10. The rate of improvement to lower the engine noise reduces with time and this is because component efficiencies and material quality levels are reaching close to their theoretical limits. The continuous growth of air transport will inevitably lead to unacceptably high noise levels in the airport suburbs. Thus, the consequent demand for significant future noise abatement makes essential the need of drastic changes in the propulsion system design. From the propulsion engineer's perspective, a redesign of the thermodynamic cycle could lead to promising result, and this is the objective of the research study completed by Mr G. Doulgeris [17].

As jet engine efficiency has increased and noise has been reduced, the effect on the size of the engine is the effective increase in fan diameter. The increase of the fan diameter is more commonly referred to increase in the bypass ratio. Bypass ratios of the earlier engines were as low as 3, where current ultra efficient engines are leading towards bypass ratios of 8 and above. The limit with these engines is the diameter of the fan required and is limited because of current aircraft configurations with engines under the wing. The engines have a diameter limit due to ground impact considerations, where a ground clearance is required in order to avoid collision damage during the landing part of the flight cycle. In addition to the size limitations, the current turbofan engine designs are reaching a plateau, where increasing the bypass ratio past a certain limit impacts the fuel efficiency of the engines, hence the study by G. Doulgeris to investigate alternate engine cycles for a lower noise propulsion system design.

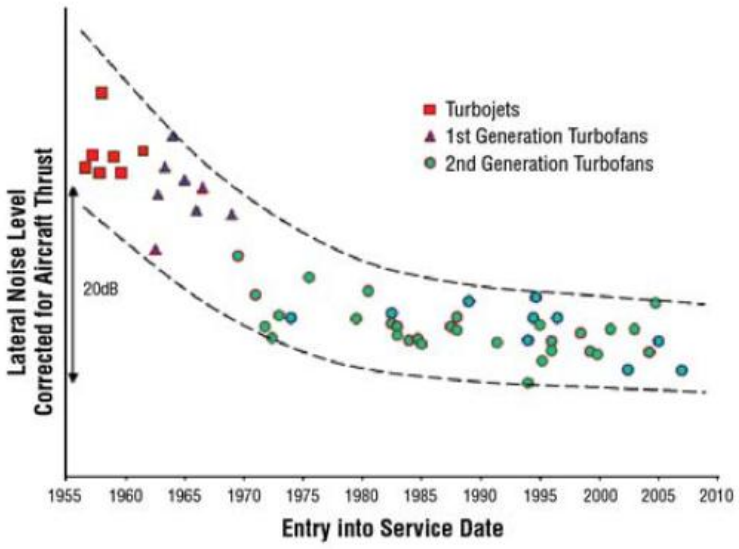

Fig 2-10: Historical progress on Jet powered aircraft noise reduction through evolution of the turbofan engine [6].

Engine noise sources are categorised as forward propagating and rearward propagating noise sources. The main contributors are the fan and jet noise, where compressor noise and turbine noise does increase at higher speeds. The major jet noise source can be reduced by incorporating chevrons at the rear of the jet to allow the hot core and cold bypass air to mix gradually, which results in lower noise.

Fan noise can be reduced through careful design of novel swept fan blades, and this combined with suitable noise liners within the engine nacelle has great potential to reduce noise. Each source of noise, whether engine or airframe has the capability of propagating in any direction, so it its not surprising to know that there are some noise components, such as engine fan noise, that has an aft and forward noise component.

2.3.3 Current Status of Aircraft Noise

Noise reduction of existing airliners has reached a stage where regardless of the number of modifications made [18], the only method to reduce noise significantly, is for a complete airframe redesign [19]. A conventional 'tube and wing' aircraft can be equipped with minor modifications to lower noise, which not only changes the performance, but increases mass and fuel burn, resulting in a less efficient aircraft; for example the use of undercarriage fairings, or addition of novel LE or TE devices.

The introduction of new technologies onto old airframes provides a basis to test and validate the designs, but applying these technologies to a fleet of older aircraft will only provide short-term noise benefits. It is more practical to invest in the development of these new technologies and integrate them into a novel airframe, which would not only complement the low noise devices, but merge their capabilities into the performance of the new airframe.

An additional noise source now mentioned, but not discussed further is the internal passenger cabin noise. The noise produced by components within the aircraft, is not considered as important as the external noise, for this study. Although internal cabin noise is considered a nuisance, it is also reassuring for example, during taxi onto the runway, checks are made using hydraulics, where the flaps are extended, and this noise is heard within the cabin; not only indicating that something is happening, but providing reassurance that checks are taking place, and 'everything is as it should be'. The main concern for passenger cabin is the engine noise, but for many medium-range flights, onboard entertainment systems keep the passengers occupied, and in many cases they become accustomed to the 'buzz-saw' noise from the engine.

2.4 Environmental Considerations

Local and global environmental considerations have recently escalated in importance within aviation, such as emissions, noise, and health concerns, and a few of these are commented on within this chapter. Local environmental concerns refer to those concentrated around communities along the aircraft flight path and depend upon daily flight frequencies. Global effects consider the flight procedures of the operators and environmental issues such as emissions, NOx, contrails, and the release of harmful emissions into the atmosphere. Emissions released during cruise flight may not be visible at present but have lasting effects on population health and the climate.

2.4.1 Environmental Effects on Local Communities

Aircraft noise is a nuisance to those who reside close to airports, where noise from take-off, fly-over, and landing aircraft create a serious impact on surrounding communities. The majority of noise is produced during take-off and landing cycles because of the proximity of the aircraft to the ground and the generation of 'dirty' airflow from deflected surfaces i.e. undercarriage, flaps, etc.. The ICAO established boundaries for which the noise across various stages of the perimeter must be measured. Reducing noise is now a new challenge from a design perspective alongside emissions and costs, and as a result international aviation regulations have changed, prohibiting the use of 'noisy' aircraft at night and in regions that they would exceed local noise limits.

2.4.2 Global Environmental Effects

The reduction of aircraft noise together with the reduction of harmful emissions is a major challenge to make the aerospace industry greener [20]. Aviation has been targeted as one of the greatest polluters in the transport sector leading to noise and green taxes and relates to the proximity of airports to residential areas [21]; where noise tends to take a back seat compared to emissions because it is a localised problem at airport perimeters. Emissions such as nitrogen-oxide (NO_x) and carbon dioxide (CO_2) are considered to be more of a long-term problem, as these gases stay in the atmosphere and are associated with enduring environmental effects. Increased green taxes affect the cost for airline operators, so in order to minimise these costs, operators have stricter requirements for the specifications of new aircraft in terms of noise, fuel consumption and environmental impact. These customer requirements directly impact new products produced by the major aircraft design companies.

2.5 Economical Effects of Aircraft Noise

Airframe manufacturers and engine developers are obliged to meet the requirements of operators. Cost is a key driver for aviation and is considered to be of equal importance as emissions compared

with reducing noise. This is primarily because the cost of development, acquisition, operations, and disposal of the aircraft is critical to aviation. Often the benefit of reducing aircraft noise is overlooked, where one beneficial scenario considers 24-hour flight operations, which would increase both aircraft manufacturers and operator revenues, and cater for growing passenger demands. The fact remains that if designers and operators want to reduce overall costs, more resources should now be invested in the development stage for greener aircraft to provide greater future returns.

Noise isolation is a critical and costly study that requires the thoughts of an aircraft design team combined with the expertise of an independent authority on noise. Isolation of noise requires identification of major noise sources emanating from the aircraft and can be divided into airframe noise and engine noise; with subdivisions under the two groups. To identify noise sources, a detailed exploration of novel airframe concepts is required, coupled with noise prediction tools. One source of noise that will not be discussed within this dissertation is the engine, where the propulsions system design is only referred to for integration purposes. The broad field of airframe and engine research is covered by two doctoral candidates, where Mr G. Doulgeris completed research into the novel propulsion systems [17] and the author investigated innovative airframe concepts.

2.6 Literature Summary

The literature study has identified a number of key issues to understand noise sources and methods that can be used to combat aircraft noise. The main emphasis of this study was to provide a broader understanding of the noise issue and to create a focus point for future design research. The key importance for designing a silent aircraft is to focus design efforts on reducing airframe noise; with a view to producing a greener and more cost effective novel airframe design.

The generation of noise produced by an airframe is now understood to the extent where a basic low-fidelity code could be found and run for given aircraft geometry. In order to fully understand the airframe noise, further research will be required to investigate the prediction of component noise. The main sources of noise have been identified as the undercarriage, TE flaps, LE slats and wing and tail lifting surfaces. Other sources of airframe noise include the interactions between the joints of various geometries, for example the wing-fuselage and the nacelle-wing interfaces. Further research is required in order to establish a possibility to predict these low noise sources or to even minimise them by altering the airframe design.

Research into legislation has provided specific requirements so that noise results can be compared to the limitations set by the aerospace industry noise regulators. Legislative requirements must be met for the development of a civil aircraft design, so that the methodology may be validated, which will

later be used in this dissertation for the analysis of future innovative airframe concepts. Validation of the methodology should indicate a degree of reliability in the results, coupled with a sensitivity analysis, which in-turn requires a screening process to check that the requirements are met.

This section has introduced the major topics related to the noise challenge for future aircraft designers. The procedure for developing a reduced noise novel conceptual aircraft design methodology will now be explained with a description to accompany an initial analysis. This process will also describe the generation of a baseline aircraft in order to understand and validate the methodology being investigated by the author. Prior to developing a methodology, a series of airframe configurations are required in order to determine the scope of airframe variations to date. Investigations into configurations using both current and future technology assumptions provide an overview of possibilities for a future airframe. The following sections provide an overview of the airframe selection process and design philosophy.

2.7 Airframe Configurations

The development of novel airframe designs was achieved through investigating multiple geometries to identify a series of innovative airframe configurations. The baseline aircraft was established within the methodology section, and alternative solutions were sought to initiate a variety of alternate airframe selections. This process began with a brainstorming session involving teaching staff and doctoral researchers, combining ideas and providing a variety of individual opinions for types of novel and futuristic airframe configurations, with the final decision made by the author.

2.7.1 Conventional variations

The benefits of investigating new technology conventional aircraft allows a comparison to be made with the current technology transports, and also enables a direct comparison with some of the newly released aircraft designs such as the Boeing 787-Dreamliner, and the Airbus A380. Comparing similar aircraft which will be released in the market enables a quantitative comparison of both old and new designs. A study to investigate a new technology conventional design will be discussed further on in the dissertation.

Through investigating the baseline aircraft configuration, the variables such as empennage, engine locations, wing locations, wing types, etc, provide a phenomenal number of alternatives for what one may expect to be a simple configuration. In order to understand the true complexity and the sheer number of arrangements, the following aircraft are simply twelve possible combinations for the baseline aircraft alone. Since the baseline design is the datum design case, we can always investigate alternate conventional aircraft configurations which have greater potential for reduced airframe noise.

Fig 2-11: New Generation 'tube and wing' aircraft; Boeing B-787-Dreamliner (left), Airbus A380 (right)

The aircraft below represent a few variations of the current tube and wing airliners and will be discussed as part of the initial down-selection process for silent airframe concepts.

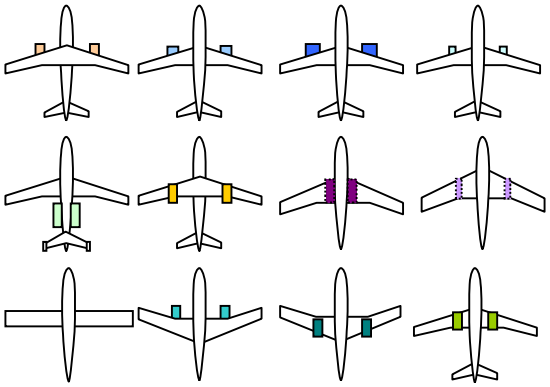

Fig 2-12: Conventional 'tube and wing' (baseline) configuration variants, where all are considered to have the same fuselage with a varying empennage layouts.

The descriptions are listed below for each row from left to right; defined by the wing type and location, followed by each engine location assuming that all have podded nacelles:

Row1: High-wing with underslung High BPR, low-wing with underslung High BPR, low-wing underslung Ultra High BPR, Conventional aircraft with upnderslung moderate BPR.

Row2: Low-wing with aft-fuselage mounted HBPR **(**DC-9), High-wing upper mounted HBPR, Low-wing with engines embedded at wing root (Comet), Low-wing with engines semi-embedded in wing semi-span (Canboro').

Row3: Un-swept low-wing with underslung HBPR, Forward sweep low-wing with underslung HBPR, forward sweep upper mounted HBPR, Low wing with upper mounted HBPR engines inboard.

2.7.2 Broad Delta variations

The Broad Delta (BD) aircraft has many variations and these are represented below. The benefits of the BD configuration is that the number of surfaces creating noise is reduced, as there is no tail-plane and therefore no requirement for trailing edge high lift devices such as flaps, or elevators mounted on a separate tail surface for pitch attitude control. This is an ideal plan-form for a reduced noise aircraft, with a similar range of combinations as with the baseline.

The BD incorporates the design of winglets to this large delta wing and discrete fuselage shape. Each design above has its own merits and the ideal configurations will be stated later as part of the initial down-selection process for the 'most' silent concepts. The descriptions for each variant are listed below for each row from left to right:

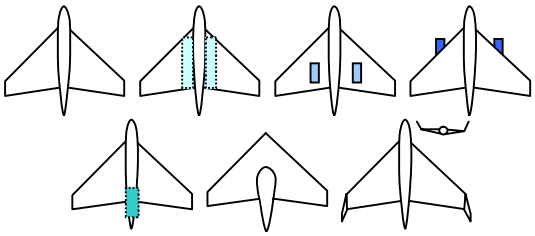

Fig 2-13: Broad Delta Configurations

Row1: Avro Vulcan Concept with conventional fuselage, Engines buried in deep wing root structure, Vulcan with upper podded engines, Vulcan with lower podded engines

Row2: Vulcan concept with buried rear engines, Flying wing with rear fuselage section only, Broad delta (Vulcan) with winglets.

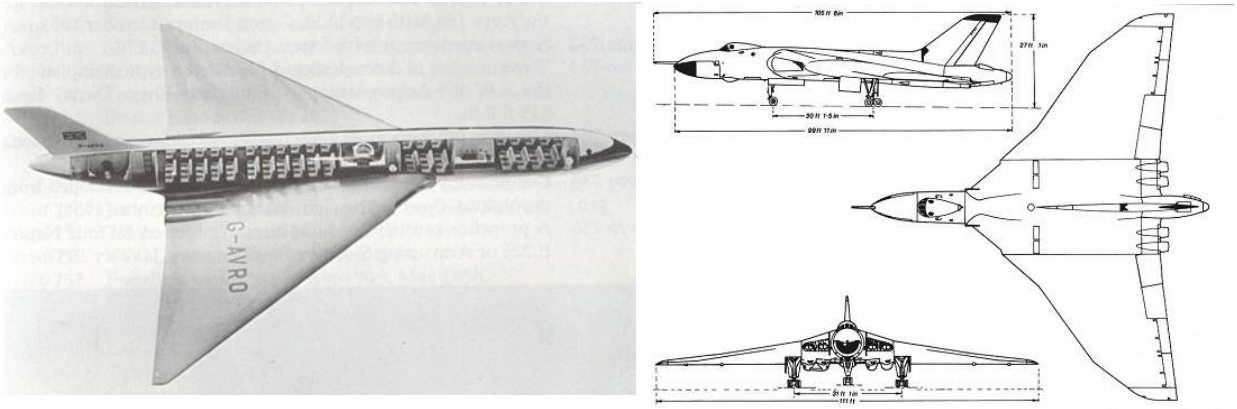

Fig 2-14: Broad Delta Aircraft; Avro Atlantic Concept aircraft (left), Avro Vulcan (right).

2.7.3 Slender Delta variations

The concept of a slender delta aircraft is not ideal for subsonic flight conditions, because it is considered to be inefficient at low speeds, and the high incidence during take-off and landings could cause unease to some passengers. The main advantage of the slender delta is the high LE sweep, where slats, flaps, or a tail are not necessary for flight, where this would be an optimum low noise configuration.

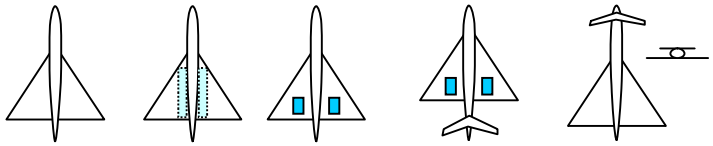

Fig 2-15: Narrow Delta Configurations

Creating a next generation subsonic variant of the Concorde could be an exciting challenge. The Concord is the baseline aircraft for the slender delta family of designs. Each design has its own merits and some resemble the concepts for a sonic cruiser aircraft. The descriptions are listed below for each row from left to right:

Row1: Concorde configuration, Upper embedded engines at wing root, Upper podded engines, upper pods with a tailplane, Long coupled canard with low main wing.

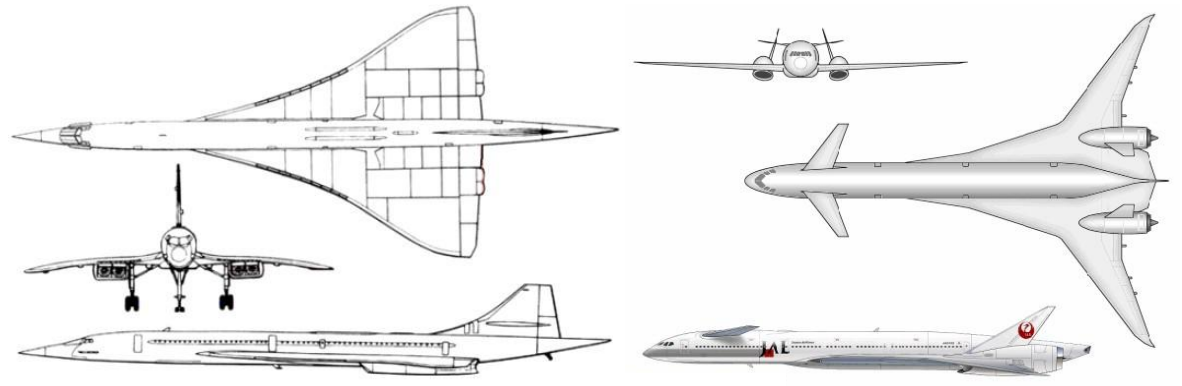

Fig 2-16: Aérospatiale-BAC Concorde (left), and Boeing Sonic Cruiser Concept (right).

2.7.4 Blended Wing Body (BWB) variations

Blended wing bodies are similar to the broad delta concept, where the main advantage is that the fuselage and wings are blended into a smooth single surface. This is an ideal low noise design because like the broad delta, this design does not require flaps or a tailplane for pitch control, thus removing the requirement for TE and possibly LE high lift devices. There are many examples of BWB concepts in the research community, where some of the most extensive studies have been

carried out at Cranfield University, as well as numerous other academic institutes across the world. Current investigations by aircraft manufacturers have led to the design and testing of low and high-speed small-scaled-powered BWB demonstrators, such as the NASA-Boeing X48B, where this design is termed to be more of a hybrid wing-body (HWB) design.

The first two designs in Fig 2-17 on the first row represent previous studies from Cranfield University for the CU-BWB-98 and the CU-BWB-01 group design projects, which are the baseline aircraft for this concept of airframe. The third concept represents the Cambridge-Massachussetts (C-MIT) SAI BWB design (SAX-40), and the fourth is the Russian TSAGI discrete fuselage blended wing body. On the second row, is a novel concept of incorporating a close coupled canard to the BWB design, the CU-BWB-Kestral, and the final BWB has podded engines mounted on the wing semi span.

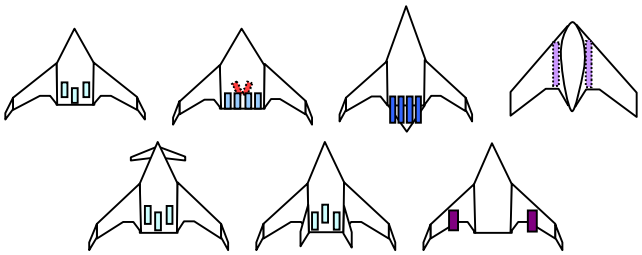

Fig 2-17: Blended Wing Body Configurations

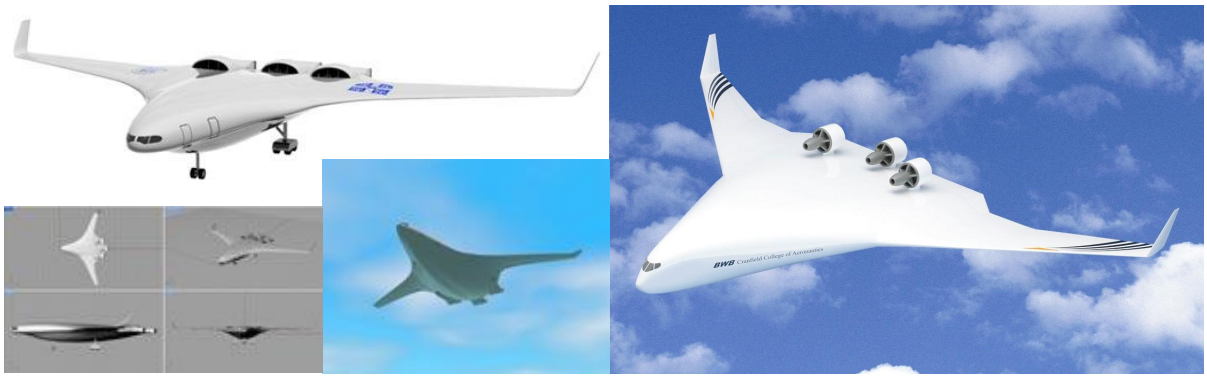

Fig 2-18: C-MIT SAI SAX-40 Concept (left), Cranfield University BWB-01 Concept (right)

2.7.5 Innovative Wing variations

The innovative wing concepts have not been explored past a conceptual design level stage but are worth-while to explore for future airframe designs. Many of the innovative wing designs consider having a 'tube' fuselage, designed to be identical to that of a conventional aircraft fuselage, which simplifies the design process. The type and variation of innovative wing transports are restricted by

the author to symmetrical aircraft. The viability of an oblique wing or an asymmetric civil airliner is not expected to be easily certifiable within the given entry into service (EIS) timeframe.

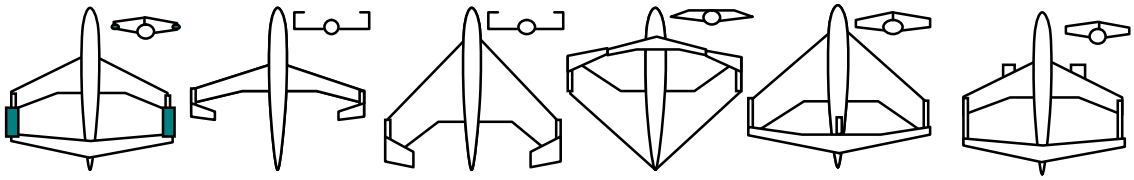

Fig 2-19: Innovative Wing configurations also referred to as joined wings

The sketches above represent concepts for innovative wings. The majority of designs are for joined wing configurations with the concept on the far left incorporating engine nacelles at the wing joins. There are two designs which are essentially 'C' wings, one being similar to a broad delta, and the other being a tail-less conventional aircraft.

Alternative wing designs that are considered to be variations of the JW concept and resemble a conventional airliner are designs such as the truss-braced, strut-braced, and three-surface wings. The strut-braced wing differs from a conventional cantilever wing by incorporating a support strut that reacts all the in-flight compression and tension loads, allowing a lighter wing to be designed. The truss-braced wing is in many ways similar to the strut-braced design, but does not consider negative loads to be transferred through the brace; such as taxi and gust response loads. The three surface wing designs have been investigated for many years, where the reason for having an additional control surface has not yet been justified; because this creates more drag even though the aircraft stability and/or manoeuvrability margins are increased.

The question is raised as to whether an aircraft can be more manoeuvrable or stable or both. Manoeuvrability indicates that the aircraft is agile and responsive, such as a military jet, where this is not the case for civil airliners. Stability indicates that the vehicle may be either statically or dynamically stable during flight where static stability is referred to later on within the dissertation and dynamic stability is not covered. A perturbation, such as a vertical gust would divert the aircraft away from equilibrium (e.g. cruise), where the difference is that a stable aircraft would revert back to its equilibrium position and an unstable aircraft would deviate further into an uncontrolled response (refer to Appendix G, pp. 368 -382). Therefore military aircraft are designed to be unstable in most cases and are highly agile and therefore manoeuvrable. Civil aircraft are designed to be highly stable and have less agility, so can an aircraft be both? The answer can not be answered by the author, however reviewing historical aircraft, the Avro Vulcan was designed as a tailless aircraft and was highly stable, and as a military bomber, the aircraft was considered to be fairly agile for the payload

that it carried, so maybe it is possible to design an aircraft that has high-to-moderate stability and manoeuvrability.

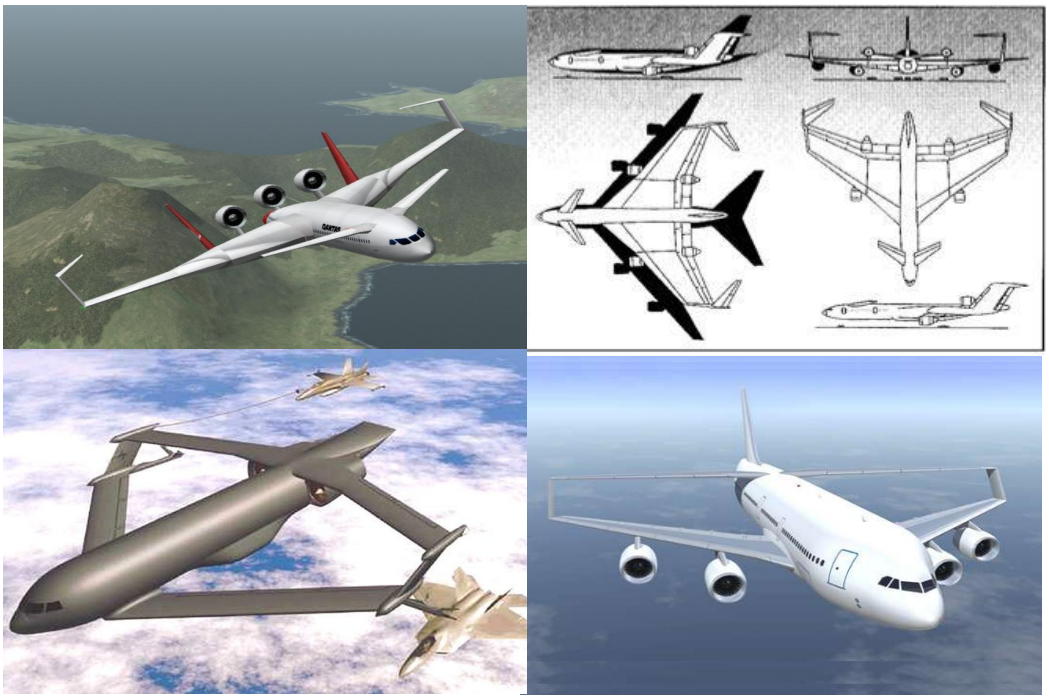

Fig 2-20: C-Wing Concept (top), Lockheed Box wing (bottom left), Airbus Joined Wing (bottom right)

Fig 2-21: Strut-braced Wing (top), Three-surface concept (bottom left), Truss-braced Wing (bottom right)

2.8 Airframe Review Process

A number of novel airframe ‘family’ groups were identified using top-level critical analysis of airframes, such as conventional ‘tube-and-wing’, Blended Wing Body (BWB), Innovative Wing (IW),

Narrow Delta (ND), and Broad Delta (BD) airframes. An aircraft family represents a number of concept variations of a specific airframe configuration[2], where the geometries were assessed in terms of performance advantages and design challenges using published data. A review process in the form of a systematic study was incorporated to investigate how each configuration would 'score' relative to a baseline for three main objective functions: noise, low emissions (green), and low cost.

The main objective function was noise, where Table 2-1 shows the weighting system for each attribute, reflecting the degree of importance; 10 being most important and 0 the least.

Attribute	***Weighting (w)***
Far-field Airframe Noise	10
Far-field Engine Noise	10
Environmental Effects	9
Cost (development, DOC, etc)	8
Minimum weight	8
Certification	8
Reliability and Maintainability	8
Familiarity / Risks	8
Passenger comfort / environment	7
Crashworthiness / Emergency egress	6
Airport Infrastructure	6
Passenger local internal noise	5
Maximum possible Aircraft Score (w×10)	***930***

Table 2-1: Attributes and weightings for Noise

The aim of this analysis was to compare each configuration in terms of design feasibility. In total 96 different concepts were identified using this systematic approach [22]. Each airframe concept was given a score out of 10 which was multiplied by the attribute weighting to provide a total aircraft score. The designs were scored and compared to the baseline (*BL*) aircraft. The scores were later used as a guide to select airframes, discarding the less promising design layouts and further investigating 'better' solutions so that the airframe design and noise analysis process could be initiated.

The systematic approach identifies the key areas of noise, performance, integration into existing airport facilities, legislation, requirements, and maintenance aspects; some of which will be either analysed or discussed later in the conceptual design process.

2 Terms: 'concept' refers to a specific airframe design with a unique layout, and 'configuration' refers to a general type of airframe layout with many permutations; i.e. many concept variations.

2.9 Airframe Review Summary

The down selection process involves reviewing the results of the systematic approach described above to determine the most ideal aircraft configuration to investigate. The optimal configurations singled out using the systematic approach are summarised below; where comparisons are discussed for similar designs for each family of aircraft. Finally the desired path of this research is defined to enable the reader to visualise the scope of the dissertation design methodology and familiarise oneself with the challenges associated with this broad area of research.

2.9.1 Baseline Configuration

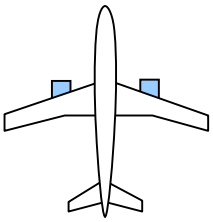

The optimal *BL* design was the high bypass ratio (*HBPR*) conventional arrangement which scored 58.7%. The reason that this score is considered ideal is not because it is the best design but because it is the most familiar solution. This design has one of the lowest scores in terms of far-field airframe and engine noise, with an extremely low rating for environmental effects, but this is expected because it is a current day aircraft and sets guidelines/presedent for the lower limits that alternate designs must improve on. The main driver for the HBPR airliner is that it is the most familiar design, which has low development costs, a reputable reliability and good maintenance record, but mostly because its is easily certifiable. However, the challenges associated with this aircraft configuration on the market are that the design is not likely to meet future emissions and noise certification targets/requirements.

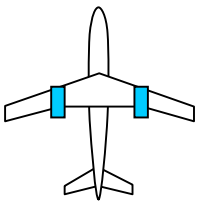

The *BL* design is closely followed by another configuration, which has a high wing and upper mounted engines pods, providing additional noise shielding. It may cause some discomfort to passengers in certain scenarios such as a ditching case, because of egress challenges, primarily because there are no civil-high wing aircraft to-date that are in the same class as the baseline. Having stated this, the BAe-146 is a smaller class high wing passenger aircraft that is certified for ditching [23]. An added benefit of the high-wing is a completely un-interrupted view across the horizon for all passengers, since passengers would be interested in viewing the up-coming landscapes below. The main engineering advantages of the high wing layout, tailors itself for egress routes that are closer to the ground, despite the main detriment being that for a ditching case, the location and buoyancy effects of the wing would force part of the fuselage to be sub-merged under water creating evacuation concerns. This does not mean that the configuration is un-certifiable, but rather that there are challenges ahead, if this configuration were to be developed further. An added advantage this configuration has over the BAe-146 is that the engines are above the wing, and would be impacted less by the ditching case, and more importantly by foreign object damage (FOD) from the ground.

2.9.2 Broad Delta Configuration

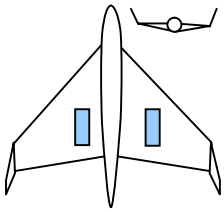

The best BD design for low noise was a tailless design with winglets and scored an impressive 61.4%. This concept scored well in almost every attribute area except for environmental consideration where the ratings sunk. In general this is an ideal configuration for low noise, because there is a large noise shielding effect produced by mounting the engines on the upper surface of the wing, combined with sideline noise shielding from the winglets. Embedding the engines within the wing root increases the configuration rating up to 63.8% and is because of an increase in passenger comfort (engines not at cabin eye-level), safety (from rotor burst scenarios), and slight reduction in local internal cabin noise. The BD concept is an ideal solution for shielding the sideline and forward propagating noise of the engines, but not so much the rearward jet noise, and is similar for most of the aircraft families. In addition, the tailless delta wing lends itself to a high sweep, large area, low wing-loading design, which does not necessarily require the use of flaps, slats, or a tail surface, removing three noise sources. The airframe is capable of a lower approach velocity than the *BL* which further reduces the noise of the configuration. The main challenge would be in certifying an unstable (refer to Appendix G, pp. 368 -382), tailless aircraft configuration for use as a passenger airliner, but this requirement may change with the development of high reliability ($\times 10^9$) active flight control systems.

2.9.3 Slender Delta Configuration

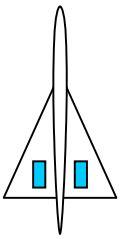

The best of the slender delta family revealed a disappointing score of 59.1% with a poor score for environmental impact (emissions), but a high score for low airframe and engine noise. This configuration scores well for noise, reliability, maintainability and certification. The score tends to drop when considering the passenger comfort and local internal noise. The major concern is the certification of a slender delta because it is a tailless subsonic design that is not optimal for low speed flight/manoeuvrability; narrow deltas are usually associated with high speed transonic and supersonic flight. The poor performance at low speed answers the major concerns about why the environmental score is so low, and the general perception is that the narrow delta is a highly uneconomical subsonic design that consumes fuel inefficiently compared to the *BL*. Challenges associated at low speed flight conditions such as landing and take-off, suggest that airflow into the over-the-wing (*OTW*) engines will be highly turbulent due to high incidence during take-off but is more of a concern for landing. Alternatively locating the engines on the lower surface provides a challenge of ingestion/foreign object damage (*FOD*) from the runway; a similar problem in addition to a poor fuel tank design caused a major incident which led to the decommissioning of the ‘Concorde’.

2.9.4 BWB Configuration

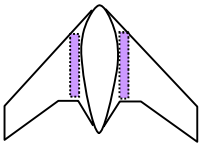

The ideal BWB configuration can be described as similar to the Russian TSAGI concept, with embedded engines, a discretely blended fuselage, and scored 64.3%. The score is very high for environmental effects, with high ratings for airframe and engine far-field noise, meaning that this layout has noise shielding benefits that translate into an extremely quiet design. The passenger comfort and internal noise has an average score, because of crashworthiness, emergency egress issues, interior window designs; where concerns are related to emergency exits/evacuation within the BWB, and the possibility of introducing window-less cabins.

A similar design to the C-MIT SAX solution was considered for analysis even though it only scored 50.8%. The interest for this airframe layout was to see whether or not the new methodology would produce values similar to the SAI team, and this would be a good method for comparing initial design methods.

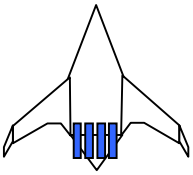

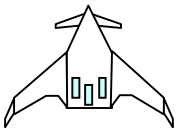

Investigating the effects of adding a canard to the SAX configuration was the initially proposed to investigate the effect of an additional control surface on vehicle noise. If an accurate model for the SAI aircraft was modelled, and was time-permitting, then a canard surface sizing process will be developed and a noise analysis for the entire configuration will be initiated.

2.9.5 Innovative wing Configuration

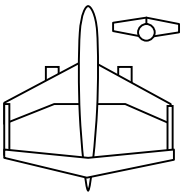

The innovative wing designs have surprisingly low scores and this is due to the designs being of an unfamiliar nature. As previously discussed for the *BL* aircraft, the development of a 'known' design is considered acceptable, but when products start to become unfamiliar such as the joined wing, concerns are raised. This is the reason why the innovative wing family scored the lowest of all the above investigated configurations families.

2.10 Airframe Selection for Silent Aircraft Analysis

The down-selection process began with analysing the strengths and weaknesses of the remaining aircraft to see the benefits of each aircraft configuration. Those designs which were not considered worth further exploration were noted for specific reasons and the remaining configurations were to be further assessed as the research progressed.

2.10.1 Down-Selection Process

The first aircraft configuration that will not be explored further is the slender delta aircraft. This aircraft is an excellent shape for low noise production but it is also extremely inefficient and would

result in a quiet un-economical and inefficient aircraft design. The advantages of noise shielding from this airframe is outweighed by the risks associated with the engine location and design inefficiencies at low flight speeds.

The second aircraft to be disregarded is the high mounted engine pods on a high wing conventional aircraft. This configuration may be ideal for noise shielding but is considered to be too similar to existing conventional airframes and time will not be spent redesigning this configuration. The *BL* aircraft with high BPR engines will be assessed in order to provide a datum model as a reference for the other novel designs. This would ensure that the methodology is working correctly and also to allow a detailed design of a current aircraft alongside a novel concept using the same principles. The broad delta (BD) and discrete fuselage BWB will also remain to be further analysed, and so too will the SAX aircraft with the additional investigation into adding a canard to the BWB. Finally the joined wing concept will be added to the group with two possible variations; one with two equal sized wings joined at the tip, and one design with a horizontal stabiliser joined on to the main wing at a semi span location.

A total of seven designs will be investigated in further detail, time-permitting, in order for the development of an innovative silent aircraft conceptual design methodology. Investigations and brainstorming sessions took place throughout the duration of the research to ensure that all possible design routes were explored. The possibilities for generating innovative airframe designs are endless because novel configuration families may be combined, for example, fusing two designs together such as the BWB and the JW concepts. An another example of one current combined solution mentioned above is the discrete fuselage BWB (TSAGI), which is simply a conventional 'tube-and-wing' delta transport (BD wing) combined with an extra wide-body fuselage blended into the wing, forming the BWB design.

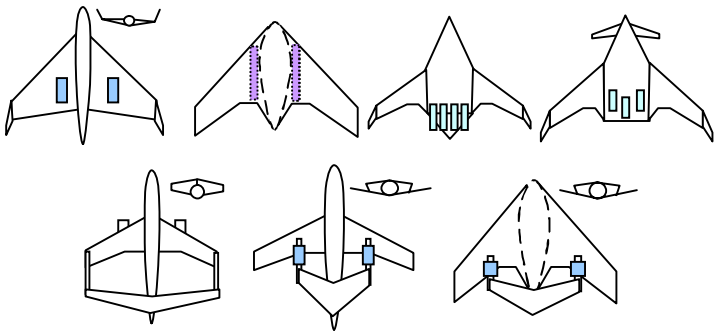

Fig 2-22: Final selection of airframe concepts chosen to develop and their ratings, from top left to bottom right: Broad Delta [61.4%], Discrete Fuselage BWB (D-BWB) [64.3%], SAX-40 [50.8%], Canard derivative of SAX-40 [59.2%], Joined wing (JW) [47%] , Partial-span Joined-Wing (PS-JW) [51.5%], and Discrete Fuselage Partial-Span-Discrete-Fuselage-Joined-Blended Wing Body (PSDFJ-BWB) [53.1%]

The final seven configurations that were chosen to further investigate are shown within Fig 2-22. A further assessment is required by means of a detailed concept design. To give an idea of results, the baseline aircraft scored 58.7%, so airframes scoring higher were considered ideal for further development, and those that score lower were not considered further as potential low noise configurations.

Each airframe concept houses different engine locations, for which a parallel engine study was completed by Doulgeris, 2008 [17], identifying novel engine solutions for specific airframe concepts; this is predominantly where the airframe-engine integration process is crucial.

2.11 Current Market Solutions to Lower Aircraft Noise

The main solution to the noise requirements is to try and combat the noise produced by the current fleet airlines use to-date, and this method is being attempted by those involved in reduced noise projects such as SILENCE(R) and QAT [9]. Another solution is to combat noise as a challenge from an initial design point, and to this date most major competitors in the aerospace industry have discussed future projects.

Boeing are due to unveil their new 787 dream-liner aircraft whereas Airbus have certified their new super jumbo A380 (Fig 2-11). Both companies are fighting for the leading spot in the industry, and both have vast experience in aircraft design. Their new aircraft designs are based on the conventional configuration of the first jet 'tube-and-wing' aircraft. This is not to say that they will not change their aircraft configurations, because in fact both companies are investigating novel concepts for the future. To create a new configuration requires time and resources for design, development, and requires reassurance that the concept would be feasible; and is why extensive research by both companies have resulted in two separate visions for of a future BWB airliner.

Alternate configurations also consider passenger comfort, speed, range, larger capacity, and at present reduced noise and emissions. The challenge is not only to keep up with changing customer/operator demands, but to see which company can develop an efficient and economical replacement for the current conventional aircraft designs.

The future of aviation depends solely upon feasible alternatives to environmental concerns we face at present. As research develops and new materials, experimental technologies, and manufacturing processes evolve, the design of novel and innovative configurations would have fewer challenges than what we now face today. Further research is required not only to bridge the gap between the 'ideal' blended wing body transport and current aircraft designs, but to implement new design drivers such as

noise, emissions, alternative fuels into the design process to increase the efficiency of current aircraft. The following chapters will describe the process undertaken by the author to initiate a study into the design of silent airframes; addressing emissions, environmental concerns, and additional factors that may influence the evolution of what we deem to be the most efficient and effective form of global transport to date: the civil airliner.

Fig 2-23: Boeing Vision of Blended Wing Body outer design geometry [24], (courtesy of http://www.promotex.ca/articles/cawthon/2006/2006-05-15_article.html)

Fig 2-24: Airbus Vision of Blended Wing Body concept design [25], (*courtesy of http://www.flug-revue.rotor.com/FRHeft /FRH0101/FR0101e.htm*).

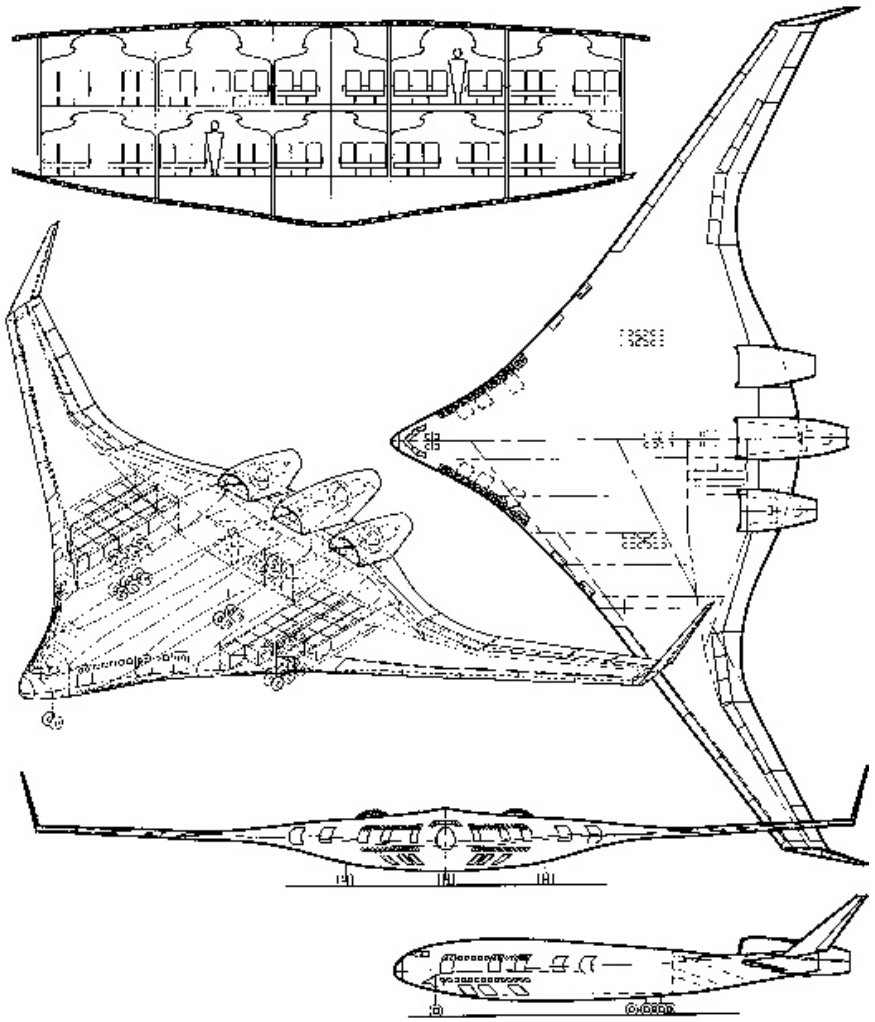

Fig 2-25: Boeing Blended Wing Body design research and interior layout [26], (*http://leehamnews.wordpress.com /2009/05/ 31/bwb-a-big-challenge/).*

References

[1] Smith M. J. T., [Smith, 1989], 'Aircraft noise', *Cambridge Aerospace Series*, Cambridge University Press, 1989, NY.

[2] Truax, B., [Truax, 1989], 'Handbook for Acoustic Ecology', Second edition: 1999, *The Soundscape Project, Simon Fraser University, & ARC Publications*, 1978, website: *http://www.sfu.ca/sonic-studio/handbook/Effective_Perceived_Noise_.html*, last accessed March 2009.

[3] Boeing internal memo (confidential), [Boeing, 2007], SAI member access only for noise validation, January 2007.

[4] ICAO website, [ICAO, 2009] *http://www.icao.int/*, last accessed March 2009.

[5] ICAO Certification Standards, [ICAO, 2006], 'Noise levels for transport category and jet airplanes under §36.103', Part 36 Appendix B and Chapter 4, Annex 16, Environmental Protection, January 2006.

[6] Environmental Unit of ICAO, [ICAO, 2007] 'ICAO environmental report 2007', Part 2 Aircraft Noise, Montreal, 2007.

[7] [flightsimaviation, 2009] *http://www.flightsimaviation.com/data/FARS/part36.html*, website last accessed March 2009.

[8] Ballal, D.R., [Ballal, 2003], 'Progress in aero engine technology (1939-2003)', *39th AIAA/ASME/SAE/ASEE Joint Propulsion Conference and Exhibit*, 20-23 July 2003, Huntsville, Alabama.

[9] Willshire B., [Willshire, 2000], 'Quiet aircraft technology (QAT) program', National Aeronautics and Space Administration (NASA), March 2000, US, http://www.aerospace.nasa.gov/library/event_archives/encompat/qat/willshire/sld001.htm, last accessed September 2005.

[10] Advisory Council for Aeronautics Research in Europe (ACARE), [ACARE, 2001], 'European aeronautics: a vision for 2020', http://www.acare4europe.org/html/documentation .asp, January 2001, Belgium.

[11] CAA website, [CAA, 2009] 'Classification of LDEN' http://www.caa.co.uk/default.aspx?catid=68&pagetype=70&qid= 69&faqid=403, last accessed March 2009.

[12] Fielding J. P., [Fielding, 2000], 'Design investigation of variable-camber flaps for high-subsonic airliners', *24th Congress of the International Council of Aeronautical Sciences (ICAS)*, ICAS2000-0124, September 2000, Harrogate, WA.

[13] Herr M., [Herr, 2007], 'Experimental study on noise reduction through trailing edge brushes', *Notes on Numerical Fluid Dynamics and Multidisciplinary Design*, 2007, Springer, Berlin.

[14] Honda website, [Honda, 2007], 'HA-420 business jet homepage', http://hondajet.honda.com/default.aspx?bhcp=1, last accessed 7th December 2007.

[15] Spearman, M.L., [Spearman, 2002], 'Some aviation growth events', *9th AIAA/ISSMO Symposium on Multidisciplinary Analysis and Optimization*, AIAA 2002-0172, September 2002, Atlanta Georgia.

[16] Centennial of flight (CoF) website, [CoF, 2007], http://www.centennialofflight.gov/essay/evolutionoftechnology/noise/tech25.htm, last accessed August 2007.

[17] Doulgeris G., [Doulgeris, 2008], 'Modelling & integration of advanced propulsion systems', *PhD Research Thesis*, March 2008, Cranfield University, UK.

[18] Porter D N, Rhodes P D, [Porter, 2006], 'Aircraft noise in london: past, present and future', *Environment Research and Consultancy Department*, CAA, London, June 2006.

[19] Reynolds T. G., Mistry S., [Reynolds, 2006], 'Low noise approach operations; steep approaches, low approach speed, displaced landing thresholds, and delayed landing gear deployment', *Silent Aircraft Initiative (SAI) Internal Report, C-MIT SAI*, Cambridge University, August 2006, Cambridge, UK.

[20] Green J., [Green, 2001], 'Air travel – greener by design: the technology challenge', *Royal Aeronautical Society (RAeS)*, 2001, UK.

[21] Berglund B. Lindvall T., Schwela D. H., [Berglund et al, 1999], 'Guidelines for community noise', *World Health Organisation (WHO)*, April 1999, London.

[22] Mistry, S., Doulgeris, G., Fielding, J. P., Pilidis, P., [Mistry *et al*, 2006], **'**Development of novel airframe concepts and innovative cycle propulsion systems for reduction in aircraft noise', *25th Congress of the International Council of Aeronautical Sciences (ICAS)*, September 2006, ICAS-2006-5.7.4, Hamburg, Germany.

[23] Flight international (FI) magazine, [FI, 1983], 'Certification of the BAe 146', 12 February 1983, page 54.

[24] Boeing Blended-Wing-Body (BWB) concept, [Boeing BWB, 2008], http://www.promotex.ca/articles/cawthon/2006/images/2006-05-15-B.jpg, last accessed March 2008.

[25] Airbus BWB concept, [Airbus BWB, 2008] http://www.flug-revue.rotor.com/FRHeft /FRH0101/FR0101e.htm, last accessed March 2008.

[26] Boeing BWB 3-view drawings, [Boeing BWB 3V, 2008], http://leehamnews.wordpress.com /2009/05/ 31/bwb-a-big-challenge/, last accessed March 2008.

Chapter 3 Aircraft Conceptual Design Methodology

Developing a novel airframe design methodology customised for a silent aircraft is a broad area of research. The design of a novel concept is a challenging process, which often uses many assumptions to predict performance and technology levels for an estimated aircraft (aircraft) release date, and also provides a large scope for errors. The design philosophy for this dissertation accepted that errors were inevitable and any assumptions would be based upon published research and not on fictitious estimates. In addition to the complexities of creating a novel concept design methodology, airframe noise analysis was integrated into the design procedure, for which the analysis was completed using a low fidelity ESDU noise prediction method [1]. The aim of the integrated design methodology was to analyse multiple airframe concepts with a low fidelity noise model and to use a higher fidelity noise model for the final silent airframe design.

The introduction of a 'baseline' (*BL*) aircraft provided a means to design a current technology airliner using a datum conceptual design methodology, with a view to adapt the methodology for novel designs. The *BL* design process is divided into two main sections within this chapter consisting of airframe design development and airframe noise analysis. A summary of the conceptual design methodology is shown within Fig 3-1, where the basic design process is similar for all novel airframe configurations, although the design analysis used may differ. The *BL* aircraft design results were compared with an existing aircraft of similar class and provided a direct sizing comparison to an aircraft that is currently in-service. The *BL* aircraft results were compared to the in-service aircraft specification and measured noise results using Federal Aviation Administration (*FAA*) published data [2], so that design procedure and noise results could be compared and validated.

Airframe noise analysis considered the landing, sideline, and take-off noise cases at a datum airport, considered in this case to be London Heathrow (LHR). Additional investigations were completed in collaboration with SAI to explore alternate approach operations for a conventional airliner without considering any airframe redesign. The aim of the study was to investigate flight limitations of the *BL* to explore the possibility of a slow and/or steep approach, possibly combined with a displaced landing threshold.

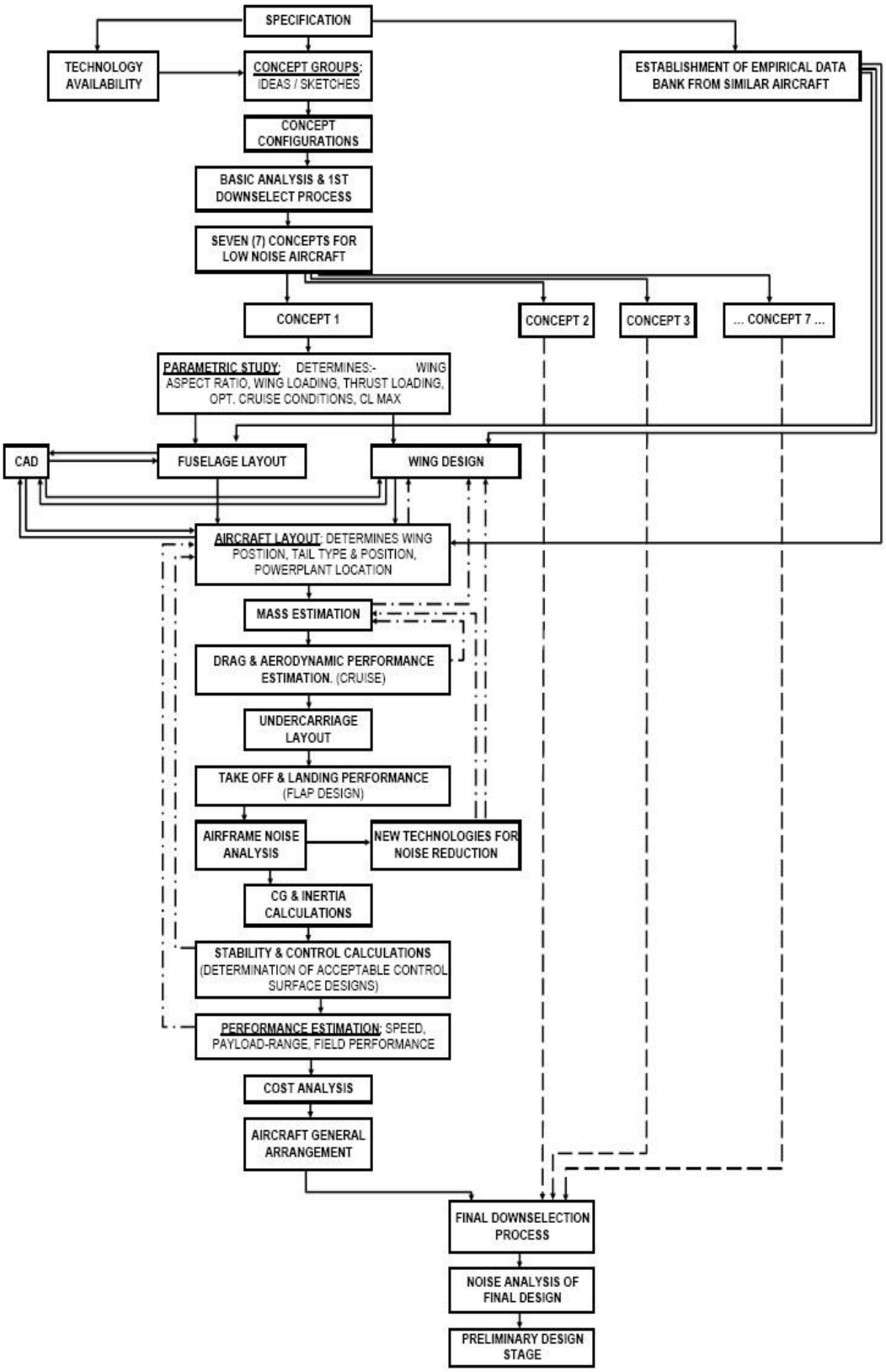

Fig 3-1: Conceptual Design Methodology

3.1 Baseline Aircraft Conceptual Design Summary

The *BL* aircraft was designed using a specification provided by SAI for a 216 passenger civil transport with a 0.8 cruise Mach providing a range of 4,000 nautical miles. The design was governed by SAI for a three-class cabin arrangement that represented the shortest and lightest possible aircraft variant. Cabin configurations such as two or single-class cabins enable a greater passenger capacity and hence a heavier aircraft, so the smallest design variant was selected with a view to stretch the cabin, providing a basis to produce a family of aircraft at a later design phase. Production of a family of aircraft drove the SAI to a 3-class configuration, mainly because it was the lighter of the three, and reduced weight reflects in a lower total airframe noise.

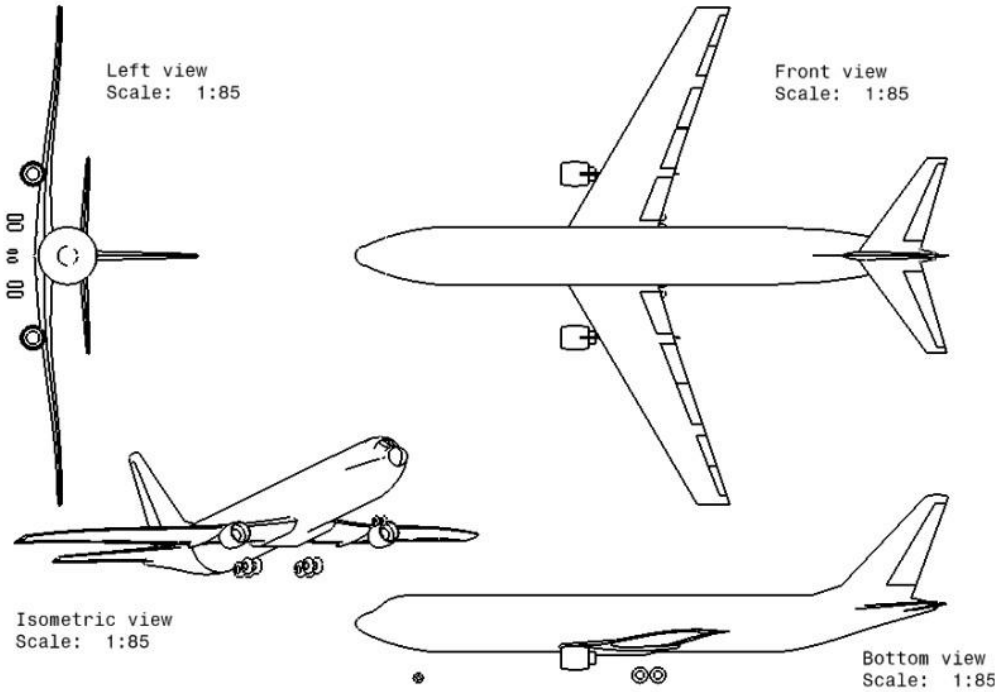

Fig 3-2: 'Datum' Baseline (*D-BL*) aircraft model and general arrangement of geometry

The *BL* aircraft was designed using a semi-empirical parametric analysis[3] methodology [3], which was tailored to meet the design specification. The design process is summarised within Appendix A and compared to the broad delta airframe concepts within Appendix B; where a description of equations used provide a guide for the development of the aircraft model. The design specification places the *BL* aircraft in a similar class as a Boeing 767-300 airliner. Published B767-300 geometrical data [4] was used for comparative purposes as a sanity check for the parametric study results. Hoerner, Pamadi, and Katz & Plotkin methods [5, 6, and 7] were used to revise aircraft drag and

3 Parametric analysis is a basis for the initial sizing of aircraft components, where a further assessment re-sizes the geometry and re-iterates performance.

performance calculations. The fuselage layout, wing, undercarriage, mass estimations, and stability and control were determined using Howe, Jenkinson *et al.*, Raymer, and Young [3, 4, 8, and 9].

Development of the *BL* aircraft evolved in parallel with the broad delta (BD) concept, where technologies introduced for the BD were integrated into the design of the *BL* model to provide alternate design solutions. The *BL* design was used as a reference vehicle, now referred to as the 'datum' baseline aircraft (*D-BL*), based on the initial specification and optimised for a cruise flight at 39,000ft. A comparison between the *D-BL* aircraft model and a new technology (*NT*) variant was considered, where an in-depth description of the *NT-BL* is provided within Appendix B.

Description	***Symbol***	***NT-BL***	***D-BL***	**B767-300**	***Units***
Wing Area	S	202.4	237.7	283.3	[m^2]
Wing Span	b	40.2	43.6	47.57	[m]
Wing Standard Mean Chord	$\bar{c}$	5.03	5.45	6.98	[m]
Wing Aspect Ratio	A	7.99	7.99	7.99	-
Wing Quarter Chord Sweep	$\Lambda_{¼}$	32.3	31.6	39.0	[deg]
Wing Taper Ratio	Λ	0.277	0.207	0.207	-
Thickness-to- Chord Ratio	t/c	0.115	0.115	0.115	-
Wing Apex location	l_{APEX}	23.6	22.9	-	[m]
Horizontal Tail Area	S_{HT}	52.6	57.1	77.7	[m^2]
Vertical Tail Area	S_{VT}	31.5	34.2	46.14	[m^2]
Wing Area Parameter	$S^{-0.1}$	0.588	0.579	0.569	[m^{-2}]
Static Wing Loading	$(Mg/S)_0$	7465	6540	5419	[N/m^2]
Static Thrust Loading	$(T/Mg)_0$	0.328	0.317	0.291	-
Lift-Drag Ratio	L/D	15.6	14.6	14.4	-
Cruise Lift Coefficient	$(c_L)_{cr}$	0.438	0.522	-	-
Mass of Wing	M_W	20,927	25,265	-	[kg]
Fuselage Mass	M_{FUS}	15,649	18,010	-	[kg]
Mass of Tail (+ winglets)	M_T	2,300	5,053	-	[kg]
Mass of Undercarriage	M_G	6,092	6,338	-	[kg]
Propulsion Systems Mass	M_{PP}	12,516	13,956	-	[kg]
Mass of Systems	M_{Sys}	16,613	19,446	-	[kg]
Operational Items Mass	M_{OP}	3,357	2,762	-	[kg]
Operational Empty Mass	M_{OEW}	77,912	95,149	87,135	[kg]
Mass of Payload	M_{Pay}	23,760	23,760	24,795	[kg]
Mass of Fuel Required	M_f	44,934	43,849	44,559	[kg]
Available Fuel in Wing Volume	M_{f_a}	47,836	47,342	-	[kg]
Total Static Thrust	T_0	495,502	492,706	447,000	[N]
Total Overall Mass	$\boldsymbol{M_0}$	**146,151**	**158,438**	**156,489**	**[kg]**

Table 3-1: Mass optimised results summary for the *D-BL* and *NT-BL* aircraft compared to B767-300 data

The idea of incorporating new technologies into the design process enabled the *D-BL* aircraft to be enhanced through the addition of winglets, manufacture of a more-composite airframe, and upgrading systems to define a more-electric aircraft concept (Appendix B). A comparison of the *NT-BL* and the *D-BL* aircraft was completed for two main reasons:

- To compare the *D-BL* with a B767-300 to validate the design methodology.
- To develop a *NT*-BL for a consistent technology level comparison with all novel airframe designs considered in this research.

The *D-BL* represents an aircraft designed over 20 years prior to currently in-service aircraft and does not provide a suitable comparison model for novel configurations. Significant delays in the design, development, manufacture, and testing phases of any new aircraft ensures that by the time of release into service, the technology used on the aircraft will be outdated. This is due to significant delays between a company's research, development, and testing (RD&T) phases and the time taken to mature technology readiness levels (TRL) for application to an aircraft program.

The *D-BL* and *NT-BL* designs, were compared with electronically published data on the B767-300 [4], and are shown above in Table 3-1.

3.2 Baseline Aircraft Operations

Modifications to current aircraft operating procedures were investigated to lower aircraft noise. A collaborative study with SAI explored alternate approach operations for a conventional airliner to investigate the boundaries of the configuration without considering airframe redesign. This study aimed to investigate the flight limitations of a B767-300 type airframe (*D-BL*) in order to explore the possibilities of completing a slow and steep approach combined with a displaced landing threshold.

3.2.1 Conventional & Unconventional Approaches

Flight operations were investigated for unconventional approach procedures. The *D-BL* airframe was used to quantify the noise impact, and determine which operation significantly affected airframe and engine noise enough to warrant a change in the operational procedures, with minimal risks associated with aircraft and airport safety. Investigations into displaced landing thresholds, steep continuous descent approaches, and reduced approach velocity are discussed within Appendix A.

3.2.2 Baseline Aircraft Approach & Noise Analysis

The aim of the *D-BL* study was to determine changes in noise produced from an approaching aircraft with variable speeds, approach angles, and through displacement of the landing threshold. The *D-BL*

aircraft was used to produce a suitable noise analysis by characterising the aerodynamic behaviour on an approach glide path.

Mass	***[kg]***
Wing	25,265
Fuselage	18,010
Tail	5,053
Undercarriage	6,338
Power-plant	13,956
Systems	19,446
Operating items	2,762
OEM	95,149
Payload	23,760
Fuel	43,849
Fuel capacity (wing)	47,342
SL static thrust	**492,706**
$MTOW_{metallic}$	**158,438**
$MTOW_{composite}$	**152,639**
Areas	$[m^2]$
Wing	237.65
H_z *tail*	57.06
V_z *tail*	34.24
Flap Area	33.64
Angles	***[deg]***
0.25_c *sweep*	31.60

Non dimensional	
A	7.99
t/c_{avg}	0.115
λ	0.207
BPR	8.0
Cl_{max}	2.939
$Cl_{approach}$	1.763
Cl_{cruise}	0.522
L/D_{cruise}	14.6
$[T/Mg]_0$	0.317
$[Mg/S]_0$	6540
$C_{Do\ ls}$	0.0164
$C_{Do\ cr}$	0.0151
$C_{Di\ ls}$	0.0510
$C_{Di\ cr}$	0.0526
$(Mn)_{cruise}$	*0.80*
$(Mn)_{to}$	*0.24*
$(Mn)_{crit}$	0.85
Velocities	***[m/s]***
V_{stall}	57.40
V_a	70.91
V_{design}	236.64

Length / chord	***[m]***
Wing span	43.60
MAC (Mean Aero Chord)	5.45
Wing $Root_c$	8.45
Wing $kink_c$	6.20
Wing tip_c	2.20
Flap span	14.97
Wing apex (from nose)	22.9
c.g. (from nose)	21.06
Tail moment arm	27.24
H_z *tail span*	17.07
H_z *tail* $Root_c$	5.19
H_z *tail* tip_c	1.50
V_z *tail span*	9.31
V_z *tail* $Root_c$	5.66
V_z *tail* tip_c	1.70
Fuselage length	53.7
Fuselage width	5.03
Fuselage breadth	5.03
Nose gear strut	2.03
Nose gear diameter	0.76
Main gear strut	2.92
Main gear diameter	1.31
Nose/main gear wheels	2/8

Table 3-2: *D-BL* aircraft geometry and performance summary [10]

D-BL data was extracted from section Chapter 3 (Table 3-1), providing a comparable model to the B767-300 aircraft, both in terms of geometry and performance. The following results are based upon the published work within Reynolds & Mistry [10].

Understanding the behaviour of the *D-BL* during flight critical phases was crucial. The main flight cases were the approach and landing, for which the performance of each case was calculated by using [3], and is summarised within Table 3-2. Detailed analysis of the wing performance was based on a NASA SC-(2)-0610 supercritical airfoil combined with high lift control devices. The wing design incorporated partial span trailing edge (TE) flaps and full span leading edge (LE) slats, with correction factors for wing taper and a finite wing. The sizing of control surfaces such as flaps, elevators, ailerons, and the rudder were input into the airframe geometry analysis using AVL [11]. *D-BL* lift, drag, and approach flap settings were used to identify the approach configuration and control

setting angles, where the airframe noise was calculated using the *ESDU 90023 Airframe Noise Prediction* code [1], and is described in further depth within Appendix A.

3.2.3 Airframe Noise Analysis

Airframe noise consists of many sources or components of noise. The major contributors are the airfoil self noise (wing), empennage, TE devices, LE devices, and undercarriage. Additional noise sources which are difficult to determine the magnitude of include interference between fuselage-wing, wing-pylons, pylons-engine nacelles, fuselage-tail, and small cavities across the aircraft, such as doors/hatches. The larger more dominant noise sources are only considered within this analysis, and provide an approximation to the overall noise produced by the airframe.

The focus of a slow and steep analysis is to analyse whether it is possible for a current tube-and-wing aircraft configuration to fly at slower approach velocities, or at higher flight path angles. The steeper approach angle increases the distance between the aircraft and the ground reducing the perceived noise propagated towards the ground or surrounding airport region. The main factor effecting noise is velocity, where all noise sources are directly related to V^n, where 'n' varies for different noise sources and is typically of magnitude 5 or 6. Noise for TE devices also varies depending on the degree of flap deflection and the overall geometry. Undercarriage noise depends on velocity, number of tyres, gear length, and its configuration. It is difficult to reduce undercarriage noise, because vortices that are produced are essential to generate drag for landing, which is used to reduce aircraft approach velocity. The slow and steep analysis aims to investigate the limitations of the *D-BL*, to see whether a lower noise signature is achievable by reducing the approach velocity, and increasing the distance of the aircraft from the ground.

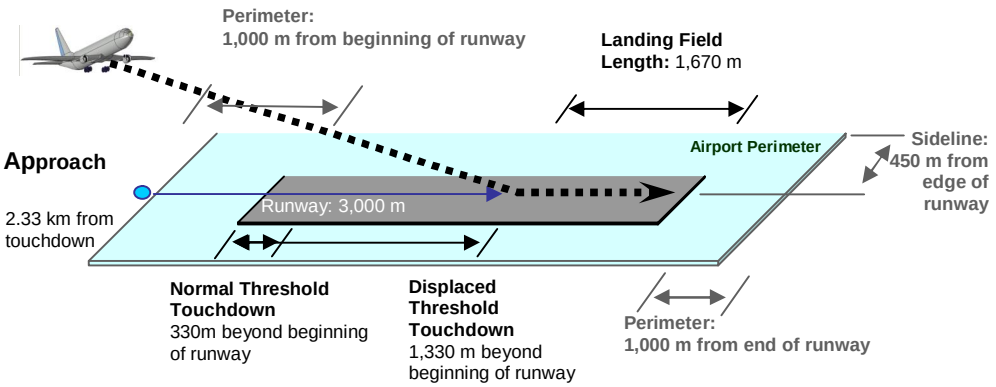

Fig 3-3: *D-BL* aircraft approach for conventional and displaced landing thresholds [10]

A series of flight cases were established to investigate aircraft noise using variable approach parameters. A standard approach considers a 3 degree flight path angle (FPA), with the aircraft

touching down at 330m beyond the beginning of the runway, as in Fig 3-3. This touchdown point is located 1km from the airport perimeter, which is a noise measuring point for SAI. ICAO limits the minimum aircraft height at the threshold to be 50ft (15.24m) above ground, more commonly referred to as the obstacle clearance distance.

The second noise measuring point is defined by ICAO and is located 2km from beginning of the runway. The requirements are clear that at this location, aircraft altitude must not fall below 120m. The noise measuring points are shown in Fig 3-4, for take-off, landing, and sideline conditions for a datum airport; considered to be London Heathrow (LHR). The main constraints for the take-off flight case are difficult to address because the climb characteristics of each aircraft are different, however the noise measuring point has a fixed location at 6.5km from the brakes release point on the runway. Sideline noise is simply 450m from the runway, but varies depending on the aircraft manoeuvre, whether it is approaching or preparing for take-off. The most critical sideline noise is for the take-off where the airframe and engine noise has a greater impact on surrounding areas compared with the noise on approach.

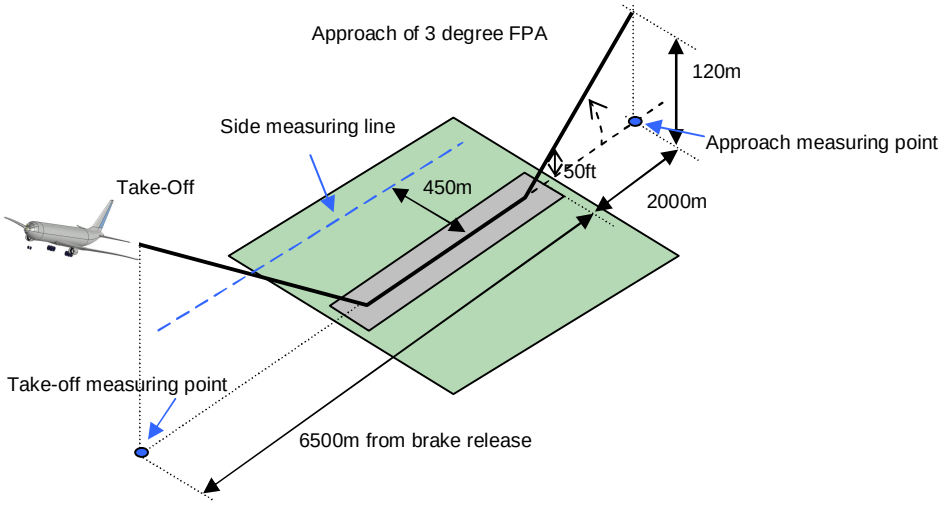

Fig 3-4: ICAO Noise Measuring points [10]

3.2.3.1 Airframe Approach Analysis

A number of flight cases must be considered for the approach analysis in addition to the two main noise measuring points defined by SAI and ICAO. An additional landing case is considered, which uses a 1km displaced threshold as shown in Fig 3-3. This enables the aircraft to land 1,330m from the beginning of the runway and increases the height of the aircraft above the noise receiver, hence reducing the noise propagated to the ground. There are numerous flight cases to consider, two measuring locations, two touch-down points, and in addition there are three approach velocities and three FPAs to consider.

Noise analysis was investigated for the *D-BL* using an ESDU airframe noise prediction method [ESDU, 2003]. The prediction of far-field airframe noise includes a calculated breakdown of airframe noise components, which consists of the landing configuration for the *D-BL* including control surface deflections. Results of the *D-BL* aircraft noise analysis study are summarised below, with a detailed description provided within Appendix A.

An interesting result for an approach with flaps and slats deployed compared with a flaps only approach reduced noise between -0.1 and -0.5 dB(A). This suggests that using flaps alone would lower the airframe approach noise, but not significantly, due to the degree of flap deflection required to produce the additional lift. Using slats adds an additional noise source but does not impact noise significantly. Another interesting result is that despite the fact that the 66.6m/s approach fails the FAR regulation lower limits on approach velocity, the noise reduction potential is as much as -2dB(A). FAR regulations state that the approach velocity cannot be less than $1.23\times V_{stall}$, and in this case 66.6m/s ($1.13\times V_{stall}$) falls below this requirement and is not advised by the FAA. This does not mean that this approach velocity is not achievable; it simply means that the safety margins are now reduced. Safety margins are in place for the security of all occupants, where for the approach case, which is a low speed manoeuvre and one of the most dangerous flight phases, these margins are put in-place to prevent the wings from stalling and keep the aircraft in the sky.

The fuselage incidence angle was found to be important, because by reducing the fuselage angle by 3 degrees, the airframe noise increased by +0.5dB(A). This is because noise generated from an airframe that is aligned parallel to the ground is directed perpendicular to the ground (90 degrees). Increasing the fuselage angle of attack or the main wing setting angle provides an increase in the angle to which noise is propagated, and hence a larger distance for noise to dissipate as it travels towards the ground. Therefore increasing the fuselage angle or wing setting angle on approach reduces noise. If the wing setting angle was fixed and a higher fuselage incidence was required on the approach, this would suggest that to achieve the approach angle, the fuselage would be set at a certain incidence during an approach. This in-turn would increase in the cabin floor incidence and so the designer must ensure that the cabin floor angle does not reach an uncomfortable angle relative to the ground, because this may affect passenger comfort. If the fuselage incidence is too high on approach, this may also affect the visibility of the pilot if there were a systems failure.

Including slow and steep approaches into the analysis suggests that if the *D*-BL approach of 72.5m/s at 3 degrees approach angle is compared with a 66.6m/s ($1.13\times V_{stall}$) case at 6 degrees, the net result is a -10dB(A) reduction in airframe noise at the perimeter (to 74.1 dB(A)). By combining this result with a displaced threshold concept, there is a further -4.9dB(A) reduction to 69.2dB(A); providing a

total of -14.9dB(A) airframe noise reduction for the *D*-BL. This noise reduction is purely for the airframe components, and engine noise is also required, but it is important to consider that smaller airframe noise sources due to interference between hatches, pylons, and adjoining structures were not considered and could add up to a few dBs.

3.2.3.2 Airframe Noise Sources on Approach

It is important to quantify which airframe noise sources are dominant for an aircraft on approach. The noise spectrum shown in Fig 3-5 below represents an ICAO noise measuring point for an aircraft on a 3 degree FPA, at 72.5m/s, with flaps deflected at 35 degrees and slats deployed, with the aircraft directly above the noise receiver.

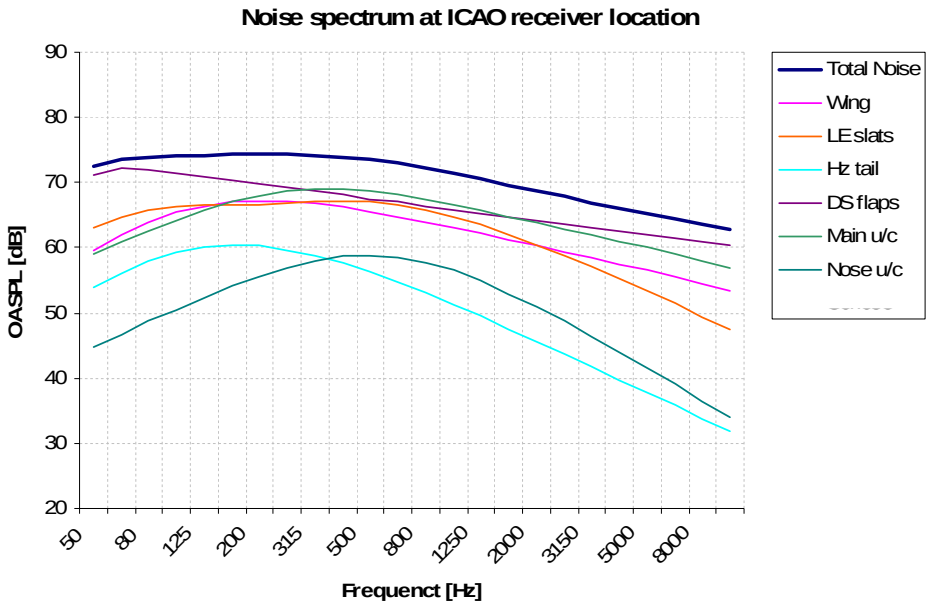

Fig 3-5: Baseline noise spectra at ICAO receiver location

The spectrum analyses the noise between a frequency range of 50Hz to 10kHz and compares the individual source components. Fig 3-5 shows how the dominant noise sources are the *TE* double slotted flaps, slats, and wing for high and low frequencies ranges, where noise is measured in overall sound pressure level, OASPL [*dB*]; calculating the total energy contained within the spectrum. At certain frequencies in the middle of the spectra, main undercarriage, slats, and flaps dominate. It is interesting that the horizontal tail has greater noise than the nose gear at low frequencies, but as frequency increases, the nose gear tends to dominate.

3.2.4 Engine Noise Analysis

Engine Noise has many different sources as per airframe noise, such as fan, jet and turbine noise. To make an estimate for noise produced by an engine on approach, thrust values were used from the force balance calculations, which typically varied between 15-30% of sea level static thrust (SLS). Noise values that were previously defined in the airframe analysis were combined with engine thrust settings at each specified FPA. Engine noise data was calculated using Doulgeris, 2008 [12], for the flight cases defined in section 3.2.3.

Detailed engine noise results predict that fan noise dominates over jet noise by as much as +10dB(A) to +31dB(A); resulting in a higher engine noise compared with airframe. In an ideal scenario, with a thrust setting of approximately 10-15% SLS, noise could reduce by 50%, however, this is not true in practice as the engine thrust would never be set to such a low setting. It is important to note that turbine noise is a high noise source for the engine during approach, and estimations for this source were not included in the analysis of Doulgeris, [12]. The predicted engine noise can be combined with airframe noise to determine the total aircraft noise as described within Appendix A.

3.2.5 Total Aircraft Noise on Approach

Airframe and engine noise components are combined to determine total aircraft noise during the specified approach conditions mentioned above. It is essential to have a benchmark to compare results of this analysis, and so FAA noise certification data was used for the B767-300. This data uses estimated maximum sound levels measured in accordance with FAA AC 36-3H, April 25, 2002 [2].

Aircraft	*Engine*	*MLW (lbs)*	*MLW (kg)*	*App Noise dB(A)*	*App flaps*
B-767-300	JT9D-7R4D(B)	320,000	145,150	92.3	30 deg
B-767-300	CF6-80A2	320,000	145,150	89.2	25 deg

Table 3-3: FAA Noise Certification Data, data courtesy of the Silent Aircraft Initiative

The data describes noise generated by the B767-300, and shows flap settings required on approach, where two noise values are for different engines, and provides an upper and lower limit for the noise calculations, allowing a reasonable margin of error. The noise measurements are taken from the ICAO measuring locations, 2km from the threshold.

Flap angle settings in Table 3-3 were compared with AVL results for the *D-BL* and were used as a reality check for the analysis. A zero fuselage incidence with a 3 degree FPA and a 72.5m/s approach provides similar flap setting values. FAA noise estimates include slats but the AVL output does not and suggests that AVL under-predicts the total lift of the *D-BL* geometry. Estimating lift from LE slats combined with the AVL outputs lowers the flap deflection angles than that set for the B767-300.

Airframe noise prediction is considered lower than it should be due to errors in using AVL. It is important to note that for the aircraft noise on approach, there are a number of errors associated with the airframe configuration and engine thrust, which transfer to into the noise calculations. A sensitivity analysis into the noise predicted by the airframe noise components provided +0.4dB(A) and -0.6dB(A) error margins. The engine noise is considered to be under-predicted because turbine noise was neglected. Airframe noise is over-predicted, because the wing geometry of the *D-BL* is larger than the B767-300, and high lift devices are deflected at a greater angle to compensate for the under-predicted lift due to AVL. Since the airframe and engine noise are associated with errors, the total aircraft noise result will be dependent on the higher more dominant noise source, and that is determined by the magnitude of each component. There are many errors contained within the total aircraft noise analysis and have been mentioned above, however, it is difficult to quantify an error margin for the entire aircraft model.

The addition of the two airframe and engine noise sources is achieved by using the cubic equation described within Appendix A, section A-3.2.7. The higher noise source is subtracted from the lowest source to provide Δx. Delta noise $\Delta dB(A)$ is then added to the maximum noise value to provide the total combined noise of the two sources. The addition of two or more noise sources is determined in this manner due to the logarithmic nature of the decibel and the fact that they cannot simply be added together.

Comparing noise from the ICAO receiver locations to that of FAA certification data for B767-300, confirms the errors associated with the design analysis. Maximum measured noise for the B767-300 is 92.3dB(A), with the minimum being 89.2dB(A). Maximum noise results calculated at ICAO measuring point were for 3 degree FPA, at 72.5m/s for a standard threshold point, which basically represents a conventional approach condition. This conventional case for the *D*-BL has a maximum noise of 93.8dB(A), which is +1.5dB(A) higher than the maximum FAA measuring noise; providing a 1.6% error.

A more effective way to represent this data is to show how noise varies with height from the ground. A descending aircraft gets closer to the ground as it approaches to land at the airfield threshold and noise increases in relation to 1/r; where ‘r’ is the height of the aircraft above ground, as shown in Fig 3-6, which represents a combination of standard and displaced thresholds. A displaced threshold SAI case is identical to that of a standard threshold ICAO case; due to the distance between receiver and threshold being 2km, or distance to touch-down being 2.33km. Therefore the heights above the ground between aircraft and receiver are the same for both cases, where different horizontal locations due to the touchdown points across the airfield, provide identical noise measured at the perimeter.

These results may be extended to show trends in varying the displaced distance further than 1km, but are only valid for airports with longer runways.

The maximum aircraft noise for a 72.5m/s, 3 degree FPA, and for a SAI measurement case is 98.8dB(A). Incorporating slower and steeper approach and comparing it to the case above suggests that for a 66.6m/s approach and at 6 degree FPA, a -11.5dB(A) reduction in aircraft noise at airport perimeter to 87.2dB(A) is achieved. By combining this result with a displaced threshold concept, there is a further -5.0dB(A) reduction to 82.3dB(A); providing a net aircraft noise reduction of -16.5dB(A).

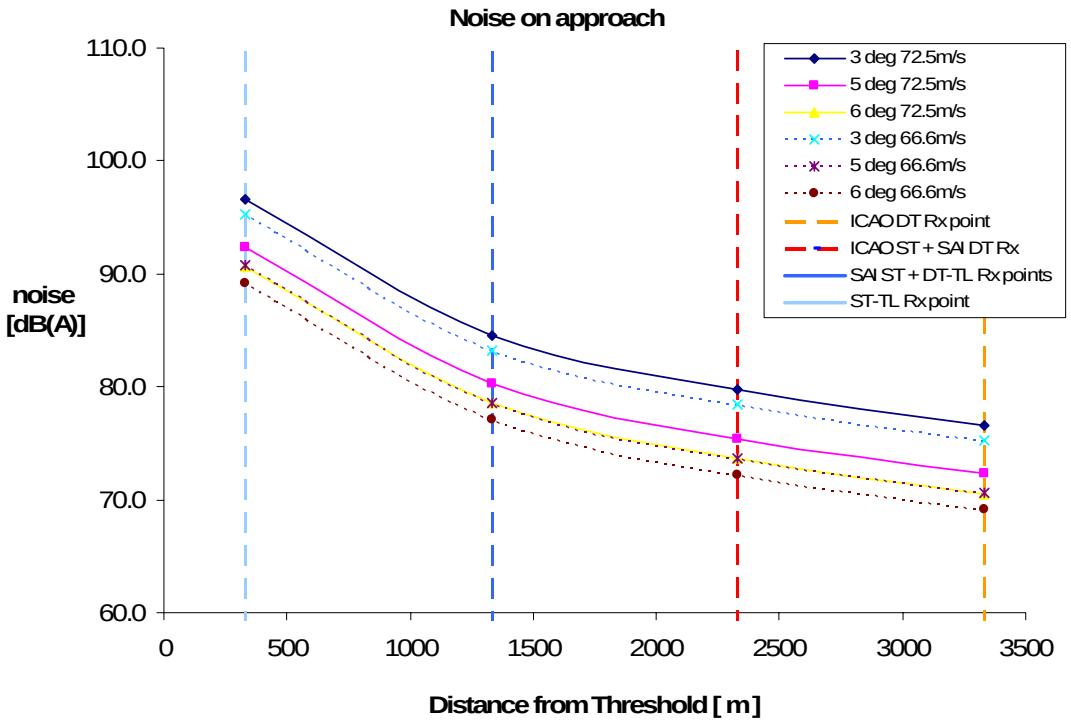

Fig 3-6: Noise Variation with distance from airfield threshold, where DT=displaced threshold, ST=standard threshold, Rx=receiver, TL=touch-down length, Reynolds & Mistry, 2006 [10]

Results also show that changing approach velocity is not a major influence for aircraft noise in comparison to steep approaches and displaced thresholds. Investigating the same scenario of a 3 degree standard threshold at 72.5m/s, and assuming that a 6 degree FPA is possible, aircraft noise is reduced by -12.0dB(A) to 86.7dB(A) at the perimeter. Combining a displaced threshold further reduces noise by -4.9dB(A) to 81.8dB(A) and the net aircraft noise reduction for a steep and displaced threshold concept is -16.9dB(A). The main emphasis of this result is that a significant noise reduction can be achieved at the airport perimeter by increasing the aircraft FPA and displacing the threshold, without changing the aircraft approach velocity. A difficulty in this, is that an approach velocity of

72.5m/s with a 6 degree FPA and displaced threshold, has a shorter runway to land on and less of a stopping distance, where this would require greater high lift and drag capability in-order not to stall the wings; emphasising a complete wing re-design, including brakes and engine thrust-reverser for the *D*-BL.

The main conclusion for this *D*-BL aircraft analysis is that combining the steep and displaced thresholds concepts, along-with a redesign of the main wings, would result in -17dB(A) net reduction in aircraft noise on the approach flight path. This provides a short-term solution to the aircraft noise challenge we have at present by changing aircraft operations. The advantage of changing operational procedures for an older aircraft to significantly reduce noise can be adapted to new airframe configurations, by optimising these new airframes along-with the engine designs to allow for these new operational procedures and would have a greater impact on total aircraft noise reduction compared to the *D*-BL configuration.

References

[1] ESDU, [ESDU, 2003], 'Airframe noise prediction', *Engineering Sciences Data Unit (ESDU) data Item 90023*, June 2003, Amendment C, Endorsed by The Royal Aeronautical Society (RAeS).

[2] Federal Aviation Administration (FAA), [FAA, 2002], 'Federal aviation regulations (FAR) noise standards; aircraft type and airworthiness certification, estimated maximum A-weighted sound levels', measured in accordance with Part 36 Appendix C Procedures, FAR 36-3H, April, 2002.

[3] Howe D., [Howe, 2000], 'Aircraft conceptual design synthesis', *Professional Engineering Publishing Ltd.*, 2000, Wiltshire, UK.

[4] Jenkinson L. R., Simpkin P., Rhodes D., [Jenkinson et al, 1999], 'Civil jet aircraft design', electronic data: *http://www.bh.com/companions/034074152X/appendices/default.htm*, *Arnold Publishing*, 1999, London, UK.

[5] Hoerner S. F., [Hoerner, 1965], 'Fluid-dynamic drag: practical information on aerodynamic drag and hydrodynamic resistance', *Hoerner*, 1965, New Jersey.

[6] Pamadi B. N., [Pamadi, 1998], 'Performance, stability, dynamics and control of airplanes', *AIAA Education Series*, NASA Langley Research Centre, 1998, Hampton, Virginia.

[7] Katz J., Plotkin A., [Katz, 2001], 'Low-speed aerodynamics', *Cambridge Aerospace Series*, 2nd Edition, Cambridge University Press, 2001, UK.

[8] Raymer D. P., [Raymer, 1992], 'Aircraft design: a conceptual approach', *AIAA Educational Series*, 1992, Washington, US.

[9] Young D., [Young, 2005], 'Messier-dowty landing gear design course', *Notes for a short course run by Messier-Dowty*, November 2005, Cranfield University, UK (contact author for details).

[10] Reynolds T. G., Mistry S., [Reynolds, 2006], 'Low noise approach operations; steep approaches, low approach speed, displaced landing thresholds, and delayed landing gear deployment', *Silent Aircraft Initiative (SAI) Internal Report, C-MIT SAI*, Cambridge University, August 2006, Cambridge, UK.

[11] Youngren H., Drela M., [Youngren, 1988], 'Athena vortex lattice (AVL): an extended vortex-lattice model for aerodynamic analysis, trim calculation, dynamic stability analysis, and aircraft configuration development', *http://web.mit.edu/drela/Public/web/avl/*, last accessed February 2007, *Massachusetts Institute of Technology (MIT)*, Boston, US.

[12] Doulgeris G., [Doulgeris, 2008], 'Modelling & integration of advanced propulsion systems', *PhD Research Thesis*, March 2008, Cranfield University, UK.

Chapter 4 Broad Delta Aircraft Concept Development

4.1 Introduction

History has shown that novel designs for civil transport aircraft were avoided due to uncertainties of passenger acceptance, technology capabilities, and development risks. In the past decade aircraft leaving the 'drawing board' and entering the manufacture and test stages are all of a conventional configuration; a cylindrical pressure-vessel fuselage with a moderate to high aspect ratio wing, rear empennage, and either under-slung or rear-mounted engines. The Broad Delta (BD) is in many ways similar to a conventional aircraft, with the main difference being the wing design, which is a low aspect ratio delta wing traditionally found on military aircraft. Although the BD concept is considered a novel design, it utilises the conventional 'tube-and-wing' characteristics, and thus has potential to serve in the immediate future as a civil transport.

This chapter contains details of the BD concept design process, utilising requirements set for the baseline aircraft model, as previously described. An initial parametric analysis provides a basis to develop detailed sizing of wing, fuselage, and airframe components. The consequence of a design evolution process is two BD configurations, where a tailed and tailless version aim to investigate the impact of a trim surface and high lift devices on airframe noise and performance.

4.2 Parametric Design Analysis

The BD design is based on a similar specification and methodology as the baseline parametric analysis, [1], as discussed in Appendix B. Unlike the baseline aircraft, there are no existing civil BD aircraft available to initiate the design process and compare data for wing aspect ratio, airfoil types, and performance. The fuselage was the common feature between the baseline and BD concept. Investigations into military aircraft provided a means to gather data on similar delta wing aircraft, one such design was the Avro Vulcan advanced tactical bomber [2], which was tailless (Fig 4-1 & Fig 4-2).

The Avro Vulcan (*AV*) had the benefit of a large wing with low wing-loading and no horizontal empennage, a capability of carrying large payloads with its ideal lifting surface plan-form, and excellent handling characteristics; especially for a tailless aircraft which required the use of four turbojet engines. The development of the BD concept design extracted data from the *AV* as a primary reference, as shown in

Table 4-1.

Fig 4-1: Avro Vulcan Mk2 Bomber (http://ourworld.compuserve.com/homepages/j_falk/vulcan.htm) [3]

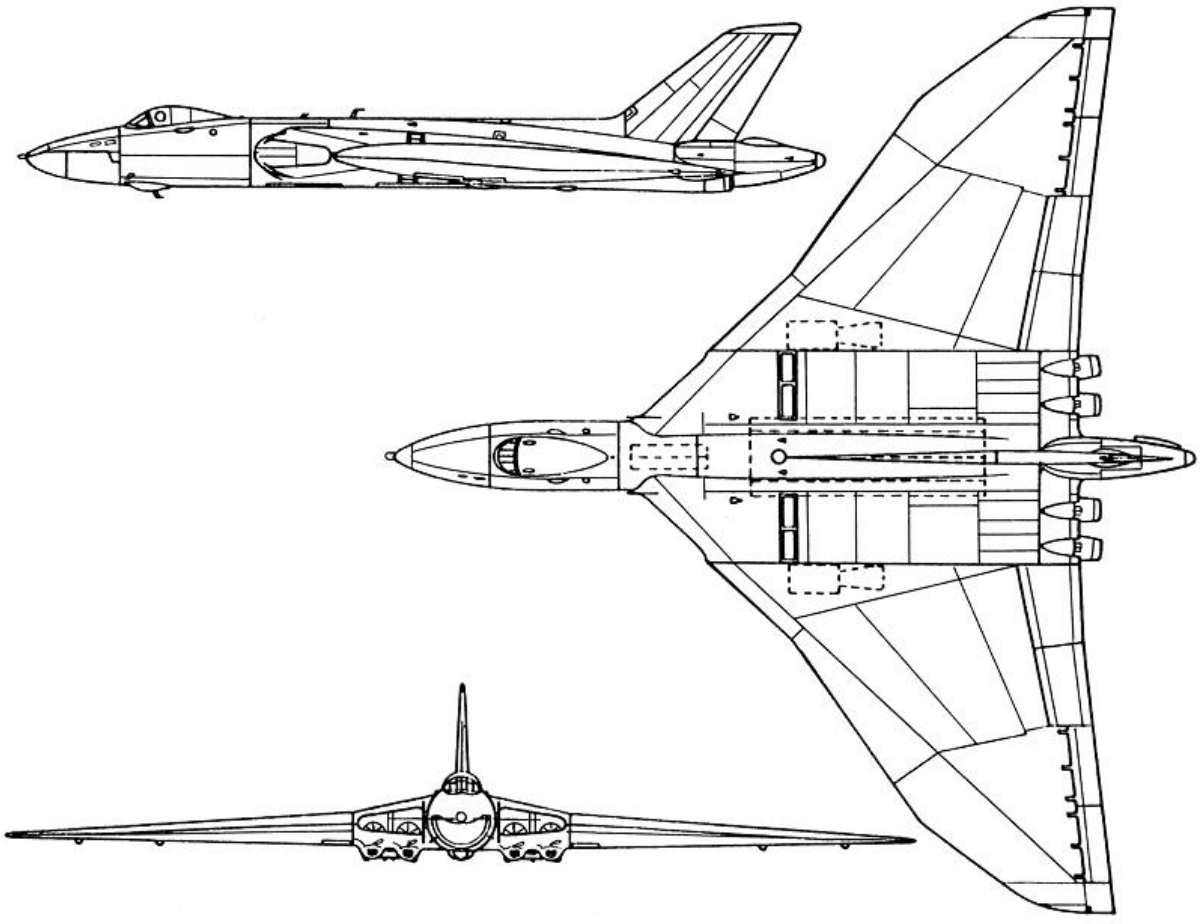

Fig 4-2: Avro Vulcan General Arrangement Diagram (http://www.raf.mod.uk/history_old/vforcespec.html) [4]

The parametric design process was similar to the baseline aircraft with minor modifications to represent a low aspect ratio wing. To understand the development of the BD concept a step-by-step analysis is required as described within Appendix B. It is the authors' decision to consider two alternative configurations of the BD concept. The primary design is a tailless BD based on the *AV* and will be referred to as the broad delta single fin (BDSF), the second derivative is the tailed variant and is referred to as the broad delta fin and tail (BDFT), where the two concepts are analysed in parallel.

Parameter	***Imperial units***	***S.I units***
Overall Length	99.9 [ft]	30.5 [m]
Overall Height	27.2 [ft]	8.3 [m]
Wing span	111 [ft]	33.8 [m]
Wing Area	3965 [ft^2]	368.4 [m^2]
Wing Aspect Ratio	3.11	3.11
V_{max}	625 [mph]	543 [knots]
Max service ceiling	55,000 [ft]	16,764 [m]
Range	3,000 [miles]	2,605 [n.miles]
AUM	170,000 [lb]	77,111 [kg]

Table 4-1: Avro Vulcan Aircraft data adapted from (http://www.aerospaceweb.org/aircraft/bomber/vulcan/) [5]

4.2.1 Initial BD Parametric Design Analysis

To initiate the design, estimates for the wing geometry, propulsion system, and flight characteristics are required. An in-depth discussion of initial design parameters is provided within Appendix B, section B-2, where the modification of Howe's first design spreadsheet provides results that are fed into the next phase of the design process.

To summarise the initial parametric phase, a comparison for change in thrust-to-weight ratio $(T/Mg)_0$ with wing loading $(Mg/S)_0$ was analysed for a range of flight cases. The flight cases investigated included the take-off, climb, cruise, and landing, where aborted landing and gust sensitivity requirements were also considered, with the results provided in Fig 4-3 and Fig 4-4 below.

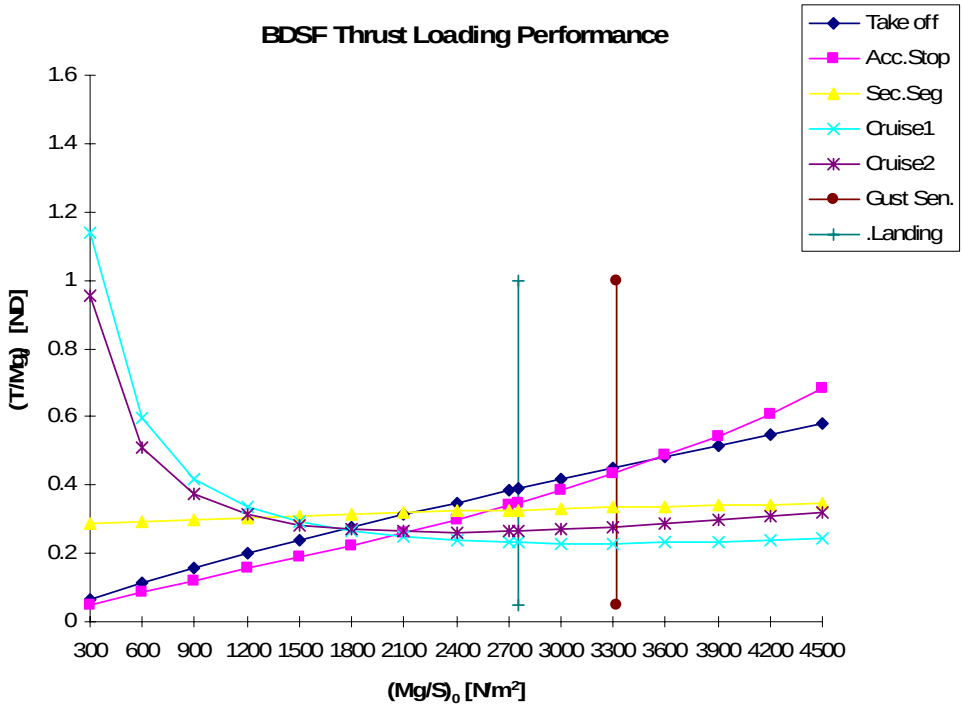

Fig 4-3: BDSF Concept Thrust Loading Performance

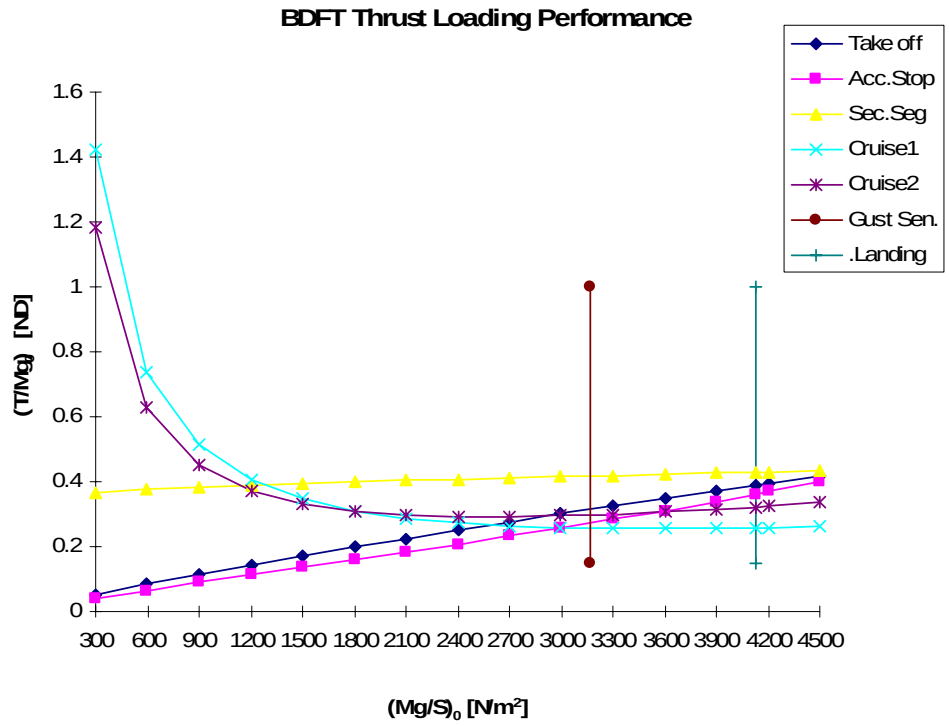

Fig 4-4: BDFT Concept Thrust Loading Performance

4.2.2 Second Phase of Parametric Design Analysis

The second phase of the parametric analysis is a direct continuation from Appendix B, section B-2 and uses detailed aircraft geometry and flight performance to provide a first estimation of the overall concept mass. Howe's second design spreadsheet is modified and used as a guide as described within Appendix B, section B-3.

Description	*Parameter*	*BDSF*	*BDFT*	*NT-BL*	*units*
Wing Area	S	1129.3	839.9	562.8	[m^2]
Wing Span	B	61.8	51.1	67.0	[m]
Wing Standard Mean Chord	$\bar{c}$	19.9	16.4	8.39	[m]
Wing Quarter Chord Sweep	$\Lambda_{¼}$	29.3	32.3	32.3	[deg]
Wing Taper Ratio	λ	0.236	0.209	0.277	-
Thickness-to- Chord Ratio	(t/c)	0.11	0.11	0.115	-
Wing Apex location	l_{APEX}	23.3	24.2	22.59	[m]
Horizontal Tail Area	S_{HT}	-	854.2	243.3	[m^2]
Vertical Tail Area	S_{VT}	353.3	199.3	145.8	[m^2]
Mass of Wing	M_W	75,742	61,697	90,533	[kg]
Fuselage Mass	M_{FUS}	16,540	16,540	17,454	[kg]
Mass of Tail components	M_T	7,574	11,105	16,296	[kg]
Mass of Undercarriage	M_G	13,809	14,152	17,899	[kg]
Propulsion Systems Mass	M_{PP}	32,250	36,500	62,282	[kg]
Mass of Systems	M_{Sys}	34,522	35,380	44,749	[kg]
Operational Items Mass	M_{OP}	2,762	2,762	2,762	[kg]
Operational Empty Mass	M_{OEW}	183,199	178,137	251,975	[kg]
Mass of Payload	M_{Pay}	23,760	23,760	23,760	[kg]
Mass of Fuel Required	M_f	138,261	151,908	191,285	[kg]
Available Fuel within Wing Volume	M_{f_a}	923,483	532,433	180,076	[kg]
Total Static Thrust	T_0	1,318,234	1,491,923	2,248,519	[N]
Total Overall Mass	$\boldsymbol{M_0}$	**345,220**	**353,806**	**467,020**	**[kg]**

Table 4-2: BD Second Phase of Parametric Study Results Summary

Initial mass estimates and geometry sizing is summarised in Table 4-2 for the tailed and tailless configurations. Results from the second stage are fed directly into the final stage of parametric analysis so that the concept can be optimised for minimum mass.

4.2.3 Final Phase of Parametric Analysis; Optimisation

The final phases of parametric analysis are based on optimising the results from Appendix B, section B-**2** and section B-3, and are tabulated below.

Description	*Symbol*	*BDSF*	*BDFT*	*NT-BL*	*units*
Wing Area	S	526.6	321.3	202.4	[m^2]
Wing Span	B	40.5	31.6	40.2	[m]
Wing Standard Mean Chord	$\bar{C}$	13.0	10.2	5.03	[m]
Wing Aspect Ratio	A	3.11	3.11	7.99	-
Wing Quarter Chord Sweep	$\Lambda_{¼}$	29.3	32.3	32.3	[deg]
Wing Taper Ratio	λ	0.240	0.209	0.277	-
Thickness-to- Chord Ratio	t/c	0.11	0.11	0.115	-
Wing Apex location	l_{APEX}	22.0	22.8	23.6	[m]
Horizontal Tail Area	S_{HT}	-	155.4	52.6	[m^2]
Vertical Tail Area	S_{VT}	76.0	36.2	31.5	[m^2]
Wing Area Parameter	$S^{-0.1}$	0.534	0.561	0.569	[m^{-2}]
Static Wing Loading	$(Mg/S)_0$	2755	4133	7465	[kg/m^2]
Static Thrust Loading	$(T/Mg)_0$	0.389	0.401	0.328	-
Lift-Drag Ratio	L/D	14.9	14.8	14.9	-
Cruise Lift Coefficient	$(c_L)_{cr}$	0.204	0.307	0.271	-
Mass of Wing	M_W	24,125	16,865	23,846	[kg]
Fuselage Mass	M_{FUS}	16,540	16,540	17,453	[kg]
Mass of Tail components + winglets	M_T	2,413	3,036	4,292	[kg]
Mass of Undercarriage	M_G	5,915	5,415	6,161	[kg]
Propulsion Systems Mass	M_{PP}	13,815	13,014	12,122	[kg]
Mass of Systems	M_{Sys}	14,789	13,537	15,402	[kg]
Operational Items Mass	M_{OP}	2,762	2,762	2,762	[kg]
Operational Empty Mass	M_{OEW}	80,359	71,169	82,039	[kg]
Mass of Payload	M_{Pay}	23,760	23,760	23,760	[kg]
Mass of Fuel Required	M_f	43,767	40,441	48,217	[kg]
Available Fuel in Wing Volume	M_{f_a}	281,233	126,009	38,919	[kg]
Total Static Thrust	T_0	564,706	531,957	495,502	[N]
Total Overall Mass	$\boldsymbol{M_0}$	**147,886**	**135,370**	**154,015**	**[kg]**

Table 4-3: BD Mass Optimised Results Summary for BDSF and BDFT (as per Table B-29)

This process aims to reduce the concept mass and increase performance through a mass optimisation process. Modifications to Howe's third spreadsheet *'the optimiser'*, characterises how a minimum mass solution is achieved through re-iteration, and is described in Appendix B, section B-4, with the final parametric results shown in Table 4-3.

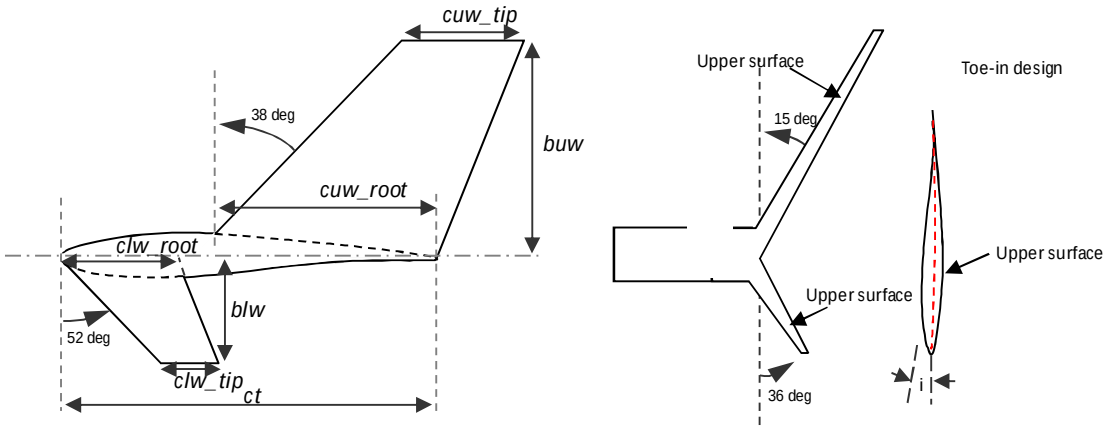

Fig 4-5: Simplification of winglet Geometry modified from McCormick [6]

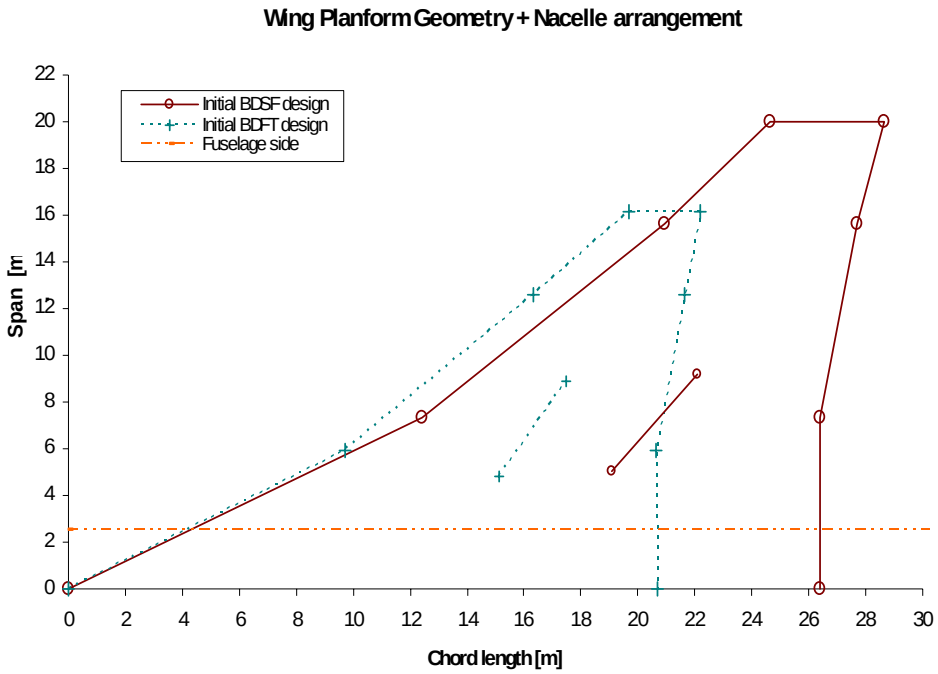

Fig 4-6: BDSF & BDFT Wing & Nacelle Layout

The minimum mass optimised design for the BDSF and BDFT is established for a wing design that includes integrated winglets, Fig 4-5, and over-the-wing (OTW) engine nacelles, Fig 4-6. The configuration development included the analysis to investigate the spanwise and chordwise positioning of podded engines over-the-wing and also the effects of winglets on the outer wing-tips. The main driver for including winglets was to minimise induced drag, primarily for cruise performance but also for directional control during low speed flight, such as take-off, flyover, and landing, with additional benefits of shielding sideline engine noise. *OTW* engine nacelles were

incorporated into the initial design, to investigate the change in aircraft drag and investigate the degree of engine noise shielding using the wing and winglets.

A minimum mass optimised solution should not be confused with the main research objective of reducing noise. The goal of the parametric process is to produce an aircraft concept using suitable design methodology, performance, and mass estimates, and not to analyse noise before there is a feasible geometry for the design. Modifications to the design process to determine aircraft noise and investigations into noise reduction technologies will be implemented into the methodology once an initial design is determined.

Having completed the parametric study an investigation into a series of flight cases was required to analyse the BD performance. Prior to establishing these flight cases, the BD required detailed wing and tail sizing, so that investigations into flight performance would reflect the true behaviour for the BDSF and BDFT configurations.

4.3 BD Concept Evolution

This section defines the evolution of the design for two key features of the BD which are the wing and empennage layout. As the design of the BD progresses it is difficult to visualise the aircraft based on results tables, despite the geometry definitions in Appendix B for the fuselage, wing, tail, and engine nacelles, the configuration as a whole is unknown.

A study into placing the wing at a high, mid, or low locations on the fuselage was investigated, and discusses concerns for aerodynamic efficiency, crashworthiness, egress, noise, maintainability, and cost. A range of empennage configurations were considered to investigate improving the BDFT efficiency.

4.3.1 BD Wing Location

A high wing produces cleaner airflow across the upper wing surface compared to a low or mid-wing design; mainly because the fuselage generates interference, separates the spanwise flow over the wing, and reduces overall section lift. The greatest disadvantage of a high wing is for a crash landing case, where the aircraft sits closer to the ground (because of fuselage mounted undercarriage), and a severe impact could push the wing down into the passenger cabin and either crush the cabin or block egress routes. Another scenario is for a water landing, more commonly referred to as ‘ditching’, where the for a low wing configuration, the wing is used as a float so the fuselage sits above water, unlike the high wing configuration where the buoyancy of the wing forces the fuselage to sink below the water level, creating challenges with the egress of passengers. It is not impossible to certify a high-wing configuration, where aircraft such as the BAe-146 [7] and Bombardier Q-series are

certified for ditching. The challenge is to certify a high-wing aircraft for ditching with greater than 70 passengers onboard.

The BD wing has potential for shielding engine noise by reflecting it upward and away from the ground. Doulgeris, 2008 [8] discusses how the correct positioning of engines on the wing provides forward fan and rearward jet noise shielding. Engine pods on the wing upper surface provide less noise shielding compared with an embedded solution, which could be ideal as there is ample volume inside the wing, however both have maintenance concerns. In addition to airframe noise, internal cabin noise must also be considered, as locating engines on the upper wing surface removes the wing shielding effect and places the engines in-line with the cabin. In the event of an engine fire, both podded and embedded solutions have egress challenges, reducing the chance of using *OTW* exits, as passengers could be exiting in close proximity to engines.

Egress is a major concern because the thickest wing root region has sufficient depth to cover 50% of the fuselage height. This provides a major challenge in using *OTW* exits for any of the BD configurations with a major concern for high or mid-wings, where the passenger cabin is likely to be inside the wing structure. Conventional Type A door exits are located at the front and rear of the fuselage, with two type I or II over wing exits for the low wing BD; positioned where there is sufficient clearance, aft of the thickest wing region, as per the requirements of CS-25.807 and CS-25.810 [9, 10].

The final concerns consider installation, maintainability, and cost for embedding or mounting engines above a high, mid, or low wing. Additional ground vehicles would be required and increase the risk of damage through carelessness/collisions from ground crew error. The challenge of implementing new procedures and safety guidelines relative to an existing low wing aircraft with under-slung engines would increase maintenance, training, and ground crew/vehicles costs, which is not ideal for the airlines.

4.3.2 BD Tail Configuration

Empennage designs were investigated to provide solutions for tail surfaces without a constraint on passenger acceptance/perception. The phrase that '*looks are irrelevant*' does not apply to aviation, as passengers tend to comply with a 'conventional' form for vehicles they wish to travel in. A conventional empennage was not considered for the BDFT, because the large delta wing at high incidence would generate vortices, which would most likely reduce the control effectiveness of the tail. Alternate and novel tail configurations were investigated, with noise playing a part in the selection process.

Two solutions were considered ideal for the BDFT, these being a *T-tail* and *V-tail* design, as shown in Fig 4-7. The *T-tail* was a conventional vertical tail with a large horizontal empennage mounted on-top, which was eventually considered too large a surface to mount on the fin, because of the size required for control and trim. A large fin design was therefore necessary to counter the lift generated by the main delta wing. The size was defined by the moment arm of the tail from the centre of gravity and the lift required for balancing the aircraft. In addition, the larger sized horizontal control surface produces more noise and propagates the sound directly down towards the ground. The *V-tail* configuration was selected because the canted tail surfaces direct noise at an angle to the ground, and significantly reduces the noise directly below the aircraft, providing a greater distance for noise attenuate before reaching the ground; the suggestion is that sideline noise will be greater and requires further investigation

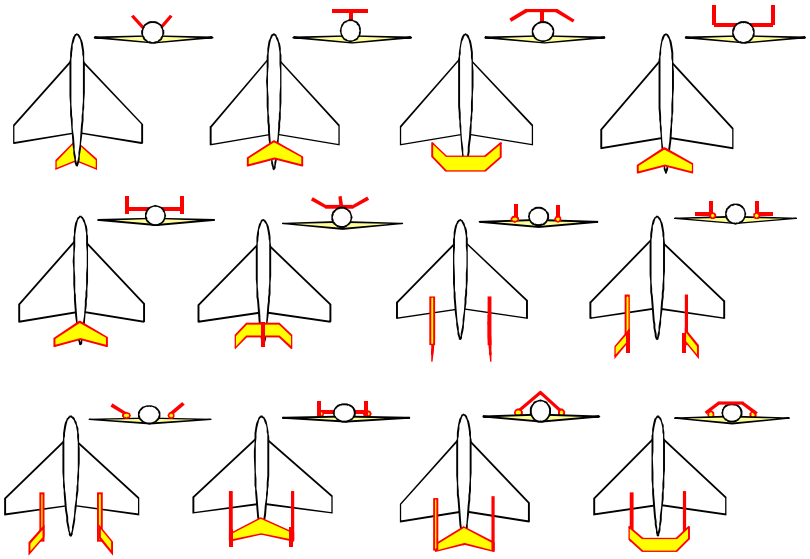

Fig 4-7: Tail Solutions for the BDFT and BDSF (from top left to bottom right: V-Tail, T-Tail, M-Tail, U-Tail, H-Tail, W-Tail, Fin-boom, L-boom, V-boom, H-boom, A-boom, N-boom)

According to [Howe, 2000], the horizontal tail aspect ratio A_{ht} for a conventional aircraft is 50-60% of the main wing, but for the low aspect ratio BD wing A_{ht} was initially assumed to be equal to the main wing, so A_{ht} =3.11. The optimisation of the main wing in section 4.4.1 provides an optimised A =4.87 and from the comment within Appendix B, 'Howe suggests for a subsonic aircraft, A should be in the region of 5 to 10', implying that A for the BDFT horizontal tail can be treated similar to a conventional aircraft. The new optimised wing A is on the lower limit for a 'conventional' subsonic aircraft, based on the statement above, and so $A_{ht} = ½A = 2.435$. The tail geometry is calculated as: b_{ht} = 21.9m, λ_t = 0.565, $(c_{ht})_{root}$ = 8.96m, $(c_{ht})_{tip}$ = 3.75m, and $\Lambda_{¼ht}$ = 48.3 degrees, from the method described in Appendix B.

A new geometry for the *V-tail* was determined by resizing the tail, where the maximum of the vertical and horizontal tail root chords were used as an equivalent *V-tail* root chord, likewise with the tip chord, and the equivalent span was calculated using:

$$(b)_{V-tail} = \sqrt{\left(b_{ht}{}^2 + b_{vt}{}^2\right)} \textbf{ [m]}$$

Equation 4-1

The geometry of the new *V-tail* empennage is calculated as:

$(b)_{V\text{-}tail}$ [m]	$(c_{V\text{-}tail})_{root}$ [m]	$(c_{V\text{-}tail})_{tip}$ [m]	$(\lambda)_{V\text{-}tail}$	$(\Lambda_{¼})_{V\text{-}tail}$ [deg]
11.96	10.77	6.09	0.565	48.3

Table 4-4: BD *V-tail* Equivalent Geometry

The BDSF was considered to have a greater noise reduction potential compared with the BDFT because of the removal of three major noise sources. The horizontal stabiliser is disconnected for the tailless design and therefore does not require the use of *TE* flaps, or slats for high lift. However, drooped *LE* devices were incorporated in the design because a significant noise reduction was achieved compared to conventional slats, and additional lift was required at low speed to achieve an increased c_{Lmax}. Investigating changing the BDSF vertical fin design by incorporating extended tail booms enables an effective increase in tail moment arm, and reduces the fin size. The tail boom was symmetrically placed at 30% wing semi-span, extending the vertical stabiliser beyond the end of the fuselage and was split into two components on each boom. Fin sweep angle was increased, moving the moment arm further aft and was considered to shield engine jet noise, significantly reducing the sideline.

Exploring the effect of canting the fins on the vertical tail booms transforms the boom design into a *V-tail*-boom with a part-span separation (for the BDFT). The main difficulty in canting the tail is that the tail control surfaces are now ruddervators, controlling yaw, pitch, and trim. This implies that similar to a conventional aircraft *TE* and *LE* devices can be used to produce a higher c_{Lmax} than the BDSF design, allowing the loading of the wing to be increased, for a slower (and a more controlled) landing performance. Simply changing the tail angle provides two noise sources compared to the fin-boom design, noise that is now produced from the tail and *TE* flaps. The majority of noise generated by *TE* flaps is caused by surface interactions as flow passes through the slot/vane of slotted flap devices. To reduce flap noise, variable camber flaps (*VCFs*) were used as described within Fielding, 2000 [11]; effectively increasing wing chord and camber by maintaining a smooth transition as the

device is extended out on a track to a specified angle, without allowing flow to pass through slots, hence reducing the noise generated.

4.3.3 BD Evolution Summary

The design evolution of the BDSF and BDFT are shown below in Fig 4-8, investigating numerous empennage configurations and wing locations, to determine the vehicle layout.

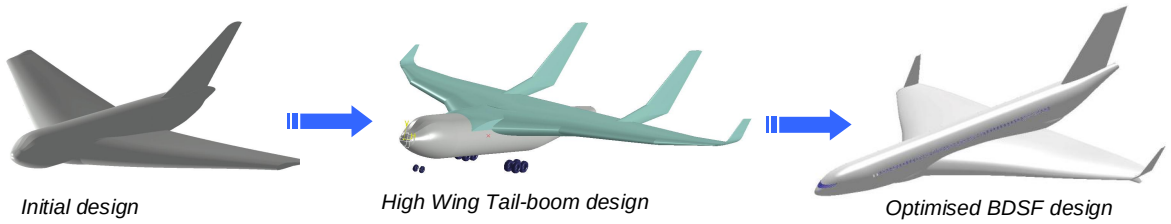

Fig 4-8: Graphical Evolution of BDSF Design

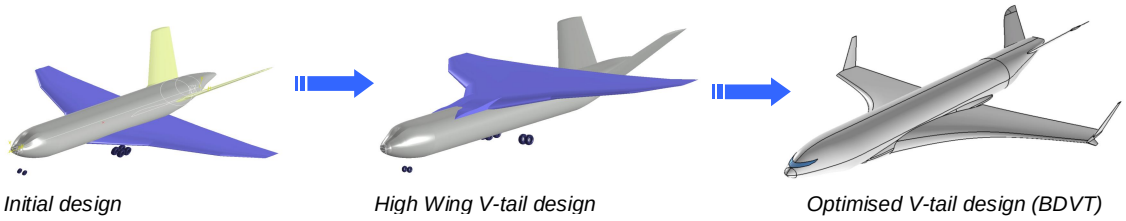

Fig 4-9: Graphical Evolution of BDFT Design - now referred to as the BDVT Design

Having discussed the potential benefits and challenges of each wing location, a low wing configuration was selected for the BD configurations to avoid challenges with egress and ditching. The tail-boom concept was not developed further because a small reduction in tail size was achieved by adding a complex tail arrangement. The acronym for the BDFT will now be changed to represent the *V-tail* empennage, and is referred to as the broad delta *V-tail* configuration (BDVT). The introduction of novel technology low noise high lift control devices has been introduced to the BD concept, where drooped *LE* devices and *TE VCF*s, are implemented to reduce airframe noise during take-off and approach.

4.4 Configuration Trade Studies

The mission specification set for the baseline aircraft was used as a datum starting point for the BD concept, but was purely for a comparative study purpose, and did not reflect the true capabilities of the BD airframe design. An investigation into alternate mission flight cases was considered because the BD has potential performance benefits, similar to that of the *AV* aircraft, such as a higher cruise altitude, increased cruise speed, steeper ascent and descent capabilities, etc. The aim of the

configuration trade study was to investigate five key areas to analyse the performance, by changing aspect ratio (A), thickness to chord ratio (t/c), cruise altitude, laminar flow, and steep continuous descent approaches. The following investigations state the relevance of each study to performance, airframe noise, and the environment.

4.4.1 Wing Aspect Ratio and Thickness-to-Chord Ratio

Investigating the ideal aspect ratio (A) and thickness-to-chord (t/c) ratio, not only provides solutions for wing lifting properties, but also loading, performance, and drag. Changing the wing t/c affects the structural efficiency, aerodynamic efficiency (lift and drag), and wing internal fuel volume. Wing drag and structural parameters are defined by changes in A, where Raymer [12], emphasises a change to stalling angles, wing tip vortices, and drag. Wing A for a subsonic aircraft should be in the region of 5 to 10, according to Howe [1], as *"the aerodynamic trend is towards high aspect ratio since this is the most efficient in reducing the inevitable drag due to lift of a finite wing. However, higher aspect ratio implies higher structural mass so that a compromise is necessary with due consideration given to aerofoil and other geometric parameters"*.

Initial inputs for the BD design were A = 3.11 and t/c = 0.11, which were then varied from A = 2 to 7 and t/c = 0.11 to 0.15, resulting in a change in $(T/Mg)_0$. The first parametric analysis methodology was used (as described in section 4.2.1), and calculated multiple cases for A and t/c, indicating a trend for the BDSF and BDVT performance. The trade study results compared changes in thrust loading $(T/Mg)_0$, wing loading $(Mg/S)_0$, lift, drag, and the structural parameter (SP). Where SP is an established value, used to indicate any likely structural limitations for a given design, and identifies direct conflicts between aerodynamic and structural requirements.

As t/c is increased, structural mass increases, zero-lift and induced drag increases, and lift is reduced, resulting in a higher thrust loading $(T/Mg)_0$, and greater aircraft mass. As A (aspect ratio) is increased there is a small change in zero-lift drag but a significant reduction in induced drag, resulting in a marginal decrease in $(Mg/S)_0$ (wing loading), a reduced $(T/Mg)_0$ (thrust loading), and a lower aircraft mass. The results tend towards a thin high aspect ratio wing, but due to the BD concept being a low aspect ratio wing design, a constraint of $A < 5$ was implemented.

Trade study results for $(T/Mg)_0$ are shown in Fig 4-10 and Fig 4-11, and a design point was selected based on the average airfoil t/c designed in section 4.5.1; $(t/c)_{avg}$ = 0.10125. Evaluation of the results provided two design points, where the final selection for the BDSF was A= 4.13, and A= 4.87 for the BDVT.

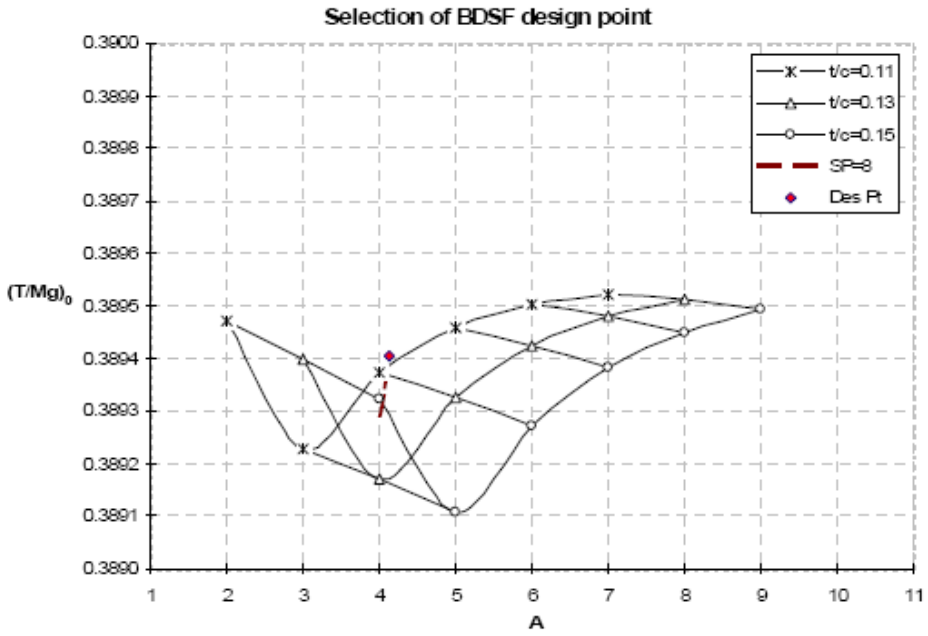

Fig 4-10**:** BDSF *A* and *t/c* Trade Study and Design Point Selection

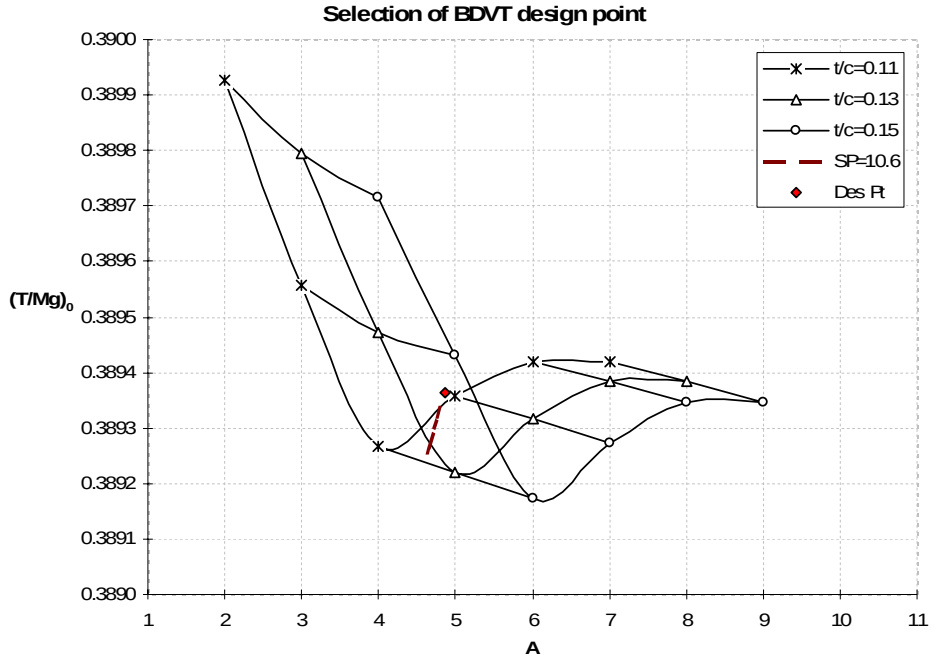

Fig 4-11**:** BDVT *A* and *t/c* Trade Study and Design Point Selection

4.4.2 Initial Altitude Selection for Cruise Optimisation

Determining an appropriate cruise altitude not only impacts cruise performance, but also climb performance, time of flight, and mission fuel, which feeds directly into the propulsion systems design,

and back into the overall vehicle mass. Standard atmosphere data, such as speed of sound, altitudes, densities, and temperatures, were extracted from Pamadi [13], to calculate relative densities for a range of cruise flight cases. There is no defined lower limit for cruise altitude of a civil airliner, and so a constraint of 38,000ft was considered the lowest cruise ceiling because this was consistent with the baseline aircraft, with a similar classification to a Boeing 767.

Flight Mach numbers varied from 0.8 to 0.85 which is typical for most subsonic passenger aircraft, with an additional case of Mach 0.9. The idea of flying slower for 'green' flight operations was considered but not developed further at this stage. Appendix C describes a detailed description of the analysis, where results for a range of altitudes and Mach numbers, were used to determine ideal cruise cases for the BDSF and BDVT.

To summarise two of the key results of this analysis, *L/D* and all-up-mass (*AUM*) variations are shown in Fig 4-12 and Fig 4-13. The altitude specified on the x-axis of each chart represents the start of cruise climb altitude, where the final cruise altitude (ceiling) is achieved after climbing a further 4,000ft, and this altitude is maintained for the remainder of the cruise range.

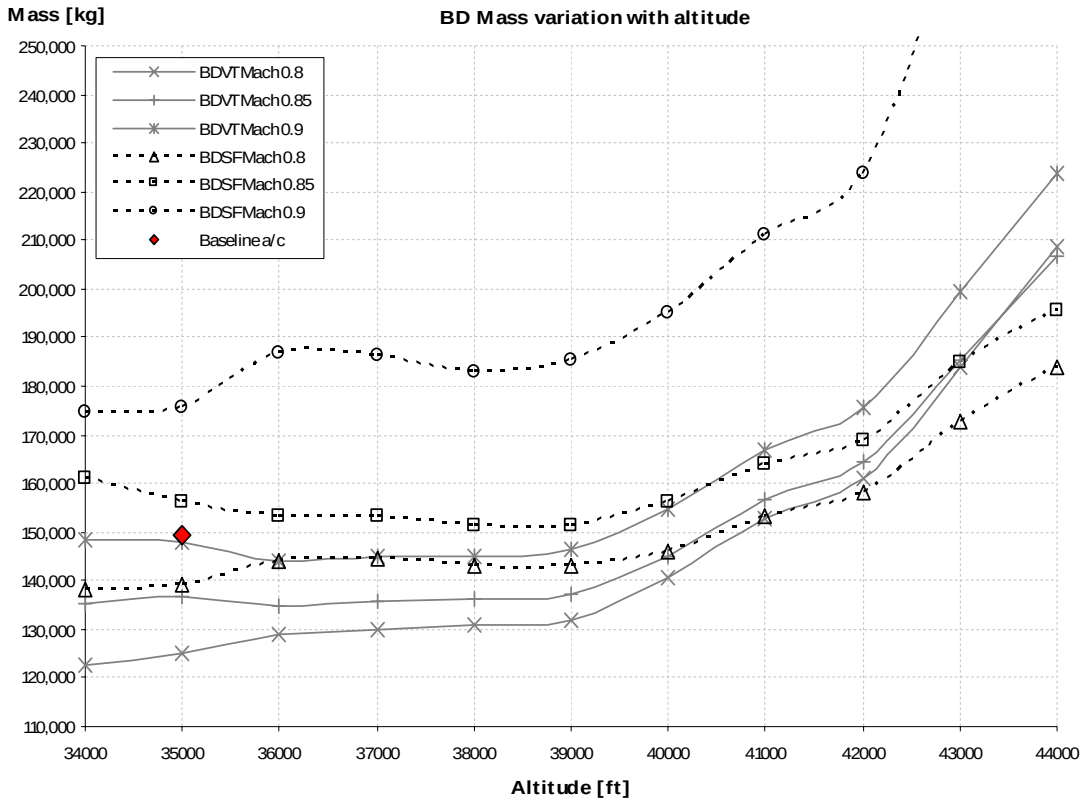

Fig 4-12**:** BD Total aircraft Mass variation by changing Cruise Altitude and Cruise Mach (Appendix C)

The most significant results are in Fig 4-13, where the *L/D* for the BDVT is above 20.2 at 0.8 Mach; for a cruise flight starting at 37,000ft and ending at a ceiling of 41,000ft. As cruise speed increases to Mach 0.85, so does *L/D* to 20.4, for a cruise of 40,000ft to 44,000ft. A similar increase in *L/D* is observed for a cruise segment at Mach 0.9 for range of cruise segments starting from 40,000ft to 43,000ft. It is necessary to cross-reference *L/D* results with *AUM* in Fig 4-12, where the mass of the BDVT increases rapidly above a cruise altitude of 41,000ft.

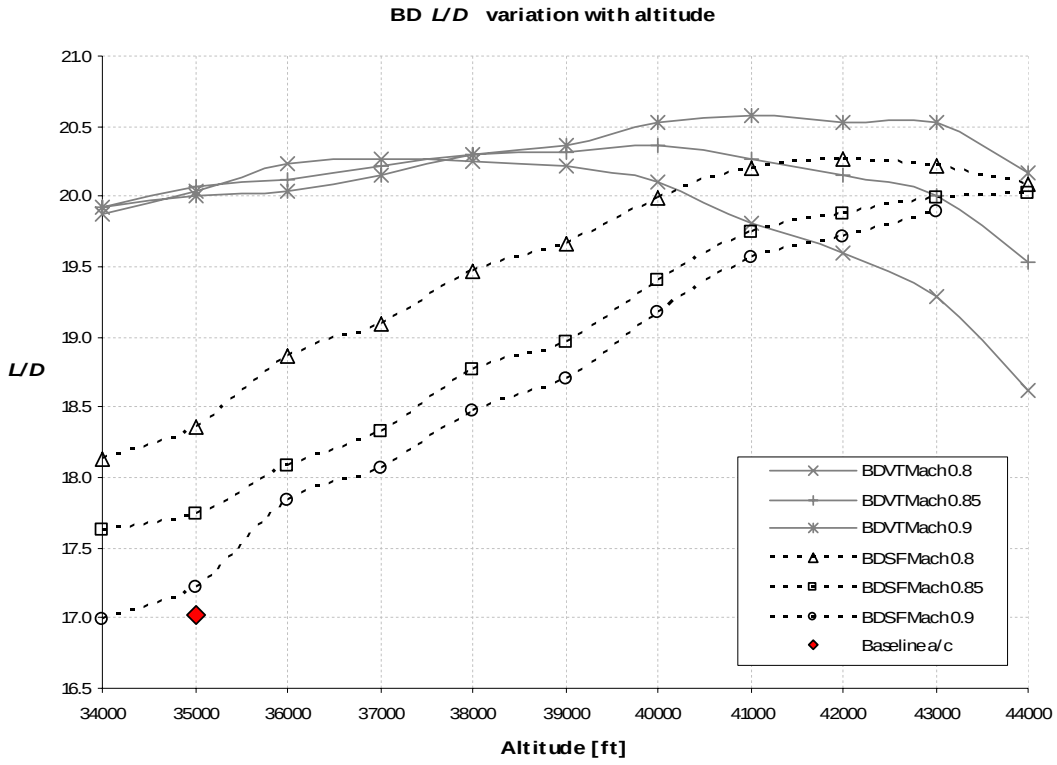

Fig 4-13: BD *L/D* variation by changing Cruise Altitude and Cruise Mach (Appendix C)

The BDSF displays similar results to the BDVT although *L/D* at lower altitudes is poor in comparison and is comparable to the baseline aircraft results. As cruise starts above 40,000ft, *L/D* and total mass for the BDSF peaks to similar values as the BDVT, with the exception at Mach 0.9, where there is a substantial mass increase due to high induced and trim drag.

A single cruise altitude was selected for the BDSF and BDVT, so that both designs could be compared in terms of performance, efficiency, and more importantly airframe noise. A cruise case at Mach 0.8 was selected for a cruise-climb altitude starting at 41,000ft and ending at a ceiling of 45,000ft. This altitude is higher than that designed for by SAI, where the BWB cruise case was for a cruise ceiling at 40,000ft [14].

This altitude and cruise Mach has been selected for three main reasons:

- To minimize aircraft *AUM* for cruise at Mach 0.8,
- To increase the performance of the BD concept at higher altitudes,
- Lower the thrust requirement and size of the engines.

Each design provided initial estimates for static engine thrust requirements, where a maximum vehicle thrust of 650kN was selected, providing a static thrust of 162.5kN for each of the four engines and was used to initiate the propulsion systems design. Engine thrust analysis was an iterative design procedure between airframe development and propulsion systems design by Doulgeris [8], where quantifying design specific fuel consumption $(c)_{des}$ and thrust requirements was critical for each designer. The BDSF and BDVT configurations use the same thrust-rated engines to simplify the design process and provide a fair comparison for the final aircraft performance.

The engine design was a high bypass ratio turbofan (*HBPR=8*) and included advanced technologies to reduce noise and increase fuel efficiency. The BDVT was considered to have more drag because of the podded engine configuration and the presence of a tail, compared to the additional trim drag of the BDSF, resulting in a higher design specific fuel consumption $(c)_{des}$ = 16 mg/N/s (0.57 N/N/h) for the BDVT, and $(c)_{des}$ = 15.85 mg/N/s (0.559 N/N/h) for the BDSF. The fuel flow rates at cruise were considered to be comparable to an efficient long range transport aircraft. An airframe-engine configuration of 4 HBPR turbofans podded at the wing root was selected; aimed to reduce asymmetric thrust for an engine out scenario and reduce the engine diameter to aid integration into the airframe. Further on in the study these specific fuel consumption assumptions were proved to be reasonable, because the drag associated with the BDVT included 4 over-the-wing podded engines as well as the trim drag of the tail, compared to the elevon deflection trim drag and the semi-embedded engine configuration for the BDSF.

Environmental and economical effects were considered to fly the BD slower and at lower altitudes; which would release emissions lower in the atmosphere, producing fewer contrails and a shorter time-frame for vapours to remain in the atmosphere. Although low and slow flight is environmentally beneficial, it was not considered to be economical for the airlines, indicating more fuel required and longer flight durations. This may not be completely true, because the time taken to climb to 40,000ft and descend may be equivalent to a low-altitude-slow aircraft; because less time is taken to reach cruise altitude and to descend for landing, where the flight duration may be similar for short-medium range operations, but not for long range.

The altitude study revealed an optimum cruise-climb altitude of 41,000ft to 45,000ft, and was selected for both BD configurations with a 0.8 cruise Mach. A lower and slower cruise may be environmentally beneficial, but the design will progress using the flight case above, unless advantages other than those already discussed will benefit the design enough to warrant further investigation.

4.4.3 Steep Approach Flight Path Angles

Descent angles were previously discussed in a slow and steep approach investigation for the baseline aircraft. The same principals apply for the BD where high approach angles place the aircraft at a greater distance from the ground and reduce the noise footprint. The BD was initially designed for a conventional 3 degree continuous descent approach, where a 6 degree steep approach angle is now considered, and aimed at investigating landing performance as well as noise. The two descent angle cases are analysed in parallel within sections 4.4.4 and 4.4.5 to compare laminar flow, steep approaches, and engine bypass modifications.

4.4.4 Engine Bypass Modifications

Higher engine bypass ratios increase efficiency and reduce noise [8]. The engine designs were modified from *HBPR* to ultra-high-bypass ratio turbofans (*UHBPR*), with a bypass range from 5 to 30. A selected BPR of 12 was integrated into the BD airframe designs, and results were compared to initial engines with a *BPR* of 8. The final design was for *UHBPR* engines with noise reduction technologies and improvements that increase fuel efficiency, where $(c)_{des}$ = 15.53 mg/N/s (0.549 N/N/h) for the BDSF, and $(c)_{des}$ = 15.68 mg/N/s (0.554 N/N/h) for the BDVT; providing a reduction in fuel consumption of 1% relative to the BPR = 8 engines. The new specific fuel consumptions were revised and re-iterated in the parametric study calculations, and combined with the steep approach and laminar flow analysis results.

4.4.5 Wing Artificial Laminar Flow

The effect of artificial laminar flow was investigated by introducing an *OTW* hybrid laminar flow control (HLFC) system to determine an increase in BD wing efficiency. Laminar flow is usually associated with un-swept wings, where for this highly swept delta laminar refers to achieving a favourable airfoil pressure gradient, hence producing the ‘laminar bucket’. The study was based on a HLFC system on the outboard wing sections and included mass penalties as well as any associated aerodynamic improvements [15].

Four engines placed either side of the wing root was thought to disturb the flow over the inboard upper surface, so it was assumed that the outboard section of the wings generated the main proportion of lift. The outboard wing was designed using modified supercritical NACA airfoils (as described in

section 4.5.1) and shows a laminar flow bucket/region. Assuming that 75% of total wing lift was generated from the outboard wing, a maximum of 75% laminar flow is achievable, only if the outboard chord was designed to be 100% laminar. In reality this is not be possible for the BD, due to the high LE sweep angles, therefore a maximum of 50% laminar flow was thought to be achievable by the wing; it was decided that a maximum laminar flow of 67% for the outboard region was possible if there was zero sweep. Therefore investigations were made into increasing the percentage of HLFC from 0 to 50% chord.

Results from the combined study of HLFC, engine BPR, and steep descent approach studies are shown in Appendix D. Laminar flow investigations assumed that hybrid laminar flow was achievable over the highly swept delta wing, and where applicable mass penalties for the system were introduced, neglecting any detriments in engine performance due to bleed and power off-takes. This assumption is based on technology release levels and the maturity of the more-electric aircraft concept by 2020. The addition of the HLFC system now incurs mass, integration, and cost concerns for the BD concept design, but is necessary to investigate the true potential of the concept.

There are four main BD design studies that represent the engine BPR and approach angle variables. The variation in *AUM, L/D, $(T/Mg)_0$,* and mission fuel mass for the laminar flow range previously mentioned are compared for the design range and cruise mission specified in section 4.4.2.

The four main BD configurations analysed are:

- BDSF - BPR=8, 3 degree approach angle,
- BDSF - BPR=8, 6 degree approach angle,
- BDSF - BPR=12, 6 degree approach angle,
- BDVT - BPR=12, 6 degree approach angle.

Increasing laminar flow reduces vehicle and fuel mass, and increases L/D and $(T/Mg)_0$ for a given powerplant. Increasing the approach angle from 3 to 6 degrees has a marginal effect on performance, with the main change being a slight increase in $(T/Mg)_0$. Increasing BPR from 8 to 12 improves fuel burn resulting in a lower fuel mass, and a slight improvement in *L/D*, with a marginal change in $(T/Mg)_0$. An additional variable is added into the trade study and this is the design $(Mg/S)_0$, and this clearly shows how the BDSF and BDVT differ for a similar range of wing-loadings. The results are shown in Appendix D and provide an insight into how the tailed and tailless designs diverge.

The trade studies revealed that using an UHBPR engine provided fuel consumption benefits at the expense of nacelle diameter, and combined with the steep 6 degree descent angle, would provide

significant reduction in airframe and engine noise during approach and landing. 12.5% wing artificial laminar flow was selected across the main wing which corresponds to 16.7% artificial laminar flow across the outboard wing section and is factored into both BD configurations from here-on.

4.5 BDSF and BDVT Concept Development

The main focus for further developing the BD concept is to finalise the wing, tail, and general arrangement for both of the tailed and tailless configurations. Lifting surface development involved investigating the design of supercritical airfoils, wing twist, control surfaces, winglets, and fuselage-wing-winglet interfaces, not to forget the four *OTW* nacelle pods; all of which are essential for optimising the concept for lift, drag, low speed, and cruise flight performance. A summary of the airfoils used is presented below, with further detailed design data collated within Appendix E.

4.5.1 BD Lifting Surface Design

Airfoil design for the BD concept were developed using Reid [15], and modified from existing NACA 5-digit airfoil data extrapolated from Harris [16]. The four main airfoils were modified to achieve the desired cruise and maximum low speed lift coefficients, and are shown in Fig 4-14; representing the root, kink1, kink2 and the tip airfoil sections for the BD wing. The design of these airfoils uses methods similar to the SAI which investigated carving out the LE to generate a nose-up pitching moment and avoid using reflex camber at the rear of the airfoil, as used on the AV aircraft. The BDSF and BDVT concepts use the same airfoils to simplify the design analysis, where the airfoil properties are shown in Appendix E, with data representing the lift, drag, pitching moment, and lift-curve slopes for each section. Caution is advised, because the airfoil design process was a top level design study on a 2-dimensional (2-D) basis and that full 3-D analysis is required to fully optimise the wing design process.

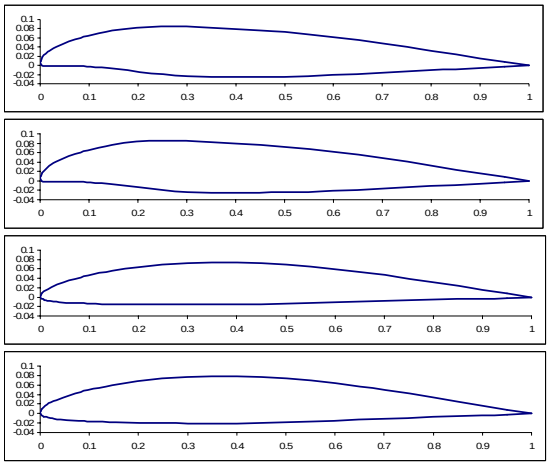

Fig 4-14**:** BD Airfoil Designs, top to bottom: Root = NACA-23011 (modified), kink1= NACA-63A0(10.5) (modified), kink2 = NACA-63A009, tip= NACA-63A010.

The outboard airfoil sections were designed to be laminar flow airfoils, as described within section 4.4.5, where the drag polar summary for the four airfoils are shown below in Fig 4-15. The laminar flow buckets can clearly be seen for the kink2 and tip airfoil sections, with a small laminar region on the inboard root and kink1 airfoils.

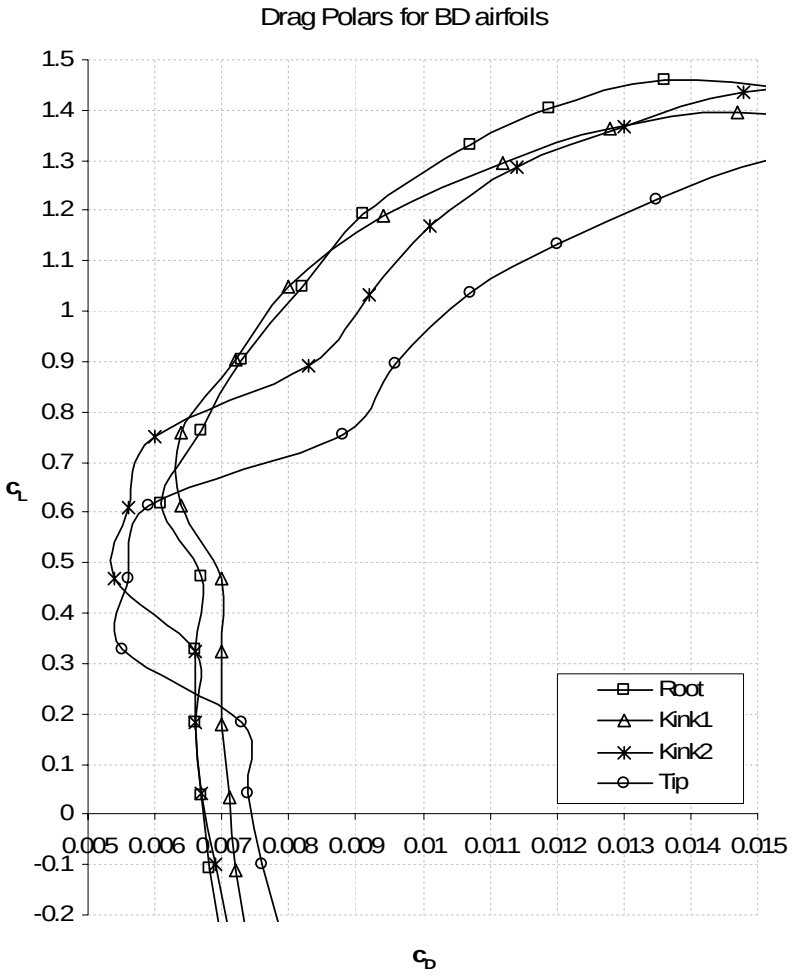

Fig 4-15**:** Designed Airfoil Drag Polar showing Laminar Flow Buckets for Outboard Airfoils

The BD wing is separated into three main segments by the four airfoil sections and represents a transition phase to blend one airfoil to the next. The blend is combined with a progressive geometric wing twist, or washout of 2 degrees at the tip. Washout is included to prevent tip stall at high angles of attack, especially for low speed manoeuvrability, where the tip airfoils stall at an incidence above 12 degrees. The BD has an estimated fuselage incidence of 4 degrees at cruise for a lift coefficient of 0.35, corresponding to an airfoil incidence of 2 degrees, and falls within the laminar flow region of the tip and kink1 airfoils, hence utilising the laminar flow capabilities outboard.

4.5.2 BD Fuselage Development and Design

The BD fuselage is a conventional cylindrical design, with a single-deck passenger compartment layout [10]. The fuselage does not produce much lift but does generate significant drag for a conventional aircraft, and the idea was to use a similar *LE* carving at the nose of the fuselage (Fig 4-16) to generate a positive pitching moment about the centre of gravity (*c.g.*). Analysis of *LE* carving effect would be an interesting scope for further research, but due to time constraints the amount of lift generated was estimated through a vortex lattice code, AVL [17], where a lift increment of 1% was achieved and factored into the design calculations.

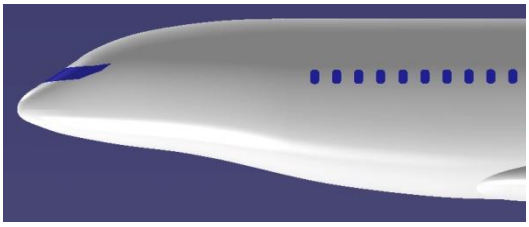

Fig 4-16: Fuselage Nose Design incorporating *LE* Carving

Cabin layout for a 3-class, single deck, and 269 passenger configuration was designed; which includes seating for 170 economy, 24 business, 15 first class, with 7 cabin attendants, and 2 pilots plus crew baggage storage.

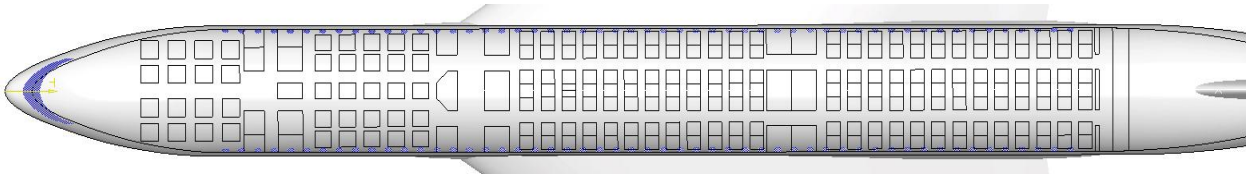

Fig 4-17: Fuselage Internal Layout for a 3 Class arrangement, with Galleys, Cross Aisles, and Toilet facilities

Cargo and baggage stowage are located below the cabin floor, with access doors at the front and rear of the fuselage. There is ample room for storing 8 LD-3 containers at the front below business class, and 16 LD-3 containers at the rear below economy (or 14 LD-3 containers plus bulk cargo space. This is a significantly larger capacity than the B767-300 equivalent which can only contain smaller LD-2 containers.

Attached to the lower fuselage is a twin wheel nose gear, located below the first and business class seating because of the track requirement and the LE nose carving on the fuselage. The main landing gear is housed within the wing and consists of two 4-wheeled bogies that retract inwards into the main wing-fuselage region. Landing gear calculations for sizing, tyre selection, and initial loading of a tri-

cycle gear layout was incorporated into the design methodology using Young, [18] and Currey [19], as described in Appendix F.

Fig 4-18: BD Concept, Showing Main and Nose Undercarriage, and Wing-Fuselage Blister

The wing-fuselage join usually incorporates the design of a belly fairing or blister and is typically used to house undercarriage for conventional aircraft, however for the BD the blister design is solely required to provide a smooth fairing between the wing and fuselage lower surface, as shown in Fig 4-18. The blister is blended into the wing and fuselage to create minimal interference drag for the lower surface and contributes to the lift produced by the wing and fuselage nose carving. Vehicle drag calculations were combined with empirically derived data and the AVL results [17], and consider a pessimistic parasitic drag assumption, which in-turn provides higher *L/D* compared to the baseline aircraft.

4.5.3 BD Design Changes and Configuration Selection

The previous sections of this chapter have described the evolutionary design of the BD concept, where numerous design changes have been made, and as a result the concept has developed into a series of variants that now suggest 8 possible design solutions. This section describes the final changes to each of the four BDSF and BDVT configurations previously mentioned, with the aim to define a single BDSF and BDVT for a final (head-to-head) design comparison.

4.5.3.1 BD Thrust-to-Weight Optimisation

The final results for the optimised BDSF and BDVT provided high $(T/Mg)_0$ of around 0.5 for the cruise flight case where ideally nominal values are in the range of 0.25 to 0.35. An investigation into the design showed that although the BD concept could potentially fly at higher altitudes, it is the thrust required to reach that cruise altitude that pushes the vehicle $(T/Mg)_0$ higher, with a resulting impact on the propulsion systems design, driving changes in the engine size, fuel consumption, and overall vehicle mass.

An ideal cruise-climb altitude was designed where maximum $(T/Mg)_0$ = 0.318 for the BDSF, with an initial Mach number climb starting at 35,000ft (10.7km), and climbing to a ceiling of 38,000ft (11.6km). Similarly for the BDVT a maximum $(T/Mg)_0$ = 0.321 was determined for an initial Mach number climb starting at 36,000ft (11.0km) and climbing to a ceiling of 39,500ft (12.0km). These design changes were part of an iterative design loop in the design methodology and hence replace previously quoted flight altitudes within this chapter.

4.5.3.2 BD Cruise Mach Optimisation

A final study was initiated, investigating a cruise Mach number range of 0.7 to 0.9 in order to optimise these new altitude cruise segments for the revised BD designs. This analysis incorporated 12.5% wing artificial laminar flow, 4 *OTW* podded engines, drooped LE slats, and *TE VCF* for the BDVT to mention a few. The results of this new optimisation study are shown below in Fig 4-19 to Fig 4-22.

A comparison of BPR of 8 to 12 engines for a cruise Mach of 0.7 shows a significant decrease in overall aircraft and fuel mass for the BDSF. The change from a conventional 3 degree approach to a steep 6 degree approach for the BDSF suggests an overall aircraft and mission fuel mass increases, a marginal change in L/D, and a reduction in $(T/Mg)_0$. The trend that is clearly shown for the BDSF is that flying at a lower cruise Mach numbers reduces *AUM* significantly and increases *L/D*. When cruise Mach is increased from 0.7 to 0.9 an *AUM* increase of up-to 40 tonnes is shown, 6 tonnes of which is additional fuel, resulting in a reduction of *L/D* from 19.8 to 17.1. The results clearly show that for the BDSF concept, a slower cruise Mach number is beneficial not only for reducing *AUM* and mission fuel, but also for increasing the lifting performance and reducing harmful aircraft emissions produced by the engines, providing significant environmental benefits.

The BDVT in comparison to the BDSF has an overall increased *AUM* but a reduced mission fuel mass and provides a better trend in results. At Mach 0.7 the aircraft mass is comparable to that of Mach 0.75, however the mission fuel required at this lower cruise speed is increased by 2 tonnes. As Mach is further increased, the mission fuel chart (Fig 4-20) represents a typical bath-tub curve, where the minimum values often represent the optimum design solution. The $(T/Mg)_0$ results (Fig 4-22) show a similar trend as the mission fuel plot, where the optimum cruise speed to minimise $(T/Mg)_0$ is clearly identified as Mach 0.8. Fig 4-21 represents the variation of *L/D*, where the BDVT *L/D* increases with Mach number and remains above a value of 19.4 for the entire Mach number range, unlike the BDSF.

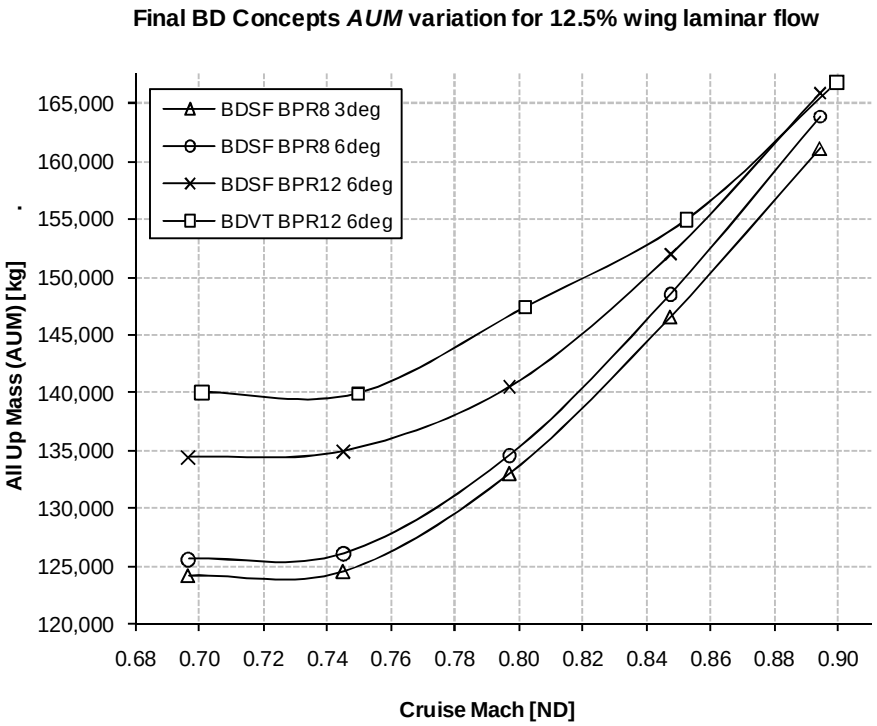

Fig 4-19**:** *AUM* variation for BDSF and BDVT final Mach number optimisation study

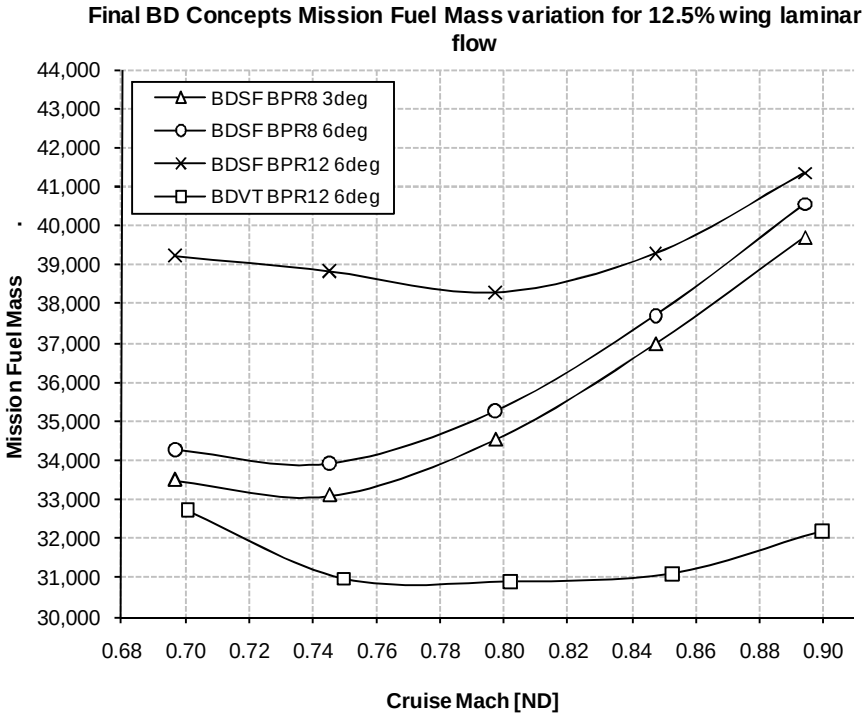

Fig 4-20**:** *Mission fuel* variation for BDSF and BDVT final Mach number optimisation study

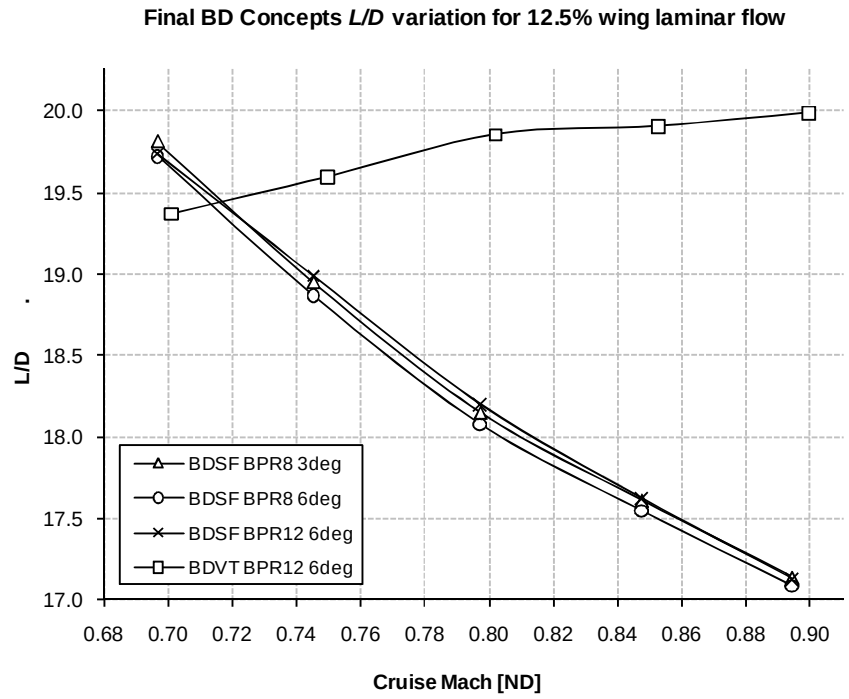

Fig 4-21**:** *L/D* variation for BDSF and BDVT final Mach number optimisation study

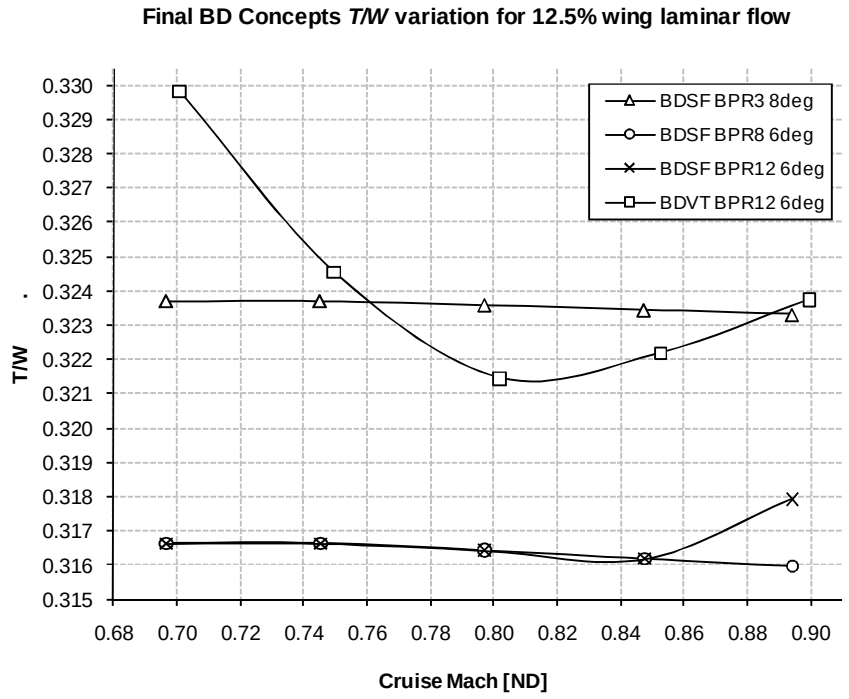

Fig 4-22**:** *T/W* variation for BDSF and BDVT final Mach number optimisation study

4.5.3.3 Podded Vs Embedded Engine Selection

The design of the BD has developed using *OTW* podded engine installations, where the increase in nacelle drag, maintenance considerations, and noise reduction has been considered. Embedding or semi-embedding the engines provides a greater noise reduction potential, but introduces design challenges; primarily with airframe integration and also for the prediction of installed drag.

Nettis [20], quantifies the drag increase due to installing embedded, semi-embedded, and podded engines on a delta wing, and compares the increase in drag. The drag increment predicted using CFD for a podded installation is 3 times the amount for a clean wing. Similarly the drag results for the semi-embedded are 2 times, and the embedded is 1.7 times that of the clean wing. This delta wing study at Mach 0.8 provided questionable results because the wing was associated with shock formations across the *LE*, and was not representative of the current geometry.

Fujino [21, 22], was used in Appendix B to predict the increase in drag due to *OTW* engine nacelles, where a 10% increase in low speed induced drag $(K_V)_o$ and a 5% increase in cruise induced drag $(K_V)_{cr}$ was factored into the design calculations.

	Podded	***Semi-embedded***	***Embedded***
$(K_V)_o$	10%	5.9%	3.8%
$(K_V)_{cr}$	5%	2.9%	1.9%

Table 4-5: Increase in induced engine installation drag adapted from Fujino, [21, 22] and Nettis [20]

A trend in the drag increment, from embedding to using engine pods, was determined using the results from Nettis [20], combined with assumptions from Fujino [21, 22], where the following characteristics were factored into the BD engine drag calculations and into the parametric design analysis. Table 4-5 represents the drag increase of using the three alternate engine installation solutions.

4.5.3.4 Final BDSF and BDVT Design Selection

The optimisation study for cruise Mach number and reducing thrust-loading determined that the BDSF and BDVT differ in terms of flight performance. Despite the BDSF being more efficient at a lower cruise Mach of 0.7, a design Mach 0.8 was selected for both variants. Steeper approaches are ideal for reducing airframe approach noise, with a marginal increase in performance for the BDSF, relative to a conventional 3 degree approach. Reducing engine noise was also a priority, achieved by integrating four UHBPR=12 engines, despite having a larger diameter and being heavier, but were

more adaptable to the airframe compared with the UHBPR=20 to 30 engines due to the fan diameter sizing.

Description	*Symbol*	*BDSF*	*BDVT*	*NT-BL*	*units*
Wing Area	S	516.2	356.6	184.8	[m^2]
Wing Span	b	46.2	41.7	38.4	[m]
Wing Standard Mean Chord	$\bar{c}$	11.2	8.56	4.81	[m]
Wing Aspect Ratio	A	4.13	4.87	7.99	-
Wing Quarter Chord Sweep	$\Lambda_{¼}$	25.6	30.2	32.3	[deg]
Wing Taper Ratio	λ	0.181	0.283	0.277	-
Thickness-to- Chord Ratio	t/c	0.1013	0.1013	0.115	-
Wing Apex location	l_{APEX}	21.8	21.9	23.5	[m]
Horizontal Tail Area	S_{HT}	-	151.3	45.5	[m^2]
Vertical Tail Area	S_{VT}	93.3	57.5	27.3	[m^2]
Wing Area Parameter	$S^{-0.1}$	0.535	0.556	0.569	[m^{-2}]
Static Wing Loading	$(Mg/S)_0$	2680	3550	7465	[N/m^2]
Static Thrust Loading	$(T/Mg)_0$	0.314	0.321	0.333	-
Lift-Drag Ratio	L/D	18.3	19.9	15.6	-
Cruise Lift Coefficient	$(c_L)_{cr}$	0.252	0.338	0.432	-
Mass of Wing	M_W	25,461	21,841	21,097	[kg]
Fuselage Mass	M_{FUS}	17,235	17,660	17,454	[kg]
Mass of Tail components +winglets	M_T	2,546	3,931	3,797	[kg]
Mass of Undercarriage	M_G	5,640	5,162	5,626	[kg]
Propulsion Systems Mass	M_{PP}	10,621	9,938	11,248	[kg]
Mass of Systems	M_{Sys}	14,329	13,065	14,230	[kg]
Operational Items Mass	M_{OP}	2,762	2,762	2,762	[kg]
Operational Empty Mass	M_{OEW}	78,594	74,359	76,215	[kg]
Mass of Payload	M_{Pay}	23,760	23,760	23,760	[kg]
Mass of Fuel Required	M_f	38,636	30,939	40,681	[kg]
Available Fuel in Wing Volume	M_{f_a}	209,781	102,215	43,967	[kg]
Total Static Thrust	T_0	434,149	406,207	459,759	[N]
Total Overall Mass	$\boldsymbol{M_0}$	**140,990**	**129,058**	**140,656**	**[kg]**

Table 4-6: BD final design summaries for BDSF and BDVT configurations with NT-BL aircraft

The final BD concept is dependent on the results from Chapter 6, where the most promising of the BDSF and BDVT solutions are compared by their airframe noise. Both BD variants are designed for a cruise Mach of 0.8, with BPR 12 engines, for a 6 degree steep approach angle, and both with 12.5% wing laminar flow incorporated. The main difference lies with the BDSF having four integrated semi-embedded UHBPR engines located at the wing root, where the BDFT has four similar UHBPR engines, but are podded OTW at different spanwise stations; because there was insufficient volume

within the BDVT wing to efficiently house four semi-embedded engines without causing significant drag penalties.

4.6 BD Mass, Centre of Gravity, Stability & Control Analysis

Appendix G describes revised mass estimates for each BD configuration, where the wing, fuselage, empennage, and systems masses are revised and compared for a metallic and composite aircraft configuration. In addition to these variables, an environmental factor was investigated through removal of the hydraulic systems and a comparison with the mass of a more-electric aircraft. The comparison of a More-Electric aircraft (*ME*) and a hydraulic aircraft in addition to composite and metallic variants raises a question as to whether the aircraft should include environmental considerations other than noise in the final selection.

Table 4-7 provides a summary of the final mass breakdown for the BDSF and BDVT with comparisons for the two materials and All Electric (*AE*) vs. hydraulic variations. An all composite airframe design was selected, considering the BD concept aircraft would enter into service in 2025, integrated with *AE* flight management and control systems.

The main concern for the BDSF is the absence of a horizontal tail for trim. Longitudinal control and stability was calculated using Howe, Raymer, and Pamadi [1, 12, 13], where a -3.88% stick free static margin was calculated for the BDSF, and a +4.45% static margin for the BDVT. BDSF stability and control implications can be solved using a flight control system at a detailed design stage. Lateral stability is outside the scope of this study, never-the-less, control surfaces were sized using Howe and Jenkinson et. al., [1, 10]. The BDSF fin and rudder were sized using volume coefficients and revised to consider low speed manoeuvrability and gusts [1, 10, 12]. Low speed performance is not as critical for the BDVT because ruddervators act as a horizontal trim surface, along-with drooped *LE* and *TE VC* flap[4] devices for high lift, enabling the configuration to perform like a conventional aircraft.

The final two designs are all composite airframe constructions with *AE* systems, designed to increase aircraft efficiency and reduce vehicle mass. Mass breakdown, centre of gravity, stability, and control surface sizing for both BD configurations were determined, where the challenges associated with both designs were: certification, being the major concern for the tailless design, and cabin noise for the BDVT. An interesting trade-off is the increased stability, reduced manoeuvrability, and increased noise from the BDVT compared to the reduced longitudinal stability and noise of the BSDF.

4 Variable camber flaps are concealed flaps that extend and arc outwards, running on tracks within the wing. The advantage of using variable camber flaps is that there are no slots, so that sufficient lift and drag is generated without turbulent flows through slot vanes generating noise.

BD Configuration description		*BDSF*	*BDVT*	*NT-BL*
Empty Mass (EM)	metallic	83,618	88,736	80,252
	composite	77,472	81,321	74,555
Operational Empty Mass (OEM)	metallic	86,975	92,093	83,609
	composite	80,829	84,678	77,912
All Up Mass (AUM) - Hydraulic	metallic	152,535	152,383	152,304
	composite	146,338	144,968	146,607
AUM – All-Electric (AE)	metallic	152,972	152,820	152,116
	composite	147,132	145,339	146,151

Table 4-7: BDSF and BDVT total mass summary and comparison with *NT*-BL aircraft [kg]

4.7 BD Cost Analysis

The final stage of the concept design is to determine a cost analysis which considers the development, manufacture, testing, and assembly phases of the BD. This is achieved by using a cost comparison for operating, acquisition, and development costs.

The cost methodology for development, acquisition and fuel operating costs was predicted using Burns [23], with guidance sought from Raymer [12], relating to the direct (*DOC*) and indirect (*IOC*) operating costs, along-with assumptions for the cost of disposal, and the DOC per seat per nautical mile.

The development costs for the BDSF were higher than the BDVT, mainly due to the increased testing and advanced technologies required for the tailless design. The tailless design has a higher engineering cost, with higher development costs, more flight testing and operations, greater manufacturing costs due to the larger wing design, and higher quality control compared to the BDVT. The main differences between the BDVT and BDSF are reflected in the cost summaries within Appendix I.

An overview of the life-cycle cost (LCC) is provided in Table 4-8 below, summarising the total cost of the BDSF compared with the BDVT for development, acquisition, operating, and disposal costs. The term DDTE refers to the design, development, test and evaluation costs.

Cost Description	***symbol***	***BDSF***	***BDVT***	***NT-BL***
DDTE per unit	C_{UDDTE}	38	39	38
Acquisition per unit	C_{UA}	203	211	206
Operating per unit	C_{UOPER}	3,289	3,016	4,326
Disposal per unit	C_{UDISP}	41	42	41
Life Cycle Cost per unit	C_P	3,571	3,308	4,611

Table 4-8: BDSF and BDVT Summary of Life Cycle Cost per aircraft [*$US Million*]

One of the main cost figures used to compare aircraft is the cost per seat per nautical mile, where both the BDSF and BDVT have significant cost savings compared with B767-300 published data. Caution is advised in using the costing methodology described within Appendix I, because the process is aimed at preliminary design level studies and not for a conceptual design level. The results shown in Table 4-9 provide an optimistic result where the cost-per-seat-per-nautical mile is 25% less than the B767-300, which is published at 0.0936lb/seat/n.mile (0.0425kg/seat/n.mile).

Cost Description	***symbol***	***BDSF***	***BDVT***	***NT-BL***
DOC *per unit* [*$US*]	C_{UDOC}	65,301	59,882	76,621
mission block fuel [*lb*]	F_{BLOCK}	21,863	20,049	28,756
block fuel/seat [*lb*]	F_{BPS}	101	93	133
DOC/block hour [*$US/hr*]	C_{UDPH}	10,846	9,946	13,743
DOC/seat [*$US*]	C_{DPS}	302	277	355
DOC/seat n.mile [*$US/n.mile*]	C_{DPSM}	0.0752	0.0690	0.0882

Table 4-9: BDSF and BDVT Summary of DOC and mission fuel per seat nautical mile; with a block time of 6.02hours and mission range of 4,020 nautical miles

The methodology predicts an optimistic solution for cost-per-seat-per-nautical mile for both of the BD configurations. A comparative study with the baseline aircraft (similar class of aircraft as B767-300), found that a cost of 0.0917 lb/seat/n.mile was calculated, providing an approximate error margin of 4% with respect to the B767-300 published data. The cost results show that both of the BD configurations could provide a significant saving to the direct operating cost, and increase the aircraft economy with little impact on the development, and manufacturing costs compared to conventional aircraft to-date.

4.8 Concept Design Summary

Two main airframe concepts were investigated for the BD concept family, where multiple design variables such as materials, engine selections, approach conditions, etc, were explored and down-

selected to two configurations. The main emphasis on the design selections were based on producing the lightest possible airframe, and introduce noise reduction technologies to develop a silent airframe, so a composite all-electric airframe was developed with a tailed BDVT and a tailless BDSF solution.

4.8.1 Summary of the BDSF Design

The tailless BD configuration is an all composite airframe optimised for a cruise Mach of 0.8, BPR 12 engines, at an altitude of 38,000ft for the specified design range. The BDSF becomes more efficient at higher cruise altitudes and Mach numbers with an L/D in excess of 20; at the expense of a heavier aircraft, more fuel, and larger engines. The benefits of a higher and faster flight is out-weighed by environmental factors such as releasing emissions higher in the atmosphere, and economical concerns related to the cost of fuel.

The BDSF is considered to be a quieter solution compared to the BDVT because fewer surfaces interfere with the free-stream, reducing vortices and noise. The BDSF is designed to reduce airframe noise through implementing novel technologies such as *TE* brushes, *VC LE*, winglets, engine noise liners, and undercarriage fairings.

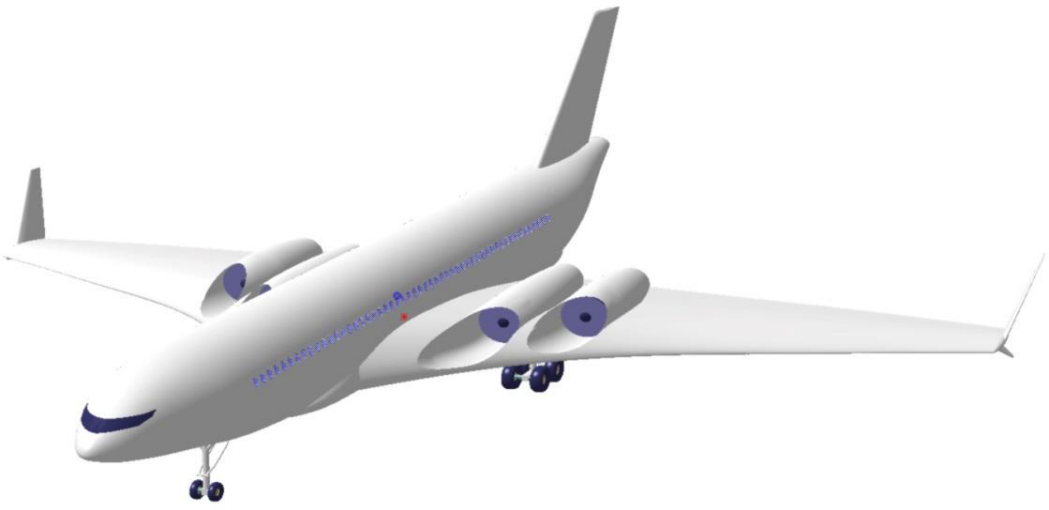

Fig 4-23: Final BDSF Concept Design

The wing design uses modified laminar flow airfoils, with *LE* carvings to produce a positive pitching moment about the c.g., reducing the required elevon deflection for trim. *VC LE* devices are deployed to increase maximum lift coefficient so avoid wing stall, assisting with the steep 6 degree approach angle. *TE* elevon and aileron deflections are coupled to increase wing camber and maintain steady flight, with spoilers assisting as air-brakes and for yaw control, and the fin and winglets providing directional stability at low speeds. A flight control system is a necessity for this design, where the control surfaces are continuously moving and would be difficult for a pilot to control.

Engine integration was a collaborative effort between airframe and engine designers, where a number of configurations were considered and the final selection was for four semi-embedded engines at the wing root. Initial design layouts were investigated by MSc researchers using *CFD* where the results were inconclusive due to an incorrect number of engines integrated and for a late change in the wing geometry.

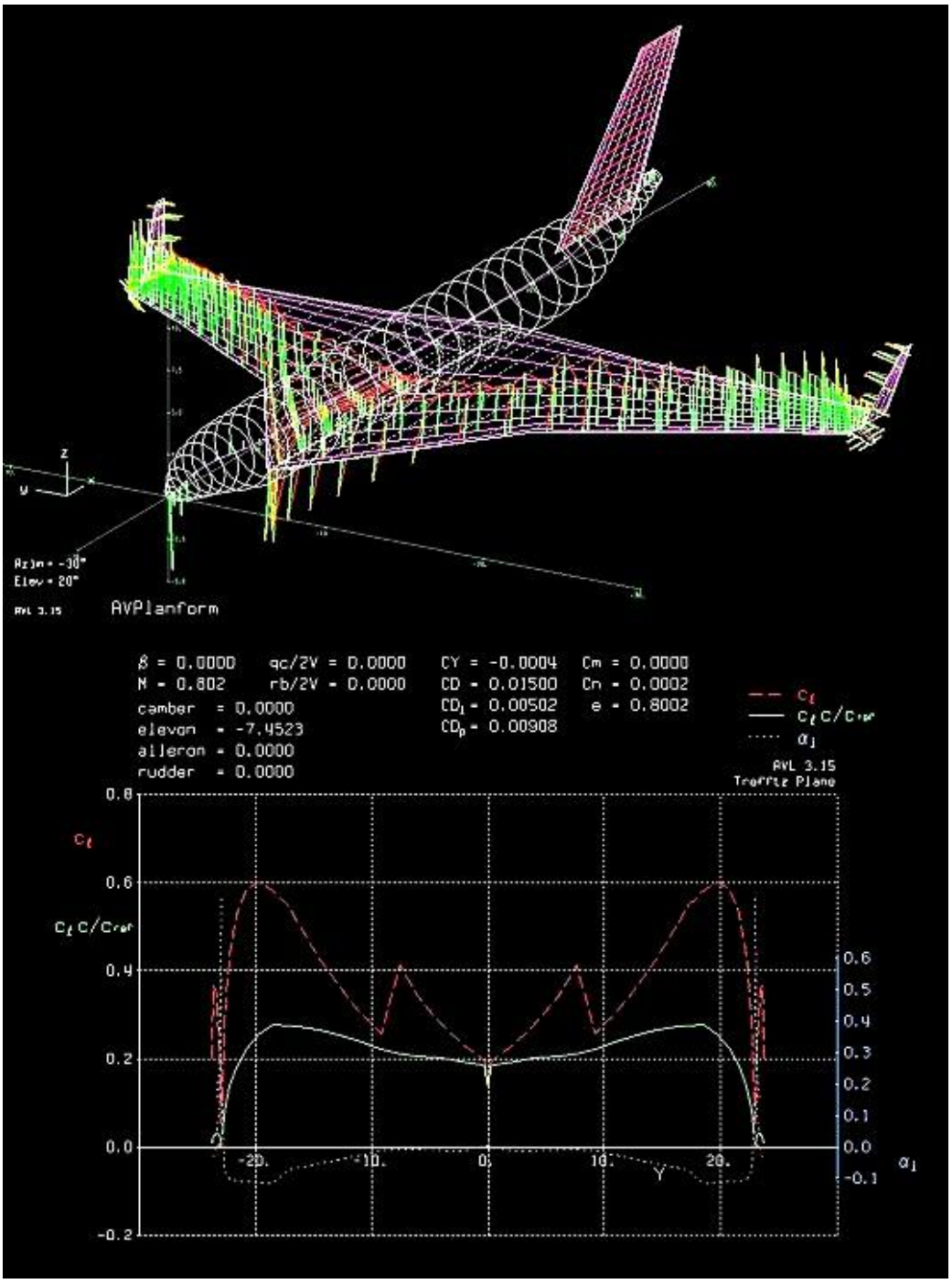

Fig 4-24**:** BDSF AVL loading and Trefftz plane plot for cruise 0.8 Mach at 38000ft

An intermediate analysis using a vortex lattice method (*AVL*) [18] was implemented to visualise the lifting properties of the BDSF lifting surfaces less engines. The vortex panel method was limited in modelling lift of *LE* devices and surface thicknesses, but provided results for the fuselage section where a comparison with a conventional fuselage, enabled the lift increase from the *LE* nose carving to be quantified. The *AVL* results are provided as a guide for the BDSF lifting properties, with further investigations required to use *CFD* for engine-wing interactions studies, and to investigate the effect of a *VC LE*.

Appendix H contains the *AVL* input files, geometry plots, and output data for the BDSF and BDVT, where the aim was to extrapolate data to determine upper and lower wing surface pressure plots to check for shock formations. Due to time constraints this was not possible and the data is provided to aid any further studies of this configuration.

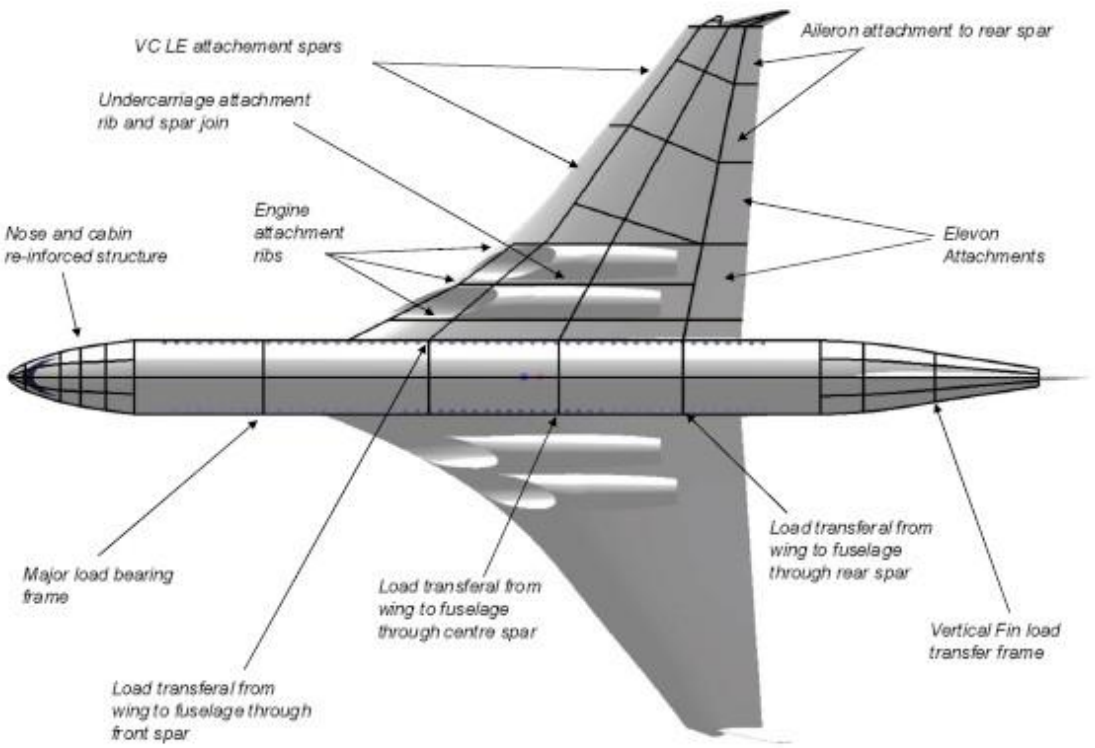

Fig 4-25: BDSF plan view layout of major structural components and critical attachment areas

The mass, c.g., stability, and control estimates were combined with the AVL model to characterise cruise and low speed performance, where investigating aircraft angle of attack, elevon deflection for trim, and increments of induced drag were compared with initial parametric design study estimates. A 10% increase in drag was found using *AVL*, where it is the authors' opinion that the true behaviour of the wing-winglet interaction, along-with thickness effects over the laminar sections is not accounted

for. Having investigated the BD geometry, mission flight cases, flight performance, component masses, and stability, the development, acquisition, operating, and disposal costs of the BD were the final phases required to complete to conclude the design study.

A preliminary study into the BDSF structural layout of major structural frames was investigated, and identifies the key load bearing regions, shown in Fig 4-25. The critical load transferral from the wing into the fuselage is combined with engine and undercarriage loads, which act on and across the same ribs and spars. The nose and tail of the fuselage requires additional large frame support structures to transfer loads from the fin and rudder, and also from the nose landing gear. The passenger cabin of the fuselage is pressurised and is represented by the region with dispersed large frames, contained by a forward and rear pressure bulkhead. There are many lighter frames spread between the larger frames and are not shown on the image.

4.8.2 Summary of the BDVT Design

The BDVT is identical to the tailless configuration in the sense that an all composite airframe is used and optimised for a cruise Mach of 0.8 and with BPR 12 engines, but has a higher cruise altitude of 39,500ft for the same design range. The BDVT is more efficient over a range of cruise altitude and Mach number cases compared with the BDSF, providing greater operational flexibility, higher *L/D*, and a reduced aircraft weight.

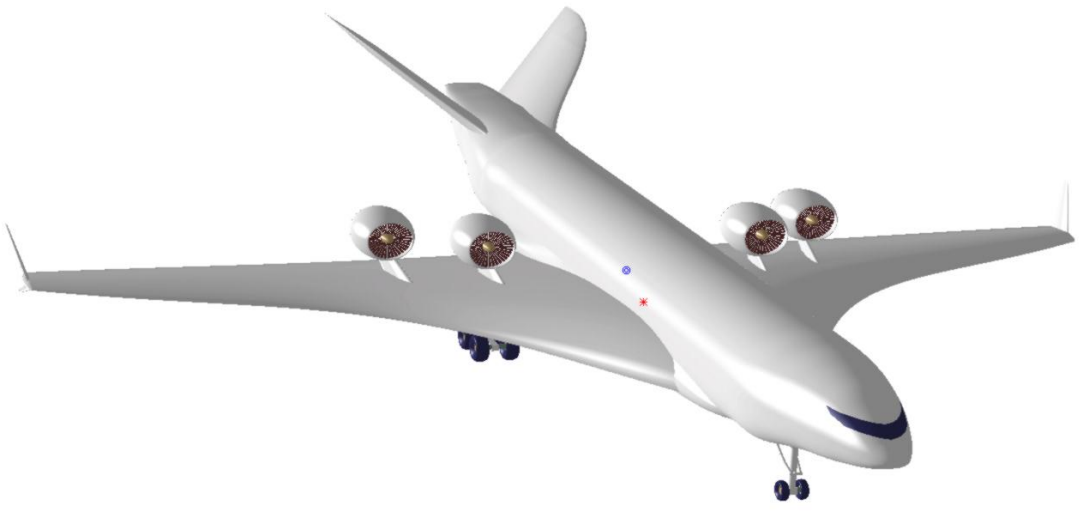

Fig 4-26: Final BDSF Concept Design

BDVT airframe noise is considered to be high, where the main wing incorporates *LE* and *TE VC* devices, combined with two ruddervators integrated into the *V-tail*. Interference caused by additional surfaces within the free-stream suggests an increase in noise, but because the wing size is smaller

relative to the BDSF, there is a noise trade-off between size and number of surfaces. Noise reduction methods such as *TE* brushes, *VC LE*, winglets, engine noise liners, and undercarriage fairings are also implemented on the BDVT design, where the addition of VCF and an all-moving tail compared to a ruddervators surface was investigated to reduce airframe noise.

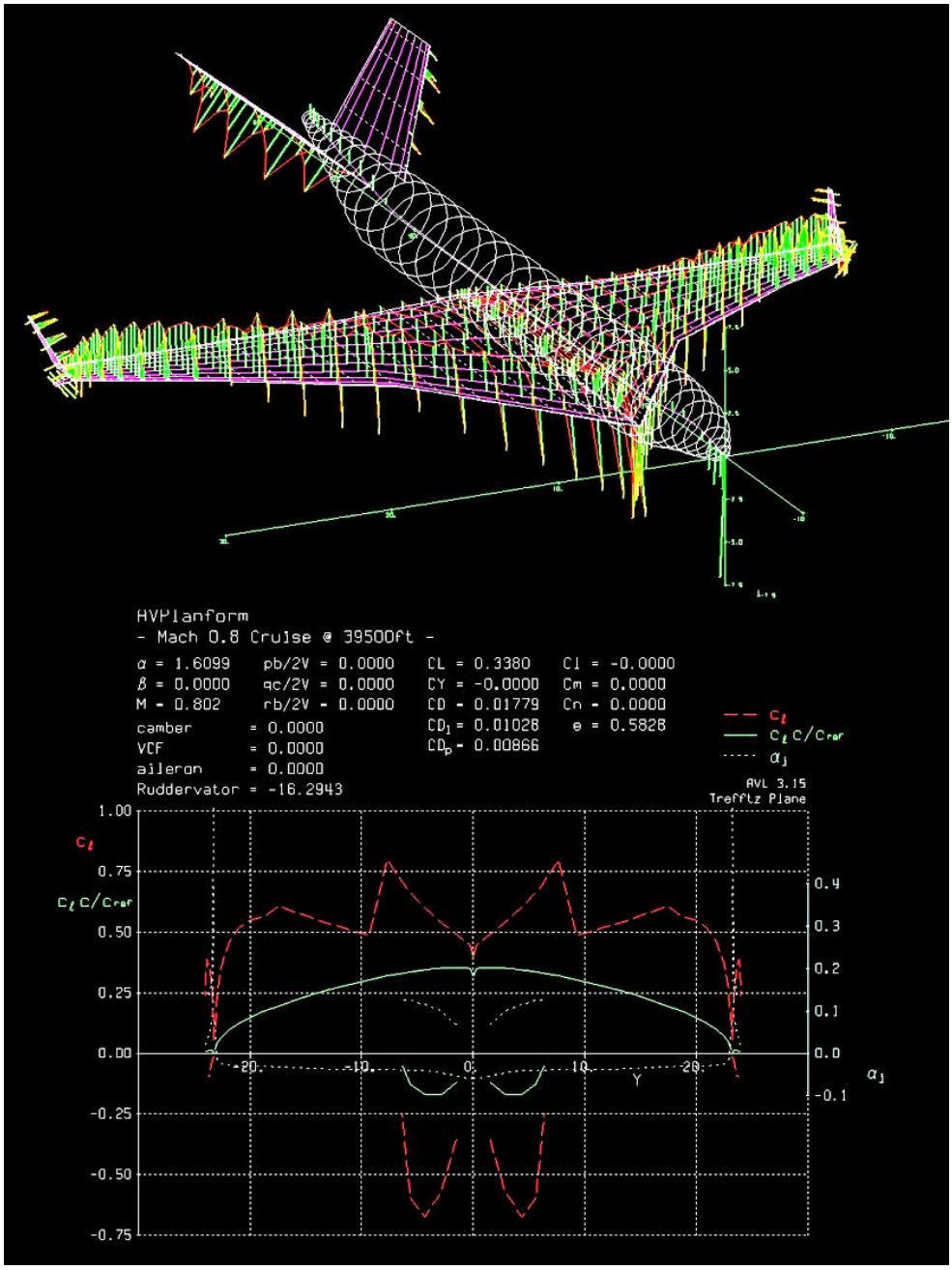

Fig 4-27: BDSF AVL loading and Trefftz plane plot for cruise 0.8 Mach at 38000ft

Implementing laminar flow airfoils outboard and re-design of the fuselage nose and inboard airfoils to have the LE carved out, was also used for the BDVT as with the BDSF, to complement the main wing lift. *VCFs* and *LE* devices are deployed to increase maximum lift coefficient to avoid wing stall,

assisting with the steep 6 degree approach angle. Aileron deflections are purely used for roll control and are coupled with spoilers to double-up as air-brakes and for yaw control. The V-tail ruddervator design provides a degree of directional stability, with the control surface used to trim the aircraft and control the pitch attitude during flight. Loss of the flight control system for the BDVT has an additional redundancy where the pilot can fully control the aircraft manually, unlike the BDSF, where the pilot may require additional training to handle the tailless aircraft.

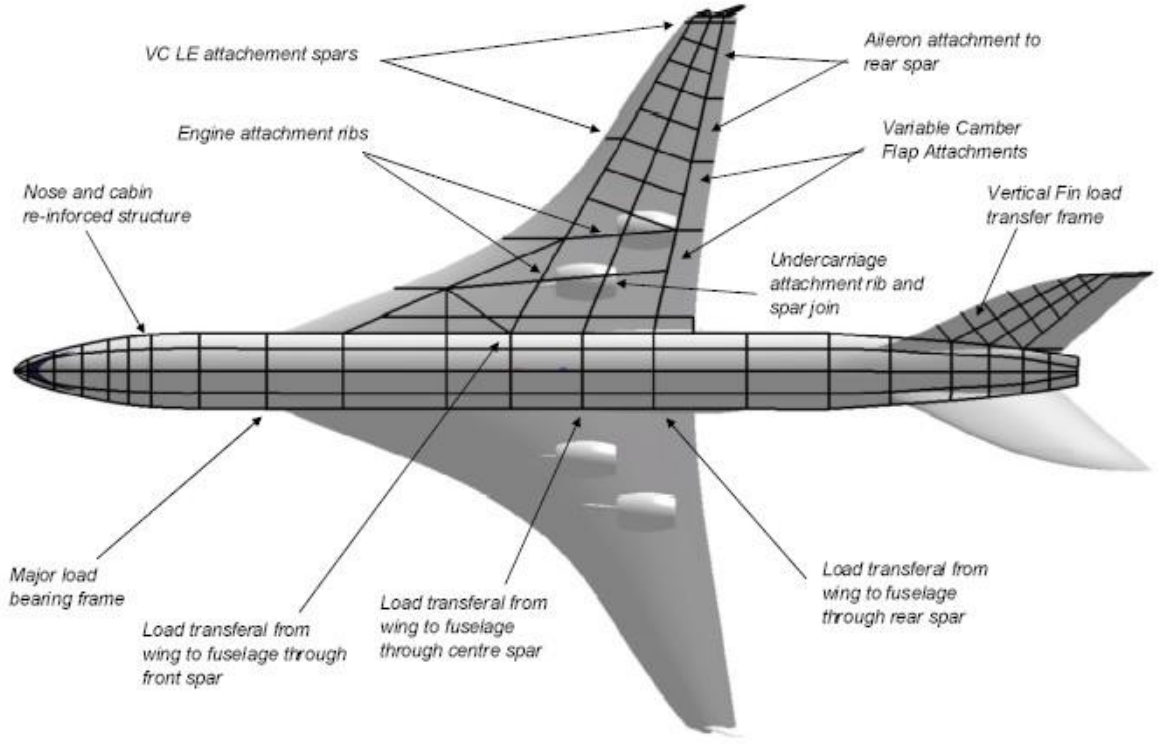

Fig 4-28**:** BDSF plan view layout of major structural components and critical attachment areas

An integration study revealed a wing depth of less than 40% of the engine diameter and was considered insufficient to semi-embed the engines. The chosen configuration for engine installation was for four *OTW* podded engines with canted pylons to reduce interference with the flow across the outboard wing.

The BDVT structural layout identifies the key load paths for the aerodynamic wing and tail loads to transfer into the fuselage. The majority of loads are similar to the BDSF, where the structural arrangement is almost identical to a conventional aircraft where all the major loads are transferred through heavy frames, ribs, spars, and the fuselage longitudinal stiffeners/longerons.

The transfer of loads from the undercarriage and engines into the structure is preferred for the BDVT aircraft configuration compared to the BDSF, mainly because landing gear loads and engine attachments are staggered and do not act on the same point. The BDSF structural arrangement stresses the centre wing-box spar by mounting two engines per side on a variable depth structural member (due to semi-embedded engines), and also contain the attachments for the main undercarriage leg. Structural challenges such as these are to be tackled during preliminary and detailed design, where for this discussion the engine torque, flight loads, and landing loads are assumed to transfer into the structure without any major design challenges.

4.8.3 Comparison of BDSF & BDVT Final Design Characteristics

Throughout this chapter, the design philosophy for the BD concept has evolved from an 'idea' to create a civil aircraft using a military bomber as a guide, to producing numerous aircraft configurations with alternate materials, engine locations, empennage designs, wing layouts etc. The final two BD configurations were developed in parallel to provide a new concept for a civil airliner, inheriting the tube and wing characteristics of current aircraft, and providing two solutions for a tailed and tailless BD.

The BD aircraft is seen as an intermediate stage to reduce noise in the medium-term, where studies into dramatic changes of the airframe design, such as blended-wing-body (BWB) aircraft boast substantial noise reduction, but require extensive research, development, and testing prior to release or certification as a passenger transport. Short-term solutions include the implementation of noise reduction technologies on current airliners, boasting 5-10dB noise reduction, which is not significant when considering future noise targets. The BD is considered as an intermediate step, primarily because the tailed variant can enter into service with little to no changes in current airline operations, with the tailless design to follow shortly after. Both configurations reduce noise considerably, and the tailless design could be used as a stepping stone for the release and certification of alternate tailless solutions, such as the BWB aircraft.

A tabulated design summary for both tailless (BDSF) and tailed (BDVT) airframe configurations are shown in Table 4-10, where a comparison suggests that at a first glance both designs have improved flight performance and a lower overall mass relative to the baseline aircraft. Improved lift-to-drag ratios above 20 were found for the clean airframes, but with nacelle drag, and the additional growth of aircraft weight as the designs developed, L/D reduced to around 18, which is above that produced by current airliners. Airframe noise analysis is required to compare the designs against each other, where presently the BDVT has the edge over the BDSF when considering certification, mass of fuel required for a 4,020 n.mile mission, and cost per seat per n.mile.

Description	***Symbol***	***BDSF***	***BDVT***	***NT-BL***	***units***
Wing Area	S	531.4	397.1	202.4	[m^2]
Wing Span	B	47.9	46.4	40.2	[m]
Wing Standard Mean Chord	$\overline{C}$	11.6	9.53	5.03	[m]
Wing Aspect Ratio	A	4.13	4.87	7.99	-
Wing Quarter Chord Sweep	$\Lambda_{¼}$	25.6	30.2	32.3	[deg]
Wing Taper Ratio	λ	0.181	0.283	0.277	-
Thickness-to- Chord Ratio	t/c	0.1013	0.1013	0.115	-
Wing Apex location	l_{APEX}	14.7	17.3	23.6	[m]
Horizontal Tail Area	S_{HT}	-	141.1	52.6	[m^2]
Vertical Tail Area	S_{VT}	87.1	59.9	31.5	[m^2]
Wing Area Parameter	$S^{-0.1}$	0.536	0.556	0.588	[m^{-2}]
Static Wing Loading	$(Mg/S)_0$	2680	3550	7465	[N/m^2]
Static Thrust Loading	$(T/Mg)_0$	0.314	0.321	0.328	-
Engine bypass ratio	BPR	12.0	12.0	12.0	-
Lift-Drag Ratio	L/D	18.3	19.9	15.6	-
Cruise Lift Coefficient	$(c_L)_{cr}$	0.241	0.316	0.438	-
Approach Lift Coefficient	$(c_L)_a$	1.13	1.45	2.01	-
Approach velocity	V_a	57.5	58.4	72.0	[m/s]
Mass of Composite Wing	M_W	25,711	21,967	20,929	[kg]
Fuselage Composite Mass	M_{FUS}	16,007	16,641	15,649	[kg]
Composite Tail + winglets Mass	M_T	2,001	2,063	2,300	[kg]
Mass of part-composite Undercarriage	M_G	5,918	5,912	6,092	[kg]
Propulsion Systems Mass	M_{PP}	11,721	12,321	12,516	[kg]
Mass of All-Electric Systems	M_{Sys}	16,857	16,788	16,613	[kg]
Operational Items Mass	M_{OP}	3,357	3,357	3,357	[kg]
Operational Empty Mass	M_{OEW}	80,829	84,678	77,912	[kg]
Mass of Payload	M_{Pay}	23,760	23,760	23,760	[kg]
Mass of Fuel Required	M_f	41,799	36,530	44,934	[kg]
Available Fuel within Wing Volume	M_{f_a}	214,493	113,781	47,836	[kg]
Total Static Thrust	T_0	447,006	454,131	495,502	[N]
Total Overall Mass	$\boldsymbol{M_0}$	**147,132**	**145,339**	**146,151**	**[kg]**
Cruise Mach Number range	$(M_N)_{cr}$	0.8 – 0.9	0.7 - 0.9	0.8 - 0.85	-
Cruise ceiling	-	38,000	39,500	39,000	[ft]
Longitudinal centre of gravity	$x_{c.g.}$	27.2	26.3	29.1	[m]
Lateral centre of gravity	$y_{c.g.}$	0.00	0.00	0.00	[m]
Vertical centre of gravity	$z_{c.g.}$	-1.35	-0.821	-1.26	[m]
Static margin	K_n	-3.88	4.45	6.20	[%]
DDTE cost	C_{DDTE}	38	39	37	[$US M]
Aircraft Life Cycle Cost	*LCC*	3,571	3,308	4,178	[$US M]
DOC per seat per nautical mile	-	0.0752	0.0690	0.0895	[$/n.mile]

Table 4-10: BDSF and BDVT final comparison of design parameters with *NT*-BL aircraft design

References

[1] Howe D., [Howe, 2000], 'Aircraft conceptual design synthesis', *Professional Engineering Publishing Ltd.*, 2000, Wiltshire, UK.

[2] Davies S. D., [Davies, 1969], 'The history of the avro vulcan', *The 14th Chadwick Memorial Lecture*, RAeS Lecture, March 1969, Institute of Science and Technology, Manchester, UK.

[3] Avro Vulcan Mk2 Bomber, [Avro Vulcan, 2007], http://ourworld.compuserve.com/homepages /jfalk/vulcan.htm, last accessed March 2007.

[4] Avro Vulcan General Arrangement Diagram, [Avro Vulcan GA, 2007], http://www.raf.mod.uk/historyold/vforcespec.html, last accessed February 2007.

[5] Avro Vulcan Aircraft data, [Aerospaceweb, 2008], http://www.aerospaceweb.org/aircraft/ bomber/vulcan/, last accessed February 2007.

[6] McCormick B. W., [McCormick, 1979], 'Aerodynamics, aeronautics, and flight mechanics', *John Wiley & Sons inc.*, 1979, Pennsylvania State University, Canada.

[7] Flight international (FI) magazine, [FI, 1983], 'Certification of the BAe 146', 12 February 1983, page 54.

[8] Doulgeris G., [Doulgeris, 2008], 'Modelling & integration of advanced propulsion systems', *PhD Research Thesis*, March 2008, Cranfield University, UK.

[9] European Aviation Safety Agency (EASA), [EASA, 2006], 'Certification specifications for large aeroplanes: CS-25', *EASA*, October 2006, Amendment 2, EU.

[10] Jenkinson L. R., Simpkin P., Rhodes D., [Jenkinson et al, 1999], 'civil jet aircraft design', electronic data: http://www.bh.com/companions/034074152X/appendices/default.htm, *Arnold Publishing*, 1999, London, UK.

[11] Fielding J. P., [Fielding, 2000], 'Design investigation of variable-camber flaps for high-subsonic airliners', *24th Congress of the International Council of Aeronautical Sciences (ICAS)*, ICAS2000-0124, September 2000, Harrogate, WA.

[12] Raymer D. P., [Raymer, 1992], 'Aircraft design: a conceptual approach', *AIAA Educational Series*, 1992, Washington, US.

[13] Pamadi B. N., [Pamadi, 1998], 'Performance, stability, dynamics and control of airplanes', *AIAA Education Series*, NASA Langley Research Centre, 1998, Hampton, Virginia.

[14] Hileman J. I., Spakovszky Z. S., Drela M., Sargeant M. A., [Hileman et al, 2007], 'Airframe design for 'silent aircraft'', *45th AIAA Aerospace Sciences Meeting and Exhibit*, AIAA 2007-453, January 2007, Reno, Nevada.

[15] Wilson, R. A. L., [Wilson, 1997], 'The introduction of laminar flow to the design and optimisation of transport aircraft', PhD Research Thesis, 1997, Cranfield University, UK.

[16] Reid D. L., [Reid, 2007], 'AeroFoil; A 2-dimensional airfoil design and analysis program', AeroFoil Version 2.1, http://AeroFoilEngineering.com , last accessed March 2007, US.

[17] Harris C. D., [Harris, 1990], 'NASA supercritical airfoils; a matrix of family-related airfoils', *National Aeronautics and Space Administration*, Technical Paper 2969, March 1990, Langley Research Centre, Hampton, Virginia.

[18] Youngren H., Drela M., [Youngren, 1988], 'Athena vortex lattice (AVL): an extended vortex-lattice model for aerodynamic analysis, trim calculation, dynamic stability analysis, and aircraft configuration development', http://web.mit.edu/drela/Public/web/avl/, last accessed February 2007, *Massachusetts Institute of Technology (MIT)*, Boston, US.

[19] Young D., [Young, 2005], 'Messier-dowty landing gear design course', *Notes for a short course run by Messier-Dowty*, November 2005, Cranfield University, UK (contact author for details).

[20] Currey N. S., [Currey, 1988], 'Aircraft landing gear design; principals and practices', *AIAA Educations Series*, 1988, Washington, US.

[21] Nettis L., [Nettis, 2007], 'The constant volume combustor: cycle optimisation and engine-airframe integration study for a silent aircraft', *MSc Research Thesis*, September 2007, Cranfield University, UK.

[22] Fujino M., Kawamura Y., [Fujino, 2003], 'Wave-drag characteristics of an over-the-wing nacelle business-jet configuration', *Journal Of Aircraft Vol. 4, No. 6, Pages 1177-1184*, December 2003, Honda R&D Americas, Inc., North Carolina.

[23] Fujino M., Kawamura Y., [Fujino, 2003], 'Wave-drag characteristics of an over-the-wing nacelle business-jet configuration', *41st Aerospace Sciences Meeting and Exhibit*, AIAA 2003-933, January 2003, Reno, Nevada.

[24] Burns J. W., [Burns, 1994], 'Aircraft cost estimation methodology and value of a pound derivation for preliminary design development applications', *53rd Annual Conference of Society of Allied Weight Engineers, Inc. (SAWE)*, Paper No. 2228, May 1994, Long Beach, CA.

Chapter 5 Novel Aircraft Concepts

5.1 Introduction

There are many alternate airframe configurations other than the conventional 'tube-and-wing' that we are now so familiar with today. Many designs are of a similar layout, but possess certain design characteristics that distinguish the aircraft from what we refer to as the baseline aircraft. This chapter identifies the main airframe configurations that satisfy the term 'Novel' airframe designs, where alternate wing arrangements and fuselage geometries are discussed and analysed. To avoid excessive repetition of formulae, the results contained within this chapter refer to the methodologies used in the previous BD analysis, and are combined with reference methodologies for the reader to view at their discretion.

5.1.1 Blended Wing Bodies

The flying wing, more commonly referred to at present as the blended wing body (BWB) is an extremely efficient lifting body. Many consider this to be a novel design, however this configuration is an established flying geometry, where the design, manufacture and flight of the 'all-wing concept' has been in use since 1946, where Northrop produced the XB-35 tailless bomber [1].

Fig 5-1: Northrop XB-35 Bomber, with the early engine pusher fan design, later upgraded to turbojets (*http://en.wikipedia.org/wiki/Northrop_YB-35*) [2]

The blended wing body (BWB) aircraft is one of the most promising solutions for an all-lifting-body airliner because of its efficiency in carrying a large amount of payload in a relatively compact configuration. The main advantage of this configuration is a lower vehicle wetted area compared with a conventional aircraft, providing reduced drag, and an improved lifting efficiency. The BWB concept has been investigated by most of the major aircraft design companies, where Boeing, NASA,

and Airbus have their own proposals for a future BWB transport. NASA and Boeing are presently the main developers of BWB configurations, with the aid of research departments such as at Cranfield University, through the development and testing by the Aircraft Design Centre (ADC) and Cranfield Aerospace. One such collaborative project is the current NASA/Boeing X-48B [3, 4] development of an unmanned flying vehicle (UAV), which is used as a test vehicle to investigate the performance and low speed capabilities of the BWB airframe. Despite the development of the small scale test vehicle, many aircraft design companies are not willing to push for the development of such a concept because of the high risks associated with the unconventional design.

Fig 5-2: NASA X-48B small scale BWB flying UAV demonstrator
(*http://www.nasa.gov/centers/dryden/research/X-48B/index.html*) [3]

The BWB in many ways is similar to the broad delta (BD) airframe, where the main difference is the absence of a clearly visible fuselage. The BWB and tailless BD (BDSF) configurations are both primarily based on a large flying delta wing which is designed to be stable by using an artificial control system. The main challenge in developing such a design for a civil aircraft is the certification of the tailless and unconventional design. An additional challenge for the BWB is the certification aspects associated with egress.

5.1.2 Innovative Wing Concepts

An additional investigation into innovative wing designs identifies the possibilities to modify the wing shape to design a Prandtl plane (box wing), joined wing, strut-braced, or truss-braced wing design. Each design has similar properties, so a comparison between the main advantages and disadvantages

is discussed below, identifying the main challenges with the designs and possible areas that need further investigation during the development of the designs.

5.1.2.1 Prandtl Plane or Box Wing Configuration

The Prandtl plane, or box-wing configuration, is a design where the wing span and tail span are essentially the same and are joined at the tips. This configuration was thought to be interesting to investigate, because in theory the noise of the airframe should not change due to the configuration. This is because the main wing and tail geometries are replaced by two equally sized smaller high aspect ratio wings. The total wing reference area of the box-wing is similar to the baseline aircraft, but there are now two larger sources of noise, which are not considered to be ideal. The noise shielding benefits of the BD or BWB configurations are not as apparent with this design, as engine noise shielding can be difficult due to the two high aspect ratio wings. Locating engines above or below either wing provides challenges in maintenance, integration, and more importantly shielding. The noise from engines can be reflected off either wing and could increase the perceived noise on the ground.

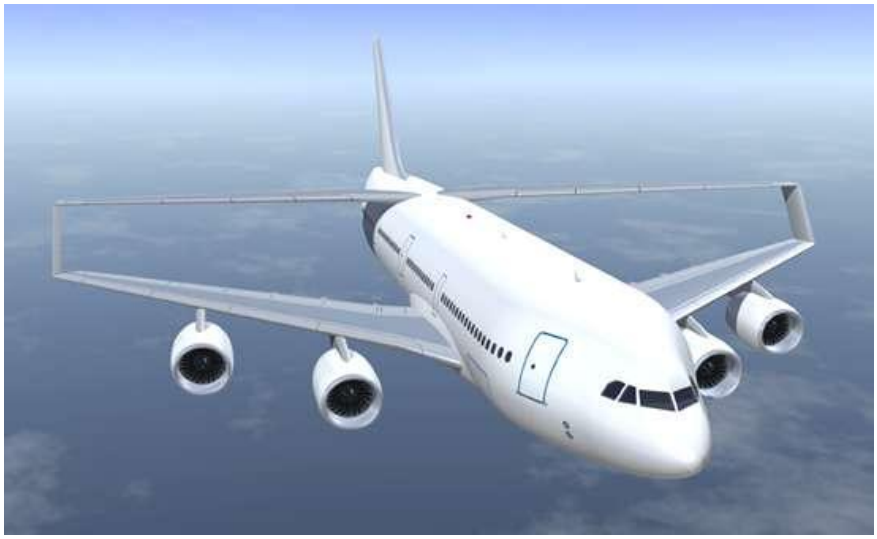

Fig 5-3: Airbus innovative "joined wing" concept design
(*http://aerospace-technology.blogspot.com/2008/12/airbus-future-airliner-concepts.html*) [5]

During flight the main wing transfers tip vortices outboard on the main wing and up the wing-tip joins and to the upper wing. This creates a constructive interference drag between the two lifting surfaces, producing a downwash over the forward swept joint-tail; increasing the wing lifting efficiency by reducing induced drag. The configuration is structurally stronger than a cantilever wing (baseline aircraft), but both wings are now subject to loading both in-flight lifting, down-loads, during gusts, manoeuvres, and ground-taxiing conditions.

Theory predicts a huge induced drag saving by investigating this Prandtl wing, as two equally sized wings with varying sweep angles joined at the tips is considered to be extremely efficient. The optimum design of the box wing uses the assumption that the total wing area required for both lift and trim for a conventional aircraft lifting surfaces can be equally shared out between the two wings, creating a shorter span vehicle with equivalent lifting characteristics and that is structurally more efficient. The reduced span high aspect ratio wings have limited lifting performance at low speeds compared to a conventional aircraft, however, the tip-joins creates a net reduction of wing induced drag, reducing the overall drag of the vehicle at cruise. This design therefore creates a shorter span, lighter and stiffer wing-box structure relative to the baseline design and has potential to explore further as a future efficient airframe, but noise is one of the main concerns.

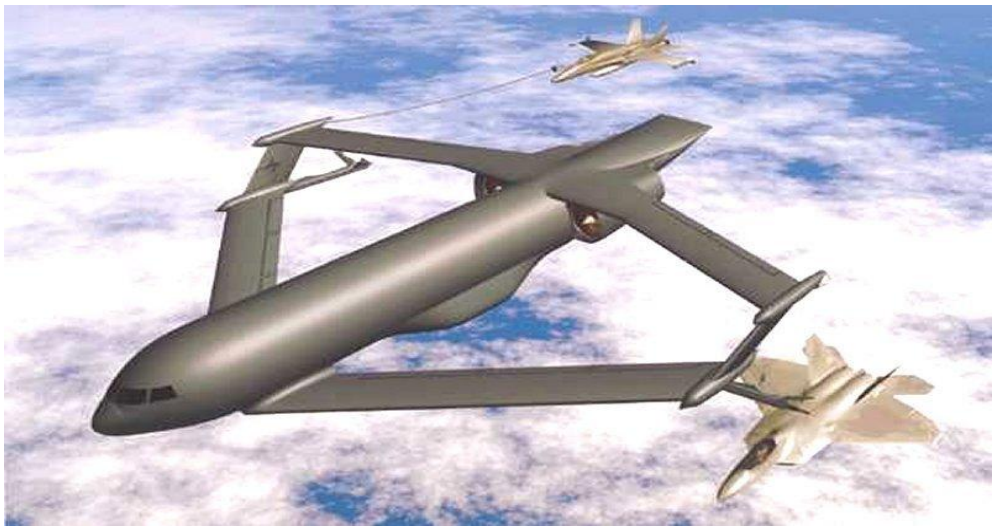

Fig 5-4: Lockheed Global Tanker aircraft program, proposed in 2004 (*http://www.globalsecurity.org/military/systems /aircraft/images/nsa3.jpg*), [6]

A major concern for the design of a box wing is that the lower (front) wing provides a pitch up lifting moment about the c.g. of the fuselage, where-as the upper (aft) wing provides a pitch down lifting moment around the same point; hence creating a large bending moment and/or torque if load is applied asymmetrically on each wing. This moment/torque depends upon the loading conditions and acts upon the longitudinal and lateral axes of the fuselage structural frame. Loads acting on the lifting surfaces are transferred and reacted through the fuselage, where the fuselage requires additional reinforcements at the wing joins to take high loading cases: depending on whether the aft wing produces down-loading or up-lifting loads. A similar effect on the fuselage would also occur for the box wing when in a roll, banked manoeuvre, or in a cross-wind gust case.

Up-loading tail = *bending moment*

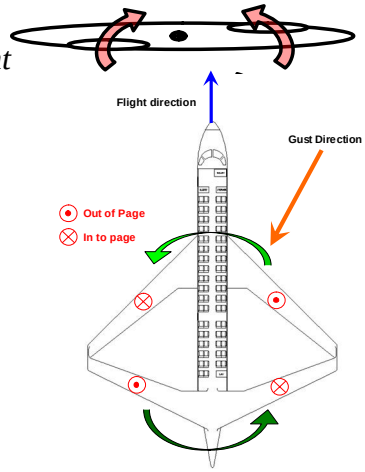

Up-loading tail + Gust = *Torque*

Fig 5-5: Bending moment and torque examples for the Joint wing loading extreme conditions

These lifting cases produce a bending effect on the fuselage that generates a strain about the c.g. location. When considering the aircraft on the ground, the weight of the wing acts in the opposite manner creating a negative (downward) bending effect around the undercarriage due to the weight of the wings, also experienced during negative gust conditions. The concentration of bending loads on the fuselage is mainly focussed around the c.g. and may cause concerns for the detailed design phase where fatigue may be a concern during airframe life-flight-cyclic loading. A similar effect on the fuselage would also occur for the box wing during roll or bank manoeuvres, as the control surfaces such as ailerons, would be located on both upper and lower wings. Roll control requires the use of four ailerons now, two upper and two lower, creating additional wing bending and torque challenges. Additional design complexities may lead to an increased structural mass because of structural reinforcements required to attach both wings to the fuselage and to each other at the wing tips.

There are some difficulties associated with the design of the joined wing, such as the location of the main undercarriage. The landing gear must be located inside a belly-fairing which is an additional drag source. The increased drag of the fairings combined with the increased structures mass due to the fuselage-wing reinforced mounting points could out-weigh the reduced drag benefits of the joint wing arrangement, creating an aircraft with better performance than the baseline, but with a greater overall mass. At a worse case condition this aircraft configuration may be equal to the baseline, which would question the need for changing the configuration if there is little-to-no benefit in the new concept design.

5.1.2.2 Strut or Truss-Braced Wing Configuration

The strut-braced wing concept involves the design of a reduced chorrd lighter wing, similar to the joint wing, but is supported by a rigid strut. This strut is designed to take the major loads of the wing

and is designed not to buckle; increasing the wing loading characteristics by transferring loads through the strut, as now the wing is no longer considered to be a simply supported cantilever beam at the root. The truss-braced concept is similar to that of the strut-braced wing, but in this case the supporting element is designed to be loaded in tension only, and does not take into consideration negative 'g' loading cases of the wings or ground taxiing loads, and the design is constrained to a high wing configuration.

The wing design of the strut and truss-braced wing provides an ideal platform to introduce a low sweep, high aspect ration wing with highly laminar flow airfoils. The aerodynamic benefit of the laminar flow sections produces a lighter unsupported wing structure that is prone to flutter at the wing-tips due to the reduced structural stiffness of the high aspect ratio wing. The location of the wing may cause concerns because a high wing design introduces challenges for the undercarriage layout (as with the joint wing concept), where for the design of the low wing the truss-braced design is not possible and a strut-braced solution is the only feasible solution. This would require a strut loaded under continuous compression, which is not ideal and would create a challenge for any design and manufacturing centres of excellence.

Fig 5-6: Strut-Brace Wing design concepts (http://www.aeronautics.nasa.gov/docs/ar99/obj8.html) [7], (http://www.aoe.vt.edu/research/groups/tbw/LMAS.jpg) [8]

The opinion of the author is that a poorly designed Truss-braced wing with a mass greater than that of a typical cantilever wing, lends itself to the solution of a strut-braced wing. This is because the truss is only designed to take the in-flight loads, and if over-designed the properties of the truss would react like a strut-braced design and would be able to withstand the compressive negative gust and taxi loads. The truss designs reduce the structural weight compared to the baseline aircraft and strut-braced design, by removing a critical negative loading case to achieve a lighter design. If the wing and truss is loaded negatively and results in the truss buckling or causes damage to the main wing, then the benefit of the lighter, smaller wing may be insignificant, especially when the wing may not be able take any further aircraft loads. The design of the truss-braced design is questionable, because in the event of the truss buckling, the truss would need replacing, or at a worse case during flight the aircraft

would be subject to a catastrophic failure. In either event, a major overhaul or maintenance would be required and this is not ideal for any operator, airframe integrator, or aviation regulator.

5.1.2.3 Joined Wing Configuration

The Joined Wing (JW) configuration is often confused with the box-wing or Prandtl plane, but these in essence are two completely difference concepts. The primary advantage of the JW is its triangulated planform wing that provides a rigid lifting surface design, combining both the properties of the box-wing and strut-braced designs. The secondary benefit is a constructive interference drag between the two surfaces where the wings are joined. The published work of authors such as Kroo, Gallman, and Nangia [9, 10, 11] consider multidisciplinary design optimisation studies, were the main focus of their studies were either to address aerodynamic benefits or structural design complications, such as aero-elastic and buckling analysis.

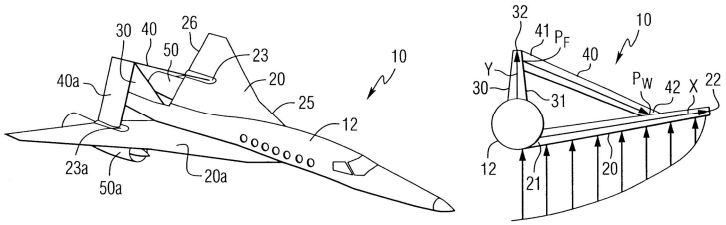

Fig 5-7: Lockheed Supersonic transport patent (http://www.freepatentsonline.com/6729577.html) [5]

Fig 5-8: Lockheed Quiet Supersonic Transport Private Jet (*http://www.aviationexplorer.com/Quiet_Supersonic_Transport_(QSST)_Private_Jet.html*) [6]

The reduced drag gain can be achieved from a joint between the two wing surfaces located around 70% of the main wing semi-span, where the total tail length has a semi-span of 60% of that of the main wing. The structure must be optimized in an unconventional manner to withstand conventional flight loads. The structure of the joint wing is a rigid triangular section, where the loads acting on the wing during flight are transmitted through to the adjoining tail structure, similar to the box-wing. Loads acting on the wing-joint are transmitted through an off-centred axis, where the structural design/material orientation must reflect non-uniform loading as shown below in Fig 5-9. A greater

stiffness is required on two of the four corners of the wing-box to support and optimize the structure with regards to stresses, torsion, and bending loads acting perpendicular to the load axis.

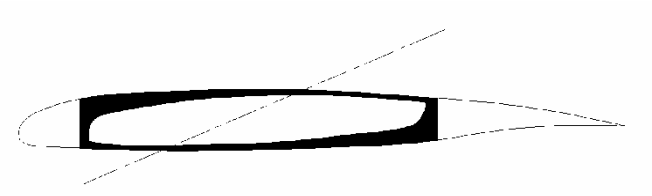

Fig 5-9: Optimal structural layout and load axis for the joint wing and box-wing designs.

The fuselage length of a JW can drive the configuration to an aft engine layout, where a longer fuselage forces the design to locate engines at alternate locations; this is mainly due to balance, c.g. considerations, and passenger comfort levels at high angles of incidence, as shown below in Fig 5-10. Engines could be located at alternate stations, such as above the main wing or even at the tip joins, however, the overall configuration layout will be explored in more depth later.

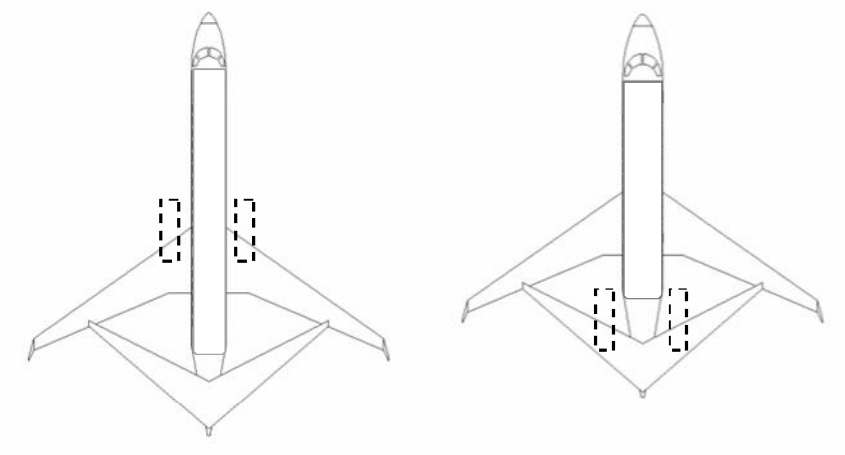

Fig 5-10: Configuration layouts for the joined wing concept

The layout of the wings lends itself to a potential capacity of pure side slip, where the aircraft would appear to fly straight (in-line with the fuselage direction), but would in reality be flying at a yaw angle in a completely different direction. This provides advantages in the event of a single engine failure and allows the airframe to fly in sideslip with minimal loss of performance. There is high structural stiffness due to the wing-joins and reduced aero-elastic problems, such as that experienced by the strut and truss-braced designs, although the aerodynamics is fairly complicated around the join regions. New methods for establishing stall or pre-stall warnings would be required as the joint and box-wing designs do not behave like the baseline configuration with the early-stall-warning tail buffet to alert pilots. There is a possibility that wing wake could interfere with tail lift at high incidence, solved by

either changing longitudinal spacing (moment arm), or increasing the height between the two wings, similar to a high tail or cruciform tail configuration.

Undercarriage may be difficult to integrate for configurations other than with an aft-engine arrangement. An aft engine configuration allows ample volume for the landing gear to retract within the main wing. Alternate engine locations may push the apex of the main wing forward for balance and c.g. considerations, causing the gear location to deviate from the traditional wing position, hence requiring an external undercarriage blister for the main gear units, impacting drag at all flight conditions.

Despite being an unconventional configuration, the design possesses many similarities to a conventional tube and wing design, making it a viable solution for marketing, customers, and passengers perception. The challenge remains to identify and generate a suitable analysis method that can be used within the design methodology.

5.2 Parametric Design Analysis

The initial airframe design analysis identified seven novel airframe concepts that were chosen to further analyse, which included the BD, as previously identified in Chapter 2 and re-iterated in Fig 5-11. The BWB, PSJBW, and JW concepts were three of the remaining six configurations selected to further develop and were subject to an initial design investigation. Initially three different BWB were considered, a re-design of the SAI SAX design to establish the methodology used, a variant with a canard for the impact of noise on the pitch control surface, and a discrete fuselage design. The analysis of three BWB variants was considered impractical due to the time limitations and a single BWB design was developed. The canard study was considered to be too detailed in terms of the aerodynamic design process of the close-coupled configuration combined with the 3-D flow challenges associated with the BWB. It was considered that the methodology to size a BWB conceptually was more important to understand and so the discrete fuselage BWB was also not studied at this stage.

The remaining two concepts chosen to develop further were the JW design and the PSJWB configuration. The development of a PSJW, which had a conventional fuselage, was not further considered because of the integration of a partial span wing onto the BWB airframe, and the fact that this configuration was too similar to the baseline aircraft.

The three novel concepts were not developed in parallel because there are not many commonalities between them, other than the PSJBW is a derivative of both the BWB and JW airframes. The

following three designs are compared together within this chapter purely because they are all characterised as novel designs.

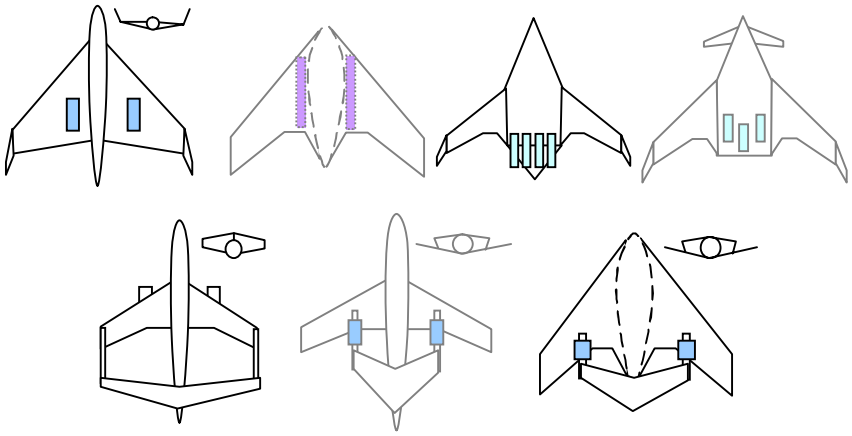

Fig 5-11: Final selection of airframe concepts to develop, adapted, but as defined as Fig 2-11

The three remaining configurations evolved using the same specification and design methodology as a datum [14], with modifications made similar to the BD and BL aircraft, as discussed within Appendix B. Design assumptions based on published data were made, where relevant, and were input into the analysis to reflect the characteristics of each novel configuration.

The BL and BD airframes are characterised as cylindrical pressure vessels attached to wings and this assumption was used for the joined wing concept, where the BWB is considered to have a non-cylindrical pressure vessel and conventional outboard wing. The challenges that the BWB introduces are, new considerations for the fuselage design, sizing of the cabin due to pressurisation, and structural layout of an all flying wing. The *NT*-BL and BD used the same slender cylindrical fuselage geometry, however for the BWB, there are challenges associated with pressurising the BWB cabin due to the loads acting on the non-cylindrical centre-body, which requires a new means to transfer loads through the structure and maintain an aerodynamically smooth surface without buckling or crumpling the upper skins.

To initialise the parametric design analysis an initial study investigated approximating the volume required for the internal cabin geometry to seat 216 passengers in a three-class arrangement. Ramburg [15] investigated the passenger effect of being housed within the BWB cabin. The internal cabin width (W_{cabin}) required for each class of passenger seating is:

$$w_{cabin} = \left(k_{pc} \cdot p_c\right) + \left(k_{ac} \cdot a_c\right)$$

Equation 5-1

The number of seats across the cabin width (p_c), cabin width factor (k_{pc}), number of aisles across the cabin (a_c), and the aisle factor (k_{ac}) are all dependent upon the cabin class investigated, where typical values are shown in Table 5-1 below.

Cabin class	k_{pc}	p_c	k_{ac}	a_c	W_{cabin} [m]
First	0.700	8	0.580	2	6.76
Business	0.625	12	0.460	4	9.34
Economy	0.525	22	0.400	5	13.55

Table 5-1: Cabin calculation for initial sizing of the BWB passenger cabin width for each seating class

The internal cabin length (L_{cabin}) required for each class of passenger seating is:

$$L_{cabin} = \left(\frac{n_{pax}}{p_c} + a_c \right) \cdot s_c + t_c + 0.5 w_c$$

Equation 5-2

The number of passengers (n_{pax}), seat pitch (s_c), number of toilets (t_c), and number of cross aisles (w_c) are all dependent upon the cabin class investigated, where typical values are shown in Table 5-2 below.

Cabin class	n_{pax}	s_c	t_c	w_c	L_{cabin} [m]
First	16	0.950	2	1	6.30
Business	24	0.900	2	1	7.90
Economy	176	0.775	6	2	17.6

Table 5-2: Cabin calculation for initial sizing of the BWB passenger cabin length for each seating class

The total cabin length is the sum of all class seating, providing a provisional cabin internal length of 31.8m, which is considered to be 75% of the total centre-body (BWB fuselage) length. The total centre-body length is estimated as 42.4 metres, which is 11.3 metres shorter than the B767-300 and *NT*-BL fuselage length, as in Fig 5-12 and Fig 5-13.

The overall fuselage width is determined by the widest section, where an additional width of 15% is added due to the leading edge the curvature near the nose, and also considers the taper region from the cabin region into the wing. The width of the fuselage is calculated at 15.9m, with a height of 5.03m, which maintains the *NT*-BL fuselage height requirement for below deck cargo and baggage storage.

The BWB wing-fuselage-join is characterised by a low-wing configuration, where the centre-body transition into the wing occurs on the upper surface; emphasising a discrete bump on the upper surface to represent the fuselage. Although many BWB configurations consider mid or high-wing

locations, the author decided on a low wing to incorporate over-the-wing exits to assist with passenger egress in the event of an emergency, and in the event of a ditching scenario the underside of the wing would serve as a float due to the buoyancy effects of the planform area.

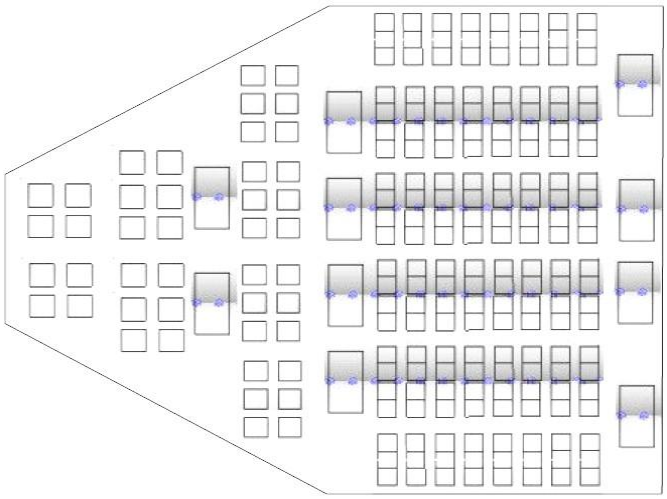

Fig 5-12: BWB Cabin layout based on initial calculations

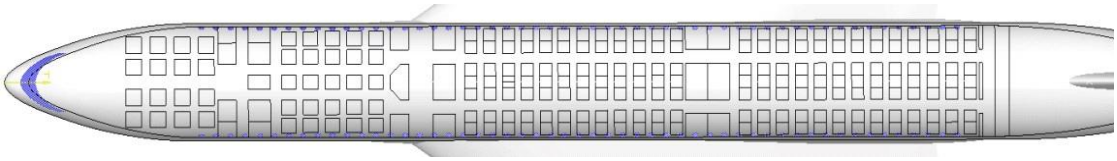

Fig 5-13: NT-BL Cabin layout for comparison with BWB layout

The initial design of the BWB airframe investigated two configurations, similar to the BD, where a conventional tailless BWB was investigated. The tailed variant was considered with two possibilities, where the first was a canard pusher design, and the second was a partial-span-joined wing-body (PSJWB). The canard concept was not considered feasible for a civil BWB aircraft not because of the installed performance, but because the location of a canard relative to the nose and challenges associated with the design of a close-coupled canard-delta configuration. The canard would introduce challenges with the (already difficult to locate) cabin doors, possibly blocking the view of the pilots, and has the additional concerns associated with passengers disembarking at conventional airport gates; whether existing airport facilities could accommodate the BWB configuration.

The alternate airframe configurations investigated herein consist of the BWB, the partial–span-joined-wing-body (PSJWB), and the joined wing (JW) concepts. The methodology used for the initial parametric analysis stage is identical to the BD concepts, where minor revisions are made to the drag,

wing area, aspect ratio, and 'equivalent' fuselage geometry for the BWB passenger cabin layout previously established.

5.2.1 Final Optimised solution for Parametric Analysis

The optimised design solutions using the parametric analysis methodology were compared for the BWB, PSJWB, and JW configurations. A direct comparison of the three designs with the *NT*-BL was not necessary because the results of the JW concept were almost identical, except for the wing and tail geometry; where the design tailors to two equally sized smaller wings joint through vertical sections to create a box wing, with an equivalent mass to that of the *NT*-BL wing and tail configuration. The main challenge with the joint wing was to stabilise the aircraft, mainly due to both wings being of a 'wet wing' nature and containing fuel. The challenge in this design is to maintain a suitable longitudinal and lateral centre of gravity range during all flight conditions. The aim is to achieve this using an artificial flight control system without the need to transfer the fuel through the extremes of the wing-tip joins. Such a design would be difficult to analyse at the conceptual design phase because of the large movement of fuel, but the technology is readily achievable and this can be investigated during the preliminary design phase. Therefore c.g. control by means of fuel transfer/migration will no longer be considered in this conceptual definition, because it is factored into the design of an artificial flight control system.

The remaining two configurations were designed with integrated winglets to reduce the main wing induced drag. All designs incorporated drooped LE devices, TE brushes and advanced liners to shield engine noise. The noise shielding effect of the wing on engine noise is far superior on the BWB than on the JW, where the large delta wing plan-form provides an ideal shielding surface. An additional shielding effect is achieved from the canted vertical fins of the BWB either side of the quad engine arrangement. The PSJWB is similar to the JW and partly reflects engine jet noise towards the ground inboard of the join because of the high rear wing location. However, the joint surface provides a degree of controllability as the rear surface is used as a pitch control device, providing a design with greater stability and control compared to the BWB design.

The mass of the BWB centre-body and structural layout is difficult to predict, where an analysis was completed to determine the internal structural arrangement of a non-cylindrical pressurised pressure-vessel. The process is best described within Howe [14], where an initial estimate for the centre-wing-body mass of the BWB was predicted based on a series of compartments separated by longerons, ribs, and spars, much similar to a conventional wing. The design of three or four semi-cylindrical sections joined via a series of arch ways was considered for the structural design, but neglected due to the mass of the design. The cylindrical shell concept would provide a series of semi-arced pressure vessels

which are ideal for pressure loads, however, if a leak were to develop the skin surrounding these shells would now be required to take the pressure loading of the cabin, and would be sized accordingly. If this is the case, the internal structure would consist of four cylindrical pressure vessels sized for pressurisation at cruise altitude, joined together by a series of equally sized arches, and surrounded by a skin also sized for this pressure case and designed to withstand in-flight loads – which is highly impractical in terms of weight, manufacturing, and design efficiency. The design of boxed cabin sections separated by chordwise ribs and spanwise frames/spars combined with a loaded skin surface and supported by longerons was preferred because the design provides a significant weight saving of 30tonnes relative to the initial design. The mass estimates are fed directly into the optimiser to replace the fuselage section and the wing geometry is optimised accordingly. The current mass estimates for the centre-body are provided below in Table 5-3.

The main results provided for the analysis show that both the BWB and PSJWB configurations with installed engines provide substantial improvements in *L/D* efficiency in excess of 60% compared with the *NT*-BL. The JW concept does not provide any change in *L/D* because there are now two equally sized smaller wings (Table 5-3) compared to the wing and stabiliser design of the *NT*-BL. The smaller wings reduce the lift per wing and also the drag, but in essence, the total drag of the two wing components is equivalent to that generated by the *NT*-BL; and the overall performance is identical despite the joined wing layout.

The all-wing configuration of the BWB significantly increases the vehicle lifting capability compared to the *NT*-BL, where the overall vehicle structural mass is less than the *NT*-BL aircraft, providing a greater lifting performance due to a reduced wetted area and therefore a significant reduction in fuel used for the specified 4,000 nautical mile range. Additional investigations into BWB aircraft aerodynamics and design principals were considered through a detailed search of current literature, the majority of research has been conducted by Robert Liebeck of the Boeing Company, and he is considered to be one of the leading experts on this vehicle [16 - 23 incl.]. Although a large amount of literature is available for the design of the BWB, the time to develop an in-depth detailed study into airfoil design and ideal altitude selection, similar to that of the BD concept is beyond the time constraints of this dissertation. The airfoil design process for the BWB cannot be accurately assessed using 2-D analysis and is a 3-D flow problem, for which CFD analysis would be the preferred route, which is currently beyond the scope of this conceptual design methodology.

Description	***Symbol***	***BWB***	***PSJWB***	***JW***	***units***
Wing Area	S	552.7	417.0	131.1	[m^2]
Wing Span	b	51.1	45.1	32.4	[m]
Wing Standard Mean Chord	$\overline{C}$	10.8	9.25	4.05	[m]
Wing Aspect Ratio	A	4.72	4.87	7.99	-
Wing Quarter Chord Sweep	$\Lambda_{¼}$	28.1	31.2	32.3	[deg]
Wing Taper Ratio	λ	0.163	0.169	0.277	-
Thickness-to- Chord Ratio	t/c	0.11	0.111	0.115	-
Wing Apex location (outer wing)	l_{APEX}	14.9	15.5	26.6	[m]
Horizontal Tail Area	S_{HT}	-	244.7	131.1	[m^2]
Vertical Tail Area	S_{VT}	136.0	91.6	30.0	[m^2]
Wing Area Parameter	$S^{-0.1}$	0.532	0.547	0.569	[m^{-2}]
Static Wing Loading	$(Mg/S)_0$	2683	3551	7465	[N/m^2]
Static Thrust Loading	$(T/Mg)_0$	0.226	0.261	0.344	-
Engine Bypass Ratio	BPR	12	12	12	-
Lift-Drag Ratio	L/D	23.5	24.7	15.2	-
Cruise Lift Coefficient	$(c_L)_{cr}$	0.243	0.322	0.271	-
Approach Lift Coefficient	$(c_L)_a$	1.51	1.57	2.00	-
Approach Velocity	V_a	49.8	56.2	72.0	[m/s]
Mass of Wing	M_W	28,875	24,762	14,020	[kg]
Fuselage/centre-body Mass	M_{FUS}	33,812	33,812	17,454	[kg]
Mass of Tail components + winglets	M_T	2,887	4,457	14,020	[kg]
Mass of Undercarriage	M_G	6,046	6,038	6,145	[kg]
Propulsion Systems Mass	M_{PP}	8,188	9,458	12,680	[kg]
Mass of Systems	M_{Sys}	15,116	15,095	15,362	[kg]
Operational Items Mass	M_{OP}	2,762	2,762	2,762	[kg]
Operational Empty Mass	M_{OEW}	97,687	96,384	82,443	[kg]
Mass of Payload	M_{Pay}	23,760	23,760	23,760	[kg]
Mass of Fuel Required	M_f	29,713	30,805	47,415	[kg]
Available Fuel in Wing Volume	M_{f_a}	239,789	153,173	48,919	[kg]
Total Static Thrust	T_0	334,679	386,610	518,302	[N]
Total Overall Mass	$\boldsymbol{M_0}$	**151,160**	**150,949**	**153,618**	**[kg]**
Cruise Mach Number range	$(M_N)_{cr}$	0.8 - 0.85	0.8 - 0.85	0.8 - 0.85	-
Cruise Ceiling	-	38,000	38,000	38,000	[ft]
Longitudinal centre of gravity	$x_{c.g.}$	23.7	24.0	29.4	[m]
Lateral centre of gravity	$y_{c.g.}$	0.00	0.00	0.00	[m]
Vertical centre of gravity	$z_{c.g.}$	-0.906	0.105	1.14	[m]
Static margin	K_n	-3.21	3.01	4.25	[%]
DDTE cost	C_{DDTE}	48.1	52.8	36.2	[$US M]
Aircraft Life Cycle Cost	LCC	2,375	2,433	4,756	[$US M]
DOC per seat per nautical mile	-	0.0603	0.0618	0.0914	[$/n.mile]

Table 5-3: BWB and Innovative wing Mass Optimised Results Summary for BWB, PSJWB, and JW

Airfoil and cruise altitude selections for the BWB, PSJWB, and JW concepts were assumed to be similar to the initial aircraft concepts previously described. The BWB and PSJWB designs use the airfoil sections previously designed with the LE carvings on the inboard wing (as per the BD concept), with the supercritical partial laminar-flow airfoil sections outboard. The JW concept uses the conventional supercritical airfoil selected for the *NT*-BL aircraft study for both wings. All novel airframe concepts are designed for a cruise ceiling of 38,000ft so that a comparison can be clearly be made with previously designed airframes. The BDVT however was optimised for 39,500ft, where the higher cruise altitude provides a heavier aircraft, but is still capable of cruising lower at 38,000ft with a slight penalty to the high L/D performance. The reduced altitude and minor change in L/D (see Fig 4-12 and Fig 4-13), provides a more efficient vehicle because the design is lighter (AUM) and burns less mission fuel relative to a design at 39,500ft before all of the optimised assumptions were integrated into the design methodology.

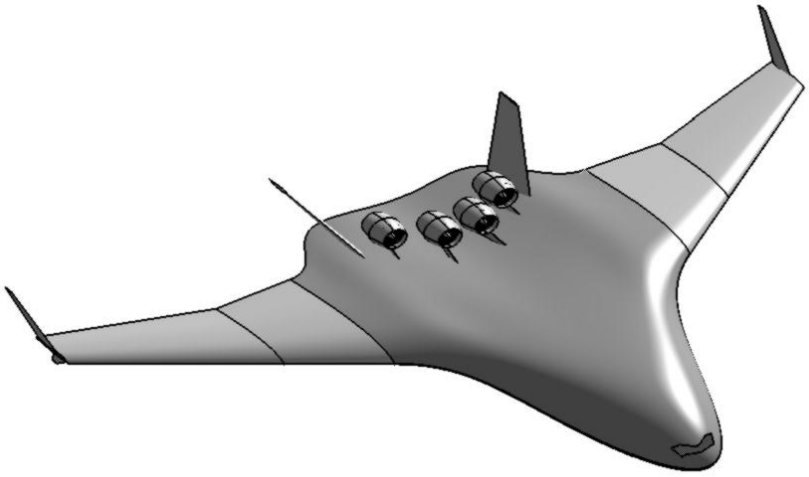

Fig 5-14: Initial design layout for the BWB geometry, sized to conduct a preliminary noise analysis.

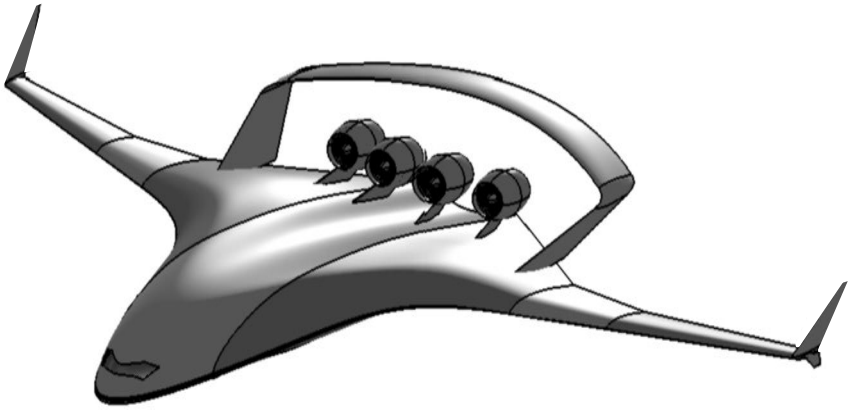

Fig 5-15: Initial design layout for the PSJWB geometry, sized to conduct a preliminary noise analysis

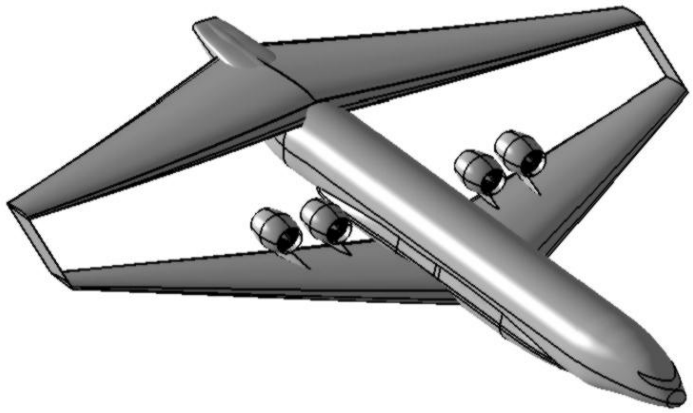

Fig 5-16: Initial design layout for the JW geometry, sized to conduct a preliminary noise analysis.

The results of this analysis enabled a comparison of each airframe based on the same flight specification, range, cruise Mach, altitude, and similar engine technology assumptions. The comparison of each airframe design provides an overview of how the various geometries perform relative to one another, and shows the limitations of the current tube-and-wing class of airframe.

The design of each novel airframe configuration is based on empirical assumptions, designed to be used to represent conventional tube and wing aircraft. The addition of design assumptions tailored for the BWB, JW, and PSJWB configurations are to be treated with caution as these are unknown designs using methodologies that are yet to be validated. The three designs described do not reflect a fair comparison of performance relative to the analysis of the BD and baseline aircraft, but allow for a trend to be deduced on how the configurations behave relative to the more conventional aircraft designs.

The sizing of the BWB and PSJWB concepts were generated into CAD models, providing geometries for each configuration, so that the designs may be optimised in more detail and to a higher level of fidelity as future work. The BWB rendered design model is illustrated within Fig 5-14 alongside the PSJWB and the JW configurations, which are also depicted within Appendix J.

References

[1] Northrop XB-35 Historical Aircraft website, [Northrop, 2008], http://www.airbornegrafix.com/HistoricAircraft/FlyingWings/XB35.htm, last accessed August 2008.

[2] Northrop XB-35, [Northrop, 2009], http://puolue.proboards.com/index.cgi?action=display&board=Asevoimat&thread=116&page=2, last accessed February 2009.

[3] NASA X-48B fact sheet, [NASA, 2009], http://www.nasa.gov/centers/dryden/research/X-48B/index.html, last accessed March 2009.

[4] Boeing X-48B Press Release, [Boeing, 2009], http://www.boeing.com/news/releases/2006/q4/061027b_nr.html, last accessed February 2009.

[5] Airbus future joint-wing concept, [Airbus, 2009], *http://aerospace-technology.blogspot.com/2008/12/airbus-future-airliner-concepts.html*, last accessed March 2009.

[6] Lockheed Global Tanker, [Lockheed, 2009], *http://www.globalsecurity.org/military/systems/aircraft/images/nsa3.jpg*, last accessed February 2009.

[7] Lockheed Strut-braced Wing Transport concept, [Lockheed, 2008], *http://www.aeronautics.nasa.gov/docs/ar99/obj8.html*, last accessed December 2008.

[8] VT, [Virginia-Tech, 2009], Virginia-Tech University Strut-braced Wing concept, *http://www.aoe.vt.edu/research/groups/tbw/LMAS.jpg*, last accessed January 2009.

[9] Kroo, I., Gallman, J., Smith, S. C., [Kroo, 1991], 'Aerodynamic and structural studies of joined wing aircraft', *Journal of Aircraft*, January 1991.

[10] Gallman, J., Kroo, I., [Gallman, 1993], 'Preliminary design optimisation of joined wing aircraft', *Journal of Aircraft*, November 1993.

[11] Nangia, R. K., Palmer, M. E., [Nangia, 2003], 'Unconventional high aspect ratio joined-wing aircraft incorporating laminar flow', *AIAA Applied Aerodynamics Meeting & Exhibit*, AIAA-2003-3297, 23-26 June 2003, Orlando.

[12] Lockheed patent for a Tail-braced wing aircraft and configurations for achieving long supersonic range and low sonic boom, [Lockheed, 2004], *http://www.freepatentsonline.com/6729577.html*, last accessed March 2008.

[13] Lockheed Martin Quiet Supersonic Transport (QSST) Private Jet Aircraft History, [Lockheed, 2003], http://www.aviationexplorer.com/Quiet_Supersonic_Transport_(QSST)_Private_Jet.html, last accessed February 2008.

[14] Howe D., [Howe, 2000], 'Aircraft conceptual design synthesis', Professional Engineering Publishing Ltd., 2000, Wiltshire, UK.

[15] Ramberg M. J., [Ramberg, 2002], 'Passenger comfort in the blended wing body', *Cranfield University School of Engineering*, MSc in Human Factors and Safety Assessment in Aeronautics, Cranfield University, UK,

[16] Liebeck, R., [Liebeck, 2002], 'Design of the blended-wing-body subsonic transport', The Boeing Company, *40th AIAA Aerospace Sciences Meeting & Exhibit*, AIAA-2002-0002, 14th–17th January 2002, Reno, Nevada.

[17] Wakayama, S., Kroo, I., [Wakayama, 2002], 'The challenge and promise of blended-wing-body optimization', *7th AIAA/USAF/NASA/ISSMO Symposium on. Multidisciplinary Analysis and Optimization*, AIAA-98-4736, August 1998.

[18] Roman D., Gilmore R., Wakayama S., [Roman et al, 2003], 'Aerodynamics of high-subsonic blended-wing-body configurations', *41st Aerospace Sciences Meeting and Exhibit*, AIAA 2003-554, January 2003, Reno, Nevada.

[19] Dodier J. A., [Dodier, 2002], 'Investigation of the effect of intakes on the drag performance of blended wing-body aircraft', *College of Aeronautics*, MSc Aerospace Vehicle Design Thesis 2001 -2002, Cranfield University, UK

[20] Gau H., [Gau, 2002], 'Blended wing body winglet design for lateral stability and aerodynamic efficiency', *MSc Research Thesis*, September 2002, Cranfield University, UK.

[21] Pambagjo E. T., Nakahashi K., Obayashi S., Matsushima K., [Pambagjo et al, 2001], 'Aerodynamic design of a medium size blended-wing-body airplane'. *39th AIAA Aerospace Sciences Meeting & Exhibit*, AIAA 2001-0129, January 2001, Reno, Nevada.

[22] Xiao-peng W. Zheng-hong G., [Xiao-peng et al, 1999], 'Aerodynamic configuration design of aircraft using multi-objective genetic algorithm', *Department of Aircraft Engineering, Northwestern Polytechnical University*, 1999, Xi'an, &10072, P.R. China.

[23] Ericsson E. L., [Ericsson, 1997], 'Effect of fuselage geometry on delta wing vortex breakdown', *35th Aerospace Sciences Meeting & Exhibit*, AIAA 97-0746, January 1997, Reno, Nevada.

Chapter 6 Noise Analysis

Reducing airframe noise is the main objective of this research, where the designs up until now have described measures to reduce noise via the implementation of new technologies and devices for the novel airframe configurations. This chapter describes how the process of analysing the noise produced by each airframe was conducted, along with the views, regulations and requirements set by authorities. Noise analysis methods used are described and the relevant references are provided, so that the reader may investigate further the ideals used for this dissertation.

The major contributors to airframe noise were previously identified as the wing, tail, undercarriage, leading edge, and trailing edge devices. Noise produced by the flaps and undercarriage were identified and confirmed to be the main sources of noise within the *D*-BL analysis. Although control devices such as flaps and slats might not be used for these new technology vehicles, such as the tailless configurations, it may be necessary to investigate the change in noise due to the absence of such devices.

The design of novel airframe geometries include conventional and new technology control devices, which regardless of their design modifications will create a disturbance to the clean airflow around the wing and generate noise. It is necessary to determine the magnitude of noise created by using new technology components, as well as existing old technology systems transferred onto the new airframes. Existing technology airframe components such as the undercarriage and main wing are noise producing critical components, where noise suppression proves to be difficult, mainly because these are two of many flight critical systems. The addition of noise suppressing technologies and advancements in control systems can aid the airframe noise reduction challenge, but prior to their integration, the clean airframe noise (prior to technology assumptions) must be identified and quantified.

6.1 Associated Noise Calculations

To accurately predict the noise of airframe components, a literature study revealed that there are many noise components to consider, as well as many flight cases and corrections required to provide an accurate assessment of aircraft noise. A few of the corrections required are associated with noise attenuation, combined with identifying mission specific phenomena which may occur during the noise certification and measurement stages for current airliners. The following sections refer to the assumptions made, deltas produced using the noise analysis code and errors which may have been produced as a result of using the analysis methods.

6.1.1 Atmospheric attenuation

Atmospheric attenuation is described as the reduction of a wave's acoustic energy as it propagates through the atmosphere as described within ESDU data items 94036, 81305, and 81306 [1, 2, 3]. Attenuation is dependent upon ambient temperature, pressure and relative humidity; where low values for these conditions result in an increase in noise attenuation. Atmospheric attenuation absorbs more sound energy at higher frequencies compared to the lower frequency of the noise spectra, and is considered to be an ideal natural method to reduce some high frequency noise.

6.1.2 Ground reflection correction

Ground reflection should only be considered for aircraft at a large distance from the receiver; primarily because the heights from receiver and aircraft relative to the ground are required. A measured spectrum is determined by incorporating a correction factor for the initial free field estimates, which includes the reflected noise back from the ground to the receiver, providing a correction factor and the new measured noise (corrected) spectrum. The ESDU 94035 [4], method has been integrated in the noise code.

6.1.3 Liner attenuation

Acoustical liners are a significant aid in noise suppression, especially in modern turbofans, where the fan is the major noise source. A model able to predict the noise absorption from current technology liners using ESDU 00012 [5] was implemented to the noise code by Doulgeris [6] and integrated into the combined airframe engine calculations to provide the total aircraft noise.

6.1.4 Noise Shielding

Over-the-wing engine installations assist in reducing forward and aft propagating fan noise. In order to study this, Doulgeris [6], investigated a noise shielding method using ESDU 79011 [7], and was integrated into the final noise solution. The model provided attenuation levels in agreement to the calculations and the measurements as discussed in Doulgeris [6].

6.2 Airframe Noise & Combination of Noise Levels

As previously discussed the aircraft is considered as a grouping of multiple noise sources each of which are calculated separately. In order to predict total aircraft noise, ESDU data item 66017 [8] is used. This method combines the sound levels resulting from two sources of known dBs. Any number of noise sources can be combined by repeated use of the method to determine the noise of a multiple component system such as an aircraft.

Estimating the noise produced from an airframe is a challenging task, even when there are software codes to assist with the process. ESDU developed a low fidelity noise analysis tool that enables the combined wing, LE, TE, undercarriage, and empennage noise to be calculated using ESDU data item 90023 [9]. Correction factors were included in the calculations based on the results from SAI final conclusions into detail aeroacoustic noise testing using small scale models and theoretical predictions [10, 11, 12]. Noise correction factors include a -5dB(A) reduction of TE flap noise due to using slot-less variable camber flaps [13], -3dB(A) for using a drooped variable camber LE, -6dB(A) for faired undercarriage [14], and a reduction of -2dB(A) for TE brushes [15] to reduce the wake vortex and associated drag.

Noise reduction technologies can also be implemented to further reduce airframe component noise. As previously mentioned both BD concepts have two 4-wheel main bogies, and a twin nose wheel. Fairing the undercarriage components provide noise shielding of around 8-10dB(A) [14]. Airfoil self noise can be reduced by using trailing edge brush technologies, which reduce main wing noise by as much as 2dB(A) [10, 11, 12].

6.3 Aircraft Noise Validation

The measurements of noise from the prediction tools used were validated against FAA noise measured data for the *D*-BL aircraft. In this manner, useful conclusions have been made on the accuracy and the error involved in the noise predictions, as described within Appendix A. The critical airframe noise case for approach and landing was determined for the *D*-BL aircraft model, and is the primary case for the noise analysis of all novel airframe designs.

6.4 FAA Noise Regulations

The noise calculation is following reference procedures, according to Federal Aviation Regulation (FAR). These procedures and conditions are specified in FAR Part 36 and are presented below:

Reference atmosphere:

- Sea level atmospheric pressure 101325 Pa
- Sea level static temperature 298 K
- Atmospheric relative humidity 70%
- Zero wind

Takeoff reference flight path, according to section B36.7:

- Maximum available thrust
- Thrust cutback at 300m

- Climb gradient of 4%
- Reference speed V2+19km/h

Approach reference flight path according to section B36.7:

- Approach angle of 3 degrees
- Steady approach speed at Vref+19km/h

Reference noise measurement positions, as shown in Fig 6-1:

- Sideline measuring point lies on a line, parallel to runway and at a distance of 450m, after lift-off of the aircraft.
- The maximum noise is calculated at an altitude of 442.5m for Stage-3 two engine aircraft, for maximum thrust available.
- Flyover reference noise measurement point is 6500m from start of takeoff roll.
- Approach measurement point is at a height of 120m.

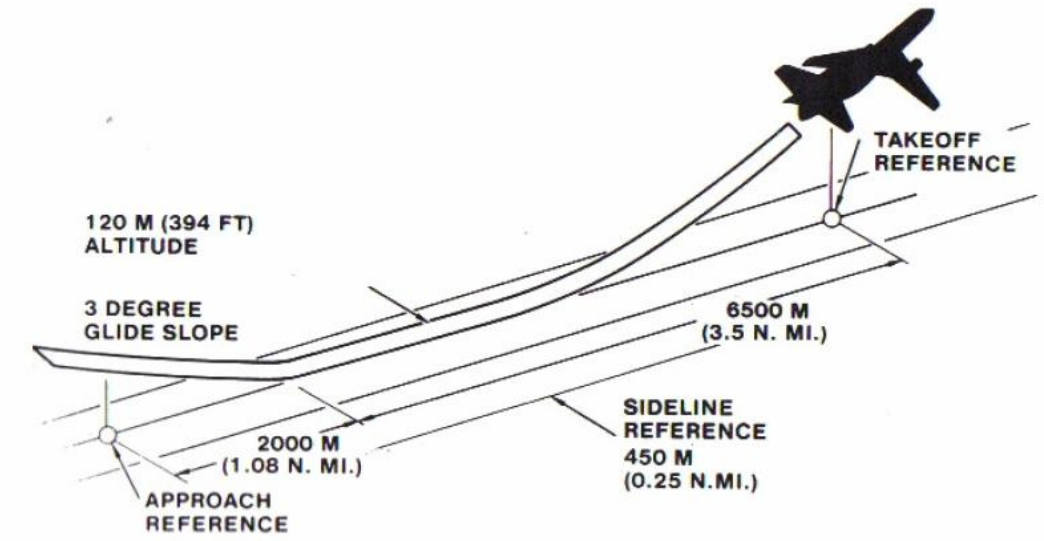

Fig 6-1: Noise Certification reference positions, Smith, 1989 [16]

Maximum noise is measured when the aircraft is at minimum vertical distance from the receiver, for example the noise for a 3 degree approach Flight Path Angle (FPA) is greater than compared to a 6 degree FPA. The position for the measurement point, is fixed at a horizontal distance of 1km from the touchdown point, where the calculation of the dB(A) noise estimates are taken. The calculations for take-off have a measurement constraint of Mach 0.3 at an altitude of 442.5m, and for the approach condition the *D*-BL aircraft is at its lowest at 120m, with an approach speed derived from the initial conceptual design results for a 3 degree approach angle.

6.5 Novel Airframe Configurations Noise Overview

The selection of a steep FPA is preferred because a lower approach velocity is achievable and reduces noise, because noise is directly related to velocity by V^n. By reducing approach velocity at high FPA, noise will be significantly reduced for the novel airframe concepts compared to the *NT*-BL. Not only will there be a noise reduction due to velocity, but for the BDSF and BWB, there is no tail and therefore no requirement for TE flaps, or LE slats (although drooped LE devices are designed for the wings), where this configuration alone has removed two-three major airframe noise sources.

The tailed airframe variants, such as the BDVT, PSJWB, and JW configurations previously defined, have the disadvantage of a tail noise source. Despite the additional tail surface, the integration of novel technologies such as the variable camber (slot-less) flaps, and drooped LE slats, TE brushes, etc, can reduce the airframe approach noise compared to the older technologies used on the *NT*-BL airframe.

6.6 Broad Delta Noise Summary

To summarise the noise analysis for the BD concepts, the three main flight variables used on the baseline noise analysis are discussed. For the tailless BD, increasing FPA from 3 to 6 degrees reduces airframe noise from 79.6dB(A) to 72.5dB(A). Geometry changes, due to increasing engine BPR, had little effect on noise. V-tail BD reduced airframe noise further to 70.4dB(A) using a 6 degree FPA. It is important to note that these results represent the noise of the airframe without including factors for low noise technology devices such as liners, brushes, etc.

The BD airframe noise for 6 degree approaches, currently exceeds the noise target, of 60dB(A). Implementing novel technologies, such as undercarriage fairings and trailing edge brushes, novel high lift devices, could potentially reduce noise by 5-6dB(A). If achievable, noise technologies would lower the approach noise of the BDVT concept to 64.6dB(A), almost meeting the noise target. The BDSF does not meet the required noise target and a calculated noise of 69.4dB(A) is achievable with maximum possible noise benefits of implementing new low noise technologies. Caution is advised when interpreting these results, because these are estimations based on the current trend in technologies, research studies, and tests completed on a few model/small-scale devices. The full extent of the integration of these devices onto a full-scale working airframe is unknown, both in terms of performance and noise reduction capabilities, so caution is advised in using these results further. A further study is required with the use of higher fidelity noise modelling of the each technology used and airframe configuration.

In addition to the noise from the airframe components, a further noise reduction is achievable through the use of a displaced threshold landing. Baseline results suggest a reduction of 5dB(A) by using a displaced threshold of 1km, and this noise reduction figure is assumed to be applicable to the BD concept, providing a minimum airframe noise level that could potentially meet the 60dB(A) target noise at the ICAO measuring point. The 60dB(A) target could be met at the ICAO/FAA noise certification point but unfortunately not at the SAI measuring point, where at the airport perimeter the noise will exceed the 60dB(A) target required, because of the distance between the aircraft and the ground. Never-the-less, to achieve a drastic reduction in noise (from a tube-and-wing class of aircraft) through introducing slight modifications to the airframe design, usable technologies, and operations, the benefits for a conventional baseline aircraft are significantly reduced compared with the same assumptions applied to a future BD aircraft concept. Therefore the BD airframe concept is considered an ideal test-bed for a quieter aircraft configuration that has a greater operational flexibility than the conventional baseline aircraft though using advanced quiet technology systems.

6.7 Novel Airframe Noise Summary

Airframe approach, take-off, and sideline noise was calculated in accordance with the ground location of ICAO noise measuring receivers. The analysis was modified to consider the design case of a six degree steep glide-slope or flight path angle (FPA) for the approach measuring point for the airframes, where this increase in FPA provides an increased distance between the aircraft and the ground, and reduces the perceived noise. Sideline noise was measured for a flyover case with the receiver located at 450m from the edge of the airport perimeter. The take-off case was the main variable, and proved to be a function of the second segment climb characteristics of the airframe. The more efficient BWB and BD concepts were able to climb at a higher ascent rate during the second segment climb phase, and increased the distance between the take-off noise receiver and the airframe at the measuring point located at a horizontal position 6.5km from brakes release.

The noise was predicted using ESDU 90023 and provides the airframe noise in overall sound pressure level (OASPL), which provides an estimate of the sound generated on the ground. Table 6-1 provides a summary of the OASPL measured at the receiver location points for each airframe, and represents a clean airframe without engine noise, ground level reflections, atmospheric attenuation, or any new technology advancements factored into the noise levels.

Airframe Configuration	***Approach Noise OASPL***	***Sideline Noise OASPL***	***Take-off Noise OASPL***
NT-BL	88.7	71.4	78.8
BDSF	72.2	64.8	71.6
BDVT	72.7	65.0	70.7
BWB	68.8	61.3	69.8
PSJWB	71.8	64.5	72.0
JW	82.6	71.1	74.7

Table 6-1: Clean Airframe Noise results for three cases: 1) approach flight path angle of 6degrees with a standard landing threshold (not displaced), 2) Sideline flyover noise at 450m from runway, 3) Take-off noise at 6.5km from brakes release. All noise measurements are given in overall sound pressure levels OASPL (dB).

Correcting the results above to factor in a suitable sound weighting scale, the OASPL can be converted into dB(A), representing the human audible sound measuring scale, and also includes ground reflections and the technology advancements for the majority of concepts. When considering technology advancements to reduce the airframe noise there are a number of specific technologies which were factored into the design of each airframe, and these are:

- Main wing is treated with TE brushes to reduce the vortex magnitude and pressure difference at the TE; used for both take-off, landing, and cruise,
- Drooped LE slats deployed for take-off and landing cases to assist with additional lift from the low lift coefficients achieved by the delta and tailless configurations,
- TE variable camber flaps (VCF) deployed for landing cases only for airframes with a tail, such as *NT*-BL, BDVT, PSJWB, and the JW concept.

In terms of airframe design, undercarriage fairings were not implemented on the final airframe selections. Undercarriage fairings were avoided because although the degree of noise reduction achieved through the fairings is significant, the loss of drag is also a major factor coupled with the additional weight of the fairings on the total aircraft mass. Placing fairings on the undercarriage main strut or over the wheels also complicates maintenance, inspection, as well as the approach/landing drag generated by the gears when fully extended. Taking into consideration the effects of the dB(A) noise scale, new technologies (excluding landing gear fairings), and the airframe geometry without engines, the breakdown of airframe noise is as follows for all three major cases:

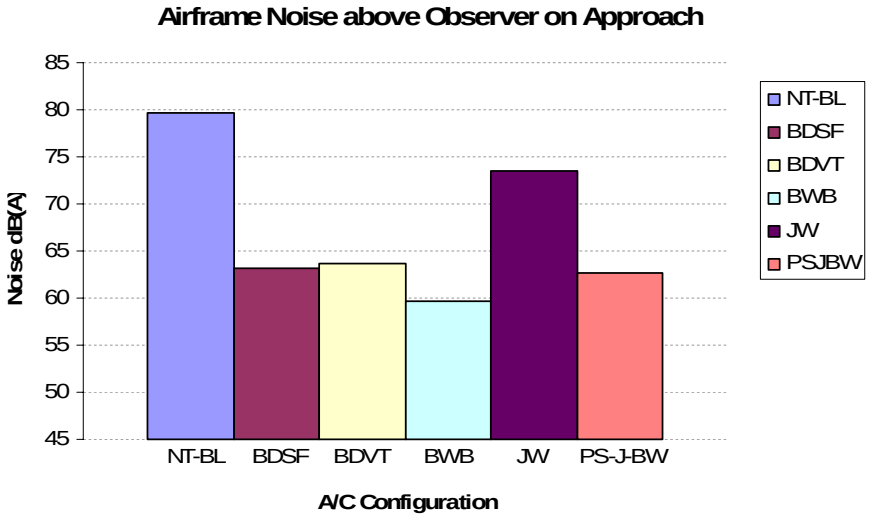

Fig 6-2: Airframe Noise variation at approach measuring point for a six degree flight path angle: includes novel technologies, ground reflections, and data converted into dB(A) to represent audible human ear range.

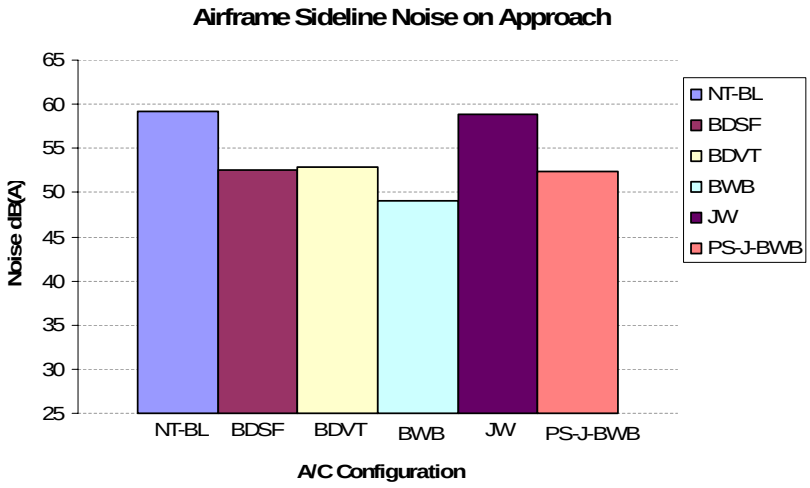

Fig 6-3: Airframe Noise variation at the sideline at the approach measuring point for a six degree flight path angle.

Fig 6-2 represents the predicted approach noise from the six main airframe configurations. The primary result is the approach noise directly above the observer where it can be clearly deduced that the *NT*-BL and JW configurations produce the most noise. The BDSF, BDVT, BWB and PSJWB are all of a similar delta wing configuration and share similar noise results, with the BWB being the quietest configuration of the group on approach. The approach noise results suggest that the noise produced through additional of a tail surface for the BDVT and PSJWB designs is not significant, compared to the BDSF and BWB for the approaching aircraft, but what the graphs do not show is the impact on stability for each of the tailless designs compared with the tailed variants.

The sideline noise produced by the airframe on an approach at the edge of the airport perimeter is documented within Fig 6-3, where the noise measured for all airframes is below 60dB(A). This magnitude indicates that the noise perceived by the human ear is no-more than that of a busy A-road, and is considered an acceptable noise limit for an aircraft located at a horizontal distance of 450m, as per the ICAO requirements.

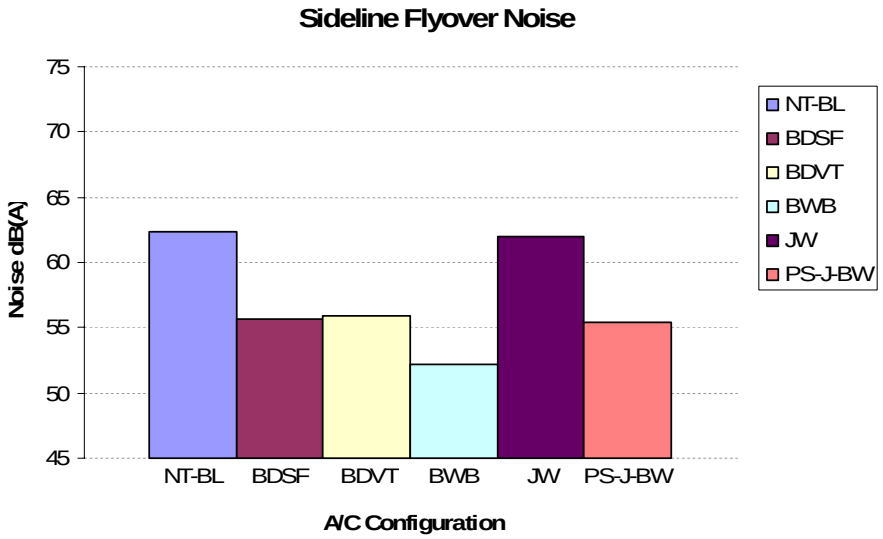

Fig 6-4: Airframe Sideline Flyover Noise variation: includes novel technologies, ground reflections, and data converted into dB(A) to represent audible human ear range.

The sideline flyover noise is when the aircraft is required to climb out from an aborted landing, and passes over the airport, with the noise measured at a distance of 450m. The noise measured at this location suggests that the BD and BWB concepts provide the least sideline airframe noise in comparison to the *NT*-BL and JW configurations.

The take-off noise produced by the airframe configurations has an equal effect to the approaching noise of each airframe as shown by Fig 6-5. The predicted noise at the 6.5km from brakes release location does not provide a fair comparison, because each airframe has a varied climb performance, placing the airframes at different altitudes above this observer point. Increasing the distance from the ground reduces the perceived noise, and once again confirms that the delta wing planforms despite having a larger wing area, produce less noise than a conventional high aspect ratio wing. In terms of the sideline noise measured from the retreating airframes at the airport perimeter, the noise predicted within Fig 6-6 is negligible, and is almost inaudible to the human ear.

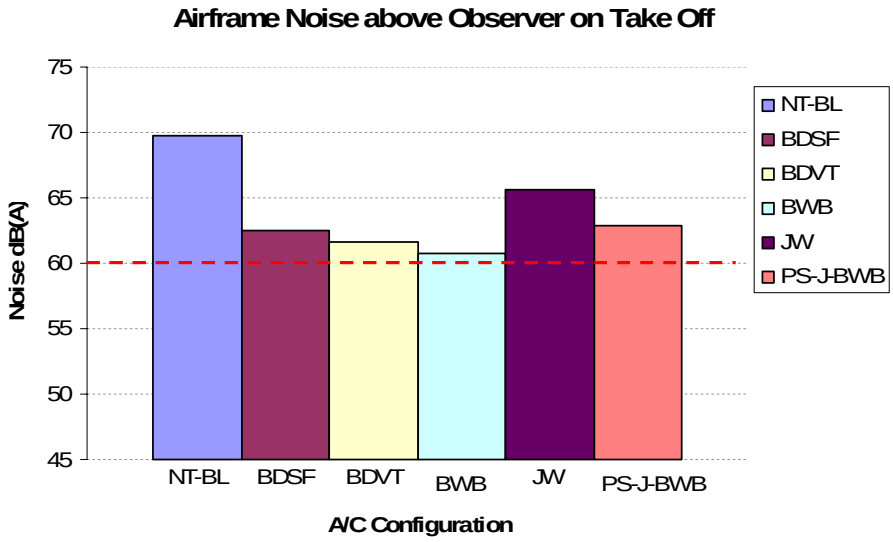

Fig 6-5: Airframe Noise variation at Take-off measured at 6.5km from brakes release: includes novel technologies, ground reflections, and data converted into dB(A) to represent audible human ear range. The red dashed line represents the noise target, as this is the worst case for engine noise.

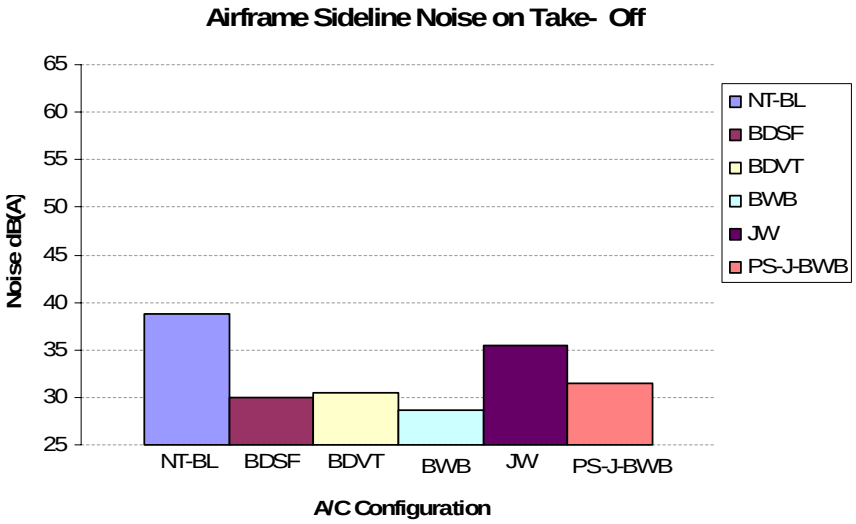

Fig 6-6: Airframe Noise variation at sideline condition during the take-off measuring point.

The noise results from the six main airframe geometries clearly describe the noise benefits of moving away from a conventional high aspect ratio wing configuration. In terms of performance, the BWB and BD families of aircraft provide a higher lifting efficiency (L/D), require less fuel for the specified 4,000 nautical mile mission, and reduce airframe noise significantly to no greater than 65dB(A). By comparing these results to the *NT*-BL variant, which has a predicted airframe noise in the region of 70-80dB(A) for take-off and landings, proves that the current configuration of airliners cannot achieve

a significant enough reduction in noise even with advanced technologies and operational approach changes.

One could argue that undercarriage fairings would provide a greater benefit to reduce the noise of the *NT*-BL further below 70dB(A) however, undercarriage is generic for most aircraft, so if there is a noise reduction potential achievable for a conventional airframe, then this can also be transferred across to the novel configurations to further reduce their noise signature. An additional noise reduction method would be to introduce a displaced landing threshold to the existing steep approach procedures and as described by the *D*-BL results, this could potentially reduce airframe noise by 10-17dB(A)

6.8 Airframe – Engine Integration

Certain challenges are associated with the location of engines above the wing for the novel airframe configurations, such as installation, maintenance, and passenger safety concerns. Engines were installed on the upper surface to increase the shielding effect of the wing, and to avoid ingestion or damage caused by foreign objects (FOD) on the ground being sucked up into the engines. Engine maintenance provides some additional challenges for accessibility, inspection and removal/replacement, which would increase cost of ownership and servicing.

With respect to passenger safety, engines are typically located for most of the novel airframes at close proximity to the passenger cabin above the wing, where rotor-bursts would be a concern. A requirement for the fan disc and more importantly the turbine, states that the pressurised cabin should not be penetrated by a five degree clearance zone around the rotor/blades. The fan should be contained by the engine cowl, whereas the turbine being a smaller high rotational velocity component, has the greatest concern for a rotor-burst; so as long as the pressurised cabin is not penetrated by a disc burst, it may be acceptable to locate the engines along the upper rear surface of the wings. In the event of engine fires, the close proximity of each propulsion system could result in a multiple engine failures, and provide additional obstacles for passengers during egress, especially in the case of the BWB concept where the geometry restricts the location of exits to the front or rear of the vehicle with no OTW exits.

Another challenge would be to shield engine noise from the passengers because engine noise is directly in-line with the cabin. The benefit of locating the engines above the wing considers cases such as an undercarriage failure or during ditching scenarios, where the majority of loads are impacted by the wing, wing box, and blister.

Integration studies of OTW engines on a high-wing BD configuration were investigated by Medicina [17] and Abreu Dos Santos [18]. A further in-depth analysis of a low-wing BD configuration including modified airfoils, and a new plan-form shape was investigated by de Bellis, Nettis, Rousselot, and Truffi [19, 20, 21, 22]. These studies investigated integrating four podded, semi-embedded, and fully-embedded engines at the wing root. Results from Nettis [20] conflicts with Fujino [22, 23] suggesting that there is an overall drag increase of *OTW* engine nacelles. It is the authors' opinion that induced drag is increased due to the incorrect placement of engines in the study relative to any shock formations. On the other hand, the results describe an increase of three times the drag of the clean wing for four engine pods near the root. The semi-embedded installation provided twice the drag, and the fully-embedded solution provided 1.7 times the drag of the clean wing, suggesting that from the three configurations, the fully embedded is the ideal solution.

Integrating the engines, nacelles, and airframe is an iterative design process, where at present CFD analysis completed at Cranfield for the BD tailless configuration is described in more depth within Doulgeris [6]. Studies to further modify the BD wing design were investigated in order to avoid the formation of shock waves over the main wing. At present a detailed CFD analysis is required to investigate whether the changes have improved the wing lifting performance and reduced the Mach range over the wing.

Two of the main integration studies investigated semi-embedded engines and upper podded engines. It was found that for greater drag reduction, the integration of semi-embedded or fully embedded engines provided the greatest benefits, but at the expense of integration, maintenance, more importantly development costs.

The podded engine solution provides a drag penalty, but with a reduced cost for development and installation, but has similar difficulties with maintenance, and at the additional cost of reduced engine noise shielding from the airframe itself. Due to time constraints for the integration of novel airframes and alternate engine configurations, the BWB, JW and PSJWB configurations were integrated with OTW podded engine nacelles, with a further area of research required to carefully integrate these airframe designs with either semi-embedded or fully-embedded engines.

A summary of the novel propulsion cycle study completed by Doulgeris [6] provides an interesting comparison between a range of engines compared against a datum 'baseline' engine. Studies into the development of Ultra High bypass ratios (UHBPR), recuperated cycles, a Constant Volume Combustor (CVC), and Inter-Cooled Recuperated (ICR) propulsion cycles, provided solutions for quiet propulsion systems that may be integrated into the novel airframes. Incorrect airframe-engine matching would provide a noisy aircraft and would negate any benefits of each individual low noise

design. Doulgeris describes how integration of all four engine variants on the *NT*-BL and the BDSF configurations provide similar total noise results calculated for both the aircraft. This suggests that the engine noise for each design is similar, approximately 63dB(A) during approach and 69dB(A) during take-off. As each engine is mounted on the same airframe the results conclude that any increase in performance due to the novel cycles would have little to no noise benefit for airframe-engine integration process.

6.9 Total Aircraft Noise Summary

Total aircraft noise is achieved by taking the noise produced from the airframe and engine at each specific or relevant flight case and combining the two values to create a final total noise summary. The airframe noise results were summarised within section 6.7 and had described the three main flight cases for the airframe noise analysis. The propulsion systems design summary in section 6.8 provides a datum guide as to how engine noise varies for the four engines during the same flight cases as per the airframe.

The integration process of airframe and engines provides a means to either pod, embed, or semi-embed the engines. A considerable amount of time and resources has been spent on integrating semi-embedded engines within the BDSF configuration. Airframe-engine integration studies included spanwise and chordwise positioning, along-with the height displacement of the nacelles/pods, coupled with low and high fidelity CFD computations; to predict how the flow over the fuselage-nacelle-wing combination would affect this lift distribution and the formation of shock waves across the delta wing. The BDSF integration study enabled the comparison of numerous variables to locate and place the engines for the one specific BD airframe, but the study proved to be time consuming and could not be duplicated for the remaining airframe configurations.

A datum engine location was decided to compare each of the remaining airframes using consistent methods. The selected engines were the UHBPR turbofan designs, considered to be mounted above the wings, with a quad engine configuration for the BDVT, BWB, JW, and PSJWB, and a twin engine configuration for the *NT*-BL aircraft. The engine and airframe noise components were combined using the quadratic function (equation A-1) described within Appendix A, and provided the following results. The final results of the Airframe engine integrated designs provide optimistic solutions for the development of future aircraft concepts and are shown below.

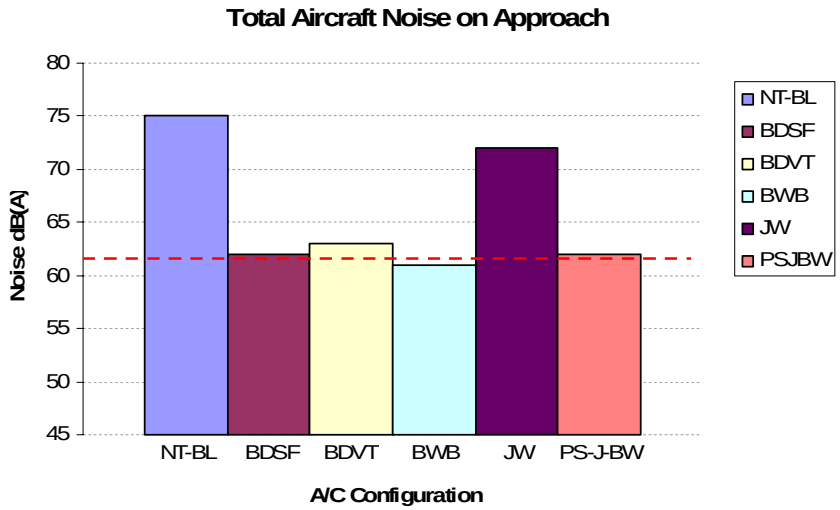

Fig 6-7: Total Aircraft Approach Noise: includes novel technologies, ground reflections, integrated UHBPR engines and data converted into dB(A) to represent audible human ear range. The red dashed line represents the final solution for the SAI SAX-40 BWB design.

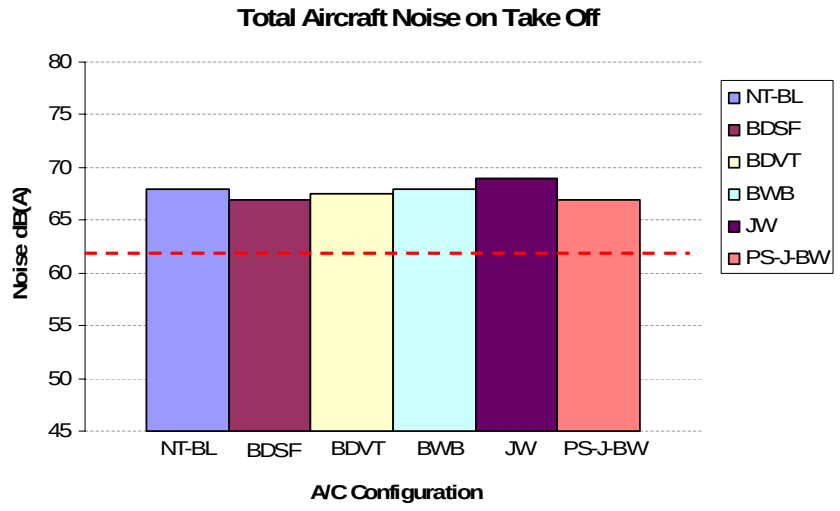

Fig 6-8: Total Aircraft Take-Off Noise: includes novel technologies, ground reflections, integrated UHBPR engines and data converted into dB(A) to represent audible human ear range. The red dashed line represents the final solution for the SAI SAX-40 BWB design.

The BD and BWB configurations appear the most promising in-terms of overall noise reduction for all flight cases analysed. The joined wing does not significantly reduce noise and is comparable to that of the *NT*-BL airframe both in terms of noise and performance. The joined wing is designed with two equally positioned high aspect ratio wings positioned fore and aft of the centre fuselage, where the two smaller high aspect ratio wings generate a larger degree of noise compared to the low aspect

ratio deltas. The two intermediate designs are the BDSF, and the PSJWB, where the designs produce significant noise reductions, but are considered potentially un-certifiable. The BDSF requires artificial control in order to maintain stability during flight, and this can be a major design draw-back in terms of certification, similarly the PSJWB is in essence a BWB design, but the partial span close-coupled joined tail raises a few questions in terms of the drag and interference over the wing, and whether the tail will be subject to stall for high incidence cases.

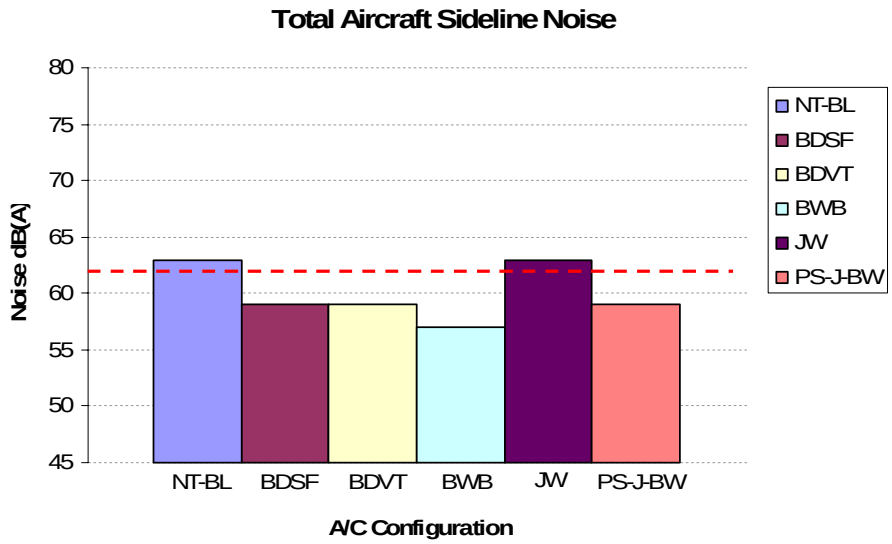

Fig 6-9: Total Aircraft Sideline Noise: includes novel technologies, ground reflections, integrated UHBPR engines and data converted into dB(A) to represent audible human ear range. The red dashed line represents the final solution for the SAI SAX-40 BWB design.

Airframe Configuration	*Approach Noise dB(A)*	*Sideline Noise dB(A)*	*Take-off Noise dB(A)*
NT-BL	74.9	62.8	67.7
BDSF	62.2	59.1	66.4
BDVT	62.8	59.2	66.7
BWB	61.7	57.3	66.8
PSJWB	62.5	58.8	66.6
JW	71.8	63.0	69.2

Table 6-2: Final Aircraft Noise results summary corrected for new technologies and for an approach flight path angle of 6degrees with a standard landing threshold (not displaced), and integrated with UHBPR engines podded above the wings

6.10 Airframe Recommendations for further Studies

This research has investigated the design of four main concepts, the baseline (*NT*-BL), broad delta (BD), blended wing body (BWB), and joined wing (JW) configurations to a parametric design level.

A more detailed investigation into the design of the BD configuration has enabled the development of two solutions, and provided a refined detailed design process. The design process has discovered that a 60dB(A) noise target is achievable for alternate airframe configurations by using a 6 degree approach FPA and noise reduction technologies. The BWB design has great potential to be a silent, economical, and green aircraft, as discovered by the SAI project, and the author's research aimed to investigate alternate future configurations by investigating how efficient and silent a selection of novel airframe designs compare to the BWB.

The most promising design or a near-future concept which provides reduced noise and potential performance improvements is the BDVT, where this design could potentially be designed, tested, and built within the next 10-15 years, and provide an ideal solution for a part-silent part-green design. Further modifications can be made by integrating the BDVT with swept un-ducted prop fan (UDF) engines, which would locally increase cabin noise, but the prop noise would be shielded from with the wing geometry, enabling a lower altitude slower cruising speed that would reflect in a reduced fuel burn, and provide a greener aircraft concept.

The design process described within this dissertation has enabled the reader to follow the design methodology used to develop a series of airframe concepts, with the view to provide a silent aircraft design methodology. In addition to developing a methodology, the challenge was to provide a solution for the most silent airframe configuration, and has been met; with a series of innovative design solutions compared in terms of performance, design feasibility, economics, global, and environmental concerns.

The ideal silent airframe, which happens to be the ideal 'greener' aircraft solution, is the BWB. This configuration has the potential to be an extremely efficient airframe, but is faced with many challenges in integrating this vehicle into current airport operations, and also acceptance from both passengers and airworthiness authorities. The future development of the BWB configuration is reliant upon concepts such as the broad delta (BD), which in many ways is a similar configuration to the BWB, but has many of the 'traditional' qualities of a current tube and wing aircraft. The development of the BD configuration may lend itself towards a tailless design in the future, and by certifying this aircraft, the potential to expand on the delta wing, and produce an all flying certifiable blended wing body airliner may enable the BWB airliner 'concept' to become a reality in the not-so-distant future.

References

[1] ESDU 94036 [ESDU, 1994], 'The prediction of sound attenuation as a result of propagation close to the ground', Engineering Sciences Data Unit (ESDU) data Item 94036, November 1994.

[2] ESDU 81305 [ESDU, 1981], 'An introduction to aircraft noise lateral attenuation', Engineering Sciences Data Unit (ESDU) data Item 81305, November 1994.

[3] ESDU 81306 [ESDU, 1989], 'The calculation of overground sound propagation in the presence of wind and temperature gradients', Engineering Sciences Data Unit (ESDU) data Item 81306, October 1989, Amendment A and B, July 1992.

[4] ESDU 94035 [ESDU, 1994], 'The correction of measured noise spectra for the effects of ground reflection', Engineering Sciences Data Unit (ESDU) data Item 94035, November 1994.

[5] ESDU 00012 [ESDU, 2000], 'The acoustic attenuation of absorbent linings in cylindrical flow ducts, Engineering Sciences Data Unit (ESDU) data Item 00012, 2000.

[6] Doulgeris G., [Doulgeris, 2008], 'Modelling & integration of advanced propulsion systems', *PhD Research Thesis*, March 2008, Cranfield University, UK.

[7] ESDU 79011 [ESDU, 1979], 'Estimation of noise shielding by barriers', Engineering Sciences Data Unit (ESDU) data Item 79011, September 1979.

[8] ESDU 66017 [ESDU, 1978], 'Combination of noise levels in dB, Engineering Sciences Data Unit (ESDU) data Item 66017, Amendment A, 1978.

[9] ESDU 90023 [ESDU, 2003], 'Airframe noise prediction', Engineering Sciences Data Unit (ESDU) data Item 90023, June 2003, Amendment C, Endorsed by The Royal Aeronautical Society (RAeS).

[10] Hileman J. I., et al., [Hileman et al, 2007], 'Development of approach procedures for silent aircraft', *45th AIAA Aerospace Sciences Meeting and Exhibit*, AIAA 2007-453, January 2007, Reno, Nevada.

[11] Lui Y., [Lui, 2007], 'Experimental study of surface roughness noise, *45th AIAA Aerospace Sciences Meeting and Exhibit*, AIAA 2007-3449, January 2007, Reno, Nevada.

[12] Herr M., Dobrzynski W., [Herr, 2004], 'Experimental investigations in low noise trailing edge design', *10th AIAAIRCRAFTEAS Aeroacoustics Conference*, AIAA-2004-2804, 2004, Manchester, UK.

[13] Fielding J. P., [Fielding, 2000], 'Design investigation of variable-camber flaps for high-subsonic airliners, *24th Congress of the International Council of Aeronautical Sciences (ICAS)*, ICAS2000-0124, September 2000, Harrogate, WA.

[14] Quayle A., [Quayle, 2007], 'Landing gear for a silent aircraft', *45th AIAA Aerospace Sciences Meeting and Exhibit*, AIAA 2007-231, January 2007, Reno, Nevada.

[15] Herr M., [Herr, 2007], 'Experimental study on noise reduction through trailing edge brushes', *notes on Numerical Fluid Dynamics and Multidisciplinary Design*, 2007, Springer, Berlin.

[16] Smith M. J. T., [Smith, 1989], 'Aircraft noise', *Cambridge Aerospace Series*, Cambridge University Press, 1989, NY.

[17] Medicina, D., [Medicina, 2006], 'Silent aircraft initiative: tip turbine driven fan integration on wing top using 3D-CFD', *MSc Research Thesis*, September 2006, Cranfield University, UK.

[18] Abreu Dos Santos M., [Abreu Dos Santos, 2006], 'Aircraft engine noise analysis and influence around the airport', *MSc Research Thesis*, September 2006, Cranfield University, UK.

[19] de Bellis F., [de Bellis, 2007], 'Variable fan nozzle area engine cycle design, optimisation, and 3D-CFD airframe integration study for a silent aircraft', *MSc Research Thesis*, September 2007, Cranfield University, UK.

[20] Nettis L., [Nettis, 2007], 'The constant volume combustor: cycle optimisation and engine-airframe integration study for a silent aircraft', *MSc Research Thesis*, September 2007, Cranfield University, UK.

[21] Truffi D., [Truffi, 2007], 'Jet engine components interaction for a silent aircraft', *MSc Research Thesis*, September 2007, Cranfield University, UK, Universita Degli Studi Di Roma 'La Sapienza', Italy.

[22] Fujino M., Kawamura Y., [Fujino, 2003], 'Wave-drag characteristics of an over-the-wing nacelle business-jet configuration', *Journal Of Aircraft Vol. 4, No. 6*, Pages 1177-1184, December 2003, Honda R&D Americas, Inc., North Carolina.

[23] Fujino M., Kawamura Y., [Fujino, 2003], 'Wave-drag characteristics of an over-the-wing nacelle business-jet configuration', *41st Aerospace Sciences Meeting and Exhibit*, AIAA 2003-933, January 2003, Reno, Nevada.

Chapter 7 Discussions and Conclusions

This chapter re-iterates some of the main discussions provided within the dissertation, highlighting the most relevant information and results leading to the completion of this study to producing a silent aircraft design methodology. The main focus, emphasis on designs, and procedures used are touched upon to provide an overview of the process, with further details provided within the accompanying appendices.

7.1 Accomplishments

The research presented within this dissertation has contributed to the evolution of multiple airframe configurations, with the primary aim to reduce airframe noise by developing novel airframe solutions to combat the challenges of ever-increasing noise, emissions, and environmental concerns around airports. The study focuses on altering the current airframe geometry, combined with investigating novel technologies to reduce airframe noise. Identifying the major contributors to noise such as the leading edge, trailing edge devices, empennage, and undercarriage, has enabled the design of the airframes to evolve and integrate new technologies such as chevrons, liners, brushes into the design. The research is separated into three distinct parts, consisting of airframe configurations, design methodologies, and finally airframe noise analysis.

Studies into current configurations, technologies, and how aviation is tackling the current noise and environmental challenge provides a way to move forward and to explore unconventional airframe geometries by thinking ‘out of the box’. A matrix of novel airframe ‘families’ initiated a review process through a systematic study, which investigated how each configuration would ‘score’ relative to a conventional datum design, based on three main objectives, to reduce noise, emissions, and cost.

The development of a design methodology using semi-empirical methods was expanded to consider novel airframe geometries, including performance enhancements such as winglets, and geometric studies to determine ideal lifting sections and airfoil design. The methodology evolved as an iterative process with the preferred use of empirical or semi-empirical methods as opposed to intelligent guestimates/assumptions, and included integration of programs to assess lifting performance through vortex panel methods, airfoil section profiles, and also combined a performance and cost model to explore the design feasibility.

Airframe noise prediction was the final goal to predict the noise produced by each configuration. Initially an automated noise analysis code was sought to integrate with the conceptual design process, however it was more practical to focus on the design methodology and use a low fidelity noise model, and so ESDU methods were used. Noise analysis of six main airframe configurations using ICAO

defined flight cases for approach, take-off, and sideline noise were completed. The BD, BWB, and JW designs were compared alongside a conventional *BL* configuration which also included the use of new technologies. The results for the noise analysis favour the BD and BWB concepts, and a review of the engine-airframe integration process allowed for the scope of the research to expand into CFD to understand the behaviour of flow around semi-embedded engines compared with podded alternatives for the BD.

The authors' main achievement from this research study was the recognition that although there are many different airframe possibilities present, the ideal solution is usually staring you straight in the face! The entire scope of the silent airframe design methodology investigated alternate airframes of all permutations, but the one design which is not far off from what the military use today is the delta wing. Out of the six final designs selected, four of these were similar to a delta wing; two of which were permutations of a conventional aircraft but with low aspect ratio wings and the other two were of a BWB design.

The main accomplishment of this research is the realisation that the most silent, efficient, and green airframe, is the most costly, and is the BWB airliner. Given current technology levels and stringent legislative requirements, the BWB will not realistically be an achievable high capacity civil transport aircraft before 2050. However, as mentioned above, a stepping-stone for say 2020 would be to develop a BD aircraft, certify a tailed and tailless version of this airframe, and the next phase of the evolution would simply be the BWB.

7.2 Discussion on Research

From the onset of this research project the focus was on achieving a single number, and that was the noise limit goal required to produce a silent aircraft concept, which was 60dB(A). Obviously closely followed the aircraft specification for passenger payload, range, and that was based upon the datum design aircraft which was the B767-300 class of aircraft.

A number of novel airframe 'family' groups were identified for this design study where a conventional 'tube-and-wing' aircraft was used as a *BL* datum design, to develop the design methodology and integrate new technologies to provide a suitable comparison for a future technology class of airframe. The *BL* aircraft was used to compare the designs of the BWB, JW, and BD airframe concepts.

The seven configurations initially chosen to investigate further were reduced to the three main designs or four configurations, due to time constraints, as shown below in Fig 2-22. The investigation of the

partial span conventional joined wing (PS-JW), canard BWB were not further developed as they were intermediate derivatives of the PSJWB. The SAX-40 design was not developed, optimised, and compared with the C-MIT study using this design methodology primarily due to time constraints. The designed BWB completed within this research was a part compromise between the discrete fuselage design and the SAI SAX-40, where further work would indicate a direct comparison using the C-MIT SAX-40 aircraft as the baseline model.

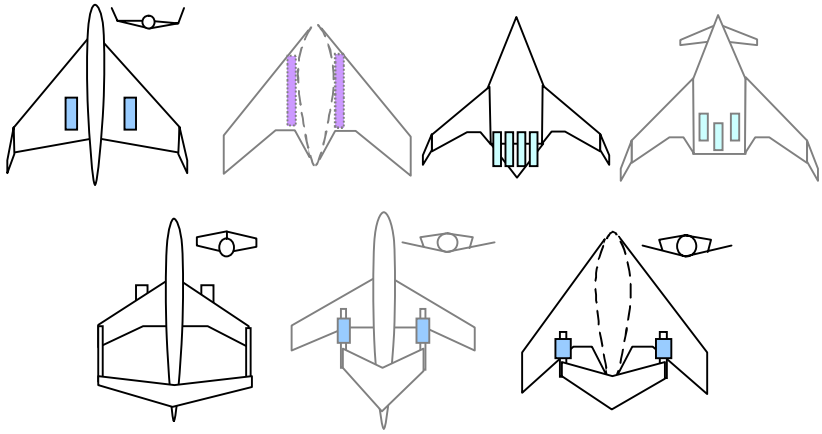

Fig 7-1: Final selection of airframe concepts to develop, from top left to bottom right: Broad Delta (BD), Discrete Fuselage BWB (D-BWB), C-MIT SAX-40, Canard derivative of SAX-40 (C-SAX), Joined wing (JW), Partial-span Joined-Wing (PS-JW), and Discrete Fuselage Partial-Span-Discrete-Fuselage-Joined-Blended Wing Body (PSDFJ-BWB)

7.3 Baseline Review

The design methodology investigated within this dissertation provided a basis to combine high fidelity analysis, alongside low fidelity noise models, so that a BL aircraft could be designed. Two BL aircraft were designed based firstly on past technology levels and a second using future 15-20 year technology predictions; where the first design was used to validate the design process and noise analysis, and the second design provided a datum design for suitable comparison with the remaining novel aircraft designs. The low fidelity noise analysis was implemented with a view for a higher fidelity model to be implemented at the end of research, but due to time constraints and the broad scope for noise analysis on multiple airframe configurations, the basic analysis using ESDU was considered satisfactory for preliminary comparative purposes.

Airframe noise analysis considered the baseline aircraft during the landing, sideline, and take-off noise cases for a standard airport, considered to be London Heathrow (LHR). An additional study was completed in collaboration with SAI to explore alternate approach operations of a conventional airliner without redesigning the airframe. It was found that for unconventional approach procedures using current aircraft, steep and slow approaches were beneficial to reduce noise around the airport

perimeter, but greater noise reduction of is potentially available by carrying out a displaced threshold landing.

Looking at incorporating the slow and steep approaches into one case, suggests that if the baseline 72.5m/s flight at 3 degrees is compared with that of 66.6m/s case at 6 degrees, the net result is a -10dB(A) reduction (to 74.1 dB(A)) in airframe noise at the perimeter. By simply combining this with a displaced threshold concept, there is a further -4.9dB(A) reduction to 69.2dB(A); providing a net airframe noise reduction of -14.9dB(A) for the baseline. However, this noise benefit is purely idealistic for the airframe components, and estimations for the engine noise are also required. It is important to note that the addition of two noise sources can not be simply assessed as mentioned above. The quadratic function must be used to see the net benefit of the total noise reduction for each technology, therefore the 14.9dB(A) noise reduction would in reality be -8dB(A) for the 3 cases mentioned above.

Detailed engine noise results predict that fan noise dominates over jet noise by as much as +10dB(A) to +31dB(A); resulting in a higher engine noise compared with airframe. In an ideal scenario, with a thrust setting of approximately half (10-15% SLS), noise could reduce by half however, this is not true in practice as the engine thrust would never be set to such a low setting. It is important to note that turbine noise is a very high noise source for the engine during landing, and estimations for this source are not included in this analysis. The predicted engine noise from Doulgeris [1] was combined with airframe noise to determine the total aircraft noise.

The main emphasis of the slow and steep approach study was that a significant noise reduction could be achieved at the airport perimeter by increasing the aircraft FPA and displacing the threshold, without changing the aircraft approach velocity. A challenge in implementing this solution is apparent when considering an approach velocity of 72.5m/s, a 6 degree FPA, and a reduced stopping distance due to a shorter runway, requiring a greater high lift and drag capability for the wings; emphasising re-design for the BL wing.

The main conclusion for the *D*-BL aircraft analysis is that combining the steep and displaced thresholds concepts, along-with a redesign of the main wings, would result in -17dB(A) net reduction in aircraft noise on the approach flight path. This provides a short-term solution to the aircraft noise challenge we have at present. However, despite this short term-solution, many aircraft designers/integrators would not be willing to redesign the wings of their entire fleet, so implementation of these measures should be placed on the design specification of the next generation transports.

7.4 Summary of the BD Designs

Two main airframe concepts were investigated for the BD concept family, where multiple design variables such as materials, engine selections, approach conditions, etc, were explored and down-selected to two the main configurations. The design selections were based on producing the lightest possible airframe, and introduce noise reduction technologies to develop a silent airframe, so an all-composite all-electric airframe was developed for two variants. The designs converged to a tailed and a tailless solution for the delta wing, where a tailed V-tail solution referred to as the BDVT was directly compared to a tailless solution, the BDSF, in terms of performance, cost, and noise.

The tailless BD configuration is an all composite airframe optimised for a cruise Mach of 0.8, BPR 12 engines, at an altitude of 38,000ft for the specified design range. The BDSF becomes more efficient at higher cruise altitudes and Mach numbers with an L/D in excess of 20; at the expense of a heavier aircraft, more fuel, and larger engines. The tailless solution has the main challenge of trim during flight, where there is a lot of trim drag associated at mostly all flight conditions. The benefits of a higher and faster flight is out-weighed by environmental factors such as releasing emissions higher in the atmosphere, producing contrails, and economical concerns related to the cost of fuel.

The BDVT is identical to the tailless configuration in the sense that an all composite airframe is used and optimised for a cruise Mach of 0.8 and with BPR 12 engines, but has a higher cruise altitude of 39,500ft for the same design range. The BDVT is more efficient over a range of cruise altitude and Mach number cases compared with the BDSF, providing greater operational flexibility, higher *L/D*, and a reduced aircraft weight. The increase in efficiency, *L/D*, and cruise performance is related to the reduced trim drag, and is because of the tail surface.

The BDSF was found to be a noisier solution compared to the BDVT because of the larger wing, and greater surface deflections required for trim of the aircraft in all flight conditions. It was initially assumed that BDSF design would have a lower airframe noise because of the absence of the tail, but the tail provides a greater scope for generating more drag, greater lift, and assists with achieving lower approach velocities by reducing the aircraft stall speed. The additional benefits of noise technologies such as *TE* brushes, *VC LE*, winglets, engine noise liners, and undercarriage fairings, were implemented. It must be noted that the maximum noise reduction levels were used, and that the degree of noise reduction may be optimistic, and therefore reduced by a few dB(A)'s with a ±2% error margin for the noise results. A sensitivity analysis was planned for the change in noise reduction due to variations in the parameters. The sensitivity study was only considered necessary once the designs of all aircraft concepts were developed to a suitable standard; namely a higher fidelity noise model than that currently used for this analysis.

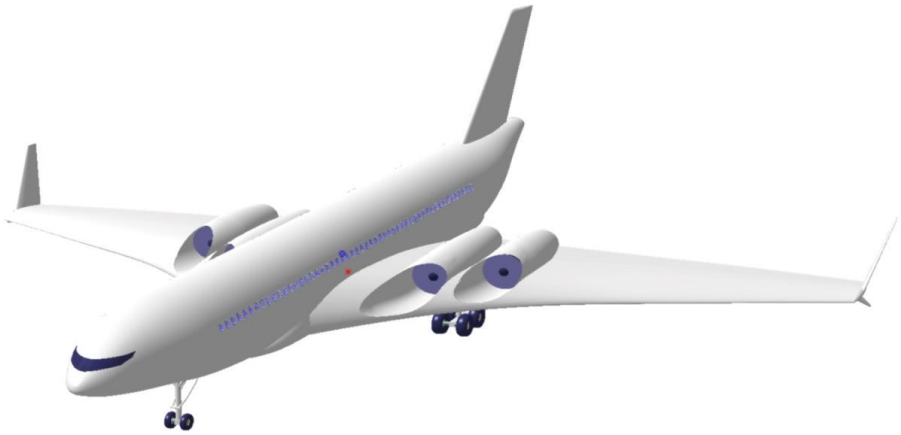

Fig 7-2: Final BDSF Concept Design

The BDSF wing design uses modified laminar flow airfoils, with LE nose carvings to produce a positive pitching moment about the c.g., reducing the required elevon deflection for trim. *VC LE* devices are deployed to increase maximum lift coefficient so to avoid wing stall, assisting with the steep 6 degree approach angle. *TE* elevon and aileron deflections are coupled to increase wing camber and maintain steady flight, with spoilers assisting as air-brakes and for yaw control, and the fin and winglets providing directional stability at low speeds. A flight control system is a necessity for this design, where the control surfaces are continuously moving and would be difficult for a pilot to control.

The BDVT incorporates similar noise reduction methods as the BDSF, such as *TE* brushes, *VC LE*, winglets, engine noise liners, and undercarriage fairings. The main differences with this configuration is the addition of variable camber flaps (VCF) and implementing an all-moving tail compared to using a conventional tail with ruddervator control surface, in order to investigate the capability of reducing airframe noise. *VCFs* and *LE* devices are deployed to increase maximum lift coefficient to avoid wing stall, assisting with the steep 6 degree approach angle. Ailerons deflections are purely used for roll control and are coupled with spoilers to double-up as air-brakes and for yaw control. The V-tail ruddervator designs coupled with the winglets provide a degree of directional stability, with the control surface used to trim the aircraft and control the pitch attitude during flight. Loss of the flight control system for the BDVT has an additional redundancy where the pilot can fully control the aircraft manually, unlike the BDSF, where the pilot would require training to handle the tailless aircraft. This was justified by the stability study investigated where for the short period mode, the time to double amplitude for the BDSF was less than one third, and for the BDVT half of that calculated for the *NT* baseline. This indicated that for a gust or an induced oscillation, the pilot has

less time to react any disturbances compared to the conventional aircraft, and this would be a critical issue if the automatic flight control system were to fail.

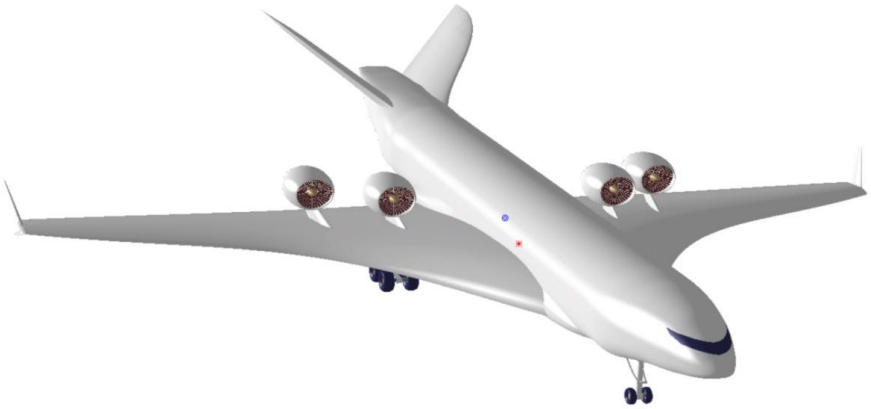

Fig 7-3: Final BDSF Concept Design

Engine integration was a collaborative effort between airframe and engine designers, where a number of configurations were considered and the final selection was for four semi-embedded engines at the wing root for the BSDF. Initial design layouts were investigated by MSc researchers using *CFD* where the results are inconclusive due to an incorrect number of engines integrated and for a late change in the wing geometry. In addition a preliminary study into the control and performance was investigated using *AVL*, where the model was used to predict the lifting capabilities for approach and landing conditions.

An engine integration study on the BDVT revealed a wing depth of less than 40% of the engine diameter and was considered insufficient to semi-embedd the engines. The chosen configuration was for four *OTW* podded engines with canted pylons to reduce interference with the flow across the outboard wing.

The mass, c.g., stability, and control estimates were combined with the AVL model to characterise cruise and low speed performance, where investigating aircraft angle of attack, elevon deflection for trim, and increments of induced drag were compared with initial parametric design study estimates. A 10% increase in drag was found using *AVL*, where it is the authors' opinion that the true behaviour of the wing-winglet interaction, along-with thickness effects over the laminar sections is not accounted for due to the limitations in using *AVL*. Having investigated the BD geometry, mission flight cases, flight performance, component masses, and stability, the development, acquisition, operating, and disposal costs of the BD were investigated to conclude the design.

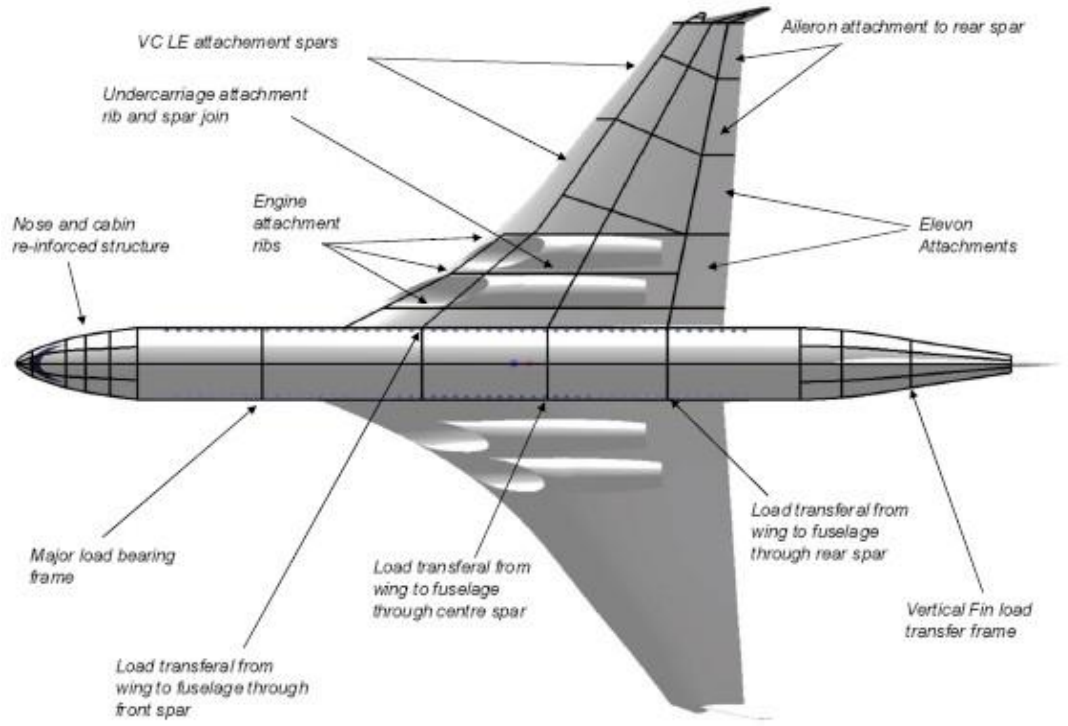

Fig 7-4**:** BDSF plan view layout of major structural components and critical attachment areas

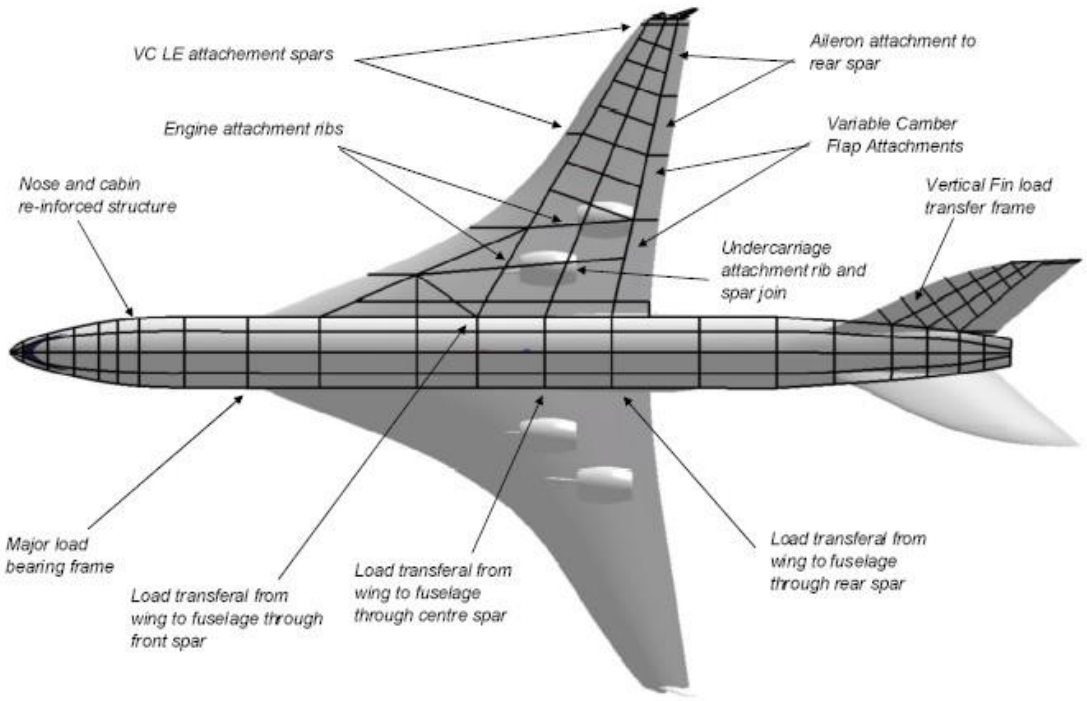

Fig 7-5**:** BDSF plan view layout of major structural components and critical attachment areas

A preliminary study into the BDSF structural layout of major structural frames was investigated, and identifies the key load bearing regions, shown in Fig 7-4. The critical load transferral from the wing into the fuselage is combined with engine and undercarriage loading which act on across the same ribs and spars. The nose and tail of the fuselage requires additional large frame support structures to transfer loads from the fin and rudder, and also from the nose landing gear. The passenger cabin of the fuselage is pressurised and is represented by the region with dispersed large frames, contained by a forward and rear pressure bulkhead.

The BDVT structural layout identifies the key load paths for the aerodynamic wing and tail loads to transfer into the fuselage. The majority of loads are similar to the BDSF, where the structural arrangement is almost identical to a conventional aircraft where all the major loads are transferred through heavy frames, ribs, spars, and the fuselage longitudinal stiffeners/longerons. The transfer of loads from the undercarriage and engines into the structure is preferred for the BDVT aircraft configuration compared to the BDSF, mainly because landing gear loads and engine attachments are staggered and do not act on the same point. The BDSF structural arrangement stresses the centre wing-box spar by mounting two engines per side on a variable depth structural member (due to semi-embedded engines), and also contain the attachments for the main undercarriage leg. Structural challenges such as these were considered to be tackled during preliminary and detailed design, where for this discussion the engine torque, flight loads, and landing loads are assumed to transfer effectively into the structure without any major design challenges.

The BD aircraft concept is seen as an intermediate stage to reduce noise in the medium-term, where studies into dramatic changes of the airframe design, such as BWB aircraft provide substantial noise reduction, but require extensive research, development, and testing prior to release or certification as a passenger transport. Short-term solutions include the implementation of noise reduction technologies on current airliners, boasting 5-10dB noise reduction, which is not significant when considering future noise targets. The BD is considered as an intermediate step, primarily because the tailed variant can enter into service with little to no changes in current airline operations, with the tailless design to follow shortly after. Both configurations reduce noise considerably, and the tailless design could be used as a stepping stone for the release and certification of alternate tailless solutions, such as the BWB aircraft.

A comparison of both BD airframes has been completed throughout this investigation, where at a first glance both designs have improved flight performance and a lower overall mass relative to the *NT*-BL aircraft. Improved lift-to-drag ratios above 20 were found for the clean airframes, but with nacelle drag, and the additional growth of aircraft weight as the designs developed, L/D reduced to around 18,

which is still at the high end of current airliners. Airframe noise analysis is required to compare the designs against each other, where presently the BDVT has the edge over the BDSF when considering certification, mass of fuel required for a 4,020 n.mile mission, and cost per seat per n.mile.

Description	***Symbol***	***BDSF***	***BDFT***	***NT-BL***	***units***
Wing Area	S	531.4	397.1	202.4	[m^2]
Wing Span	B	47.9	46.4	40.2	[m]
Wing Standard Mean Chord	$\bar{c}$	11.6	9.53	5.03	[m]
Wing Aspect Ratio	A	4.13	4.87	7.99	-
Thickness-to- Chord Ratio	t/c	0.1013	0.1013	0.115	-
Horizontal Tail Area	S_{HT}	-	141.1	52.6	[m^2]
Vertical Tail Area	S_{VT}	87.1	59.9	31.5	[m^2]
Static Wing Loading	$(Mg/S)_0$	2680	3550	7465	[N/m^2]
Static Thrust Loading	$(T/Mg)_0$	0.314	0.321	0.328	-
Lift-Drag Ratio	L/D	18.3	19.9	15.6	-
Cruise Lift Coefficient	$(c_L)_{cr}$	0.241	0.316	0.438	-
Approach Lift Coefficient	$(c_L)_a$	1.13	1.45	2.01	-
Approach velocity	V_a	57.5	58.4	72.0	[m/s]
Mass of Composite Wing	M_W	25,711	21,967	20,929	[kg]
Fuselage Composite Mass	M_{FUS}	16,007	16,641	15,649	[kg]
Composite Tail + winglets Mass	M_T	2,001	2,063	2,300	[kg]
Mass of part-composite Undercarriage	M_G	5,918	5,912	6,092	[kg]
Propulsion Systems Mass	M_{PP}	11,721	12,321	12,516	[kg]
Mass of All-Electric Systems	M_{Sys}	16,857	16,788	16,613	[kg]
Operational Items Mass	M_{OP}	3,357	3,357	3,357	[kg]
Operational Empty Mass	M_{OEW}	80,829	84,678	77,912	[kg]
Mass of Payload	M_{Pay}	23,760	23,760	23,760	[kg]
Mass of Fuel Required	M_f	41,799	36,530	44,934	[kg]
Total Static Thrust	T_0	447,006	454,131	495,502	[N]
Total Overall Mass	$\boldsymbol{M_0}$	**147,132**	**145,339**	**146,151**	**[kg]**
Cruise Mach Number range	$(M_N)_{cr}$	0.8 – 0.9	0.7 - 0.9	0.8 - 0.85	-
Cruise ceiling	-	38,000	39,500	39,000	[ft]
Longitudinal centre of gravity	$x_{c.g.}$	27.2	26.3	29.1	[m]
Lateral centre of gravity	$y_{c.g.}$	0.00	0.00	0.00	[m]
Vertical centre of gravity	$z_{c.g.}$	-1.35	-0.821	-1.26	[m]
Static margin	K_n	-3.88	4.45	6.20	[%]
DDTE cost	C_{DDTE}	38	39	37	[$US M]
Aircraft Life Cycle Cost	*LCC*	3,571	3,308	4,178	[$US M]
DOC per seat per nautical mile	-	0.0752	0.0690	0.0895	[$/n.mile]

Table 7-1: BDSF and BDVT final comparison of design parameters with *NT*-BL aircraft design

7.5 Novel Airframe design Summary

The optimised design solutions using the parametric analysis results were compared for the BWB, PSJWB, and JW configurations. The three configurations were designed to incorporate winglets, where for the JW concept the winglets were integrated as the attachment points between upper and lower wings, referred to previously as the box-wing. All designs incorporated drooped or variable camber leading edge devices, trailing edge brushes and advanced liners to shield engine noise. The noise shielding effect of the wing on engine noise is far superior on the BWB than on the JW, where the large delta wing plan-form provides an ideal shielding surface. An additional shielding effect is achieved from the vertical fins of the BWB located at either side of the quad engine arrangement, where the PSJBW is similar to the JW and partly reflects engine jet noise down to the ground, partially removing any wing shielding benefits.

The mass of the BWB centre-body and structural layout is difficult to predict, where an analysis was completed to determine the internal structural arrangement of a non-cylindrical pressurised pressure-vessel. The process described within Howe [2], was used to determine an initial estimate for the centre-body mass of the BWB, with the aim to further refine the results. The current mass estimates for the centre-body are provided below in Table 7-2.

The main results provided for this interim analysis stage show that the BWB configurations, both partial-span-tailed and tailless provide substantial improvements in efficiency in excess of 60% of that of the *NT*-BL configuration. The JW concept does not provide any change in L/D because the two equally sized wings which were sized previously within Table 7-2, do not enhance lifting performance, but increase control sizing requirements for flight cases.

Despite significantly increasing the lifting capability for the BWB, the overall vehicle mass increases, along-with the structural volumes, longerons, and heavy frames associated with the design of a non-circular pressure vessel. Additional investigations into aircraft aerodynamics by can be determined by searching literature such as Roman *et al*, Dodier, Gau, Panbagjo *et al.*, Xiao-Peng, and Ericsson [3 – 8 incl.]. Although a large amount of literature is available for the design of the BWB configuration, the time to develop an in-depth detailed study similar to that of the BD concept is beyond the time constraints of this dissertation. The preliminary sizing of the BWB and PSJWB concepts were generated into CAD models so that the design may be further assessed at a later stage.

Description	***Symbol***	***BWB***	***PSJWB***	***JW***	***units***
Wing Area	S	606.7	465.2	131.3	[m^2]
Wing Span	B	53.5	47.6	25.1	[m]
Wing Standard Mean Chord	$\bar{C}$	11.3	9.77	5.23	[m]
Wing Aspect Ratio	A	4.72	4.87	7.99	-
Wing Quarter Chord Sweep	$\Lambda_{¼}$	28.1	31.2	32.3	[deg]
Wing Taper Ratio	λ	0.163	0.169	0.277	-
Thickness-to- Chord Ratio	t/c	0.11	0.111	0.115	-
Wing Apex location	l_{APEX}	14.7	3.08	23.6	[m]
Horizontal Tail Area	S_{HT}	-	3.15	131.3	[m^2]
Vertical Tail Area	S_{VT}	157.5	109.2	36.1	[m^2]
Wing Area Parameter	$S^{-0.1}$	0.527	0.541	0.569	[m^{-2}]
Static Wing Loading	$(Mg/S)_0$	2683	3551	7465	[kg/m^2]
Static Thrust Loading	$(T/Mg)_0$	0.226	0.261	0.328	-
Lift-Drag Ratio	L/D	23.7	24.2	14.9	-
Cruise Lift Coefficient	$(c_L)_{cr}$	0.243	0.322	0.272	-
Mass of Wing	M_W	32,747	28,703	14,069	[kg]
Fuselage/centre-body Mass	M_{FUS}	39,014	39,014	17,454	[kg]
Mass of Tail components + winglets	M_T	3,275	5,166	14,069	[kg]
Mass of Undercarriage	M_G	6,637	6,736	6,161	[kg]
Propulsion Systems Mass	M_{PP}	9,010	10,552	12,122	[kg]
Mass of Systems	M_{Sys}	16,593	16,840	15,402	[kg]
Operational Items Mass	M_{OP}	2,762	2,762	2,762	[kg]
Operational Empty Mass	M_{OEW}	110,038	109,772	82,039	[kg]
Mass of Payload	M_{Pay}	23,760	23,760	23,760	[kg]
Mass of Fuel Required	M_f	32,131	34,863	48,217	[kg]
Available Fuel in Wing Volume	M_{f_a}	275,773	168,395	38,919	[kg]
Total Static Thrust	T_0	368,285	431,294	495,502	[N]
Total Overall Mass	$\boldsymbol{M_0}$	**165,928**	**168,395**	**154,015**	**[kg]**

Table 7-2: BWB and Innovative wing Mass Optimised Results Summary for BWB, PSJWB, and JW

The development of the novel airframe designs requires further investigation to a similar level as the BD concepts, where this would provide a greater comparison of all concepts which would be compared directly to the *NT*-BL aircraft design. The results presented within this dissertation are a means to understand the behaviour of the vehicle at an initial conceptual level. The author has identified that the design of BWB, PSJWB, and JW airframe concepts are design challenges that require more than a semi-empirical approach, where detailed 3-dimensional analysis for flow interactions such as a 3-D flow over a wing-body and flow around wing-tip joins are required. The detailed investigations into these airframe concepts were not possible due to the time constraints, limitation of resources, and broad scope investigated within this research, however, the author will continue to develop means to understand the behaviour of such configurations, and develop alternate

solutions for these airframe challenges within the near future. As a preliminary comparison, the SAI blended wing body results were used as a comparison, where it was found that the mass of the current design is much greater than that published for the SAX-40, implying that the noise would be greater for all flight conditions than previously predicted using the ESDU method.

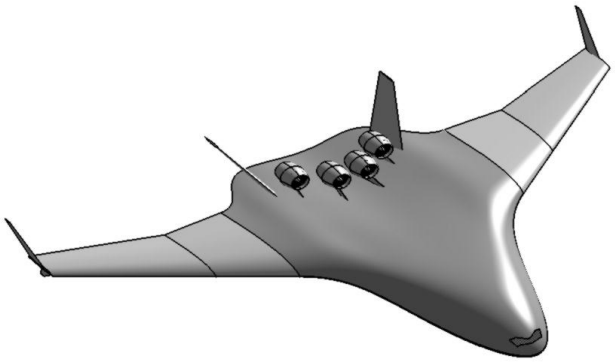

Fig 7-6: Initial design layout of the BWB geometry, sufficiently sized with analysis to conduct a preliminary noise analysis.

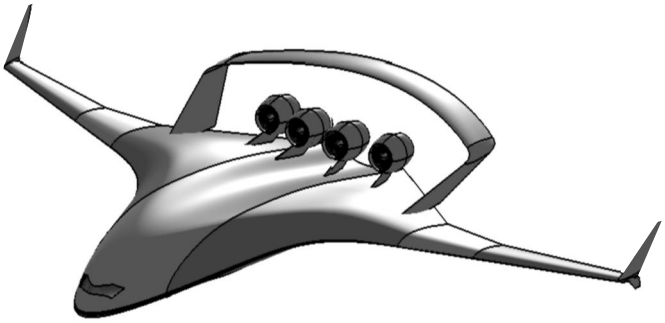

Fig 7-7: Initial design layout of the PSJWB geometry, sufficiently sized with analysis to conduct a preliminary noise analysis.

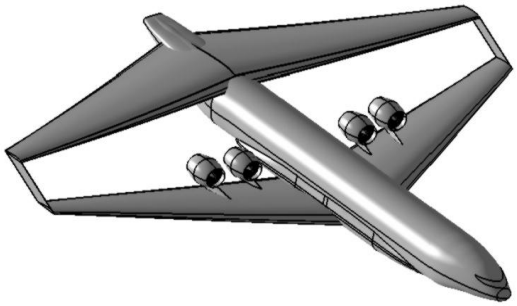

Fig 7-8: Initial design layout of the JW geometry, sufficiently sized with analysis to conduct a preliminary noise analysis.

7.6 Noise Analysis Summary

Airframe approach, take-off, and sideline noise were calculated in accordance with ICAO noise measuring points. The results provided a guide as to how the noise of each configuration compares to each other using a similar design methodology.

Airframe Configuration	*Approach Noise dB(A)*	*Sideline Noise dB(A)*	*Take-off Noise dB(A)*
NT-BL	80.2	76.4	77.9
BDSF	69.4	62.2	67.2
BDVT	64.6	64.2	62.1
BWB	63.1	61.5	59.7
PSJWB	66.9	65.9	65.2
JW	82.8	72.1	80.1

Table 7-3: Final Airframe Noise results corrected for new technologies and for an approach flight path angle of 6degrees with a standard landing threshold (not displaced)

It is estimated that the noise produced by the BWB is higher than should be for the design and is primarily because of the greater mass of the vehicle compared with the other configurations. Further work is required to provide and integrate a detailed structural mass model for the BWB within the current design methodology to investigate noise implications.

The implementation of the noise analysis into the alternate configurations has been completed at a low-fidelity level, and the results provide an interesting outcome, especially for the BD configurations. The main result of this research was to develop a silent airframe design methodology and to investigate how the each configuration compares to one another.

In addition, it was necessary to identify whether the Silent Aircraft Initiative research chose to develop the right configuration for their study. This research confirms that for an airframe geometry point of view, the most silent design of those investigated within this dissertation, is the BWB. The most interesting outcome of this research is to identify that a fairly conventional design, such as the BDVT airframe concept is, or has the potential to be as silent as the BWB. This is providing that the slow and steep design approach can be implemented by airworthiness authorities, and that air-traffic control do not influence the aircraft to approach on a conventional 3 degree flight path angle (FPA).

The design and application of a future BD airliner would enable significant fuel savings of 10-12tonnes per flight when considering the design of a 4,020 nautical mile mission for the above designs. This saving in fuel does not actually mean much in the aviation industry, as the designers have no influence in how the operators use their aircraft, and many aircraft are currently used for the ‘wrong’ or ‘off optimum’ design missions and burn more fuel because of these off-design missions.

The potential to save a large amount of fuel, with the accompanying reduction in fuel costs, emissions, and noise, enables the author to conclude that the BD concept is a viable solution for a short-term quiet airframe configuration that could enter into service by 2020. Alternatively, the optimal solution for the future is the design, development, and integration of the BWB airframe into commercial aviation, but certification, regulations, and application of this high capacity civil airframe would not be possible prior to 2050.

7.6.1 Airframe – Engine Integration

Certain challenges are associated with the location of engines above the wing for the novel airframe configurations, such as installation, maintenance, and passenger safety concerns. Engines were installed on the upper surface for most of the airframe configurations to increase the shielding effect of the wing, and to avoid ingestion of foreign objects on the ground into the engines. The BDSF incorporated a detailed study into semi-embedding the engines at the wing root, which enabled a greater noise benefit, and allowed for an aerodynamically cleaner integration, despite the loss of lift over the wing root region due to the intakes. Engine maintenance provides some challenges for accessibility, inspection and removal/replacement, which would increase cost of ownership, servicing, and repair.

With respect to passenger safety, engines are located at close proximity to the cabin where rotor-bursts would be a concern. In the event of engines fires, the close proximity of each engine could result in a twin engine failure, and provide an obstacle for passengers to egress using the over-wing exits. Another challenge would be to shield engine noise from the passengers, as engine noise is directly in-line with the cabin. The benefits of locating the engines above the wing consider cases such as undercarriage failure and during ditching scenarios, where the loads are impacted by the wing.

Integrating the engines, nacelles, and airframe is an iterative design process, where CFD analysis completed at Cranfield for the BD tailless configuration is described in more depth within Doulgeris [1]. Studies were investigated to further modify the wing design of the BD to avoid the formation of shock waves over the main wing. At present a detailed CFD analysis is required to investigate whether the changes have improved the wing lifting performance and reduced the Mach range over the wing.

Two of the main integration studies investigated semi-embedded engines compared to upper-mounted podded engines. It was found that for greater drag reduction, integration of semi-embedded or fully embedded engines provided the greatest benefits, but with at the expense of complex integration, maintenance, and development costs. Podded engines provide a drag penalty, but have a reduced cost

for development and installation, with similar difficulties with maintenance, and reduced airframe noise shielding.

7.6.2 Total Aircraft Noise Summary

The airframe and engine noise results described in the preceding chapters were combined to determine the overall aircraft noise signature. The embedded engines of the BDSF configuration have little impact on the noise signature of the airframe, as the main drivers pushing the noise up is the large wing area and control surface deflections required during low speed flight cases. The remaining configurations were designed with podded engines above the wing, with the *NT*-BL having conventional under-slung engines.

The final results of the Airframe engine integrated designs provide optimistic solutions for the development of future aircraft concepts. The BDVT and BWB configurations appear the most promising in-terms of overall noise reduction throughout all three take-off sideline and approach noise measuring cases. As a contrast, the joined wing does not significantly reduce the noise and is mainly due to the airframe. The joined wing is a design with two equally sized high aspect ratio wings positioned fore and aft of the centre of gravity, where the two smaller wings generate greater noise compared with the low aspect ratio delta wings. The two intermediate designs are the BDSF, and the PSJWB, where the designs produce significant noise reductions, but are considered potentially un-certifiable. The BDSF requires artificial control in order to maintain stability during flight, and this can be a major design draw-back in terms of certification, similarly the PSJWB is in essence a BWB design, but the partial span close-coupled joined tail raises a few questions in terms of the drag over the wings, and whether the tail will be subject to stall for high incidence cases.

Airframe Configuration	***Approach Noise dB(A)***	***Sideline Noise dB(A)***	***Take-off Noise dB(A)***
NT-BL	78.5	77.2	78.9
BDSF	67.4	65.2	63.2
BDVT	63.6	67.2	59.8
BWB	61.7	64.7	58.7
PSJWB	66.6	66.3	64.2
JW	84.8	74.8	82.1

Table 7-4: Final Aircraft Noise results corrected for new technologies and for an approach flight path angle of 6degrees with a standard landing threshold (not displaced), and integrated with UHBPR engines

7.7 Limitations and Future Work

The research contained within this dissertation was developed to a detailed level for the conventional classification of aircraft, which includes the two BL aircraft and the two BD airframes. The BD

airframe was developed extensively with a detailed study into the ideal cruise altitude and cruise Mach to optimise the design. A detailed cruise optimised investigation into the airfoil design was also completed for the BD, which initiated the study into CFD to investigate alternate engine integration techniques. This detailed analysis assisted with and drove the mass, c.g., and cost models that were developed. An initial study into the alternate wing configurations of the JW, BWB, and PS-JWB configurations was completed, but not optimised using the airfoil design methodology, or for cruise altitude and Mach. This is identified as a key area of concern by the author, as the off-designed models used in the airframe comparisons are conservative design estimates and the airframes may have greater potential once optimised. Further work is therefore required to identify the optimum cruise altitude, Mach, and tailor the airfoils for the novel airframes so that the mass, c.g., and cost models truly reflect the optimised vehicle solutions.

Ideally the comparison of seven airframe family solutions would have provided a broader design space for the current research activity. Time limitations prevented the author from developing three alternate solutions, which included the re-design of the SAI SAX-40 aircraft so that it may be used as a benchmark to compare the BWB design methodology, and to also integrate a canard into the design. An investigation was completed to add an additional tail surface onto the BD, where the BDSF and BDVT were compared in terms of performance, noise, and airworthiness considerations. The conclusion of the study was that having an additional tail did not significantly increase the noise, but did solve stability issues and reduced the drag required to trim the aircraft during most flight conditions. The behaviour of the BD concept and the BWB concept are relatively similar, but the design of an aft tail on a tube-and-wing can not be directly compared with a canard on a BWB, and therefore this study would be an interesting area to explore for further work.

The main challenge in developing a conceptual design methodology for silent and novel airframes was to identify the process to calculate noise. At the on-set of the project the challenge was apparent that noise estimations for airframe components was not a simple task, and by attending an aero-acoustics workshop, the author was exposed to the difficulties associated with accurate acoustic predictions. The decision at the beginning of the project was made to use a low-fidelity ESDU noise prediction tool, combined with correction factors to determine the major airframe component noise. The use of the low fidelity model enabled a fast calculation of the airframe noise, with the aim to integrate a higher fidelity noise model at a later date, which was soon realised to be unachievable, because of time limitations. It is therefore suggested that a higher-fidelity noise analysis method should be implemented on these conceptual designs, using the optimised airframe geometries, and would enable a detailed estimate of the noise of each concept.

It is necessary to identify that there may be errors associated within the semi-empirical methods used within this dissertation. The combination of these errors and the use of the noise prediction tools increase the error margin, where it should be noted that the noise results published within this text are initial guides on how the airframes should behave in terms of performance, noise, cost, stability and control. The results of this dissertation should be used as a guide and not an absolute, where the design process is a stepping-stone that enables future designs to progress given the direction of development within the aviation sector over the foreseeable future.

7.8 Airframe Conclusions

This research has investigated the design of four main concepts, being the BL, BD, BWB, and JW configurations to a parametric design level. A more detailed investigation into the design of the BD has investigated two airframe solutions with alternate engine integrations, and provided a refined detailed design process, which has successfully reached the noise targets produced by the Silent Aircraft Initiative. The 60dB(A) noise target initially set as by the SAI project leaders produced the solution of a BWB airframe with 62dB(A) noise measured outside the airport perimeter. The solutions presented within this dissertation enabled the author to compare alternate airframes and use a low fidelity noise model to achieve three airframe solutions that achieved 62-68dB(A) around the airport perimeter.

The airframes designed were all designed using the slow and steep approach procedures enabling the noise of even the conventional *NT*-BL aircraft to be reduced by over 10dB(A) relative to the *D*-BL aircraft initially designed to validate the design tool. The 6 degree steep approach combined with novel noise reduction technologies such as VCF, TE brushes, and noise liners were implemented into the airframe-engines to achieve a noise reduction of over 12-18dB(A) relative to the *D*-BL aircraft.

The blended wing body design was initially studied as the most silent aircraft by the SAI, and this consideration has now been confirmed by this research, where the BWB is the most promising design, and may even have a greater potential once the design process of this configuration matures. The aim of this study was to compare how efficient and silent the BWB design was compared with alternate airframe solutions, and the conventional airframes we use to date. The quest to find a solution for the most silent solution has been met, and in the process, alternate solutions have been developed which show great potential for near-future concepts that can not only assist in gradually reducing the noise footprint of most airframe geometries, but also assist in the design, development, and understanding of tailless solutions, so that the blended wing body may mature and become a viable concept for future civil airliners.

To conclude, the most promising design or a near-future concept, say for release into service in 2020, which provides reduced noise and potential performance improvements is the BDVT. This design could be designed, tested, and built within the next 10-15 years, and provide a solution for a part-silent, part-green design. Further modifications can be made by integrating the BDVT with swept un-ducted prop fan engines, which would increase cabin noise despite improving performance, shield the prop noise from the ground by using the wing geometry, reduce fuel burn, and provide a greater impact on the evolution of a greener concept. The most silent airframe design is the BWB airframe, which could be a realised solution if the development and certification of the BDVT leads to a new BDSF solution, which in-turn will aid the certification of future tailless aircraft such as the BWB.

To conclude, the research contained within this dissertation has enabled the author to develop a methodology that incorporates a flexibility of creating conceptual designs of alternate conventional and unconventional airframe configurations. The methodology developed enabled the conceptual design of conventional tube-and-wing, innovative wing, and blended wing body designs, which provides the flexibility to calculate, analyse, identify, and compare each configuration to the next to identify the most silent airframe solution. The ideal 'silent' airframe design was identified by combining the airframe design methodology completed by the author with the 'silent' engine technologies developed by Doulgeris [1], enabling the total aircraft noise to be predicted. The final design solution for a future 2050 silent aircraft, which was both environmentally and economically viable in terms of green and cost implications, was the BWB. A short-term quiet airframe solution was also identified for release in 2020, which was the BDVT concept, with a further development of a BDSF in 2030 to enable the certification process of tailless aircraft to mature before release of the BWB in 2050.

7.9 Recommendations for Future work

This research has investigated the conceptual design process for unconventional vehicles, where this is top level analytical analysis to predict the main difference and identify the challenges associated with each alternate airframe design. There are a number of studies that would be beneficial for the development of the alternate concepts mentioned above, and these would also assist in the design, testing, and development of scaled or mock-up models in order to create a feasible product that could be introduced to the market. The following tasks are what the author perceives as being beneficial to the development of the novel airframe design methodology.

- A complete CFD analysis of the BD airframes
- detailed CFD analysis, redesign and optimisation of the BD airfoils used

- detailed CFD analysis and optimisation of the location of alternate engines on the BD configurations.
- Detailed design of the BD concept to enable a like for like comparison of structures weight, performance, stability relative to a baseline similar to a Boeing 767 class of vehicle.
- Detailed assessment of the static and dynamic behaviour of the tailless concepts.
- Lateral control challenges with the tailless vehicles
- Sizing of the control surfaces for the unconventional vehicles and how the critical design and certification issues would be considered.
- Design and development of a flight control system for the tailless vehicles and how their systems architecture would differ from a conventional aircraft.
- Detailed study into the impact of laminar flow from an engine and systems installation point of view on the BD airframe, tailed and tailless designs.
- Study on the safety, reliability, and installation of systems for the BD concepts.
- Technology studies into the design, implementation and technology readiness levels for all new and innovative systems implemented in the designs, such as artificial laminar flow, variable camber flaps, ultra-high bypass ratio engines, etc.

Therefore the activities listed above consider a few areas of interest and would aid the development of any of the novel airframes mentioned to the next level of detail, and would be beneficial to the aviation scientific community. At the same time, these would be great candidates for a research Masters or PhD projects.

References

[1] Doulgeris G., [Doulgeris, 2008], 'Modelling & integration of advanced propulsion systems', *PhD Research Thesis*, March 2008, Cranfield University, UK.

[2] Howe D., [Howe, 2001], 'Blended wing body airframe mass prediction', *College of Aeronautics*, Cranfield University, Cranfield, Bedfordshire, UK.

[3] Roman D., Gilmore R., Wakayama S., [Roman et al, 2003], 'Aerodynamics of high-subsonic blended-wing-body configurations', *41st Aerospace Sciences Meeting and Exhibit*, AIAA 2003-554, January 2003, Reno, Nevada.

[4] Dodier J. A., [Dodier, 2002], 'Investigation of the effect of intakes on the drag performance of blended wing-body aircraft', *College of Aeronautics*, MSc Aerospace Vehicle Design Thesis 2001 -2002, Cranfield University, UK

[5] Gau H., [Gau, 2002], 'Blended wing body winglet design for lateral stability and aerodynamic efficiency', *MSc Research Thesis*, September 2002, Cranfield University, UK.

[6] Pambagjo E. T., Nakahashi K., Obayashi S., Matsushima K., [Pambagjo et al, 2001], 'Aerodynamic design of a medium size blended-wing-body airplane'. *39th AIAA Aerospace Sciences Meeting & Exhibit*, AIAA 2001-0129, January 2001, Reno, Nevada.

[7] Xiao-peng W. Zheng-hong G., [Xiao-peng et al, 1999], 'Aerodynamic configuration design of aircraft using multi-objective genetic algorithm', *Department of Aircraft Engineering, Northwestern Polytechnical University*, 1999, Xi'an, &10072, P.R. China.

[8] Ericsson E. L., [Ericsson, 1997], 'Effect of fuselage geometry on delta wing vortex breakdown', *35th Aerospace Sciences Meeting & Exhibit*, AIAA 97-0746, January 1997, Reno, Nevada.

Thesis References & Bibliography

Authors Publications

Mistry S., Fielding J. P., Smith H., [Mistry *et al.*, 2008], 'Novel design concepts for aircraft with reduced noise and global warming characteristics', *26th Congress of the International Council of Aeronautical Sciences (ICAS)*, September 2008, Alaska.

Rousselot S., Truffi D., Doulgeris G., **Mistry S.**, Pachidis V., Pilidis P., [Rousselot *et al*, 2008], 'Generation of a quasi-3-D map of a half-embedded ultra high bypass ratio turbofan intake of the wing of a broad delta wing airframe', *Turboexpo 2008: Power for Land, Sea and Air*, June 2008, Berlin, Germany.

Mistry S., Doulgeris G., Fielding J. P., **[**Mistry *et al.*, 2008], **'**The broad delta aircraft – part 1: a viable solution for reducing airframe noise', *Cranfield Multi-Strand Conference*, Cranfield University, May 2008, Bedfordshire, UK.

Doulgeris G., **Mistry S.**, Pilidis P., [Doulgeris, *et al.*, 2008], 'The broad delta aircraft – part 2: silent propulsion systems design methodology', *Cranfield Multi-Strand Conference*, Cranfield University, May 2008, Bedfordshire, UK.

Doulgeris G., **Mistry S.**, Fielding J. P., Pilidis P., [Doulgeris *et al.*, 2007], 'Development of a broad delta airframe and propulsion concepts for reducing aircraft noise around airports', *Society of Automotive Engineers (SAE) AeroTech Congress and Exhibition*, SAE-2007-01-3806, September 2007, Los Angeles, US.

Mistry S., Fielding J. P., Smith H., [Mistry *et al.*, 2007], **'**Development of novel aircraft concepts to reduce noise and global warming effects', *7th AIAA Aviation Technology, Integration and Operations Conference (ATIO)*, AIAA-2007-7753, September 2007, Belfast, Ireland.

Mistry S., Fielding J. P., Smith H., [Mistry *et al.*, 2007], **'**Commercial aircraft design for reduced noise and environmental impact', International School of Mathematics, Guido Stamp Acchia, *47th Workshop on Variation Analysis and Aerospace Engineering*, July 2007, Sicily.

Mistry S., Doulgeris G., Fielding J. P., Pilidis P., [Mistry et al., 2007], **'**A future silent and green aircraft', *Milton Keynes Science Festival*, Cranfield University, May 2007, Bedfordshire, UK.

Mistry, S., Doulgeris, G., Fielding, J. P., Pilidis, P., [Mistry *et al.*, 2006], **'**Development of novel airframe concepts and innovative cycle propulsion systems for reduction in aircraft noise', *25th Congress of the International Council of Aeronautical Sciences (ICAS), September 2006*, ICAS-2006-5.7.4, Hamburg, Germany.

Reynolds T. G., **Mistry S.**, [Reynolds & Mistry, 2006], 'Low noise approach operations; steep approaches, low approach speed, displaced landing thresholds, and delayed landing gear deployment', *Silent Aircraft Initiative (SAI) Internal Report*, C-MIT SAI, Cambridge University, August 2006, Cambridge, UK.

References and Bibliography

A

Abreu Dos Santos M., [Abreu Dos Santos, 2006], 'Aircraft engine noise analysis and influence around the airport', *MSc Research Thesis*, September 2006, Cranfield University, UK.

ACARE, [ACARE, 2001], 'European aeronautics: a vision for 2020', *Advisory Council for Aeronautics Research in Europe (ACARE)*, *http://www.acare4europe.org/html/documentation.asp*, January 2001, Belgium.

ADC, [ADC, 2006], 'Technical study of new aircraft concepts for low total operating cost, and environmentally friendly aviation – final report', *Cranfield Aircraft Design Centre (ADC)*, Confidential Report NFP-0512, September 2006, Cranfield University, UK.

Agarwal A., Dowling A. P., [Agarwal & Dowling, 2005], 'Low frequency acoustic shielding of engine noise by the silent aircraft airframe', *43rd AIAA Aerospace Sciences Meeting and Exhibit*, AIAA 2005-2996, January 2005, Reno, Nevada.

AIAA, [AIAA, 2002], 'A collection of the 18th AIAA applied aerodynamics conference technical papers, volume 2', *American Institute of Aeronautics and Astronautics (AIAA)*, August 2000, Denver, Colorado.

AIAA, [AIAA, 2004], 'A collection of the 4th AIAA aviation technology, integration, and operations forum technical papers, volume 1', *American Institute of Aeronautics and Astronautics (AIAA)*, September 2004, Chicago, Illinois.

AIAA/CEAS, [AIAA/CAES, 2004], 'SILENCE(R) significantly lower community exposure to aircraft noise – half way to success'. *10th AIAA/CEAS Aeroacoustics Conference*, 2004, Manchester, UK.

Airbus BWB, [Airbus, 2008], 'Airbus blended wing body concept' *http://www.flug-revue.rotor.com/FRHeft /FRH0101/FR0101e.htm*, last accessed March 2008.

Airbus JW, [Airbus, 2009], Airbus future joint-wing concept, *http://aerospace-technology.blogspot.com /2008/12/airbus-future-airliner-concepts.html*, last accessed March 2009.

Anhalt C., Breitbach E., Sachau D., [Anhalt et al., 2000], 'Realization of shape variable fowler flap for transport aircraft', *2000 World Aviation Conference*, AIAA 2000-01-5572, October 2000, San Diego, California.

Antoine N. E., Kroo I. M, [Antoine & Kroo, 2005], 'Framework for aircraft conceptual design and environmental performance studies', *AIAA Journal*, Vol. 43, No. 10, October 2005.

Antoine N. E., Kroo I. M, [Antoine & Kroo, 2004], 'Aircraft optimisation for minimal environmental impact', *Journal of Aircraft, 2004*, Vol. 41, No. 4, pp. 790-797.

Antoine N. E., Kroo I. M, Wilcox K., Barter G., [Antoine *et al.*, 2004], 'A framework for aircraft conceptual design and environmental performance studies', *10th AIAA/ISSMO Multidisciplinary Analysis and Optimisation Conference*, AIAA 2004-4314, August 2004, Albany, NY.

Association of European Airlines (AEA), [AEA, 1989], 'Short-medium range aircraft – AEA requirements', *AEA*, December 1989, Europe.

Avro, [Avro, 1953], 'The avro atlantic', *Civil Aircraft Design Proposal document*, A.V. Roe & Co Ltd, 1953, Manchester, UK (contact Prof J. P. Fielding, Cranfield University).

Avro, [Avro, 2008], 'Avro vulcan aircraft data', *aerospaceweb.org*, *http://www.aerospaceweb.org /aircraft/ bomber/vulcan/*, last accessed February 2007.

Avro, [Avro GA, 2007], 'Avro vulcan general arrangement diagram', *http://www.raf.mod.uk /historyold/vforcespec.html*, last accessed February 2007.

Avro, [Avro, 2007], 'Avro vulcan Mk2 bomber', *http://ourworld.compuserve.com/homepages/jfalk /vulcan.htm*, last accessed March 2007.

AvWST, [AvWST, 1974], 'ALPA opposes two-segment approaches', *Aviation Week and Space Technology*, May 1974, Vol. 100, No. 6, p. 29.

AvWST, [AvWST, 1974] 'Two-segment approach views concern FAA', *Aviation Week and Space Technology*, August 1974, Vol. 101, No. 6, p. 42.

B

Ballal, D. R., [Ballal, 2003], 'Progress in aero engine technology (1939-2003)', *39th AIAA/ASME/SAE/ASEE Joint Propulsion Conference and Exhibit*, 20-23 July 2003, Huntsville, Alabama.

Bangert H. L., Krivec K. D., Segall N. R., [Bangert *et* al., 1983], 'Effect of nacelle configuration/position on performance of subsonic transport', *NASA Contractor Report 3743*, November 1983, Langley Research Centre, Hampton, Virginia.

Barns J. P., [Barnes, 1997], 'Semi-empirical vortex step method for the lift and induced drag loading of 2D or 3D wings', *1997 World Aviation Congress*, AIAA 975559, October 1997, Anaheim, California.

de **Bellis F.**, [de Bellis, 2007], 'Variable fan nozzle area engine cycle design, optimisation, and 3D-CFD airframe integration study for a silent aircraft', *MSc Research Thesis*, September 2007, Cranfield University, UK.

Berglund B., Lindvall T., Schwela D. H., [Berglund et al., 1999], 'Guidelines for community noise', *World Health Organisation (WHO)*, April 1999, London.

Berry P., [Berry, 2000], 'Sizing the landing gear in the conceptual design phase', *AIAA World Aviation Conference*, AIAA 2000-01-5601, October 2000, San Diego, CA.

de la Rosa **Blanco E.**, Hall C. A., Crichton D., [de la Rosa Blanco et al., 2007], 'Challenges in the silent aircraft engine design', *45th AIAA Aerospace Sciences Meeting and Exhibit*, AIAA 2007-454, January 2007, Reno, Nevada.

Boeing, [Boeing, 2009], 'Boeing X-48B blended wing body UAV test vehicle', *The Boeing Company*, *http://www.boeing.com/news/releases /2006/q4/061027b_nr.html*, Boeing X-48B Press Release, last accessed February 2009.

Boeing, [Boeing BWB, 2008], 'Boeing blended wing body concept', *The Boeing Company*, *http://www.promotex.ca/articles/cawthon/2006/images /2006-05-15-B.jpg*, last accessed March 2008.

Boeing, [Boeing BWB 3V, 2008], 'Boeing blended wing body 3-view drawing', *The Boeing Company*, *http://leehamnews.wordpress.com /2009/05/31/bwb-a-big-challenge/*, last accessed March 2008.

Boeing, [Boeing, 2007], 'Boeing internal memo (confidential)', SAI member access only: data for noise comparison and validation, *The Boeing Company*, January 2007.

Boeing, [Boeing, 1967], 'Study of aircraft in short haul transportation systems: final report', *The Boeing Company*, August 1967, US. CA.

Burns J. W., [Burns, 1994], 'Aircraft cost estimation methodology and value of a pound derivation for preliminary design development applications', *53rd Annual Conference of Society of Allied Weight Engineers, Inc. (SAWE)*, Paper No. 2228, May 1994, Long Beach, CA.

Bowers M. P., [Bowers, 1984], 'Unconventional aircraft', *Airlife Publishing Limited*, 1st edition, 1984, Shrewsbury, UK.

Brown B. R., Whitehead B. L., [Brown et al., 2001], 'Powered glider design for proposed palomar international airport carlsbad', *AIAA Subcommittee on Aircraft Design*, June 2001, Borrego Springs, California.

Brown B. R., Swihart M. J., [Brown, 1998], 'Design solutions for 50% reduction in per-passenger fuel consumption of long range commercial aircraft', *1998 Conference on the Atmospheric Effects of Aviation*, April 1998, Virginia Beach Resort Hotel and Conference Centre Virginia Beach, Virginia.

C

CAA website, [CAA, 2009] 'Classification of LDEN' *http://www.caa.co.uk/default.aspx?catid =68&pagetype =70&gid=69&faqid=403*, last accessed March 2009.

Catalano F. M., Ceron-Munoz H. D., [Catalano, 2005], 'Experimental analysis of aerodynamics characteristics of adaptive multi-winglets', *43rd AIAA Aerospace Sciences Meeting and Exhibit*, AIAA 2005-1231, January 2005, Reno, Nevada.

Caves R. E., Rhodes D. P., [Caves, 1995], 'Steeper approaches: a contribution to alleviating airport environmental and physical capacity constraints', *1st AIAA Aircraft Engineering Technology and Operations Congress*, AIAA 1995-3907. September, 1995, Los Angeles, CA.

Centennial of flight website, [CoF, 2007], *http://www.centennialofflight .gov/essay/evolutionof technology/noise/tech25.htm*, last accessed August 2007.

Chudoba B., Cook M. V., [Chudoba, 2003], 'Identification of design-constraining flight conditions for conceptual sizing of aircraft control effectors', *AIAA Atmospheric Flight Mechanics Conference and Exhibit*, AIAA 2003-5386, August 2003, Austin, Texas.

Coppinger R., [Coppinger, 2004], 'Noise reduction', *Flight International (FI) subscription*, *www.flightinternational.com*, June 2004.

Cranfield, [Cranfield, 1999] 'The turbomatch scheme; for aero/industrial gas turbine engine design point/off-design performance calculation', *Cranfield User Manual*, October 1999, Cranfield University, UK.

Crichton D., de la Rosa Blanco E., Law T. R., [Crichton *et al*, 2007], 'Design and operation for ultra low noise take-off', *45th AIAA Aerospace Sciences Meeting and Exhibit*, AIAA 2007-456, January 2007, Reno, Nevada.

Currey N. S., [Currey, 1988], 'Aircraft landing gear design; principals and practices', *AIAA Educations Series*, 1988, Washington, US.

D

DAC, [DAC, 1971], 'Airplane characteristics for airport planning', *Douglas Aircraft Company (DAC)*, DAC-67803, December 1971, Long Beach, California.

Dalton W. N. III, [Dalton, 2003], 'Ultra high bypass ratio engine noise study', *National Aeronautics and Space Administration (NASA)*, NASA/CR-2003-212523, November 2003, Allison EDR 16083, Langley Research Center, Hampton, Virginia.

Davies S. D., [Davies, 1969], 'The history of the avro vulcan', *The 14th Chadwick Memorial Lecture*, RAeS Lecture, March 1969, Institute of Science and Technology, Manchester, UK.

Denery D. G., Bourquin K. R., Whie K. C., Drinkwater III F. J., [Denery *et al.*, 1973], 'Flight evaluation of three-dimensional area navigation for jet transport noise abatement', *Journal of Aircraft (JoA)*, 1973, Vol. 10, No. 4, pp. 226-231.

Denisov E. V., Bolsunovsky L. A., Buzoverya P. N., Gurevich I., B., Shkadov M.L., [Denisov et al., 1996], 'Conceptual design for passenger airplane of very large passenger capacity in flying wing layout', *AIAA/ICAS 1996*, ICAS – 96-4.6.1, Sorrento, Italy.

DfT, [DfT, 2003], 'The future of air transport – white paper and the civil aviation bill', *Department for Transport*, CM-6046, www.dft.gov.uk/aviation/whitepaper, December 2003, UK Government.

Diedrich A., Hileman J. I, Tan D., Willcox K., Spakovszky Z. S., [Diedrich *et al.*, 2006], 'Multidisciplinary design and optimisation of the silent aircraft', *44th AIAA Aerospace Sciences Meeting and Exhibit*, AIAA 2006-1323, January 2006, Reno, Nevada.

Dodier J. A., [Dodier, 2002], 'Investigation of the effect of intakes on the drag performance of blended wing-body aircraft', *College of Aeronautics*, MSc Aerospace Vehicle Design Thesis 2001 -2002, Cranfield University, UK.

Dodier J. A., [Dodier, 2002], 'Investigation of the effect of intakes on the drag performance of blended wing-body aircraft', *College of Aeronautics*, MSc Aerospace Vehicle Design Thesis 2001 -2002, Cranfield University, UK

Doulgeris G., [Doulgeris, 2008], 'Modelling & integration of advanced propulsion systems', *PhD Research Thesis*, March 2008, Cranfield University, UK.

Dowling A. P., Ffowcs Williams J. E., [Dowling, 1983], 'Sound and sources of sound', *Ellis Horwood Publishers Limited*, 1983,UK.

Drela M., [Drela, 2000], 'X-FOIL subsonic development system', *Massachusetts Institute of Technology (MIT)*, December 2000, Boston, http://web.mit.edu/drela/Public/web/xfoil/, last accessed June 2006.

E

EASA, [EASA, 2006], 'Certification specifications for large aeroplanes: CS-25', *European Aviation Safety Agency (EASA)*, October 2006, Amendment 2, EU.

Elson B. M., [Elson, 1973], 'Two-segment approach method studies', *Aviation Week & Space Technology* (AvWST), February 2003, pp 47-53.

Ericsson E. L., [Ericsson, 1997], 'Effect of fuselage geometry on delta wing vortex breakdown', *35th Aerospace Sciences Meeting & Exhibit*, AIAA 97-0746, January 1997, Reno, Nevada.

ESDU 90023, [ESDU, 2003], 'Airframe noise prediction', Engineering Sciences Data Unit (ESDU) data Item 90023, June 2003, Amendment C, Endorsed by The Royal Aeronautical Society (RAeS).

ESDU 01004, [ESDU, 2001], 'Computer-based estimation procedure for co-axial jet noise, including far-field subsonic jet mixing noise database for stationary, coplanar conical nozzles', *Engineering Sciences Data Unit (ESDU) data Item 01004*, May 2001.

ESDU 00012, [ESDU, 2000], 'The acoustic attenuation of absorbent linings in cylindrical flow ducts, Engineering Sciences Data Unit (ESDU) data Item 00012, 2000.

ESDU 94035, [ESDU, 1994], 'The correction of measured noise spectra for the effects of ground reflection', Engineering Sciences Data Unit (ESDU) data Item 94035, November 1994.

ESDU 94036, [ESDU, 1994], 'The prediction of sound attenuation as a result of propagation close to the ground', Engineering Sciences Data Unit (ESDU) data Item 94036, November 1994.

ESDU 81306, [ESDU, 1989], 'The calculation of overground sound propagation in the presence of wind and temperature gradients', Engineering Sciences Data Unit (ESDU) data Item 81306, October 1989, Amendment A and B, July 1992.

ESDU 98008, [ESDU, 1988], 'Prediction of noise generated by fans and compressors in turbojet and turbofan engines', *Engineering Sciences Data Unit (ESDU) data Item 98008*, April 1988.

ESDU 81305, [ESDU, 1981], 'An introduction to aircraft noise lateral attenuation', Engineering Sciences Data Unit (ESDU) data Item 81305, November 1994.

ESDU 79011, [ESDU, 1979], 'Estimation of noise shielding by barriers', Engineering Sciences Data Unit (ESDU) data Item 79011, September 1979.

ESDU 66017, [ESDU, 1978], 'Combination of noise levels in dB, Engineering Sciences Data Unit (ESDU) data Item 66017, Amendment A, 1978.

ESDU 76011, [ESDU, 1976], 'First approximately to take-off field length of multi-engined transport aeroplanes', Engineering Sciences Data Unit (ESDU) data Item 76011, May 1976, Amendment A, May 1985.

ESDU RG 2/1, [ESDU, 1962], 'Reduction of take-off and landing measurements to standard conditions', *Engineering Sciences Data Unit (ESDU) data Item RG 2/1*, November 1981.

Eshelby E. M., [Eshelby, 2000], 'Aircraft performance theory and practice', *Published by Arnold publishers*, 2000.

F

FAA, [FAA, 2002], 'Federal aviation regulations (FAR) noise standards; aircraft type and airworthiness certification, estimated maximum A-weighted sound levels', measured in accordance with Part 36 Appendix C Procedures, *Federal Aviation Administration (FAA)*, FAR 36-3H, April, 2002.

FAA, [FAA, 2002], 'FAR noise standards; aircraft type and airworthiness certification, Part 36, *Federal Aviation Administration (FAA), web link for majority of standards located at:* *http://www.flightsimaviation.com/data/FARS/part36.html*, website last accessed March 2009.

FI, [FI, 1983], 'Certification of the BAe 146', *Flight international (FI) magazine*, 12 February 1983, page 54.

Fielding J. P., [Fielding, 2000], 'Design investigation of variable-camber flaps for high-subsonic airliners, *24th Congress of the International Council of Aeronautical Sciences (ICAS)*, ICAS2000-0124, September 2000, Harrogate, WA.

Fielding J. P., [Fielding, 1999], 'Introduction to aircraft design', *Cranfield College of Aeronautics*, January 1999, Bedfordshire, UK.

Fielding J. P., [Fielding, 1983], 'Advanced 150 passenger short – range aircraft a-82', *Cranfield College of Aeronautics*, Doc Id: Des 8200, January 1983, Bedfordshire, UK.

Fujino M., Kawamura Y., [Fujino, 2003], 'Wave-drag characteristics of an over-the-wing nacelle business-jet configuration', *Journal Of Aircraft Vol. 4, No. 6, Pages 1177-1184*, December 2003, Honda R&D Americas, Inc., North Carolina.

Fujino M., Kawamura Y., [Fujino, 2003], 'Wave-drag characteristics of an over-the-wing nacelle business-jet configuration', *41st Aerospace Sciences Meeting and Exhibit*, AIAA 2003-933, January 2003, Reno, Nevada.

Filippone A., [Fillippone, 2007], 'Wings for all speeds: wing tip devices, 1999-2004', http://www.aerodyn.org/Drag/tipdevices.html , last accessed 4th September 2007.

Fraport, [Fraport, 2006], 'Research and innovation management: HALS / DTOP – high approach landing system/dual threshold operation', http://www.fraport.com/cms/company/dok/81/81482.halsdtop @en.htm, last accessed June 2006.

Fujino M., Kawamura Y., [Fujino, 2003], 'Wave-drag characteristics of an over-the-wing nacelle business-jet configuration', *Journal Of Aircraft Vol. 4, No. 6*, Pages 1177-1184, December 2003, Honda R&D Americas, Inc., North Carolina.

Fujino M., Kawamura Y., [Fujino, 2003], 'Wave-drag characteristics of an over-the-wing nacelle business-jet configuration', *41st Aerospace Sciences Meeting and Exhibit*, AIAA 2003-933, January 2003, Reno, Nevada.

G

Gallman, J., Kroo, I., [Gallman, 1993], 'Preliminary design optimisation of joined wing aircraft', *Journal of Aircraft*, November 1993.

Gau H., [Gau, 2002], 'Blended wing body winglet design for lateral stability and aerodynamic efficiency', *MSc Research Thesis*, September 2002, Cranfield University, UK.

Gern H. F., Ko A., Sulaeman E ., Mason H. W., Kapania R., Grossman B., Haftka T. R., [Gern et al., 2000], 'Passive load alleviation in the design of a strut-braced wing transonic transport', *8th AIAA/USA/NASA/ISSMO Symposium on Multidisciplinary Analysis and Optimization*, AIAA2000-4826, September 2000, Long Beach, California.

Gern H. F., Ko A., .Mason H. W., Kapania R., Grossman B., Haftka T. R., [Gern et al., 2000], 'Transport weight reduction through MDO: the strut-braced wing transonic transport', *35th AIAA Fluid Dynamics Conference and Exhibit*, AIAA2005-4667, June 2005, Ontario, Canada.

Gern H. F., Gundlach F.J., Ko A., Gundlach F.J., Mason H. W., Kapania R., Grossman B., Haftka T. R., Naghshineh-Pour A., Grossman B., [Gern et al., 1999], 'Multidisciplinary design optimization of a transonic commercial transport with a strut-braced wing', *1999 World Aviation Conference*, 1999-01-5621 , October 1999, San Francisco, California.

Gliebe P. R., Janardan B. A., [Gliebe, Janardan, 2003], 'Ultra-high bypass engine aeroacoustic study', *National Aeronautics and Space Administration (NASA)*, NASA-2003-212525, October 2003, Langley Research Center, Hampton, Virginia.

Grasmeyer M. J., Naghshineh-Pour A., Tetrault A-. P., Grossman B., Haftka T. R., Kapina K. R., Mason m H. W., Schetz A. J., [Grasmeyer et al., 1998], 'Mulitdisciplinary design optimization of a strut-braced wing aircraft with tip-mounted engines', MAD 98-01-01, *Virginia Polytechnic Institute and State University*, April 1998, Blacksburg, Virginia, USA.

Grasmeyer M. J., [Grasmeyer, 1998], 'Truss-braced wing code description and user's manual', Department of Aerospace and Ocean Engineering, *Virginia Polytechnic Institute and State University*, April 1998, Blacksburg, Virginia, USA.

Grasmeyer M. J., [Grasmeyer, 1998], 'Multidisciplinary design optimization of a strut-braced wing aircraft', Department of Aerospace and Ocean Engineering, *Virginia Polytechnic Institute and State University*, April 1998, Blacksburg, Virginia, USA.

Grasmeyer M. J., [Grasmeyer, 1998], 'Multidisciplinary design optimization of a transonic strut-braced wing aircraft', Department of Aerospace and Ocean Engineering, *Virginia Polytechnic Institute and State University*, April 1998, Blacksburg, Virginia, USA.

Grasmeyer M. J., [Grasmeyer, 1998], 'Stability and control derivative estimation and engine-out analysis', VPI-AOE-245, *Virginia Polytechnic Institute and State University*, January 1998, Blacksburg, Virginia, USA.

Green J., [Green, 2001], 'Air travel – greener by design: the technology challenge', *Royal Aeronautical Society (RAeS)*, 2001, UK.

Guillon E., [Guillon, 1997], 'Blended wing body – conceptual design', *College of Aeronautics*, MSC Thesis 1997 -1998, Cranfield University, UK.

Gundlach F. J., Tetrault P-A., Gern F., Nagshineh-pour A., Ko A., Schetz A. J., Mason H. W., Kapania R., Grossman B., Haftka T. R., [Gundlach et al., 2000], 'Multidisciplinary Design Optimization of a Strut-Braced Wing Transonic Transport', *38th Aerospace Sciences Meeting & Exhibit*, AIAA2000-0420, January 2000, Reno, Nevada.

Gunston B., [Gunston, 1977], 'Modern Military Aircraft: A Technical directory of today's major warplanes', *Salamander Books Limited*, 1977, London, UK.

Guynn D. M., Olson D. Erik., [Guynn et al., 2002], 'Evaluation of an aircraft concept with over-wing, hydrogen-fueled engines for reduced noise and emissions', *National Aeronautics and Space Administration (NASA)*, NASA/TM-2002211926, September 2002, Hampton, Virginia.

H

Hall C. A., Crichton D., [Hall, 2006], 'Engine design studies for a silent aircraft', *ASME Turbo Expo*, GT2006-90559, 2006, Barcelona, Spain.

Hall C. A., Crichton D., [Hall, 2005], 'Engine and installation configurations for a silent aircraft', *17th International Symposium on Air Breathing Engines*, ISABE-2005-1164, September 2005, Munich, Germany.

Harris C. D., [Harris, 1990], 'NASA supercritical airfoils; a matrix of family-related airfoils', *National Aeronautics and Space Administration*, Technical Paper 2969, March 1990, Langley Research Centre, Hampton, Virginia.

Hedlund-Astrom A., Luttropp C., [Hedlund-Astrom, 2006], 'Metal inserts and hazardous content in light weight composite structures in the context of recycling', *13th CIRP International Conference on Life Cycle Engineering (LCE)*, May 2006, Belgium.

Herr M., [Herr, 2007], 'Experimental study on noise reduction through trailing edge brushes', *notes on Numerical Fluid Dynamics and Multidisciplinary Design*, 2007, Springer, Berlin.

Herr M., Dobrzynski W., [Herr, 2004], 'Experimental investigations in low noise trailing edge design', *10th AIAAIRCRAFTEAS Aeroacoustics Conference*, AIAA-2004-2804, 2004, Manchester, UK.

Hileman J. I., Spakovszky Z. S., Drela M., Sargeant M. A., [Hileman et al., 2007], 'Airframe design for 'silent aircraft'', *45th AIAA Aerospace Sciences Meeting and Exhibit*, AIAA 2007-453, January 2007, Reno, Nevada.

Hileman J. I.., Spakovszky Z. S., Drela M. Sargeant M. A., [Hileman *et al.*, 2006], 'Aerodynamic and aeroacoustic three-dimensional design for a "silent" aircraft', *44th AIAA Aerospace Sciences Meeting and Exhibit*, AIAA 2006-241, January 2006, Reno, Nevada.

Hileman J. I., Spakovszky Z. S., Drela M. Sargeant M. A., [Hileman *et al.*, 2006], 'Multidisciplinary design and optimisation of the silent aircraft', *44th AIAA Aerospace Sciences Meeting and Exhibit*, January 2006, Reno, Nevada.

Hoerner S. F., Borst S. F., [Hoerner & Borst, 1975], 'Fluid-dynamic lift: practical information on aerodynamic and hydrodynamic lift', *Hoerner*, 1975, New Jersey.

Hoerner S. F., [Hoerner, 1965], 'Fluid-dynamic drag: practical information on aerodynamic drag and hydrodynamic resistance', *Hoerner*, 1965, New Jersey.

Honda, [Honda, 2007], 'HA-420 business jet', *Honda HA-420 Business Jet homepage*, http://hondajet.honda.com/default.aspx?bhcp=1, last accessed 7th December 2007.

Hosder S., Schetz A. J., Grossman B., Mason H, W., [Hosder et al., 2004], 'Airframe noise modelling appropriate for multidisciplinary design and optimization', *42st Aerospace Science Meeting and Exhibit*, AIAA 2004-0698, January 2004, Reno, Nevada.

Howe D., [Howe, 2001], 'Blended wing body airframe mass prediction', *College of Aeronautics*, Cranfield University, Cranfield, Bedfordshire, UK.

Howe D., [Howe, 2000], 'Aircraft conceptual design synthesis', *Professional Engineering Publishing Ltd.*, 2000, Wiltshire, UK.

I

ICAO, [ICAO, 2009] 'International civil aviation organization (ICAO)', *ICAO*, http://www.icao.int/, website last accessed March 2009.

ICAO, [ICAO, 2007], 'ICAO environmental report 2007, part 2 aircraft noise', *Environmental Unit of ICAO*, Montreal, 2007.

ICAO, [ICAO, 2006], 'ICAO noise certification standards: noise levels for transport category and jet airplanes under §36.103', *ICAO, Part 36 Appendix B and Chapter 4, Annex 16, Environmental Protection*, January 2006.

J

Jenkinson L. R., Simpkin P., Rhodes D., [Jenkinson et al., 1999], 'Civil jet aircraft design', electronic data: http://www.bh.com/companions/034074152X/appendices/default.htm, *Arnold Publishing*, 1999, London, UK.

Jenkinson L. R., Rhodes D., [Jenkinson, 1993], 'Beyond future large transport aircraft', *AIAA Aircraft Design, Systems and Operations Meeting*, AIAA 93-4791, August 1993, Monterey, California, USA.

Jepson J. K., Gopalarathnam A., [Jepson, 2003], 'Inverse airfoil design via specification of the boundary-layer transition curve', *41st Aerospace Science Meeting and Exhibit*, AIAA 2003-212, January 2003, Reno, Nevada.

Joiner A. C., [Joiner . 1997], 'A critical analysis of the proposals and impact of future aircraft noise regulation', *College of Aeronautics*, MSC Thesis 1996 -1997,Cranfield University. UK

K

Katz J., Plotkin A., [Katz, 2001], 'Low-speed aerodynamics', *Cambridge Aerospace Series*, 2nd Edition, Cambridge University Press, 2001, UK.

Keen B. E., Mason H. W., [Keen et al., 2005], 'A conceptual design methodology for predicting the aerodynamics of upper surface blowing on airfoils and wings', *23rd AIAA Applied Aerodynamics Conference*, AIAA 2005-5216, June2005, Toronto, Ontario, Canada.

Ko A. Y. Y., [Ko, 2000], 'The role of constraints and vehicle concepts in transport design: a comparison of cantilever and strut-braced wing airplane concepts', Department of Aerospace and Ocean Engineering, *Virginia Polytechnic Institute and State University*, April 1998,Blacksburg, Virginia, USA.

Ko A. Y. Y., [Ko, 2003], 'The multidisciplinary design optimization of a distributed propulsion blended-wing-body aircraft', Department of Aerospace and Ocean Engineering, *Virginia Polytechnic Institute and State University*, April 2003, Blacksburg, Virginia, USA.

Kors E., [Kors, 2004], 'Significantly lower community exposure to aircraft noise – halfway towards success', *10th AIAA/CEAS Aeroacoustics Conference*, Guest speaker, March 2004, Manchester, UK.

Kraft R. E., Janardan B. A., Gliebe P. R. [Kraft et al., 1997], 'Estimate of aircraft flyover noise reduction by application of active noise control to engine fan tones', *35th Aerospace Sciences Meeting & Exhibit*, AIAA 97-0489, January 1997, Reno, Nevada.

Kroo I., [Kroo, 1984], 'A general approach to multiple lifting surface design and analysis', *AIAA/AHS/ASEE Aircraft Design Systems and Operating Meeting*, AIAA-84-2507, October 1984, San Diego, California.

Kubrynski K., [Kubrynski, 2003], 'Wing-winglet design methodology for low speed applications', *41st Aerospace Sciences Meeting and Exhibit*, AIAA 2003-215, January 2003, Reno, Nevada.

L

Laban M., [Laban, 2001], 'AIRcraft drag and thrust analysis (AIRDATA); publishable synthesis report', *National Aerospace Laboratory NLR*, NLR-TP-2000-473, June 2001, Netherlands.

Lajux V., [Lajux, 2007], 'Methodology for the Design of Leading Edge Devices Applied to Variable Camber', *PhD Research Thesis*, March 2007, Cranfield University, UK.

Lajux V., Fielding J. P., [Lajux, 2005], 'Development of a variable camber leading edge device design methodology', *5th Aviation, Technology, Integration, and Operations Conference (ATIO)*, AIAA-2005-7356, September 2005, Virginia.

Law T. R., Dowling A. P., [Law, 2006], 'Optimisation of traditional and blown liners for a silent aircraft', *12th AIAA/CEAS Aeroacoustics Conference*, 8-10th May 2006, AIAA-2006-252593, Cambridge, MA**.**

Leiffson T. L., Mason H. W., [Leifsson, 2003], 'The blended wing body aircraft', *Polytechnic Institute and State University*, 2003, Blacksburg, Virginia, USA

Liebeck, R., [Liebeck, 2002], 'Design of the blended-wing-body subsonic transport', The Boeing Company, *40th AIAA Aerospace Sciences Meeting & Exhibit*, AIAA-2002-0002, 14th–17th January 2002, Reno, Nevada.

Lockheed GT, [Lockheed, 2009], Lockheed Global Tanker, *http://www.globalsecurity.org/military /systems /aircraft/images/nsa3.jpg*, last accessed February 2009.

Lockheed SBW, [Lockheed, 2008], Lockheed Strut-braced Wing Transport concept, *http://www. aeronautics.nasa.gov/docs/ar99/obj8.html*, last accessed December 2008.

Lockheed TBW, [Lockheed, 2004], 'Lockheed patent for a tail-braced wing aircraft and configurations for achieving long supersonic range and low sonic boom', *http://www.freepatentsonline.com /6729577.html*, last accessed March 2008.

Lockheed QSST, [Lockheed, 2003], 'lockheed martin quiet supersonic transport (qsst) private jet aircraft history', *http://www.aviationexplorer.com/Quiet_Supersonic_Transport_(QSST)_Private_ Jet.html*, last accessed February 2008.

Lighthill M. J., [Lighthill, 1952], 'On sound generated aerodynamically (part 1: general theory)', *Proceedings of the Royal Society of London*, Series A: Mathematical and Physical Sciences, vol.211, pp 564-587, 1952.

Lin W. F., Chen A. W., Tinoco E. N., [Lin et al., 1990], '3D transonic nacelle and winglet design', *8th Applied Aerodynamics Conference*, AIAA-90-3064-CP, August 1990, Portland, Oregon.

Lockard P. D., Lilley M. G., [Lockard, 2004], 'The airframe noise reduction challenge', *National Aeronautics and Space Administration (NASA)*, NASA/TM-2004-213013, April 2004, Langley Research Center, Hampton, Virginia.

Low J. K. C., [Low, 1994], 'Ultra high bypass ratio jet noise', *National Aeronautics and Space Administration (NASA)*, NASA CR-195394, 1994, Langley Research Center, Hampton, Virginia.

Lundbladh A., Sjunnesson A., [Lundbladh, 2003], *Heat Exchanger Weight and Efficiency Impact on Jet Engine Transport Applications*, ISABE-2003-1122, 2003.

Lui Y., [Lui, 2007], 'Experimental study of surface roughness noise, *45th AIAA Aerospace Sciences Meeting and Exhibit*, AIAA 2007-3449, January 2007, Reno, Nevada.

M

de **Mattos B. S.**, Macedo A. P., da Silva Filho D. H., [de Mattos *et al.*, 2003], 'Considerations about winglet designs', *21st Applied Aerodynamics Conference*, AIAA 2003-3502, June 2003, Orlando, Florida.

Mavis D. [Mavis, 1998], 'Formulation of a stochastic approach to aircraft design', School of Aerospace Engineering, *Georgia Institute of Technology*, 1998, Atlanta.

Maughmer M. D., Swan T. S., Willits S. M., [Maughmer *et al.*, 2001], 'The design and testing of a winglet airfoil for low-speed aircraft', *19th Applied Aerodynamics Conference*, AIAA 2001-2478, June 2001, Anaheim, California.

McCormick B. W., [McCormick, 1979], 'Aerodynamics, aeronautics, and flight mechanics', *John Wiley & Sons inc.*, 1979, Pennsylvania State University, Canada.

Medicina, D., [Medicina, 2006], 'Silent aircraft initiative: tip turbine driven fan integration on wing top using 3D-CFD', *MSc Research Thesis*, September 2006, Cranfield University, UK.

Melin T., [Melin, 2000], 'A vortex lattice MATLAB implementation for linear aerodynamic wing applications', Master Thesis, Department of Aeronautics, *Royal Institute of Technology (KTH)*, December 2000, Stockholm, Sweden.

Mistry, S., Doulgeris, G., Fielding, J. P., Pilidis, P., [Mistry *et al.*, 2006], **'**Development of novel airframe concepts and innovative cycle propulsion systems for reduction in aircraft noise', *25th Congress of the International Council of Aeronautical Sciences (ICAS)*, September 2006, ICAS-2006-5.7.4, Hamburg, Germany.

Mukhopadhyay V., [Mukhopadhyay, 2005], 'Blended-wing-body(BWB) fuselage structural design for weight reduction', *46th AIAA/ASME/ASCE/AHS/ASC Structures*, Structural Dynamics and Materials Conference, AIAA 2005-2349, April 2005, Austin, Texas.

Mukhopadhyay V., Sobieszczanski-Sobieski J., Kosaka I. Quinn G., Charpentier C., [Mukhopadhyay et al., 2002], 'Analysis design and optimiszation of non-cylindrical fuselage for blended-wing- body (BWB) vehicle', *9th AIAA/ISSMO Symposium on Multidisciplinary Analysis and Optimization*, AIAA 2002-5664, September 2002, Atlanta, Georgia.

N

Nangia, R. K., Palmer, M. E., [Nangia, 2003], 'Unconventional high aspect ratio joined-wing aircraft incorporating laminar flow', *AIAA Applied Aerodynamics Meeting & Exhibit*, AIAA-2003-3297, 23-26 June 2003, Orlando.

NASA, [NASA, 2009], NASA X-48B fact sheet, http://www.nasa.gov/centers/dryden/research/X-48B/index.html, last accessed March 2009.

Nettis L., [Nettis, 2007], 'The constant volume combustor: cycle optimisation and engine-airframe integration study for a silent aircraft', *MSc Research Thesis*, September 2007, Cranfield University, UK.

Nicolai M. L., [Nicolai, 1975], 'Fundamentals of aircraft design', June 1975, Aerospace Engineering, *University of Dayton*, 1975, Dayton, Ohio.

Northrop, [Northrop, 2009], Northrop XB-35, http://puolue.proboards.com/index.cgi?action=display&board=Asevoimat&thread=116&page=2, last accessed February 2009.

Northrop, [Northrop, 2008], Northrop XB-35 Historical Aircraft website, http://www.Airbornegrafix.com/HistoricAircraft/FlyingWings/XB35.htm, last accessed August 2008.

P

Pamadi B. N., [Pamadi, 1998], 'Performance, stability, dynamics and control of airplanes', *AIAA Education Series*, NASA Langley Research Centre, 1998, Hampton, Virginia.

Pambagjo E. T., Nakahashi K., Obayashi S., Matsushima K., [Pambagjo et al., 2001], 'Aerodynamic design of a medium size blended-wing-body airplane'. *39th AIAA Aerospace Sciences Meeting & Exhibit*, AIAA 2001-0129, January 2001, Reno, Nevada.

Philpot G. M., [Philpot, 2000], 'Future challenges for powerplant aerodynamic integration in combat aircraft', *Defence Evaluation and Research Agency (DERA)*, 2000, Farnborough, UK.

Plas A. P., Madani V., Sargeant M. A., Greitzer E. M., Hall C. A., Hynes T. P., [Plas et. al., 2007], 'Performance of a boundary layer ingesting propulsion system', *45th AIAA Aerospace Sciences Meeting and Exhibit*, AIAA 2007-0450, January 2007, Reno, Nevada.

Porter D. N., Rhodes P D, [Porter, 2006], 'Aircraft noise in london: past, present and future', *Environment Research and Consultancy Department*, CAA, London, June 2006.

Powell C. A., Preisser J. S., [Powell & Preisser, 2000], 'NASA's subsonic jet transport noise reduction research', *NASA Langley Research Center*, Hampton, Virginia.

Prasetyo E., [Prasetyo, 2005], 'A flow control for advanced technology regional aircraft (ATRA) using a variable camber wing with hybrid laminar flow control', *Proceedings of the 3rd IASME/WSEAS International conference on Fluid Dynamics and Aerodynamics*, pp96-101, Corfu, Greece, August 20-22nd 2005.

Q

Quayle A., [Quayle, 2007], 'Landing gear for a silent aircraft', *45th AIAA Aerospace Sciences Meeting and Exhibit*, AIAA 2007-231, January 2007, Reno, Nevada.

R

Ramberg M. J., [Ramberg, 2002], 'Passenger comfort in the blended wing body', *Cranfield University School of Engineering*, MSc in Human Factors and Safety Assessment in Aeronautics, Cranfield University, UK,

Raymer D. P., [Raymer, 1992], 'Aircraft design: a conceptual approach', *AIAA Educational Series*, 1992, Washington, US.

Reid D. L., [Reid, 2007], 'AeroFoil; A 2-dimensional airfoil design and analysis program', AeroFoil Version 2.1, *http://AeroFoilEngineering.com* , last accessed March 2007, US.

Reneaux J., [Reneaux, 2004], 'Overview of drag reduction technologies for civil transport aircraft', *European Congress on Computational Methods in Applied Sciences and Engineering*, ECCOMAS 2004, Jyvaskyla, 24-28th July 2004.

Reubush E. D., [Reubush, 1979], 'An experimental and theoretical investigation of the effect of non-metric over-the-wing nacelles on wing-body aerodynamics', *NASA Technical Paper 1503*, August 1979, Hampton, Virginia.

Reynolds T. G., Mistry S., [Reynolds, 2006], 'Low noise approach operations; steep approaches, low approach speed, displaced landing thresholds, and delayed landing gear deployment', *Silent Aircraft Initiative (SAI) Internal Report, C-MIT SAI*, Cambridge University, August 2006, Cambridge, UK.

Roman D., Gilmore R., Wakayama S., [Roman et al., 2003], 'Aerodynamics of high-subsonic blended-wing-body configurations', *41st Aerospace Sciences Meeting and Exhibit*, AIAA 2003-554, January 2003, Reno, Nevada.

Roskam J., [Roskam, 1988], 'Airplane design part VII: determination of stability, control and performance characteristics: FAR and military requirements', *University of Kansas*, 1988, Lawrence, Kansas.

Roskam J., [Roskam, 1987], 'Airplane design part VI: preliminary calculation of aerodynamic thrust and power characteristics', *University of Kansas*, 1987, Lawrence, Kansas.

Roskam J., [Roskam, 1986], 'Airplane design part III: layout design of cockpit, fuselage, wing and empennage: cutaways and inboard profiles', *University of Kansas*, 1986, Lawrence, Kansas.

Roskam J., [Roskam, 1979], 'Airplane flight dynamics and automatic flight controls Part I', *University of Kansas*, 1979, Lawrence, Kansas.

Rousselot S., [Rousselot, 2007], 'Etude numerique des deformations do profil de pression en entrée de la soufflante pour un projet d'avion silencieux', MSc Research Thesis, September 2007, *Cranfield University*, UK, *Universite de Nantes*, France.

Rudolph C. K P., [Rudolp, 1996], 'High-lift systems on commercial subsonic airlines', *NASA Contractor Paper 4746*, September 1996, Seattle, Washington.

S

SAI, [SAI, 2007], 'The 'silent aircraft initiative' (SAI) – a new approach', Cambridge and Massachusetts Institute of Technology (C-MIT) Official website, http://silentaircraft.org/, February 2007, Cambridge, UK, US.

Santos G., Barbosa J. R., Pilidis, P., [Santos et al., 2005], 'Analysis of turbofan empirical noise prediction methods', *43rd AIAA Aerospace Sciences Meeting and Exhibit*, AIAA 2005-3076, January 2005, Reno, Nevada.

Smith C. F., Snyder P. H., Emmerson C. W., Nalim M. R., [Smith et al., 2002], 'Impact of the constant volume combustor on a supersonic turbofan engine', *9th AIAA/ISSMO Symposium on Multidisciplinary Analysis and Optimization*, AIAA-2002-3916, 2002.

Smith C. P., [Smith, 2005], 'The environmental challenge – bringing technology to the market', *17th International Symposium on Air Breathing Engines*, ISABE-2005-1008, September 2005, Munich, Germany.

Smith M. J. T., [Smith, 1989], 'Aircraft noise', *Cambridge Aerospace Series*, Cambridge University Press, 1989, NY.

Snyder P. H., Nalim M. R., Alparsian B., [Snyder et al., 2002], 'Gas dynamic cycle of the CVC, a novel detonation cycle', *9th AIAA/ISSMO Symposium on Multidisciplinary Analysis and Optimization*, AIAA-2002-4069, 2002.

Spearman, M.L., [Spearman, 2002], 'Some aviation growth events', *9th AIAA/ISSMO Symposium on Multidisciplinary Analysis and Optimization*, AIAA 2002-0172, September 2002, Atlanta Georgia.

Stone J. R., Krejsa E. A., Berton J. A., Kim, H. D., [Stone *et al.*, 2008], 'Initial noise assessment of an embedded-wing-propulsion concept vehicle', *National Aeronautics and Space Administration*, NASA/TR-2008-215140, April 2008, Glenn Research Centre, Ohio.

Strohmeyer D., Seubert R., Heinze W., Osterherld C., Fornasier L., [Strohmeyer et al, 2000], 'Three surface aircraft – a concept for future transport aircraft', *38th AIAA, Aerospace Sciences Meeting and Exhibit*, AIAA-00-0566, January 2000, Reno, Nevada.

T

Torenbeek E., [Torenbeek, 1976], 'Synthesis of subsonic airplane design', *Delft University Press*, 1976, Netherlands.

Truax, B., [Truax, 1989], 'Handbook for Acoustic Ecology', Second edition: 1999, *The Soundscape Project, Simon Fraser University, & ARC Publications*, 1978, website: *http://www. sfu.ca/sonic-studio/handbook/Effective_Perceived_Noise_.html*, last accessed March 2009.

Truffi D., [Truffi, 2007], 'Jet engine components interaction for a silent aircraft', *MSc Research Thesis*, September 2007, Cranfield University, UK, Universita Degli Studi Di Roma 'La Sapienza', Italy.

V

Vigneron Y., [Vigneron, 2003], 'Commercial aircraft for the 21st century – A380 and beyond', *43rd AIAA/ICAS International Air & Space Symposium and Exposition*, AIAA 2003-2886, July 2003, Dayton, Ohio, US.

VT, [Virginia-Tech, 2009], Virginia-Tech University Strut-braced Wing concept, *http://www.aoe.vt.edu /research/groups/tbw/*, last accessed January 2009.

W

Wagnon S., [Wagnon, 2001], 'Aerodynamic design of a winglet for the cranfield blended wingbody', *MSc Research Thesis*, September 2001, Cranfield University, UK.

Wakayama, S., Kroo, I., [Wakayama, 2002], 'The challenge and promise of blended-wing-body optimization', *7th AIAA/USAF/NASA/ISSMO Symposium on. Multidisciplinary Analysis and Optimization*, AIAA-98-4736, August 1998.

Walter R. S., [Walter, 1993], 'Conceptual design of an economical multirole aircraft for patrol and surveillance missions', *College of Aeronautics*, MSc Research Thesis, August 1993, Cranfield University, UK.

Wedderspoon R. J., [Wedderspoon, 1980], 'High lift and its application to aircraft design', ICAS-80-12-1, British Aerospace, Aircraft Group, Weybridge, UK.

Whitcomb R. T., [Whitcomb, 1958], 'Special bodies added on a wing to reduce shock-induced boundary-layer separation at high subsonic speeds', *National Advisory Committee for Aeronautics*, Technical Note 4293, June 1958, Langley Aeronautical Laboratory, Hampton, Virginia.

Willshire B., [Willshire, 2000], 'Quiet aircraft technology (QAT) program', National Aeronautics and Space Administration (NASA), March 2000, US, *http://www.aerospace.nasa.gov/library/event_archives/encompat/qat/willshire/sld001.htm*, last accessed September 2005.

Wong H. T., Waters M., [Wong, Waters, 2003], 'Constant volume combustor implementation on a 50 passenger commercial regional transport mission simulation', *43rd AIAA/ICAS International Air & Space Symposium and Exposition*, AIAA-2003-4413, 2003.

Wong R. L. M., [Wong, 1982], 'Experimental and analytical studies of shielding concepts for point sources and jet noises', *PhD Thesis*, University of Toronto, 1982.

WvAR, [WvAR, 2006], *www.eng-tips.com/viewthread.cfm?qid=87793&page=8*, Winglets Vs. Aspect Ratio (WvAR), March 2006.

X

Xiao-peng W., Zheng-hong G., [Xiao-peng et al., 1999], 'Aerodynamic configuration design of aircraft using multi-objective genetic algorithm', *Department of Aircraft Engineering, Northwestern Polytechnical University*, 1999, Xi'an, &10072, P.R. China.

Y

Young D., [Young, 2005], 'Messier-dowty landing gear design course', *Notes for a short course run by Messier-Dowty*, November 2005, Cranfield University, UK (contact author for details).

Young T., Humphreys B., [Young, 2004], 'Liquid anti-contamination systems for hybrid laminar flow control aircraft – a review of the critical issues and important experimental results', Proceedings of the Institute of Mechanical Engineers (IMechE) Vol. 218 Part G pp267-277, *Journal of Aerospace Engineering*, IMechE 2004.

Young T., Mahony B., Humphreys B., Totland E., McClafferty A., Corish J., [Young et al., 2002], 'Durability of hybrid laminar flow control (HLFC) surfaces', Aerospace Science and Technology 7, *Elsevier Scientific and Medical editions*, (2002) 181-190, December 2002.

Young T., Humphreys B., Fielding J. P. F., [Young et al., 2001], 'Investigation of hybrid laminar flow control (HLFC) surfaces', Aircraft Design 4, *Elsevier Science Ltd.*, (2001) 127-146, 2001.

Youngren H., Drela M., [Youngren, 1988], 'Athena vortex lattice (AVL): an extended vortex-lattice model for aerodynamic analysis, trim calculation, dynamic stability analysis, and aircraft configuration development', *http://web.mit.edu/drela/Public/web/avl/*, last accessed February 2007, *Massachusetts Institute of Technology (MIT)*, Boston, US.

APPENDICES

Table of Contents

Appendix A Baseline Aircraft Design Study

A.1 Background

The baseline (BL) aircraft analysis is divided into two main sections, where a summary of the design methodology is discussed, followed by an investigation into altering current aircraft operational procedures to address noise and establish performance limits of the BL aircraft design.

A.2 Design Summary of the Baseline Aircraft

The baseline (BL) aircraft design was developed in parallel with the broad delta (BD) airframe concept and is described within Appendix B. The BL aircraft was generated from a parametric design analysis using [Howe, 2000] and electronic data from [Jenkinson et. al., 1999] which provided data for similar aircraft as a comparative aid. The aircraft design results are compared with an existing aircraft (aircraft) of a similar class to the BL, identified as the Boeing 767-300 (Fig A-1), with a detailed comparison provided against published data.

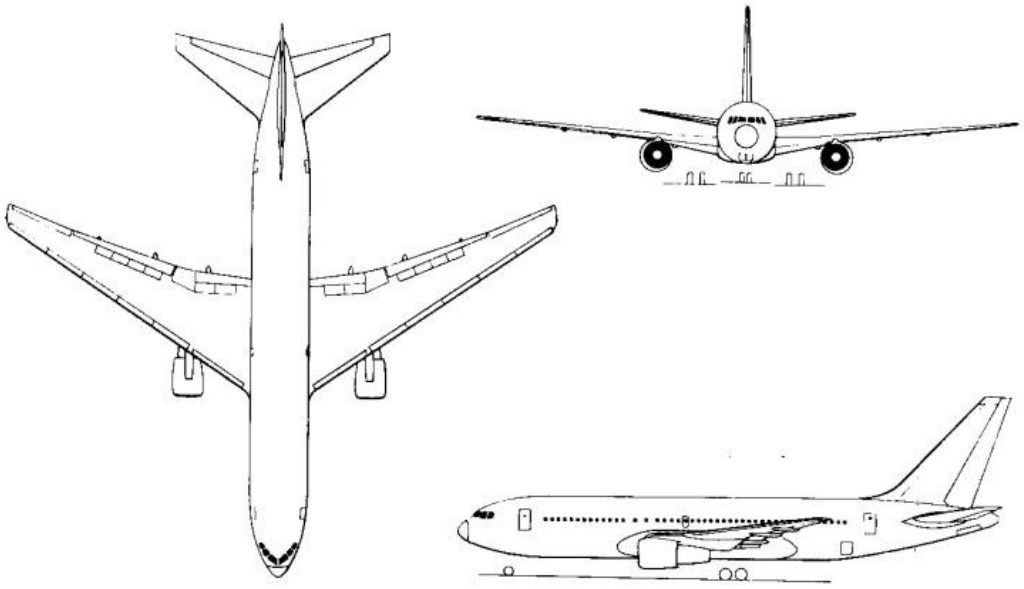

Fig A-1: Boeing 767-300 General Arrangement (http://www.aviastar.org/pictures/usa/boeing-767.gif).

The BL aircraft design summary is provided below in Table A-1, where data obtained from [Jenkinson et. al, 1999] for the B767-300 airliner is directly compared with the parametric study results. The results shown are comparable between the BL and B767-300 and they also identify significant differences for the wing geometry and performance.

Description	***Symbol***	**BL (with winglets)**	**BL (no winglets)**	**B767-300**	***Units***
Wing Area	S	196.2	237.7	283.3	[m^2]
Wing Span	b	39.6	43.6	47.57	[m]
Wing Standard Mean Chord	$\bar{c}$	4.96	5.45	6.98	[m]
Wing Aspect Ratio	A	7.99	7.99	7.99	-
Wing Quarter Chord Sweep	$\Lambda_{¼}$	32.3	31.6	39.0	[deg]
Wing Taper Ratio	Λ	0.277	0.207	0.207	-
Thickness-to- Chord Ratio	t/c	0.115	0.115	0.115	-
Wing Apex location	l_{APEX}	23.5	22.9	-	[m]
Horizontal Tail Area	S_{HT}	49.9	57.1	77.7	[m^2]
Vertical Tail Area	S_{VT}	29.9	34.2	46.14	[m^2]
Wing Area Parameter	$S^{-0.1}$	0.569	0.579	0.569	[m^{-2}]
Static Wing Loading	$(Mg/S)_0$	7465	6540	5419	[N/m^2]
Static Thrust Loading	$(T/Mg)_0$	0.349	0.317	0.291	-
Lift-Drag Ratio	L/D	14.8	14.2	14.4	-
Cruise Lift Coefficient	$(c_L)_{cr}$	0.271	0.342	-	-
Mass of Wing	M_W	22,869	25,265	-	[kg]
Fuselage Mass	M_{FUS}	17,454	18,010	-	[kg]
Mass of Tail (+ winglets)	M_T	4,116	5,053	-	[kg]
Mass of Undercarriage	M_G	5,973	6,338	-	[kg]
Propulsion Systems Mass	M_{PP}	12,516	13,956	-	[kg]
Mass of Systems	M_{Sys}	14,932	19,446	-	[kg]
Operational Items Mass	M_{OP}	2,762	2,762	-	[kg]
Operational Empty Mass	M_{OEW}	80,622	95,149	87,135	[kg]
Mass of Payload	M_{Pay}	23,760	23,760	24,795	[kg]
Mass of Fuel Required	M_f	44,934	43,849	44,559	[kg]
Available Fuel in Wing Volume	M_{f_a}	47,919	47,342	-	[kg]
Total Static Thrust	T_0	511,604	492,706	447,000	[N]
Total Overall Mass	$\boldsymbol{M_0}$	**149,316**	**158,438**	**156,489**	**[kg]**

Table A-1: Mass optimised results summary for the baseline aircraft compared to B767-300 data

The main difference is the wing sizing where the BL has a 7m shorter wing span and is because of two key differences in the design. The first reason is because the B767-300 wing is oversized due to the fuselage capacity being restricted with the capability of adding extensions to the fuselage for a stretched variant. The larger wing reflects the capability of using a common wing for a family of aircraft, so that development and manufacturing costs are reduced, where the BL aircraft wing is specifically tailored for the design mission provided by the initial specification.

The second factor that results in a shorter wing span is the addition of winglets to the aircraft, where the addition of these wing-tip extensions provides an effective increase in wing aspect ratio, without providing an excessive increase in wing span. The addition of winglets, combined with the design tailored for one design mission, justifies the shorter span of the BL aircraft. The resulting effects of

this smaller wing on performance suggests that for an aircraft of equivalent mass to the B767-300, the BL would have a higher wing-loading, where the wing is required to provide greater lift (works harder) throughout all flight conditions, creates greater drag, and uses more fuel for a specified mission range.

Fig A-2: Baseline CATIA model generated using results from the initial parametric analysis study

A.3 Baseline Aircraft Operational Analysis to Reduce Noise

This second section refers to an additional study that was completed in collaboration with the SAI to explore alternate approach operations for a conventional airliner without redesigning the airframe. The study aimed to investigate the flight limitations of the B767-300 airframe in order to examine the performance of a slow and steep approach, with an additional variable of a displaced landing threshold. An initial investigation into alternate conventional and unconventional approach procedures is discussed followed by the slow and steep approach analysis.

A.3.1 Conventional & Unconventional Approaches

Approach angle and speed are dependent upon each other and will be considered together in this discussion. The slow approach investigates the reducing the approach velocity of an existing tube-and-wing aircraft without stalling the wing and determining the resulting impact on noise. A steep approach concept investigates the effect of increasing the approach glide path angle above the current civil aircraft datum of 3 degrees.

A.3.1.1 Approach angle & Low Approach Speed

Steep approach profiles have been investigated for many years. In the late 1960's Short Take Off and Landing (STOL) concepts were developed to utilise airfields with shorter runways [Boeing, 1967], where reducing approach speeds to meet the shorter landing requirements, enabled steeper approaches while maintaining a given descent rate.

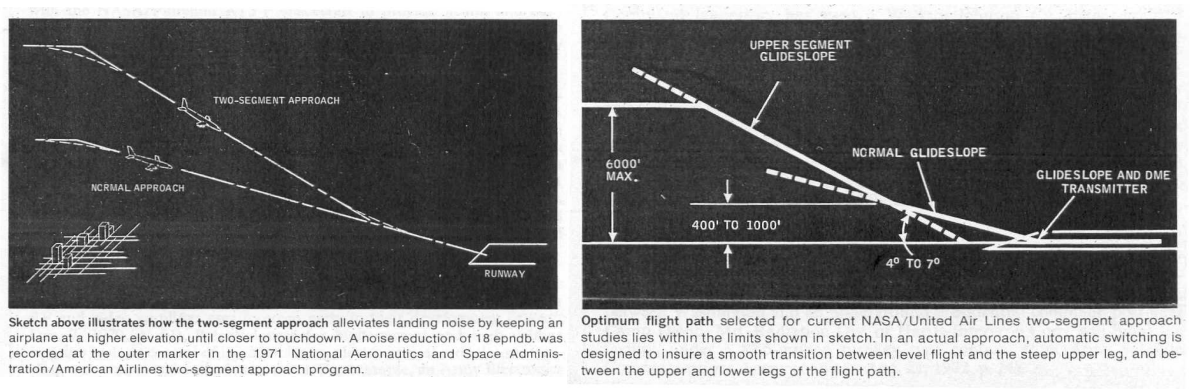

Sketch above illustrates how the two-segment approach alleviates landing noise by keeping an airplane at a higher elevation until closer to touchdown. A noise reduction of 18 epndb. was recorded at the outer marker in the 1971 National Aeronautics and Space Administration/American Airlines two-segment approach program.

Optimum flight path selected for current NASA/United Air Lines two-segment approach studies lies within the limits shown in sketch. In an actual approach, automatic switching is designed to insure a smooth transition between level flight and the steep upper leg, and between the upper and lower legs of the flight path.

Fig A-3: NASA two-segment approach studies [Elson, 1973]

Studies such as the NASA "two-segment" approaches were investigated involving a 4-7° initial approach segment followed by a transition to a conventional 3° final approach at 400-1000 ft, as shown in Fig A-3. Flight trials with Boeing 720 aircraft (109 passengers, 175,000 lb maximum gross landing weight) suggested that noise reductions were obtained using this approach (Fig A-4) due to a higher altitude and lower thrust level for part of the approach.

Despite these apparent noise benefits, they were not introduced operationally, mostly due to pilot union opposition to the fact they "*would require pilots to make un-stabilised approaches close to the ground - a practice that has been branded as 'unsafe' for many years*" [AvW&ST, 1974] referring to the requirement for the transition from the steep to conventional segment at low altitude. Additional concerns were also expressed [AvW&ST, 1974], including icing, wind, wake turbulence, and noise reduction, further details of which are discussed in [Reynolds & Mistry, 2006].

During the 1990s, studies examining the potential for one segment steep approaches for reduced noise and increased system capacity were conducted by [Caves & Rhodes, 1995], [Rhodes, 1996], [Caves *et al.*, 1997], and [Rhodes, 1998]. The study investigated steep approaches up to 6° with regional jet and B757-sized aircraft (Fig A-5).

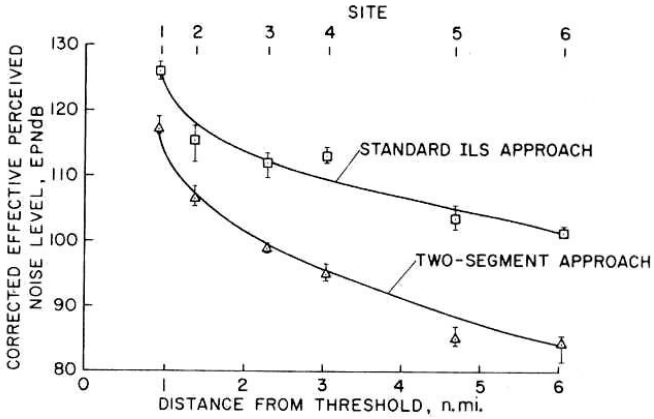

Fig A-4: Measure Noise Benefits of a two-segment approach [Denery et al., 1973]

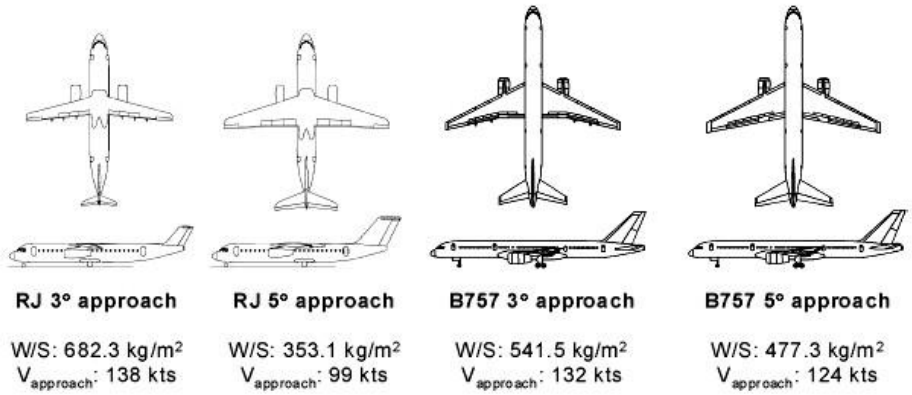

Fig A-5: Regional jet and B757 steep approach studies [Caves, Rhodes, 1995], [Rhodes, 1996]

Passenger comfort was the main driver behind constraining the vertical descent rates to change from a conventional to a steep approach, which required lower approach flight speeds, resulting in larger wing areas and/or reduction of the landing weight. The changes to aircraft geometry are represented below, where the steep approach results in a larger wing and lower wing loading in the 5° aircraft designs shown.

Noise benefits of up to -6dB(A) were predicted for the one segment steep approach, with a reduction in peak noise at the approach certification point due to increased distance between aircraft and ground; assuming that engines were at lower thrust settings. Capacity benefits of allowing commercial aircraft to land on shorter runways at smaller airfields is associated with potential STOL characteristics of steep/slow approaches. The studies also suggested that steep approaches improve safety through greater margin over obstacles, longer glide times in the event of engine failure, and less energy absorption required on landing due to lower approach speeds.

More detailed optimization approaches are under development [Antoine & Kroo, 2004] and [Antoine *et al.*, 2004], making it possible to explore the potential gains of steep approaches by including

approach angle as an optimization variable. Conceptual designs offering the optimal combination of approach profile, engine characteristics, and aircraft performance can then be developed, and is similar to the research completed within this research study. Additional investigations into the UK Civil Aviation Authority (CAA) guidance on steep approaches and operational performance of current airliners [Lutz & Wieser (2006)], is further discussed within [Reynolds & Mistry, 2006].

A.3.1.2 Displaced Landing Threshold

Displaced threshold analysis looks into 'displacing' or pushing back the touch-down point of the aircraft further than a conventional landing. Current Joint and Federal Aviation Regulations are identified within [Reynolds & Mistry, 2006]. Displacing the landing threshold decreases the runway length available, affects exit, and taxi times for landing aircraft; which must be accounted for when determining which aircraft types can use the procedure and how much displacement is feasible on a runway of a given length.

Frankfurt Airport (FRA) in Germany has been conducting displaced threshold approaches since 1999 as part of its High Approach Landing System/Dual Threshold Operation (HAL/DTOP) programme [Fraport, 2006]. Because the two parallel runways (25L and 25R) at FRA have a lateral separation of only 518 m (1700 ft) from one another, independent landing operations between them are not permitted.

Wake vortex separation criteria must be applied as if approaches were on the same runway, preventing the airport from making maximum use of its runway capacity. They have tested a system that utilises a displaced threshold on runway 25L to reduce the likelihood of wake vortex interaction between approaches to the parallel runways, potentially allowing the lost capacity to be regained (Fig A-6). The displaced landing approach can only be used by "large" and "small" weight category aircraft, i.e. those with a maximum gross take-off weight of 255,000 lb or less. The second landing threshold (26L) is displaced by 1500 m to distinguish it from the conventional threshold 25L (which can be used at the same time) and is equipped with a new lighting and marking systems, shown in Fig A-7, and described within [Reynolds & Mistry, 2006].

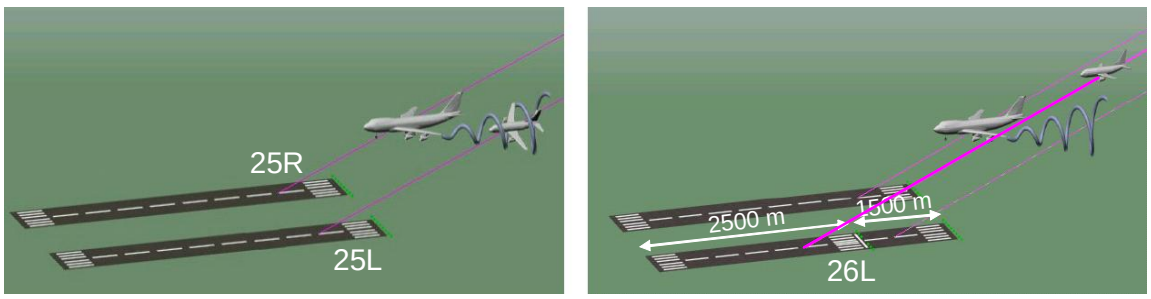

Fig A-6: Displacing landing threshold at FRA for wake vortex avoidance, adapted from [Fraport, 2006]

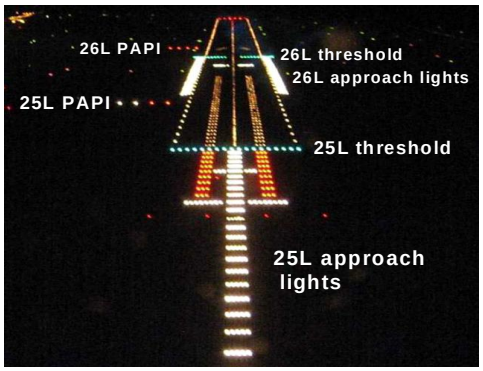

Fig A-7: Lighting system for FRA displaced landing threshold, adapted from [Fraport, 2006]

A.3.2 Baseline Aircraft Approach & Noise Analysis

The baseline (BL) study aims to determine changes in noise produced from an approaching aircraft with variable speed, approach angles, and consider displaced thresholds. In order to produce a suitable noise analysis a baseline aircraft design is required to determine the aerodynamic behaviour of the aircraft on an approach glide path. The baseline aircraft model is adapted from section A-2 where removal of the winglets (including all drag and geometry assumptions) provides a comparable model to the B767-300 aircraft both in terms of geometry and performance. The following information is based upon results published within [Reynolds & Mistry, 2006].

A.3.2.1 Baseline Aircraft Model

The design of the BL aircraft calculated the maximum low speed lift coefficient which included the use of high lift devices such as trailing edge (TE) flaps and leading edge (LE) slats. The initial calculations used within the parametric analysis study estimated the maximum lifting performance of the wing by using [Howe, 2000], where data from exiting aircraft, were used to establish drag and lift increments for each TE and LE device.

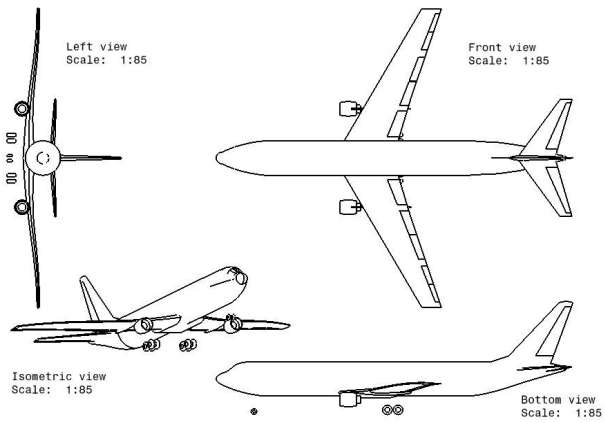

Fig A-8: Baseline aircraft design without winglets [Reynolds & Mistry, 2006]

A detailed analysis into the lifting performance of the BL aircraft was determined, so that the true low speed lifting characteristics during the approach and landing could be investigated, with a noise analysis to follow. The following sections provide a summary of the detailed analysis completed by the author for the SAI conventional aircraft operations report [Reynolds & Mistry, 2006].

The result of the baseline (BL) aircraft for this analysis is defined below from Fig A-8 and Table A-2

Mass	***[kg]***
Wing	25,265
Fuselage	18,010
Tail	5,053
Undercarriage	6,338
Power-plant	13,956
Systems	19,446
Operating items	2,762
OEM	95,149
Payload	23,760
Fuel	43,849
Fuel capacity (wing)	47,342
SL static thrust	**492,706**
$MTOW_{metallic}$	**158,438**
$MTOW_{composite}$	**152,639**
Areas	***[m²]***
Wing	237.65
H_z *tail*	57.06
V_z *tail*	34.24
Flap Area	33.64
Angles	***[deg]***
0.25_c *sweep*	31.60

Non dimensional	
A	7.99
t/c_{avg}	0.115
λ	0.207
BPR	8.0
Cl_{max}	2.939
$Cl_{approach}$	1.763
Cl_{cruise}	0.342
L/D_{cruise}	14.2
$[T/Mg]_0$	0.317
$[Mg/S]_0$	6540
$C_{Do\ ls}$	0.0164
$C_{Do\ cr}$	0.0151
$C_{Di\ ls}$	0.0510
$C_{Di\ cr}$	0.0526
$(Mn)_{cruise}$	*0.80*
$(Mn)_{to}$	*0.24*
$(Mn)_{crit}$	0.85
Velocities	***[m/s]***
V_{stall}	57.40
V_a	70.91
V_{design}	236.64

Length / chord	***[m]***
Wing span	43.60
MAC (Mean Aero Chord)	5.45
Wing $Root_c$	8.45
Wing $kink_c$	6.20
Wing tip_c	2.20
Flap span	14.97
Wing apex (from nose)	22.9
c.g. (from nose)	21.06
Tail moment arm	27.24
H_z *tail span*	17.07
H_z *tail* $Root_c$	5.19
H_z *tail* tip_c	1.50
V_z *tail span*	9.31
V_z *tail* $Root_c$	5.66
V_z *tail* tip_c	1.70
Fuselage length	53.7
Fuselage width	5.03
Fuselage breadth	5.03
Nose gear strut	2.03
Nose gear diameter	0.76
Main gear strut	2.92
Main gear diameter	1.31
Nose/main gear wheels	2/8

Table A-2: Baseline aircraft geometry and performance summary [Reynolds & Mistry, 2006]

A.3.2.1.1 Airfoil Analysis

The BL was assumed to have a supercritical airfoil wing design, where the chosen airfoil to represent the wing was a NASA designed SC(2)-0610 section with 10 percent thickness and a design lift coefficient of 0.6 [Harris, 1990].

The SC(2)-0610 airfoil stall velocity is 62.2m/s, which in practice does not represent a wing section. Introducing a sweep variable to the lift coefficient, allows for an estimate of swept airfoil stall velocity, where airfoil sweep angle, θ_{sw} = 30 degrees. The maximum achievable lift coefficient for a

swept SC(2)-0610 airfoil is reduced by 25% to 1.71 and the stall velocity increases by 15.4% to 71.8m/s. Typically a supercritical swept airfoil which has aspect ratio and taper ratio corrections, produces a maximum lift coefficient of 1.5.

FAR 25.125 states that approach velocity of an aircraft is 1.23 times stall velocity. In this instance approach velocity for the un-swept airfoil is 76.5m/s and for the swept airfoil 88.3m/s; representing clean airfoils with no high lift devices.

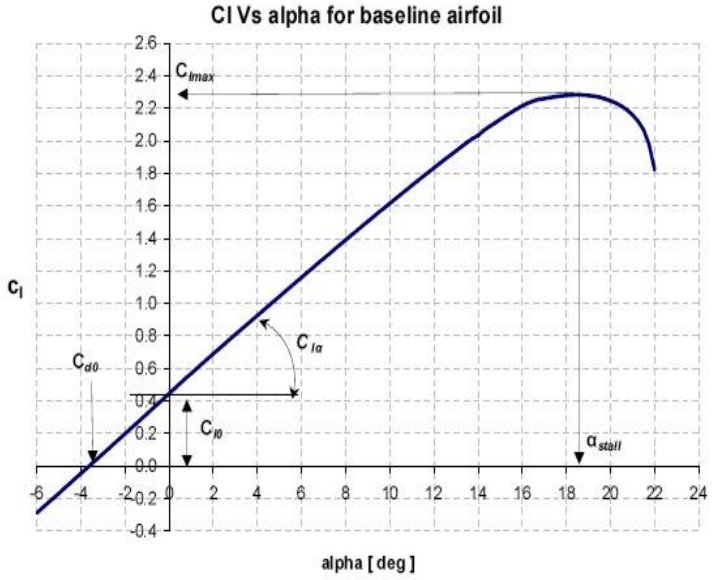

Fig A-9: BL aircraft SC(2)-0610 2-Dimensional lift curve slope, where c_{l0} = 0.446, $c_{l\alpha}$ = 6.904 rad^{-1}, $c_{l.max}$ = 2.28 and (α_{stall}) =18.5 deg [Reynolds & Mistry, 2006]

A.3.2.1.2 Trailing Edge (TE) High Lift Devices

The addition of high lift devices to a SC(2)-0610 airfoil increases maximum lift and reduces stall velocity. To determine lift effectiveness of TE devices a semi-empirical approach for TE flaps was used, correlating experimental data with thin airfoil theory [Torenbeek, 1976]. Glauert's linearised theory for thin airfoils with flaps determines flap effectiveness, allowing delta increases in C_l to be calculated.

The single slot (SS) lift effectiveness is very sensitive to flap and slot geometry, with a main constraint being location of the flap hinge line. A lower hinge line produces a more effective flap, with slot design also being a critical issue, and a limited maximum deflection angle of 40 degrees.

Double slotted (DS) flaps are essentially single slots with an added extension or turning vane in the slot. This additional vane recovers loss of effectiveness experienced for the SS above 40 degree

deflections, further reduces the hinge line and increases chord-wise extension; achieving 60 degrees of deflection before lift effectiveness is reduced.

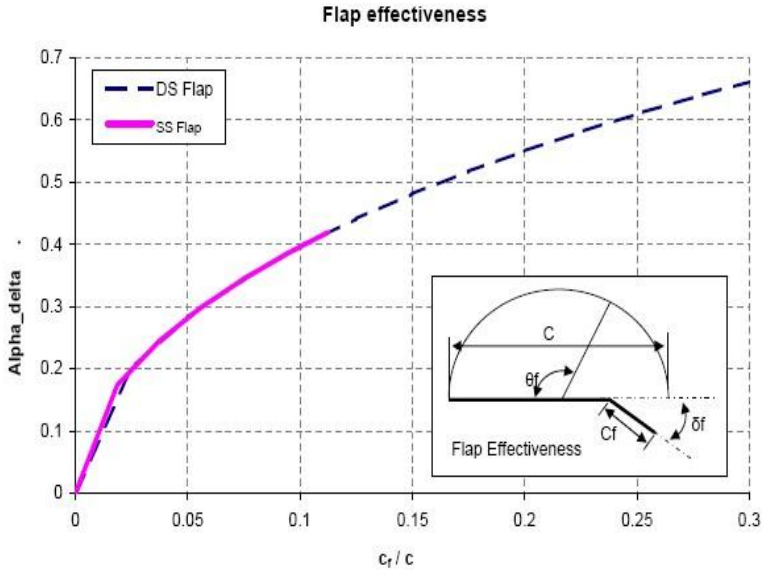

Fig A-10: Flap effectiveness [Reynolds & Mistry, 2006]

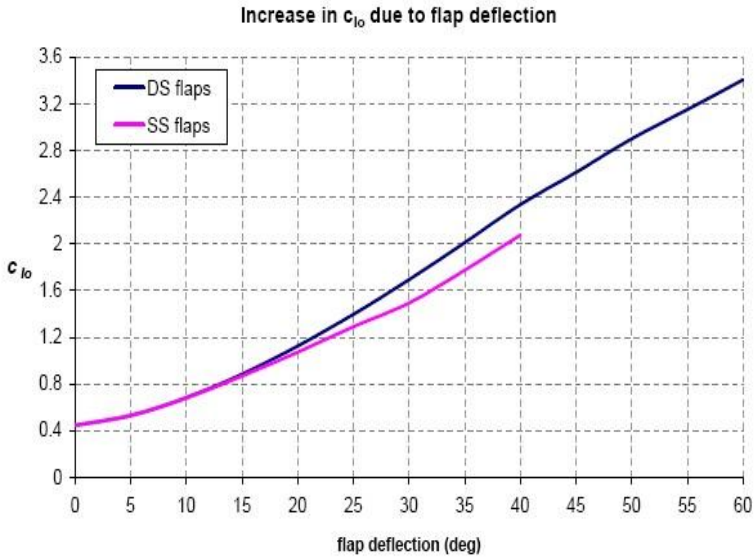

Fig A-11: Increase in c_{l0} for single and double slotted flap deflections [Reynolds & Mistry, 2006]

Maximum lift produced from a deflected flap section is also important to determine stall characteristics for an airfoil-flap combination. The resulting lift increments due to deflecting SS and DS flaps can be added to airfoil maximum lift and superimposed over the SC(2)-0610 lift curve slope. Corrections are required to convert this 2-dimensional airfoil-flap device into a 3-dimensional finite wing section.

A.3.2.1.3 Leading Edge (LE) High Lift Devices

Leading edge (LE) high lift devices are also required for the BL aircraft wing to further increase maximum achievable lift. The addition of LE slats to the SC(2)-0610 airfoil-flap combination introduces an increase in C_{lmax}, which is calculated using [Torenbeek, 1976].

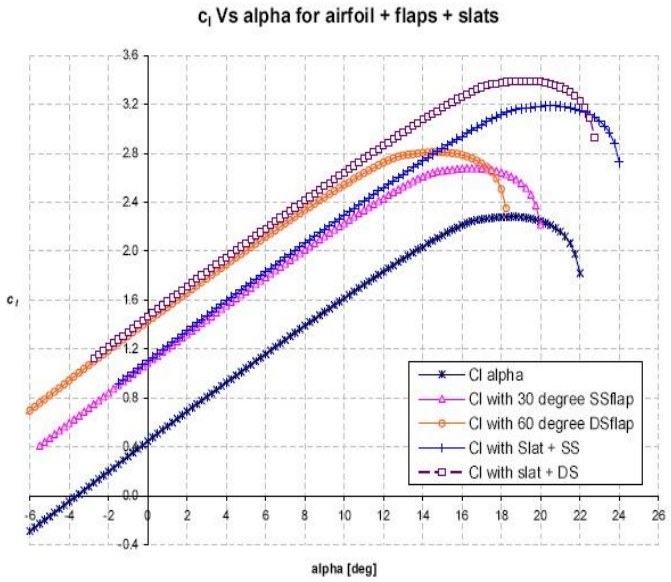

Fig A-12: 2-Dimensional analysis results for the change in lift-curve of an un-swept airfoil slope due leading edge Slats combined with single (SS) and double slotted (DS) trailing edge flaps [Reynolds & Mistry, 2006]

The maximum lift from a combination of flaps and slats are compared within Table A-3, representing overall effectiveness of high lift devices, and reductions in both stall and approach velocities. The results from swept and un-swept airfoil cases are also compared within Table A-3, showing net aerodynamic benefits for aircraft with zero-swept wings. Swept wings are essential for cruise performance in delaying shocks on the wing, where an ideal scenario would be to have a wing with variable sweep; to improve both low speed and cruise performance.

One of the key results to bear-in-mind from Table A-3 is where a combination of slats and DS flaps deflected at a maximum of 60 degrees provides a 72.4m/s (140.8 knots) approach velocity. The baseline parametric analysis calculated an approach velocity of 70.9m/s (137.8 knots) and was compared with the 72.5m/s (141.0 knots) taken to be the B767-300 approach velocity [Jenkinson *et al.*, 2000].

The results for swept wings with DS flaps and slats, indicates that deployment/deflection of high lift devices for an approach setting produces a maximum lift coefficient which is reasonable compared to the B767-300 published data. The BL parametric results slightly differ to this analysis, but are due to

the assumptions made for the airfoil and high lift devices basic estimation methods. The results from this section were used to analyse the aircraft performance for numerous approach cases.

Configuration	C_{Lmax}	V_{stall} [m/s]	V_a [m/s]	C_{La}
Airfoil	2.282	62.18	76.48	1.508
Airfoil + SS Flap	2.679	57.38	70.58	1.771
Airfoil + DS Flap	2.810	56.03	68.92	1.857
Airfoil + SS Flap + Slat	3.187	52.62	64.72	2.106
Airfoil + DS Flap + Slat	***3.392***	***51.00***	***62.73***	***2.242***
$Airfoil_{swept}$	1.712	71.79	88.31	1.131
$Airfoil_{swept}$ *+ SS Flap*	2.009	66.26	81.50	1.328
$Airfoil_{swept}$ *+ DS Flap*	2.107	64.70	79.59	1.393
$Airfoil_{swept}$ *+ SS Flap + Slat*	2.390	60.76	74.73	1.580
$Airfoil_{swept}$ + DS Flap + Slat	***2.544***	***58.89***	***72.43***	***1.681***

Table A-3: Comparison of stall characteristics for BL SC(2)-0610 airfoil with TE and LE high lift devices [Reynolds & Mistry, 2006]

A.3.2.2 BL Aircraft Analysis

The following analysis considers the effect of wing sweep, partial span flaps and wing twist, where a vortex lattice code, *AVL*, [Youngren & Drela, 1988] was used to analyse the baseline. Lifting performance for the BL aircraft is not empirically calculated because the wing incorporates aerodynamic twist with wingtip downwash, dihedral, and has a partial span TE flaps with full span LE slats. These variables complicate the analysis and *AVL* allows the BL geometry to be analysed relatively easily and with reasonable accuracy.

Lift is underestimated by *AVL*, because the flap is defined as a slot-less surface, similar to a hinged flat plate, where the air that should flow through slots vanes and increase the flap lifting capability, is not modelled. *AVL* does not predict increments in lift due to LE devices, so a slat correction factor $\Delta C_{Lslat} = 0.535$, was introduced and corresponds to a change in angle of attack of $\Delta\alpha_{slat} = +4.5$ degrees.

Increasing TE flap deflection results in a reduction of approach velocity (Fig A-13), causing a nose down pitch; causing the incidence of fuselage datum line to fall compared to the zero flap deflection setting.

Fig A-14 represents the effect of increasing flap deflection on induced drag. As velocity is reduced, the induced drag associated with the geometry increases, which implies that slower approach velocities with larger control surface deflections generate more induced drag. High drag at low

speeds is essential for an aircraft on an approach flight path, where additional benefits of this, such as reduced noise will be discussed towards the end of this appendix.

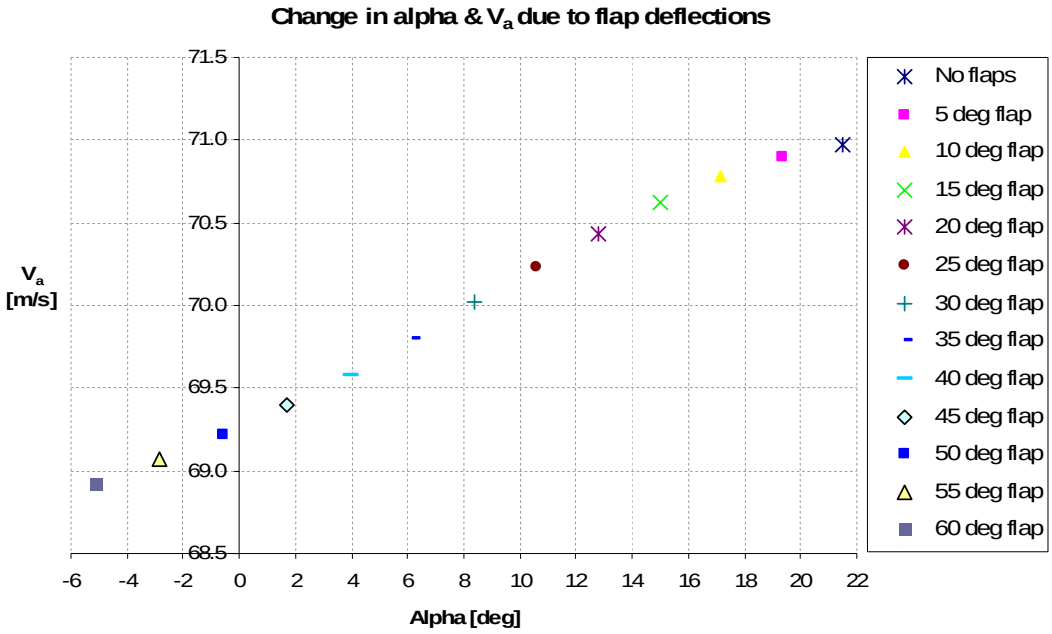

Fig A-13: Aircraft angle of attack variation due to deflecting flaps [Reynolds & Mistry, 2006]

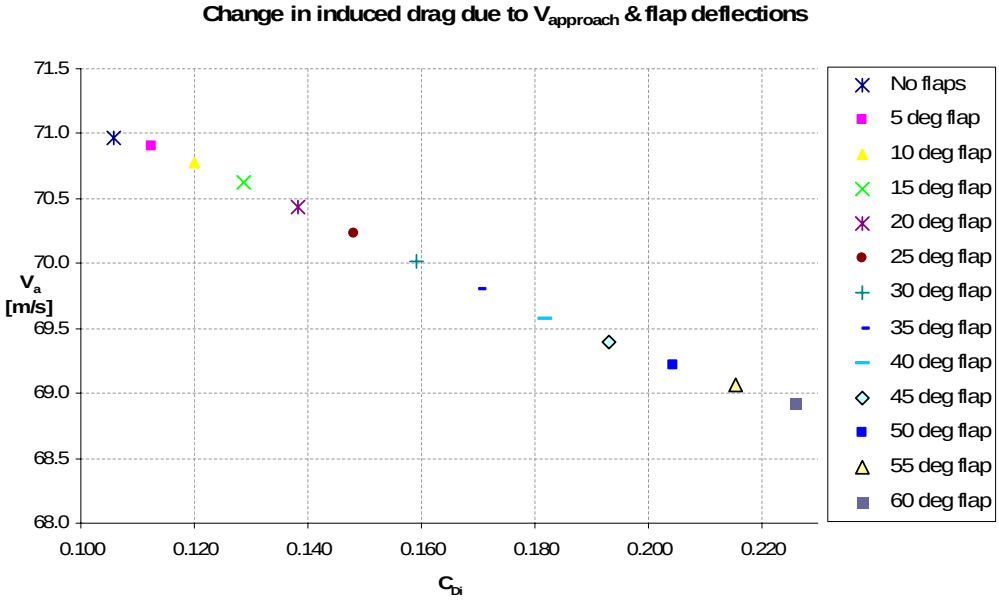

Fig A-14: Induced drag variation of BL aircraft geometry due to flap deflection [Reynolds & Mistry, 2006]

A.3.2.3 BL Aircraft Drag Analysis

Total aircraft drag has many components other than the induced drag calculated from *AVL*. Drag components such as the zero-lift, interference, airfoil thickness, fuselage, engine nacelles, horizontal and vertical empennage, and the undercarriage drag sources are determined using semi-empirical methods from [Torenbeek, 1976] and [Hoerner, 1965].

A.3.2.4 Approach Analysis

Investigation of slow and steep approaches introduced a new variable, which was the flight path angle, referred to as FPA or θ_{FPA}. FPA is often also referred to as the glide slope and is the angle between aircraft direction of flight and the ground line (horizontal).

A conventional FPA is usually between 3 to 4 degrees, where the steep approach analysis considers 3, 5 and 6 degree FPAs. Aircraft designed to approach at steeper angles, require larger wings and a slower approach velocity to maintain an acceptable descent rate for passenger comfort. Investigations into steep approaches for the BL aircraft does not consider wing re-design, but tests the boundaries of the current geometry to confirm whether alternate approach operations are possible, and to quantify the resulting impact on noise.

The FPA analysis investigated variables such as the flap deflection required for any given approach speed and angle (ranging from 0 to 60 degrees). These angles also assist in identifying the resulting fuselage incidence, so that the internal passenger cabin angle can be determined, and checked alongside levels of passenger comfort. Finally *AVL* is used to trim the BL aircraft using the elevators to produce a zero pitch moment and represents a steady approach flight condition. The main purpose of this analysis to determine degree of flap deflection required to achieve maximum wing lift by constraining aircraft incidence.

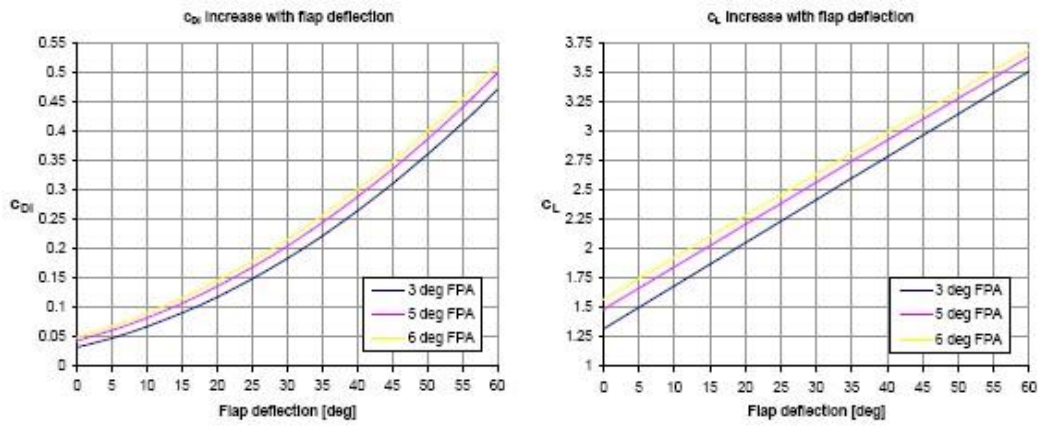

Fig A-15: Lift and Drag variation with increasing flap deflections for an approach FPA of 6 degrees and at an approach velocity of 72.5m/s [Reynolds & Mistry, 2006]

Studies to investigate the lift (C_L) and drag (C_{Di}) produced for the BL aircraft with a 3 degree fuselage constraint and 72.5m/s approach velocity are summarised below in Fig A-15. The results show a linear lift increase caused by deflecting TE flaps for each FPA. C_{Di} increase is more parabolic, indicating a gradual increase in drag due to the incremental deflection of flaps compared with the lift.

The final variable for the approach analysis was to investigate the flight speed. The flight case described above was for a 72.5m/s case (Va_1), where a minimum approach velocity of 55m/s (Va_3) as considered. The SAI target approach case of 55m/s was chosen to quantify the effects of reducing the approach velocity on noise, where the BL airframe noise could be compared to the SAI blended wing body airframe. An intermediate case investigated a 66.6m/s approach velocity (Va_2), which was an 8m/s reduction compared with Va_1, which is $1.13V_{stall}$, which investigates the possibility of changing the FAR flight requirements from $1.23V_{stall}$ to $1.13V_{stall}$ and the resulting impact on noise. The change of the requirements is to relax the safety margins to allow for this lower approach velocity. The implications of doing so are that there is a reduced factor of safety for the aircraft as it approaches at a lower speed, this being closer to the stall speed and allows for less room for pilot error or change in ambient flying conditions. If for example there was a head-wind, the aircraft would not be approaching at $1.13V_{stall}$, but at a lower velocity and could be prone to stall, leading to the aircraft plummeting to the ground at one of the most dangerous phases of flight. The approaching aircraft has a fairly slim chance of recovering due to the proximity of the vehicle to the ground and there would not be enough speed or altitude to dive and recover from this situation.

The results below show a range of flap deflections for all velocities and FPA settings. It is interesting to note that although the 55m/s case is not possible, the wing does not stall; because the maximum lift coefficient is never reached. Lift produced for a flap is non-linear above a 30 degree deflection, so for the 55m/s results the wing would stall much earlier; conflicting with the results previously shown.

FPA	$V_{approach}$	*Flap angle*	$C_{Lapproach}$	*stall with Flaps*
3	72.5	10	1.683	35 deg
	66.6	20	2.044	45 deg
	55.0	45	2.941	No stall
5	72.5	5	1.663	30 deg
	66.6	15	2.019	45 deg
	55.0	40	2.900	No stall
6	72.5	5	1.743	25 deg
	66.6	15	2.095	40 deg
	55.0	40	2.967	No stall

Table A-4: Airfoil flap & slat settings for a 3 degree fuselage incidence constraint [Reynolds & Mistry, 2006]

FPA	$V_{approach}$	*Flap angle*	$C_{Lapproach}$	*stall with Flaps*
3	72.5	15	1.624	40 deg
	66.6	25	1.994	50 deg
	55.0	50	2.915	No stall
5	72.5	10	1.602	35 deg
	66.6	20	1.966	50 deg
	55.0	45	2.872	No stall
6	72.5	10	1.683	35 deg
	66.6	20	2.044	45 deg
	55.0	45	2.941	No stall

Table A-5: Airfoil flap & slat settings for zero degree fuselage incidence constraint [Reynolds & Mistry, 2006]

The only method which can be used to produce such a high lift coefficient as that required for 55m/s case is to use blown flaps. This would increase the lift coefficient a value in the order of 5.0. Blown flaps are not ideal for low noise, and are not often considered for civil applications.

An approach velocity of 72.5m/s for 3 degree FPA requires a 10 degree flap deflection combined with a deployed slat. Removal of the slats results in the flap deflection angle doubling to generate a similar lift coefficient. Increased FPA results in less flap deflection, where for a 6 degree FPA zero flap deflection is required with a slat deployed, but by retracting the slat, a 15 degree flap deflection is required to produce the required lift coefficient.

The lower fuselage angle of attack constraint requires a greater degree of flap deflection to produce the required approach lift coefficient. BL aircraft with no slats deployed would not stall for a 3 degree FPA 66.6m/s case with a 60 degree deflection, but has a lift coefficient lower than the required C_{Lmax} = 3.012. When slats are deployed, stall occurs with a 50 degree deflection for the same FPA. This result questions the use of slats because if an aircraft could approach without slats deployed, and only TE flaps deflected then that would eliminate a single noise source. But what is the effect be of removing slat noise compared to increasing the deflection of TE flaps? This comparison would provide a beneficial result to determine a low noise approach.

A.3.2.5 ESDU Airframe Noise Prediction Methodology

This section relays information about the noise prediction methodology used within the dissertation, where the majority of information has been extracted from the ESDU data item 90023. The ESDU method may be used to predict airframe noise for discrete airframe elements and by summation for any selected combination of the following aircraft components (as shown within Fig A-17):

- wing (conventional or delta)
- slats
- horizontal tail
- vertical tail
- flaps (single-, double- or triple-slotted)
- main landing gear
- nose landing gear

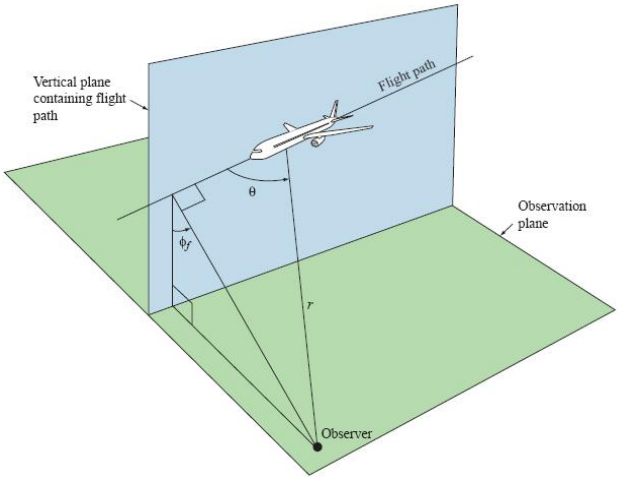

Fig A-16: Aircraft noise calculation vectors for an approach flight condition [ESDU 90023, 2003]

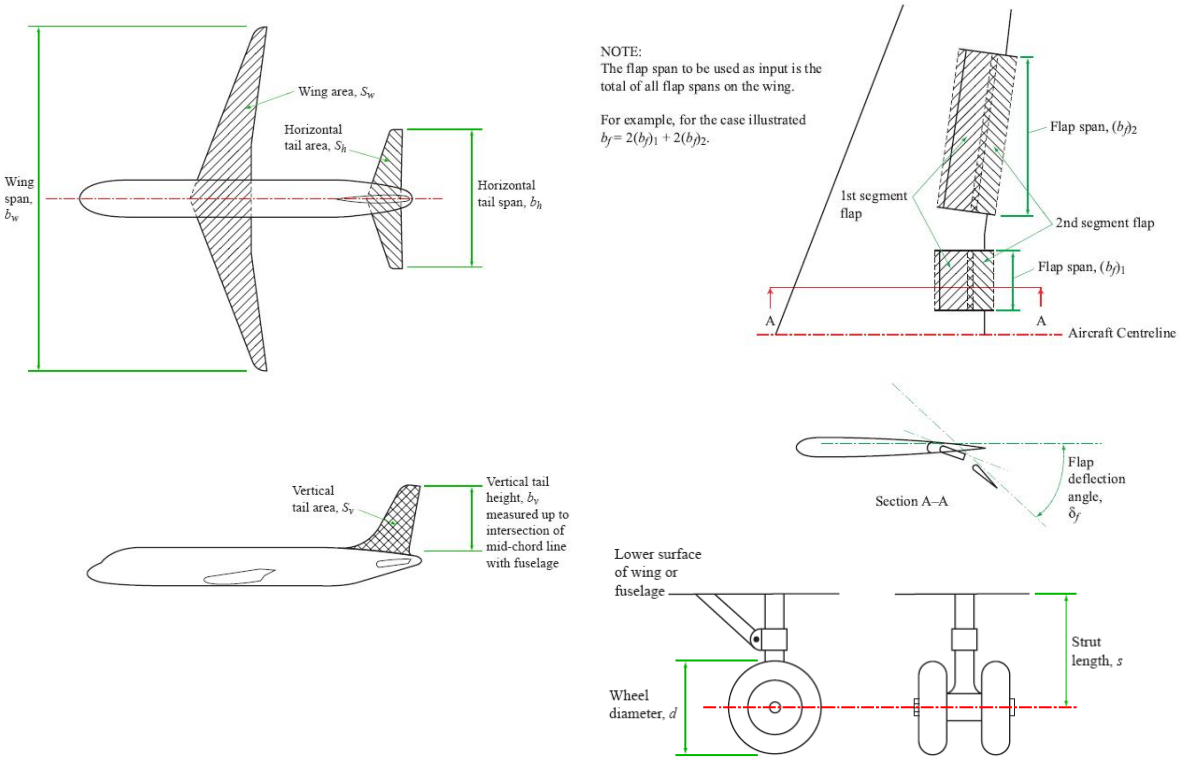

Fig A-17: Wing and tail surfaces (left), Trailing edge flaps and Undercarriage (right) [ESDU 90023, 2003]

An example of the outputs are shown below in Fig A-18 the landing gear spectrum representing the sound pressure level (SPL) measured in (SPL dB) against a specified frequency range (Hz).

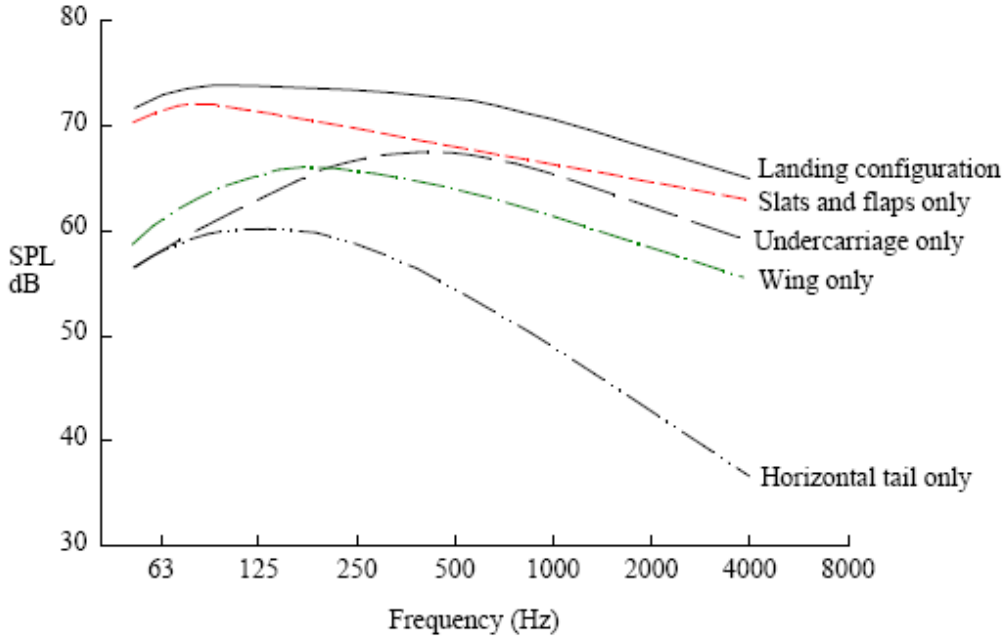

Fig A-18: Breakdown of airframe landing noise spectrum [ESDU 90023, 2003]

A.3.2.5.1 Background to Method

The prediction method works by modelling individual components of the airframe as elementary sources of source distributions. The spectral and directivity characteristics of these sources have been derived analytically or empirically, or have been assumed to be similar to sources of known characteristics.

The individual components of the airframe that are considered are the wing, flaps, slats, tail and landing gear; no interaction between components is assumed. The executable code provided with ESDU 90023 allows the discrete computation and output of the noise emanating from any of these components before summing the contributions for the selected combination. As an example, a clean flight configuration, such as during cruise, would have contributions from the wing, horizontal and vertical tail components. For the landing configuration, additional contributions from the landing gear, leading edge slats and trailing edge flaps must be added to the noise of the clean configuration.

A.3.2.5.2 Method of Calculation

The method of calculating the broad-band noise contribution from each of the various airframe components are similar to the derivations made within [Fink, 1977] and

[Zorumski, 1990]. The same basic sequences of steps are followed for each component but with appropriately different values of constants and functions.

The general method of calculation is described in this section. Specific constants and functions for each component are also described within this Appendix.

The sound pressure level (SPL) at the reception point, adjusted for the difference in ambient pressures at the aircraft and reception point locations is given by the equation:

$$SPL = 10\log p^2 + 10\log\frac{\rho^2 c^4}{p_{ref}^2} - 20\log\frac{p_1}{p_0}$$

Equation 1

Where p^2 is the mean-square acoustic pressure non-dimensionalised by $\rho^2 c^4$, where c is the ambient speed of sound at aeroplane location at minimum range. In this form it is given by:

$$p^2 = \frac{P \cdot b^2 \cdot D(\phi_f, \theta) \cdot F(Sr)}{4\pi \cdot r^2 (1 - M \cdot \cos\theta)^4}$$

Equation 2

The term $P \cdot b^2$, in Equation 2 is a function of Mach number and has the form:

$$P \cdot b^2 = k_1 \cdot M^{k_2} \cdot k_3$$

Equation 3

Where k_1, k_2 are constants and k_3 is a function depending on the airframe component under consideration. The acoustic power. P, has been non-dimensionalised by $P \cdot c^3 b^2$.

The Strouhal number (Sr) has the form:

$$Sr = \frac{f \cdot l}{M \cdot c}(1 - M\cos\theta)$$

Equation 4

Where l is a length scale characteristic of the airframe component.

Each airframe component also has its own directivity function, $D(\phi_f, \theta)$, and spectrum function, $F(Sr)$. Motion of the source is accounted for by the Doppler frequency factor $(1 - M\cos\theta)$, and a source amplification factor $(1 - M \cdot \cos\theta)^4$.

Values of ambient density and kinematic viscosity required by the calculations method are computed from input values of pressure and temperature using the relationships given in [ESDU 77021, 1977].

Airframe Element	k_1	k_2	k_3
Wing	4.464×10^{-5}	5	$0.37 S_w \left(\frac{V S_w}{v b_w} \right)^{-0.2}$
Horizontal tail	4.464×10^{-5}	5	$0.37 S_h \left(\frac{V S_h}{v b_h} \right)^{-0.2}$
Vertical tail	4.464×10^{-5}	5	$0.37 S_v \left(\frac{V S_v}{v b_v} \right)^{-0.2}$
For gliders, $k_1 = 7.075 \times 10^{-6}$ for the above components. Constants k_2 and k_3 remain unchanged.			
Single- or double-slotted trailing edge flaps	2.787×10^{-4}	6	$S_f \sin^2 \delta_f$
Triple-slotted trailing edge flaps	3.509×10^{-4}	6	$S_f \sin^2 \delta_f$
One- or two-wheel landing gear unit	4.349×10^{-4}	6	$n\, d^2$
Four-wheel landing gear unit	3.414×10^{-4}	6	$n\, d^2$
Landing gear strut	2.753×10^{-4}	6	$s\, d$

Table A-6: Constants and Geometry functions (parameters used in equation 3) [ESDU 90023, 2003]

	Directivity, $D(\phi_f, \theta)$	*Strouhal number, Sr*	*Spectrum function, F (Sr)*
Conventional wing	$4\cos^2\phi_f\cos^2(\theta/2)(1-\cos\theta)$ $(\theta < 90°)$	$f \cdot 0.37 \cdot \frac{S_w}{b_w}\left(\frac{V\,S_w}{\nu\,b_w}\right)^{-0.2}\frac{(1-M\cos\theta)}{V}$	$0.613(10Sr)^5[(10Sr)^{1.5}+0.5]^{-4}$
	$4\cos^2\phi_f\cos^2(\theta/2)$ $(\theta > 90°)$		
Delta wing	$4\cos^2\phi_f\cos^2(\theta/2)(1-\cos\theta)$ $(\theta < 90°)$	$f \cdot 0.37 \cdot \frac{S_w}{b_w}\left(\frac{V\,S_w}{\nu\,b_w}\right)^{-0.2}\frac{(1-M\cos\theta)}{V}$	$0.485(10Sr)^4[(10Sr)^{1.35}+0.5]^{-4}$
	$4\cos^2\phi_f\cos^2(\theta/2)$ $(\theta > 90°)$		
Horizontal tail	$4\cos^2\phi_f\cos^2(\theta/2)$	$f \cdot 0.37 \cdot \frac{S_h}{b_h}\left(\frac{V\,S_h}{\nu\,b_h}\right)^{-0.2}\frac{(1-M\cos\theta)}{V}$	$0.613(10Sr)^4[(10Sr)^{1.5}+0.5]^{-4}$
Vertical tail	$4\sin^2\phi_f\cos^2(\theta/2)$	$f \cdot 0.37 \cdot \frac{S_v}{b_v}\left(\frac{V\,S_v}{\nu\,b_v}\right)^{-0.2}\frac{(1-M\cos\theta)}{V}$	$0.613(10Sr)^4[(10Sr)^{1.5}+0.5]^{-4}$
Leading-edge slats	$4\cos^2\phi_f\cos^2(\theta/2)$	$f \cdot 0.37 \cdot \frac{S_w}{b_w}\left(\frac{V\,S_w}{\nu\,b_w}\right)^{-0.2}\frac{(1-M\cos\theta)}{V}$	$0.613(2.19Sr)^4[(2.19Sr)^{1.5}+0.5]^{-4}$
Single- and double-slotted flaps	$3(\sin\delta_f\cos\theta+\cos\delta_f\sin\theta\cos\phi_f)^2$ $(\theta < 90°)$	$\frac{fS_f}{b_f V}\quad(1-M\cos\theta)$	$0.0480\,Sr$ $(Sr < 2)$ $0.1406\,Sr^{-0.55}$ $(Sr \geq 2)$
Triple-slotted flaps	$\frac{3(\sin\delta_f\cos\theta+\cos\delta_f\sin\theta\cos\phi_f)^2}{(1-\cos\theta)^{-4}}$ $(\theta < 90°)$	$\frac{fS_f}{b_f V}\quad(1-M\cos\theta)$	$0.0257\,Sr$ $(Sr < 2)$ $0.0536\,Sr^{-0.0625}$ $(Sr \geq 2)$
One- and two-wheel landing gear unit	$1.5\sin^2\theta$ $(\theta < 90°)$	$\frac{fd}{V}(1-M\cos\theta)$	$13.59Sr^2(30.0+Sr^2)^{-2.25}$
	$1.5\sin^2\theta(1-\cos\theta)^4$ $(\theta > 90°)$		
One- and two-wheel landing gear strut	$3\sin^2\theta\sin^2\phi_f$ $(\theta < 90°)$	$\frac{fd}{V}(1-M\cos\theta)$	$5.325Sr^2(30.0+Sr^8)^{-1}$
	$3\sin^2\theta\sin^2\phi_f(1-\cos\theta)^4$ $(\theta > 90°)$		
Four-wheel landing-gear unit	$1.5\sin^2\theta$ $(\theta < 90°)$	$\frac{fd}{V}(1-M\cos\theta)$	$0.0577Sr^2(5.0+0.25Sr^2)^{-1.5}$
	$1.5\sin^2\theta(1-\cos\theta)^4$ $(\theta > 90°)$		
Four-wheel landing-gear strut	$3\sin^2\theta\sin^2\phi_f$ $(\theta < 90°)$	$\frac{fd}{V}(1-M\cos\theta)$	$1.280Sr^3(1.06+Sr^2)^{-3}$
	$3\sin^2\theta\sin^2\phi_f(1-\cos\theta)^4$ $(\theta > 90°)$		

Table A-7: Directivity, Strouhal number and spectrum functions for Airframe noise (parameters used in equations 1 through 4) [ESDU 90023, 2003]

A.3.2.5.3 Accuracy and Limitations

The airframe noise prediction procedure described by the ESDU procedure is not suitable for propeller-driven aeroplanes. The principal reason for this is unsuitability is that installation effects associated with propellers are likely to be very different from those associated with the turbofan aeroplanes used to develop the prediction method. The prediction method is not designed to account for either tonal components or to consider interaction between different airframe elements. The prediction method does not address airbrake or winglet noise, or the effect of podded undercarriages. Wing incidence effects have been neglected in the derivation of the method.

Although there are no explicit limits on take-off weights of airspeed, this prediction method has been validated for multi-engined turbofan aeroplanes with maximum take-off weights ranging from 42,000 kg to 390 000 kg and flying at airspeeds ranging from 70 m/s to 145 m/s. Wherever possible, data for runs in which engines had been set to flight idle were used for the validation purposes.

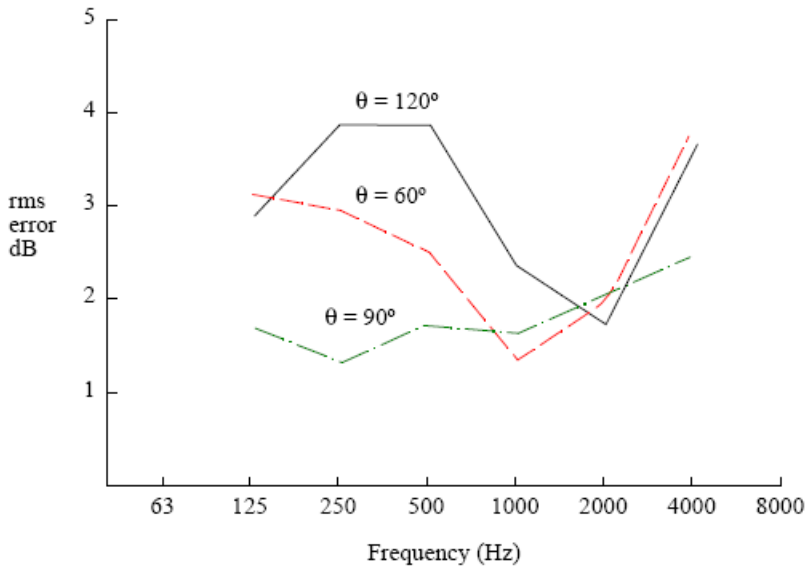

Fig A-19: Rms error from eight recent ESDU flyover data sets [ESDU 90023, 2003]

The airframe noise component is at its maximum fraction of the total aircraft noise during the final approach, because all the high lift devices are usually deployed, the undercarriage is lowered, and the engines are set at the minimum thrust setting required for maintaining the desired glide slope. In this configuration the root mean-squared (rms) error between estimated and measured one-third octave band sound pressure levels has been estimated for the range of aircraft flyovers in the available ESDU database. The corresponding values of rms error for the overall sound pressure level were of the order of 2 dB at θ =60 degrees, 1 dB at θ =90 degrees, and 3 dB at θ =120 degrees. The rms error is shown as a function of frequency for three different values of polar angle, θ , as shown in Fig A-19.

A.3.2.5.4 ESDU Executable program

There are two executable codes associated with ESDU data item 90023, and these are A9023 and B3023. The program A9023 provides a means of estimating the airframe noise generated by an aeroplane. Program B9023 can be run to create input files easily. Further details on the ESDU executable methods are noted within [ESDU 90023, 2003].

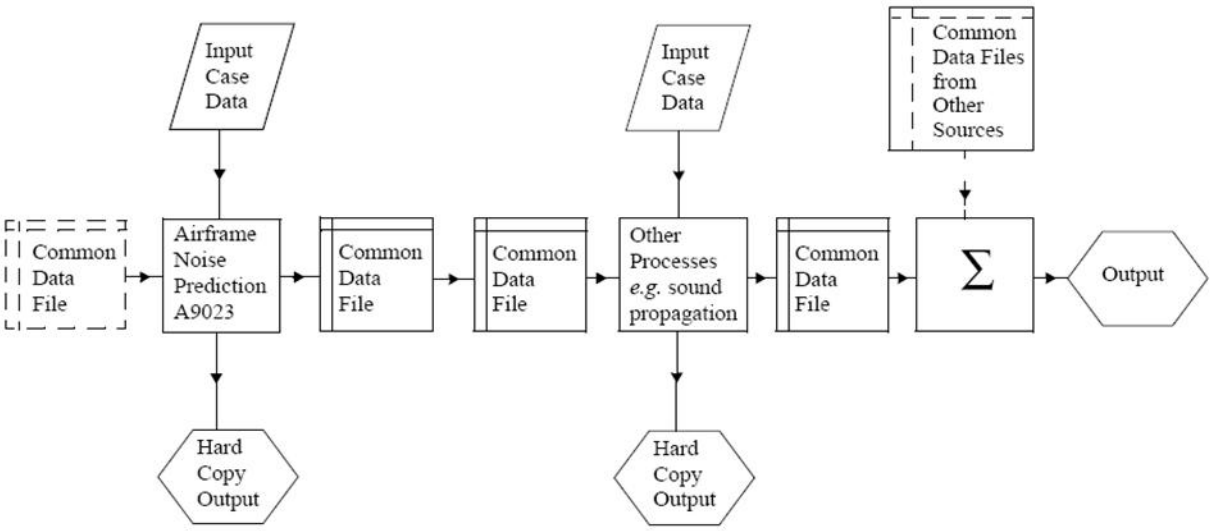

Fig A-20:ESDU program flow chart to summarise the procedure of noise calculations [ESDU 90023, 2003]

A.3.2.6 Airframe Noise Analysis

Noise produced by an airframe is divided into many components, the major sources being airfoil self noise (wing), empennage, TE devices, LE devices, and undercarriage. Additional noise sources which are difficult to determine magnitude of include interference between fuselage-wing, wing-pylons, pylons-engine nacelles, fuselage-tail, and small cavities across the aircraft, such as doors/hatches.

The focus of this slow and steep analysis is to identify whether current aircraft configurations could fly an approach at a slower velocity, or at higher flight path angles; to lower noise generated on surrounding airport regions. Main factor effecting noise is velocity, with all sources directly related to V^n, where 'n' varies for different noise sources. Noise for TE devices also varies depending on the degree of flap deflection. Undercarriage noise also depends on number of tyres, gear length and arrangement.

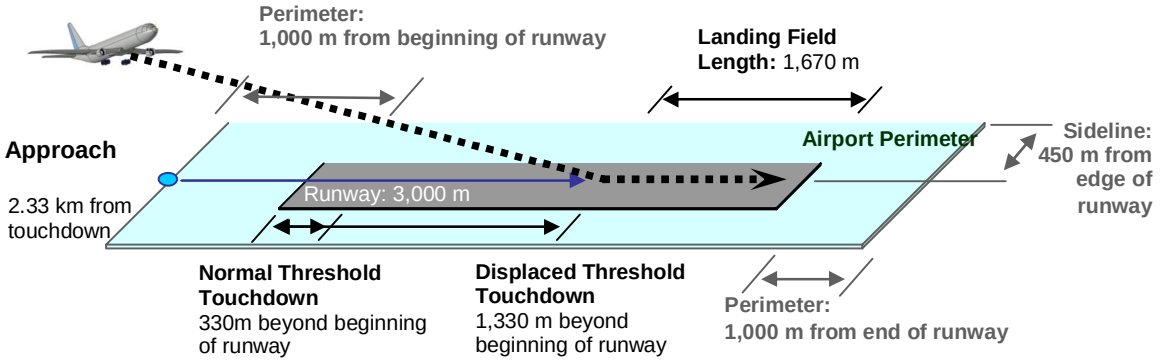

Fig A-21: BL aircraft on approach for a conventional and displaced landing threshold [Reynolds & Mistry, 2006]

A series of flight cases were established to determine aircraft noise. A standard approach considers an aircraft on a 3 degree FPA, with an aircraft touching down at 330m beyond the beginning of the runway, as shown in Fig A-21. This touchdown point is located 1km from the airport perimeter, which is considered as a noise measuring point for SAI. The ICAO limits aircraft height at the perimeter to be a minimum of 50ft (15.24m) above ground.

The second noise measuring point is defined by ICAO, located 2km from beginning of the runway. The requirements are clear that at this location, aircraft altitude must not fall below 120m. The noise measuring points are shown in Fig A-22, for take-off, landing, and sideline conditions for a datum airport; considered as London Heathrow (LHR).

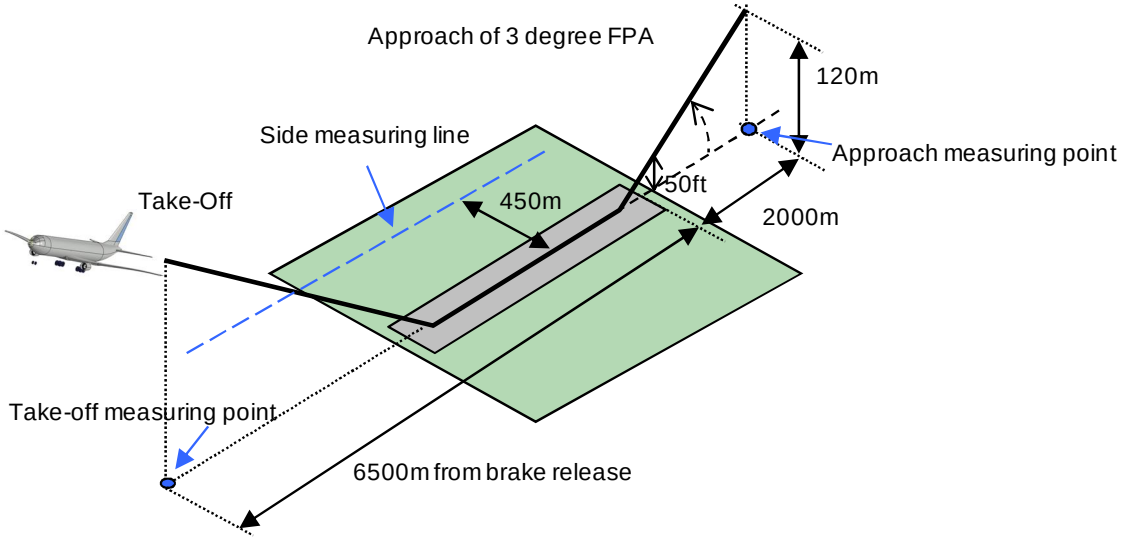

Fig A-22: ICAO Noise Measuring points [Reynolds & Mistry, 2006]

Two main noise measuring points are identified however, as shown in Fig A-22, there is an additional landing case using a 1km displaced threshold. This allows the aircraft to land 1,330m from the

beginning of the runway. There are now two measuring points and two landing conditions; however, there are also three approach velocities and three FPA to consider for a noise analysis.

Noise analysis is completed using ESDU Airframe Noise Prediction code [ESDU, 2003], as described within A-3.2.5 above, which predicts far-field airframe noise, including a breakdown of aircraft components for a landing configuration.

Determining altitude above ground is essential for using this code, so height at the perimeter is calculated for a standard and displaced threshold for each of the three FPA cases; 3, 5 and 6 degrees. The same cases are then recalculated for ICAO landing noise measuring point, or receivers (Rx); to ensure that minimum ground clearance is retained. The heights are shown below, where, *SAI Rx* refers to noise measurements at the airport perimeter and *ICAO Rx* refers to measurements taken a further 1km away.

We now have the height for each FPA case, each *Rx*, and we also have results for flap deflections at alternate approach velocities; for wing-flap and wing-flap-and-slat combinations. It is now possible to run the noise analysis using the ESDU method, using the undercarriage geometry from Table A-2.

Approach analysis considers the baseline aircraft on a specified approach FPA and velocity, with undercarriage deployed, DS flaps deflected by a given amount, and a choice to whether the slats will be deployed. The undercarriage noise is input as two components; nose and main gear, consisting of two 4-wheel bogie main gears, and a twin wheel nose gear.

FPA	Height at Standard threshold (S)		Height at Displaced threshold (D)	
	SAI Rx [m]	*ICAO Rx [m]*	*SAI Rx [m]*	*ICAO Rx [m]*
3	69.61	121.94	121.94	174.28
5	115.92	203.07	203.07	290.23
6	139.02	243.55	243.55	348.08

Table A-8: Height of aircraft above receivers for all FPA and threshold cases [Reynolds & Mistry, 2006]

Running the noise code produces far-field noise results for wing, undercarriage, slats, flaps and horizontal tail. The noise is output in overall sound pressure level OASPL [dB], which calculates the total energy contained within the spectrum, and is converted into the 'A' weighting scale, dB(A). The A-weighting scale assesses the frequencies that the human ear responds to more; "*to weight the sound pressure level in each frequency band by a factor which takes into account the ears sensitivity to that frequency range*" [Dowling & Ffowcs Williams, 1983].

The results produced by the aircraft directly above the receivers are shown below in Table A-9 and Table A-10; where these results are for a 3 degree fuselage constraint. The results show that maximum noise is generated from the BL on a 3 degree FPA at Va_1. As approach velocity reduces to 66.6m/s, noise is reduced by -1.5dB(A). As FPA changes, measured noise also reduces in the order of -2dB(A) per degree of FPA increase. Introducing displaced threshold and comparing results with a standard threshold produces a -4.8dB(A) reduction in noise.

Where:

H_s = height at standard threshold

H_d = height at displaced threshold

H_rs = height at ICAO receiver at standard threshold

H_rd = height at ICAO receiver at displaced threshold

$_1$ = FPA of 3 degrees

$_2$ = FPA of 5 degrees

$_3$ = FPA of 6 degrees

Case		H_s_1	H_s_2	H_s_3	H_d_1	H_d_2	H_d_3
		69.61	***115.92***	***139.02***	***121.94***	***203.07***	***243.55***
With slats and flaps deployed	***Va_1***	84.5	80.3	78.5	79.7	75.4	73.6
	Va_2	83.2	78.6	77.1	78.4	73.7	72.2
	Va_3	79.7	75.4	74.0	74.9	70.6	69.1
With flaps only deployed	***Va_1***	84.2	79.3	77.8	79.3	74.5	73.0
	Va_2	83.0	78.8	76.8	78.1	73.9	71.9
	Va_3	78.3	74.4	73.0	73.4	69.5	68.1

Table A-9: Noise in dB(A) for 3 degree fuselage incidence at SAI Rx location [Reynolds & Mistry, 2006]

Case		H_rs_1	H_rs_2	H_rs_3	H_rd_1	H_rd_2	H_rd_3
		121.94	***203.07***	***243.55***	***174.28***	***290.23***	***348.08***
With slats and flaps deployed	***Va_1***	79.7	75.4	73.6	76.6	72.3	70.5
	Va_2	78.4	73.7	72.2	75.3	70.6	69.1
	Va_3	74.9	70.6	69.1	71.8	67.8	66.0
With flaps only deployed	***Va_1***	79.3	74.5	73.0	76.2	71.4	69.9
	Va_2	78.1	73.9	71.9	75.0	70.8	68.8
	Va_3	73.4	69.5	68.1	70.3	66.4	65.0

Table A-10: Noise in dB(A) for 3 degree fuselage incidence at ICAO Rx location [Reynolds & Mistry, 2006]

An interesting result is that for an aircraft with flaps and slats deployed, noise produced compared with only flaps deployed varies between -0.1 and -0.5dB(A). This suggests that using flaps alone would slightly lower the approach noise, but not significantly due to the degree of flap deflection

needed to produce lift. Using slats adds an additional noise source, but does not impact noise significantly. Another interesting result is that although the 66.6m/s approach is considered to fail the FAR regulation on approach velocity, the noise reduction between similar flight cases is as much as -2dB(A).

The second case with a zero degree fuselage incidence provides the following results within Table A-11 and Table A-12. Results from this zero degree fuselage constraint, show similar trends to those for the 3 degree constraint. The expectation was that noise generated from this second study would increase due to additional flap deflection required for an approach FPA. The actual results agree with this statement, but noise produced varies between 0dB(A) to +0.4dB(A) by deflecting the flaps a further 5 or 10 degrees. The implication that flap deflection angles would significantly affect noise, are not true, according to these results. The fuselage angle is important, and reducing incidence by 3 degrees increases noise by +0.5dB(A). Therefore, increasing the fuselage angle on approach should lower noise; but this would have an impact on the cabin angle and would affect passenger comfort.

Case		H_s_1	H_s_2	H_s_3	H_d_1	H_d_2	H_d_3
		69.61	***115.92***	***139.02***	***121.94***	***203.07***	***243.55***
With slats and flaps deployed	Va_1	84.9	80.3	78.8	80.0	75.4	73.9
	Va_2	83.6	79.0	77.5	78.8	74.1	72.6
	Va_3	79.7	75.5	74.1	74.8	70.7	69.2
With flaps only deployed	Va_1	85.2	80.5	78.4	80.3	75.6	73.5
	Va_2	83.3	79.1	77.3	78.5	74.3	72.4
	Va_3	78.3	74.2	72.7	73.4	69.3	67.9

Table A-11: Airframe Noise dB(A) for zero degree fuselage incidence constraint at SAI Rx location [Reynolds & Mistry, 2006]

Case		H_rs_1	H_rs_2	H_rs_3	H_rd_1	H_rd_2	H_rd_3
		121.94	***203.07***	***243.55***	***174.28***	***290.23***	***348.08***
With slats and flaps deployed	Va_1	80.0	75.4	73.9	76.9	72.3	70.8
	Va_2	78.8	74.1	72.6	75.7	71.0	69.5
	Va_3	74.8	70.7	69.2	71.7	67.6	66.1
With flaps only deployed	Va_1	80.3	75.6	73.5	77.2	72.5	70.4
	Va_2	78.5	74.3	72.4	75.4	71.1	69.3
	Va_3	73.4	69.3	67.9	70.3	66.2	64.8

Table A-12: Airframe Noise dB(A) for zero degree fuselage incidence constraint at ICAO Rx location [Reynolds & Mistry, 2006]

Looking at incorporating the slow and steep approaches into one case, suggests that if the baseline 72.5m/s flight at 3 degrees is compared with that of 66.6m/s case at 6 degrees, the net result is a -10dB(A) reduction (to 74.1 dB(A)) in airframe noise at the perimeter. By combining this with a

displaced threshold concept, there is a further -4.9dB(A) reduction to 69.2dB(A); providing a net airframe noise reduction of -14.9dB(A) for the baseline. However, this noise benefit is purely for the airframe components, and estimations for the engine noise are also required.

This study into airframe slow and steep approach analysis has found that:

- BL aircraft on a 3 degree FPA, approach velocity of 72.5m/s, undercarriage extended, flaps deflected to 15 degrees, and slats deployed produces 84.9dB(A) of airframe noise at the airport perimeter.
- Reducing approach velocity to 66.6m/s, or $1.13V_{stall}$, reduces airframe noise by 1.3dB(A) to 83.6dB(A), with flaps deflected at 25 degrees.
- Reduction of approach speed is possible if FAR requirements are changed, but will not significantly affect the airframe noise issue.
- Displaced thresholds provide a large benefit for approach airframe noise by increasing distance between aircraft and ground, resulting in -3dB(A) noise reduction.
- Steep approach flight paths result in a -2dB(A) noise reduction per additional FPA degree; e.g. a further 10 degree increase in FPA would indicate a -20dB airframe noise reduction! This of course is totally unrealistic and is purely mentioned to illustrate the point.
- Varying the fuselage incidence does not significantly affect noise, as with increased deflection of the TE DS flaps.
- Combining two or more concepts, i.e. a 6 degree FPA, approach velocity of 1.13Vstall, and a displaced threshold as mentioned above; results in a -15dB(A) noise reduction for current aircraft.

To comment on this noise analysis, the baseline airframe is currently at its limits with regard to reducing the approach velocity. Airframe noise is under-predicted due to limitations in AVL for flap lift, and should be slightly higher than that indicated in the results above. Noise benefits of slow approaches have been investigated, along with steep approaches. A greater airframe noise benefit is achieved through the use of displaced thresholds, for which wing redesign is required to further increase the maximum achievable lift. Alternatively if the concepts analysed above, for slow, steep, and displaced thresholds were combined, along-with a redesign of the main wings, there would be a greater net reduction in airframe noise on the approach flight path.

A.3.2.7 Engine Noise Analysis

Engine noise has many different sources as per airframe noise, such as fan, jet and turbine noise. To make an estimate for noise produced by an engine on approach, thrust values were used from the force balance calculations, which typically varied between 15-30% of sea level static thrust (SLS). Noise measurements used values previously described in the airframe analysis, combined with engine thrust settings at each specified FPA. Engine noise data was calculated using methods within [Doulgeris, 2008].

Flight cases are identical as per airframe analysis; with three flight velocities, three FPA settings, and using standard and displaced thresholds. The following results describe a fuselage incidence set at zero, because the previous airframe analysis has shown that altering the fuselage angle does not affect noise significantly. The analysis uses ESDU methods to predict far-field fan and jet noise, which are shown below in Table A-13 and Table A-14.

Case		H_rs_1	H_rs_2	H_rs_3	H_rd_1	H_rd_2	H_rd_3
		69.61	***115.92***	***139.02***	***121.94***	***203.07***	***243.55***
Engine Noise 20% SLS	Va_1	98.5	91.8	86.0	93.5	86.9	81.0
	Va_2	97.2	91.0	86.7	92.1	86.1	81.8
	Va_3	95.8	89.0	88.4	90.9	84.2	83.5

Table A-13: Engine Noise dB(A) at SAI Rx location [Reynolds & Mistry, 2006]

Case		H_rs_1	H_rs_2	H_rs_3	H_rd_1	H_rd_2	H_rd_3
		121.94	***203.07***	***243.55***	***174.28***	***290.23***	***348.08***
Engine Noise 20% SLS	Va_1	93.5	86.9	81.0	90.4	83.8	77.9
	Va_2	92.1	86.1	81.8	88.7	83.0	78.6
	Va_3	90.9	84.2	83.5	87.7	81.0	80.4

Table A-14: Engine Noise dB(A) at ICAO Rx location [Reynolds & Mistry, 2006]

The results are as expected, showing a reduction in engine noise as distance between engines from the ground is increased. As velocity decreases, the noise produced by engines decrease; due to a reduced thrust requirement for the lower approach speeds.

Detailed engine noise results predict that fan noise dominates over jet noise by as much as +10dB(A) to +31dB(A); resulting in a higher engine noise compared with airframe. In an ideal scenario, with a thrust setting of approximately half (10-15% SLS), noise could reduce by half, however, this is not true in practice as the engine thrust would never be set to such a low setting. It is important to note that turbine noise is a very high noise source for the engine during landing, and estimations for this source are not included in this analysis.

The predicted engine noise can be combined with airframe noise to determine the total aircraft noise; using results within sections 6.8 and 6.9.

A.3.2.8 Aircraft Noise on Approach

Having identified airframe and engine noise components, and estimated noise during an approach condition, they are combined to determine total aircraft noise. It is essential to have a benchmark to compare results of this analysis, and so FAA noise certification data was used for the B767-300. This data uses estimated maximum sound levels measured in accordance with FAR AC 36-3H, April 25, 2002.

Aircraft	*Engine*	*MLW (lbs)*	*MLW (kg)*	*App Noise dB(A)*	*App flaps*
B-767-300	JT9D-7R4D(B)	320,000	145,150	92.3	30 deg
B-767-300	CF6-80A2	320,000	145,150	89.2	25 deg

Table A-15: FAA Noise Certification Data, courtesy of the Silent Aircraft Initiative [FAR AC 36-3H, 2002]

This data shows noise generated by the B767-300 aircraft, and shows flap settings required on approach, where two noise values for different engines are shown. This provides an upper and lower limit for the noise calculations within this report; allowing a reasonable error margin. The measurements are taken from the ICAO measuring locations, 2km from the threshold.

Comparing flap angle settings in table 8.16 with those determined using AVL for a zero degree fuselage incidence, 3 degree FPA, and at 72.5m/s, shows similar values. However, the FAA noise estimates include slats, whereas the AVL output does not, and this reinforces the statement that AVL under-predicts lift; due to misrepresentation of flaps as variable camber sections with zero slots. Estimating lift from LE slats along-with AVL outputs lowers the flap deflection angles than that set for a B767-300. Airframe noise prediction is lower than it should be due to errors in using AVL. It is important to note errors associated with prediction of engine thrust, and the use of ESDU methods for both analyses. Since the airframe noise is under-predicted and engine noise is possibly over-predicted, the higher noise source will dominate the combined noise.

Addition of the two noise sources can simply be achieved using a cubic equation. The higher noise source is subtracted from the lowest source to provide Δx. The following equation [ESDU 66017, 1978] is then used to determine $\Delta dB(A)$:

$$\Delta dB(A) = -0.0005\Delta x^3 + 0.0275\Delta x^2 - 0.4809\Delta x + 2.9925$$

Equation A-5

$\Delta dB(A)$ is then added to the maximum noise value to provide the total combined noise of the two sources.

Since the zero fuselage incidence constraint is only considered, aircraft noise can be determined by combining engine and airframe noise using Equation A-5 above. Airframe noise analysis identified that using flaps alone compared to a flap-slat combination does not significantly reduce airframe noise. Therefore the following aircraft noise analysis will only consider an airframe with flaps and slats. Table A-16 and Table A-17 below show the results for using this method of combining airframe and engine noise components.

Case		H_rs_1	H_rs_2	H_rs_3	H_rd_1	H_rd_2	H_rd_3
		69.61	***115.92***	***139.02***	***121.94***	***203.07***	***243.55***
With slats and flaps deployed	Va_1	98.8	92.2	86.7	93.8	87.3	81.8
	Va_2	97.5	91.3	87.2	92.3	86.4	82.3
	Va_3	96.1	89.3	88.7	91.2	84.4	83.8

Table A-16: Aircraft noise dB(A) for zero degree fuselage incidence constraint at SAI Rx location [Reynolds & Mistry, 2006]

Case		H_rs_1	H_rs_2	H_rs_3	H_rd_1	H_rd_2	H_rd_3
		121.94	***203.07***	***243.55***	***174.28***	***290.23***	***348.08***
With slats and flaps deployed	Va_1	93.8	87.3	81.8	90.7	84.1	78.7
	Va_2	92.3	86.4	82.3	89.0	83.3	79.1
	Va_3	91.2	84.4	83.8	88.0	81.3	80.6

Table A-17: Aircraft noise dB(A) for zero degree fuselage incidence constraint at ICAO Rx location [Reynolds & Mistry, 2006]

Results above show that maximum noise is generated by the baseline aircraft on a 3 degree FPA at Va_1 is 98.8dB(A) at SAI receiver. Compared with airframe noise results, total combined noise has less of a variation as velocity is reduced, and this is due to the dominant engine noise. Noise provided by engine is +13.6dB(A) relative to airframe noise; for a 3 degree, standard threshold, 72.5m/s case. Reducing approach velocity to 66.6m/s lowers aircraft noise by -1.3dB(A) from 98.8dB(A) to 97.5dB(A). Further reduction to 55m/s lowers aircraft noise by -1.4dB(A) to 96.1dB(A). These results show that lowering approach speed does not significantly reduce aircraft noise.

As FPA changes, aircraft noise maintains a greater reduction compared with airframe noise. As FPA increases from 3 degrees to 5 degrees, noise reduces by -6.6dB(A) for the Va_1 case mentioned above; from 98.8dB(A) to 92.2dB(A). As FPA increases to 6 degrees, aircraft noise reduces further by -5.4dB(A) to 86.7dB(A). These reductions also vary depending on approach velocity; on average they are in the order of -3.3dB(A) per degree of FPA increase.

Displaced thresholds compared with a standard threshold for a 3 degree, 72.5m/s case results in a -4.9dB(A) reduction in noise from 98.8dB(A) to 93.8dB(A). On average displacing the threshold by 1km provides a -5.0dB(A) reduction in aircraft approach noise at SAI noise receiver.

Comparing noise from the ICAO receiver locations to that of FAA certification data for B767-300, identifies an error in results. The maximum noise for a B767-300 aircraft is 92.3dB(A), with the minimum measured noise being 89.2dB(A). Maximum noise results at ICAO measuring point were for 3 degree FPA, at 72.5m/s for a standard threshold point, which basically represents a conventional approach condition. This conventional case has a maximum noise of 93.8dB(A), which is +1.5dB(A) higher than the maximum FAA measuring noise; providing a 1.6% error. This error is partially due to calculations used and airframe noise generated from AVL lift and flap modelling. Alternate or smaller noise sources due to interference between airframe components, hatches, and pylons, were not considered and could add up to a few dBs. Another major source of error would be the engine noise calculations.

A more effective way to represent this data is to show how noise varies with height from the ground. An aircraft on approach FPA obviously gets closer to the ground as it approaches the airfield threshold, and as a result noise increases in relation to 1/r; where ‘r’ is the height of the aircraft above ground, as shown in Fig A-23.

Fig A-23 represents a combination of standard and displaced thresholds, because some of the previous tabulated results are replicated. For example, a displaced threshold SAI case is identical to that of a standard threshold ICAO case; due to the distance between receiver and threshold being 2km, or distance to touch-down being 2.33km. Therefore the height above the ground between aircraft and receiver are the same for each case, hence identical noise. These results may be further extended to show trends in varying displacement further than 1km initially estimated, but are only valid for airports with longer runways.

Fig A-18 includes an additional approach case for the threshold location (0m), for each FPA and velocity variation; where displaced threshold calculations were not made as this would duplicate existing results for the height of an aircraft at SAI standard case. These results show how aircraft noise at threshold peaks above 110dB(A) for a 3 degree, 72.5m/s approach case.

Maximum aircraft noise for zero fuselage incidence constraint, with 72.5m/s flight velocity at 3 degree SAI measurement case is 98.8dB(A). Incorporating slow and steep approaches into a single flight case, suggests that this case compared with a 66.6m/s approach case at 6 degrees, results in a -11.5dB(A) reduction in aircraft noise to 87.2dB(A) at airport perimeter. By combining this result

with a displaced threshold concept, there is a further -5.0dB(A) reduction to 82.3dB(A); providing a net aircraft noise reduction of -16.5dB(A).

Results have also shown that changing approach velocity is not a major influence for aircraft noise compared with steep approaches and displaced thresholds. Investigating the same scenario of a 3 degree standard threshold case at 72.5m/s, and assuming that a 6 degree FPA is possible; aircraft noise is reduced by -12.0dB(A) to 86.7dB(A) at the perimeter. Combining a displaced threshold further reduces noise by -4.9dB(A) to 81.8dB(A). Therefore net aircraft noise reduction by using displaced threshold and a 6 degree FPA is -16.9dB(A).

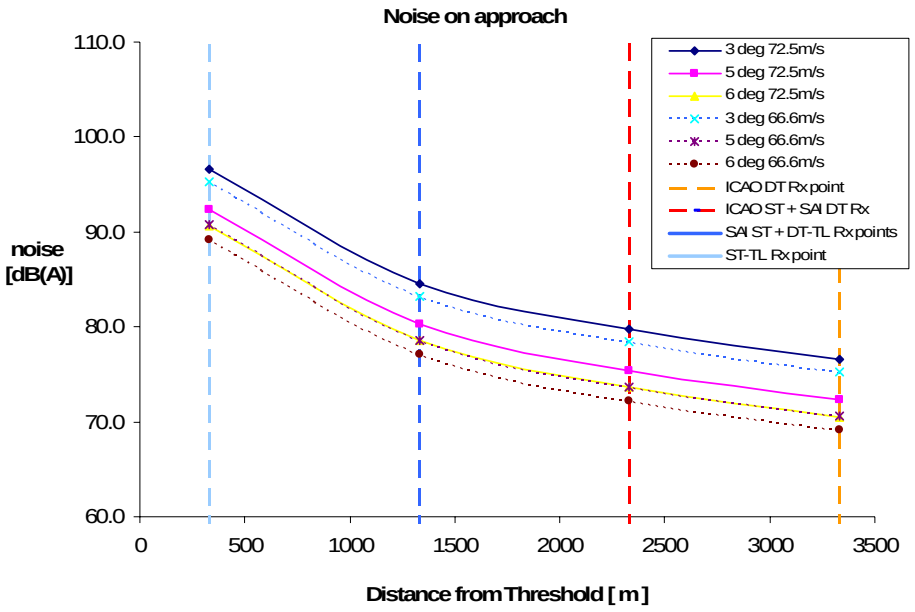

Fig A-23: Noise Variation with distance from airfield threshold, where DT=displaced threshold, ST=standard threshold, Rx=receiver, TL=touch-down length [Reynolds & Mistry, 2006]

The main emphasis of this result is that a significant noise reduction can be achieved at the airport perimeter by increasing the aircraft FPA and displacing the threshold, without changing the aircraft approach velocity. A contradiction to this is that an approach velocity of 72.5m/s, on a 6 degree FPA, with a shorter runway to land on, and less of a stopping distance, would require greater high lift and drag capability for the wings; emphasising wing re-design.

This study into aircraft slow and steep approach analysis has found that:

- BL aircraft on a 3 degree FPA, approach velocity of 72.5m/s, undercarriage extended, flaps deflected to 15 degrees, slats deployed, and engines throttled at 28% SLS produces 98.8dB(A) of noise at the airport perimeter.

- BL aircraft analysed on a conventional approach at ICAO *Rx* location produces 93.8dB(A) with a +1.6% error compared with the FAA noise certification data having a maximum noise of 92.3dB(A).
- Reducing approach velocity to 66.6m/s, or $1.13V_{stall}$, does not significantly reduce aircraft noise to warrant a change in FAR regulations, but does have an influence on airframe noise. Regulations would be difficult to change because of reduced safety margins at low speeds.
- Displaced thresholds provide a large benefit for aircraft approach noise by increasing distance between aircraft and ground, resulting in -5dB(A) noise reduction.
- Steep approach flight paths result in a -3.3dB(A) noise reduction per additional FPA degree; e.g. a further 5 degree increase in FPA would indicate a -16.5dB aircraft noise reduction!
- Varying the fuselage incidence does not significantly affect noise, as is the case with increased deflection of TE DS flaps.
- Adding an extra noise source from LE slats compared with using increased flap deflection does impact the noise significantly.
- Combining two or more concepts, i.e. a 6 degree FPA, approach velocity of 1.13Vstall, and a displaced threshold as mentioned above; results in -16.5dB(A) noise reduction for current aircraft.
- Noise results above show varying velocity does not influence aircraft noise significantly. For a standard 72.5m/s approach velocity, with a 6degree FPA, and displaced threshold results in a -16.9dB(A) aircraft noise reduction; which is achievable for current flying aircraft.

To comment on this noise analysis, the BL aircraft is currently at its limits with regard to reducing the approach velocity. Airframe analysis emphasised benefits of slower approaches, and engine noise is still the dominant noise source. Steep approaches have been investigated with the main result reflecting a reduction in noise for every degree the FPA is increased. However, a great aircraft noise benefit is achieved through the use of displaced thresholds, for which wing redesign is required to further increase the wing maximum achievable lift.

The main conclusion for this analysis is that combining the steep and displaced thresholds concepts, along-with a redesign of the main wings, would result in -17dB(A) net reduction in aircraft noise on

the approach flight path. This provides a short-term solution to the aircraft noise challenge we have at present.

The analysis above represents changes to current practice approach procedures and impact on noise. This method is a complex and detailed procedure which has established an approach noise measurement method, and can be implemented to any aircraft configuration. The main benefit for conducting this analysis is to establish errors in the design process and in the tools used. This allows alternative novel concepts to be analysed with a certain margin of error, and these new configurations can be compared with the BL aircraft.

A.3.2.9 Approach Airframe Noise components

Airframe noise components have previously been described, but it is important to determine which noise sources are dominant for an approaching aircraft. The ICAO noise measurement location with an aircraft on a 3 degree FPA, at 72.5m/s, with flaps deflected at 35 degrees, is analysed; directly above the noise receiver, with the noise spectrum shown in Fig A-24 below. The spectrum analyses the noise between 50Hz and 10kHz frequency range and compares the individual source components to each other.

Fig A-24 shows how the dominant noise sources are the TE double slotted flaps, slats and wing for high and low frequencies ranges. At certain frequencies in the middle of the spectra, main undercarriage, slats, and flaps dominate. It is interesting to see that horizontal tail noise has a greater magnitude than the nose undercarriage at low frequencies, but as frequency increases, the nose gear tends to dominate.

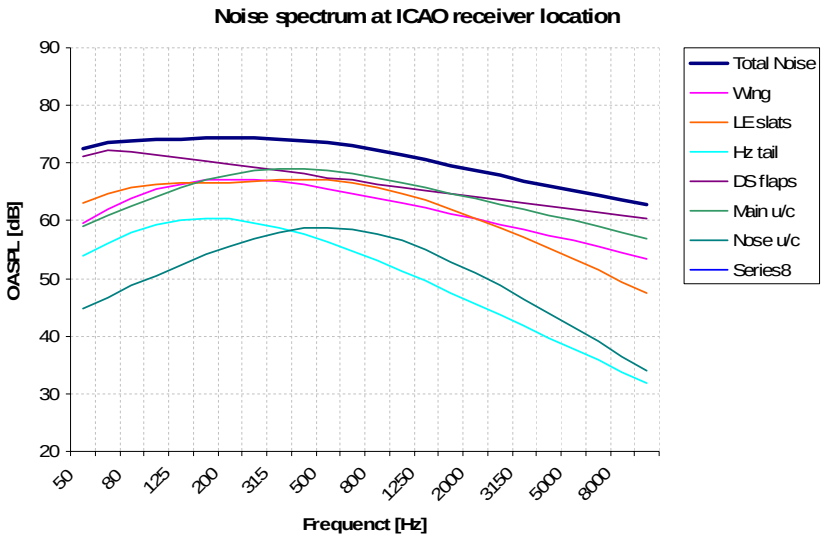

Fig A-24: Baseline noise spectra at ICAO receiver location [Reynolds & Mistry, 2006]

Airframe noise analysis was completed in more depth than that described above for single point cases. Approach noise was considered along a flight path, where over the 2km distance between the ICAO measuring point and airport threshold a series of four observers were stationed along the ground at 0m, 100m, 200m, 300m, 400m, and 450m to the sideline. The resultant 24 noise receivers were used to estimate the airframe noise of the BL as it approached on a 3 degree flight path at 72.5m/s.

Fig A-25 represents noise measured as the BL flies over each receiver. Maximum noise is measured directly below the aircraft when comparing noise with each sideline case, and peak noise measured at each receiver is when the aircraft is orientated at 87degrees. Noise variations from Fig A-25 show that as the aircraft approaches a receiver noise increases, and stays at a high level even after the aircraft has started to retreat. Noise then decreases rapidly as the aircraft flies past the range of this receiver and enters the range of the next receiver.

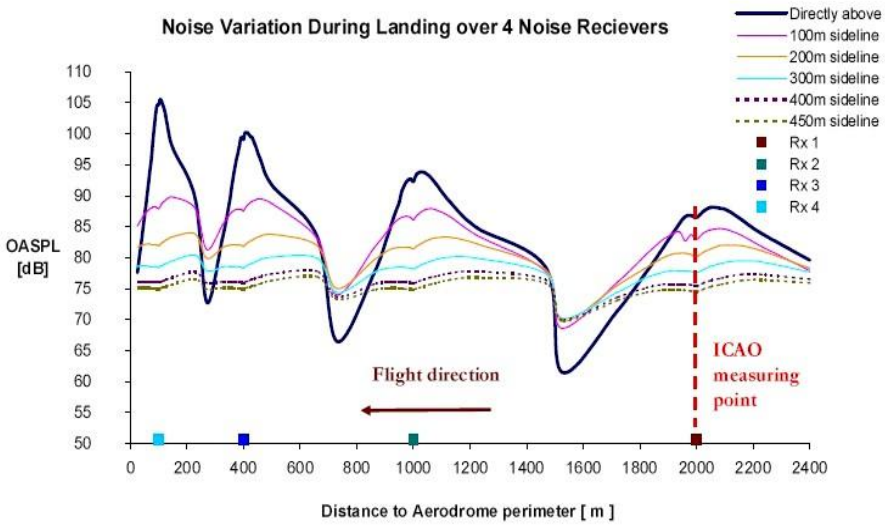

Fig A-25: Airframe noise for a 3 degree approach flight path at 72.5m/s

The range limit of each receiver is clearly represented by dips in noise levels, and indicates the cross between an approaching aircraft noise measurement and a retreating noise measurement between the two receivers. It is interesting to note that noise measured at a sideline case is much higher at these cross-over locations and is due to ground reflections amplifying the noise measured at these locations.

These noise measurements can be analysed and interpolated to determine points for which airframe noise reaches a 90dB limit. These 90dB margins have been identified to produce a ground contour plot for an approaching aircraft. These plots are usually provided by aircraft manufacturers as part of their specifications, as shown in Fig A-26.

Fig A-27 represents the baseline noise contour plots corresponding to a 3 degree approach condition. Fig A-27 is the calculated noise contour for the BL and relates to the left hand section of the Airbus noise plots for approach and landing noise. This plot represents airframe noise alone and does not include estimates for engine noise on approach idle setting. The addition of engine noise will be combined with the airframe noise once the take-off flight condition has been finalised and a complete contour plot can be produced for the BL aircraft.

Airframe noise sources have been identified for the BL aircraft, with a detailed landing analysis for the dominant airframe approach flight case. These results have been compared with FAA noise certification data and show slight errors in the order of 1.6% for aircraft noise calculations. Aerodynamic analysis of the BL aircraft approach configurations has been completed and can be repeated for all novel airframe concepts. The main emphasis now is to complete the next airframe concept and conduct a similar approach analysis for the new design and compare noise results.

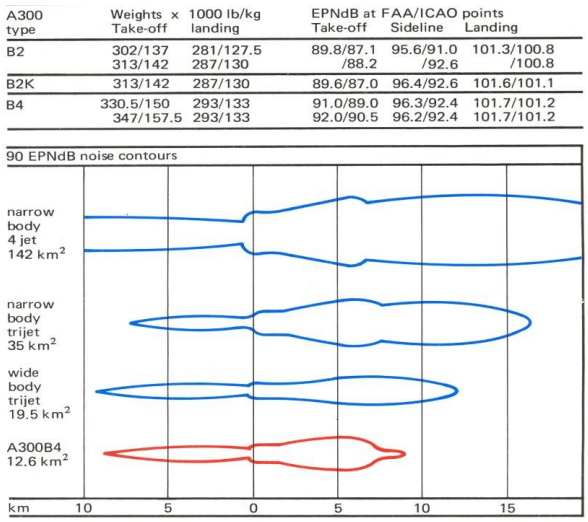

Fig A-26: Airbus A300 noise contour plot

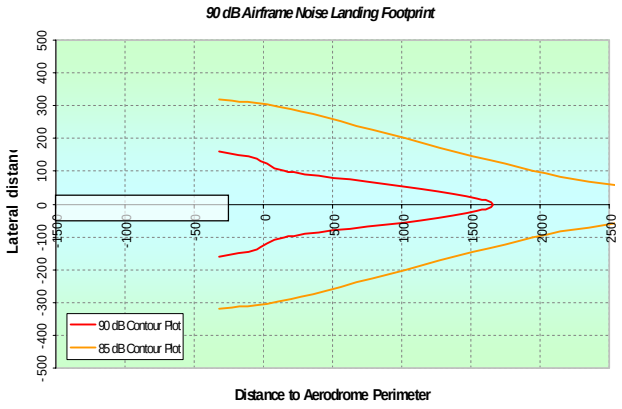

Fig A-27: Baseline landing noise contour plot

Appendix B BL and BD Parametric Analysis

This Appendix describes the parametric analysis process for the baseline aircraft and the broad delta airframe concept. The decision to combine the analysis for these two designs enables a detailed comparison of each design from the initial analysis phase through to airframe optimisation. An in-depth account of how the baseline and broad delta designs deviate is described, where comparisons with the baseline aircraft cease, as the detailed optimisation process for the broad delta airframe begins.

B.1 Background

The targets set by the Silent Aircraft Initiative (SAI) provided an aircraft specification for a 4,000 nautical mile medium-range civil transport, capable of cruising at 0.8 Mach, and for the smallest possible variant with a 216 passenger 3-class cabin arrangement. The main goal of the aircraft design process was to establish suitable integrated airframe and engine solutions to reduce the noise outside the perimeter to 60dB(A).

B.1.1 The Baseline Aircraft

The design of a new technology baseline (*NT*-BL) and a datum baseline (*D*-BL) were compared with an existing aircraft of a similar class, the Boeing 767-300 (Fig B-1), where the results of the parametric analysis were compared with published aircraft data in **Appendix A**. Airframe noise analysis defines the *D*-BL aircraft landing, sideline, and take-off noise cases for a standard airport, defined as London Heathrow (LHR), and are presented within **Chapter 6**. The BL aircraft designs use published data from the B767-300, where wing loading and thrust-to-weight ratio are obtained from the [Jenkinson et. al, 1999] electronic data link, to initiate the design process (Table B-1).

Parameter	*Imperial units*	*S.I units*
Overall Length	176.1 [ft]	53.7 [m]
Overall Height	37.7 [ft]	11.5 [m]
Wing span	156.2 [ft]	47.6 [m]
Wing Area	3,049 [ft^2]	283.3 [m^2]
Wing Aspect Ratio	7.99	7.99
V_{max}	562.8 [mph]	251.6 [m/s]
Max service ceiling	39,000 [ft]	11,887 [m]
Range	3,493 [miles]	4,020 [n.miles]
AUM	345,000 [lb]	156,489 [kg]

Table B-1: Baseline aircraft; (*http://www.bh.com/companions/034074152X/appendices/default.html/*)

The parametric design methodology is based on semi-empirical calculations using a conceptual design analysis method from [Howe, 2000]. This parametric analysis was the basis for an initial study of all airframe concepts. The *D*-BL and *NT*-BL aircraft were designed in parallel with the broad delta (BD) airframe, where two variants of a BD were investigated, providing a total of three simultaneous working designs.

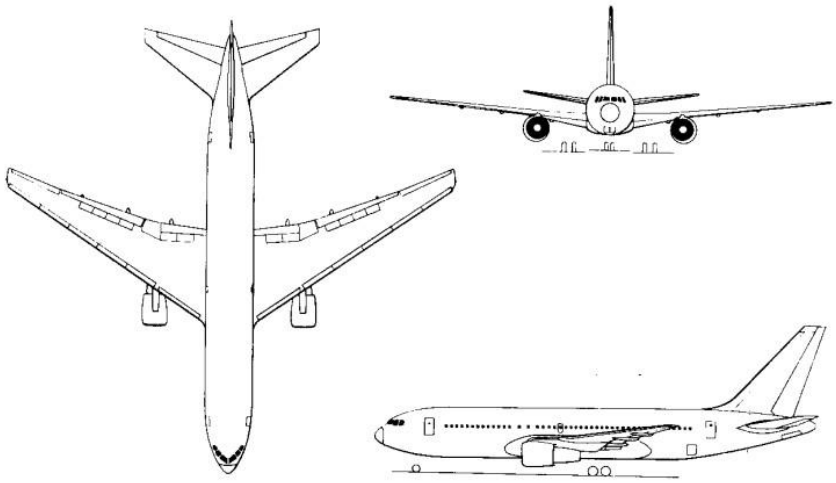

Fig B-1: Boeing 767-300 General Arrangement (http://www.aviastar.org/pictures/usa/boeing-767.gif).

B.1.2 The Broad Delta Aircraft Concept

The broad delta (BD) design was based on the same specification as the baseline parametric analysis [Howe, 2000]. Unlike the BL aircraft no existing civil aircraft to-date was available to compare wing aspect ratio, airfoil types, and performance data to initiate the design process. The fuselage was the one commonality between the BL and BD concept. Investigations into military aircraft provided a means to gather data on similar delta winged aircraft, one such design was the Avro Vulcan advanced tactical bomber [Davies, 1969], which was tailless (Fig B-2).

Parameter	*Imperial units*	*S.I units*
Overall Length	99.9 [ft]	30.5 [m]
Overall Height	27.2 [ft]	8.3 [m]
Wing span	111 [ft]	33.8 [m]
Wing Area	3965 [ft^2]	368.4 [m^2]
Wing Aspect Ratio	3.11	3.11
V_{max}	625 [mph]	543 [knots]
Max service ceiling	55,000 [ft]	16,764 [m]
Range	3,000 [miles]	2,605 [n.miles]
AUM	170,000 [lb]	77,111 [kg]

Table B-2: Avro Vulcan Aircraft data adapted from (http://www.aerospaceweb.org/aircraft/bomber/vulcan/).

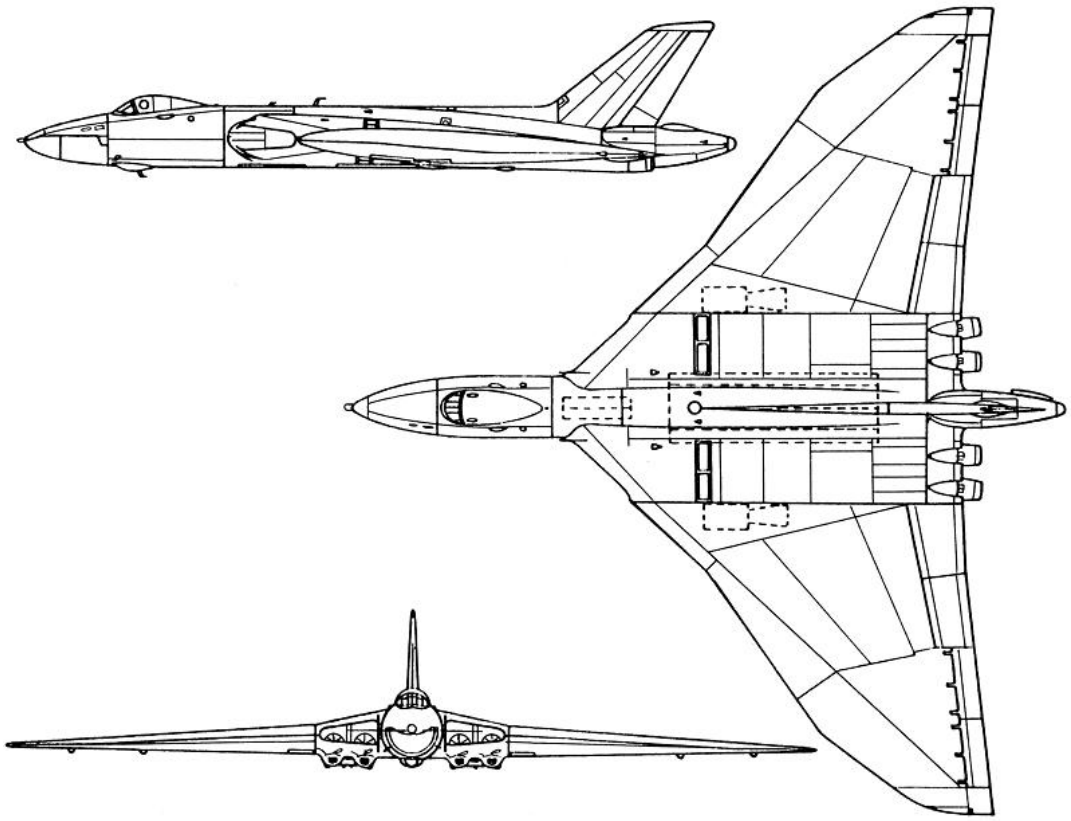

Fig B-2: Avro Vulcan General Arrangement Diagram (http://www.raf.mod.uk/history_old/vforcespec.html).

This delta-wing aircraft had benefits of a large wing design without the need for horizontal empennage, a capability of carrying large payloads with its ideal lifting surface planform, and excellent handling characteristics; especially for an aircraft which required the use of four turbojet engines. The development of the BD concept utilised data from the Vulcan as the primary source of initial design data as shown in Table B-2.

The parametric design methodology is similar to that used on the BL with minor modifications to equations. It is the decision of the author to consider two alternative configurations for the BD concept. The primary design is a tailless BD and is referred to as the broad delta single fin arrangement (BDSF), with the second derivative being a tailed variant and will be referred to as the broad delta fin and tail configuration (BDFT). The two concepts will be analysed in parallel from this point onwards.

B.2 Initial Parametric Design Analysis

To initiate the design, estimates for the wing geometry, propulsion system, and flight characteristics are required. A summary of these initial design parameters are provided in the following analysis, where the use of Howe's first design spreadsheet is combined with modifications by the author to

initiate the first stage of the parametric design. This Appendix contains data extracted from electronic references for the design of the *NT*-BL aircraft, where a link by [Jenkinson et al., 1999] is referred to as '(source 1)' and for the Avro Vulcan, data extracted from [Davies, 1969] is referred to as '(source 2)'.

B.2.1 Input Variables

Three major design variables are wing aspect ratio (A), thickness-to-chord (t/c), and engine by-pass ratio (BPR). Using (source 1) the *NT*-BL aircraft A = 7.99 and t/c = 0.115, compared to (source 2), where the BD concepts have the same A = 3.11 and t/c = 0.11. All designs use the same engine design of a moderate to high bypass ratio ($BPR = 8$).

B.2.2 Required Data

Data essential to the design of each configuration reflects the flight velocities, Mach numbers, range requirements, and take-off and landing characteristics.

B.2.2.1 Velocity Profiles

Defining mission velocities and Mach numbers (M_N) is necessary to set limits on operating flight conditions for the concept design. For initial cruise calculations, a limit of 460knots (237m/s) was set at 39,000ft, relating to a cruise $(M_N)_{cr}$ of 0.801. A critical flight M_N for the same altitude was established using the design speed (V_D), being 489knots (252m/s), providing $(M_N)_{crit}$ of 0.852.

A critical value for landing performance and more importantly for this study, noise, is the approach velocity (V_a). The maximum approach velocity for all concepts is considered to be similar to a current conventional aircraft, where $V_{a.max}$ = 72m/s. The actual approach velocity, V_a, is a function of the landing to take-off mass ratio (M_L/M_0) and approach lift coefficient (c_{La}), as shown in Equation B-1.

$$V_a = 1.278 \cdot \left(\left(\frac{1}{c_{L.a}} \right) \cdot \left(\frac{Mg}{S} \right)_0 \cdot \left(\frac{M_0}{M_L} \right) \right)^{1/2} \text{ [m/s]}$$

Equation B-1

(M_L/M_0) for medium range flight is a function of design range $(s)_{\text{des.range}}$, (Equation B-2).

$$\left(\frac{M_L}{M_0} \right) = \left(1 - 2 \cdot (s)_{range} \times 10^{-5} \right)$$

Equation B-2

Given that the range requirement is the same, $M_L/M_0 = 0.851$ for all three configurations.

The take-off wing loading $(Mg/S)_0$ varies depending on which configuration is considered. The *NT*-BL take-off wing loading of $(Mg/S)_0 = 5418.8$ kg/m^2 was an initial input value from (source 1). An estimate from (source 2) provided an $(Mg/S) = 2053$ *N/m*^{2} for the BDSF, so a value of $(Mg/S)_0 = 2000$ *N/m*^{2} was used for an initial design input. The BDFT resembles a conventional aircraft because it has a tail, but would not have a similar wing loading as the *NT*-BL because of the low aspect ratio wing, neither would it be similar to the BDSF, so an estimate of $(Mg/S)_0 = 3000$ *N/m*^{2} was used as a first approximation.

The importance of calculating c_{La} from Equation B-1, is to achieve a low V_a on approach, whilst generating enough drag to safely land the aircraft without stalling the wing. The calculation of c_{La} is dependent on the wing and empennage configuration, resulting in three outputs, one for the *NT*-BL, BDSF and the BDFT.

The BDSF has no horizontal empennage, making the aircraft a naturally stable tailless design, without the requirement to use high lift devices such as flaps or slats. The trailing edge (TE) devices used for the BDSF are a combination of elevators to establish trim and pitch, and ailerons for roll authority; referred to as elevons.

The BDFT configuration is identical to the *NT*-BL, with a horizontal empennage stabilising the aircraft on approach, the use of elevators for pitch control, TE flaps and ailerons for trim and roll control, and the addition of LE slats to increase c_{La}, drag, and reduce the approach velocity.

Equation B-3 is used to calculate c_{La}, which is 70% of the maximum low speed lift coefficient ($c_{L\,max}$), for a calculated wing quarter-chord sweep angle ($\Lambda_{¼}$).

$$c_{L.a} = 0.7 \cdot c_{L.\max} \cdot \cos \Lambda_{1/4}$$

Equation B-3

The *NT*-BL maximum achievable lift coefficient ($c_{L\,max}$) is calculated for a high aspect ratio swept wing at low speeds, where:

$$c_{L.\max} = \left(1.5 + \Delta_{LEL} + \Delta_{TEL}\right) \cdot \cos\left(\Lambda_{1/4}\right)$$

Equation B-4

The maximum achievable lift coefficient ($c_{L\ max}$) for a low aspect ratio delta wing aircraft at low speeds is given by Equation B-5.

$$c_{L.\max} = \left[\left(\frac{A}{2} \right)^{1/2} \cdot \cos \Lambda_{1/4} + \Delta_L \right]$$

Equation B-5

An additional high speed military combat manoeuvre lift coefficient can be calculated for the delta wing, but is not investigated further as this is a civil aircraft concept, with restricted manoeuvrability.

The *NT*-BL aircraft utilises both leading edge (LE) and trailing edge (TE) high lift devices on the wing to increase the maximum achievable lift coefficient and avoid wing stall at low speeds. Δ_L is the increment in lift due to LE and TE devices. The high aspect ratio *NT*-BL wing is integrated with LE slats and TE double-slotted flaps (DSF), where Δ_{LEL} = 0.65 and Δ_{TEL} = 1.35, providing a total lift increment of $\Delta_{L\ NT\text{-BL}}$ = 2.0 for the *NT*-BL.

It was necessary to increase Δ_L through using LE devices on the BDSF to increase $c_{L\ max}$ so that the effect of wing stall would be minimised and to reduce V_a for noise implications. A drooped LE device extension (*LEX*) was incorporated into the BDSF wing design, where $\Delta_{L\ BDSF} = \Delta_{LEL}$ = 0.3, but because of the tailless configuration the wing has no requirement for additional TE high lift devices.

The BDFT is similar to the *NT*-BL aircraft and incorporates both LE and TE devices, where drooped *LEX* devices are used alongside TE variable camber flaps (*VCF*), where the lift increment for a *VCF* is estimated as an intermediate value between a single slotted flap and a plain flap arrangement; where Δ_{TEL} = 0.4, providing $\Delta_{L\ BDFT} = \Delta_{TEL} + \Delta_{LEL}$ =0.7.

The remaining unknown from the above analysis $\Lambda_{¼}$ is calculated using Equation B-6, where $c_{L\ use}$ is the useable lift coefficient during cruise.

$$\Lambda_{1/4} = \cos^{-1}\left(\frac{0.95 - (0.1 \cdot c_{L.use}) - t/c}{M_{N.crit}} \right)^2 \text{ [deg]}$$

Equation B-6

	$\Lambda_{¼}$ [deg]	$c_{L\,max}$	c_{La}	V_a [m/s]
NT-BL	32.3	2.96	2.07	70.8
BDSF	29.3	1.39	0.971	62.8
BDFT	32.3	1.75	1.23	68.4

Table B-3: Calculated data for Velocity profile analysis

A typical value for $c_{L\,use}$ for a high aspect ratio civil airliner wing is 0.6, however for the BD concept, the low aspect ratio wing requires less lift due to the large wing area. It is not to suggest that less work is done during cruise, but that a larger wing area allows the airfoils to work at a lower lift coefficient, compared to a conventional high aspect ratio wing. Therefore two initial estimates for $c_{L.use}$ were selected to start the analysis for BDSF (0.44), and BDFT (0.57); due to the addition of a tail.

B.2.2.2 Cruise Altitude and Range

Design range for the BD concept is 4,020 nautical miles (7449 km) which is consistent with the baseline. Cruise flight is split into two segments, for which the relative atmospheric density ($\sigma = \rho/\rho_0$) is required for the start of cruise (σ_{cr1}) and at the second cruise altitude stage (σ_{cr2}). Typically σ_{cr1} is at an altitude below 11km, and σ_{cr2} above 11km, where for an initial design study σ_{cr1} = 0.3829 (10km) and σ_{cr2} = 0.2971 (11.5km).

B.2.2.3 Factored Take-Off Length (*ToL*)

The factored take-off length (ToL) includes a 15% increase in take-off length to consider bad weather conditions (Equation B-7). The first term includes the ground run to reach lift-off speed (s_g), the distance covered during rotation, and the distance to climb to a 15.3m obstacle clearance height (determined by the 170 constant value).

$$ToL = \underbrace{\frac{k_e}{c_{L.us}}\left(\frac{T}{Mg}\right)_0^{-1.35} \cdot \left(\frac{Mg}{S}\right)_0}_{1^{st}} + \underbrace{6 \cdot \left(\frac{Mg_0}{S \cdot c_{L.us}}\right)^{1/2}}_{2^{nd}} + \underbrace{170 \cdot \left[1 - \left(\frac{T}{Mg}\right)_0\right]}_{3^{rd}} \text{ [m]}$$

Equation B-7

Engine thrust coefficient (k_e) is representative of a turbofan engine where k_e = 0.1. The thrust-to-weight ratio at take-off $(T/Mg)_0$ = 0.3 for all three configurations, with the wing-loading $(Mg/S)_0$ defined in section B-2.2.1. The remaining unknown from Equation B-7 is the unstick lift coefficient ($c_{L\,us}$), calculated by using Equation B-8. $c_{L\,us}$ represents the lift coefficient generated at low speed or take-off conditions and is 80% of $c_{L\,max}$.

$$c_{L.us} = 0.8 \cdot \left(c_{L.\max}\right)$$

Equation B-8

Using the equations above, the *NT*-BL, BDSF, and BDFT take-off lengths and low speed lift coefficients can be determined, as shown in Table B-4 below.

	ToL [m]	$c_{L\,us}$
NT-BL	1,903	2.47
BDSF	1,482	1.11
BDFT	1,289	1.40

Table B-4: Calculated data for *ToL* and low speed lift coefficient

A realistic aircraft design always consults current requirements and legislation, for which the main compliance for European aircraft is, CS-25; Certification Specification for Large Aeroplanes [EASA, 2006]. For take-off conditions CS-25.107-(e)-(4) states "*Reasonably expected variations in service from the established take-off procedures for the operation of the aeroplane (such as over-rotation of the aeroplane and out-of-trim conditions) may not result in unsafe flight characteristics or in marked increases in the scheduled take-off distances established in accordance with CS 25.113(a). "*.

To trim the BDSF throughout take-off and climb, it is necessary to develop an active control system to stabilise the flight. The military use this technology for combat aircraft, however, the author's perception is that for a civil aircraft, failure of an active flight control system at this critical flight phase would be catastrophic. The "*take-off and climb are two of the most critical safety phases of the aircraft flight*" [Jenkinson et al, 1999]. To design a tailless civil concept would not be a challenge, but, to certify that aircraft as a passenger transport may have complications. Having considered safety implications, the decision to design two variants of the BD civil aircraft concept is justified, providing a comparison of a tailless solution with a relatively easier or 'safer' tailed design alternative.

B.2.2.4 Factored Landing Length (*LL*)

Factored landing field length (*LL*) is determined for a worse case scenario, where reverse engine thrust is not used for ground deceleration, which also estimates bad weather conditions with the use of reverse thrust [Howe, 2000], where:

$$LL = \frac{25.55}{\tan\gamma} + 4.5 \cdot V_a + 0.0255 \cdot L_L \cdot V_{a_{\max}}^2 \quad [\text{m}]$$

Equation B-9

The term 'γ' represents the descent angle set at 3 degrees for the maximum approach speed ($V_{a.max}$) defined in section B-2.2.1. The landing length factor (L_L) is a function of the landing mass ratio (M_I/M_0), static installed thrust-to-weight ratio $(T/Mg)_0$, and the braking coefficient (μ_G), as shown in Equation B-10. M_I/M_0 was previously calculated using Equation B-2, assuming that the runway is hard, smooth, and dry; where μ_G =0.38. The descent angle 'γ' is used to determine the distance covered in the air from the landing threshold to the touchdown point on the ground, where the rest of the equation considers ground friction effects and the ground rolling distance taken to bring the aircraft to rest.

$$L_L = \left(\frac{1}{\left(\frac{\mu_G}{0.38}\right)} + \frac{5.59}{\left\{\left(\frac{\mu_G}{0.38}\right) + 1.2 \cdot \left(\frac{T}{Mg}\right)_0 \cdot \left(\frac{M_0}{M_L}\right)\right\}} + 20.6 \cdot \tan\gamma \right) \text{ [m]}$$

Equation B-10

It is important to note that if reverse thrust is not required for this calculation, then $(T/Mg)_0$ must equal to zero, otherwise a calculated value implies reverse engine thrust is factored into the landing length calculation, reducing the overall landing field length.

The landing field length (*LL*) without using thrust reversal is calculated to be 1,825 m, where L_L = 7.67 for all three aircraft configurations. With thrust reversal on landing for a $(T/Mg)_0$ = 0.3, *LL* is reduced to 1,632m and L_L = 6.21 for the *NT*-BL aircraft, and for both the BDSF and BDFT *LL* = 1,606m and L_L = 6.01. From here-on, calculations involving *LL* will be without the use of reverse thrust, providing worse case landing results.

B.2.3 Empirical Assumptions

To initiate an aircraft design, data is required to define how the aircraft should behave during flight. It is essential to develop approximations of vehicle performance so that as the detail of the design develops, these estimates are revised and updated.

B.2.3.1 General Concept Data

Information regarding the vehicle type, wing, and mass data are required to initiate the concept designs. The BD concepts like the *NT*-BL aircraft are classified as jet airliner configurations, where it is safe to assume the characteristics are similar to a conventional tube-and-wing configuration, with

no external stores or additional landing gear blisters, resulting in an aircraft type factor parameter T_f = 1.1, as described within [Howe, 2000].

The zero lift drag term wing area parameter ($S^{-0.1}$) is calculated by estimating wing area for the *NT*-BL using (source 1), where S = 283.3m^2 and provides $S^{-0.1}$ = 0.569. The BD configurations require an estimate of wing area ($S_{BD\_Estimate}$), where using data from (source 2), the *NT*-BL aircraft mass ($M_{Baseline}$) is divided by the AV wing loading $(Mg/S)_{AV}$ to provide an equivalent wing area for the BD variants. The assumption is made that the maximum mass of the BD configuration is equal to the baseline aircraft, with a similar wing-loading as the AV aircraft. In principal, this approximates the delta wing area required to support a similar mass of aircraft as the *NT*-BL design.

$$(S)_{BD\_Estimate} = \left(\frac{(M_{Baseline} \cdot g)}{(M \cdot g/S)_{AV}} \right) = \left(\frac{(M_{Baseline}) \cdot S_{AV}}{M_{AV}} \right) \text{ [m}^2\text{]}$$

Equation B-11

The *NT*-BL aircraft mass from (source 1) is 156,489kg, which is used to determine the wing area estimates for both BD configurations, providing the solution $S^{-0.1}$ = 0.516 given that $(S)_{BD\_Estimate}$ = 747.6 m^2, S_{AV} =368.4 m^2, and M_{AV} =77,111kg.

Wetted area (R_w) corresponds to the friction drag of the aircraft, where the *NT*-BL is considered as a conventional civil airliner and R_w = 5.5. The BDSF has a lower estimate for and is due to its tailless configuration, where R_{w_SF} = 3.0 and because of the wetted area contribution of the tail, the BDFT has an estimated R_{w_FT} = 4.0.

B.2.3.2 Take-Off Parameters

As well as establishing the aircraft type, it is necessary to determine initial parameters for the take-off, such as the ratio between start of climb and take-off mass (M_1/M_0), where an estimate of 1% of the maximum take-off mass is used and M_1/M_0 = 0.99.

Take-off Mach number $(M_N)_{TO}$ is calculated from the aircraft stall speed (V_{stall}) using the previous result of $V_{a.max}$ from section B-2.2.1, where:

$$V_a = 1.23 \cdot V_{stall} \text{ [m/s]}$$

Equation B-12

Take-off velocity (V_{TO}) can therefore be calculated from V_{stall}, using:

$$V_{TO} = 1.15 \cdot V_{stall} \text{ [m/s]}$$

Equation B-13

$(M_N)_{TO}$ can be calculated for both BD configurations, given that the speed of sound for a sea level (*SL*) take-off condition is 340.29 m/s, and by using the equation:

$$(M_N)_{TO} = \frac{V_{TO}}{a}$$

Equation B-14

The final take-off consideration is the flap factor (F_F), representing the drag produced by *TE* flaps. The high lift arrangement is discussed in B-2.2.1, where drag from *LE* devices is considered negligible at take-off. In the case of the BDSF flaps are not present but there is drag due to deflected elevons at take-off where F_F = 0.133. The BDFT incorporates *VCF*s which are a relatively new technology device yet to be implemented on any aircraft so the behaviour during take-off is unknown. Drag produced is considered to be less than that of a double slotted flap (F_F=1.2), and equivalent to a single slotted arrangement (F_F=1.0). It is assumed that *VCF*s would provide less drag than that of a single slotted flap at take-off, corresponding to a 5% reduction where F_F = 0.95, as shown within Table B-5.

The discussion above described the process of calculating the take-off Mach number, providing us with the following data:

	V_a [m/s]	V_{stall} [m/s]	V_{TO} [m/s]	$(M_N)_{TO}$	F_F
NT-BL	70.9	57.6	66.3	0.195	1.20
BDSF	62.8	51.1	58.8	0.173	0.133
BDFT	68.5	55.7	64.0	0.188	0.950

Table B-5: Calculated data for take-off Mach, velocity profiles, and *TE* drag.

B.2.3.3 Climb, Cruise, and Loading Parameters

Second segment climb can be a critical case for determining the required engine thrust for climb out, especially for an engine failure on a twin engine aircraft such as the *NT*-BL, where the second segment climb-out factors are:

$$\alpha_{SS} = 2.74, \text{ and } \gamma_{SS} = 0.020.$$

The BD concepts are designed with 4 engines to improve the climb-out performance in the event of an engine failure after take-off, and to reduce the size of the engines so that it may be possible to embed them within the wing root. The BDSF reflects a naturally stable delta wing for which certification as a civil airliner would be a challenge. Four (4) engines enable additional yaw control power by using differential thrust and reduce the workload on the fin in the event of an engine failure. The BD wing has sufficient room to embed or semi-embed 4 engines, where maximising the use of internal wing volume provides efficient use of space at the same times as providing wing span-wise bending relief. The main disadvantages would be engine maintenance and ingestion of foreign objects from the runway. A four (4) engine configuration was selected for the BD configurations for which the second segment climb-out factors are:

$$\alpha_{SS} = 1.83, \text{ and } \gamma_{SS} = 0.025.$$

Another critical phase of flight is the climb-out up to the cruise, as this dictates how quickly the aircraft can reach a cruising height, and the amount of fuel burnt to reach that point. The following assumptions are required to progress with the design of the two BD configurations.

Constant equivalent air speed climb (C_{1_EAS}) is the next stage of flight where a calculation for relative air density (σ_{C1_EAS}) is required. C_{1_EAS} is considered to be at 8.5km altitude, where $\rho_{8.5km}$ = 0.4947 kg/m^3, corresponding to σ_{C1_EAS} = 0.4045.

The speed of sound at initial cruise altitude (a_{cruise}) was selected based upon an altitude study for the BDSF design **(**Appendix C**)**, for which an optimum start of cruise altitude was selected, providing the following data:

Altitude [ft]	*Altitude [m]*	ρ_{cruise} *[kg/m^3]*	T_{cruise} *[K]*	P_{cruise} *[bar]*
36,000	10,973	0.3652	216.83	0.2232

Table B-6: Data for Initial cruise altitude.

The data within Table B-6 represents the density, temperature, and atmospheric pressure at the specified initial start of cruise altitude. Using the results within Equation B-15 below, we can determine the speed of sound at cruise a_{cruise}, given that the gas constant (R) = 287.05 J/kg/K, and γ = 1.4.

$$a_{cruise} = \sqrt{(\gamma \cdot R \cdot T_{cruise})} = 295.19 \text{ [m/s]}$$

Equation B-15

The ultimate normal manoeuvre factor (N) is one of the critical parameters that will affect the aircraft structural design. CS-25 requirements for this class of aircraft specify that the maximum positive N = 3.75, and maximum negative manoeuvre load is 1.0.

The power-plant altitude dependence power factor ($PP_{Fac\text{-}s}$) describes the work done by a high bypass ratio (HBPR) engine, where if the flight is above 11km, $PP_{Fac\text{-}s}$ = 0.6, after 11km $PP_{Fac\text{-}s}$ tends to unity.

The proportion of wing laminar flow (c_l) over the wing is optional, but not considered for the initial design synthesis. Laminar flow airfoils were investigated for the BD concept, the results of which are discussed within **Chapter 4** and **Appendix E**.

Another design parameter is the gust sensitivity, where *"it is desirable to ensure that aircraft will not possess unacceptable responses to atmospheric turbulence"* [Howe, 2000]. Gust sensitivity was included in the BD designs to ensure a suitable flight quality for passengers in the event of turbulence.

B.2.4 Initial Calculations and Input Data

Calculations using the results above provide the mass properties at take-off and landing, in addition to detailed estimates of the lift and drag coefficients. Landing mass to take-off mass ratio (M_L/M_0) is calculated as a function of the design range, as shown below:

$$\left(\frac{M_L}{M_0}\right) = 1 - 2 \cdot (s) \times 10^{-5} = 0.851$$

Equation B-16

The ratio of initial cruise to take-off mass (M_{cr}/M_0) is calculated using Equation B-17. M_{cr}/M_0 uses the start of climb to take-off mass ratio, the relative density at the end of *EAS* climb, and relative density at the start of cruise, as shown below:

$$\left(\frac{M_{cr}}{M_0}\right) = \left(\frac{M_1}{M_0}\right) \cdot \left(\sigma_{C1._{EAS}}{}^{0.016}\right) \cdot \left[\left(\frac{\sigma_{cr1}}{\sigma_{C1._{EAS}}}\right)^{0.02}\right] = 0.975$$

Equation B-17

The following analysis investigates the changes in lift coefficient at low speed and cruise flight conditions to compare the tailless and tailed BD configurations.

The un-swept maximum lift coefficient is calculated from the initial swept result, where:

$$\left(c_{l_{.\max}}\right)_0 = \left(\frac{c_{L_{.\max}}}{\cos\left(\Lambda_{1/4}\right)}\right)$$

Equation B-18

The zero sweep un-stick lift coefficient is given by:

$$\left(c_{l_{.us}}\right)_0 = 0.8 \cdot \left(c_{l_{.\max}}\right)_0$$

Equation B-19

The zero sweep approach lift coefficient is given by:

$$\left(c_{l_{.a}}\right)_0 = \left(\frac{c_{L_{.a}}}{\cos\left(\Lambda_{1/4}\right)}\right)$$

Equation B-20

Zero sweep useable lift coefficient in cruise uses delta wing combat aircraft approximations, where this takes into account a possibility for high speed combat manoeuvres, which are not a requirement from the design specification.

$$\left(c_{l_{.use}}\right)_0 = 0.4 \cdot \left(c_{l_{.\max}}\right)_0 \cdot \left(1 - 0.25 \cdot \left(M_{N_{.cr}}\right)\right)$$

Equation B-21

The low speed zero lift drag coefficient is calculated by:

$$\left(c_{d_{.z}}\right)_{ls} = 0.005 \cdot \left(1 - \frac{2c_l}{R_w}\right) \cdot \bar{\tau} \cdot \left[1 - 0.2\left(M_N\right)_{TO} + 0.12\left\{\frac{\left(M_N\right)_{TO}\sqrt{\cos\left(\Lambda_{1/4}\right)}}{\left(A_f - t/c\right)}\right\}^{20}\right] \cdot R_w \cdot T_f \cdot S^{-0.1}$$

Equation B-22

Where in Equation B-22 there are two new parameters, firstly an airfoil design factor (A_f), and a wing thickness correction factor ($\bar{\tau}$), where:

$$\bar{\tau} = \left[\frac{(R_w - 2)}{R_w} + \frac{1.9}{R_w} \cdot \left\{ 1 + 0.526 \cdot \left(\frac{t}{c} \Big/ 0.25 \right)^3 \right\} \right]$$

Equation B-23

A_f is a design factor that depends on whether the airfoil is a specially designed advanced section (A_f = 0.93), or whether it is an older airfoil designed for incompressible flow conditions (A_f = 0.75). The airfoil sections for the *NT*-BL and BD configurations are assumed to be fairly advanced sections of A_f =0.9. Table B-7 shows the results for the un-swept lift coefficients of the BD concepts using the formulae above:

	$(c_{l.max})_0$	$(c_{l.us})_0$	$(c_{l.a})_0$	$(c_{l.use})_0$	$(c_{d.z})_0$	$\bar{\tau}$
NT-BL	3.50	2.80	2.45	1.12	0.0160	0.999
BDSF	1.59	1.27	1.11	0.509	0.00818	0.995
BDFT	2.07	1.66	1.45	0.663	0.0103	0.996

Table B-7: Initial calculations and input data for *NT*-BL and BD configurations

The swept lift coefficients have previously been calculated, except for the usable lift coefficient at cruise, where multiplying $(c_{l.use})_0$ with the cosine of wing quarter chord sweep provides $c_{l.use}$ = 0.947 for the *NT*-BL, $c_{l.use}$ = 0.444 for BDSF, and $c_{l.use}$ = 0.561 for the BDFT. The final parameter required is the relative air density at start of cruise (σ_{cr}), where this was initially calculated within section B-2.2.2, as the first cruise altitude (σ_{cr1}).

B.2.5 Preliminary Calculations

This section represents the analysis required prior to initiating the concept design, where the drag, wing loading, and flight critical characteristics need to be calculated.

B.2.5.1 Drag Factors

The lift coefficients for initial design calculations were previously established, and now drag characteristics are required for various flight conditions, before analysis of the concept can be initiated. The primary drag terms required, are wave drag (F_{wave}), zero lift drag at cruise $(c_{d.z})_{cr}$, equivalent zero lift drag at climb-out $(c_d)_{co}$, low speed induced drag $(K_v)_0$, and cruise induced drag $(K_v)_{cr}$ factors.

The wave drag factor is found within Equation B-22, from the term:

$$F_{wave} = 0.12 \cdot \left[\frac{M_{N_{cr}} \cdot \sqrt{\cos\left(\Lambda_{1/4}\right)}}{A_f - \frac{t}{c}} \right]^{20}$$

Equation B-24

The zero lift drag coefficient in cruise $(c_{d.z})_{cr}$ is determined by:

$$\left(c_{d_z}\right)_{cr} = 0.005\left(1 - \frac{2c_l}{R_w}\right) \cdot \bar{\tau} \cdot \left[1 - 0.2\left(M_N\right)_{cr} + F_{wave}\right] \cdot R_w \cdot T_f \cdot S^{-0.1}$$

Equation B-25

The equivalent zero lift drag term during climb-out $(c_d)_{co}$ is given by:

$$\left(c_d\right)_{co} = \left(c_{d_z}\right)_{ls} + \left(\frac{0.03 \cdot F_F - 0.004}{A^{0.33}}\right)$$

Equation B-26

The low speed induced drag factor $(K_v)_0$ is given by:

$$\left(K_v\right)_0 = \left[\frac{1 + 0.12 \cdot \left(M_N\right)_{TO}^6}{\pi}\right] \cdot f\left(A\right)$$

Equation B-27

$f(A)$ is the wing aspect ratio function for four engines (N_e) mounted above the wing:

$$f\left(A\right) = \frac{1}{A} \cdot \left\{1 + \frac{0.142 + f\left(\lambda\right) \cdot A \cdot \left(10 \cdot \frac{t}{c}\right)^{0.33}}{\left(\cos\Lambda_{1/4}\right)^2} + \frac{0.1 \cdot \left(3 \cdot N_e + 1\right)}{\left(4 + A\right)^{0.8}}\right\}$$

Equation B-28

$f(\lambda)$ is the taper ratio function and is given by:

$$f\left(\lambda\right) = 0.005 \cdot \left[1 + 1.5 \cdot \left(\lambda - 0.6\right)^2\right]$$

Equation B-29

The taper ratio (λ) is calculated as a first approximation by:

$$\lambda = 0.2 \cdot A^{1/4} \cdot \cos^2 \Lambda_{1/4}$$

Equation B-30

The final drag term to calculate is induced drag at cruise $(K_v)_{cr}$, identical to the procedure used within Equation B-27, except this time using Mach number at cruise conditions:

$$(K_v)_{cr} = \left[\frac{1 + 0.12 \cdot (M_N)_{cr}^6}{\pi} \right] \cdot f(A)$$

Equation B-31

	F_{wave}	$(c_{dz})_{cr}$	$(c_d)_{co}$	$(K_v)_0$	$f(A)$	$f(\lambda)$	λ	$(K_v)_{cr}$
NT-BL	0.462	0.0216	0.0319	0.0548	0.172	0.00578	0.277	0.0565
BDSF	0.0411	0.00746	0.00817	0.147	0.462	0.00600	0.236	0.152
BDFT	0.0303	0.00935	0.0271	0.147	0.462	0.00614	0.209	0.152

Table B-8: Drag characteristics for *NT*-BL and BD configurations

The drag results for the *NT*-BL aircraft and two BD variants were calculated and are compared within Table B-8, where at this early stage of the design it is clear to say that there is greater zero lift drag generated by the tailed BD at cruise and climb-out, but the BDFT produces less low speed induced and wave drag compared to the BDSF. Despite the small variations in drag components, both concepts produce the same induced drag for cruise flight conditions.

B.2.5.2 Thrust Factors

Thrust factors (τ) are dependent on flight speed, altitude, and engine operational conditions. The BD concepts consider two cruise segments, where for the cruise Mach number is defined in section B-2.2.1, and relative density $\sigma = \sigma_{cr1}$, providing:

$$\tau = F_\tau \cdot \left[K_{1\tau} + K_{2\tau} R + \left(K_{3\tau} + K_{4\tau} R \right) \cdot M_N \right] \cdot \sigma^S$$

Equation B-32

Equation B-32 introduces five new thrust parameters, where F_τ represents the use of afterburning on the engine, and is not required for civil aircraft, where for basic dry operating conditions is unity. The four remaining parameters are dependent on ($PP_{Fac\text{-}s}$), where as described in B-2.3, above 11km, $PP_{Fac\text{-}s}$ = 0.6, and is unity above this altitude. $K_{1\tau}$, $K_{2\tau}$, $K_{3\tau}$, and $K_{4\tau}$, are constants for a given propulsion system with defined operating conditions and Mach number range. Using [Howe, 2000] as an initial guide the following values for thrust parameters for a Mach range from 0.4-0.9 are used:

BPR	$K_{1\tau}$	$K_{2\tau}$	$K_{3\tau}$	$K_{4\tau}$
8	0.89	-0.014	-0.3	0.005

Table B-9: Thrust Parameters 0.9< M_N >0.4

Therefore for initial cruise τ_{cr1} = 0.320, and by replacing $\sigma = \sigma_{cr2}$, the second thrust factor for a cruise segment above 11km, can be calculated to be τ_{cr2} = 0.275. The *NT*-BL, BDSF, and BDFT all have the same flight cases hence the thrust factors are the same.

B.2.5.3 Take-Off and Approach Calculations

The two most critical phases of flight are the take-off and landing, where the wing loading, actual approach velocity, and actual landing lengths are required. Maximum approach velocity ($V_{a.max}$) was determined in section B-2.2, where an initial calculation for the approach velocity, V_a, is shown within Table B-3. To check the calculation for approach velocity ($V_{a.calc}$), we can combine the assumptions made within B-2.2, and rearrange Equation B-9 and Equation B-10, to provide:

$$V_{a_{.(calc)}} = -11.5 + \left[132.2 - 5.11 \cdot \left(488 - LL\right)\right]^{0.5} \text{ [m/s]}$$

Equation B-33

The actual approach velocity is the lower of the solutions and is used to calculate the correct landing length (LL_{cor}):

$$LL_{cor} = 488 + 4.5 \cdot V_a + 0.196 \cdot V_a^2 \text{ [m]}$$

Equation B-34

The take-off wing loading $(Mg/S)_{0.ld}$ is defined by limiting approach velocity, approach lift coefficient and landing to take-off mass ratio, as shown below in Equation B-35:

$$\left(\frac{Mg}{S}\right)_{0_{.ld}} = \tfrac{1}{2} \cdot \rho_0 \cdot \left(V_a\right)^2 \cdot c_{l_a} \cdot \left(\frac{M_0}{M_L}\right) \text{ [N/m}^2\text{]}$$

Equation B-35

To meet gust sensitivity requirements, the take-off wing loading is calculated using:

$$\left(\frac{Mg}{S}\right)_{0_{.gt}} = \frac{2.7 \cdot V_D \cdot A}{\left(0.32 + 0.16A/\cos\Lambda_{1/4}\right) \cdot \left\{1 - \left(\left(M_N\right)_{cr} \cos\Lambda_{1/4}\right)^2\right\}^{1/2}} \text{ [N/m}^2\text{]}$$

Equation B-36

The results for the above analysis are shown below in Table B-10. Initial comparison shows that the actual approach velocities for both concepts are lower than the initial assumption of $V_{a.max}$ =72m/s. This lower approach velocity reflects a reduced LL_{cor}, compared to the initial calculations where LL = 1,825 m.

	$V_{a.calc}$ [m/s]	LL_{cor} [m]	$(Mg/S)_{0.ld}$ [N/m^2]	$(Mg/S)_{0.gt}$ [N/m^2]
NT-BL	70.8	1,791	7465	4005
BDSF	62.8	1545	2755	3316
BDFT	68.4	1714	4133	3164

Table B-10: Revised Take-off and Approach considerations

The BDFT has a longer LL_{cor} compared to the BDSF and this is due to the higher approach velocity, hence producing a greater momentum to retard, without using thrust reversal upon landing. The greater approach velocity also applies greater loads on the wing, and is reflected by the $(Mg/S)_{0.ld}$ results.

Gust sensitivity is a concern for the BDSF, where $(Mg/S)_{0.ld} \geq (Mg/S)_{0.gt}$, representing undesired gust response characteristics at low speeds. Gust responses and control of a civil aircraft is critical at low speeds, and would be a 'show-stopper' for the BDSF. As this research is based on a silent and green aircraft study, the comparison of the two BD variants will continue, assuming that the gust challenge can be resolved prior to the aircraft preliminary design stage.

B.2.6 Parametric Analysis

The parametric analysis for the BD concepts involves evaluating changes in take-off wing loadings $(Mg/S)_0$, with installed static thrust-to-weight ratios $(T/Mg)_0$, for the following performance conditions:

- Take-off - factored runway length,
- Accelerate-stop – runway length,
- Second segment climb – worse case scenario,
- Start of cruise - residual rate of climb,
- Reverse thrust landing – maximum $(T/Mg)_0$

The above performance conditions are analysed for a range of thrust-to-weight ratios to determine the behaviour of the BD concepts. The following analysis will only describe the process to investigate $(T/Mg)_0$ using $(Mg/S)_{0.ld}$ calculated within Table B-10.

B.2.6.1 Take-Off Analysis $(T/Mg)_0$

The take-off thrust-to-weight ratio is calculated for a factored runway length, and is an iterative calculation, where for a first approximation the initial thrust-to-weight ratio from section B-2.2.3 of 0.3, is used as an input in Equation B-37 below:

$$\left(\frac{T}{Mg}\right)_0 = \left[\frac{c_{l.us}}{k_e\left(Mg/S\right)_0}\cdot\left[ToL - 170\cdot\left\{1-\left(\frac{T}{Mg}\right)_{0.input}\right\}\right] - \frac{6}{k_e}\cdot\left(\frac{c_{l.us}}{\left(Mg/S\right)_0}\right)^{1/2}\right]^{-0.7407} \quad [\mathrm{N/m^2}]$$

Equation B-37

The value of 170 represents a factor required for an obstacle clearance height of 15.3m as specified in CS-25, and JAR requirements for civil aircraft. If this design were to address a short take-off run, the factor 6 in the rotation term would be replaced with 2.3.

Once an initial calculation for $(T/Mg)_0$ is made, a second iteration is required using the results from the first calculation as the input thrust-to-weight. This second value is considered to be adequate for the performance analysis to continue, although if preferred further iterations can be made. The results for $(T/Mg)_0$ at a take-off conditions are shown below in Table B-11.

	$(T/Mg)_{0.input.1}$	$(T/Mg)_{0.input.2}$	$(T/Mg)_0$
NT-BL	0.3	0.325	0.323
BDSF	0.3	0.395	0.389
BDFT	0.3	0.393	0.389

Table B-11: Take-off results for $(T/Mg)_0$

B.2.6.2 Accelerate-to-Stop Analysis for $(T/Mg)_0$

The Accelerate-to-stop thrust-to-weight ratio is calculated for the distance required to stop during an engine failure on the ground at take-off.

$$\left(\frac{T}{Mg}\right)_0 = \left[\frac{1.22\cdot c_{l.us}}{k_e\left(Mg/S\right)_0}\cdot ToL - 2.2\right]^{-0.7407} \quad [\mathrm{N/m^2}]$$

Equation B-38

The accelerate-to-stop condition is calculated for the *NT*-BL aircraft as $(T/Mg)_0$ = 0.367, where the BDSF $(T/Mg)_0$ = 0.349, and $(T/Mg)_0$ = 0.362 for the BDFT.

B.2.6.3 Second Segment Climb Analysis for $(T/Mg)_0$

The second segment climb analysis thrust-to-weight ratio is calculated for a worse case scenario, where hot and high climb conditions are considered, combined with a single engine failure. The thrust loading for this condition is calculated using:

$$\left(\frac{T}{Mg}\right)_0 = \frac{\alpha_{ss}\cdot\left\{\left[\frac{(c_d)_{co}}{c_{l_{.us}}}\right]+\frac{0.71\cdot(\overline{\beta})_{co}}{\left[(c_d)_{co}/c_{l_{.us}}\right]}+\gamma\right\}}{\tau_{co}}$$

Equation B-39

There are two unknowns to calculate $(T/Mg)_0$, firstly the drag term $(\overline{\beta})_{co}$ is given by:

$$(\overline{\beta})_{co} = (c_d)_{co}\cdot(K_v)_0$$

Equation B-40

The final unknown is the thrust factor at climb-out condition (τ_{co}) as previously described by Equation B-32. The worse case for a twin engine aircraft such as the *NT*-BL would be for 'hot and high' climb-out conditions for a single engine failure, where σ = 0.8. The BD concepts are not affected by this 'hot and high' case because of the quad engine configuration. The climb out Mach number is given therefore given by:

$$(M_N)_{co} = 1.1\cdot\left(\frac{V_{LOF}}{a}\right)$$

Equation B-41

V_{LOF} represents the speed at which the aircraft lifts off the ground, where lift equals the weight, and the lift coefficient is assumed to be that at climb-out conditions.

$$V_{LOF} = \left(\frac{2}{\rho_0\cdot c_{l_{.us}}}\cdot\left(\frac{Mg}{S}\right)_0\right)^{1/2}$$

Equation B-42

Using the assumptions above, Equation B-32 can be re-written as:

$$\tau_{co} = F_\tau\cdot\left[K_{1\tau}+K_{2\tau}R+(K_{3\tau}+K_{4\tau}R)\cdot(M_N)_{co}\right]\cdot\sigma^S$$

Equation B-43

Where for the climb-out condition, the thrust parameters are for a lower Mach number range of 0-0.4, and are shown below.

BPR	$K_{1\tau}$	$K_{2\tau}$	$K_{3\tau}$	$K_{4\tau}$
8	1	0	-0.595	-0.03

Table B-12: Thrust Parameters 0.4< M_N >0

Table B-13 provides the results for the second segment climb with a single engine failure.

	$\left(\overline{\beta}\right)_{co}$	V_{LOF} *[m/s]*	τ_{co}	$(T/Mg)_0$
NT-BL	0.00175	71.8	0.778	0.442
BDSF	0.00120	63.7	0.828	0.328
BDFT	0.00399	69.4	0.813	0.430

Table B-13: Second Segment Climb results for $(T/Mg)_0$

B.2.6.4 Start of Cruise Analysis $(T/Mg)_0$

The start of cruise thrust-to-weight ratio is calculated using:

$$\left(\frac{T}{Mg}\right)_{0-1} = \left(\frac{M_1}{M_0}\right)\cdot\left(\frac{T}{Mg}\right)_0$$

Equation B-44

$$\left(\frac{T}{Mg}\right)_0 = \frac{\sigma_{C1_{EAS}}^{S}}{\tau_1}\left[\frac{0.00294\left(1-0.153\left(M_N\right)_{cr}^2\sigma_{cr_{.1}}^{0.23}\right)\sigma_{cr_{.1}}^{-(s+0.1)}\left(V_V\right)_C}{\left(M_N\right)_{cr}} + Q_M\sigma_{cr_{.1}}^{(1.23-s)} + \frac{\left(\overline{\beta}\right)_{cr}}{Q_M}\sigma_{cr_{.1}}^{-(1.2+s)}\right]$$

Equation B-45

$$\left(\overline{\beta}\right)_{cr} = \left(c_{dz}\right)_{cr}\cdot\left(K_V\right)_0$$

Equation B-46

The vertical velocity at the climb ceiling $(V_v)_c$, and the thrust-to-weight evaluation factor (Q_M), are the two main unknowns, where $(V_v)_c$ is limited to 1.5m/s, and Q_M is given by:

$$\left(Q_M\right) = \frac{70910\cdot\left(M_N\right)_{cr}^2\cdot\left(c_{dz}\right)_{cr}}{\left(Mg/S\right)_1}$$

Equation B-47

The second cruise segment up to a climb ceiling above 11km is calculated using:

$$\left(\frac{T}{Mg}\right)_{0-2} = \frac{\left(M_1/M_0\right)}{\tau_1\left(\sigma_{cr_2}/\sigma_{cr_1}\right)^{0.02}}\left[\left\{\frac{0.001\left(\sigma_{cr_2}^{-0.98}\right)}{\left(M_N\right)_{cr}}\right\}\left(V_V\right)_C + 0.223Q_M + 0.404\left(\frac{\left(\overline{\beta}\right)_{cr}}{Q_M}\right)\sigma_{cr_2}^{-1.96}\right]$$

Equation B-48

The lift coefficient at the start of cruise is:

$$\left(c_l\right)_{cr} = \left(\frac{M_{cr}}{M_0}\right)\cdot\left(\frac{Mg}{S}\right)_0 \cdot \frac{2}{\rho_0 \cdot \sigma_{cr} \cdot \left[\left(M_N\right)_{cr} \cdot a_{cruise}\right]^2}$$

Equation B-49

The drag coefficient at the start of cruise is:

$$\left(c_d\right)_{cr} = \left(c_{dz}\right)_{cr} + \left(K_V\right)_{cr} \cdot \left(c_l\right)_{cr}^2$$

Equation B-50

Where the lift and drag coefficients at cruise are used to determine the lift-to-drag ratio at the start of cruise, and is multiplied by the Mach number as a performance parameter:

$$M_N \cdot \frac{L}{D} = \left(M_N\right)_{cr} \cdot \frac{\left(c_l\right)_{cr}}{\left(c_d\right)_{cr}}$$

Equation B-51

The results for the thrust-to-weight ratios at the two cruise conditions are shown below.

	Q_M	$\left(\overline{\beta}\right)_{cr}$	$(T/Mg)_{0\text{-}1}$	$(T/Mg)_{0\text{-}2}$	$(c_l)_{cr}$	$(c_d)_{cr}$	$(L/D)_{cr}$	$M_N(L/D)_{cr}$
NT-BL	0.130	0.00122	0.310	0.421	0.675	0.0473	14.3	11.4
BDSF	0.123	0.00113	0.232	0.267	0.204	0.0138	14.8	11.9
BDFT	0.103	0.00142	0.258	0.322	0.307	0.0236	13.0	10.4

Table B-14: Initial Cruise results for $(T/Mg)_0$

The results show that the lift-to-drag ratio for all three configurations is comparable with conventional civil transports which have L/D of between 14 and 18. This low figure is not a concern at this stage as the parametric study has not been completed and the design is yet to be optimised.

B.2.6.5 Reverse Thrust Landing Analysis for $(T/Mg)_0$

The thrust-to-weight ratio for a reverse thrust landing is taken to be the maximum value from the five previous cases; which were take-off, acceleration to stop, second segment climb, start of first cruise,

and final cruise settings. The maximum thrust-to-weight is the second segment climb case, which is used to determine the reverse thrust landing length, as shown below:

$$LL_{RT} = \frac{25.55}{\tan\gamma} + 4.5(V_a) + 0.0255\left[\frac{1}{\left(\frac{\mu_G}{0.38}\right)} + \frac{5.59}{\left\{\left(\frac{\mu_G}{0.38}\right) + 1.2\left(\frac{T}{Mg}\right)_0\left(\frac{M_0}{M_L}\right)\right\}} + 20.6\tan\gamma\right](V_a)^2$$

Equation B-52

The results for the thrust-to-weight ratios at the two cruise conditions are shown below.

	LL_{corr} [m]	$(T/Mg)_{0\ Max}$	LL_{RT} [m]
NT-BL	1,791	0.442	1,513
BDSF	1,545	0.389	1,343
BDFT	1,714	0.430	1,459

Table B-15: Reverse thrust landing results for $(T/Mg)_0$

B.2.6.6 Summary of $(T/Mg)_0$ Results

The thrust-to-weight calculations were established for a number of different cases, where a range of wing-loadings between 600N/m^2 and 9000N/m^2, were analysed for the *NT*-BL aircraft and the results are summarised below in Fig B-5. The thrust-to-weight range for the BD configuration wing-loadings range from 300N/m^2 to 4500N/m^2 and are summarised in Fig B-3 and Fig B-4.

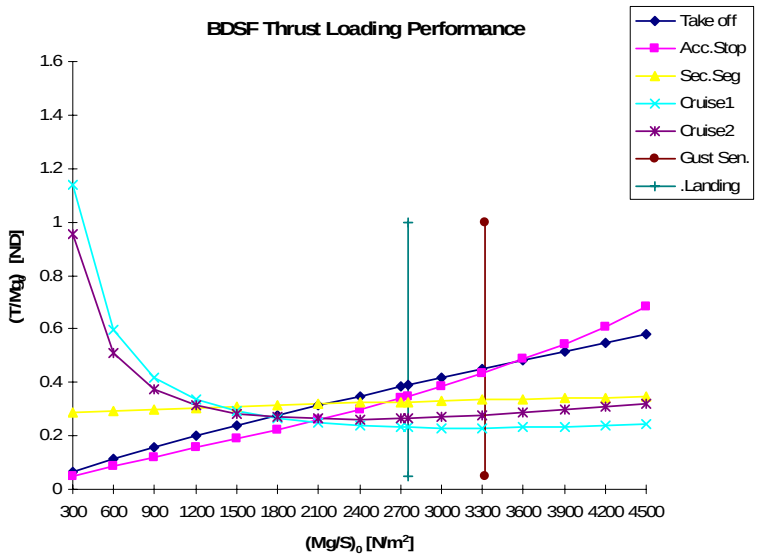

Fig B-3: BDSF concept thrust loading performance

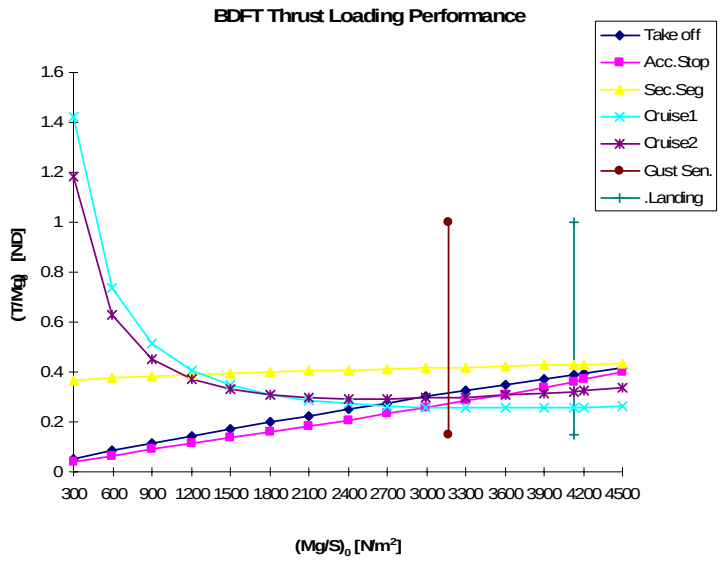

Fig B-4**:** BDFT concept thrust loading performance

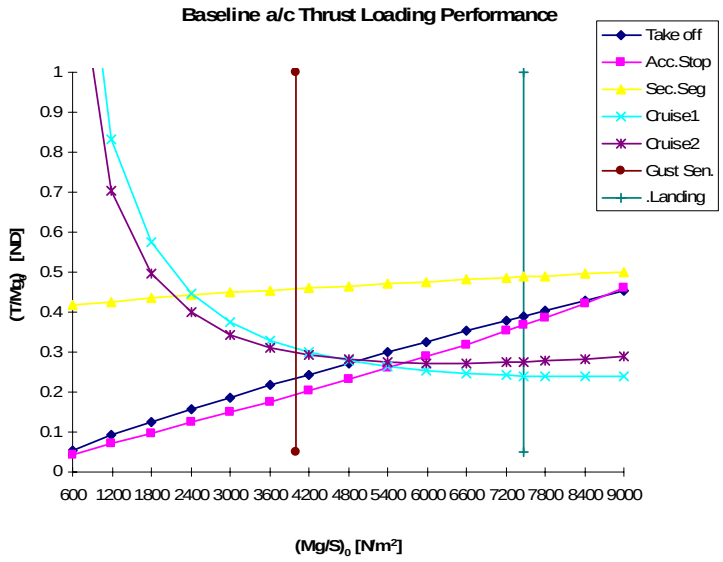

Fig B-5**:** *NT*-BL concept thrust loading performance

A Comparison of the variation in thrust by altering the wing-loading is shown for a range of flight conditions. A digital version of the summary and analysis can be viewed by reviewing Howe SS1 worksheet in the accompanying digital documents.

One final calculation involves an investigation into the *NT*-BL and BD structural design parameters. The structural design parameter (*SP*) is established to indicate likely structural limitations for a given design, and identifies direct conflicts between aerodynamic and structural requirements.

$$SP = \sec \Lambda_{1/4} \cdot \left\{ \frac{N \cdot A^{1.25}}{\left(t/c\right)^{0.5}} \right\}^{0.5}$$

Equation B-53

Where the ultimate normal acceleration factor (*N*), aspect ratio (*A*), wing thickness-to-chord (*t/c*), and quarter chord sweep ($\Lambda_{1/4}$) are defined in the paragraphs above. The value of SP is calculated where SP = 14.4 for the *NT*-BL aircraft, 7.83 for the BDSF, and 8.07 for the BDFT configurations.

According to Howe, *"the value of SP should not be an absolute design constraint, but it is useful in establishing a set of parameters for detailed investigation"* [Howe, 2000]. SP for a conventional aircraft is considered to be in the range of 10-16, but typical values may not apply to the BD aircraft configurations, and further analysis will reflect why the structural parameter results are low.

B.3 Second Phase of Parametric Design Analysis

The second phase of the parametric analysis is a direct continuation of section B-2, which uses detailed aircraft geometry and flight performance calculations to develop the design, so that the concept can be later optimised for minimum mass. The following analysis uses Howe's second design spreadsheet combined with modifications to develop the three design configurations.

B.3.1 Initial Requirement Parameters

Initial requirement parameters are required to progress with the design, which includes information on the payload, performance, and specific geometry assumptions. The majority of this data has been previously described above, and to avoid repetition, the following information provides solutions for the unknowns.

B.3.1.1 Payload

The number of passengers and payload was provided within the specification, where the objective was to establish how mass and performance of the BD concept compares to the *NT*-BL. The design was tailored for 216 passengers in a mixed three-class arrangement, with an overall passenger weight of 75kg and a luggage allowance of 35kg per passenger, providing a total payload ($M_{PAY.L}$) of 23,760kg.

B.3.1.2 Flight Characteristics

The start of cruise Mach number and relative density was determined at 36,000 ft, as in section B-2.3.3, where the cruise ended at a final altitude of 42,000 ft (12.5 km), where $\sigma_{Fin\ cr}$ = 0.235. The structural design speed V_D = 251.6 m/s, and the ultimate normal acceleration factor N = 3.75, which we can use to calculate the effective factored wing normal acceleration factor; $\overline{N}$ = 4.125, using Equation B-54 below.

$$\overline{N} = 1.65 \cdot \left(N_{\lim it}\right) = 1.65 \cdot \left(\frac{N_{ultimate}}{1.5}\right)$$

Equation B-54

B.3.1.3 Climb Path Characteristics

The climb stage calculations require the constant equivalent airspeed ($V_{C1.EAS}$), which is limited to 127 m/s (250knots) at the initial phase of flight by air traffic control (*ATC*) up to an altitude of 3.05km, where $V_{C1.EAS}$ = 170m/s. To simplify the analysis for initial calculation purposes, the ATC requirement is neglected, and will be re-introduced upon analysis of the optimised solutions. At the end of equivalent airspeed (*EAS*) flight, the start of cruise climb altitude is 8,500 ft, where the relative density is $\sigma_{C1.EAS}$ = 0.405, and the climb Mach number is $(M_N)_{cr}$.

B.3.1.4 Assumed Characteristics

Engine performance, operational items, fuel considerations, and tail properties are a few of the assumptions that are taken into account for the *NT*-BL and BD configurations. The basic thrust-to-weight ratio of propulsion system $(T/Mg)_{eng}$, is taken as highest value for civil transport engines, indicating greater thrust produced from a smaller engine mass, where for the two concepts, $(T/Mg)_{eng}$ = 6.5.

A civil aircraft houses many operational items, consisting of freight equipment, food, water, personal items of the crew, and safety equipment, such as emergency oxygen and life rafts. The mass of operational items is calculated using a operating items factor (F_{op}), where F_{op} = 12 for a medium range civil passenger aircraft.

Tail coefficients are used to size the tail surfaces of the three configurations, where the horizontal tail ($\overline{V}$) and vertical tail ($\overline{V_V}$) coefficients, are shown below in Table B-16 for a subsonic jet transport. To re-iterate, the BDSF only incorporates a vertical stabiliser, where-as the BDFT is like the *NT*-BL and also has a horizontal stabiliser.

	$\overline{V}$	$\overline{V_V}$
NT-BL	1.2	0.09
BDSF	-	0.09
BDFT	1.2	0.09

Table B-16: Horizontal and Vertical tail coefficients

The final assumption is that the approach fuel allowance mass ratio is taken to be 1% of the total aircraft mass, which is typical for the fuel burnt by a civil transport aircraft during the descent, approach, and landing phases of flight, not to forget the final reserve fuel.

B.3.2 Additional Input Data

Additional input data characterising the fuselage geometry, mass factors, and location, for major aircraft components, are considered essential in order to progress with the design. The BD mass coefficients are broken down into five main characteristics, where the lifting surface mass, fuselage mass, propulsion systems installation, systems, and secondary lifting surface factors are described below.

B.3.2.1 Fuselage Geometry

The fuselage for the two BD configurations is considered in many ways identical to that of the *NT*-BL aircraft, where the fuselage length is determined by the internal passenger capacity requirements, and is fixed at 53.7 metres. The fuselage width and height uses the assumption that a cylindrical section of 5.03m diameter is sufficient for the passenger cabin, freight stowage, and structure.

B.3.2.2 Mass Factors

The lifting surface mass factor (C_1) for a short-to-medium range subsonic jet transport aircraft is initially assumed to be C_1 = 0.0009. The fuselage mass coefficient (C_2) considers that the fuselage layout has been prepared, for an airliner with four or more abreast seating with wing mounted landing gear, where C_2 = 0.79. Propulsion system installation factor (C_3) includes the basic engines, mountings, nacelles, cowlings, and the fuel system, where C_3 = 1.56. The systems factor (C_4) takes into account passenger furnishings, equipment, and undercarriage, where C_4 = 0.14. The secondary lifting surfaces factor (C_5) is combined with C_1, taking into consideration the tail surfaces and configuration of the aircraft concept. The BDSF is a tailless concept, where C_5 = 1.1, and the *NT*-BL and BDFT have horizontal tail surfaces, where C_5 = 1.18.

B.3.2.3 Component Locations

Components within the BD are initially located by their position along the *x*-axis or centreline of the fuselage. The fuselage mass (l_{Fus}) is estimated at 45% of the overall fuselage length, and so are the systems (l_{Sys}), operational items ($l_{Op\ it}$), and payload (l_{Pay}), because they are all assumed to be evenly distributed along the fuselage length. The tail mass (l_{Tail}) is located at 90% of the overall fuselage length.

Incremental position of the wing mass (Δl_w) and fuel mass (Δl_{Fuel}) is taken to be 10% of the wing mean aerodynamic chord ($\bar{c}$) quarter chord sweep line for the *NT*-BL, BDSF, and BDFT. The propulsion systems mass (Δl_{PP}), is located forward of the crossing point of the quarter chord sweep angle and the mean aerodynamic chord. The engine location for the *NT*-BL aircraft, is characterised by a conventional pair of under-slung engine nacelles ahead of the wing leading edge, where X_{PP} = -0.85.

$$\Delta l_{PP} = X_{PP} \cdot \left(\frac{\bar{c}}{\cos\left(\Lambda_{1/4} \right)} \right)$$

Equation B-55

The BDSF and BDFT configurations house a quad engine arrangement at the wing root, consisting of two semi-embedded engines on each wing which are located at X_{PP} = -0.25, ahead of the where the quarter chord sweep angle crosses the mean aerodynamic chord.

B.3.3 Concept Flight Analysis & Mass Calculations

The mass breakdown is determined via further analysis where the process is described in this section and refers to the calculations necessary to determine the overall aircraft mass. Specific calculations for the propulsion system, EAS climb, cruise, and general data, are required prior to calculating the overall aircraft mass.

B.3.3.1 General Data

The wing loading factor for lifting surface mass is calculated using the result from $(Mg/S)_{0\ ld}$, where the factor is calculated from:

$$\left(\frac{S}{M_0} \right)^{0.45} = \left[\frac{g}{(Mg/S)_{0_{ld}}} \right]^{0.45} \quad [\mathrm{m^2/kg}]$$

Equation B-56

The location of quarter mean aerodynamic chord point on the wing centreline chord is calculated from Equation B-57 below, where the wing aspect ratio (A), taper ratio (λ), and quarter chord sweep ($\Lambda_{1/4}$) have all been determined.

$$\frac{\overline{x_{1/4}}}{c_0} = \frac{\left\{(1+2\lambda)\cdot A\tan\left(\Lambda_{1/4}\right)\right\}}{12} + 0.25$$

Equation B-57

Fuselage is designed with a pressurised passenger cabin which has a relative cabin differential pressure ($\overline{p}$). The differential pressure is defined by the maximum cruise relative density ($\sigma_{Fin\ cr}$), with an internal cabin pressure estimate at 6000ft, given by:

$$\overline{p} = 0.8 - \left(\sigma_{Fin.cr}\right)^{1.235}$$

Equation B-58

Results for the analysis above are shown below and used to calculate component masses.

	$(S/M_0)^{0.45}$	$\overline{p}$	$\overline{x_{1/4}}/c_0$
NT-BL	0.0495	0.608	0.2602
BDSF	0.0791	0.577	0.2534
BDFT	0.0659	0.577	0.2536

Table B-17: General data for mass breakdown calculations

B.3.3.2 Propulsion Systems Characteristics

The required propulsion systems thrust-to-weight ratio $(T/Mg)_{req}$ during cruise can initially be estimated as the inverse of the cruise lift-to-drag ratio. The available cruise thrust to weight ratio $(T/Mg)_{av}$ is calculated using $(T/Mg)_0$ and assumptions made for thrust factor (τ) calculated in Equation B-32, where:

$$\left(\frac{T}{Mg}\right)_{av} = \left(\frac{T}{Mg}\right)_0 \cdot \tau$$

Equation B-59

A ratio (*Av/req*) between the available and required thrust-to-weight ratios is a reality check to see whether there is a sufficient thrust range.

	$(T/Mg)_{req}$	$(T/Mg)_{av}$	*Av/req*
NT-BL	0.0705	0.118	1.67
BDSF	0.0675	0.125	1.85
BDFT	0.0770	0.138	1.79

Table B-18: General data for mass breakdown results (part I)

A conventional HBPR baseline turbofan engine was modelled by the propulsion systems designer [Doulgeris, 2008] and was based on a General Electric CF6-80C2 engine with a design specific fuel consumption of $(c)_{des}$ = 17.2 mg/N/s (0.607 N/N/h) to integrate with the *NT*-BL aircraft. The BDSF engine was slightly modified for better fuel consumption, where $(c)_{des}$ = 15.85 mg/N/s (0.559 N/N/h), like-wise with the BDFT where $(c)_{des}$ = 16 mg/N/s (0.57 N/N/h); comparable to the cruise performance of a long range transport aircraft.

The factor (*c'*) describes fuel consumption of a propulsion system at a critical datum condition, and is typically used to calculate $(c)_{des}$, but is reversed to provide:

$$c' = \frac{(c)_{des}}{\left(1-0.15R^{0.65}\right)\cdot\left[1+0.28\cdot\left(1+0.63R^{2}\right)\cdot M_{N}\right]\cdot\sigma_{cr1}{}^{0.08}} \text{ [N/N/h]}$$

Equation B-60

The datum sea level static specific fuel consumption $(c)_0$, was analysed by [Doulgeris, 2008], where $(c)_0$ = 9.80 mg/N/s (0.346 N/N/h) for the *NT*-BL aircraft, $(c)_0$ = 8.77 mg/N/s (0.31 N/N/h) for the BDSF, and for the BDFT configuration $(c)_0$ = 9 mg/N/s (0.32 N/N/h). Equation B-61 is used to determine the critical static sea level factor $(c)_0$'.

An off design specific fuel consumption, $(c)_{OD}$, is used where for a non-specific flight condition, the engine is operating at a thrust less than that of the design value, and the specific fuel consumption tends to increase.

$$c_{OD} = c\cdot\left[1+0.01\cdot\left(\frac{T}{T_{OD}}-1\right)\right] \text{ [N/N/h]}$$

Equation B-61

Where T/T_{OD} has a value less than 10, and is taken to be the *Av/req* thrust value previously calculated. Table B-19 below shows the results for the analysis above for the engine characteristics for the BDSF and BDFT configurations.

	$(c)_{des}$ [N/N/h]	c' [N/N/h]	$(c)_0$ [N/N/h]	$(c)_0$' [N/N/h]	$(c)_{OD}$ [N/N/h]
NT-BL	0.572	0.787	0.332	0.823	0.576
BDSF	0.560	0.675	0.310	0.737	0.564
BDFT	0.565	0.681	0.318	0.756	0.570

Table B-19: General data for mass breakdown results (part II)

B.3.3.3 Equivalent Air Speed Climb Characteristics

Equivalent air speed (EAS) climb was previously discussed in sections B-2.3.3 and B-3.1.3. The ratio for constant EAS climb to datum value (*Z*), is calculated using:

$$Z = \frac{V_{EAS}}{1.458 \cdot Q_V}$$

Equation B-62

Where the constant Q_V is calculated from the wing loading at EAS climb conditions, and low speed drag using the following equations:

$$Q_V = \left[\left(\frac{Mg}{S} \right)_0 \left(\frac{M_1}{M_0} \right) \frac{\overline{\beta}_0^{0.5}}{(c_{dz})_{ls}} \right]^{0.5}$$

Equation B-63

$$\overline{\beta_0} = (K_V)_0 \cdot (c_{dz})_{ls}$$

Equation B-64

The thrust factor at constant EAS climb ($\tau_{C1\ EAS}$) is calculated using Equation B-32, where the relative density, Mach number, and thrust constants for $0.4<M_N>0.9$ have previously been established, and the results are shown below.

	$\overline{\beta_0}$	Q_V	Z	$\tau_{C1\ EAS}$
NT-BL	0.000873	111.0	1.05	0.293
BDSF	0.00120	99.7	1.17	0.377
BDFT	0.00152	115.2	1.01	0.377

Table B-20: EAS and climb results (part I)

The mean constant EAS rate of climb $(V_V)_{EAS}$ is given by:

$$(V_V)_{EAS} = \frac{0.73 \cdot Z \cdot Q_V}{1 + 0.12 \cdot \left(\frac{Z \cdot Q_V}{100}\right)^2} \cdot [f(Thrust) - f(Drag)] \text{ [m/s]}$$

Equation B-65

Where the two factors *f(Thrust)* and *f(Drag)* represent thrust and drag correction factors for the propulsion system, where for a HBPR engine:

$$f(Drag) = 1.16 \cdot \overline{\beta_0}^{1/2} \cdot \left[Z^2 \cdot \left(1 + 0.9 \cdot \sigma_{C1_{.EAS}}^{-0.42}\right) + \frac{0.66 n^2}{Z^2} \cdot \left(1 + \sigma_{C1_{.EAS}}^{-0.38}\right) \right]$$

Equation B-66

Where *n*, is the normal acceleration factor during climb which is assumed to be unity, and the thrust factor for a HBPR engine is given by:

$$f(Thrust) = \left(\frac{T}{Mg}\right)_0 \cdot \frac{M_0}{M_1} \cdot \tau_{C1_{.EAS}} \cdot \left(1 + \left[\frac{(0.64 - 0.016R)}{(0.76 - 0.016R)} \cdot \sigma_{C1_{.EAS}}^{(s-0.42)}\right]\right)$$

Equation B-67

The ground distance covered during constant EAS climb phase, $(S_G)_{EAS}$, is found from:

$$(S_G)_{EAS} = \frac{0.5 \cdot H_2 \cdot V_{EAS}}{(V_V)_{EAS}} \left(1 + \sigma_{C1_{.EAS}}^{-0.5}\right) \cos\left[\sin^{-1}\left\{\frac{2(V_V)_{EAS}}{(V_V)_{EAS}\left(1 + \sigma_{C1_{.EAS}}^{-0.5}\right)}\right\}\right] \text{ [km]}$$

Equation B-68

The fuel mass ratio $W_F/(Mg)_0$ for constant EAS climb provides a calculation for the fraction of fuel burnt during climb, where the constants α = 1.45, β = 0.22, and γ = 0.82, represent a HBPR engine, where $(c)_0$ was previously calculated in section B-3.3.2:

$$\left(\frac{W_F}{(Mg)_0}\right)_{EAS} = \frac{0.1 \cdot \alpha (c)_0 H_2}{(V_V)_{EAS}} \cdot \left(\frac{T}{Mg}\right)_0 \tau_{C1_{.EAS}} \left[1 + \gamma \sigma_{C1_{.EAS}}^{(s+0.08)} + \beta \left\{1 + \gamma \sigma_{C1_{.EAS}}^{(s-0.537)}\right\} \left(\frac{V_{EAS}}{100}\right)\right]$$

Equation B-69

	f(Thrust)	*f(Drag)*	$(V_V)_{EAS}$ *[m/s]*	$(S_G)_{EAS}$ *[km]*	$(W_F/(Mg)_0)_{EAS}$
NT-BL	0.289	0.140	10.9	187.8	0.0124
BDSF	0.291	0.174	8.51	217.7	0.0138
BDFT	0.321	0.178	10.5	176.7	0.0127

Table B-21: EAS and climb results (part II)

A comparison of the results is presented within Table B-21 above. The BDSF travels a further horizontal distance to achieve the same altitude, due to the lower vertical ascent velocity compared to the *NT*-BL and BDFT, resulting in a greater mass fraction of fuel burnt for the EAS climb phase.

B.3.3.4 Constant Mach Number Climb Characteristics

The factor in constant Mach number climb (Q_M) has previously been calculated for a first estimate, where a newly revised calculation can be made re-using Equation B-47, where in this instance the wing-loading can be re-defined to incorporate the fuel used for the constant EAS climb, $W_F/(Mg)_0$.

$$\left(\frac{Mg}{S}\right)_1 = \left(\frac{Mg}{S}\right)_0 \cdot \left[\frac{M_1}{M_0} - \left(\frac{W_F}{(Mg)_0}\right)\right]$$

Equation B-70

Thrust factor for constant Mach number climb ($\tau_{Mn.1}$) is calculated using Equation B-32, where the relative density for the initial constant Mach climb is where the EAS climb phase has ended. Since the BD concepts both have the same inputs, when $\sigma = \sigma_{C1.EAS}$, the thrust factor for constant Mach number climb $\tau_{Mn.1} = 0.297$.

The mean constant Mach number rate of climb is calculated using:

$$(V_V)_{M_{N.1}} = \frac{170 \cdot (M_N)_{cr}}{\left(1 + 0.153 \cdot (M_N)_{cr}^2 \sigma_{C1_{EAS}}^{0.23}\right)} \cdot \overline{X} \text{ [m/s]}$$

Equation B-71

$$\overline{X} = \left[\frac{T_0}{Mg_1} \cdot \frac{\tau_{M_{N1}}}{\sigma_{C1_{EAS}}^{(s-0.02)}} \cdot \left\{\sigma_{C1_{EAS}}^{(s+0.1)} + \sigma_{cr2}^{(s+0.12)}\right\} - Q_M\left(\sigma_{C1_{EAS}}^{1.38} + \sigma_{cr2}^{1.35}\right) - \frac{\overline{\beta}}{Q_M}\left(\sigma_{C1_{EAS}}^{-1.1} + \sigma_{cr2}^{-1.08}\right)\right]$$

Equation B-72

The drag term $\overline{\beta}$ has been previously calculated within section B-2.6.4, and the cruise thrust-to-weight ratio during the initial constant Mach number climb T_0/Mg_1 is given by:

$$\frac{T_0}{Mg_1} = \left(\frac{T}{Mg}\right)_0 \cdot \left(\frac{M_1}{M_0} - \frac{W_F}{(Mg)_0}\right)^{-1}$$

Equation B-73

The ground distance covered during the first phase of constant Mach number climb $(S_G)_{cr1}$, is calculated using:

$$(S_G)_{cr1} = \frac{170(M_N)_{cr}}{(V_V)_{M_{N1}}}(H_2 - H_1)\left(\sigma_{cr1}^{0.117} + \sigma_{cr2}^{0.117}\right)\cos\left[\sin^{-1}\left\{\frac{(V_V)_{M_{N1}}}{170(M_N)_{cr}\left(\sigma_{cr1}^{0.117} + \sigma_{cr2}^{0.117}\right)}\right\}\right] \text{ [km]}$$

Equation B-74

The specific fuel consumption in constant Mach number climb $(c)_1$ is provided by:

$$(c)_1 = \frac{(c)_{des}}{\sigma_{cr1}^{0.08}} \text{ [N/N/h]}$$

Equation B-75

Where, $(c)_1$ is used to calculate the fuel fraction used for the first phase of constant Mach number climb, using:

$$\left(\frac{W_F}{(Mg)_0}\right)_{M_{N1}} = \frac{0.139(H_2 - H_1)\cdot\tau_{M_{N1}}(c)_1}{(V_V)_{M_{N1}}} \cdot \left(\frac{T}{Mg}\right)_0 \left[1 + \left(\frac{\sigma_{cr1}}{\sigma_{C1_{.EAS}}}\right)^{(s+0.08)}\right]$$

Equation B-76

The results for the first phase of the constant Mach number climb are shown below in Table B-22, where the BDSF travels a greater horizontal distance at a lower ascent speed, and burns a higher fuel fraction compared to the BDFT.

	Q_M	T_0/Mg_1	$(V_V)_{MN1}$[m/s]	$(S_G)_{cr1}$[km]	$(c)_1$	$(W_F/(Mg)_0)_{MN1}$
NT-BL	0.149	0.530	19.9	18.2	0.628	0.00164
BDSF	0.148	0.465	21.2	17.2	0.604	0.00150
BDFT	0.123	0.513	28.2	15.1	0.610	0.00147

Table B-22: Constant Mach number climb results (first phase)

For the second phase of constant Mach number climb, the thrust factor for constant Mach number climb ($\tau_{Mn.2}$) is calculated using Equation B-32, where the result is the same for both BD configurations, where $\tau_{Mn.2} = 0.320$.

The mean constant Mach number rate of climb at the second phase is:

$$\left(V_V\right)_{M_{N.2}} = 148 X_2 \left(M_N\right)_{cr} \overline{\overline{X}} \text{ [m/s]}$$

Equation B-77

$$X_2 = \left[\frac{\left\{ \frac{T_0 \cdot \tau_{M_{N2}}}{Mg_1} - 0.223 Q_M - 4.48 \frac{\overline{\beta}}{Q_M} \right\}}{\left\{ 3.36 \sigma_{cr2}^{0.98} \cdot \left(\frac{T_0 \cdot \tau_{M_{N2}}}{Mg_1} - 0.22 Q_M \right) - 4. \frac{1.36 \overline{\beta}}{Q_M \sigma_{cr2}^{0.98}} \right\}} \right]^{-0.11}$$

Equation B-78

$$\overline{\overline{X}} = \left[\frac{T_0 \cdot \tau_{M_{N2}}}{Mg_1} \left\{ 1 + \frac{\sigma_{cr2}^{(s-0.02)}}{0.297^{(s-0.02)}} \right\} - 0.223 Q_M \left(1 - 3.29 \sigma_{cr2}^{0.98}\right) - 4.48 \frac{\overline{\beta}}{Q_M} \left(1 + 0.304 \sigma_{cr2}^{-0.98}\right) \right]$$

Equation B-79

The drag term $\overline{\beta}$ and climb T_0/Mg_1 has previously been calculated in the first phase of climb, and the ground distance $(S_G)_{cr2}$, is calculated from:

$$\left(S_G\right)_{cr1} = \frac{295 \left(M_N\right)_{cr}}{\left(V_V\right)_{M_{N2}}} \left(H_2 - 11\right) \cos\left[\sin^{-1} \left\{ \frac{\left(V_V\right)_{M_{N2}}}{295 \left(M_N\right)_{cr}} \right\} \right] \text{ [km]}$$

Equation B-80

The fuel fraction used for the second phase of constant Mach number climb is given by:

$$\left(\frac{W_F}{(Mg)_0} \right)_{M_{N2}} = \frac{0.139 \left(H_2 - 11\right)}{\left(V_V\right)_{M_{N2}}} \cdot \tau_{M_{N2}} \cdot \left(\frac{(c)_1}{\sigma_{cr2}^{0.08}} \right) \cdot \left(\frac{T}{Mg} \right)_0 \cdot \left[1 + 3.37 \sigma_{cr2}\right]$$

Equation B-81

Results for the second phase of the constant Mach number climb can only be calculated using the equations above if the first phase of climb starts above 11km altitude.

B.3.3.5 Cruise & Descent Characteristics

The start of cruise mass ratio (M_{cr1}/M_0), is calculated using three weight fractions previously determined, where M_{cr1}/M_0 is:

$$\frac{M_{cr1}}{M_0} = \left(\frac{M_1}{M_0}\right) - \left[\frac{W_f}{(Mg)_0}\right]_{EAS} - \left[\frac{W_f}{(Mg)_0}\right]_{M_{N1}} - \left[\frac{W_f}{(Mg)_0}\right]_{M_{N2}}$$

Equation B-82

The horizontal distance covered whilst descending from cruise $(S_G)_{desc}$ is calculated using an assumption for a continuous descent approach angle of 4 degrees, where:

$$(S_G)_{desc} = \frac{H_2}{\tan(4)} = 14 \cdot H_2 \text{ [km]}$$

Equation B-83

M_{cr}/M_0 and $(S_G)_{desc}$ results are shown below, where the ground distance for descent is the same for both concepts, because they share the same climb ceiling, and descent angle.

	(M_{cr}/M_0)	$(S_G)_{desc}$ [km]
NT-BL	0.837	166
BDSF	0.837	161
BDFT	0.839	161

Table B-23: cruise mass ratio and ground distance for descent Results

B.3.3.6 Evaluation of Mass Breakdowns

The breakdown of mass is divided into structures, systems, and fuel, where the analysis above is used to determine the overall *NT*-BL aircraft and BD mass. Fuselage mass is determined using the fuselage factor (C_2), cabin maximum working differential pressure ($\overline{p}$), and fuselage length (L), width (B), and height (H) in the following equation:

$$M_{FUS} = C_2 \cdot \overline{p} \cdot (9.75 + 5.84B) \cdot \left(\frac{2L}{(B+H)} - 1.5\right) \cdot (B+H)^2 \text{ [kg]}$$

Equation B-84

The fuselage is identical for all three configurations with a calculated mass of 16,540 kg.

An evaluation factor ($\overline{C_1}$) is required to determine the lifting surface mass which uses C_1 previously calculated in section B-3.2.2, where:

$$\overline{C_1} = C_1 \cdot \left[A^{0.5} \sec \Lambda_{1/4} \left(\frac{1+2\lambda}{3+3\lambda} \right) \cdot \overline{N}^{0.3} \left(\frac{V_D}{(t/c)} \right)^{0.5} \right]^{0.9}$$

Equation B-85

Total installed propulsion systems mass ratio (M_{PP}/M_0) is calculated using the engine coefficient (C_3), and the estimated thrust-to-weight ratio for the engine, where:

$$\frac{M_{PP}}{M_0} = C_3 \cdot \left(\frac{T}{Mg} \right)_0 \left(\frac{T}{Mg} \right)_{ENG}^{-1}$$

Equation B-86

The systems mass ratio (M_{Sys}/M_0) was previously defined by C_4, and the operational item mass is calculated using the number of passengers (n_{pax}) and operational items factor (F_{OP}), as defined within section B-3.1.4, where M_{OP} is 2762 kg.

$$M_{OP} = 170 + n_{pax} \cdot F_{OP} \text{ [kg]}$$

Equation B-87

The 'fixed' mass (M_{fixed}) refers to the total of fuselage (M_{FUS}), payload (M_{PAY}), and operational items (M_{OP}) mass and are identical for all three variants M_{fixed} = 43,062 kg.

The Net range $(s)_{NET}$ requirement is calculated as the required total range $(s)_{des.range}$ less the horizontal distances required for climb and descent.

$$(s)_{NET} = (s)_{des.range} - (S_G)_{EAS} - (S_G)_{M_{N1}} - (S_G)_{M_{N2}} \text{ [km]}$$

Equation B-88

The cruise fuel ratio (M_{cr1}/M_{cr2}) can be determined using the net range requirement $(s)_{NET}$, where by rearranging Equation B-89 below, we can determine the logarithm (to base 10) of the cruise fuel mass ratio, and thereafter M_{cr1}/M_{cr2} for each configuration.

$$(s)_{NET} = 2445 \cdot \frac{(M_N)_{cr}}{(c)_{OD}} \cdot \frac{L}{D} \cdot \log_{10} \left(\frac{M_{cr1}}{M_{cr2}} \right) \text{ [km]}$$

Equation B-89

The ratio of end of cruise mass to take-off mass ratio (M_{cr2}/M_0) is a product of the initial cruise mass ratio (M_{cr1}/M_0) and the inverse of the cruise fuel ratio (M_{cr2}/M_{cr2}), calculated above using Equation B-89.

The ratio of fuel to take-off mass (M_{fuel}/M_0) is the difference between unity and the sum of M_{cr2}/M_0 and a 1% approach fuel ratio.

The ratio of all masses directly proportional to the total mass (κ_{M0}), is calculated as the sum of the systems mass ratio (M_{Sys}/M_0), installed propulsion systems mass ratio, and the fuel mass ratio (M_{fuel}/M_0). The results of the mass ratios discussed in the above analysis are shown below in Table B-24, where for the same design range the BDFT has a 40km longer cruising distance than the BDSF and is due to a more efficient climb performance because of the control available from the horizontal tail surface. The *NT*-BL aircraft proves this with similar results as the BDFT, where the *NT*-BL has a 70km longer cruise distance compared with the BDFT, and a 130km difference compared with the BDSF.

	$\overline{C_1}$	(M_{PP}/M_0)	$(S)_{NET}$ [km]	(M_{cr1}/M_{cr2})	(M_{cr2}/M_0)	(M_{fuel}/M_0)	(κ_{M0})
NT-BL	0.0553	0.107	7076.7	1.40	0.596	0.414	0.661
BDSF	0.0352	0.0934	7053.2	1.37	0.609	0.401	0.634
BDFT	0.0357	0.103	7096.2	1.44	0.581	0.429	0.673

Table B-24: Mass breakdown results

B.3.4 Mass, Centre of Gravity Analysis & Summary

The mass, centre of gravity, and design summary is the final step for the second phase of the parametric study. This is necessary to determine the overall masses of major structural and systems components, their location along the aircraft length, and to note any assumptions made during this process of determining the centre of gravity location. The following analysis will conclude with a summary of the *NT*-BL aircraft and BD configurations.

B.3.4.1 Total Mass Estimate

The first estimate for the total mass $(M_0)_{EST-1}$ is based on the assumption that the lifting surface mass is approximately 12% of the total mass of the vehicle, where:

$$(M_0)_{EST-1} = \frac{(M)_{fixed}}{0.88 \cdot \kappa_{M_0}} \text{ [kg]}$$

Equation B-90

A second mass estimate is required, where for initial calculation purposes, $(M_0)_{EST-2}$ is a direct numerical transfer of the $(M_0)_{EST-1}$ result. The mass of items proportional to the overall mass $(M_0)\kappa_{M0}$ is the product of $(M_0)_{EST-2}$ and κ_{M0}, and the mass of the lifting surfaces $M_{lift-surf}$ is determined by:

$$M_{lift-surf} = \overline{C_1} \cdot (M_0)_{EST-2}^{1.35} \cdot \left(\frac{S}{M_0} \right)^{0.45} \text{ [kg]}$$

Equation B-91

Calculated mass $(M_0)_{Calc}$ is the sum of $(M_0)\kappa_{M0}$, $(M_0)_{EST-2}$, and $M_{lift-surf}$, where the '(*error*)' between calculated and second mass estimate is used as an optimisation parameter, and adjusted to provide a minimum value for $(M_0)_{Calc}$.

	$(M_0)_{EST-1}$	$(M_0)_{EST-2}$	$(M_0)\kappa_{M0}$	$M_{lift-surf}$	$(M_0)_{Calc}$	*Error*
NT-BL	200,412	419,846	277,339	106,829	428,144	8,298
BDSF	174,993	345,220	218,842	83,316	345,220	2.54×10^{-5}
BDFT	207,548	353,806	237,941	72,802	353,806	8.62×10^{-5}

Table B-25: Initial total aircraft mass results, all mass values in [kg]

B.3.4.2 Component Mass Estimate

The overall mass of the three configurations have been established, and now it is possible to break-down this total mass and provide estimates for the wing, tail, undercarriage, systems, fuel masses, etc. The mass of the wing is calculated using:

$$M_W = M_{lift-surf} / C_5 \text{ [kg]}$$

Equation B-92

The mass of the tail is the remainder of the lifting surface mass, where:

$$M_T = M_{lift-surf} - M_W \text{ [kg]}$$

Equation B-93

The undercarriage mass (M_G) is considered to be 4% of the total mass $(M_0)_{calc}$, where 15% of this is used for the nose gear, and the other 85% split between the two main gears. The propulsion systems mass is calculated as the product of the installed propulsion systems mass ratio (M_{PP}/M_0) and $(M_0)_{calc}$. The systems mass is similarly given as the product of systems mass ratio (M_{Sys}/M_0) and $(M_0)_{calc}$, where in this instance 4% is subtracted from M_{Sys}/M_0 because the initial estimate factored in the undercarriage mass.

Using the above calculations the operational empty mass, which is the total mass of the aircraft less payload and fuel is given by:

$$M_{OEW} = M_W + M_{FUS} + M_T + M_G + M_{PP} + M_{Sys} + M_{OP} \text{ [kg]}$$

Equation B-94

The mass of fuel used is calculated as the product of the ratio of fuel mass to take-off mass ratio (M_f/M_0) and the total mass $(M_0)_{calc}$. The fuel mass (M_f), payload mass (M_{Pay}), and operational empty mass (M_{OEW}) are then combined, and provide an accurate estimate for the final mass (M_0), as shown in the design summary Table B-27.

Results for the wing area, span, mean standard chord, static thrust-to-weight ratio, and available fuel volume within the wing are expressed in Table B-27. The wing reference area (S) is simply calculated as the product of $(M_0)_{calc}$ and gravitational acceleration (g), divided by the take-off wing loading $(Mg/S)_0$ calculated within section B-2.5.3. Wing span (b) is calculated using the wing aspect ratio (A) and wing area (S), allowing the standard mean chord ($\bar{c}$) to be calculated by dividing S by b. The static engine thrust (T_0) is calculated as the product of static thrust-to-weight ratio $(T/Mg)_0$, g, and $(M_0)_{calc}$.

The actual volume available for fuel within the wing depends on the geometry, systems arrangement, structural design, and provision for four embedded engines near the root section, where for a typical airliner the maximum available wing fuel mass is:

$$M_{f\_a} = \frac{420bS \cdot \left(\frac{t}{c}\right) \cdot \left(1 - 0.89\lambda + 0.49\lambda^2\right)}{A} \text{ [kg]}$$

Equation B-95

The available internal fuel mass results for the *NT*-BL aircraft, BDSF, and BDFT configurations are shown within Table B-27.

B.3.4.3 Tail, Wing, and Centre of Gravity Estimates

At this stage of the analysis, the BD geometry consists of numbers with no physical location or dimensions for the wing, tail, or their locations on the aircraft. Without this data, it is difficult to visualise or even create a graphical representation of the aircraft, because component locations are fundamental to the design and performance of the vehicle.

The overall centre of gravity position (*c.g.*) is calculated by taking moments, where the mass and location of each major component relative to the nose of the aircraft, provides the following equation.

$$M_0 l_{cg} = M_W l_W + M_{FUS} l_{FUS} + M_T l_T + M_G l_G + M_{PP} l_{PP} + M_{Sys} l_{Sys} + M_{OP} l_{OP} + M_{Pay} l_{Pay} + M_f l_f$$

Equation B-96

The major mass components above represent the wing (M_W), fuselage (M_{FUS}), tail (M_T), undercarriage (M_G), propulsion system (M_{PP}), flight systems (M_{Sys}), operational items (M_{OP}), payload (M_{Pay}), and fuel (M_f). The lengths correspond to the distance of each component *c.g.* from the nose, and for the majority of those listed above, the distances were established within section B-3.2.

The component which does not have any data is the undercarriage, where at this stage of the conceptual design analysis, the gear is an unknown. Preliminary estimates for landing gear are required to approximate the *c.g.* location. The gear mass is assumed as 4% of M_0, where $0.034M_0$ is for the main gears, and $0.006M_0$ is for the nose gear. The nose gear location is calculated as 10% of the overall fuselage length; aft of the nose, and the main gear is 1.1 times the length of the calculated *c.g.* position.

$$M_G l_G = M_0 \left(0.00374 l_{cg} + 0.0006 l_{FUS}\right)$$

Equation B-97

The wing, propulsion system, fuel, and undercarriage, are four components that use the overall *c.g.* length to determine their locations along the fuselage. The moments for these components using section B-3.2, are:

$$M_W l_W + M_f l_f = M_W \left(0.1\bar{c} + l_{cg}\right) + M_f \left(0.1\bar{c} + l_{cg}\right)$$

Equation B-98

$$M_{PP} l_{PP} = M_{PP} \left(-\frac{0.25\bar{c}}{\cos \Lambda_{1/4}} + l_{cg} \right)$$

Equation B-99

$$M_W l_W + M_f l_f + M_{PP} l_{PP} + M_G l_G = l_{cg} \left(M_W + M_f + M_{PP} + 0.00374 M_0\right) + \bar{c}\left(\overline{M}\right) + 0.0006 M_0 l_{FUS}$$

Equation B-100

$$\overline{M} = \left(0.1 M_W + 0.1 M_f - \frac{0.25\bar{c}}{\cos \Lambda_{1/4}} M_{PP} \right)$$

Equation B-101

Substituting the mass and length components from the above approximations into Equation B-96 provides l_{cg}:

$$l_{cg} = \frac{\left[\bar{c}\left(\overline{M}\right) + l_{FUS}\left(0.45\left\{M_{FUS} + M_{Sys} + M_{OP} + M_{Pay}\right\} + 0.9M_T + 0.0006M_0\right)\right]}{\left[0.9626M_0 - M_W - M_f - M_{PP}\right]}$$

Equation B-102

Having determined the *c.g.* location, the wing apex, or root chord leading edge, can be determined as the distance from the nose to the start of the root airfoil. This is a function of the mean aerodynamic chord (*MAC*), which is calculated using the standard mean chord ($\bar{c}$) and taper ratio (λ), as shown below.

$$l_{APEX} = l_{cg} - \left(\frac{\overline{x_{1/4}}}{c_0}\right) \cdot MAC = l_{cg} - \left(\frac{\overline{x_{1/4}}}{c_0}\right) \cdot 4\bar{c} \cdot \frac{\left(1 + \lambda + \lambda^2\right)}{\left\{3\left(1 + \lambda\right)^2\right\}}$$

Equation B-103

The tail moment arm ($l_{T\text{-}arm}$) is simply calculated as the difference between the *c.g.* location, and the tail length (l_T) calculated from the nose, as described in section B-3.2.

The areas of the horizontal and vertical tail surfaces are calculated using the same equation, where the constant '*x*' represents the wing span (*b*) for the vertical tail, and the mean standard chord ($\bar{c}$), for the horizontal tail surface, where:

$$S_T = \frac{\overline{V_V} \cdot S \cdot x}{\left(l_T\right)} \ [\mathrm{m}^2]$$

Equation B-104

The results for the *c.g.*, wing apex, and tail analysis are shown below:

	l_{cg} [m]	l_{APEX} [m]	$l_{T\text{-}arm}$ [m]	S_{HT} [m^2]	S_{VT} [m^2]
NT-BL	26.29	23.92	22.01	241.0	144.4
BDSF	28.96	23.28	19.34	-	353.5
BDFT	28.92	24.16	19.39	854.2	199.3

Table B-26: Centre of gravity, tail area & wing location results

B.3.4.4 Design Summary

Description	*Parameter*	*NT*-BL	*BDSF*	*BDFT*	*units*
Wing Area	S	538.5	1129.3	839.9	[m^2]
Wing Span	B	65.6	61.8	51.1	[m]
Wing Standard Mean Chord	$\bar{c}$	8.21	19.9	16.4	[m]
Wing Quarter Chord Sweep	$\Lambda_{¼}$	32.3	29.3	32.3	[deg]
Wing Taper Ratio	λ	0.277	0.236	0.209	-
Thickness-to- Chord Ratio	(t/c)	0.115	0.11	0.11	-
Wing Apex location	l_{APEX}	23.9	23.3	24.2	[m]
Horizontal Tail Area	S_{HT}	241.0	-	854.2	[m^2]
Vertical Tail Area	S_{VT}	144.4	353.3	199.3	[m^2]
Mass of Wing	M_W	90,533	75,742	61,697	[kg]
Fuselage Mass	M_{FUS}	17,454	16,540	16,540	[kg]
Mass of Tail components	M_T	16,296	7,574	11,105	[kg]
Mass of Undercarriage	M_G	17,126	13,809	14,152	[kg]
Propulsion Systems Mass	M_{PP}	45,712	32,250	36,500	[kg]
Mass of Systems	M_{Sys}	42,814	34,522	35,380	[kg]
Operational Items Mass	M_{OP}	2,762	2,762	2,762	[kg]
Operational Empty Mass	M_{OEW}	232,697	183,199	178,137	[kg]
Mass of Payload	M_{Pay}	23,760	23,760	23,760	[kg]
Mass of Fuel Required	M_f	177,168	138,261	151,908	[kg]
Available Fuel in Wing Volume	M_{f_a}	178,902	923,483	532,433	[kg]
Total Static Thrust	T_0	1,892,416	1,318,234	1,491,923	[N]
Total Overall Mass	$\boldsymbol{M_0}$	**433,625**	**345,220**	**353,806**	**[kg]**

Table B-27: Second phase of parametric study results summary

The design of the *NT*-BL aircraft and BD configurations has reached a stage, where initial mass estimates, and geometry sizing is available to summarise for each the configurations. This marks the end of the second phase of the parametric study, where an initial design can be established, only requiring optimisation in order to finalise a minimum mass solution. The analysis above describes the process of generating the summary table above for the *NT*-BL aircraft design and the two BD variants, where the mass breakdown and geometries are the basis for an optimisation process.

B.4 Final Phase of Parametric Analysis; Optimisation

The final phase of the parametric analysis involves an optimisation process, which is used to reduce mass and increase aircraft performance. Iterating the design by means of taking any assumptions or estimated characteristics from sections B-2 and B-3, and refining them based on initial output results from Table B-27, is the basis of the optimisation process.

Optimisation is required to lower mass and increase flight performance, and should not be confused with the main research objective of reducing noise. The goal of this process is to produce an aircraft concept with a suitable design methodology, performance, and mass estimates, and not to start tackling noise before there is a feasible design. Modifications to the design to determine aircraft noise, and investigations into noise reducing technologies are investigated further within Chapter 6, where the final phase of the parametric analysis, the optimisation of the design, is discussed in more detail.

B.4.1 Wing Geometry

The wing area (*S*) and span (*b*) are known for each configuration where a detailed breakdown of the wing geometry can now be established. The airfoil selection for the *NT*-BL aircraft identifies the use of a supercritical airfoil section which is continuous from root to tip. The BD airfoil selection describes four main airfoil sections with varying *t/c* and lift characteristics, where (source 2) provides a geometry guide for the wing layout. The BD wing was divided into three main sections using the span ratios listed in Table B-28, where the divide identifies transition regions between airfoil sections along the span.

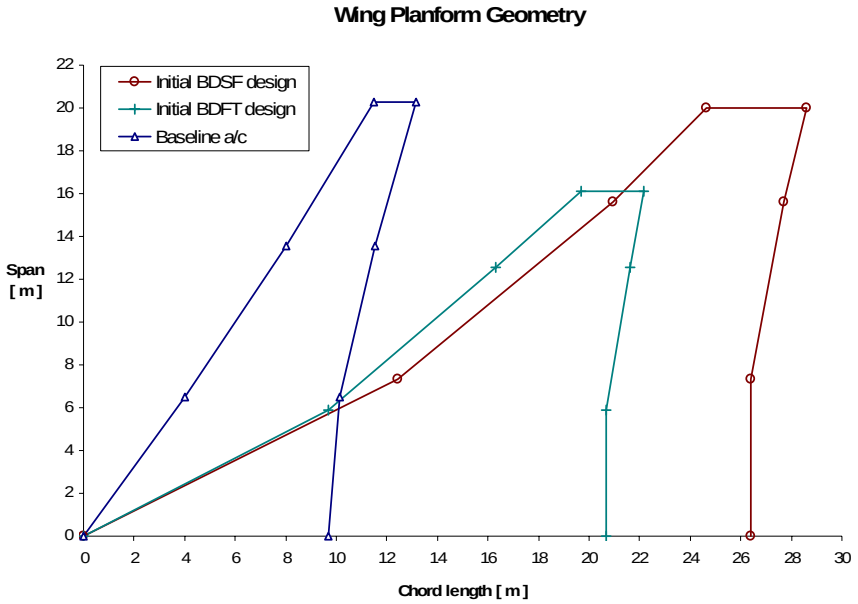

Fig B-6: *NT*-BL aircraft, BDSF, & BDFT Wing Geometries

Root-kink1	*Kink1-Kink2*	*Kink2-Tip*
0.366	0.414	0.220

Table B-28: Division of the BD wing span into three main components

The chord lengths for each airfoil section were located at the span-wise positions tabulated above, where the first kink region chord was 53% of the root chord length and the second kink was 25.7%. The tip chord defines the geometry of the winglets design and is not provided as a function of the root chord. Varying the tip chord affects the winglet geometry and the drag of the winglet. It was assumed that the tip chord was fixed at 4 metres for the BDSF and 2.5 metres for the BDFT. The BD wing geometries are plotted in Fig B-6 to compare the *NT*-BL aircraft, BDSF, and BDFT wing geometries.

B.4.2 Tail Geometry

The tail geometry is split into two calculations, firstly for the sizing of the BDSF and BDFT vertical fin, and secondly for the BDFT horizontal stabiliser. Using the results for calculated tail areas from Table B-27, it is possible to work backwards to determine the tail span (b_t), aspect ratio (A_t), taper ratio (λ_t), and quarter chord sweep ($\Lambda_{¼t}$) for both the vertical and horizontal tail components.

B.4.2.1 BDSF Vertical Tail Layout

[Howe, 2000] describes the vertical fin of a transport aircraft with a A_{vt} in the range of 0.9 to 3.0 where A_{vt} = 1.2 or above is for multiple engine configurations. A_{vt} = 1.4 was used for the BDSF vertical fin and the simplification that $A_{vt} = b_{vt}^2/S_{vt}$ can be used to determine the tail span (b_{vt}).

A mass optimisation process included modifying the aircraft drag, providing a revised calculation for the tail span, as described in section B-4.3. The new optimised tail span takes into account the addition of winglets, where the winglet area was subtracted from the vertical tail area because winglets provide directional stability, reducing the size of the vertical stabiliser; which does not necessarily mean the effectiveness of the tail is compromised, it only implies that the rudder will occupy a larger fraction of the total vertical tail area. To further increase the effectiveness of the vertical tail a higher sweep angle is incorporated moving the tail moment arm aft and providing greater control authority. The quarter chord sweep ($\Lambda_{¼vt}$) is increased to 1.25 times that of the main wing and the tail moment arm is increased by moving the tail surface from 90% to 95% of the fuselage length; which takes the increased sweep effect into consideration.

The tail geometry is a simplified trapezoidal section and the total area and span estimates are used to calculate the tip and root chord lengths. The vertical tail taper ratio for a conventional high aspect ratio wing transport aircraft is usually half that of the main wing and cannot be used on the BDSF as the taper is too high; providing a large thin and flimsy tail design which is unsuitable for a directional control surface. The taper ratio for the BDSF was considered to be twice that of the main wing. The vertical fin tip chord is constrained as the product of λ_{vt} and the fin root chord. The final vertical tail geometry for the BDSF is defined within Table B-29 and Fig B-7.

B.4.2.2 *NT*-BL aircraft & BDFT Horizontal & Vertical Tail Layout

The *NT*-BL aircraft and BDFT use a similar method for the fin sizing as described by the BDSF, where for this design case, the horizontal component is the critical surface to size mainly because it is used to balance the aircraft during flight. According to [Howe, 2000] A_{ht} for a conventional high aspect ratio aircraft such as the *NT*-BL is 50-60% of the main wing, but for the low aspect ratio BD wing, A_{ht} is assumed to be equal to the main wing. The BDFT horizontal tail span is sized using the same method as discussed in B-4.2.1, where the taper ratio is twice that of the main wing defining the root and tip chord lengths and $\Lambda_{¼ht}$ is 1.2 times that of the main wing.

The vertical tail sizing is similar to the methods used above, where the vertical tail area considers the size of the winglets, taper ratio is the same as the horizontal tail, sweep is 1.3 times the main wing $\Lambda_{¼vt}$, and A_{vt} are the same as that defined for the BDSF. Using these assumptions the overall geometry of the horizontal and vertical tail components can be established, and are shown within Table B-29 and Fig B-7.

B.4.2.3 *NT*-BL aircraft, BDSF, & BDFT Tail Comparison

The analysis above provides an insight into how the empennage was initially sized for the *NT*-BL and BD configurations; based on simplifications for the tail volume coefficients and moment arms. The geometry of each vertical and horizontal tail surface is defined within Table B-29 and a visual representation of each of the tail surfaces is shown in Fig B-7.

Comparing the tail geometries shows how the BDSF tail is larger compared with the *NT*-BL aircraft and BDFT. The BDFT has a larger horizontal tail for balancing lift during flight compared with the *NT*-BL aircraft. A concern at this stage is the location of the horizontal tail component for the BDFT, because sufficient vertical clearance is required so that the wake from the main wing at high incidence will not disturb or stall the flow over the tail surface, otherwise effects could be catastrophic. Investigations into types of tail discuss the advantages and disadvantages, where the ideal solution was found to be a V-tail.

	A	b [m]	c_{root} [m]	c_{tip} [m]	λ	$\Lambda_{¼}$
NT-BL h_t	1.98	7.03	4.91	2.18	0.443	38.8
NT-BL v_t	1.49	6.67	6.20	2.75	0.443	38.8
BDSF v_t	1.41	8.98	8.72	4.11	0.471	37.7
BDFT h_t	2.67	9.27	8.88	5.02	0.565	42.2
BDFT v_t	1.40	8.17	7.45	4.21	0.565	39.2

Table B-29: *NT*-BL, BDSF, and BDFT Empennage geometry results

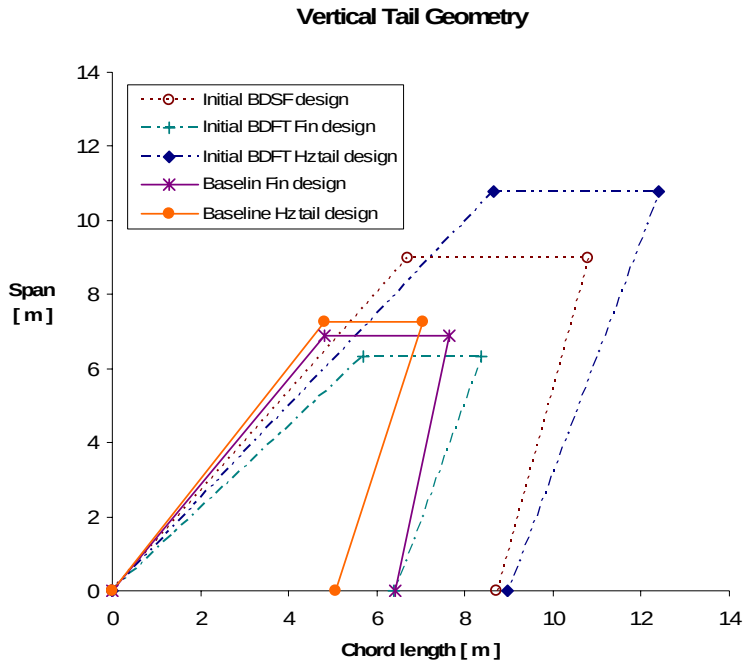

Fig B-7: BDSF & BDFT Tail Geometry Comparison

B.4.3 Optimisation Process

Optimisation begins by taking the results from the first and second stages of the parametric analysis, and refining the calculations so that the design can be iterated using specific results, such as the wing area (S), taper ratio (λ), thickness to chord (t/c) ratio etc. The optimisation begins by ensuring that the second mass estimate $(M_0)_{EST\text{-}2}$ equals the calculated value $(M_0)_{Calc}$, using the goal seek tool and results for the mass and geometry are equal to that in Table B-27. This process is referred to as a 'mass optimised' solution.

B.4.3.1 Zero Lift Wing Area Parameter

The wing area (S) calculated in Table B-27 is used in a revised calculation of the zero lift drag wing area parameter ($S^{-0.1}$), and this result is used as an input and re-iterated until a mass optimised solution is found for each of the BD configurations.

B.4.3.2 Winglet Design & Drag

The low speed and cruise induced drag is recalculated by investigating the potential drag reduction of winglets using [McCormick, 1979]. It is important to note the limitations of using McCormick as the methodology is described for first generation transport aircraft and may not necessarily reflect a true

drag reduction[1]. Never-the-less, recently published methodologies for winglet designs are scarce, and literature revealed that current methods use detailed finite element methods (FE) and viscid computational fluid dynamics (CFD) to quantify the effect of winglets. Detailed FE and CFD investigation was not considered effective time management so the empirical method by McCormick was used.

Winglet design is difficult as the aim is to lower induced drag, reduce wing-tip vortices by improving performance at cruise, and enhancing low speed handling characteristics. Detailed design of winglets includes evaluating cant angles, toe-in or toe-out designs, and the wing-tip geometry. Literature describes how to design a winglet but methods are not available to integrate their performance benefits into a conceptual design methodology.

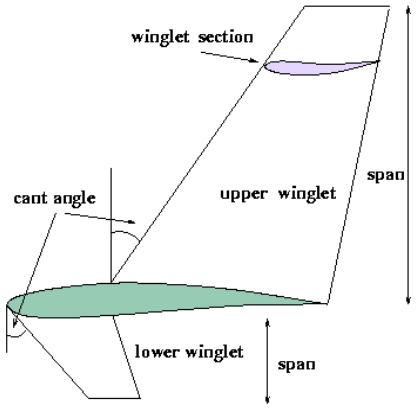

Fig B-8: Winglet Geometry [Fillippone, 2004]

The following summary is based on a literature study on winglet design, using [Lin et. al, 1990], [Maughmer et. al, 2001], [Wagnon, 2001], [Gau, 2002], [de Mattos et. al, 2003], [Kubrynski, 2003], [Filippone, 2004], and [Catalano, Ceron-Munoz, 2005], where:

- Low speed induced drag reduced by 5%
- Cruise induced drag reduced by 20% at Mach 0.76
- L/D increases between 4-8%
- Range increases by 7%
- Wing mass increase 1.55%

[1] The analysis describes how at low lift coefficients, induced drag may be increased by adding winglets, and may cancel any benefits. A high winglet aspect ratio is desirable, but McCormick's analysis suggests that by continuously increasing the aspect ratio, drag is further reduced. This is not true as an excessively large winglet has a large span, greater profile drag, and would create increased interference with the wing, negating any benefits of induced drag reduction.

- Sweep angle of winglet = 26 degrees at Mach 0.85.
- Effective Aspect Ratio (*EAR*) increase: $EAR = \frac{(b + 2h_w)}{S}$
- Effective Dihedral Angle (*EDA*) increase: $EAR = \frac{(20h_w)}{S}$

Where h_w is the height of winglets, S is the total wing reference area plus area of winglets, and b is the wing span.

[McCormick, 1979] provides approximations for sizing the winglets based on the tip chord (c_t) of the main wing. The winglet design is divided into an upper and lower segment, with each set at an incidence (i) to the chord-line; referred to as a 'toe-in' angle, as shown in Fig B-9.

The upper and lower winglet geometries are given as a fraction of c_t, and include the corresponding LE and side cant angles, as shown in Table B- B-30.

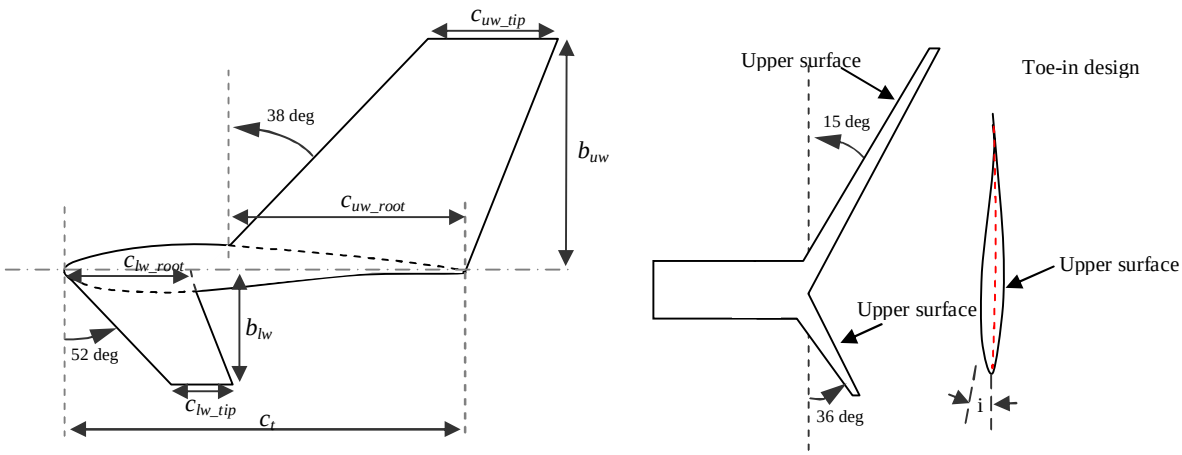

Fig B-9: Simplification of winglet Geometry modified from [McCormick, 1979]

Parameter	*upper winglet (×c_t)*	*lower winglet (×c_t)*
Span (b)	1.0	0.23
root chord ($c_{\_root}$)	0.65	0.40
tip chord ($c_{\_tip}$)	0.21	0.16
LE cant angle [deg]	38	52
side cant angle [deg]	15	36
root toe-in angle (i) [deg]	-4	-7
tip toe-in angle (i) [deg]	-4	-11

Table B- B-30: Winglet geometry defined as fractions of wing tip chord length, cant angles, and toe-in angles

To summarise the design of the winglets there are two winglets, one upper and one lower, on each wing, canted at a desired angle to the fuselage with a setting angle specified in the design calculations above. The geometry is specified above and can be used to calculate the winglet aspect ratios and winglet reference areas accordingly. The winglet airfoil is a continuation of the tip chord airfoil, where the drag coefficients are known from the airfoil analysis. The increment in drag due to the winglets is given by:

$$\Delta(c_d)_{wl} = -\frac{S_{wl}}{S}\left((c_l)_{wl}\cdot\alpha_{wl} - (c_{d_0})_{wl} - \frac{(c_l)^2_{wl}}{\pi A_{wl}}\right)$$

Equation B-105

Where the subscripts (*wl*) represent the winglet reference area (S_{wl}), aspect ratio (A_{wl}), lift coefficient $(c_l)_{wl}$ at a specified incidence (α_{wl}), and finally the zero lift drag $(c_{do})_{wl}$. The drag increments for the BDSF and BDFT are calculated below in Table B-31, where the upper winglet $\Delta(c_d)_{wl\_upper}$, and the lower winglet $\Delta(c_d)_{wl\_lower}$ drag increments are calculated per wing, and the total provides the drag reduction for one wing. $\Delta(c_d)_{wl}$ represents the total induced drag reduction for both wings, each having upper and lower winglets. The analysis indicates that the winglets reduce the overall drag of the lifting surfaces, and this is factored into the induced cruise and low speed drag, by a reduction of the specified amount.

	$\Delta(c_d)_{wl\_upper}$	$\Delta(c_d)_{wl\_lower}$	$\Delta(c_d)_{wl}$
NT-BL	-0.0045	-0.0074	-0.024
BDSF	-0.0084	-0.0140	-0.045
BDFT	-0.0034	-0.0056	-0.018

Table B-31: Induced Drag Reduction due to the addition of Winglets

B.4.3.3 Nacelle Drag

The calculation for nacelle drag of 4 over-the-wing (*OTW*) semi-embedded engines, mounted at the root, was considered for the BD configurations. Alternate arrangements were investigated by [Doulgeris, 2008] to investigate how embedded, semi-embedded or podded engine configurations would affect the integration process. Integration between airframe and engine is a difficult and lengthy process, especially when considering an incorrect selection or location could be detrimental to the design performance, so a basic engine configuration was considered.

Placing engine nacelles *OTW* was considered an ideal location for noise and was considered to be the datum configuration for initial analysis of the BD configurations. Investigations into podded engine

configurations allowed a study on the integration, location, and performance of the *OTW* layout, to produce a suitable drag model for integration into the design methodology. The designed location of the nacelles were made using assumptions from journal and conference papers by [Fujino, 2003], which later proved to be implemented on the Honda HA-420 business jet [Honda, 2007], and is currently an in-service aircraft. Fujino investigated three main variables for the location of the engines was the position along the chord, height above the wing, and the location along the span. Conclusions of this twin engine business jet conference paper described that "*over-the-wing nacelle configuration can reduce wave drag and increase drag-divergence Mach number. The nacelle front face should be located near the shock position on the clean wing and the vertical distance should be a third to half the maximum height of the nacelle. For this nacelle location, adding a pylon improves the drag-divergence characteristics and a contoured pylon, aligned with the local flow improves the aerodynamic interference at lower Mach numbers*" [Fujino, 2003].

The ideal chordwise location of the nacelles was determined to be 75% of the local chord and the spanwise location is more difficult to predict as analysis of the wing shock formation is required. In addition the BD concepts have 4 engines mounted above the wing, and interaction studies for the flow between the nacelles would be required to determine separation distance, performance, and drag data. The quad nacelle arrangement layout was estimated as shown above. The outboard nacelles were located on the BDSF at 46%, and 55% of the BDFT wing spans, and the inboard nacelles were mounted at 25% and 30% of the BDSF and BDFT wing spans.

The drag estimates were extrapolated from [Fujino, 2003], where for a high aspect ratio clean wing at Mach 0.8, the wave drag was found to be $(c_d)_{wave}$ = 0.0412, and for an *OTW* aft mounted contoured pylon, wave drag was reduced to 0.0374. The results suggest that a 9% reduction in wave drag is achieved by the OTW configuration. The author considered that although the BD houses four HBPR engines and is a civil airliner, the drag reduction seen on the business jet can be recreated for the BD, by correctly aligning the propulsion systems to achieve a 10% reduction in wave drag. A four engine configuration suggests more wave drag, but only if incorrectly located along the wing, therefore nacelles, pylons, and location, would have to be optimised using integration analysis to achieve this drag reduction.

Integration of *OTW* engine pods produces a change in the wing lift and drag, implying that not only does this effect wave drag, but also induced drag. The induced drag effect of nacelles is best described by [Hoerner, 1965], where "*any bluff obstacle placed in a certain point of a wing, somehow changes the spanwise lift distribution. Provided that the change takes place in a direction away from the elliptical optimum of that distribution, the induced drag of the wing is consequently increased"*.

Integrating *OTW* engine nacelles on a low-wing BD was investigated by [Nettis, 2007], and documents results that conflict with [Fujino, 2003], suggesting that there is a drag increase of three times the clean wing. It is the authors' opinion that due to the incorrect placement of engines in the study, the increase in drag is excessive and so a more in-depth analysis is required, but for the final BD design configuration. A 10% increase in low speed induced drag and a 5% reduction of cruise induced drag at high subsonic speeds is assumed for the *OTW* podded configuration; as concluded within [Whitcomb, 1958], with the aim to conduct a detailed CFD integration study on the final BD concept design.

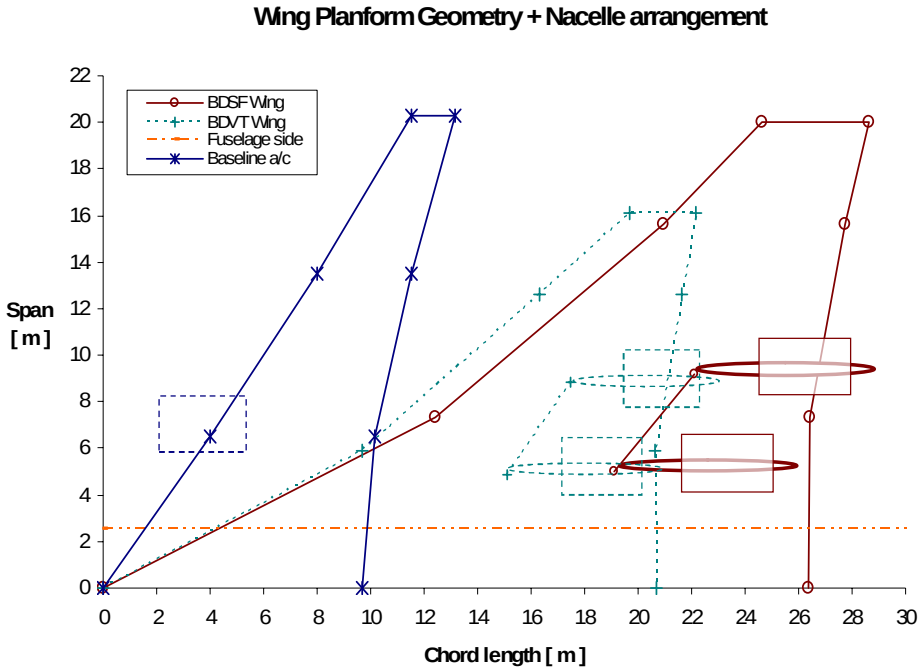

Fig B-10: BDSF & BDFT Wing & Nacelle Layout

B.4.3.4 Wetted Area Ratio

The wetted area (R_w) was initially estimated using assumptions made from [Howe, 2000], where a detailed estimate can now be calculated using [Raymer, 1992]. R_w is defined as the exposed surface area where Raymer describers it as *"the external parts of the aircraft that would get wet if it were dipped into water"*. An accurate estimation for R_w is essential as this defines the friction drag.

The wing wetted area (S_{wet}) is calculated using the exposed area ($S_{exposed}$) rather than the total reference area (S), where it is assumed that 90% of the wing area is exposed, and the other 10% is buried within the fuselage. S_{wet} is calculated by using the wing average thickness to chord ratio $(t/c)_{av}$, and $S_{exposed}$, where:

$$\left(S_{wet}\right)_{wing} = S_{\exp osed} \cdot \left[1.977 + 0.52 \cdot \left(\frac{t}{c}\right)\right] \text{ [m}^2\text{]}$$

Equation B-106

The horizontal and vertical tail surfaces and winglets are all calculated for the BDSF and BDFT using this method. The tail surfaces also have 90% of their exposed area outside the fuselage, and the winglets are fully exposed as they are joined to the wing-tips.

The fuselage wetted area is the remaining airframe component, and is calculated by estimating the top and side view areas, assuming it is an elliptic body, where:

$$\left(S_{wet}\right)_{FUS} = \pi \cdot \left(\frac{A_{top} + A_{side}}{2}\right) \text{ [m}^2\text{]}$$

Equation B-107

The remaining wetted area calculation is for the engine nacelles, and this is estimated as four elliptical bodies above the wing. As a simplification, the nacelle geometry was defined as a 2.3m by 1.9m ellipse, with a length of 5m. The wetted area is calculated using the same formula as for the fuselage. The wetted area calculations for wings, winglets, horizontal tail, and nacelles are calculated for one side, with the fuselage and vertical tail calculated as a complete section. The total wetted area represents both sides, where the wings, horizontal tail, nacelles, and winglet wetted areas are doubled and added to the calculations of the other components.

	$(S_{wet})_{FUS}$	$(S_{wet})_{Htail}$	$(S_{wet})_{Vtail}$	$(S_{wet})_{winglets}$	$(S_{wet})_{wing}$	$(S_{wet})_{nacelle}$	$(S_{wet})_{Total}$
NT-BL	747.8	50.8	60.8	6.4	259.7	33.0	1574.3
BDSF	712.2	-	123.5	15.8	464.9	66.0	1929.2
BDFT	712.2	136.8	-	6.6	324.4	66.0	1780.7

Table B-32: Wetted area results for iterated designs, where $(S_{wet})_{Htail}$ represents the V-tail for the BDFT

The total wetted areas are then divided by the corresponding wing reference areas to complete the revised calculation for $R_w = S_{wet} / S$, where for the *NT*-BL aircraft R_w = 5.52, the BDSF R_w = 3.79, and for the BDFT R_w = 2.52.

B.4.4 Optimised BD Design Summary

The design of the BD has been modified from the initial output from section B-3.4.4, where the wing geometry, tail, winglets, and nacelles have all been factored into the design, alongside new estimates for the wetted area and wing parameter ratios. The design requires mass optimisation for the design

flight case, and this is achieved using the goal-seek method within the worksheet "Howe Ss3 – Optimiser".

Description	***Symbol***	***BDSF***	***BDFT***	***NT*-BL**	***units***
Wing Area	S	526.6	321.3	196.2	[m^2]
Wing Span	b	40.5	31.6	39.6	[m]
Wing Standard Mean Chord	$\bar{c}$	13.0	10.2	4.96	[m]
Wing Aspect Ratio	A	3.11	3.11	7.99	-
Wing Quarter Chord Sweep	$\Lambda_{¼}$	29.3	32.3	32.3	[deg]
Wing Taper Ratio	Λ	0.240	0.209	0.277	-
Thickness-to- Chord Ratio	t/c	0.11	0.11	0.115	-
Wing Apex location	l_{APEX}	22.0	22.8	23.5	[m]
Horizontal Tail Area	S_{HT}	-	155.4	49.9	[m^2]
Vertical Tail Area	S_{VT}	76.0	36.2	29.9	[m^2]
Wing Area Parameter	$S^{-0.1}$	0.534	0.561	0.569	[m^{-2}]
Static Wing Loading	$(Mg/S)_0$	2755	4133	7465	[kg/m^2]
Static Thrust Loading	$(T/Mg)_0$	0.389	0.401	0.349	-
Lift-Drag Ratio	L/D	14.9	14.8	14.8	-
Cruise Lift Coefficient	$(c_L)_{cr}$	0.204	0.307	0.271	-
Mass of Wing	M_W	24,125	16,865	22,869	[kg]
Fuselage Mass	M_{FUS}	16,540	16,540	17,454	[kg]
Mass of Tail components + winglets	M_T	2,413	3,036	4,116	[kg]
Mass of Undercarriage	M_G	5,915	5,415	5,973	[kg]
Propulsion Systems Mass	M_{PP}	13,815	13,014	12,516	[kg]
Mass of Systems	M_{Sys}	14,789	13,537	14,932	[kg]
Operational Items Mass	M_{OP}	2,762	2,762	2,762	[kg]
Operational Empty Mass	M_{OEW}	80,359	71,169	80,622	[kg]
Mass of Payload	M_{Pay}	23,760	23,760	23,760	[kg]
Mass of Fuel Required	M_f	43,767	40,441	44,934	[kg]
Available Fuel within Wing Volume	M_{f_a}	281,233	126,009	47,152	[kg]
Total Static Thrust	T_0	564,706	531,957	511,604	[N]
Total Overall Mass	**M_0**	**147,886**	**135,370**	**149,316**	**[kg]**

Table B-33: Mass optimised results summary for *NT*-BL, BDSF, and BDFT

Reiteration requires the results from section B-4.3 to be used as design inputs, but tend to generate circular references using the spreadsheet method, so a relatively manual iteration is required. There are four (4) main cells that are used to optimise the BD design for minimum mass. First and foremost is the overall mass estimate M_0, where cell AB99 must be equal to $(M_0)_{est2}$ and have a zero error (cell AB102) by changing the value input in cell U90 (using goal-seek). Similarly, the wing area

calculated in cell AE89, is used to define a revised wetted area calculation, wing area parameter, and define the size of the winglets, so the value of this cell must be equal to cell J95, where the error (should equal zero) is calculated in cell J94. Also for the wetted area calculations, the fin area is required, and cell X104 must be equal to cell AE118. Finally the last iteration required is only for the BDFT design, where the horizontal empennage is sized and is used to define the wetted area calculation by changing the value in cell V121 to achieve the target tail area in cell X118, by reducing the error in cell X121 to zero.

Replicating this process by changing the necessary cell values allows the design to converge to a single mass solution for each of the *NT*-BL, BDSF, and BDFT designs. The final converged solution for each of the optimised configurations is shown in Table B-33, where the three concepts can be compared at this stage of the analysis.

This marks the end of the parametric study, where a minimum mass optimised design for the BDSF and BDFT is established with the newly integrated winglets and engine nacelles. Having completed the parametric study, the conceptual design process is continued by conducting a series of trade studies aimed to optimise the BD concept so that an ideal flight case can be established.

Appendix C Broad Delta Cruise Altitude Trade Study

C.1 Background

The success of the *AV* as a military aircraft provided a basis to design a civil variant namely the 'Avro Atlantic' [Avro, 1953]; which had great potential as a high subsonic Mach number passenger aircraft, with a cruise Mach of 0.91, and a cruise altitude in excess of 40,000ft. The aim of the altitude study was to investigate how the BD concept would behave, given that more design knowledge is available now compared with the 1950's[†]. Challenges such as stability and control of a tailless aircraft can now be addressed with active flight control systems, high fidelity design and testing methods, and with compliance of certification legislation, can reduce the chances of such catastrophic failures before the first flight stage. The challenge is not meeting certification requirements, but justifying the design of a tailless passenger aircraft, and removing the mind-set that this configuration should remain only for high-speed military vehicles.

C.2 Altitude Selection for Cruise Optimisation

Optimum cruise altitude was selected for each BD configuration using the parametric analysis mass optimisation method. Establishing an appropriate cruise altitude not only impacts cruise performance, but also climb performance, time of flight, and mission fuel, which feeds directly into the propulsion systems design, and to the overall vehicle mass. Standard atmosphere data, such as speed of sound, altitudes, densities, and temperatures, were extracted from [Pamadi, 1945], and used to calculate relative densities for a range of cruise flight cases. There is no defined lower limit for cruise altitude of a civil airliner, and so 38,000ft was considered the lowest final cruise altitude.

Flight Mach numbers were varied from 0.8 to 0.85 which is typical for most subsonic passenger aircraft, with an additional case of Mach 0.9, although the idea of flying slower for 'green' flight operations was considered, it was not developed any further mainly due to implications that the benefits of the slower concept did not out-weigh the disadvantages.

C.2.1 Altitude Selection for Cruise Optimisation

The methodology described within Appendix B was used to investigate changes in cruise altitude by varying the design inputs. The initial flight case was identical to the baseline design, where at

[†]In the 1950's, development of tailless aircraft was trial and error, involving short design, assembly, and testing phases, where on some occasions flight tests ended with pilot fatalities. The design process has changed substantially, and 'trial and error' is not acceptable, cost efficient, or practical for present day aircraft design.

the end of EAS climb, σ_{EAS} = 0.4045 at an altitude of 8.5km (28,000ft). The initial cruise climb then starts at 10km (33,000ft), where σ_{cr1} = 0.3829, and the final cruise altitude, or ceiling, was at 11.5km (38,000ft), where σ_{cr2} = 0.2971.

Optimising the cruise altitude was achieved by increasing the EAS climb ceiling to 9.1km (30,000ft), where σ_{EAS} = 0.3722. The initial start of cruise altitude was increased to 10.4km (34,000ft), where σ_{cr1} = 0.321, and reached the same cruise ceiling as the initial case of 11.5km. The mass optimisation process was completed for each design with increments of 1,000ft altitude added to the initial and final cruise altitudes. The lowest cruise case was for 10-11.5km climb case (as discussed above), and the upper limit was for an cruise segment starting at 13.4km (44,000ft) and ending at a ceiling of 14.6km (48,000ft). This point was chosen as the upper limit due to time constraints, but it was assumed that the BD concept could achieve a cruise altitude ceiling of up to 50,000ft, but with a significant mass increase; mainly due to the amount of fuel required to reach this desired cruising altitude.

The altitude study results for the cases of 34,000ft to 44,000ft initial cruise were combined with the results of changing the cruise Mach number from 0.8 to 0.9 and are compared for both the BDSF and BDFT configurations. The following results show the changes in critical design parameters, such as aircraft all-up mass: *AUM*, mission fuel: M_{fuel}, lift-to-drag ratio: *L/D*, wing loading: $(Mg/S)_0$, drag at zero lift: $c_{dz\ cr}$, cruise induced drag: $(K_v)_{cr}$, cruise lift coefficient: c_L, and aircraft thrust-to-weight ratio: *T/W*. The solid lines on each figure represent the BDFT configuration, whilst the dashed lines represent the BDSF, with a point mass for the baseline a/d design as a reference point. The altitude indicated by the ‘x’ axis, refers to the start of cruise altitude, not the final climb ceiling.

C.2.2 Results for Cruise Altitude and Mach number Analysis

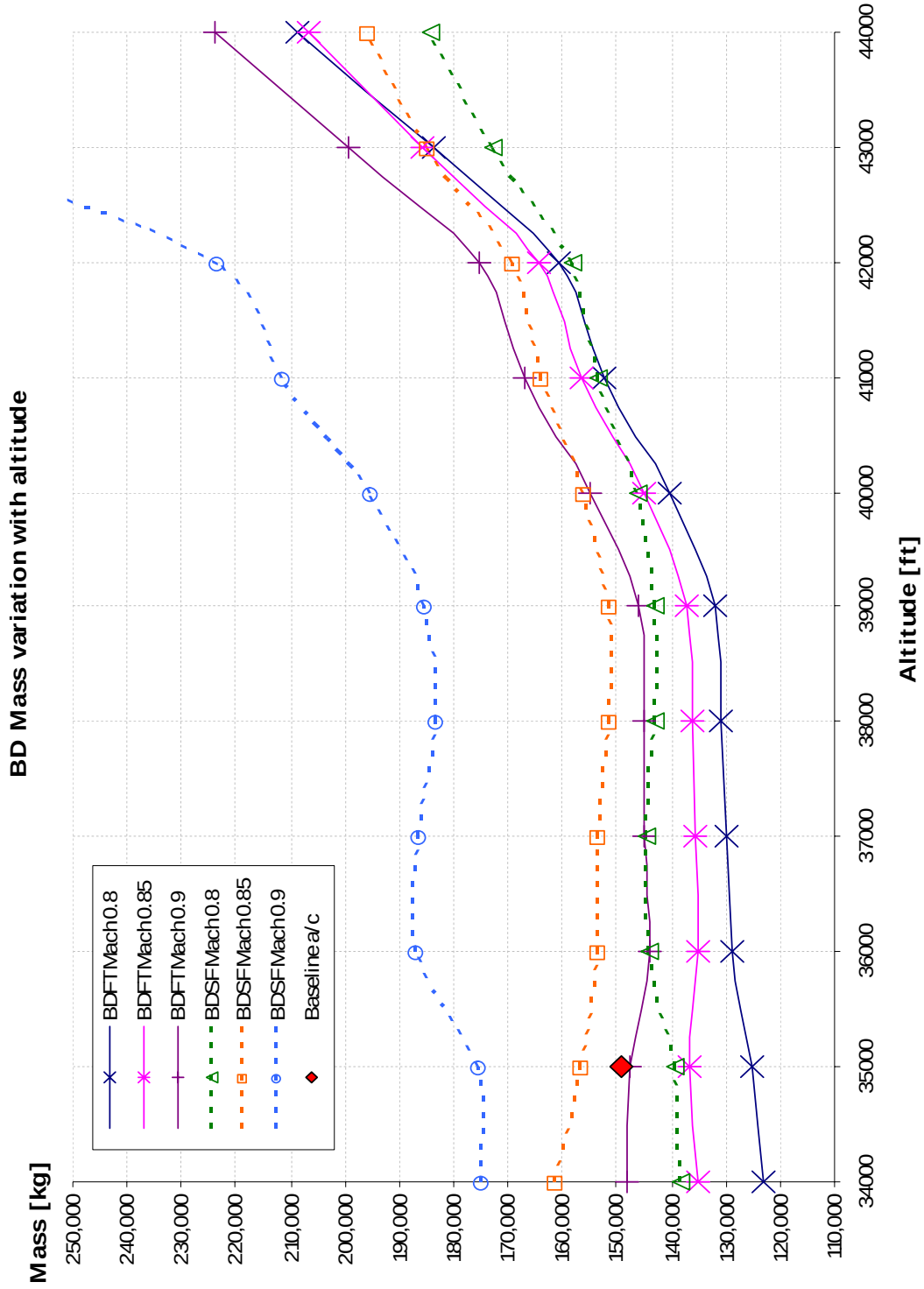

Fig C-1: BD Total aircraft Mass variation by changing Cruise Altitude and Cruise Mach

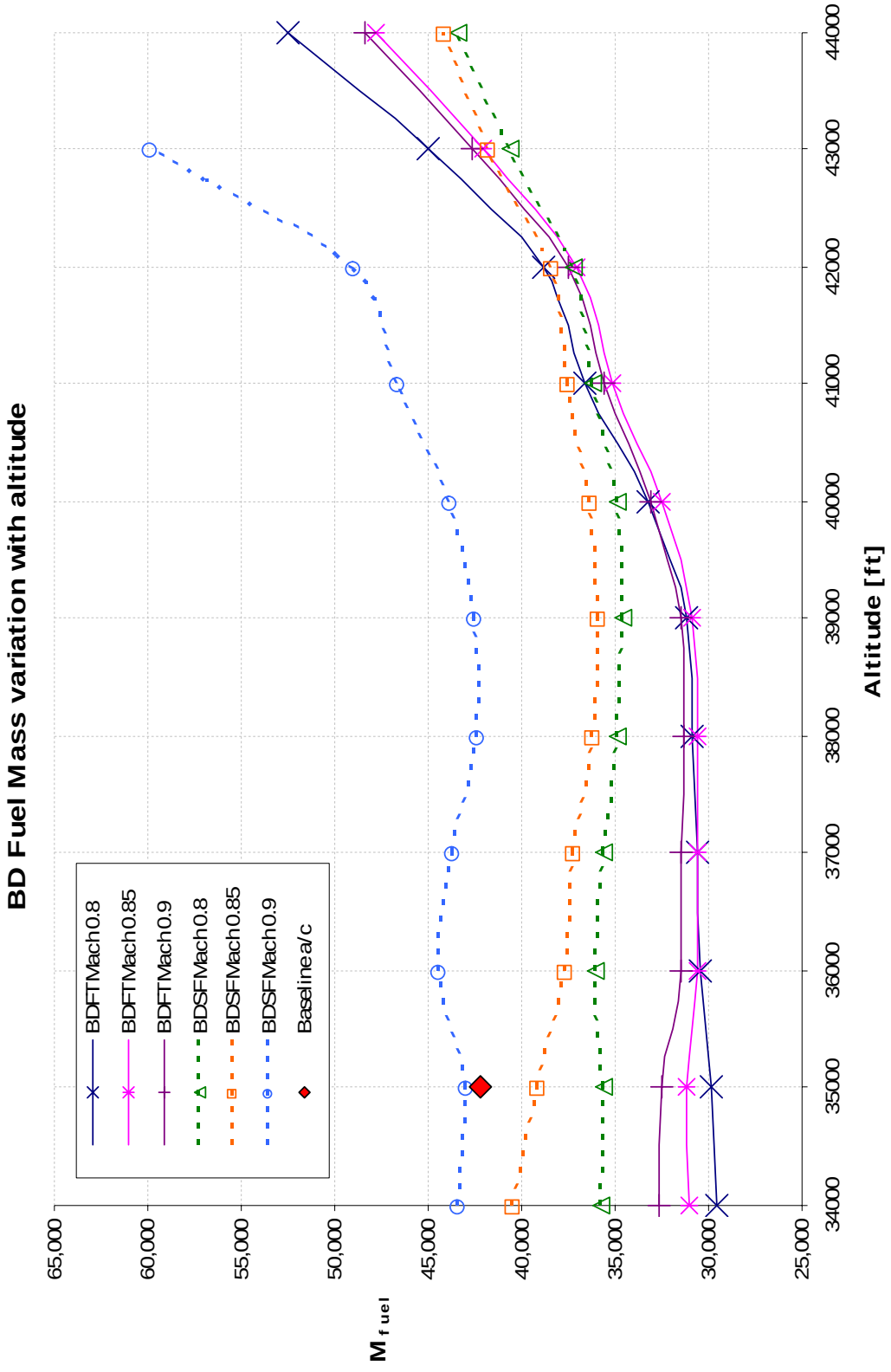

Fig C-2: BD Fuel Mass variation by changing Cruise Altitude and Cruise Mach

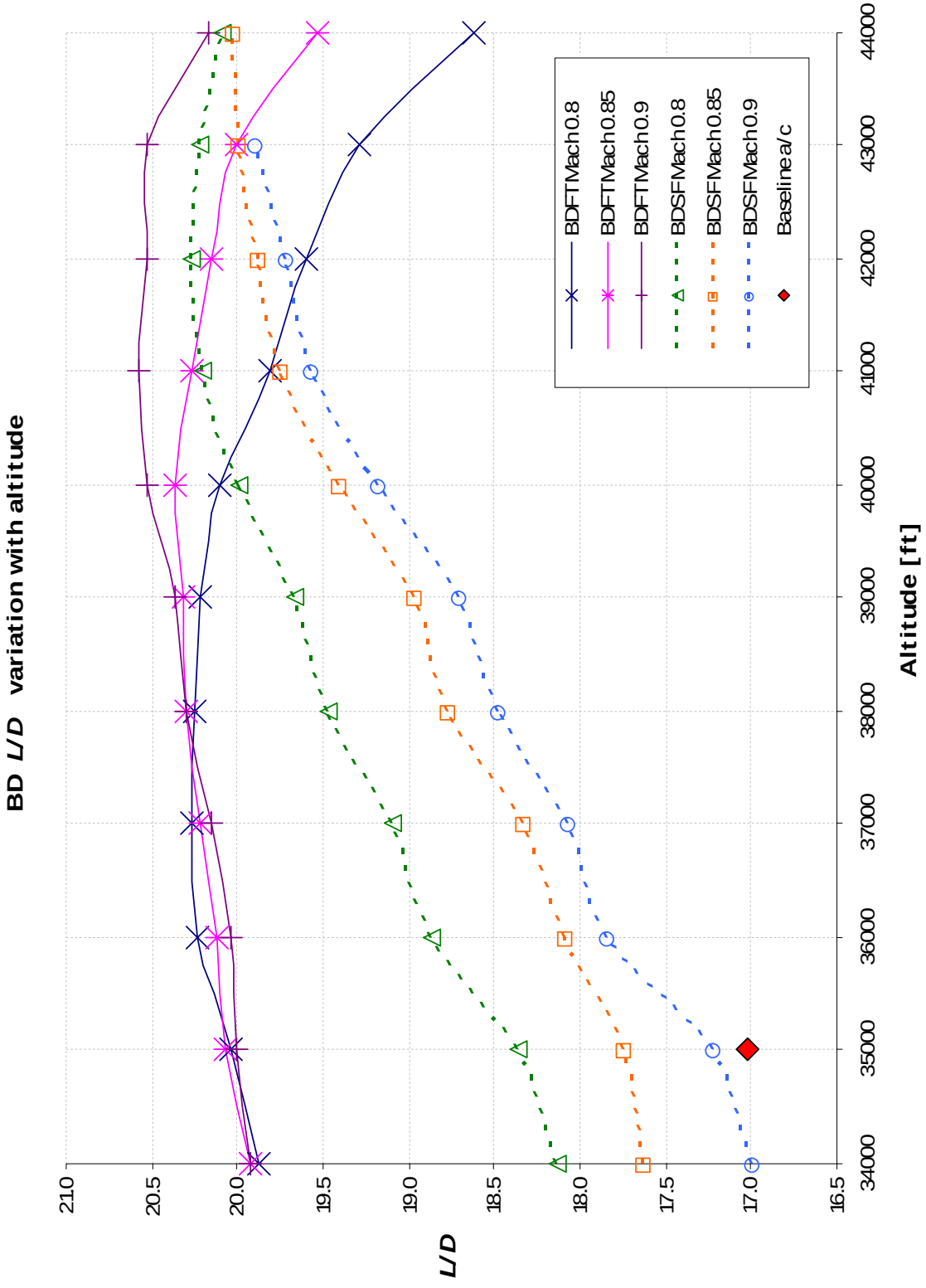

Fig C-3**:** BD *L/D* variation by changing Cruise Altitude and Cruise Mach

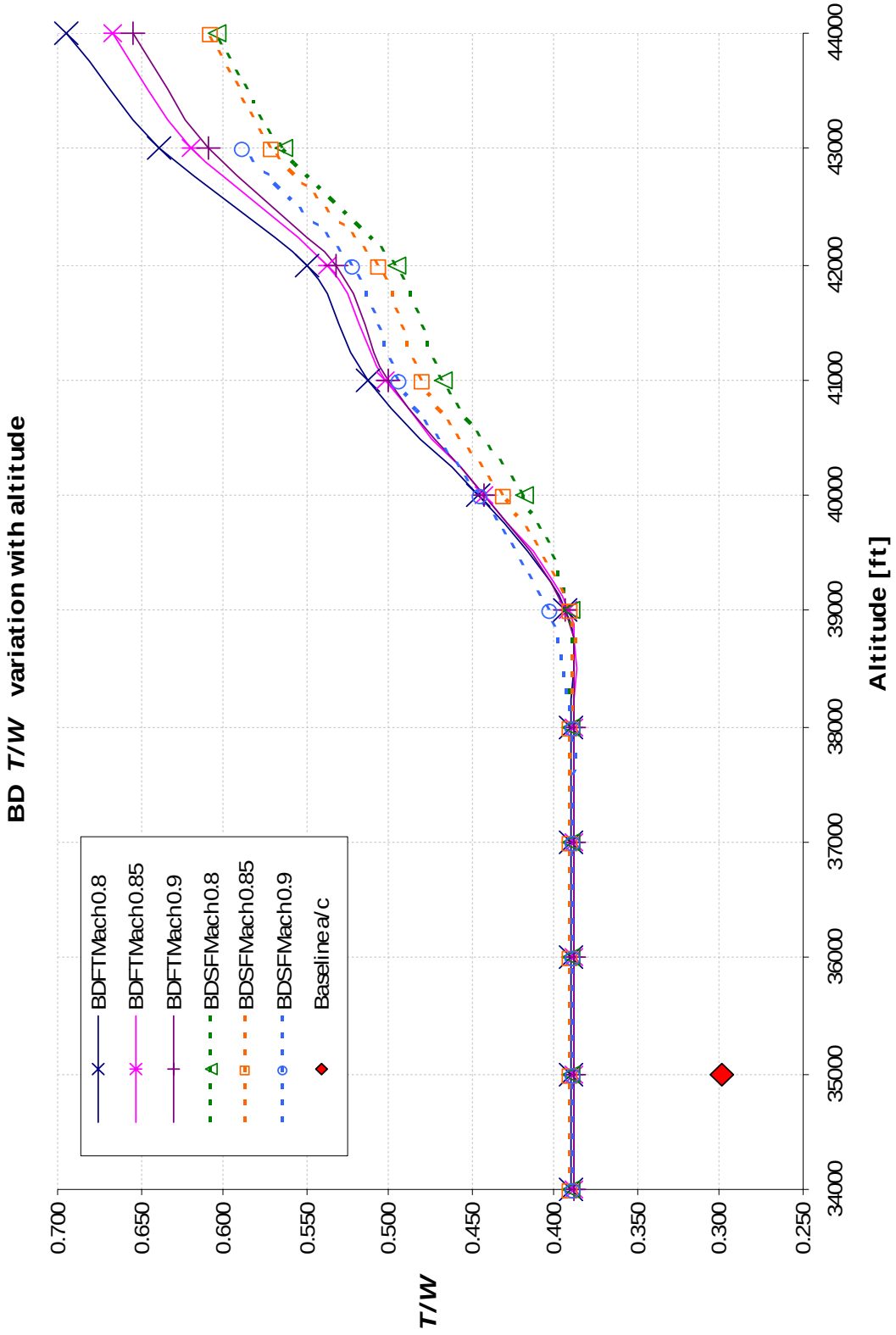

Fig C-4: BD *T/W* variation by changing Cruise Altitude and Cruise Mach

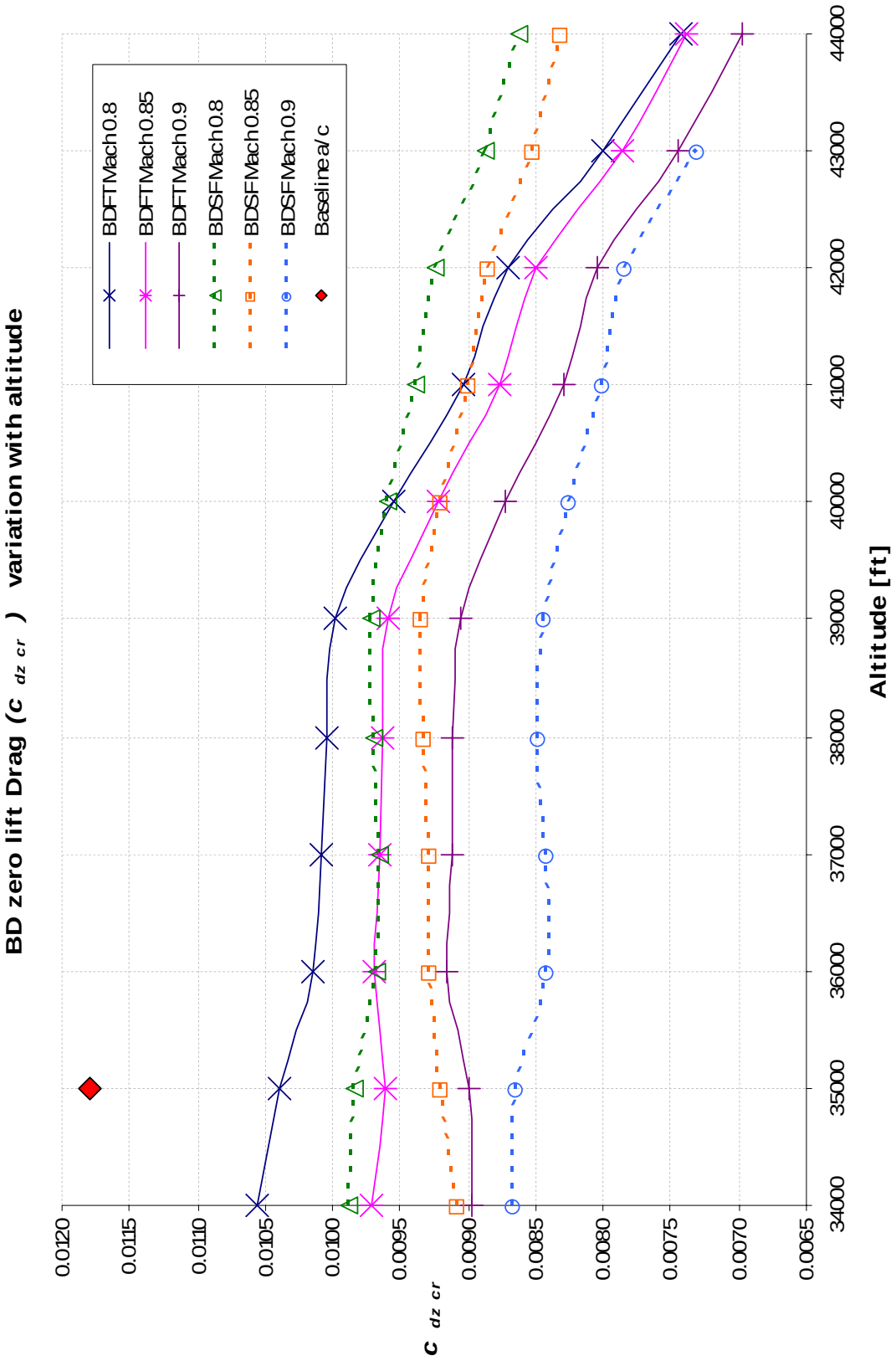

Fig C-5: BD Zero Lift Drag ($c_{dz\ cr}$) variation by changing Cruise Altitude and Cruise Mach

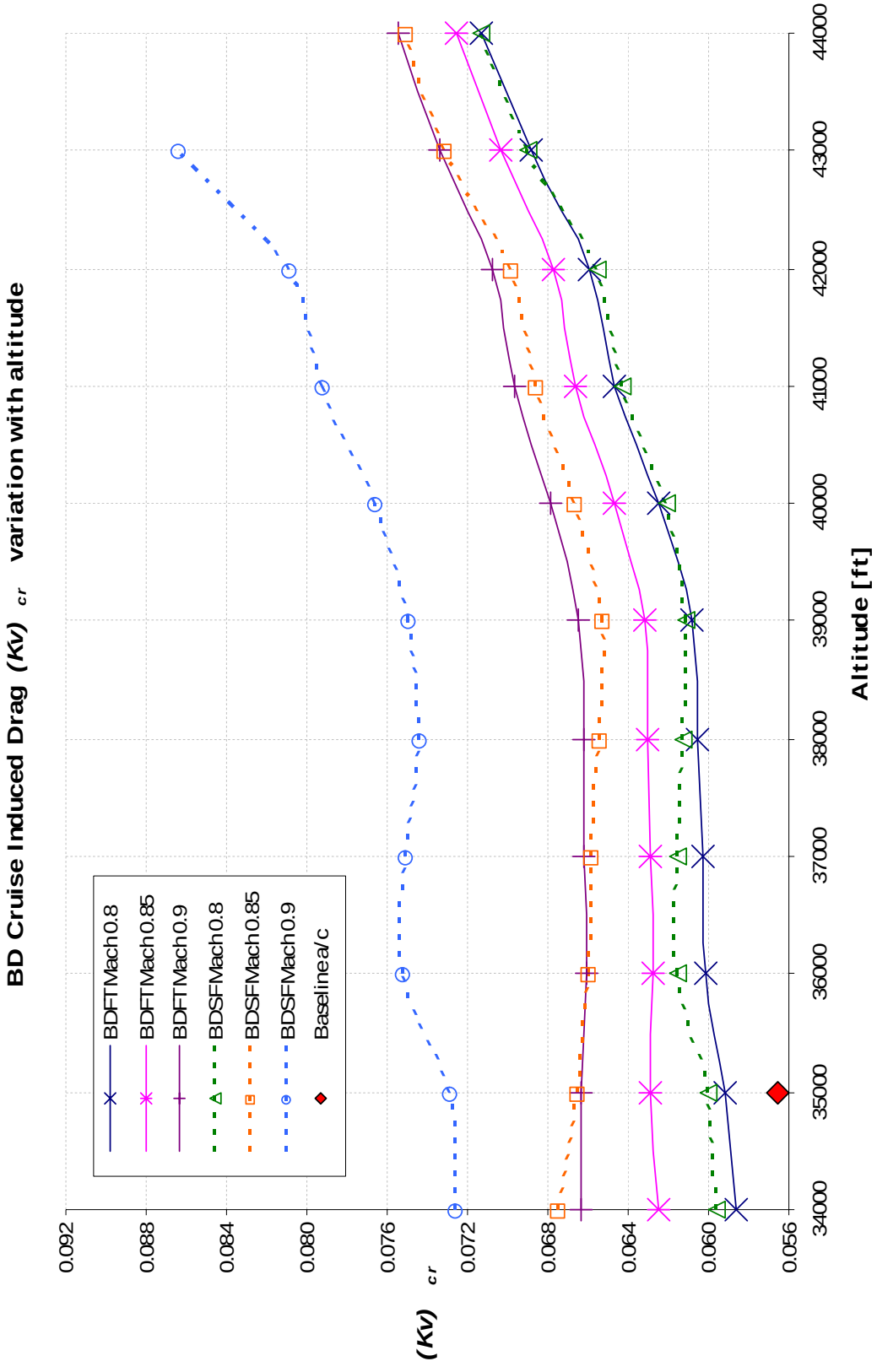

Fig C-6: BD Cruise Induced Drag $(Kv)_{cr}$ variation by changing Cruise Altitude and Cruise Mach

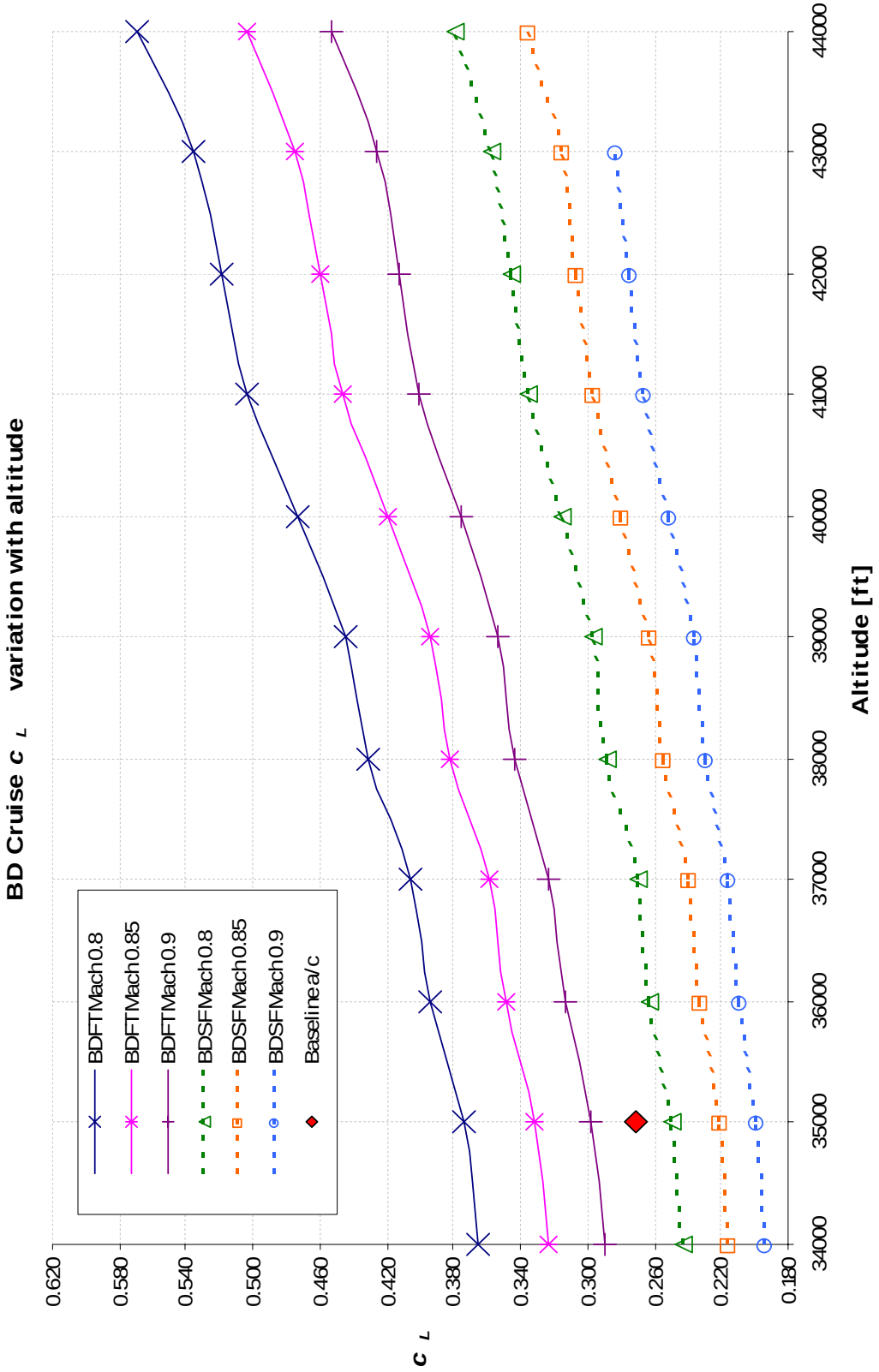

Fig C-7**:** BD Cruise c_L variation by changing Cruise Altitude and Cruise Mach

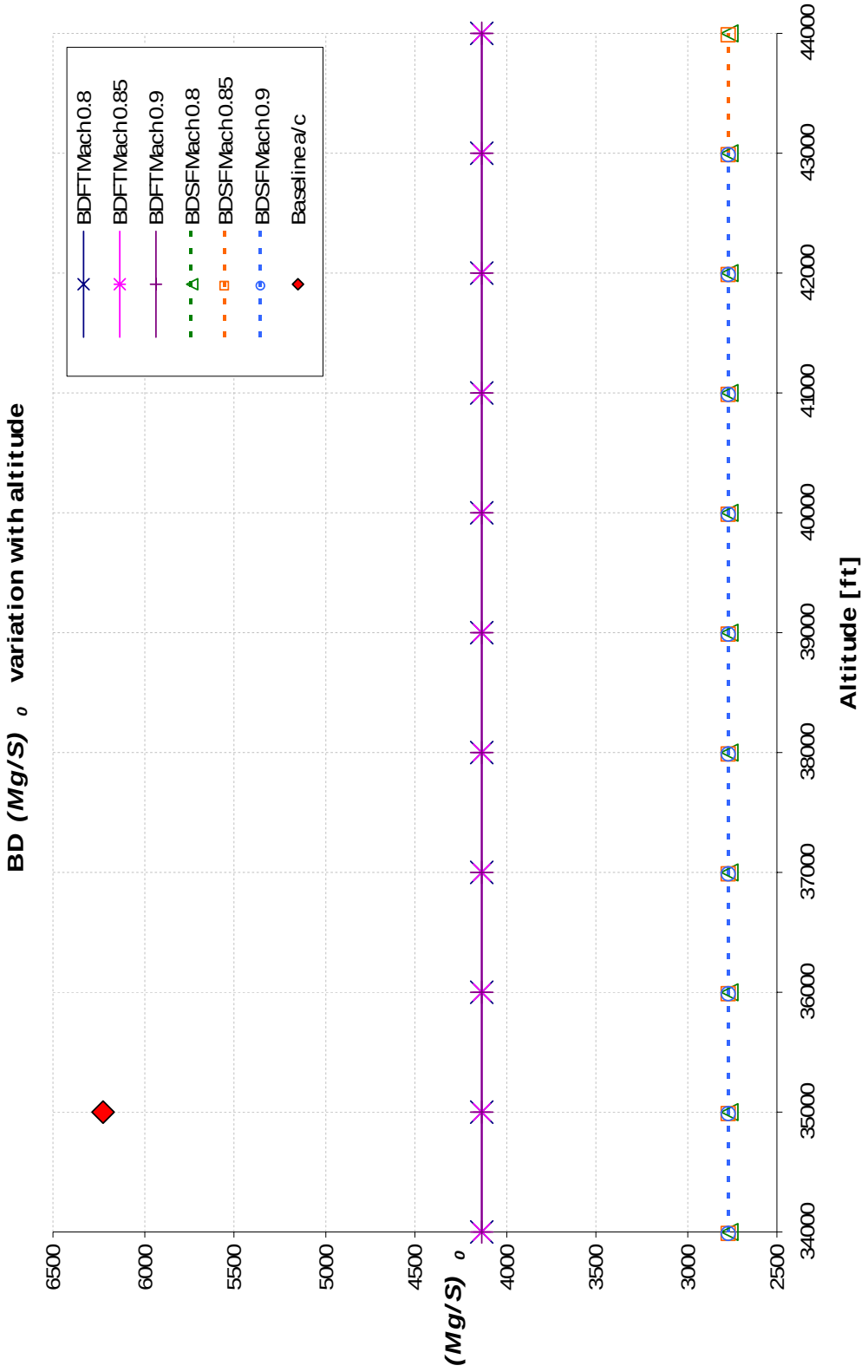

Fig C-8: BD Wing Loading variation by changing Cruise Altitude and Cruise Mach

C.2.3 Discussion on Cruise Altitude & Mach number Analysis

The altitude study results revealed that as cruise Mach increased total aircraft mass or All-Up-Mass (*AUM*) also increases, and the same result applies for increasing the cruise altitude (

Fig C-1). The BD requires more thrust to reach higher cruise altitudes and for higher cruise Mach numbers (Fig C-4), where more fuel is burnt to achieve the design range (Fig C-2). Lift increases almost linearly by increasing altitude and cruise Mach (Fig C-7), as with induced drag (Fig C-6), however zero-lift drag due to lift reduces as altitude and cruise Mach increases (Fig C-5). The wing loading results (Fig C-8) are not significant in selecting an ideal cruise altitude or Mach, as these parameters are independent of the design unless considering low speed and climb performance.

The most significant set of results are for L/D in Fig C-3, where the BDFT design has an L/D in excess of 20.2 whilst cruising at Mach 0.8; starting cruise at an altitude of 37,000ft and ending at a ceiling of 41,000ft. As Mach number is increased to 0.85, L/D peaks at 20.4 for a start of cruise at 40,000ft, ending at a ceiling of 44,000ft. Like-wise at Mach 0.9, cruise performance is increased to an L/D of 20.6 when climb starts in the range of 40,000 to 43,000ft and ends at a ceiling range of 44,000 to 47,000ft. Despite the increase in L/D at selected altitudes, it is important to cross reference results with

Fig C-1, where the BDFT mass rapidly increases beyond an initial cruise of 41,000ft. The BDSF displays similar results as the BDFT although L/D performance is poor at lower altitudes and is comparable to the baseline aircraft result. As the cruise altitude starts above 40,000ft, L/D and total mass is similar to the BDFT results, with the exception at Mach 0.9, where there is a substantial mass increase due to a high induced drag of the BDSF.

C.2.4 Design Point for Cruise Altitude & Mach number

A single cruise altitude was selected for the BDSF and BDFT, to provide an equal basis to compare both designs for performance, efficiency, and finally noise. The selected cruise case was for a 0.8 Mach cruise climb starting at 41,000ft and ending at a cruise ceiling of 45,000ft. This is a higher altitude than that designed for by SAI, where the SAI cruise case was a level cruise at a 40,000ft ceiling [Hileman, 2007], and not for a cruise climb scenario as described above.

This altitude has been selected for three main reasons:

- To minimize aircraft *AUM* for cruise at Mach 0.8,
- To increase the performance of the BD concept at higher altitudes,
- Lower the thrust requirements and size of the propulsion systems, compared with higher altitudes and higher cruise Mach numbers.

C.2.5 Environmental Considerations for Cruise

Environmental and economical effects were considered for flying the BD slower and at a reduced altitude. Low altitude flight releases emissions lower in the atmosphere causing less long-term damage, fewer contrail formations, and vapours stay in the atmosphere for a shorter time period. Although a low and slow flight is environmentally beneficial, it is not an economical solution that some airlines would agree with; implying burning more fuel and taking longer to carry out the design mission. The time of flight is actually not as big a concern as the airlines would suggest, as by the time you climb to 40,000ft, the lower cruise aircraft would already be at cruise, and would take less time than the higher cruising aircraft to land. Never-the-less, the flight time may be similar for both aircraft for a medium range mission, but not for long ranges. An initial study found that by reducing the BDFT cruise altitude to 34,000ft and Mach 0.7, the main benefit (of an optimised design to this mission) was a reduction in *AUM*, with a resultant increase in fuel required. Even though flying slower improves the fuel burn efficiency, engines would be operating at off design conditions requiring more thrust at lower altitudes and the aircraft would carry more fuel, negating any weight and performance benefits.

Appendix D BD Configuration Trade Studies

D.1 Trade Study Overview

The configuration trade study described in this appendix investigates increasing wing laminar flow, engine BPR, and approach flight path angles (*FPA*). A laminar flow wing was investigated to determine an increase in wing efficiency for realistic design assumptions. A conventional approach was considered as a three degree continuous descent approach, which is typical for most civil airliners, with the exception of smaller business jets and short range vehicles. Increasing engine BPR was a noise related exercise, as higher BPR reduces noise, but increases fuel efficiency, size, and engine mass, and it is this mass increase that is of interest for the airframe design.

D.1.1 Steep Approach Flight Path Angles

Descent angles were used to investigate slow and steep approaches for the baseline aircraft. The same principals apply for the BD, where high approach angles place the aircraft at a greater distance from the ground, reducing noise. The baseline study investigated slower approach velocities, however, the BD approach velocity is 6-18% less than the baseline 72m/s, so further reduction was not considered. The BD descent was designed for a six degree steep approach.

D.1.2 Engine Bypass Modifications

Higher engine BPR increases efficiency and reduces noise, as described in [Doulgeris, 2008] investigating ultra-high-bypass ratios (*UHBPR*) for a range of 5 to 30. A *BPR* of 12 was factored into the airframe design and compared with *BPR* = 8 engines. Increasing *BPR* also increases engine mass and diameter, so a detailed account is required to calculate the weight penalty of using *UHBPR* engines.

D.1.3 Effect of Artificial Laminar Flow Over-the-Wing

Increasing laminar flow *OTW* was investigated to quantify any changes in wing efficiency. Having four engines at the wing root disturbs the flow over the inboard upper surface where the outboard section generates the main proportion of lift. The outboard wing was designed with modified supercritical laminar flow airfoils. 75% of total wing lift is generated by the outboard wing, so if the outboard section was 100% laminar, the entire wing would achieve a maximum of 75% laminar flow. In reality a fully laminar wing is not possible for the BD because of the high sweep of the wing, so a maximum of 67% artificial laminar flow outboard was considered possible; corresponding to 50% laminar flow over the entire wing. This study investigates

increasing the percentage of laminar flow *OTW* from a range of zero (0) to 50% chord. Laminar flow on this highly swept delta was considered achievable by using the method described in [Wilson, 1997], which describes the mass and design implications of incorporating a hybrid laminar flow control system into the wing design process for commercial aircraft.

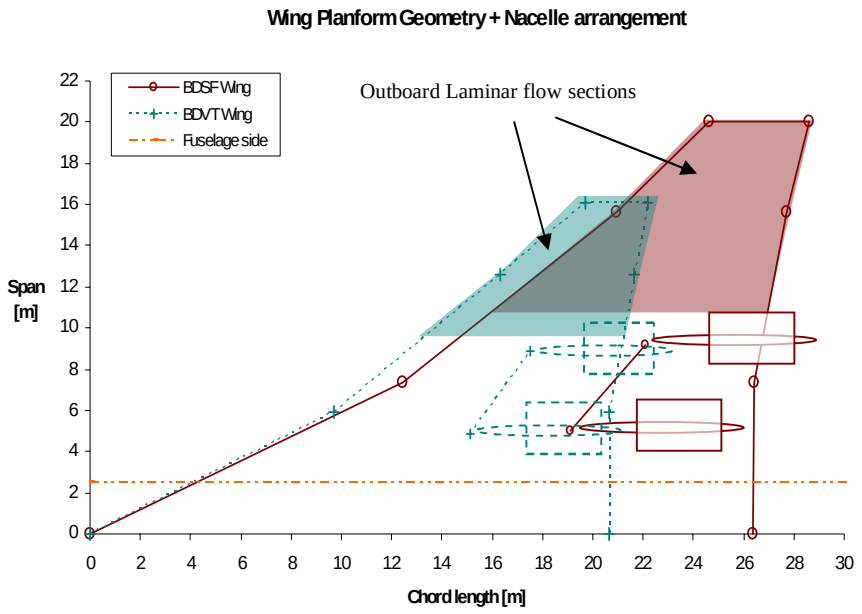

Fig D-1: BDSF and BDVT Wing spanwise laminar flow regions

Four main BD design derivatives reflect changes in the engine BPR and approach angles. The results of the study compare *AUM*, *L/D*, $(T/Mg)_0$, and mission fuel mass.

The four main BD configurations analysed are:

- BDSF - HBPR=8, 3 degree approach angle (conventional),
- BDSF - HBPR=8, 6 degree approach angle (steep),
- BDSF - UHBPR=12, 6 degree steep approach,
- BDVT - UHBPR=12, 6 degree steep approach.

D.1.4 Results for Laminar Flow, Steep Approach, and BPR Analysis

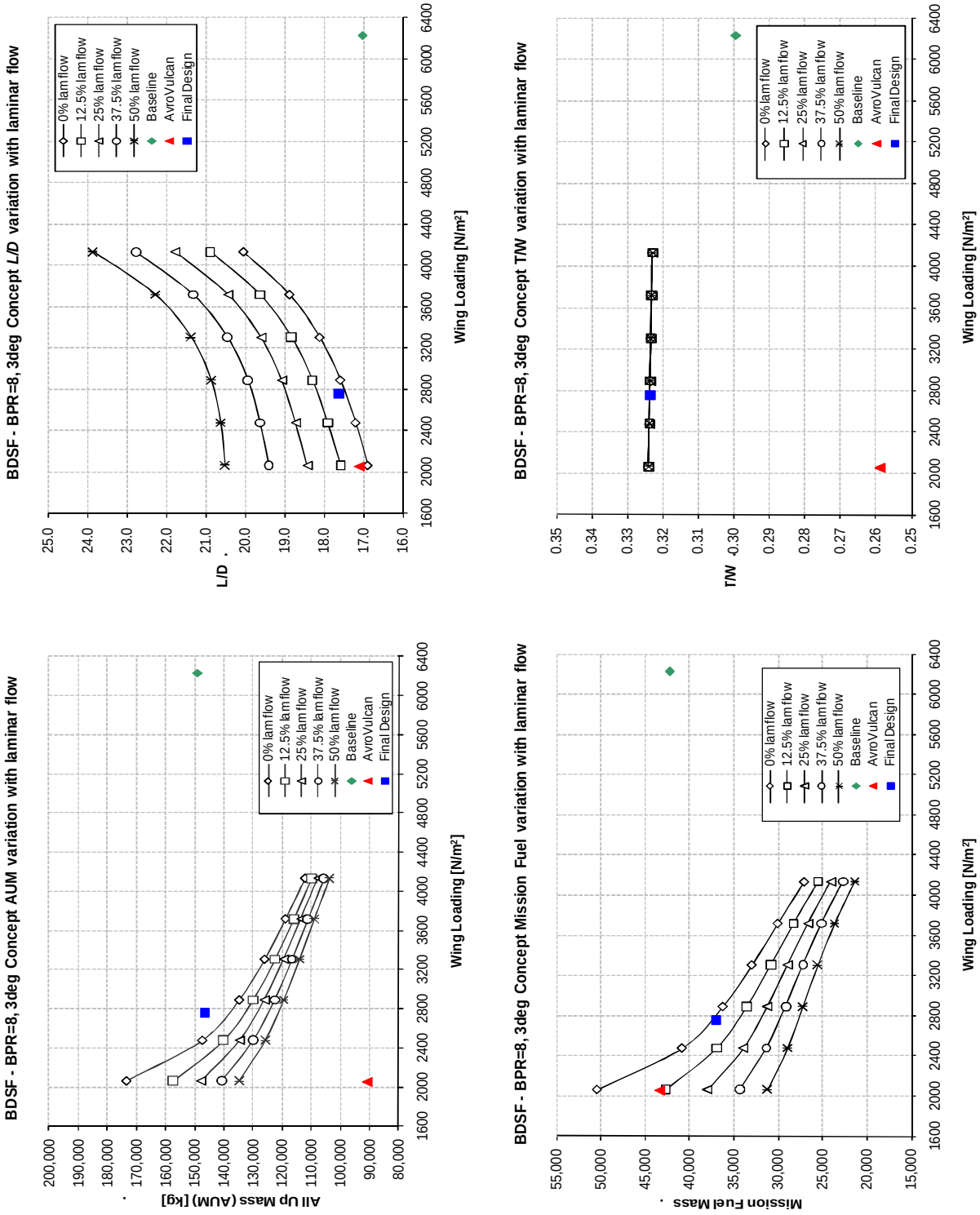

Fig D-2**:** Results for **BDSF** with **BPR=8** Engines, for a **Conventional 3 degree Approach**, and Variation of **Laminar Flow between 0-50%**

Fig D-3**:** Results for **BDSF** with **BPR=8** Engines, for a **Steep 6 degree Approach**, and Variation of **Laminar Flow between 0-50%**

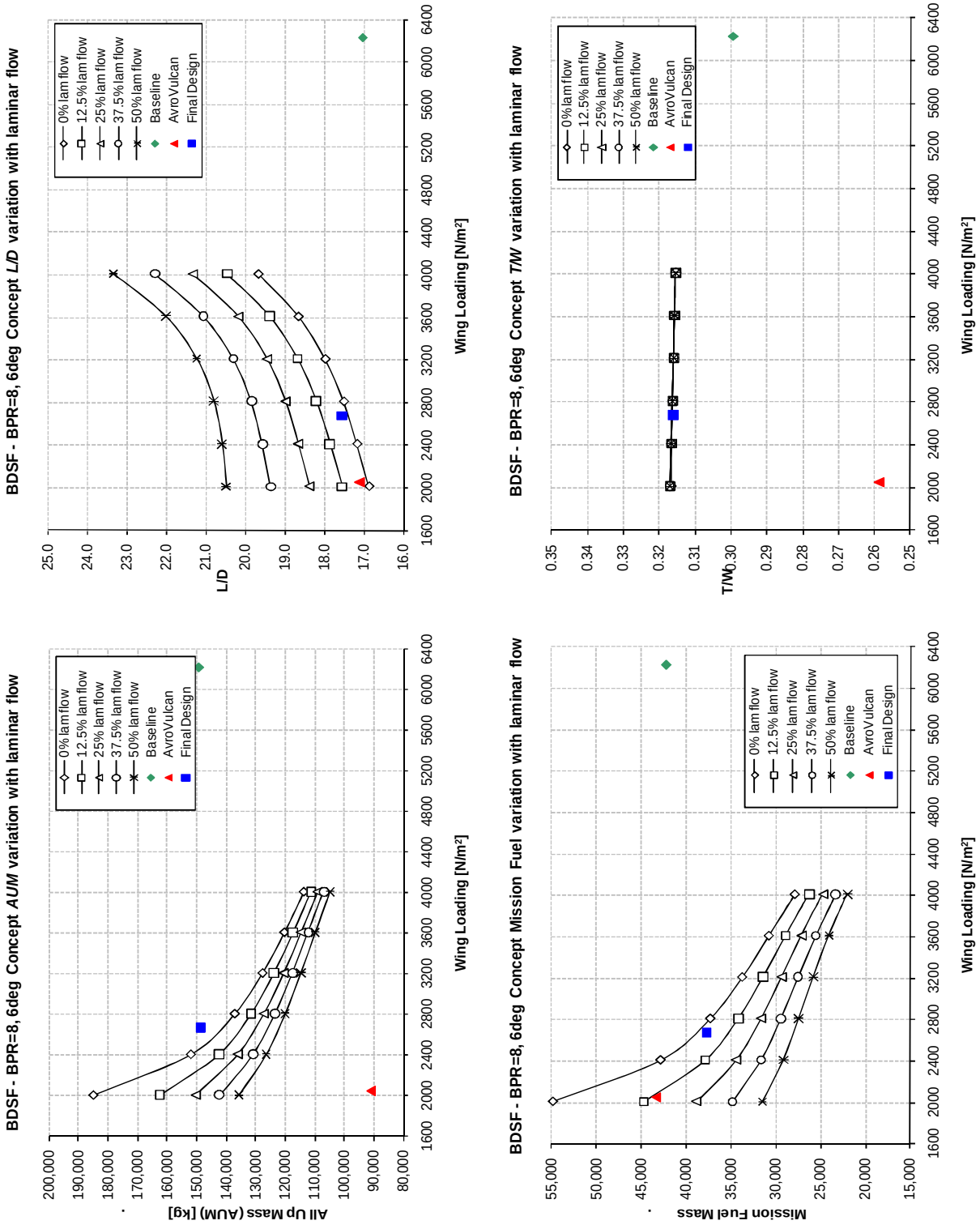

Fig D-4**:** Results for **BDSF** with **BPR=12** Engines, for a **Steep 6 degree Approach**, and Variation of **Laminar Flow between 0-50%**

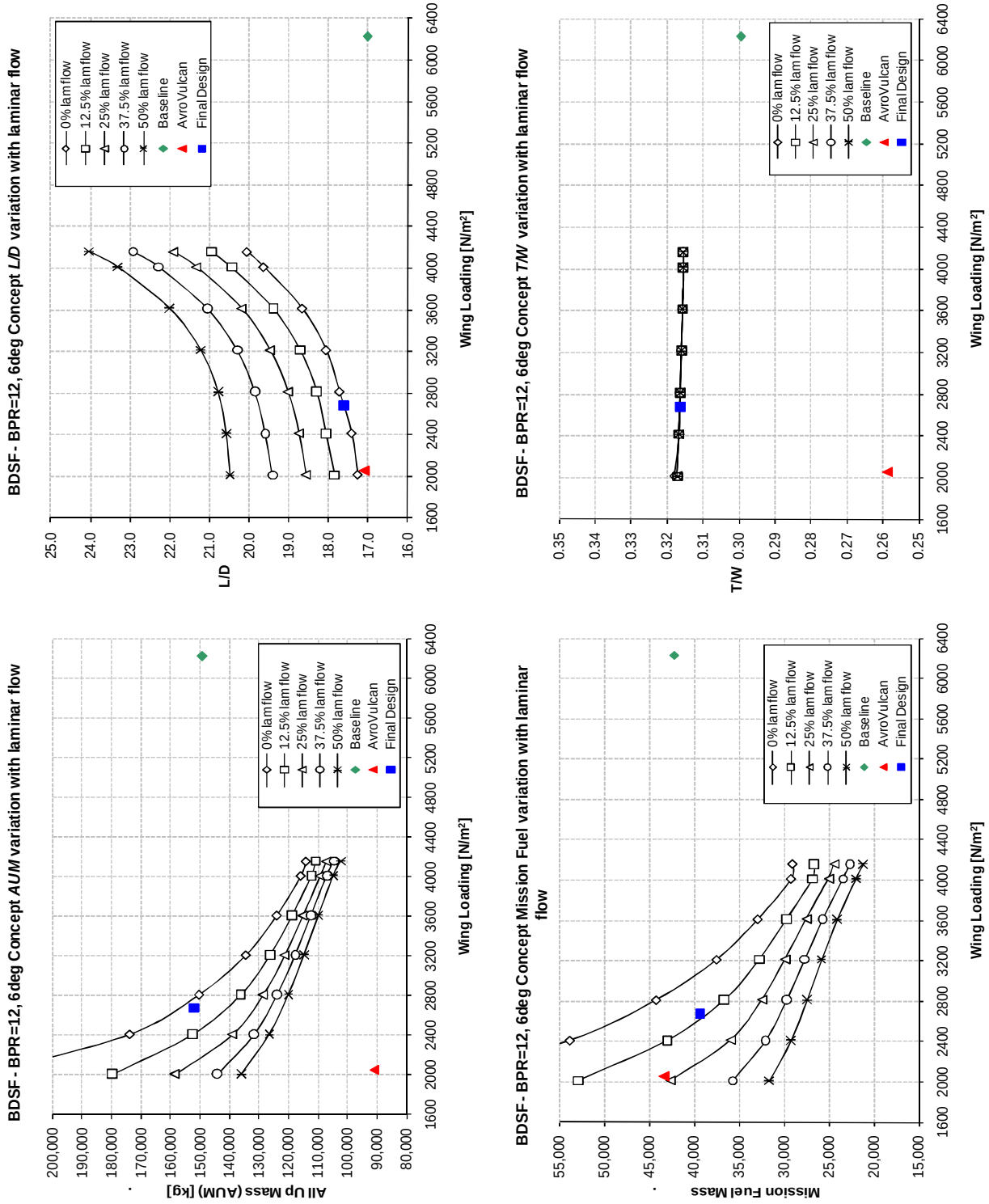

Fig D-5**:** Results for **BDVT** with **BPR=12** Engines, for a **Steep 6 degree Approach**, and Variation of **Laminar Flow between 0-50%**

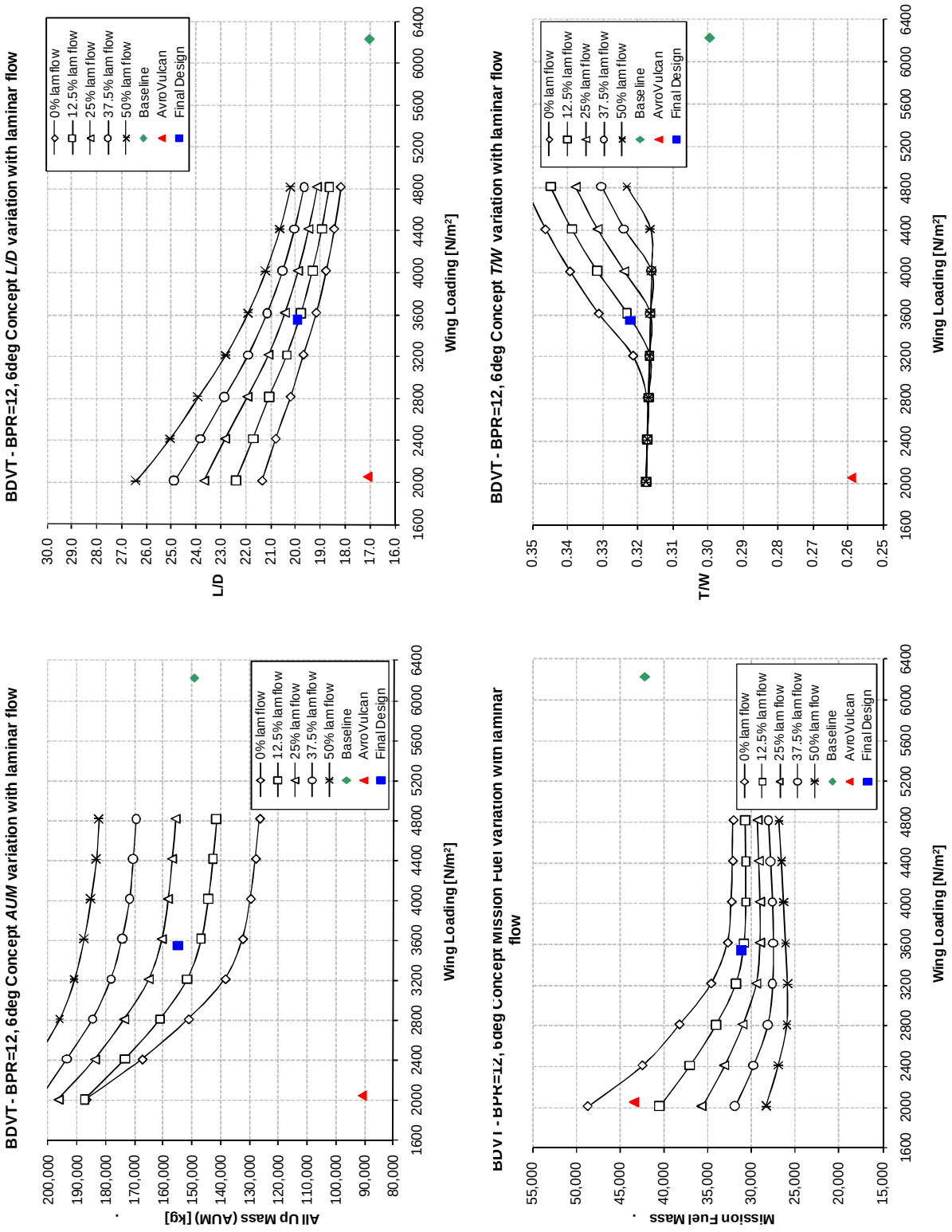

D.1.5 Trade Study Discussion

An additional variable is added into the trade study analysis, as shown in

Fig D-2 through to Fig D-5, and is the design wing-loading $(Mg/S)_0$, which clearly shows how the BDSF and BDVT differ. The results provide an interesting insight into how the behaviour of the tailed and tailless BD diverges, mainly because the BDVT behaves similarly to a conventional aircraft due to its higher aspect ratio wing and tail, compared with the tailless design. Each figure compares the final selected BD design against the trade study results along-with the baseline and AV aircraft data.

Analysing the results of the BDSF, shows that increasing laminar flow reduces vehicle and fuel mass, and increases L/D (

Fig D-2). Laminar flow has no effect on the static thrust loading $(T/Mg)_0$, because as the lifting performance increases, *AUM* and static thrust requirement decrease proportionally. There is a marginal change in performance by increasing approach angle from 3 to 6 degrees (

Fig D-2, Fig D-3, and Fig D-3), and increasing BPR from 8 to 12 improves fuel burn resulting in a lower fuel mass, and a slight improvement in *L/D* as shown within

Fig D-4.

The BDVT results in Fig D-5 for *AUM* and mass of fuel show similar trends as the BDSF with the main difference being the change in *L/D* as $(Mg/S)_0$ is increased. A higher design $(Mg/S)_0$ provides a greater *L/D* for the BDSF, where-as for the BDVT, higher $(Mg/S)_0$ reduces *L/D*, and tends towards the baseline aircraft design value. The BDSF does not provide a significant change in $(T/Mg)_0$ as $(Mg/S)_0$ is increased, however for the BDVT, as $(Mg/S)_0$ is increased beyond 2800N/m^2, $(T/Mg)_0$ increases and varies for each laminar flow case.

Examining both BD designs in terms of landing performance and noise, indicates that for a steep 6 degree approach, the BDSF approach velocity increases relative to a conventional approach angle; suggesting that airframe noise will be increased. The steep approach does however allow the BD to land on shorter runways, as the landing distance is reduced by 100m. To summarise, an increased approach speed, combined with greater distance between the noise sources and the ground, and the shorter landing distance would provide a quieter approach, and widen the operation of the BDSF to shorter runways. Despite the BDVT having a greater number of noise sources compared to the tailless variant, the approach velocity for a 6 degree *FPA* is 58.7m/s, compared to 63.3m/s for the BDSF. The additional benefit of having a tail surface for trim, makes the BDVT more appealing at low speeds, especially for gust cases, where an artificial control system would need to be implemented to maintain stability of the BDSF.

BD Configuration	Landing Field Length [m]	V_a [m/s]
BDSF, HBPR=8, 3 deg	1825.4	64.2
BDSF, HBPR=8, 6 deg	1724.5	63.3
BDSF, UHBPR=12, 6 deg	1724.5	63.3
BDVT, UHBPR=12, 6 deg	1724.5	58.7

Table D-1: BD Approach speed and Landing distances for each configuration

D.1.6 Design Point for Laminar Flow, BPR, and Descent Angle

The trade study results revealed that using an UHBPR engine provided fuel consumption benefits, and combined with the steep 6 degree descent angle, would provide significant reduction in aircraft noise during approach and landings. A 12.5% wing artificial laminar flow was selected across the main wing, which corresponds to 16.7% hybrid laminar flow across the outboard wing chord section, and is factored into the designs for both BDSF and

BDVT. Increasing engine BPR from 8 to 12 provides a noticeable change in performance, where the BD with 12.5% laminar flow achieves a 3.5% increase in overall aircraft and engine mass, 7.1% increase in fuel used, and an increase of 0.5% L/D. These results emphasise a slight aerodynamic performance benefit for increasing BPR with a 1% reduction in specific fuel consumption.

Appendix E Broad Delta Airfoil Design

E.1 BD Airfoil Geometry

Airfoil designs for the BD concept were designed using [Reid, 2007], and modified from NACA 5-digit airfoils data from [Harris, 1990]. Both BD configurations use the same airfoils to simplify analysis, designed to cruise and maximum low speed lift coefficients.

Configuration	$(c_l)_{max}$	$(c_l)_{cruise}$
BDSF	1.34	0.192
BDVT	2.07	0.338

Table E-1: Maximum and cruise lift coefficients for the BDSF and BDVT.

The four airfoils represent the root, kink1, kink2 and tip sections of the BD wing, and are shown in Fig E-1.

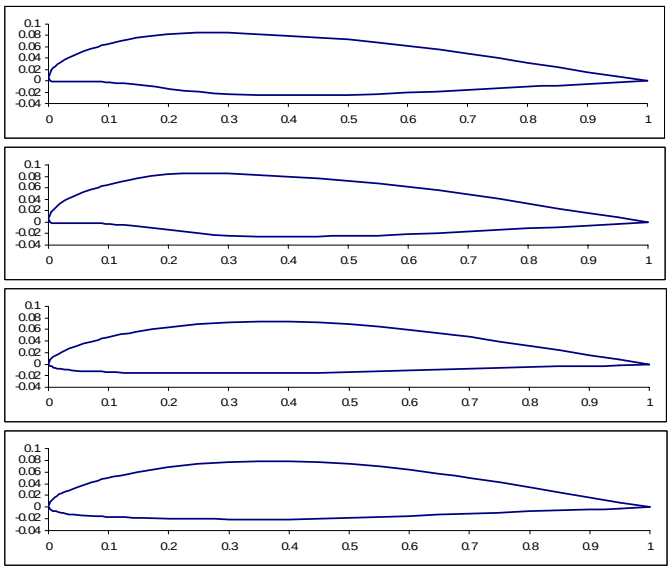

Fig E-1**:** BD Airfoil Designs, top to bottom: Root = NACA-23011 (modified), kink1= NACA-63A-0(10.5) (modified), kink2 = NACA-63A-009, tip= NACA-63A-010.

E.2 Airfoil Performance Data

The following sections provide graphical and tabulated results produced for each airfoil design, starting from the root, kink1, kink2, and finally the tip.

E.2.1 Root Airfoil Section; centre-line station, y=0

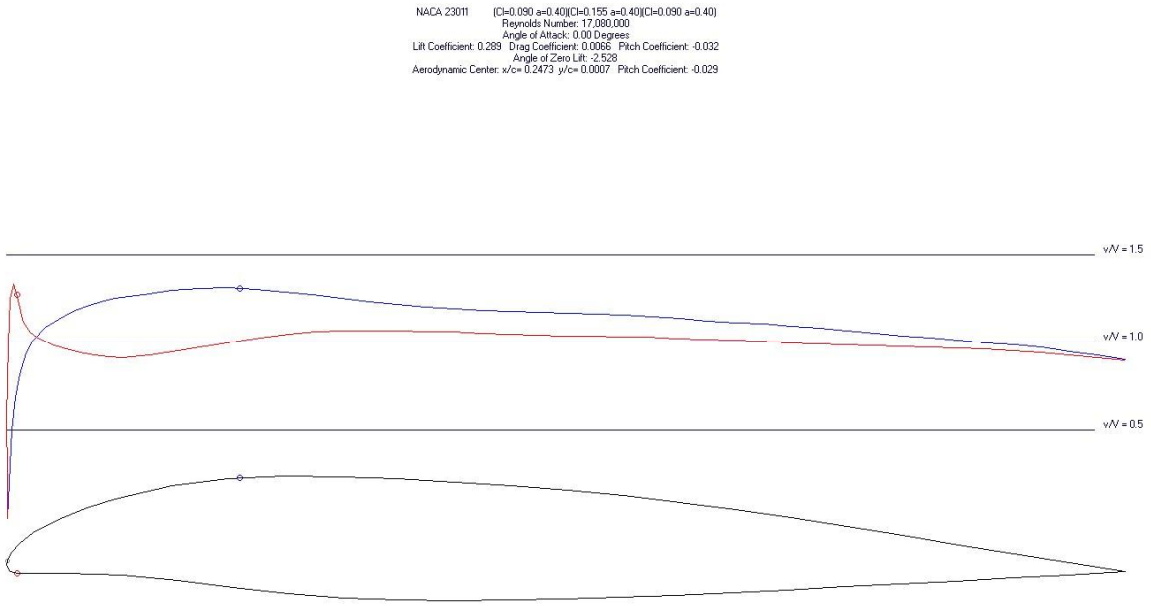

Fig E-2**:** BD Root Airfoil: NACA 23011 lift at zero incidence

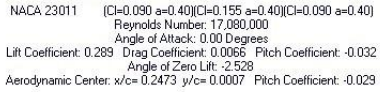

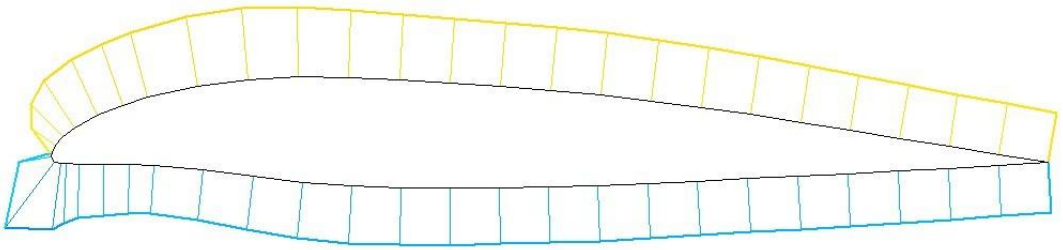

Fig E-3**:** BD Root Airfoil: NACA 23011 Viscosity effect

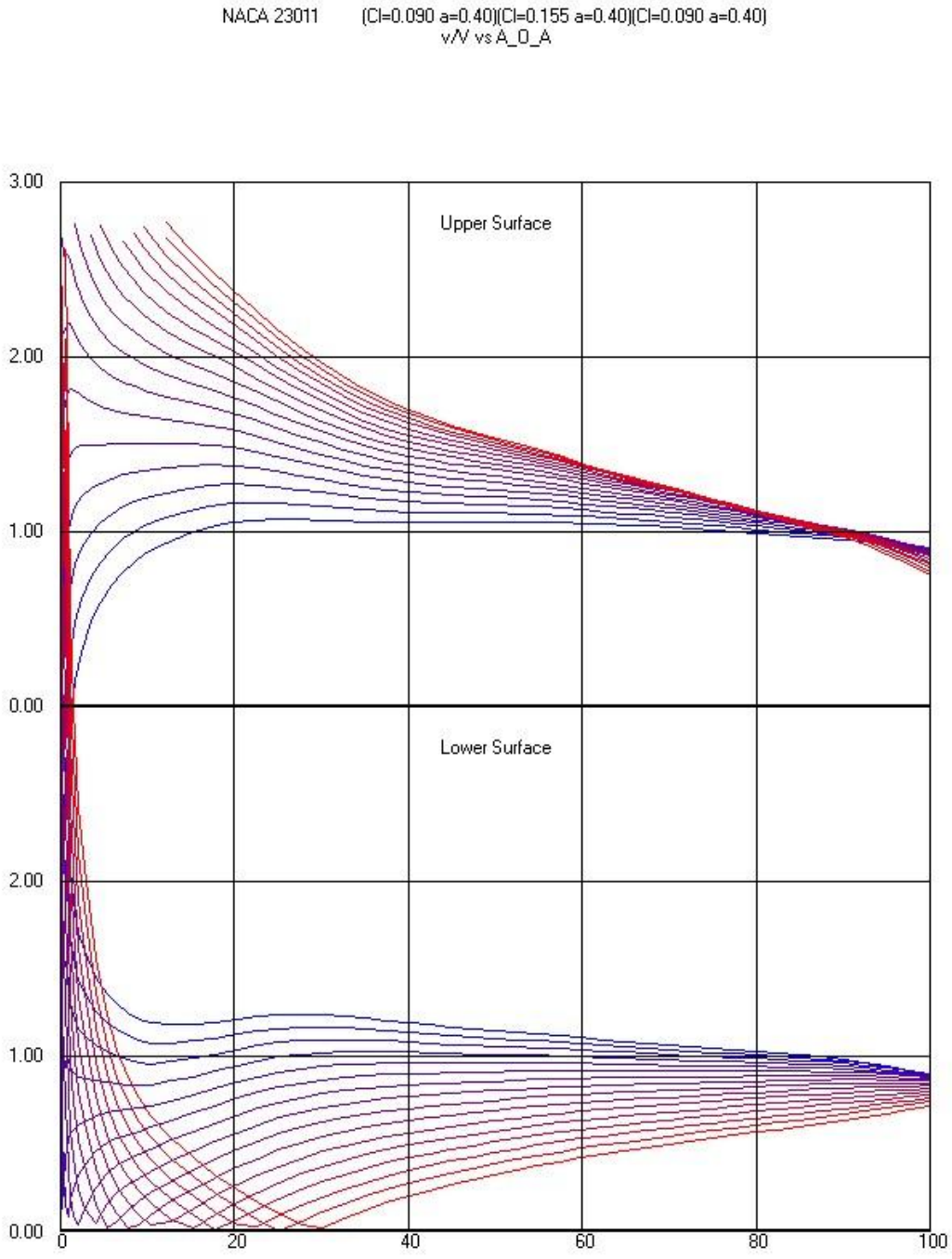

Fig E-4**:** BD Root Airfoil: NACA 23011 Pressure distributions

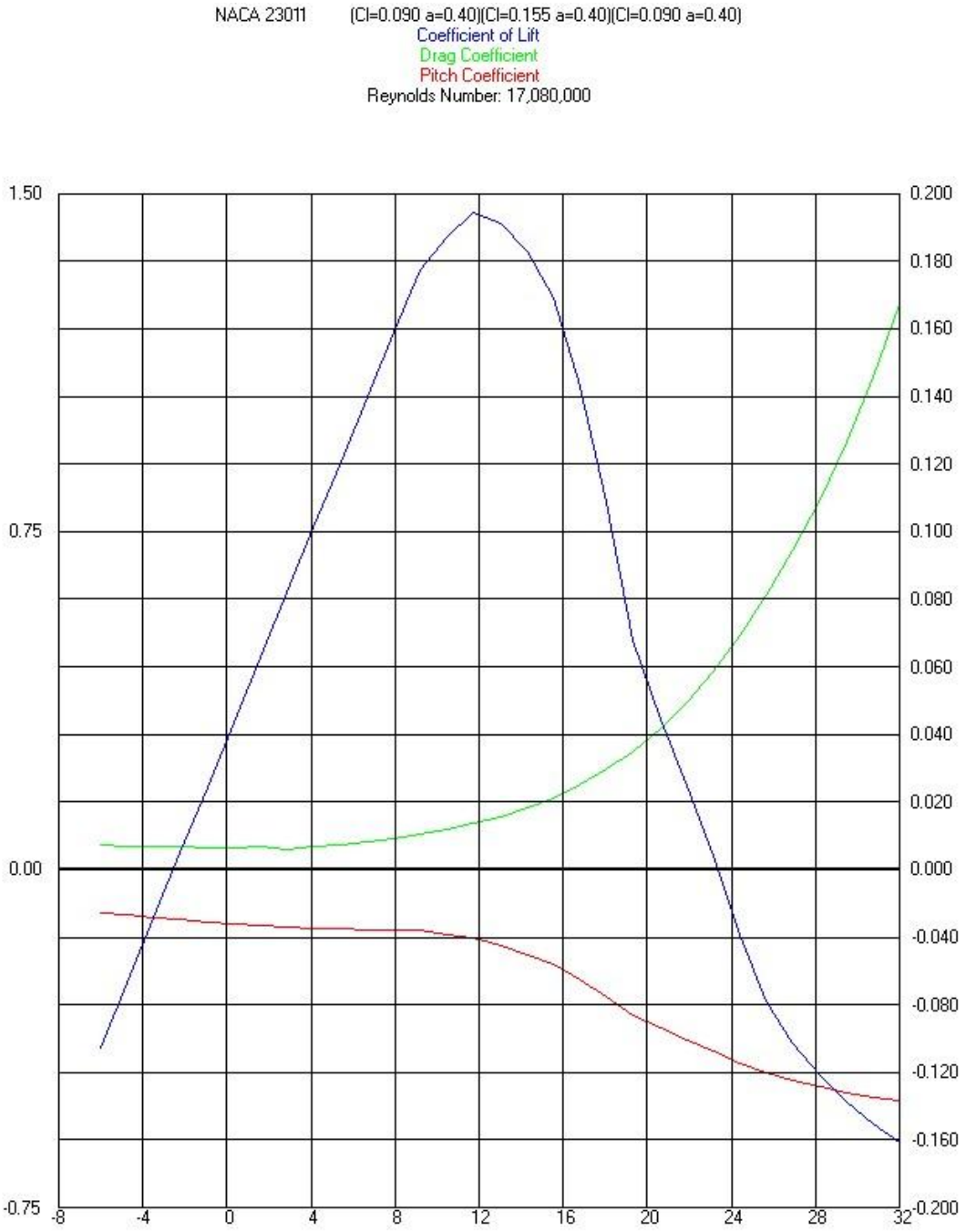

Fig E-5**:** BD Root Airfoil: NACA 23011 coefficients for lift, drag, and pitching moment

E.2.2 Kink 1 Airfoil Section; Inboard-mid station, y=0.366

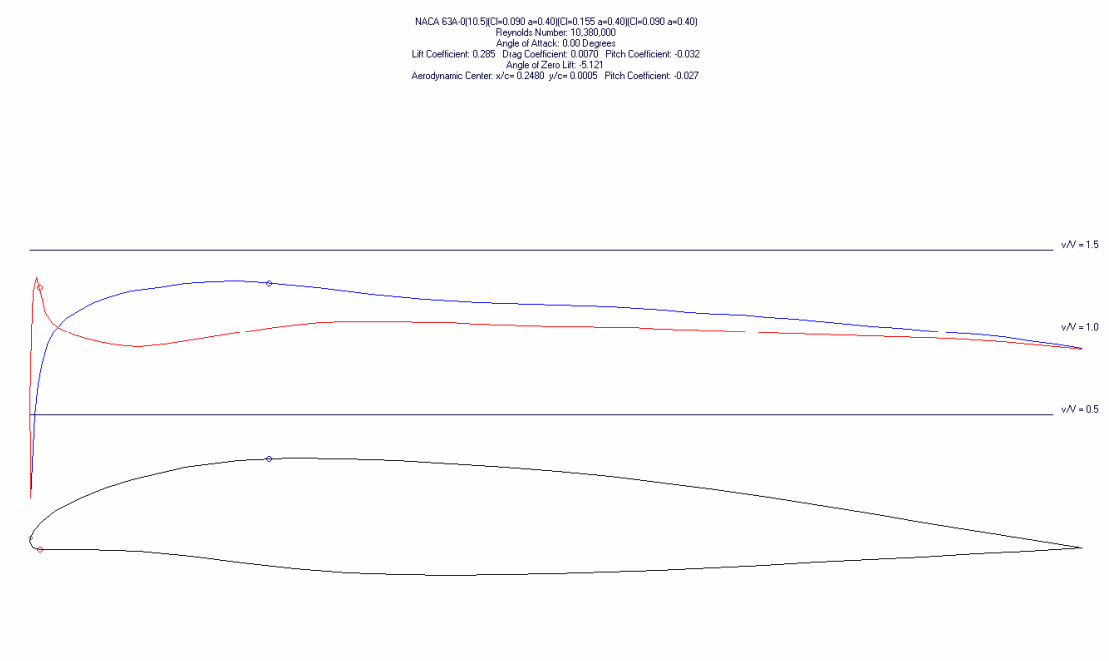

Fig E-6**:** BD Kink 1 Airfoil: NACA 63A-0(10.5) lift at zero incidence

NACA 63A-0(10.5)(Cl=0.090 a=0.40)(Cl=0.155 a=0.40)(Cl=0.090 a=0.40)
Reynolds Number: 10,380,000
Angle of Attack: 0.00 Degrees
Lift Coefficient: 0.285 Drag Coefficient: 0.0070 Pitch Coefficient: -0.032
Angle of Zero Lift: -5.121
Aerodynamic Center: x/c= 0.2480 y/c= 0.0005 Pitch Coefficient: -0.027

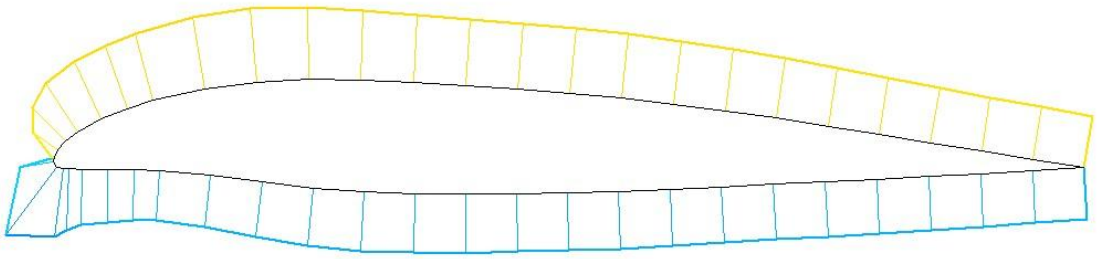

Fig E-7**:** BD Kink 1 Airfoil: NACA 63A-0(10.5) Viscosity effect

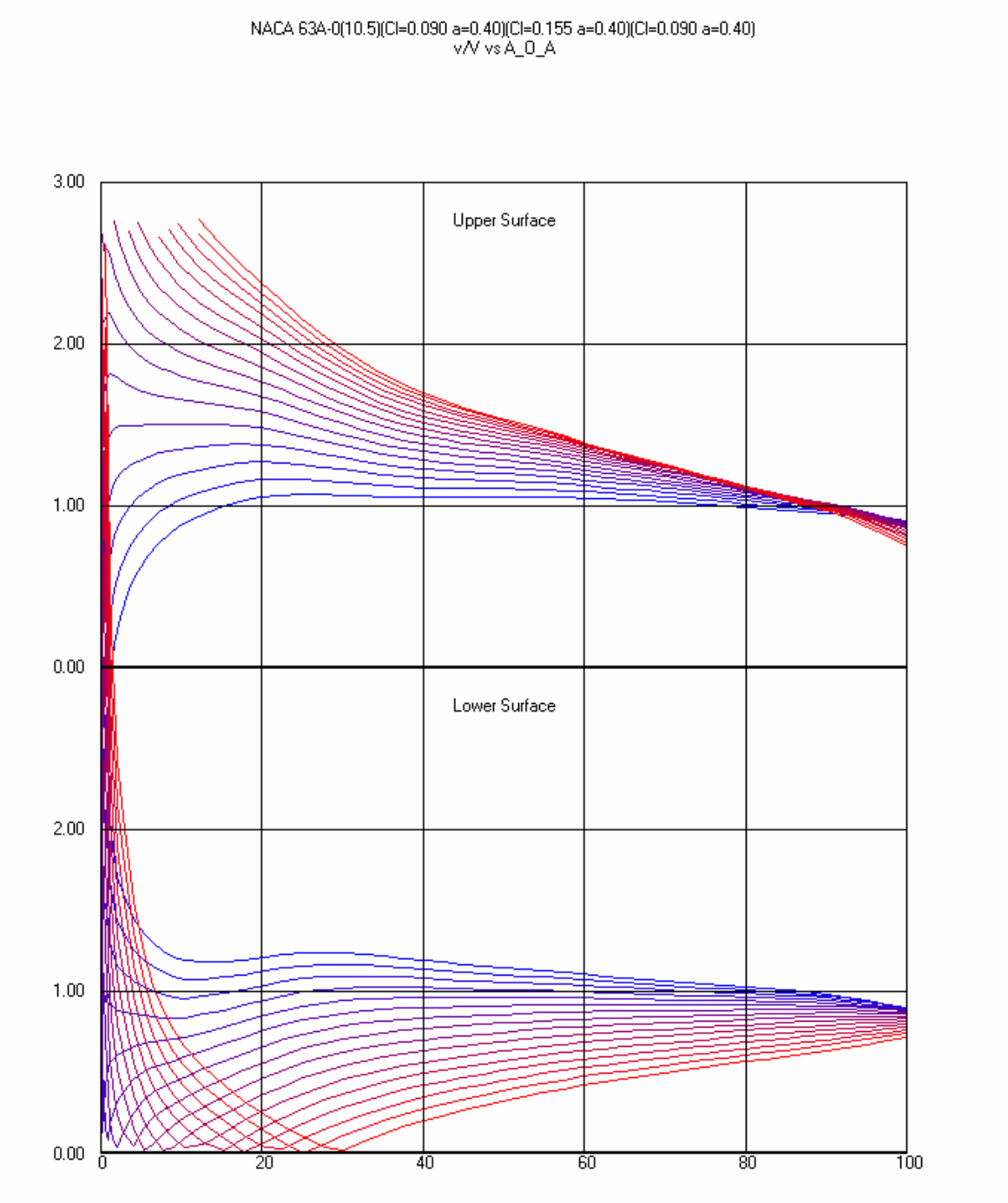

Fig E-8**:** BD Kink 1 Airfoil: NACA 63A-0(10.5) Pressure distributions

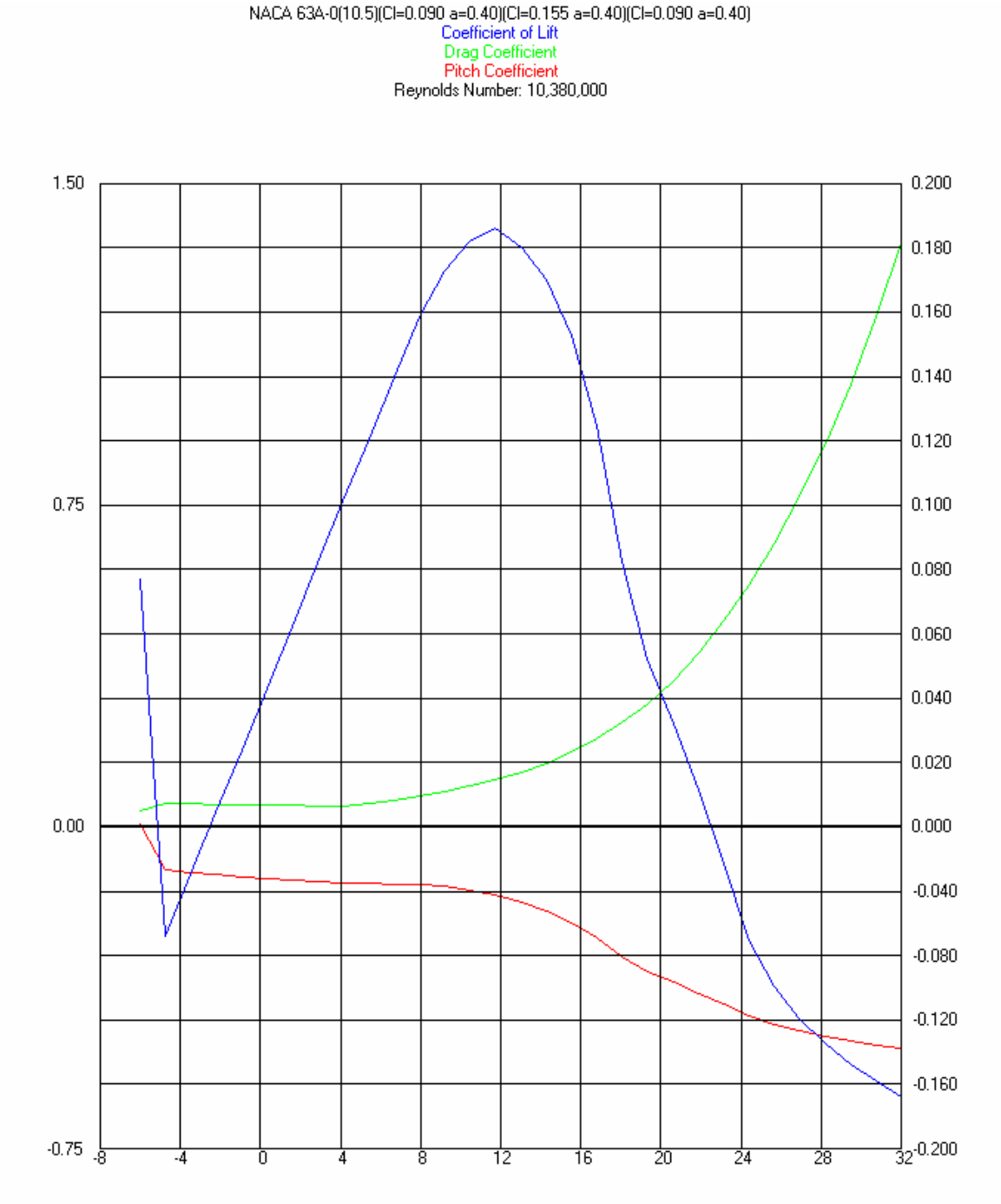

Fig E-9**:** BD Kink 1 Airfoil: NACA 63A-0(10.5) coefficients for lift, drag, and pitching moment

E.2.3 Kink 2 Airfoil Section; Outboard-mid station, y=0.781

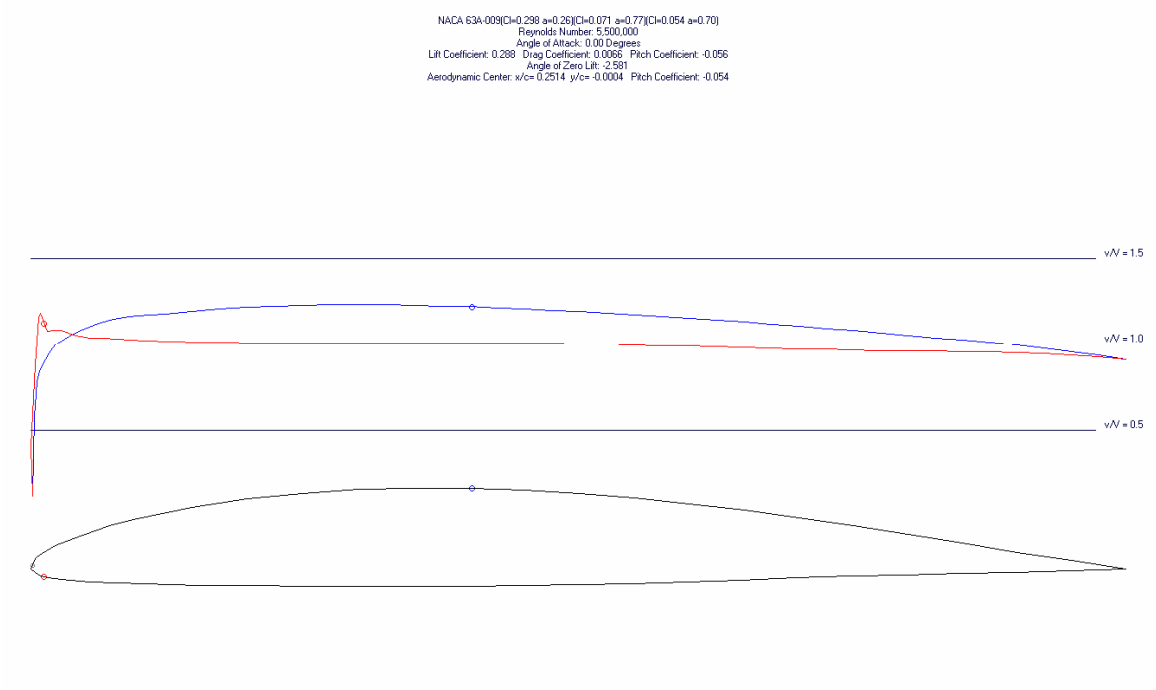

Fig E-10**:** BD Kink 2 Airfoil: NACA 63A-009 lift at zero incidence

NACA 63A-009(Cl=0.298 a=0.26)(Cl=0.071 a=0.77)(Cl=0.054 a=0.70)
Reynolds Number: 5,500,000
Angle of Attack: 0.00 Degrees
Lift Coefficient: 0.288 Drag Coefficient: 0.0066 Pitch Coefficient: -0.056
Angle of Zero Lift: -2.581
Aerodynamic Center: x/c= 0.2514 y/c= -0.0004 Pitch Coefficient: -0.054

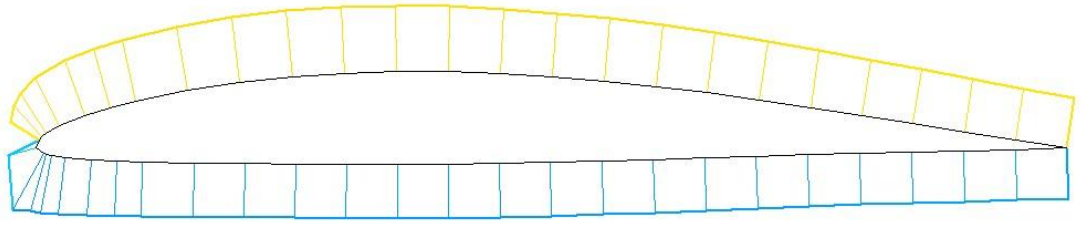

Fig E-11**:** BD Kink 2 Airfoil: NACA 63A-009 Viscosity effect

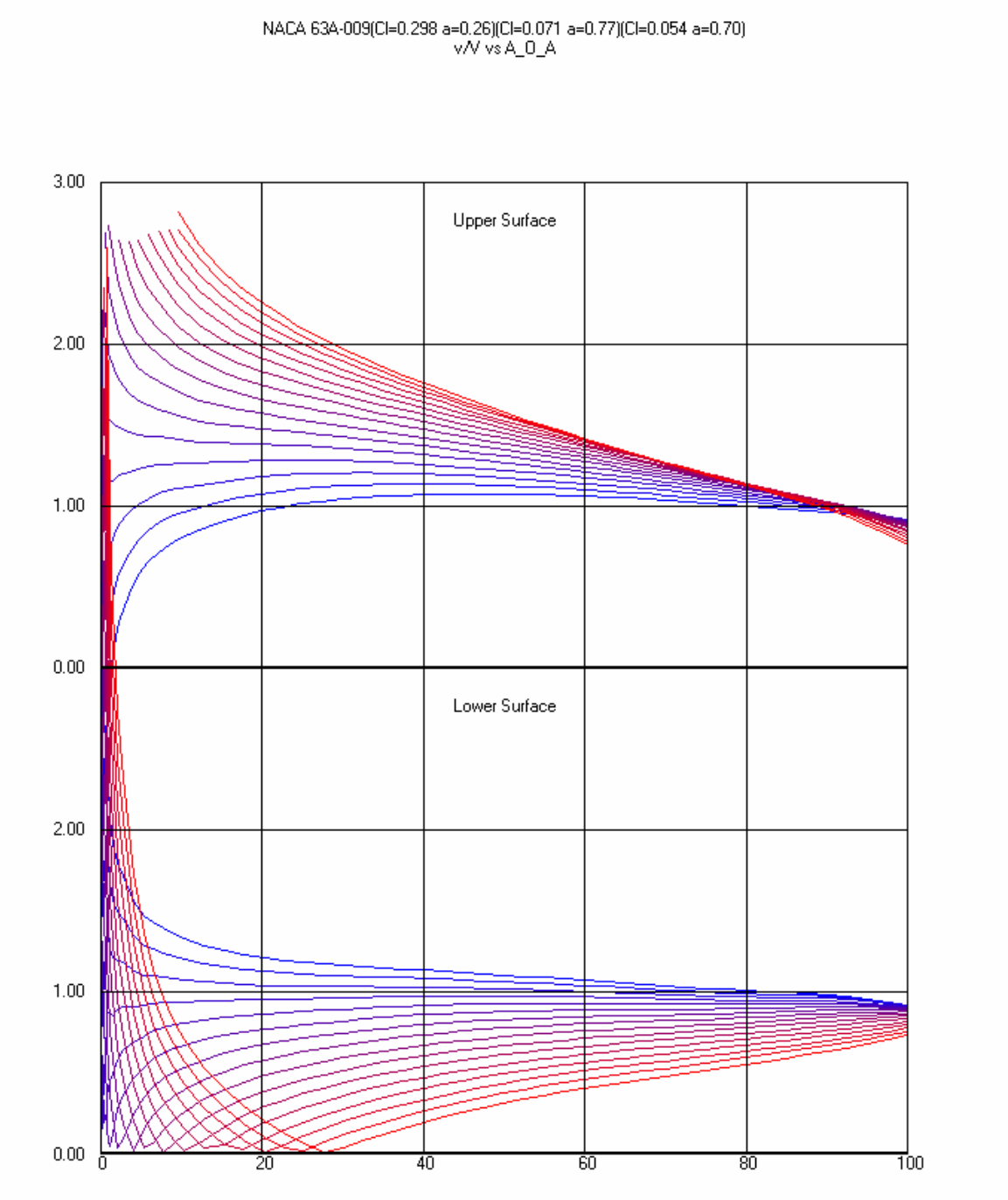

Fig E-12**:** BD Kink 2 Airfoil: NACA 63A-009 Pressure distributions

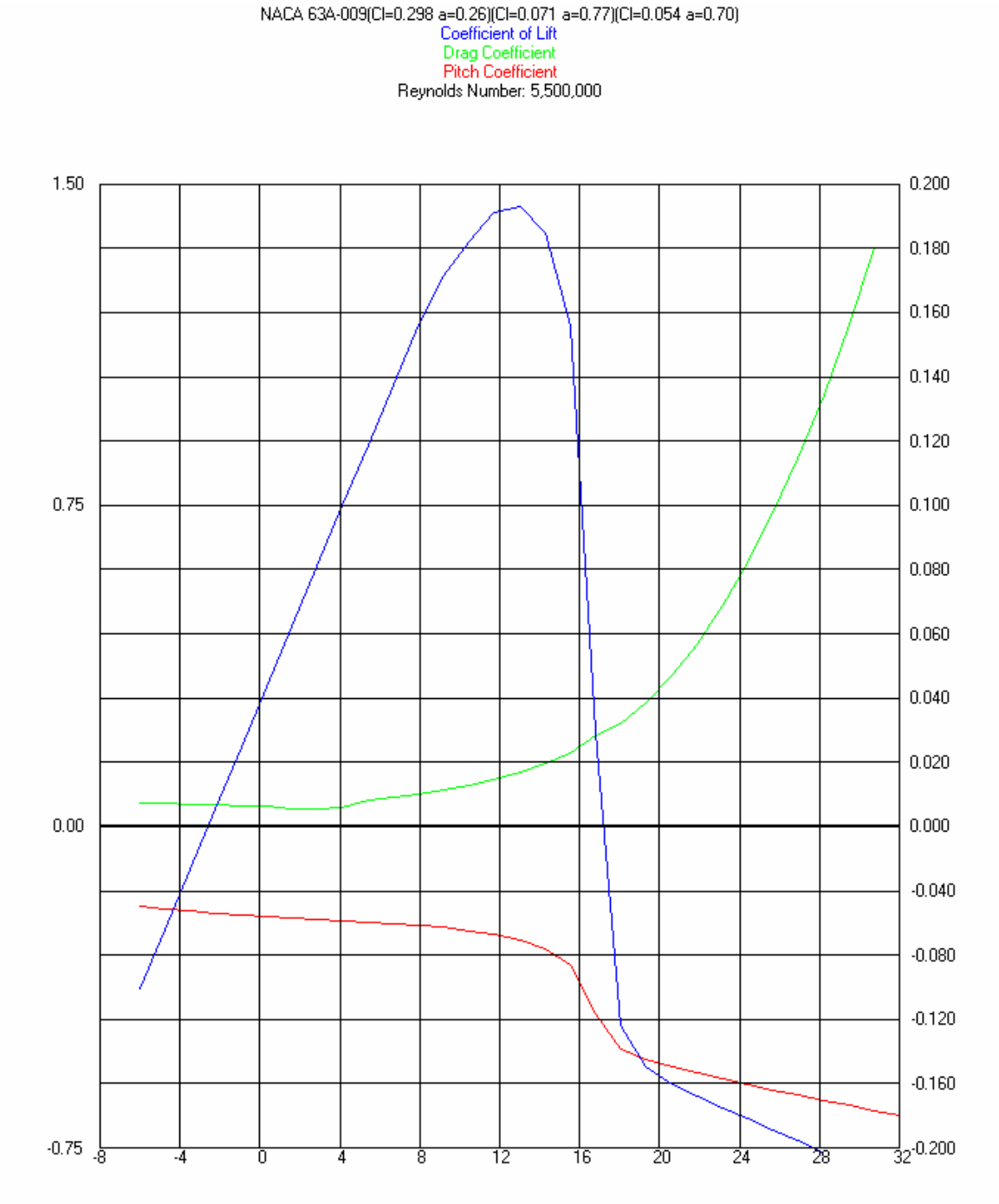

Fig E-13**:** BD Kink 2 Airfoil: NACA 63A-009 coefficients for lift, drag, and pitching moment

E.2.4 Tip Airfoil Section; Outboard station, y=1.0

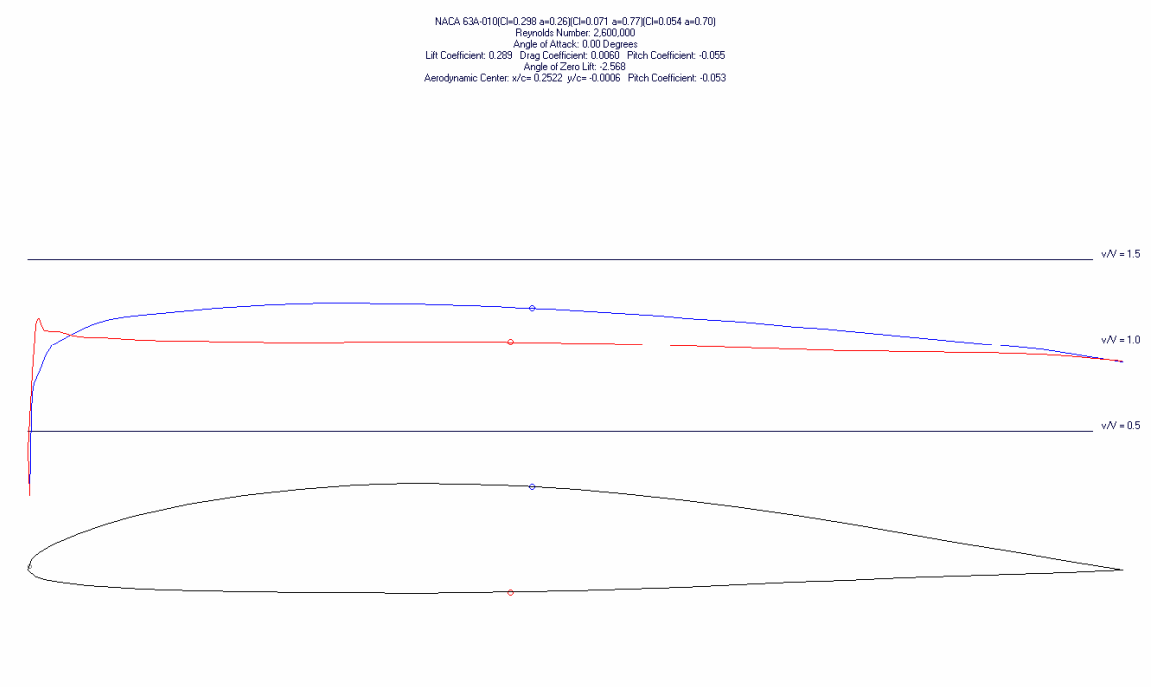

Fig E-14**:** BD Tip Airfoil: NACA 63A-010 lift at zero incidence

NACA 63A-010(Cl=0.298 a=0.26)(Cl=0.071 a=0.77)(Cl=0.054 a=0.70)
Reynolds Number: 2,600,000
Angle of Attack: 0.00 Degrees
Lift Coefficient: 0.289 Drag Coefficient: 0.0060 Pitch Coefficient: -0.055
Angle of Zero Lift: -2.568
Aerodynamic Center: x/c= 0.2522 y/c= -0.0006 Pitch Coefficient: -0.053

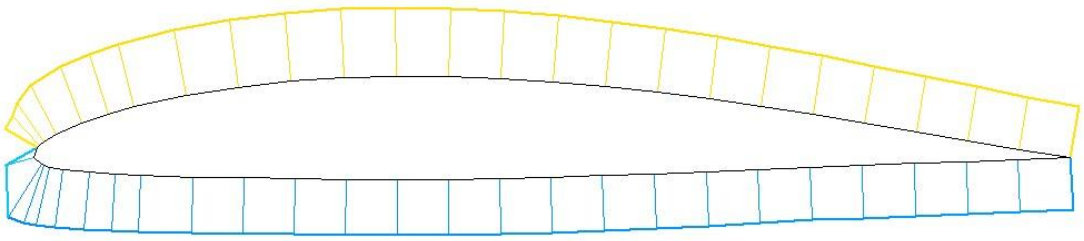

Fig E-15**:** BD Tip Airfoil: NACA 63A-010 Viscosity effect

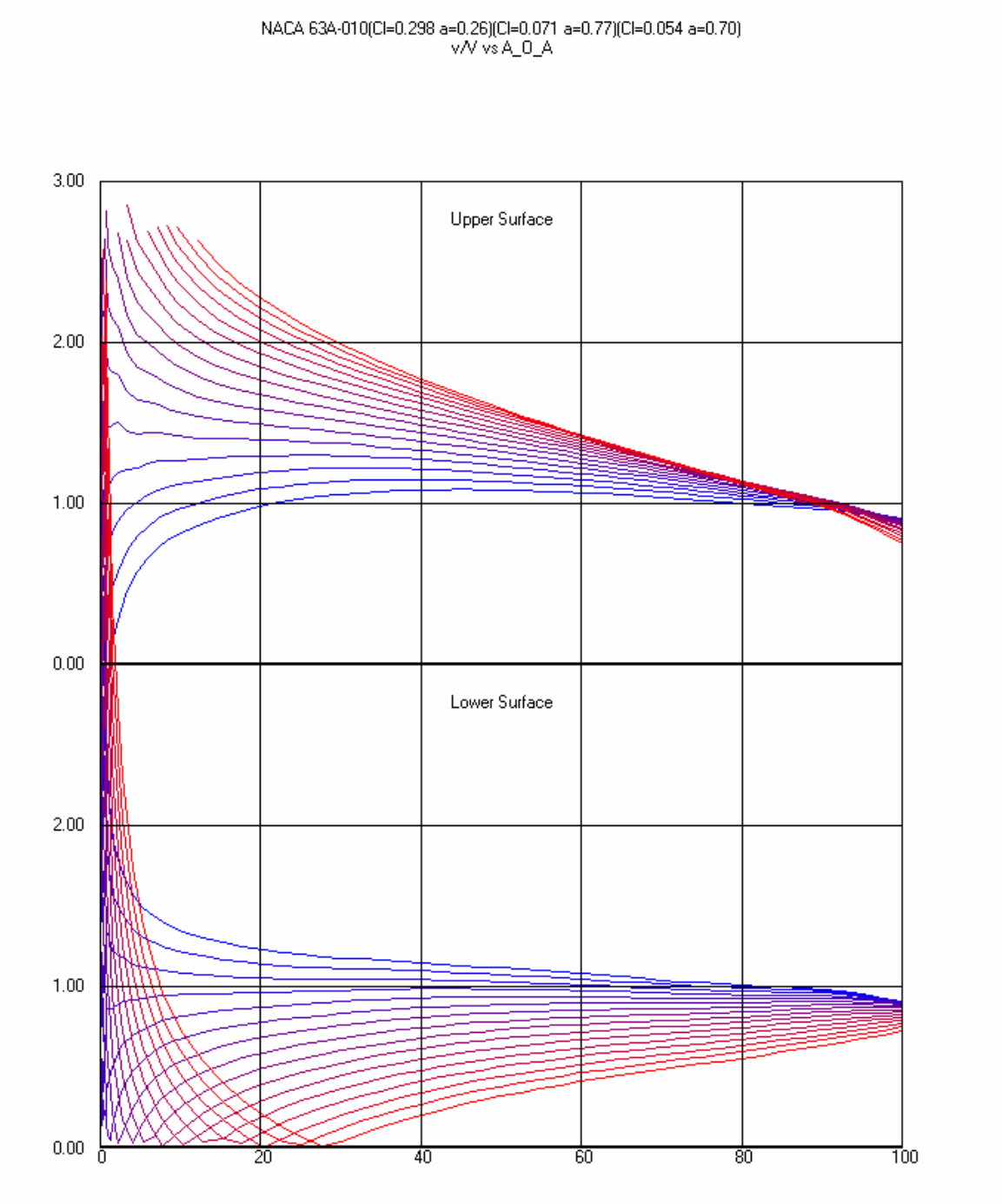

Fig E-16**:** BD Tip Airfoil: NACA 63A-010 Pressure distributions

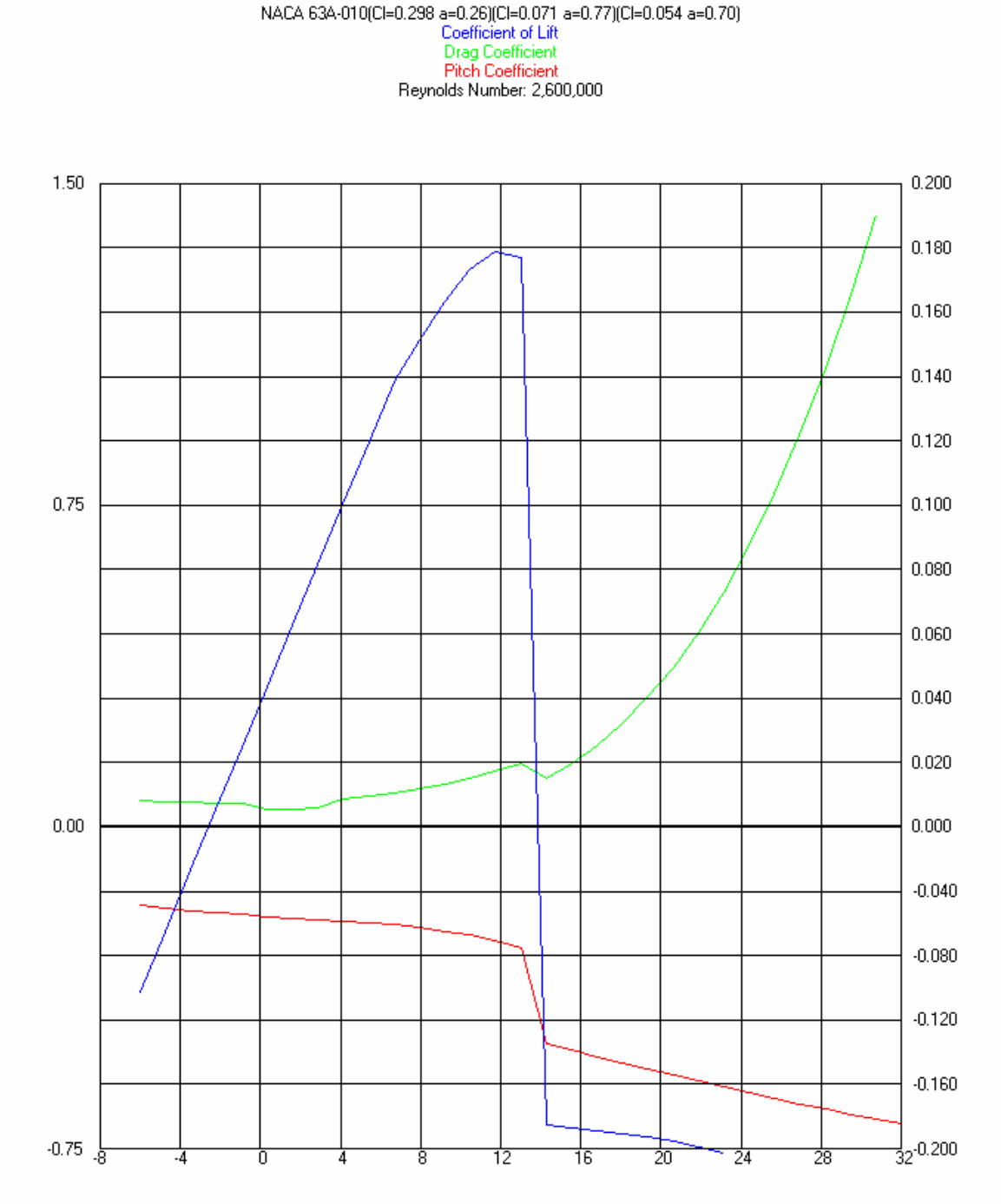

Fig E-17**:** BD Tip Airfoil: NACA 63A-010 coefficients for lift, drag, and pitching moment

E.3 Summary of Airfoil Performance

The following charts compare all four airfoils in terms of lift, drag, pitching moment, *L/D*, and their corresponding drag polars.

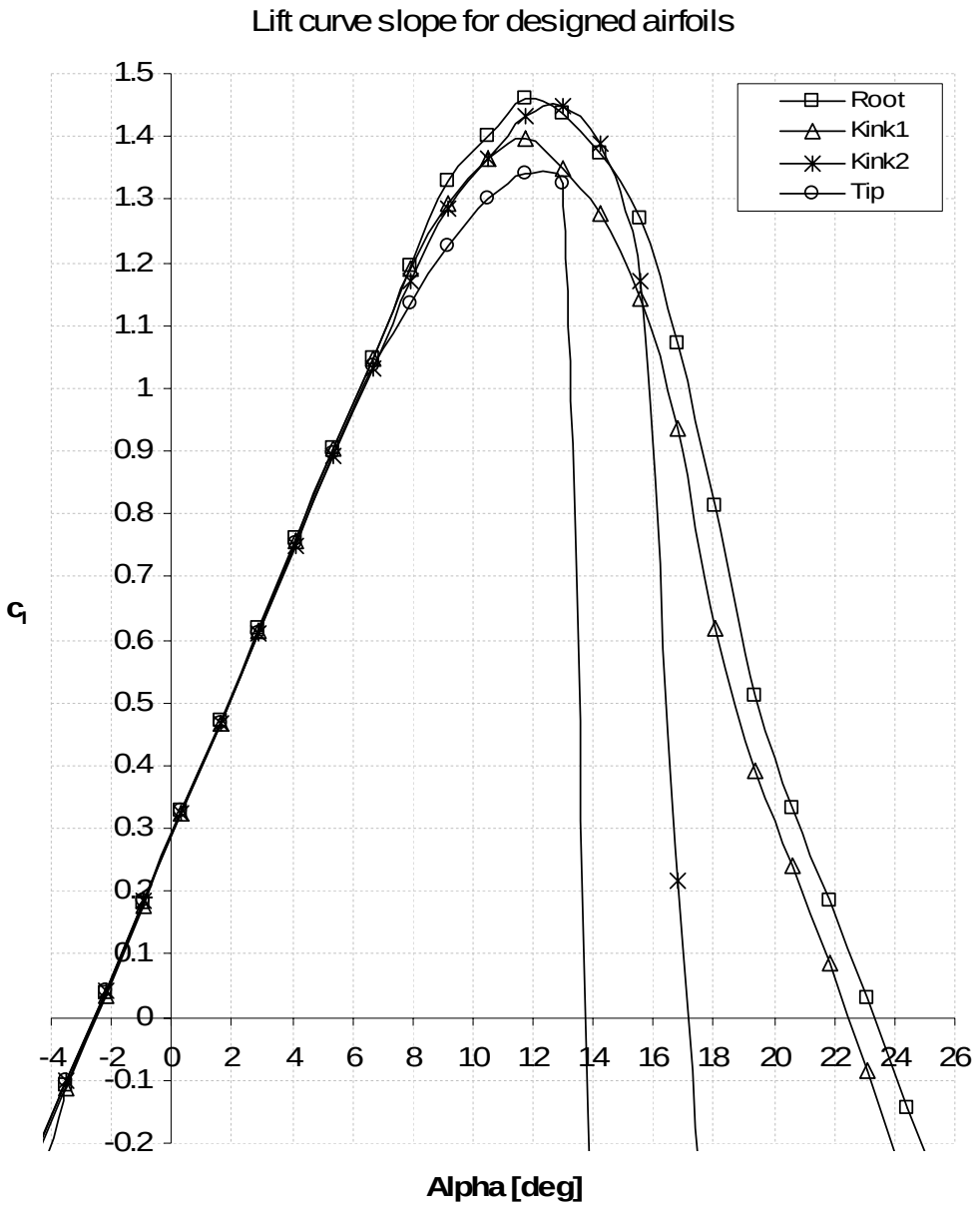

Fig E-18**:** Designed Lift Curve Slopes for all four Airfoil sections

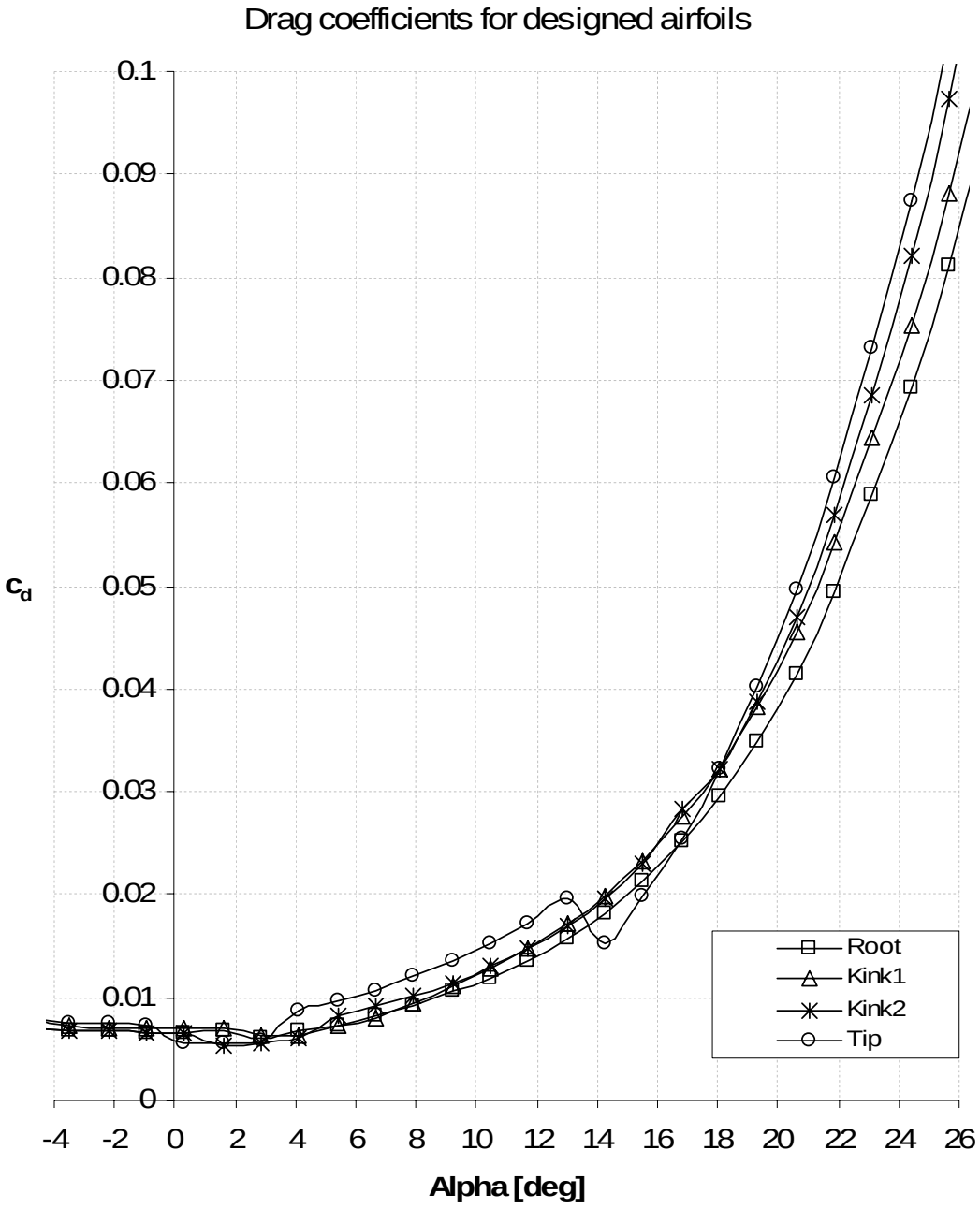

Fig E-19**:** Designed Drag Coefficients for all four Airfoil sections

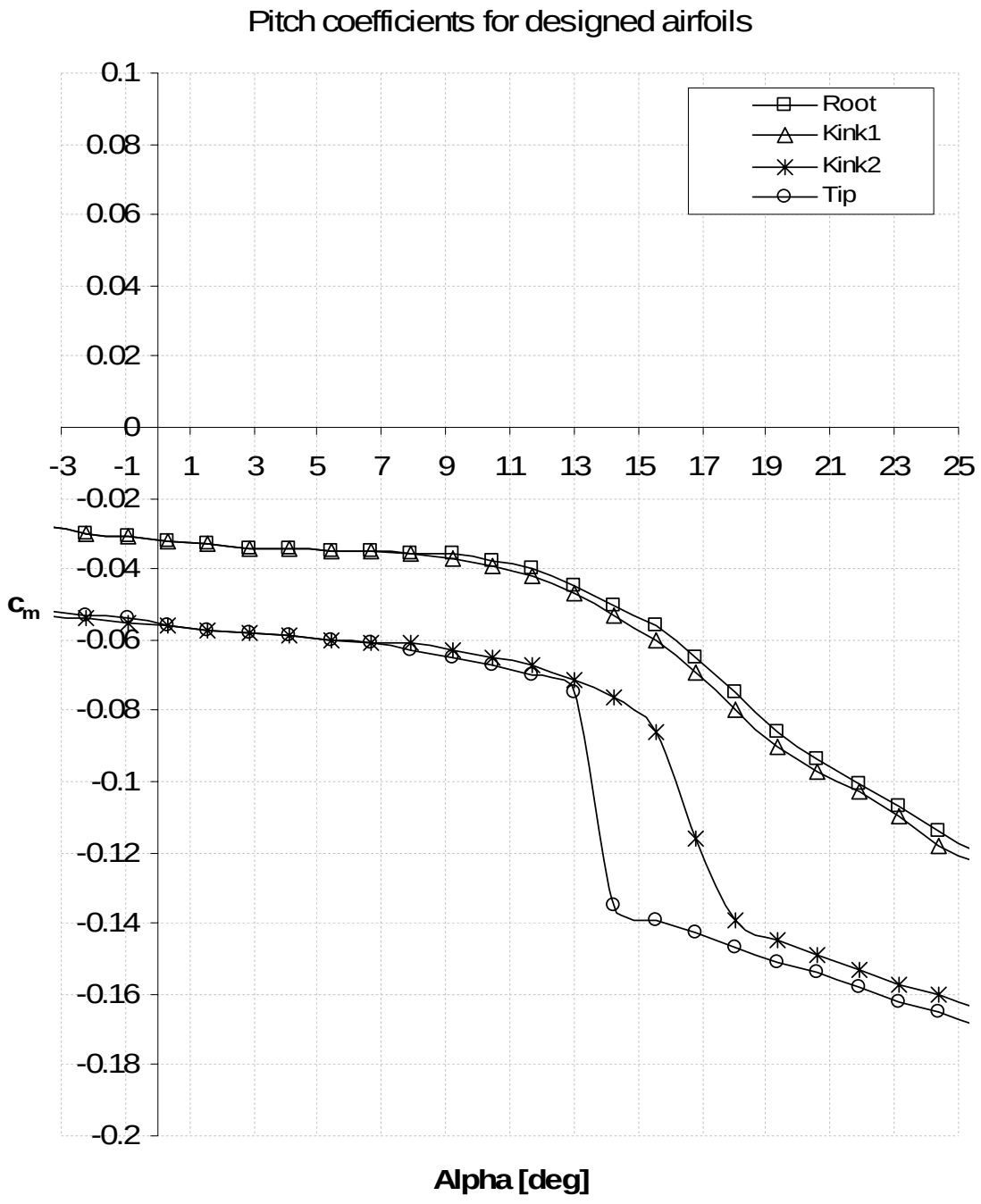

Fig E-20**:** Designed Airfoil Pitch Coefficients for all four Airfoil sections

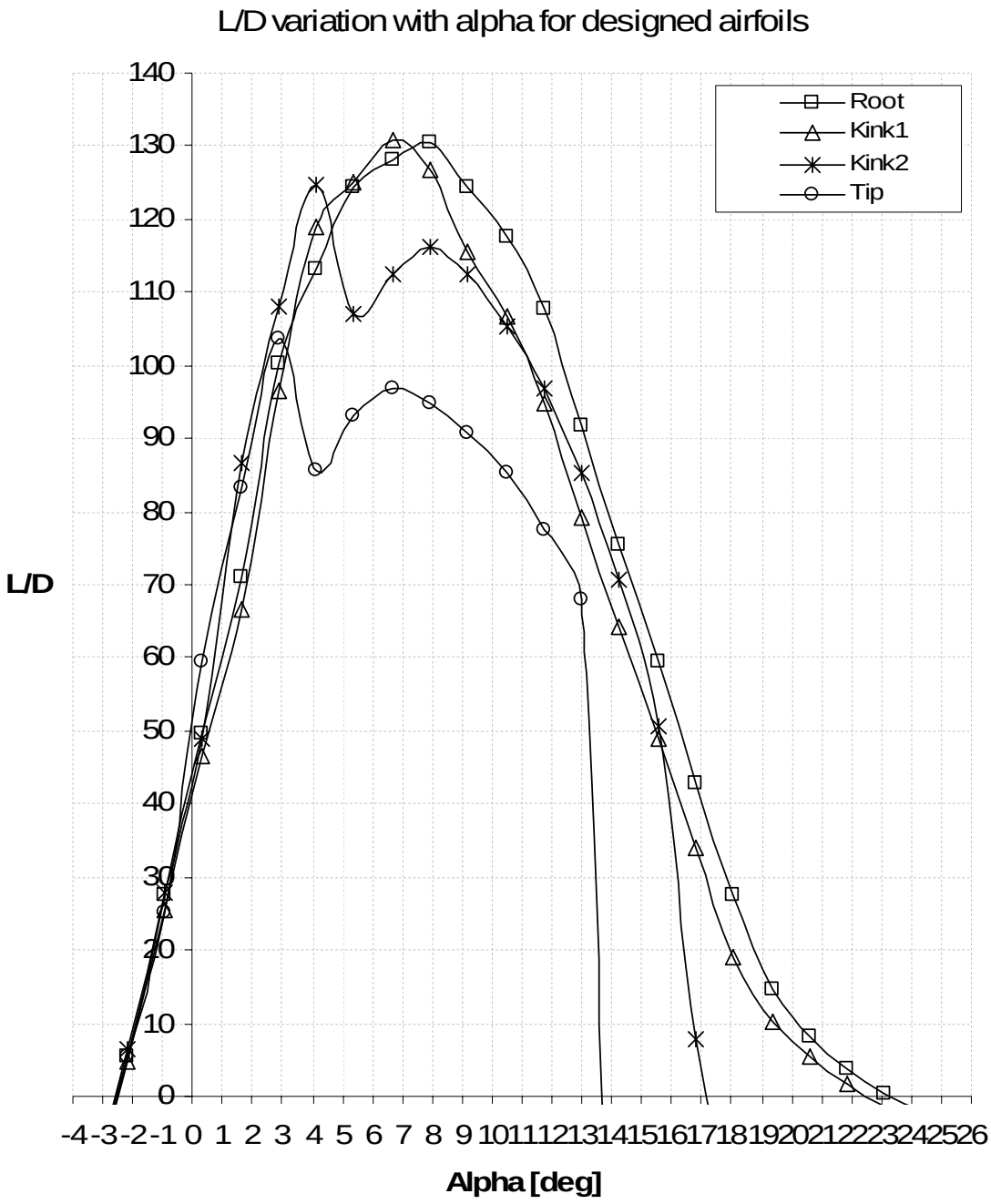

Fig E-21**:** Designed Airfoil Lift-to-Drag Ratio for all four Airfoil sections

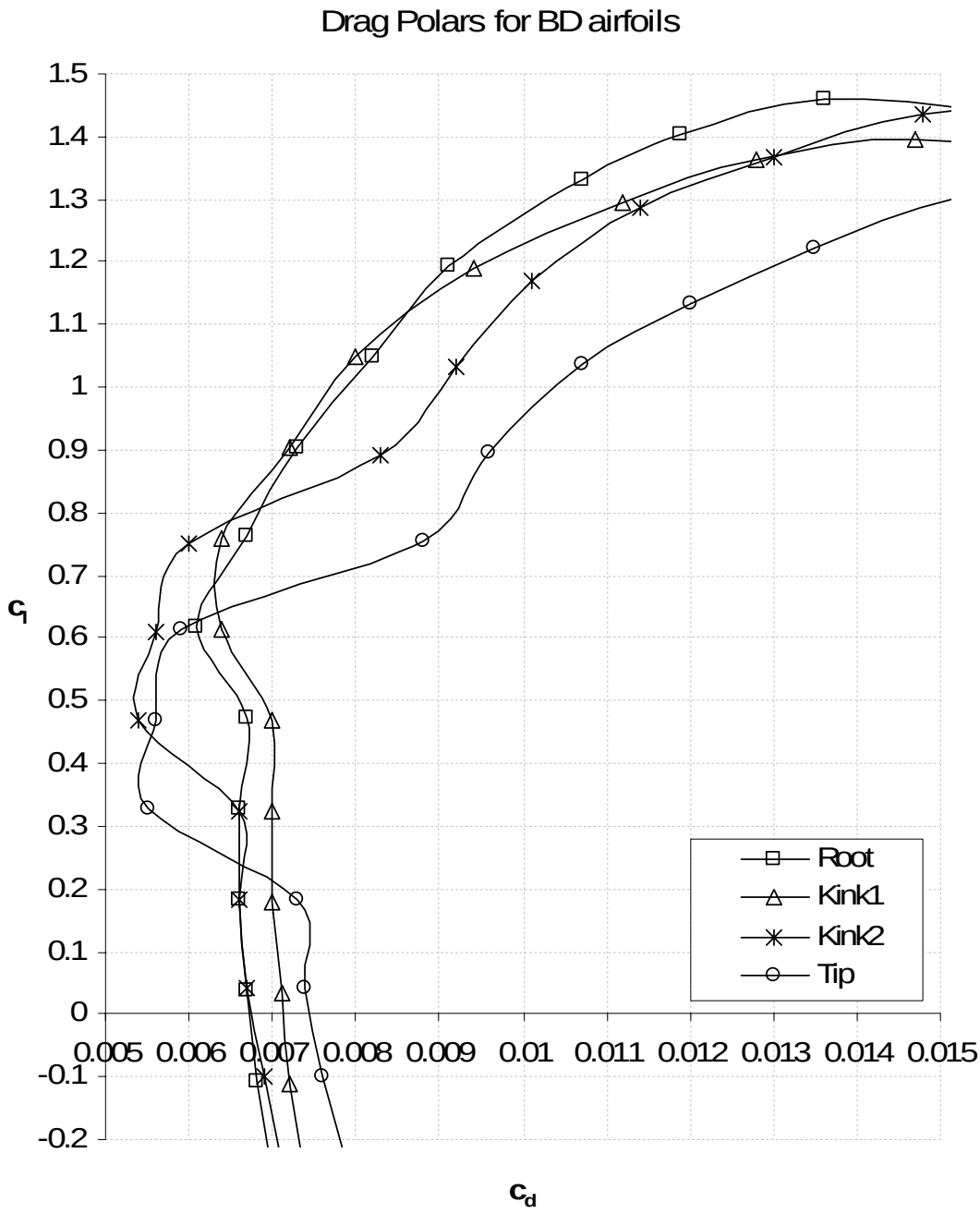

Fig E-22**:** Designed Airfoil Drag Polar showing Laminar Flow Buckets for Outboard Airfoils

Appendix F Broad Delta Undercarriage Design

F.1 Background

This section focuses on the undercarriage (u/c) size, location and an initial estimate for the loads transferred into the airframe. U/c design is an essential part of the generic design process, where the performance of the gear is required to determine how the aircraft will behave on the ground during taxi, take-off, landing, and the effectiveness of the braking system. A conventional design approach to designing the u/c was undertaken, using [Howe, 2000] for initial mass estimates, followed by [Currey, 1988], [Berry, 2000], and [Young, 2005] to detail the layout, positioning and ground clearance. As with many aircraft to date, the design of the u/c is a traditional tricycle gear, consisting of two four-wheel bogies for the main gear, and a twin nose wheel for steering.

At the beginning of the research phase the design of a novel u/c solution to reduce noise was considered, however, time was more productively spent investigating noise reduction technologies, compared to producing a new design. Noise technologies to lower the airframe noise contribution from the u/c are discussed within **Chapter 6**.

F.2 Undercarriage Design Process

The design process for the BD u/c is identical for the tailed and tailless variants where the main differences are with the landing velocity and vehicle mass. The following analysis compares the design of the BDSF alongside the BDVT to show the variation in component sizing and loading on the airframe.

F.2.1 Basic Assumptions

To initiate a first design solution for the u/c the loading on each gear was estimated with revisions to be made at a later stage when more accurate data is known. The design take-off weight (M_{DTOW}) was equivalent to *AUM*, for which 10% was the load acting on the nose gear (p_n) and 45% on each of the main gear units (p_m), and the design landing weight (M_{DLW}) was assumed to be 85% of M_{DTOW}. The landing gear reaction factor (λ_G) was considered equal for the nose and main gears and as a first estimate λ_G =1.3. One of the major parameters is the vertical descent velocity (V_V), where for a typical 3 degree continuous descent approach, V_V is equivalent to a conventional aircraft, where V_V =3.05m/s. When considering the BD design for a steep 6 degree approach, we can assume that the change in V_V is equal to the change in approach velocity (V_a), where:

$$(V_V)_{6\deg} = \left[\left\{ \frac{(V_a)_{6\deg} - (V_a)_{3\deg}}{(V_a)_{3\deg}} \right\} \cdot (V_V)_{3\deg} \right] + (V_V)_{3\deg} \text{ [m/s]}$$

Equation F-1

Approach velocity decreases as the descent angle increases, and a similar trend in descent velocities are expected for the BDSF and BDVT, as shown below.

	$(V_a)_{3deg}$ [m/s]	$(V_a)_{6deg}$ [m/s]	$(V_V)_{6deg}$ [m/s]
BDSF	58.29	57.49	3.008
BDVT	59.51	58.40	3.008

Table F-1: BDSF and BDVT vertical descent velocities (V_V) for 6 degree approach angles

The final assumption is to estimate the centre of gravity (*c.g.*) height from the ground (*H*). This was achieved using the BDSF and BDVT CAD models, where both concepts shared the same value for *H*, but not the horizontal *c.g.* location, where H = 4.08m.

F.2.2 Aircraft Landing Gear Footprint Geometry

The initial layout of the u/c uses the assumptions above combined with the following calculations so that the basic gear location can be determined. The horizontal location between the *c.g.* and the main landing gear (*MLG*) centroid to avoid tip-back, where tip-back angle α = 18 degrees, is calculated using:

$$l_m = H \cdot \tan(\alpha) \text{ [m]}$$

Equation F-2

The wheel-base (*WB*) calculation assumed that there is a 6% *MLG* load, where:

$$WB = \frac{l_m}{0.10} \text{ [m]}$$

Equation F-3

The horizontal location between the *c.g.* and nose landing gear (*NLG*) centroid is:

$$l_n = WB - l_m \text{ [m]}$$

Equation F-4

The track (T_G) is the distance between the two main gears governed by a gear orientation angle (β), where β = 47 degrees, and the minimum MLG track required is:

$$(T_G)_{Min} = 2 \cdot WB \cdot \tan\left[\sin^{-1} \cdot \left(\frac{H}{l_n \cdot \tan(\beta)}\right)\right] \text{ [m]}$$

Equation F-5

The u/c layout for both BDSF and BDVT are identical, and the geometry footprint is:

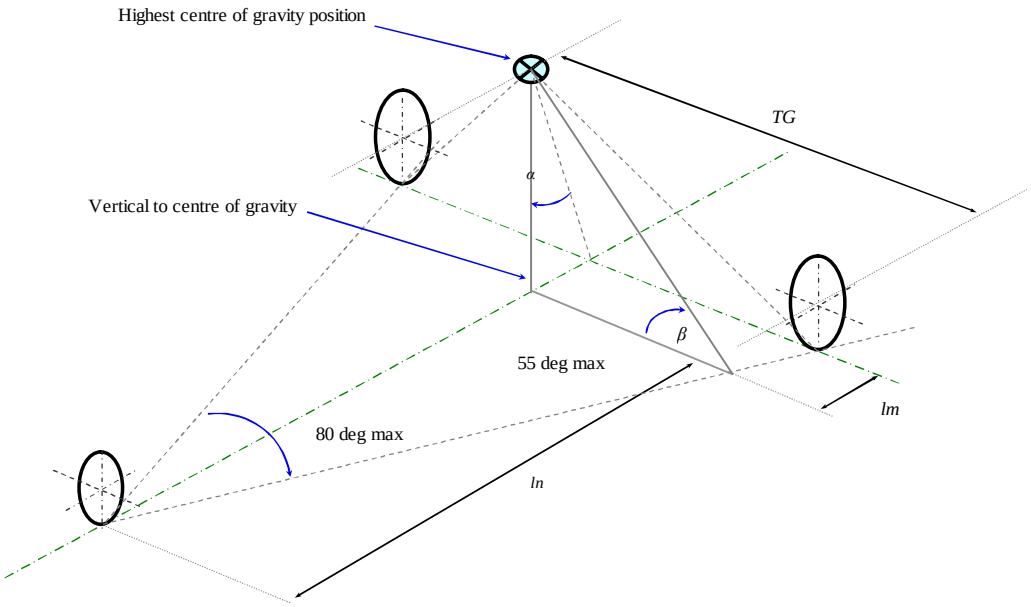

Fig F-1: U/c footprint geometry

l_m [m]	l_n [m]	WB [m]	$(T_G)_{Min}$ [m]
1.33	20.8	22.1	9.52

Table F-2: Landing gear geometry footprint for both BDSF and BDVT

F.2.3 Preliminary Landing Gear Loads

The loading on the *MLG* and *NLG* is categorised into two main cases, where there is the static load, and the dynamic load acting on the gear. The static loads on each of the u/c legs are calculated from:

$$R_{N_{Static}} = p_n \cdot M_{DTOW} \text{ [kg]}$$

Equations F-6

$$R_{M_{Static}} = p_m \cdot M_{DTOW} \text{ [kg]}$$

Equations F-7

The dynamic loads acting on each gear leg are given by:

$$R_{N_{Dynamic}} = M_{DLW} \cdot \lambda_G \cdot \left[\frac{(l_m + 0.25 \cdot h)}{(l_m + l_n)} \right] \text{ [kg]}$$

Equation F-8

$$R_{M_{Dynamic}} = 0.5 \cdot M_{DLW} \cdot \lambda_G \text{ [kg]}$$

Equation F-9

Where *h* is the static height of the *c.g.* under static rolling conditions, and *h* = 3549mm for the BDSF and for the BDVT *h* = 3576 mm, calculated by using:

$$h = H - T_{RR_{Static}} \text{ [mm]}$$

Equation F-10

NLG steady brake load acts as a vertical contribution on the nose, caused by the moment produced by the *MLG* braking force about the c.g., calculated using:

$$R_{N_{Steadybrake}} = M_{DTOW} \cdot \left[\frac{(l_m + 0.31 \cdot H)}{(l_m + l_n)} \right] \text{ [kg]}$$

Equation F-11

Parameter	*BDSF*		*BDVT*	
	MLG	*NLG*	*MLG*	*NLG*
R_{Static}	66,950	14,878	61,757	13,724
$R_{Dynamic}$	82,200	16,479	75,823	15,312
$R_{.Steadybrake}$	-	17,443	-	16,090

Table F-3: Landing gear geometry footprint for both BDSF and BDVT

F.2.4 Tyre Calculations

Tyre calculations are used to determine the tyre sizes for different load cases, where static and dynamic load cases are considered, with higher loading resulting in larger tyre sizes.

The tyre diameter for the *MLG* and *NLG* static load case is calculated by:

$$D_0 = \frac{27.891}{T_p} \cdot \sqrt{T_p \cdot \frac{R_{Static}}{N_W}} \text{ [mm]}$$

Equation F-12

The required tyre inflation pressure (T_p) for *MLG is* T_p = 8 bar and for *NLG* T_p = 6 bar, for which the number of wheels (N_W) per *MLG* leg is a four-wheel bogie, and a twin (2) wheel arrangement for the *NLG*. The tyre width is calculated using:

$$W = 0.35 \cdot D_0 \text{ [mm]}$$

Equation F-13

Tyre deflection under load (δ_T) is calculated using a load parameter (P_L), where the *MLG* static load deflection is determined by using P_L = 0.0896, and for the NLG a maximum (dynamic) tyre deflection is given by P_L = 0.21.

$$\delta_T = P_L \cdot D_0 \text{ [mm]}$$

Equation F-14

The maximum dynamic tyre deflection for the *MLG* is calculated by:

$$\left(\delta_{T_{Dynamic}}\right)_M = \left(\delta_{T_{Static}}\right)_M \cdot \left\{\frac{R_{M_{Dynamic}}}{R_{M_{Static}}}\right\} \text{ [mm]}$$

Equation F-15

The static tyre deflection for the *NLG* is similarly calculated using:

$$\left(\delta_{T_{Static}}\right)_N = \left(\delta_{T_{Dynamic}}\right)_N \cdot \left\{\frac{R_{N_{Static}}}{R_{N_{Dynamic}}}\right\} \text{ [mm]}$$

Equation F-16

The tyre rolling radius calculations for static loading is described below, where the *MLG* and *NLG* rolling radius under static load is given by:

$$T_{RR_{Static}} = \frac{D_0}{2} - \delta_{T_{Static}} \text{ [mm]}$$

Equation F-17

Similarly, for the dynamic loading of both *MLG* and *NLG* rolling radius is calculated by substituting $\delta_{Tstatic}$ for $\delta_{Tdynamic}$, where Table F-4 shows the results for parameters above to the nearest millimetre [mm].

Parameter	*BDSF*		*BDVT*	
	MLG	*NLG*	*MLG*	*NLG*
D_0	1276	600	1225	577
W	447	210	429	202
$\delta_{T.static}$	114	114	110	109
$\delta_{T.Dynamic}$	140	126	135	121
$T_{RR.static}$	524	186	503	179
$T_{RR.Dynamic}$	498	174	478	167

Table F-4: Landing gear tyre sizing and deflections under load

F.2.5 Vertical Axle Travel (VAT) for JAR25

To calculate vertical axle travel (*VAT*) according to JAR25, vertical descent velocity (V_V), shock absorber efficiency (η_o), and tyre efficiency (η_t) are required. V_V was previously discussed in section F.2.1 where a decent velocity for a steep 6 degree approach angle was estimated for both the BDSF and BDVT. Detailed iterative analysis of the u/c design or manufacturers data is required to determine η_o and η_t, however for a preliminary design study, estimates for η_o = 0.8 and η_t = 0.47 were used.

The calculation for *VAT* is the same for both *NLG* and *MLG*, where:

$$VAT = \frac{\left(\frac{V_V{}^2}{2 \cdot g \cdot \lambda_G} - \frac{\delta_{T_{Dynamic}}}{1000} \cdot \eta_t \right)}{\eta_o} + 0.25 \text{ [mm]}$$

Equation F-18

VAT is calculated in metres [m], and it is important to convert values for tyre deflections under dynamic loads into the correct units, the results for which are shown below.

Parameter	*BDSF*		*BDVT*	
	MLG	*NLG*	*MLG*	*NLG*
VAT	0.611	0.416	0.614	0.419

Table F-5: Landing gear VAT results in [m]

F.2.6 Shock Absorber Calculations

To calculate the shock absorber characteristics, the 'dry' polytropic gas index (γ_G) is required to define the shock compression ratio, where γ_G = 1.1. The extended gas force is calculated using a shock absorber ratio (R_S), where R_S = 3.5 for the *NLG*, and R_S = 4.0 for the MLG under static loading.

$$P_{extended} = \frac{R_{Static}}{R_S} \text{ [kg]}$$

Equation F-19

The shock absorber compression ratio (*CR*) can be calculated by:

$$CR = \left(\frac{1.30 \cdot R_{Dynamic} \cdot R_S}{R_{Static}} \right)^{\frac{1}{\gamma_G}}$$

Equation F-20

Static closure (S_{static}) is the vertical distance between static and extended axle positions:

$$S_{Static} = VAT \cdot \left[1 - \left\{ \frac{\left(\frac{P_{extended} \cdot CR}{R_{Static}} - 1 \right)}{(CR - 1)} \right\} \right] \text{ [m]}$$

Equation F-21

Shock absorber results are analysed for both *NLG* and *MLG*, and are compared for the BDSF and BDVT variants.

Parameter	*BDSF*		*BDVT*	
	MLG	*NLG*	*MLG*	*NLG*
$P_{extended}$ [kg]	16,738	4,251	15,439	3,921
CR	5.39	4.35	5.39	4.36
S_{static} [m]	0.563	0.386	0.565	0.388

Table F-6: Shock absorber compression characteristics

F.2.7 Piston Diameter Calculation

To determine the diameter of the piston, a few assumptions are required for the distance (*B*) between the wheel axle centreline and the closed stop on the shock absorber piston, where *B* = 0.07 m for the *MLG* and *B* = 0.045 m for the *NLG*. Thickness ratio (*D/t*) for the piston is 18, where the ratio of inside-to-outside (D_i/D_o) piston diameter is 0.89. The moment arm (*Arm*) for a piston diameter designed at high drag is calculated from:

$$Arm = 0.85 \cdot VAT + B + 0.25 \text{ [m]}$$

Equation F-22

The assumed load causing piston bending for this high drag case is given by:

$$HD_{load} = 0.64 \cdot R_{Dynamic} \cdot g \text{ [N]}$$

Equation F-23

The overall piston diameter designed for strength is calculated using:

$$D_{Piston} = \sqrt[3]{\frac{32 \cdot Arm \cdot HD_{load} \cdot 1000}{1124 \cdot \pi \cdot \left(1 - \left(D_i / D_o\right)^4\right)}} \text{ [mm]}$$

Equation F-24

Static pressure increases provide solutions for the piston diameter, where the denominator (*d*) is replaced to give *d* = 1.2655 for1800 psi, and *d* = 1.1249 for 1600 psi, where:

$$D_{Piston} = \sqrt{\frac{R_{Static}}{d \cdot 0.7854}} \text{ [mm]}$$

Equation F-25

The piston diameter calculations provide the change in diameter required for different load cases, where the maximum is used for the preliminary u/c design layout, as shown below in Table F-7.

Parameter	*BDSF*		*BDVT*	
	MLG	*NLG*	*MLG*	*NLG*
Arm [m]	0.614	0.424	0.617	0.426
HD_{load} [N]	52,608	10,547	48,527	9,751
$(D_{Piston})_{strength}$ [mm]	78	40	90	47
$(D_{Piston})_{1600}$ [mm]	275	130	264	125
$(D_{Piston})_{1800}$ [mm]	260	122	249	118

Table F-7: Landing gear piston diameter sizing, designed on strength and pressure on compression

F.3 Undercarriage Design Summary

The design process for the BD u/c provided a basis to develop a preliminary gear layout, consisting of sizing and layout for tyres, shock absorbers, and pistons; all with loading calculations. The overall *NLG* and *MLG* gear layouts are best described by Fig F-2, where the wheel axial and longitudinal spacing is shown.

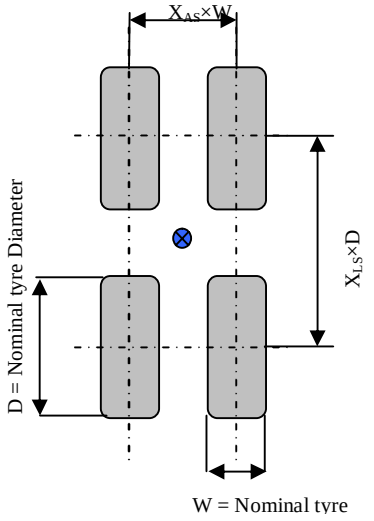

Fig F-2**:** Undercarriage Main 4-wheel bogey layout

Longitudinal spacing between the tyres is mainly used for the *MLG* because tyres under load expand and require sufficient clearance so that contact is not made between them. Axial spacing is necessary on the *NLG*, but more importantly on *MLG* because brakes require sufficient clearance along the axle, so that visual and physical maintenance checks are possible, and so that contact is not made between the wheels.

Parameter	*BDSF*		*BDVT*	
	MLG	*NLG*	*MLG*	*NLG*
Tyre diameter (D)	1.292	0.608	1.225	0.577
Tyre width (W)	0.452	0.213	0.429	0.202
Axial Spacing (X_{AS})	1.153	0.266	1.094	0.253
Longitudinal Spacing (X_{LS})	1.835	0.760	1.740	0.722

Table F-8: Landing gear summary and wheel spacing requirements, all dimensions in metres [m]

The final undercarriage layout is shown below in Fig F-3, where the two main four-wheeled bogies and twin nose wheel are clearly shown at their designed locations along the base of the BDSF airframe design.

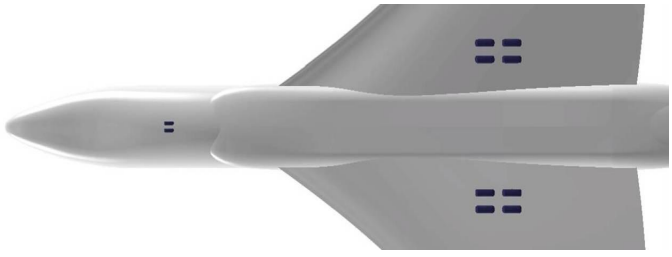

Fig F-3**:** Underside of BD Concept, Showing Main and Nose Undercarriage, and Wing-Fuselage Blister

Appendix G Broad Delta Mass & Stability Calculations

G.1 Background

This Appendix initially focuses on a revised mass estimate for each of the BD configurations, where the wing, fuselage, empennage, and systems masses are revised and compared for a metallic and composite aircraft configuration. In addition to these variables, an environmental factor was investigated through removal of the hydraulic systems and a comparison with the mass of a more-electric aircraft. The comparison of a more-electric aircraft and a hydraulic aircraft in addition to a composite and metallic variant raises a question as to whether the aircraft should include environmental considerations other than noise in the final selection.

The second focus of this Appendix is to investigate the centre of gravity (*c.g.*) and provide an estimate for the stability of each aircraft concept. Stability is critical for the BDSF, where a small static margin change and *c.g.* range is required during flight. The BDVT c.g. range is not as critical because the tail surface is used to trim the aircraft. The stability margin for both concepts should be similar because the internal arrangement of fuel, cargo, passengers, and equipment, etc are all common between variants; providing a similar stability range for one statically stable and one statically unstable configuration.

G.2 BD Component Mass Breakdown

The mass breakdowns for the BD aircraft configurations were broken down into major items and were compared for a number of aircraft variants. Mass estimates were revised and detailed below for calculating the wing, fuselage, empennage, undercarriage, propulsion systems (including integration), flight systems, equipment, furnishings, operational items, and finally the mass of disposable items.

G.2.1 Wing Mass

The wing mass is broken down into three main sections which are *IPS*, *AM*, and *SS* mass components and are used to provide the total wing mass estimate, where:

- M_{IPS} is the ideal primary structural mass,
- M_{AM} is alternate materials mass allowing for departure from a structural ideal,
- M_{SS} is the allowance for secondary structural mass.

The ***IPS* mass** is the sum of two key parameters, where the first term (m_C) represents the structural wing box covers and includes the spanwise shear webs, and the second term (m_r) represents the ribs required to support the first webs.

$$\left(\frac{M_{IPS}}{M_0}\right) = m_C + m_r$$

Equation G-1

where the wing box covers and spanwise shear web mass ratio is calculated by:

$$m_C = 1920 \cdot A^{1.5} \cdot S^{0.5} \cdot \overline{N} \cdot r \cdot \frac{(1+\lambda)\cdot \sec\phi \cdot \sec\varphi}{\tau \cdot f_a}$$

Equation G-2

and the rib support mass ratio is:

$$m_r = \frac{3S^{1.5}\tau^{0.5}}{M_0 A^{0.25}}\left[\left(1-0.34\lambda+0.44\lambda^2\right)+2.2\tau\left(\frac{S}{A}\right)^{0.5}\left(1-\lambda+0.72\lambda^2\right)\right]$$

Equation G-3

Results from the final aircraft configuration analysis are required, where *A*, *S*, and λ are provided, with $\tau = t/c$ of wing root and $\sec\Phi = \cos^{-1}(\Lambda_{¼})$, found within **Appendix B.**

The effective ultimate manoeuvre factor ($\overline{N}$) is the greater value of 1.65 times the limit manoeuvre load or:

$$\overline{N} = 1.65 + \frac{6.45 V_D S}{M_0\left(\frac{2}{A}+\sec\varphi\right)}$$

Equation G-4

Structural sweep parameter (φ) is calculated using the structural parameter previously established within the parametric analysis phase, where *SP* = 9.24. φ is found by rearranging Equation G-5:

$$SP = \sec\varphi \cdot \left[\frac{\overline{N} A^{1.25}}{\left(t/c\right)^{0.5}}\right]^{0.5}$$

Equation G-5

The allowable working stress of the airframe material (f_a) for a light alloy, where:

$$f_a = 1.12\left[\frac{\overline{N}rA^{1.75}M_0}{S^{0.75}\tau^{1.5}}(1+\lambda)^{2.5}\sec\varphi\sec\phi\right]^{0.5}\times 10^5 \text{ [N/m}^2\text{]}$$

Equation G-6

Inertial relief factor (r) is calculated for four (4) wing-mounted engines which provide a significant contribution to the wing relief. Calculation of r requires using the design zero fuel mass (M_{ZW}) at maximum payload condition, where r is given by:

$$r = 1-\left[0.22+\left(1+\frac{M_{ZW}}{M_0}\right)\right]$$

Equation G-7

	M_{IPS}/M_0	m_C	M_r	$\overline{N}$	$\sec\varphi$	f_a	R
BDSF	0.0443	0.00820	0.0361	5.35	0.9997	1.43e9	0.508
BDVT	0.0239	0.00656	0.0174	4.35	0.9996	1.88e9	0.540

Table G-1: BDSF and BDVT summary of M_{IPS} calculation

***AM* mass** is a mass penalty on the idealised primary wing structure, where attachments such as for engines and landing gear add to the ideal structural mass. The main contributor is the undercarriage, where the landing gear attachment provides a penalty of 0.4%, with a 1% penalty for the landing gear cut-out structure, where $M_{AM}/M_0 = 0.014$.

The allowance for secondary wing structure ***SS* mass** considers contributions from the secondary structural items such as:

- Ailerons ($M_{aileron}/M_0$) = 0.002,
- drooped LE slats ($M_{LEdroop}/M_0$) = 0.005,
- TE VCFs (M_{VCF}/M_0) = 0.0045,
- spoilers/airbrakes ($M_{spoiler}/M_0$) = 0.0015,
- tips/fairings ($M_{fairing}/M_0$) = 0.002,
- Composite moving surfaces ($M_{CompSurf}/M_0$) = -0.005.

Total ***SS* mass** is the sum of all components above where there is an additional weight penalty for aircraft with an *AUM* of less than 140 tonnes of (M_{Pen}/M_0) = 0.005. Total SS mass for the BDSF is (M_{SS}/M_0) = 0.009, and for the BDVT (M_{SS}/M_0) = 0.013 due to the addition of variable camber flaps.

The total wing mass is corrected to consider the inboard wing box structure contained within the fuselage width. Calculation of the wing correction factor (f_w) uses the fuselage width to wingspan ratio (β_w) and λ, where:

$$f_w = 1.13 \cdot \left[\left(1 - 5\beta^2\right) - 0.0027 \cdot \left(1 + 43\beta\right) \cdot \lambda\right]$$

Equation G-8

The three components of wing structural mass and the correction factor are known, so the total structural mass of the wing can be calculated by:

$$M_W = \left(M_{IPS} + M_{AM} + M_{SS} + f_w\right) \cdot M_0$$

Equation G-9

The corrected wing structure mass for the BDSF and BDVT is representative of metallic light alloy structures, where a composite reduction factor is included in the design to represent manufacturing advances for large structural components, with an associated 12% reduction in overall structure mass.

Metallic and composite structural mass estimates are shown in Table G-2 and compared with the initial metallic wing structural mass estimation.

	$(M_W)_{metallic}$	$(M_W)_{composite}$	*Initial* $(M_W)_{calc}$
BDSF	28,456	25,307	24,986
BDVT	25,847	21,813	21,766

Table G-2: BDSF and BDVT metallic and composite wing structural mass estimates [kg]

G.2.2 Fuselage Mass

The mass of the fuselage is calculated by simplifying the geometry to provide an ideal layout, in Fig G-1, where the assumed geometry is the same for the BDSF and BDVT.

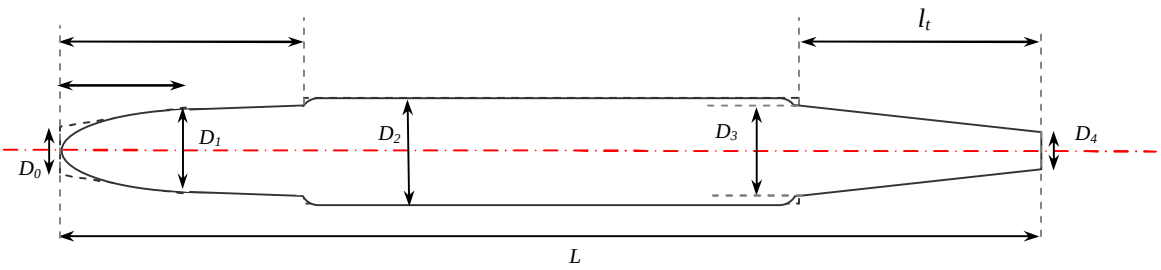

Fig G-1: Idealised representation of BD fuselage geometry

l_n = distance aft of the nose where the nose effectively blends into a parallel section,

l_p = distance aft of the nose where a cross sectional discontinuity occurs,

l_t = distance forward of the aft fuselage where the cross-section fairs down,

L = overall fuselage length,

D_0 = equivalent diameter at the nose,

D_1 = diameter where the nose locally ends at l_n,

D_2 = maximum equivalent diameter either at l_p, or (L- l_t),

D_3 = diameter at l_t,

D_4 = diameter at the tail.

The equivalent dimensions for diameter, height, and width of the fuselage at each station (i = 0-4) are related to a coefficient that depends on the cross-sectional fuselage shape.

$$D_i = k_i \cdot \frac{\left(B_i + H_i\right)}{2} \text{ [m]}$$

Equation G-10

The fuselage dimensional parameters can be summarised assuming that the shape varies between an elliptical and a rectangular cross-section, providing:

section (i)	D_i	H_i	B_i	k_i
0	0.00	0.00	0.00	1.0
1	4.72	3.88	4.71	1.1
2	6.25	5.50	5.10	1.18
3	5.07	4.73	5.03	1.04
4	1.01	0.81	1.22	1.0

Table G-3: Dimensions for BD fuselage diameter, width, and breadth [m]

where the fuselage station lengths are:

l_n	l_p	l_t	L
5.53	17.86	11.64	53.67

Table G-4: Dimensions for BD fuselage station lengths [m]

The structural surface area on the fuselage (S_f) is calculated using:

$$S_f = \pi \cdot D_1^2 \cdot \left[\left(\frac{l_p - l_n}{D_1} \right) + \left(\frac{L - l_t - l_p}{D_2} \right) \cdot \left(\frac{D_2}{D_1} \right)^2 + N_S + T_S \right] \text{ [m}^2\text{]}$$

Equation G-11

where, N_S is a function of the area at the nose for a pointed nose region, given by:

$$N_S = 0.325 \cdot \left(4 \cdot \left(\frac{l_n}{D_1} \right)^2 + 1 \right)^{0.5}$$

Equation G-12

and, T_S is a function of the tail area, where for a truncated tail:

$$T_S = k_5 \cdot \left(\frac{l_t}{D_2} \right) \cdot \left\{ 1 + \left(\frac{D_4}{D_3} \right) \right\} \cdot \left(\frac{D_3}{D_1} \right)^2$$

Equation G-13

The fuselage structural surface area (S_f) is calculated for a rear fuselage design that merges into the tail-rudder region, where $k_5 = 0.66$, resulting in $S_f = 834.7\text{m}^2$.

The dominant loading case for a civil passenger aircraft fuselage is due to pressurisation, where alternate flight loading cases are not continuous for the duration of flight, unlike cabin pressurisation, where the mass is calculated using:

$$M_{FUS} = k_6 \cdot \left(\frac{3.56p}{\bar{\sigma}^{0.75}} \cdot S_f \cdot B_{\max} \right) \cdot \left[1 + \left(3.12 - 0.354 \cdot B_{\max} \right) \cdot \frac{2\bar{\sigma}}{\left(1 + \bar{\sigma} \right)} \right] \text{ [kg]}$$

Equation G-14

The fuselage mass calculation requires the maximum fuselage breadth (B_{max}) and the structural surface area calculated above. The nominal tensile stress in the fuselage as a fraction of 100 MN/m^2, is $\bar{\sigma}$ =1.0 for a fuselage diameter in excess of 6m. The class of aircraft (passenger rating and vehicle type) and incorporated design features is represented by the coefficient k_6, where for a civil passenger airliner with wing-mounted *MLG* units, $k_6 = 1.0$.

[Howe, 2000] suggests that the ideal internal pressure of the fuselage should be between 6000 to 8000ft, with a pressure differential (p) range of 0.37bar to 0.58bar for aircraft at altitudes between 25,000ft and 43,000ft. The cruise altitude for the BDSF is 38,000ft and using linear interpolation, a cabin differential pressure is estimated at p_{BDSF} = 0.522 bar. The BDVT has a higher cruise at 39,500ft which corresponds to p_{BDVT} = 0.539 bar. The fuselage mass estimates for the two BD configurations slightly differ due to the cabin differential pressures which are shown in table.

	$(M_{FUS})_{metallic}$	$(M_{FUS})_{composite}$	*Initial* $(M_{FUS})_{calc}$
BDSF	18,190	16,007	17,235
BDVT	18,910	16,641	17,660

Table G-5: BDSF and BDVT metallic and composite fuselage structural mass estimates [kg]

G.2.3 Empennage Mass

The empennage design for both BDSF and BDVT are completely different, where the BDSF only has a vertical stabiliser, and the BDVT has two effective control surfaces that are canted; which essentially have been sized as the equivalent of the horizontal and vertical tail components required for stability and control.

The **BDVT *V-tail*** mass is assumed to be equal to an equivalent size of horizontal tail and angled to the horizontal. The effective mass of the V-tail is calculated using the structural design speed (V_D), where:

$$M_{V-tail} = 0.047 \cdot V_D \cdot \left(S_{V-tail}\right)^{1.24} \text{ [kg]}$$

Equation G-15

V-tail reference area ($S_{V\text{-}tail}$) is calculated as the effective area of tail outside the fuselage boundary, where the root, tip, and fuselage side chord and height from the centre-line are shown below in Table G-6.

Dimension	*Tip*	*Fuselage side*	*Root*
c	5.14	8.36	9.09
h	10.29	157	0.00

Table G-6: BDVT *V-tail* equivalent tail surface geometry [m]

The mass estimate for the BDVT equivalent *V-tail* surfaces is provided in Table G-8, where the mass of a metallic construction is compared to a composite design.

The BDSF vertical fin mass is calculated using:

$$M_{Vf} = 0.065 \cdot k_{12} \cdot V_D \cdot \left(S_{Vf}\right)^{1.15} \text{ [kg]}$$

Equation G-16

where k_{12} is a factor representing the vertical location of the horizontal tail surface relative to the height of the fin. For the case of the BDSF, there is no horizontal tail, and so k_{12} is unity. The vertical stabiliser geometry is required to calculate the fin reference area, and is provided within Table G-7 below:

Dimension	*Tip*	*Fuselage side*	*Root*
c	3.67	9.28	10.15
h	9.73	1.51	0.00

Table G-7: BDSF vertical stabiliser geometry [m]

BDSF vertical stabiliser mass estimate is provided in Table G-8, showing a comparison between a metallic and composite design.

	$(M_T)_{metallic}$	$(M_T)_{composite}$	*Initial* $(M_T)_{calc}$
BDSF	1,555	1,369	2,499
BDVT	8,541	7,516	3,918

Table G-8: BDSF and BDVT metallic and composite Tail mass (M_T) estimates [kg]

G.2.4 Winglet Mass

The winglet mass estimates were calculated using the same procedure for the BDSF vertical stabiliser, where the BDSF and BDVT upper and lower winglet masses are combined to provide the structural mass shown below in Table G-9.

	$(M_{winglet})_{metallic}$	$(M_{winglet})_{composite}$	*Initial* $(M_{winglet})$
BDSF	550	484	-
BDVT	133	117	-

Table G-9: BDSF and BDVT metallic and composite upper and lower winglet mass estimates [kg]

G.2.5 Undercarriage Mass

The undercarriage mass is typically estimated as 4% of the AUM estimates for the BDSF and BDVT variants. Although a preliminary u/c design study was completed within **Appendix F,** detailed mass estimates were not completed due to time constraints, so the estimated u/c mass is shown in below.

	$(M_G)_{metallic}$	$(M_G)_{composite}$	*Initial* $(M_G)_{calc}$
BDSF	6,020	5,839	5,562
BDVT	6,052	5,870	5,149

Table G-10: BDSF and BDVT metallic and composite undercarriage estimates [kg]

An assumption that 25% of the gear mass was suitable for a redesign using composite materials, where this percentage of the overall undercarriage structure has a 12% composite mass reduction.

G.2.6 Propulsion Systems Installation Mass

The propulsion systems mass calculated within **Appendix B**, suggests that the estimated mass for four engines is 7.7% of the *AUM*, providing a total mass of 12,256 kg for the BDVT, and 11,565kg for the BDSF. Typically this mass includes the engine installation components, such as the basic engine, pipe-work, removable panels, accessories, etc.

Removal of the basic propulsion system components provides the installation mass for the airframe. The engine mass for a conventional civil transport aircraft is increased by a factor of 1.56, where dividing the total engine mass by this factor provides the basic mass of the four engines; where the mass per engine for the BDSF is M_{engine} = 1,679 kg, and for the BDVT, M_{engine} = 1,964 kg.

The total installation mass for the propulsion systems is the difference between the total installed engine mass (M_{PP}), and the mass of the four engines ($4\times M_{engine}$). The calculated installation mass for the BDVT was increased by 5% to reflect the installation of four *OTW* podded engines, where M_{Pinst} = 4,399 kg for the BDVT. The BDSF considered four semi-embedded engines installed at the wing root, where the installation mass was increased by 2%, where M_{Pinst} = 4,850 kg.

G.2.7 Mass of Systems, Equipment, and Furnishings

There are many systems associated with a civil passenger aircraft, and all fall under a main system structure, which is broken down into sub-systems such as the fuel, flight control, hydraulics, auxiliary power, electrical, environmental control, and entertainment systems. Further sub-components identify individual components such as the flight control computers, hydraulic or electric actuators, instruments, avionics, air-conditioning, seats, batteries, wiring etc. To simplify the analysis, all sub-components and sub-systems are included within the major systems, furnishing, and equipment hierarchy.

System description	BDSF	BDVT
Fuel system	602	605
Flight Control system	1,204	1,210
Hydraulic/Pneumatic system	1,204	1,210
More electric actuation system	1,636	1,644
Auxiliary Power system	451	454
Electrical and Avionics systems	3,762	3,782
Environmental control systems	1,505	1,513
Cabin Furnishings	7,560	7,560

Table G-11: BDSF and BDVT systems and furnishings mass estimates [kg]

An important study into replacing conventional hydraulic and pneumatic systems with a ‘greener’ more-electric system has been investigated [ADC, 2006] using current technology release levels. At

present replacing the hydraulic and pneumatic systems with their electrical counterparts will provide environmental benefits, but the cost of doing so along with the system reliability and performance is a concern. The mass of the more electric solution is currently higher than a conventional hydraulic system.

	$(M_{Sys})_{hydraulic}$	$(M_{Sys})_{electic}$	Initial $(M_{Sys})_{calc}$
BDSF	16,069	16,501	13,904
BDVT	16,109	16,542	12,873

Table G-12: BDSF and BDVT total hydraulic and electric system and furnishing mass estimates [kg]

G.2.8 Operational Items Mass

Operational items mass is simply described as the equipment and facilities required for the aircraft to operate as a civil airliner, including items such as freight, safety equipment, emergency equipment i.e. life vests, water and food, crew and associated items/facilities, and can also include residual fuel, although this is sometimes assumed to be included with the propulsion systems mass. The operational items mass is a function of the number of passengers (P), crew (n_C), and operating items factor (F_{OP}), where F_{OP} = 12 for a medium range transport.

$$M_{OP} = 85n_C + F_{OP}P \text{ [kg]}$$

Equation G-17

The fuselage capacity was broken down into three viable configurations for possible airline operations, where a 3-class, 2-class, and single class seating arrangements were considered.

	3 class seating		*2 class seating*		*Single class seating*	
	P	n_C	P	n_C	P	n_C
Economy	175	5	245	7	287	8
Business	25	1	10	1	-	-
1st class	16	1	-	-	-	-
Total	**216**	**9**[3]	255	10^3	287	10^3

Table G-13: Number of passengers and flight attendants for varied internal class configurations

Where n_C represents the number of cabin crew required per passenger number (P) seated in the designated class areas. The greater the passenger number, the more cabin crew are required to control passenger evacuation in the event of an emergency, to satisfy the airline licensing authority, as described in [Jenkinson et al., 1999]. The operational items mass (M_{OP}) is the same for both BDSF and BDVT where M_{OP} = 3,357 kg.

3The total number of crew (n_C) includes the Pilot and Co-pilot, alongside the number of flight attendants required to control passengers in the event of an emergency, as listed in Table G-13.

G.2.9 Mass of Disposable Items

The disposable items mass are essentially the two main contributions to weight that will never be the same for two consecutive flights, which are the fuel mass, and the payload. The payload mass (M_{pay}) was one of the fist sets of data calculated at the beginning of the BD parametric design analysis, where the baggage requirement for 216 was established, as defined by the initial specification. The payload mass therefore remains as previously stated, where M_{pay} = 23,760kg.

The fuel mass (M_f) in this case is the mass of fuel required to perform the design mission, where M_f = 40,977 kg for the BDSF, and for the BDVT M_f = 36,329 kg. The total disposable items mass for the BDSF is therefore M_{disp} = 64,737kg, and M_{disp} = 60,089kg for the BDVT configuration.

G.2.10 BD Mass Summary

The total mass of each major component was analysed and compared for the BDSF and BDVT configurations, where introducing two alternate design constructions, one metallic and one composite layout has provided a mass target for each variant. A study into the replacement of hydraulic and pneumatic systems has been summarised, where an all-electric system replacement introduces mass penalties, but has a great potential for producing a 'greener' aircraft concept.

BD Configuration description		BDSF	BDVT
Empty Mass (*EM*)	metallic	82,406	87,846
	composite	76,336	80,502
Operational Empty Mass (*OEM*)	metallic	85,763	91,203
	composite	79,693	83,859
All Up Mass (*AUM*) - Hydraulic	metallic	150,500	151,292
	composite	144,430	143,948
AUM – All-Electric (*AE*)	metallic	150,381	151,725
	composite	144,862	144,200

Table G-14: BDSF and BDVT total mass summary and comparison [kg]

Table G-14 provides the final mass breakdown summary for both BDSF and BDVT with the material and more-electric vs. hydraulic variations compared. With considerations that the BD concept aircraft would be entering into service in 2025 and that the majority of airframe components can be manufactured using composites, a decision was made to use the composite mass predictions for developing the BD c.g. and stability models.

The all-electric concept considered to use electrical actuators, fly-by-light, and novel technology advancements to reduce airframe emissions and produce a 'greener' flight. The notion of producing a silent airframe design with the addition of 'green' technologies is the preferred route for the BD

concept, despite the increase in mass due to the all-electric systems. The increase in mass is due to the technologies being at an adolescent stage, where as the technology matures, systems will become lighter, and far superior to the pneumatic and hydraulic systems, and would reduce the mass of internal pipe-work, compensated of course by additional wiring looms.

The final two designs for the BDSF and BDVT to analyse for airframe noise are both designed to integrate an all-electric aircraft concept, combined with a composite airframe design to reduce overall vehicle mass.

G.3 BD Centre of Gravity (c.g.) and Stability Calculations

Major equipment and systems positioned across the BD airframe consisted of the main passenger cabin, flight deck, cargo hold, undercarriage, and propulsion systems. Three main fuel tanks are located within the wing, two tanks in the outboard wing sections, and one centrally located trim tank ahead of the wing aerodynamic centre.

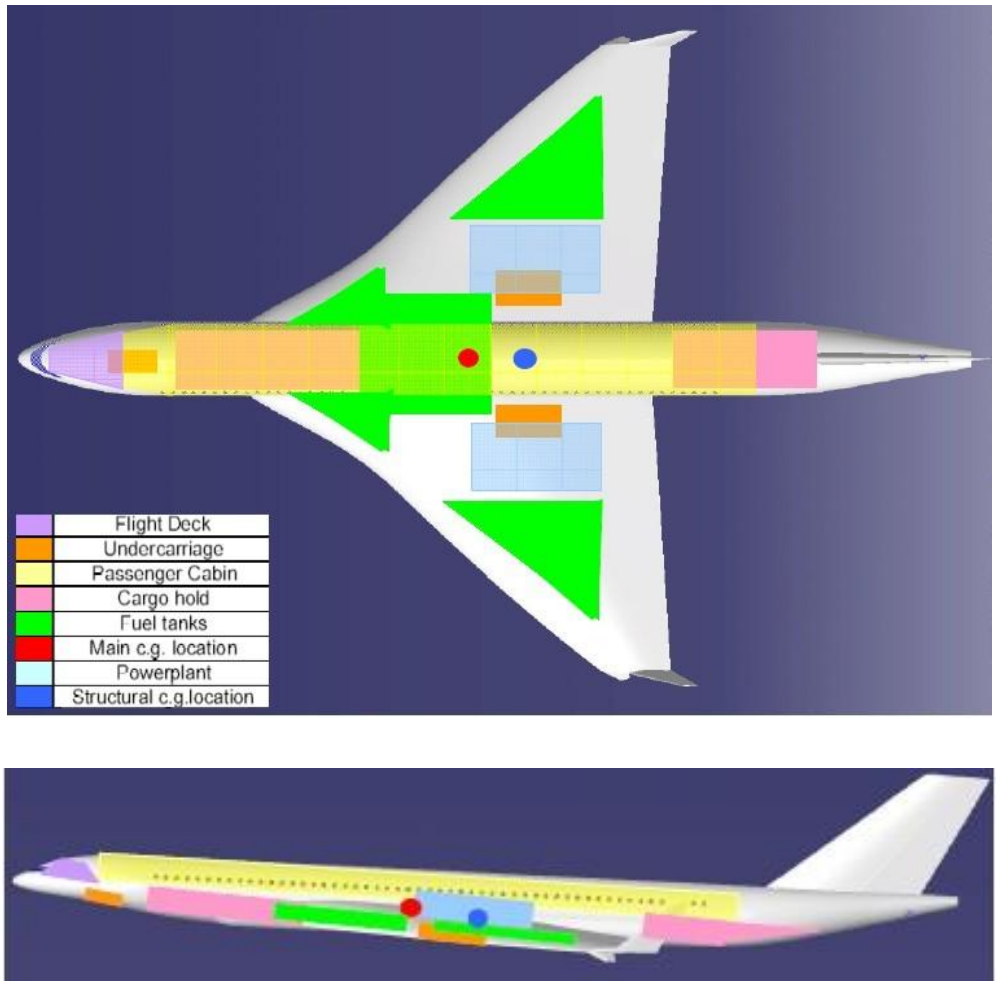

Fig G-2: BDSF Systems layout for initial c.g. and stability estimates

Fig G-2 represents a simplified layout for the BDSF configuration, where the aircraft is broken into four main groups for calculating the c.g.: structures, systems, operational items, and disposable items.

G.3.1 BDSF c.g. and Inertia Estimates

The BDSF major structural items for an all composite airframe were positioned along the geometry using the CAD model. Point mass estimates were used for each component to determine the overall structural c.g. estimate and the results summarised in Table G-15.

Structural components	*Mass* [kg]	$x_{c.g.}$ [m]	$y_{c.g.}$ [m]	$Z_{c.g.}$ [m]
Wing	25,307	29.52	0.00	-1.88
Fuselage	16,007	24.15	0.00	-0.25
Vertical tail	1,369	50.99	0.00	6.00
Winglets	484	34.03	0.00	-2.07
NLG	876	6.34	0.00	-2.66
MLG – port	2,482	28.42	4.76	-2.66
MLG – starboard	2,482	28.42	-4.76	-2.66
Total Structures	**49,006**	**27.88**	**0.00**	**-1.22**

Table G-15: BDSF Structural Mass [kg] and major component c.g. locations relative to the aircraft nose [m]

The BDSF major systems were similarly positioned to the structures, considering an all-electric (AE) actuation system, with complete removal of hydraulics. The AE system does not include the instrumentation (*IS*), or avionics (*AS*) devices. The total systems breakdown is shown in Table G-16.

Systems components	*Mass* [kg]	$x_{c.g.}$ [m]	$y_{c.g.}$ [m]	$z_{c.g.}$ [m]
Engine #1 – port	2,891	30.45	8.00	-1.38
Engine #2 – port	2,891	27.42	5.00	-1.38
Engine #3 – starboard	2,891	27.42	-5.00	-1.38
Engine #4 – starboard	2,891	30.45	-8.00	-1.38
Fuel system	602	22.27	0.00	-1.88
FCS & *AE* actuation	2,840	24.19	0.00	-2.18
Auxiliary power unit	452	50.99	0.00	0.68
Electrical, *IS*, & *AS*	3,763	16.38	0.00	-1.05
Airconditioning	984	28.41	0.00	-0.86
De-icing system	301	24.27	0.00	-1.88
Internal Furnishings	7,560	25.23	0.00	1.11
Total Systems	**28,065**	**25.92**	**0.00**	**-0.71**

Table G-16: BDSF Systems Mass [kg] and major component c.g. locations relative to the aircraft nose [m]

Operational Items	*Mass* [kg]	$x_{c.g.}$ [m]	$y_{c.g.}$ [m]	$z_{c.g.}$ [m]
Passengers + crew	**3,357**	**25.23**	**0.00**	**1.11**
Disposable Items				
Forward cargo bay	11,880	12.18	0.00	-1.27
Rear cargo bay	11,880	35.52	0.00	-0.98
Fuel tank #1 – port	16,391	32.14	11.91	-2.43
Fuel tank #2 – starboard	16,391	32.14	-11.91	-2.43
Fuel tank #3 – central	8,195	18.22	0.00	-1.66
Total Disposable	**64,737**	**27.34**	**0.00**	**-1.81**

Table G-17: BDSF Operational and Disposable items Mass [kg] and c.g. locations relative to aircraft nose [m]

The operational items and disposable items are shown in Table G-17, which were used along-side the structural and systems estimates to determine the overall mass, balance properties, and stability for the BDSF design.

A summary of the BDSF mass, c.g. locations, moments, inertias, and percentage of *MAC* for a series of cases are shown within Table G-18. These results are for a series of flight cases which provide a basic summary of how the c.g. location changes for the aircraft; investigating the change from take-off when there is full fuel (AUM), to cruise, and finally at a worse case scenario when the aircraft is diverted to another airport to land, and the mass is close to the operational empty mass (OEM), or zero fuel.

	AUM	***MLM***	***SoC***	***OEM***	***EM***
Mass [kg]	145,166	123,391	134,800	80,428	77,071
$x_{c.g.}$ [m]	27.2	27.16	27.18	27.09	27.09
$y_{c.g.}$ [m]	0.00	0.00	0.00	0.00	0.00
$z_{c.g.}$ [m]	-1.35	-1.21	-1.29	-0.946	-1.04
M_x [kg.m]	3.95×10^{6}	3.35×10^{6}	3.66×10^{6}	2.18×10^{6}	2.09×10^{6}
M_y [kg.m]	0.00×10^{0}	0.00×10^{0}	0.00×10^{0}	0.00×10^{0}	0.00×10^{0}
M_z [kg.m]	-1.96×10^{5}	-1.49×10^{5}	-1.74×10^{5}	-7.61×10^{4}	-7.98×10^{4}
I_{xx} [kg.m^2]	5.00×10^{3}	2.09×10^{2}	2.03×10^{3}	3.87×10^{3}	1.30×10^{3}
I_{yy} [kg.m^2]	5.21×10^{3}	2.09×10^{2}	2.09×10^{3}	4.28×10^{3}	1.31×10^{3}
I_{zz} [kg.m^2]	2.07×10^{2}	1.81×10^{-1}	6.43×10^{1}	4.06×10^{2}	8.05×10^{0}
I_{xy} [kg.m^2]	-1.02×10^{3}	-6.14×10^{0}	-3.61×10^{2}	-1.25×10^{3}	1.02×10^{2}
I_{xz} [kg.m^2]	-8.57×10^{-15}	3.51×10^{-15}	6.92×10^{-14}	1.24×10^{-13}	-1.87×10^{-14}
I_{yz} [kg.m^2]	-8.57×10^{-15}	3.51×10^{-15}	6.92×10^{-14}	1.24×10^{-13}	-1.87×10^{-14}
$x_{c.g.}/\ x_{MAC}$ [%]	21.9	27.2	21.8	21.2	21.7

Table G-18: BDSF Mass [kg], c.g. estimates [m], Moments [kgm], and Inertias [kgm^2] for vehicle flight conditions; AUM=All-Up Mass, MLM=Maximum Landing Mass, SoC=Start of Climb Mass, OEM=Operating Empty Mass, EM=Empty Mass.

Raymer [1992], Howe [2000], and [Jenkinson, 1999] suggest that a typical range for the mean aerodynamic chord (*MAC*) should vary between 15% and 35% *of MAC* through flight, where this requirement is satisfied for the BDSF with a range of 20.1% to 22.1%, despite being an unstable design.

The main challenge with the BDSF configuration is the static instability of the design, which will be calculated later on in this appendix, where an artificial control system is required to continuously balance and trim the aircraft throughout all flight cases. The two main flight critical cases are for the landing and take-off, where controllability at low speeds is critical for a civil airliner, and requires compliance with [EASA, 2006] certification requirements. At present there are no existing tailless civil aircraft transports, and to certify the first design would be a major achievement, but also a huge challenge. There are not just issues of compliance with the regulations to consider, but the major concerns are with flight control systems development and reliability for control of the aircraft, and more importantly passenger acceptance.

The author decided to investigate passenger perception on a random group of passengers waiting to travel from LHR. A discussion on the comparisons of pictures for the delta wing design compared to a current aircraft aimed to investigate opinions. The main first response was "*what's different*" because the design doesn't differ much from the current tube-and-wing airliner, so most of the general public were oblivious to the appearance of a conventional aircraft. It is not always the common responses that are critical, but the opinions of a few often with pessimistic opinions, can be critical in the downfall of advancing with new technologies. One of the most interesting comments/questions raised was that "*you usually see a wing like this on a fighter plane, and we normally see this on TV where it gets hit and goes down, explodes, etc … so do us passengers get ejector seats as well as the pilots?*". Despite raising a few eyebrows and being quite hilarious, if one person can think this, then others opinions may not be far off. Passenger acceptance is therefore considered to be equally critical as with the compliance of certification regulations.

G.3.2 BDVT c.g. & Inertia Estimates

The BDVT structural breakdown and c.g. locations were calculated in an identical manner to the BDSF, where an all composite airframe design was considered and the empennage mass and c.g. reflects the equivalent *V-tail* geometry. The results are summarised below in Table G-19.

The BDVT major systems and component breakdowns were positioned according to the CAD model, including a similar design assumption to the BDSF with an *AE* actuation system and removal of any hydraulic components. The systems breakdown and overall c.g. location is shown below in Table G-20.

Structural components	*Mass* [kg]	$x_{c.g.}$ [m]	$y_{c.g.}$ [m]	$Z_{c.g.}$ [m]
Wing	21,739	23.08	0.00	-1.88
Fuselage	16,641	23.08	0.00	-0.25
Vertical tail	7,155	50.99	0.00	6.00
Winglets	234	33.03	0.00	-2.07
NLG	876	6.01	0.00	-2.66
MLG – port	2,483	4.76	4.76	-2.66
MLG – starboard	2,483	-4.76	-4.76	-2.66
Total Structures	**51,612**	**27.14**	**0.00**	**-0.35**

Table G-19: BDVT Structural Mass [kg] and major component c.g. locations relative to the aircraft nose [m]

Operational and disposable items c.g. estimates are summarised in Table G-21 and are used to determine the overall mass and balance properties of the BDVT. An overall summary of the BDSF mass, c.g. locations, moments, inertias, percentage *MAC*, and static margin positions are summarised in Table G-22, where for the BDVT the same flight cases were investigated as the BDSF.

Systems components	*Mass* [kg]	$x_{c.g.}$ [m]	$y_{c.g.}$ [m]	$z_{c.g.}$ [m]
Engine #1 – port	3,057	31.75	6.67	0.38
Engine #2 – port	3,057	28.22	4.92	0.38
Engine #3 – starboard	3,057	28.22	-4.92	0.38
Engine #4 – starboard	3,057	31.75	-6.67	0.38
Fuel system	602	20.27	0.00	-1.88
FCS & *AE* actuation	2,841	22.19	0.00	-2.18
Auxiliary power unit	452	50.99	0.00	0.68
Electrical, *IS*, & *AS*	3,765	16.38	0.00	-1.05
Airconditioning	984	26.84	0.00	-0.86
De-icing system	301	24.25	0.00	-1.88
Internal Furnishings	7,560	23.08	0.00	1.11
Total Systems	**28,733**	**25.57**	**0.00**	**0.024**

Table G-20: BDVT Systems Mass [kg] and major component c.g. locations relative to the aircraft nose [m]

The BDVT is a statically stable design, and is due to the centre of lift being ahead of the centre of gravity, providing a positive pitching moment, which is accordingly balanced by the lift produced from the *V-tail*. The BDVT static margin range is between 3% and 6% for all flight cases. As the static margin increases to around 10% the handling of the aircraft becomes more difficult, so lower static margins in the region of 3-5% are desired for better handling, where these are ballpark figures suggested by pilots.

Operational Items	*Mass* [kg]	$x_{c.g.}$ [m]	$y_{c.g.}$ [m]	$z_{c.g.}$ [m]
Passengers + crew	3357	23.08	0.00	1.11
Disposable Items				
Forward cargo bay	11,880	12.18	0.00	-1.27
Rear cargo bay	11,880	35.52	0.00	-0.98
Fuel tank #1 – port	13,765	30.14	10.62	-2.43
Fuel tank #2 – starboard	13,765	30.14	-10.62	-2.43
Fuel tank #3 – central	8,364	18.22	0.00	-1.66
Total Disposable	**59,985**	**25.92**	**0.00**	**-1.82**

Table G-21: BDVT Operational and Disposable items Mass [kg] and c.g. locations relative to aircraft nose [m]

The challenges associated with certifying the BDVT are far less of a concern compared to the BDSF, where compliance of regulations and passenger acceptance are still considered, but not seen as a show-stopper and this is because there is a tail surface on the aircraft. The main benefit of the tail in this case is to provide natural stability to the aircraft configuration, and that provides a redundancy where if the flight control system fails, there could still be an manual over-ride, and the pilot would still have full control over the aircraft handling, compared to the tailless concept.

	AUM	***MLM***	***SoC***	***OEM***	***EM***
Mass [kg]	143,687	122,134	117,795	83,702	80,345
$x_{c.g.}$ [m]	26.22	26.29	26.31	26.44	26.58
$y_{c.g.}$ [m]	0.00	0.00	0.00	0.00	0.00
$z_{c.g.}$ [m]	-0.848	-0.617	-0.561	-0.164	-0.217
M_x [kg.m]	3.77×10^{6}	3.21×10^{6}	3.10×10^{6}	2.21×10^{6}	2.14×10^{6}
M_y [kg.m]	-3.64×10^{-12}	0.00×10^{0}	-7.28×10^{-12}	-3.64×10^{-12}	-3.64×10^{-12}
M_z [kg.m]	-1.22×10^{5}	-7.54×10^{4}	-6.60×10^{4}	-1.37×10^{4}	-1.75×10^{4}
I_{xx} [kg.m^2]	1.93×10^{4}	2.26×10^{3}	7.40×10^{2}	8.43×10^{3}	5.61×10^{3}
I_{yy} [kg.m^2]	2.23×10^{4}	3.00×10^{3}	1.19×10^{3}	8.87×10^{3}	9.23×10^{3}
I_{zz} [kg.m^2]	2.99×10^{3}	7.47×10^{2}	4.53×10^{2}	4.34×10^{2}	3.63×10^{3}
I_{xy} [kg.m^2]	-7.59×10^{3}	1.30×10^{3}	5.79×10^{2}	1.91×10^{3}	4.51×10^{3}
I_{xz} [kg.m^2]	-2.04×10^{-13}	-3.36×10^{-13}	1.94×10^{-13}	-5.00×10^{-14}	-1.73×10^{-13}
I_{yz} [kg.m^2]	-2.04×10^{-13}	-3.36×10^{-13}	1.94×10^{-13}	-5.00×10^{-14}	-1.73×10^{-13}
$x_{c.g.}/\ x_{MAC}$ [%]	31.7	32.4	32.4	33.5	34.7

Table G-22: BDVT Mass [kg], c.g. estimates [m], Moments [kgm], and Inertias [kgm^2] for vehicle flight conditions; AUM=All-Up Mass, MLM=Maximum Landing Mass, SoC=Start of Climb Mass, OEM=Operating Empty Mass, EM=Empty Mass.

Challenges with passenger acceptance would still be an issue with this configuration, but for different reasons, where the engines are mounted above the wings and are level with the passenger cabin. Although strategically placed to reduce noise on the ground, more methods are required to provide

internal cabin noise reduction, as the engine noise would be a nuisance for longer flights. This challenge is also a concern with the BDSF, as embedding the engines within long nacelle ducts does reduce the cabin noise, there will still be a higher noise from the engines compared with a conventional aircraft. Other than passenger noise, it is critical to address the issue of engine rotor burst and engine fires.

G.4 BD Mass, c.g., & Inertia Summary

The total mass was calculated for different BD design variants, where composite and metallic designs were investigated, and comparisons between hydraulic and all-electric (*AE*) actuation systems were considered. The selection of composite structures was made primarily to produce a lighter airframe design, so that a lower noise could be achieved, although metallic structures would provide a greener option, because metals can be recycled compared to the disposal concerns of composites structures [Hedlund-Astrom, Luttropp, 2006]. *AE* actuation was selected over the use of conventional hydraulics, where an all-electric aircraft would have environmental benefits of reducing emissions and the use of toxic hydraulic fluids within the aircraft, providing that technology advancements for electrical actuation develops in the next 15 years.

The final two designs are an all composite airframe construction with integrated AE systems designed to increase the efficiency of the aircraft and reduce vehicle mass. The mass breakdown, inertias, and centre of gravity for both BDVT and BDSF configurations has been identified, where both designs are associated with challenges; certification being the major concern for the tailless design, and cabin noise for the BDVT.

G.5 BD Control Surface Devices

The BD configuration, like all conventional aircraft requires a number of control surfaces to carry out manoeuvres, providing a crucial means to maintaining lateral and longitudinal stability. Control surfaces are used primarily to control the aircraft in pitch, roll, and yaw, where in many flight cases these are coupled for example sustaining a banked turn, and are sized accordingly. There are two main flight critical cases considered for the sizing the majority of control surfaces, the first was low speed manoeuvrability, and the second investigated gust cases. Additional loading cases were considered but unlike military aircraft where high ‘g’ combat manoeuvres at high speed dominate control requirements, civil aircraft manoeuvrability is restricted to limit uncomfortably high ‘g’ loading on the passengers.

G.5.1 BDVT Control Devices

The configuration of the BDVT provides a control surface layout which is very similar to the baseline aircraft design. The main wing has *LE* and *TE* high lift devices, ailerons, spoilers, and the *V-tail* has an elevator and rudder combined into a single surface, referred to as the ruddervators.

The main wing requires the use of high lift devices, such as *TE* flaps ad *LE* slats to increase the maximum wing lift coefficient at low speeds. The type of *TE* device selected is two variable camber (*VC*) flaps[4] per wing positioned inboard behind the engines [Fielding, 2000], with a similar selection of *LE* device of two almost complete span *VC* or drooped *LE* sections [Lajux, 2007]. The outboard *TE* region houses two ailerons per wing to provide asymmetric roll control and the inboard sections can be used symmetrically to enhance the flap effectiveness at low speed. Each outboard wing section is equipped with two conventional spoilers/air brakes. The complete trailing edge of the wing has fibres extending out, known as *TE* brushes, aimed to reduce the wing and control surface noise and reduce vortex shedding noise [Herr, 2007].

The empennage layout for a *V-tail* combines an elevator for trim and pitch control with a rudder for directional (yaw) control. The merger of horizontal and vertical tails to produce a *V-tail* is more often observed on military aircraft, where coupling the pitch and yaw controls, is effective for manoeuvrability and for low radar signature (stealth). There are no such requirements for civil transport aircraft, where this tail solution was primarily selected to reduce airframe noise directly below the aircraft.

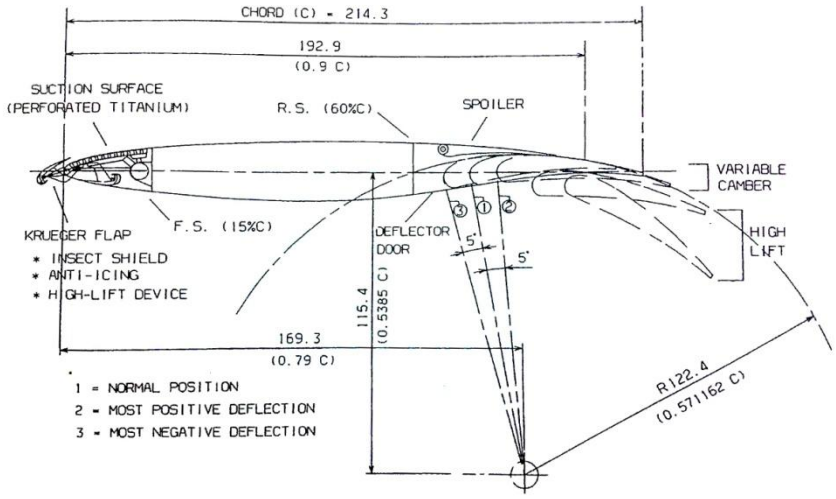

Fig G-3: Variable Camber flap Schematic, courtesy of [Fielding, 2000]

4 Variable camber flaps are concealed flaps that extend and arc outwards, running on tracks within the wing. The advantage of using variable camber flaps is that there are no slots, so that sufficient lift and drag is generated without turbulent flows through slot vanes generating noise.

G.5.2 BDVT Control Devices

The BDSF control surface layout provides an alternate solution which strays from the baseline aircraft and BDVT configuration described above. The main wing has *LE* high lift devices, *TE* ailerons and elevons, and outboard spoilers. The absence of a horizontal tail surface transforms the role of *TE* devices, and the vertical tail is a conventional design for directional yaw control using a rudder.

The main wing requires the use of *LE* high lift devices, namely a full-span *VC LE*, to increase the maximum wing lift coefficient at low speeds. *TE* devices are used to increase wing lift, but are coupled with the use of the elevator to keep the aircraft at a trimmed or stable state. The absence of a tail surface modifies the *TE* device usage by combining ailerons and elevators to be used simultaneously, both symmetrically and asymmetrically for pitch and roll control, referred to as elevons. Similar to the BDVT, *TE* brushes are once again implemented to reduce noise and each outboard wing section is equipped with two conventional spoilers/air brakes; one upper and one lower per wing to avoid nasty pitch up or uncontrollable loads, which is critical for the tailless design.

G.5.3 BD Control Surface Summary

Both BDSF and BDVT have many similarities, and yet many differences when stability and control is considered. The more naturally stable BDVT provides a reduced risk design solution that could be integrated alongside the existing fleet of airliners. Challenges that are associated with certifying a tailless civil passenger airline could be a major draw-back where aircraft controllability and reliability rely solely on the capabilities of the aircraft flight control system; so the BDSF faces many compliance concerns with regards to certification regulations. A summary of the devices used for the BDVT and BDSF to control the aircraft configurations in pitch, roll, and yaw are provided in Table G-23 below, where an overview of the control surface areas are compared to the wing and tail(s).

Control Surface	No.of devices	*BDSF*	*BDVT*
Aileron	2	11.7	11.3
TE VC Flap	2	-	36.0
VC LE	1	28.5	27.6
Spoiler	2	15.9	15.4
Rudder/Ruddervator	1	44.8	45.4
Elevon	1	33.6	-
Wing (S)	1	531.5	397.1
Vertical/*V-tail* (S_T)	1	87.1	78.4

Table G-23: BDSF and BDVT control surface areas for port wing only (double for total aircraft), all results in [m^2]

The ailerons and elevons for the BDSF were split into two segments along the wing, both with inboard and outboard sections totalling to four control surfaces on each wing, where the chord lengths were 11% with respect to the local wing chord. A similar arrangement of four control surfaces on the

TE was used for the BDVT, where the ailerons and *VCF TE* devices were designed with a 20% wing local chord length. The BDSF rudder is assumed to be 37% of the fin local chord, with a span of 90% of the fin height. The BDVT ruddervators consist of two control surfaces with 22% local chord of the *V-tail* sections acting across 90% of the tail span.

The final control surface layout has been identified, where the total mass, c.g., stability, and control estimates can be combined to summarise the overall vehicle performance for the BDSF and BDVT configurations. The main comparison is the noise of each design solution, where an interesting trade-off will be to see the effect on noise from an additional tail surface for the *V-tail* compared to the tailless BD, and shall be described within **Chapter 6**.

G.6 BD Stability Calculations

The BD control surfaces have been identified so that manoeuvring the aircraft would be possible, to ensure that the control surfaces are correctly located and sized, the lateral and longitudinal stability must be assessed. The critical case for control is considered to be the longitudinal stability, both static and dynamic, where lateral effects are not a concern because the BD concepts are fairly conventional and symmetrical about the centre-line.

The following section analyses the static and dynamic behaviour of the BD configurations, where a comparison is set not only between the BDSF and the BDVT, but also alongside the baseline, to establish a reality check for the calculations used.

G.6.1 BDVT Stability Calculations

The stability of the BDVT was established using a combination of modified longitudinal static trim and stability equations from Howe [2000], Raymer [1992], the Roskam, volumes VI and VII, [1987] and the ESDU data sheet methods, combined with results output from the AVL analysis. The aim of this procedure was to define the cruise trim, take-off rotation, and stability margins for the BDVT, where th results of the AVL analysis used are shown within Appendix H.

The fundamental equations to determine the aircraft static and dynamic stability for only the cruise flight condition were obtained from Howe [2000] and are described below, with references made to other sources for specific detailed analysis. The stick fixed static margin (K_n) is defined by:

$$K_n = \frac{l_H \cdot S_T}{c \cdot S \cdot G} \cdot \left[\frac{a_{1T}}{a_1} \cdot \left(1 - \frac{d\varepsilon}{d\alpha} \right) \right] - \left(h + H_0 \right)$$

Equation G-18

The following lengths are all measured aft of the leading edge of the mean aerodynamic chord, where 'l_H' is the length of the moment arm of the tail, 'h' is the centre of gravity position, and 'H_0' is the location of the mean aerodynamic centre. The term 'a_{1T}' is the horizontal surface lift curve slope due to incidence, 'a_1' is the wing-body lift curve slope, $\frac{d\varepsilon}{d\alpha}$ is the elevator lift curve slope, and 'G' is short-hand form for the following equation:

$$G = \left[1 + \frac{a_{1T}}{a_1} \cdot \frac{S_T}{S}\left(1 - \frac{d\varepsilon}{d\alpha}\right)\right]$$

Equation G-19

AVL was used to determine the control surface parameters above, including the lift curve slopes and the location of the mean aerodynamic centre. These results were then used to calculate the stick fixed static stability for the baseline aircraft and the BDVT. The stick free static stability was calculated using the same methodology as above, where for this instance the terms G, a_{1T}, and K_n are now replaced with $\bar{G}$, $\overline{a_{1T}}$, and Kn, where the only two terms that change within Equation G-18 above are:

$$\overline{a_{1T}} = a_{1T} + a_2\left(\frac{b_1}{b_2}\right)$$

Equation G-20

$$\bar{G} = \left[1 + \frac{\overline{a_{1T}}}{a_1} \cdot \frac{S_T}{S} \cdot \left(1 - \frac{d\varepsilon}{d\alpha}\right)\right]$$

Equation G-21

Where the equation for static stability stick free is given by:

$$K'_n = \frac{l_H \cdot S_T}{c \cdot S \cdot \bar{G}}\left[\frac{\overline{a_{1T}}}{a_1} \cdot \left(1 - \frac{d\varepsilon}{d\alpha}\right)\right] - (h + H_0)$$

Equation G-22

The horizontal surface lift curve slope due to deflection (a_2), found in Equation G-20 was calculated by rearranging the trim equation (Equation G-23) and using the inputs from the AVL analysis.

$$a_2 = \frac{1}{\eta}\left[\frac{c\left\{G\left[\frac{T z_T}{c} + qSC_{M0}\right] + Mg(h - H_0)\right\}}{qS_T l_H} - \left(\frac{Mg a_{1T}}{qSa_1}\left(1 - \frac{d\varepsilon}{d\alpha}\right)\right) - a_{1T}(\alpha_T - \alpha_W)\right]$$

Equation G-23

The author investigated alternate methods to calculate the elevator hinge moment coefficients due to incidence *(b_1)* and deflection *(b_2)* by using the following ESDU data items: 89009, 70011, AERO-W.01.01.05, AERO-C.01.01.03, AERO-C.04.01.01, AERO-C.04.01.02, AERO-C.04.01.04.

In order to determine the take-off rotation, the elevator angle required to rotate the aircraft during take-off, *'η'* is calculated by:

$$\eta_{TO} = \frac{1}{a_2} \cdot \left[\frac{\left\{ \frac{T z_T}{c} - qS\left(C_{M0} - \alpha_W (H_G - H_0)\right) \right\} + Mg\left\{ H_G + h + \frac{0.1 k_B^2}{l'_H c} \right\}}{qS_T \left(H_G - \frac{l'_H}{c} \right)} - a_{1T} \cdot \left(\alpha_T + \alpha_W \cdot \frac{d\varepsilon}{d\alpha} \right) \right]$$

Equation G-24

Where in this case, the thrust (T), engine thrust line (z_T), position of the last main landing gear wheel relative the leading edge of the aerodynamic chord (H_G), and the pitch radius of gyration (k_B) is required, along with the wing and the tail incidence angles (α_W, α_T) relative to the aircraft body. The radii of gyration were estimated using Raymer [1992], where for a conventional transport aircraft typical values were extracted from the text as shown below in Table G-24.

Aircraft type	$\overline{R_x}$ (k_B)	$\overline{R_y}$	$\overline{R_z}$
Fuselage mounted Engines	0.24	0.36	0.44
2 Wing mounted Engines	0.25	0.38	0.46
4 Wing mounted Engines	0.31	0.33	0.45

Table G-24: Radii of gyration (k_B) values extracted from Raymer [1992].

The dynamic stability behaviour of the BDVT was also investigated at a top level, where the short period and phugoid motions were assessed. The short period dynamic stability is calculated by determining the short period frequency *(ω_{SP})* and damping ratio *(ζ_{SP})* for the vehicle, where the damping ratio is:

$$\zeta_{SP} = \frac{\left[\frac{a_1}{4} + \frac{a_{1T}}{4} \left(\frac{l_n}{k_B} \right)^2 \left(1 + \frac{d\varepsilon}{d\alpha} \right) \frac{S_T}{S} \right]}{\left[\frac{M a_1 c}{2\rho S k_B^2} \left\{ (H_0 - h) + \left[\frac{a_{1T} l_H}{G a_1 c} \left(1 - \frac{d\varepsilon}{d\alpha} \right) + \frac{\rho S a_{1T} l_H^2}{2Mc} - \rho \frac{l_H^2}{c} \frac{S^2}{S_T} m_{\dot{\theta}} \right] \left(\frac{S_T}{S} \right) \right\} \right]^{\frac{1}{2}}}$$

Equation G-25

And the short period frequency is given by:

$$\omega_{SP} = \rho \left(\frac{SV}{2\pi M} \right) \left[\frac{M a_1 c}{2\rho S k_B^2} \left\{ (H_0 - h) + \left[\frac{a_{1T} l_H}{G a_1 c} \left(1 - \frac{d\varepsilon}{d\alpha} \right) + \frac{\rho S a_{1T} l_H^2}{2Mc} - \rho \frac{l_H^2}{c} \frac{S^2}{S_T} m_{\dot{\theta}} \right] \left(\frac{S_T}{S} \right) \right\} \right]^{\frac{1}{2}}$$

Equation G-26

The above equations use most of the parameters identified, except for the derivative of pitching moment of the wing body due to the pitch velocity ($m_{\dot{\theta}}$), where this was obtained using Roskam [1987], part VI and part VII, and part I of 'airplane flight dynamics'. This is using the following approximation, where the term ($C_{m_{\dot{\theta}}}$), is the pitching moment coefficient due to pitch velocity:

$$m_{\dot{\theta}} = \frac{qSc^2 C_{m_{\dot{\theta}}}}{2I_{yy}V}$$

Equation G-27

The phugoid motion is the second dynamic stability behaviour investigated, which is calculated by determining the frequency *(ω_L)* and damping ratio *(ζ_L)* for the vehicle, where the damping ratio is:

$$\zeta_L = F_1 C_{D0} + F_2 C_L^2$$

Equation G-28

And the phugoid frequency is given by:

$$\omega_L = \frac{Mc}{2SK_B^2} \cdot \frac{a_{1T}}{2} \cdot k_n$$

Equation G-29

Where the two functions F_1 and F_2 are considered to be a function of the dynamic viscosity *(v)*, as shown by the following equations:

$$F_1 = 0.5 + \frac{\omega_L}{2(2\omega_L + a_1 v)}$$

Equation G-30

$$F_2 = \left[\frac{3\omega_L - a_1 v}{4\omega_L + 2a_{1T} v}\right]\left(\frac{C_{D0} - C_D}{C_L^2}\right) - \frac{a_1}{2}\frac{\left\{\omega_L - v^2\left\{1 + \frac{d\varepsilon}{d\alpha}\right\}\right\}}{(2\omega_L + a_1 v)^2}$$

Equation G-31

$$v = \frac{a_1}{2} \cdot \frac{S_T}{S} \cdot \left(\frac{l_H}{k_B}\right)^2$$

Equation G-32

This basic analysis for the BDVT behaviour under static and dynamic motion have been identified and applied within the conceptual design code. This analysis is also applicable to the baseline aircraft, where the configuration is similar to the baseline with a main wing and horizontal empennage for trim and control. The main difficulty is the comparison of these two configurations with the

BDSF, and how the analysis of the tailless vehicle compares to the static and dynamic behaviour of the two tailed variants.

G.6.2 BDSF Stability Calculations

[Howe 2000] describes that for a tailless vehicle, the absence of a tail surfaces implies a need to reorganise the basic trim equations used for a tailed vehicle (Equation G-23), such as the BDVT and baseline. It is assumed that longitudinal control is provided by an elevon at the trailing edge of the wing, where this device combines the functions of a traditional aileron and an elevator. The elevator has a lift curve slope (a_2), for a specified wing area, and supplies an increment in lift located at a distance $l_\eta^{'}$, aft of the LE of the mean aerodynamic chord. Howe suggests that the downwash effect described in the calculations for the BDVT is not relevant and that a_{1T} is zero.

$$l_T = \frac{l_\eta}{c}$$

Equation G-33

$$l_\eta = l_\eta^{'} - h \cdot c$$

Equation G-34

Where the trim equation now becomes:

$$a_2 = \frac{c}{\eta \cdot l_\eta}\left[\frac{\left(\frac{Tz_T}{c} + qSC_{M0}\right) + Mg\left(h - H_0\right)}{qS} - \left(h - H_0\right)\right]$$

Equation G-35

The static stick fixed stability can easily be determined for the tailless vehicle as being:

$$K_\eta = \left(H_0 - h\right)$$

Equation G-36

The stick free stability is calculated using:

$$K'_{\eta} = (H_0 - h) + \frac{l_{\eta}}{c} \cdot \frac{\overline{a_{1T}}}{a_1}$$

Equation G-37

Since $a_{1T} = 0$, Equation G-20 now becomes:

$$\overline{a_{1T}} = a_2 \cdot \left(\frac{b_1}{b_2} \right)$$

Equation G-38

The take-off rotation angle can therefore be defined as with the BDVT, but for the tailless BDSF, Equation G-24 now becomes:

$$\eta_{TO} = \left[C_{M0} - \frac{Th_T}{qSc} - a_1 \alpha_W (H_G - h) - \frac{Mg}{qS} \left(H_G - h + \frac{0.1 k_B^2}{l'_{\eta}} \right) \right] \cdot \frac{1}{a_2 \left[H_G - \frac{l'_{\eta}}{c} \right]}$$

Equation G-39

The dynamic stability equations also change with the tailless concept, where the following equations represent the short period and the phugoid characteristics, where Equation G-25 now becomes:

$$\zeta_{SP} = \frac{\left[\frac{a_1}{4} - \left(\frac{l_n}{k_B} \right)^2 \left(\frac{m_{\dot{\theta}}}{2} \right) \right]}{\left[\frac{M a_1 c}{2 \rho S k_B^2} \left\{ (H_0 - h) - \rho \frac{S l'_{\eta}}{c} m_{\dot{\theta}} \right\} \right]^{\frac{1}{2}}}$$

Equation G-40

Equation G-26 is now:

$$\omega_{SP} = \frac{\rho S V}{2 \pi M} \cdot \left[\frac{M a_1 c}{2 \rho S k_B^2} \left\{ (H_0 - h) - \rho \frac{S l'_{\eta}}{c} m_{\dot{\theta}} \right\} \right]^{\frac{1}{2}}$$

Equation G-41

Equation G-27 remains unchanged for the short period calculations.

The dynamic phugoid motion equations remain unchanged for Equation G-28 and Equation G-30, however Equation G-29 now changes to:

$$\omega_L = \frac{Mc}{\rho S k_B^2} \cdot \frac{a_1}{2} \cdot (H_0 - h)$$

Equation G-42

And Equation G-31 becomes:

$$F_2 = \left[\frac{3\omega_L - a_1 v}{4\omega_L + 2a_1 v}\right]\left(\frac{C_{D0} - C_D}{C_L^2}\right) - \frac{a_1}{2}\frac{(\omega_L - v)}{(2\omega_L + a_1 v)^2}$$

Equation G-43

And Equation G-32 becomes:

$$v = \left(\frac{l_\eta}{k_B}\right)^2 \cdot m_{\dot{\theta}}$$

Equation G-44

G.6.3 BD Stability Comparisons

The equations listed above represent the methodology used to calculate the stability of the baseline, BDVT, and the BDSF aircraft concepts. The process has shown that the stability calculations are not as straight forward as possible, because without the AVL results, there would have been a number of assumptions leading to incorrect stability results. Having been said, one should not disregard the fact that the AVL analysis or running of the vortex lattice code did not produce errors; errors which could be transferred into the calculations listed above creating unrealistic results. Therefore the reader is advised to use caution with these results and to follow the empirical calculations wherever possible.

In order to provide a comparison between the three aircraft concepts, the stability results for both static and dynamic behaviours are tabulated along with the main calculated parameters investigated by the analysis documented above. These results are combined with the take-off rotation angles required to rotate the aircraft on the runway and produce enough lift to allow the aircraft to be airborne.

The static margin (K_n,K_η) represents the degree of static stability of the concept, where a suitable range is usually between 3% and 5% according to [Howe, 2000] and [Raymer, 1992]. The BDSF is statically unstable shown by a negative static margin of -3.88% of the mean aerodynamic chord; where the centre of lift acts ahead of the centre of gravity, causing a nose up moment (-ve pitching moment) about the c.g.. Elevon deflection is required to balance the aircraft and provide a zero pitching moment for a trimmed flight, where the LE carving used on the airfoil design provides a positive pitching moment and assists by reducing the elevon deflection angle required to trim, where a smaller elevon deflection reduces trim drag. A similar principal applies to the BDVT design, where for this case the additional lift and the LE pushes forward the centre of lift on the wing, reduces the

lifting moment, and is located behind the centre of gravity. The BDVT configuration helps generate a nose down (positive) pitching moment, and hence a statically stable aircraft concept, as with the *N-T* baseline.

Table G-25 represents the characteristic described above:

Parameter	Baseline	BDVT	BDSF
C_{M0}	0.0578	0.0578	-0.0861
η_{Trim}	2.187	2.06 deg	-6.56 deg
$\frac{d\varepsilon}{d\alpha}$	0.050	0.0253	-0.0201
a_1	7.81	6.51	6.51
a_2	1.20	0.319	0.399
a_{1T}	0.00489	0.00439	-
$\overline{a_{1T}}$	1.92	0.438	0.543
G	1.00	1.00	-
$\bar{G}$	1.06	1.03	-
K_n, K_η	6.20%	4.45%	-3.88%
K'_n, K'_η	18.2%	10.7%	14.3%
k_B	0.250	0.310	0.31
η_{TO}	15.0 deg	3.93 deg	-6.07 deg
$m_{\dot{\theta}}$	$-9.57\text{x}10^{-10}$	$-1.26\text{x}10^{-9}$	$8.2\text{ax}10^{-6}$
$c_{m_{\dot{\theta}}}$	-5.65	-4.35	38567.9
ω_{SP}	5.84 Hz	5.66 Hz	2.79 Hz
ζ_{SP}	0.021	0.047	0.032
t_2	30.6 sec	13.4 sec	9.74 sec
C_D	0.0174	0.0146	0.0133
C_{D0}	0.0147	0.00856	0.00909
C_L	0.271	0.338	0.243
v	1.08	0.794	0.0170
F_1	0.573	0.517	0.751
F_2	0.0247	0.203	3.45
ζ_L	0.0102	0.0276	0.210
ω_L	1.73 Hz	1.84 Hz	10.2 Hz

Table G-25: Comparison of stability data calculated for each concept.

A study to investigate and compare the short period mode on each configuration was considered, where if an oscillation was induced, perhaps by a gust, what response time would there be for each aircraft to either diverge or converge. The short period mode time to double amplitude (t_2) was therefore considered and is also shown in Table G-25. This shows that as the aircraft configuration changes from the baseline to the BDVT, the time to double amplitude is decreased by almost half, and

the further reduced for the BDSF. This indicates that the tailless aircraft could be a challenge to control under gust conditions and that an artificial flight control system is a necessity for the functionality of this configuration. The BDVT is not as bad as the BDSF, but never-the-less the time to double amplitude is still below half that of the baseline, and an artificial control system should be fed into the design architecture for the stability and control laws for the delta wing concept.

Appendix H Broad Delta Airframe Analysis using *AVL*

H.1 Background

An intermediate analysis using a vortex lattice code 'Athena Vortex Lattice' (*AVL)* [Drela, 2007] was implemented to visualise the properties of the wing lifting surfaces less engines. This Appendix contains input files and *AVL* results for the BDSF and BDVT analyses. The vortex panel method is limited in modelling lift of *LE* devices and surface thicknesses, but provided results for the fuselage section where a comparison with a conventional fuselage, enabled the lift increase from the *LE* nose carving to be quantified. Two main flight cases are considered where cruise, and a low speed case is assumed, representing both the landing and take-off wing and high-lift control surface settings.

The *AVL* results are provided as a guide for the BDSF lifting properties, with further investigations required to use *CFD* for engine-wing interactions studies, and to investigate the effect of a *VC LE.*

H.2 BDSF AVL Anlaysis

H.2.1 BDSF Input AVL file

```
AVPlanform
0.800               !  Mach
0    0    0.0      !  iYsym  iZsym  Zsym
509.02   11.10   45.85      !  Sref   Cref   Bref   reference area, chord, span
27.162   0.0   -1.165      !  Xref   Yref   Zref   moment reference location (arb.)
0.020               !  CDp
#
#============================================================
#
SURFACE
Wing
10  1.0  22  1.0   ! Nchord   Cspace   Nspan  Sspace
#
# reflect image wing about y=0 plane
YDUPLICATE
    0.00000
#
# twist angle bias for whole surface
ANGLE
    0.00000
#
SCALE
  1.0   1.0   1.0
#
# x,y,z bias for whole surface
TRANSLATE
   10.849199     0.00000     -1.88
#
#------------------------------------------------------------
#   Xle         Yle         Zle         chord       angle   Nspan  Sspace
SECTION
    0.0         0.0         0.0         27.214      0.000   9     -0.75

AFIL
BD1-63A-0(10.5)A-Mod34.dat
```

```
#Cname   Cgain  Xhinge  HingeVec      SgnDup
CONTROL
camber   1.0    0.70    0.0 1.0 0.0     1.0

CONTROL
elevon     1.0   0.70     0.0 1.0 0.0     1.0
#------------------------------
SECTION
   14.18289     8.38723     -0.694269       13.241309       0.000   7     -1.25

AFIL
BD2-63A-0(10.5)A-Mod34.dat

CONTROL
camber   1.0    0.70    0.0 1.0 0.0    1.0

CONTROL
elevon     1.0    0.7     0.0 1.0 0.0    1.0
#------------------------------
SECTION
   21.257631    17.89723       -1.170379     6.93518      0.000   5     -1.25

AFIL
BD3-63A-009A.dat

CONTROL
camber   1.0    0.70    0.0 1.0 0.11    1.0

CONTROL
elevon     0.3   0.70     0.0 1.0 0.0   -1.0
#------------------------------
SECTION
   24.468    22.92723      -1.330143      4.000      0.000   5     -1.25

AFIL
BD4-63A-010A.dat

CONTROL
camber   1.0    0.70    0.0 1.0 0.11    1.0

CONTROL
aileron  -1.0   0.70    0.0 1.0 0.11   -1.0
#
#============================================================
#
SURFACE
Vertical Stabilisor
8  1.0  14  0.75  ! Nchord   Cspace
#
# x,y,z bias for whole surface
TRANSLATE
  42.540757     0.00000     1.00
#-------------------------------------------------------------
#    Xle         Yle         Zle         chord       angle   Nspan  Sspace
SECTION
  0.0         0.0         0.0         8.714094      0.000     4      1.50

AFIL
SC2-0010hs.dat

CONTROL
rudder    1.0    0.40    0.0 0.0 1.0
#------------------------------
SECTION
  9.553453  0.0     9.149519        4.357047      0.000     6     -1.50

AFIL
SC2-0010hs.dat

CONTROL
rudder    1.0    0.40    0.0 0.0 1.0
#
#============================================================
#
SURFACE
Upper Winglet
4  1.0  5  1.0   ! Nchord   Cspace   Nspan  Sspace
#
# reflect image wing about y=0 plane
YDUPLICATE
```

```
    0.00000
#
# twist angle bias for whole surface
ANGLE
    -4.00000
#
SCALE
  1.0   1.0   1.0
#
# x,y,z bias for whole surface
TRANSLATE
    36.720    22.927         -3.210143
#
#------------------------------------------------------------
#    Xle         Yle         Zle         chord       angle   Nspan  Sspace
SECTION
    0            0         0         2.6      0.000   9     -0.75

AFIL
BD4-63A-010A.dat

#-----------------------------
SECTION
  3.063331    0.847232         3.793222         0.84      0.000   9     -0.75

AFIL
BD4-63A-010A.dat
#
#============================================================
#
SURFACE
lower Winglet
2  1.0  4  1.0   ! Nchord   Cspace   Nspan  Sspace
#
# reflect image wing about y=0 plane
YDUPLICATE
    0.00000
#
# twist angle bias for whole surface
ANGLE
    0.00000
#
SCALE
  1.0   1.0   1.0
#
# x,y,z bias for whole surface
TRANSLATE
    35.317597     22.927     -3.210143
#
#------------------------------------------------------------
#    Xle         Yle         Zle         chord       angle   Nspan  Sspace
SECTION
    0      0         0         1.6      -7.000   9     -0.75

AFIL
BD4-63A-010A.dat

#-----------------------------
SECTION
  1.110467    0.659175         -0.90         0.64      -11.000   9     -0.75

AFIL
BD4-63A-010A.dat
#
#============================================================
#

BODY
fuselage
37  1
#
TRANSLATE
   0.00000     0.00000     0.00000
#
BFIL
fusemodAVPB767.dat

#============================================================
```

H.2.2 BDSF Primary Run Case and Results for Cruise

```
---------------------------------------------
Run case  1:  - Mach 0.8 Cruise @ 38000ft -

 alpha        ->  CL          =  0.2423148
 beta         ->  beta        =  0.00000
 pb/2V        ->  pb/2V       =  0.00000
 qc/2V        ->  qc/2V       =  0.00000
 rb/2V        ->  rb/2V       =  0.00000
 camber       ->  camber      =  0.00000
 elevon       ->  Cm pitchmom =  0.00000
 aileron      ->  aileron     =  0.00000
 rudder       ->  rudder      =  0.00000

 alpha     =  0.00000
 beta      =  0.00000
 pb/2V     =  0.00000
 qc/2V     =  0.00000
 rb/2V     =  0.00000
 CL        =  0.00000
 CDo       =  0.009079E+00
 bank      =  0.00000
 elevation =  0.00000
 heading   =  0.00000
 Mach      =  0.802
 velocity  =  236.6444
 density   =  0.33100
 grav.acc. =  9.81000
 turn_rad. =  0.00000
 load_fac. =  0.00000
 X_cg      =  27.184
 Y_cg      =  0.00000
 Z_cg      =  -1.288
 mass      =  134800.
 Ixx       =  2.03000E+03
 Iyy       =  2.09000E+03
 Izz       =  6.43000E+01
 Ixy       =  -3.6100E+02
 Iyz       =  6.92000E-14
 Izx       =  6.92000E-14
 visc CL_a =  0.00000
 visc CL_u =  0.00000
 visc CM_a =  0.00000
 visc CM_u =  0.00000
```

H.2.2.1 BD Initial Results for primary cruise case

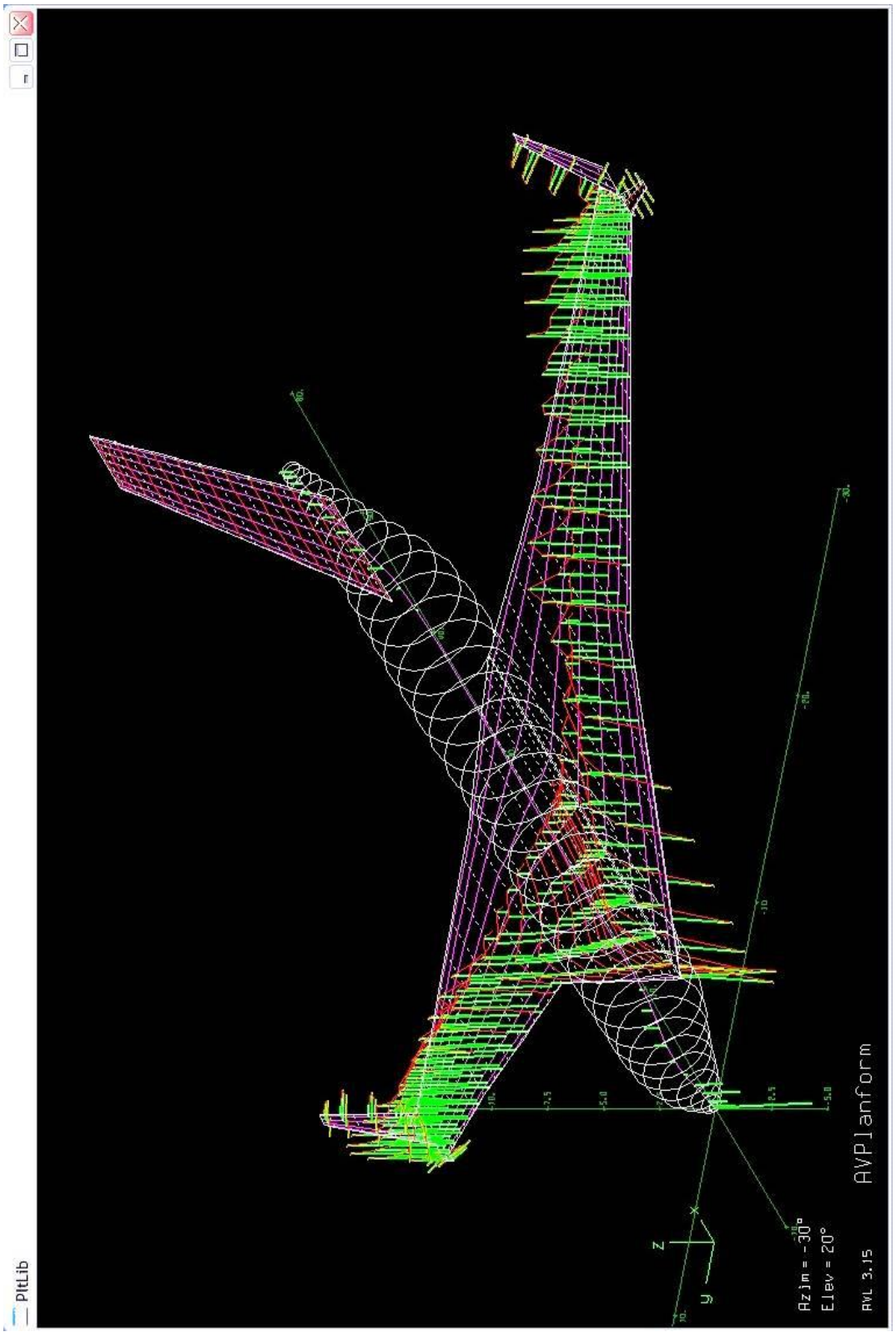

Fig H-1: BDSF Geometry for flight case of Mach 0.8 with cruise @ 38,000 ft

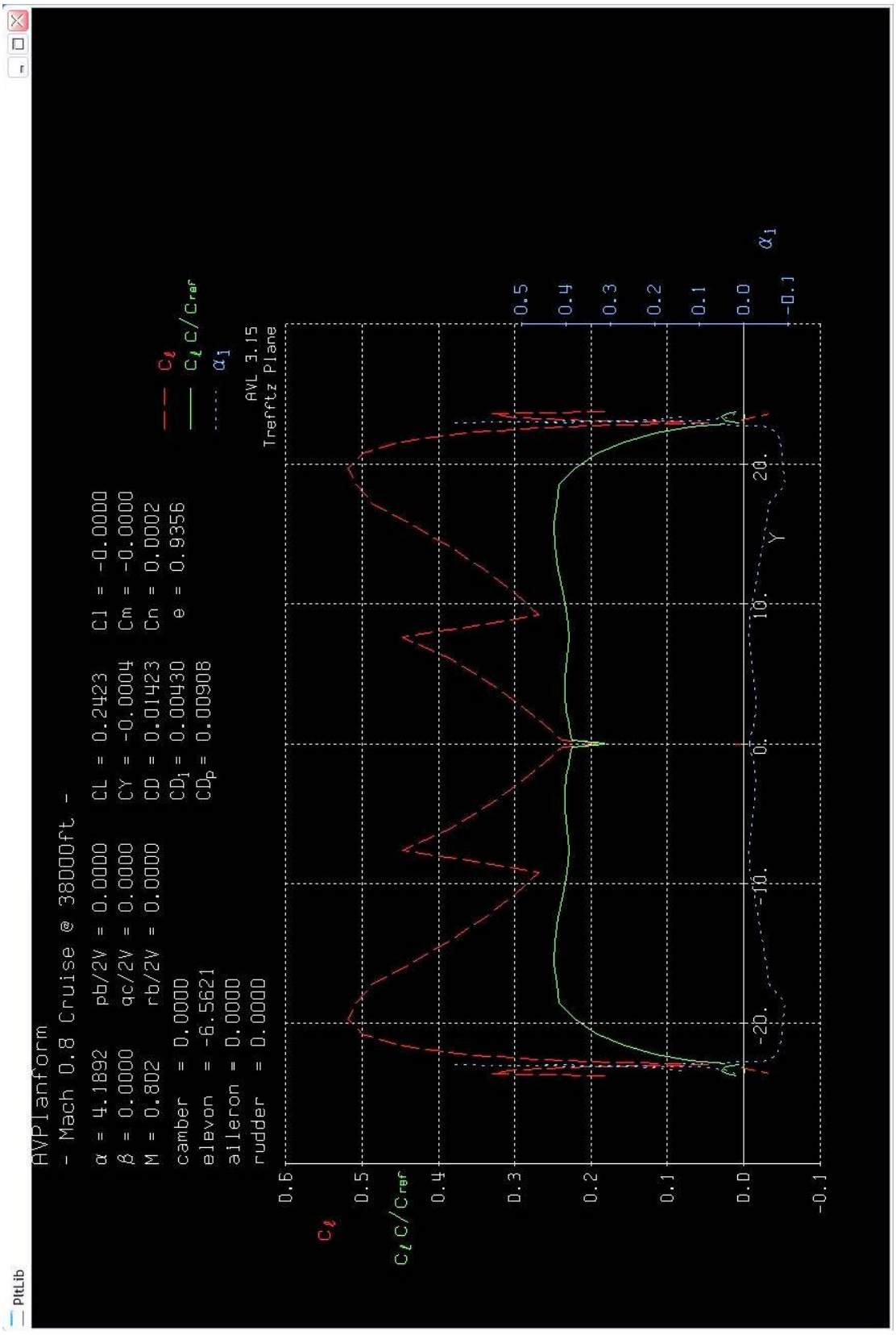

Fig H-2: BDSF Trefftz plane plot for flight case of Mach 0.8 with cruise @ 38,000 ft

H.2.2.2 CRUISE STABILITY RESULTS

```
---------------------------------------------------------------
 Vortex Lattice Output -- Total Forces

 Configuration: AVPlanform
    # Surfaces =   7
    # Strips   =  76
    # Vortices = 608

  Sref =  509.02       Cref =  11.100       Bref =  45.850
  Xref =  27.184       Yref =  0.0000       Zref = -1.2880

 Standard axis orientation,  X fwd, Z down

 Run case: - Mach 0.8 Cruise @ 38000ft -

  Alpha =   4.18922     pb/2V =   0.00000     p'b/2V =   0.00000
  Beta  =   0.00000     qc/2V =   0.00000
  Mach  =     0.802     rb/2V =   0.00000     r'b/2V =   0.00000

  CXtot =   0.00351     Cltot =  -0.00005     Cl'tot =  -0.00003
  CYtot =  -0.00045     Cmtot =   0.00000
  CZtot =  -0.24271     Cntot =   0.00025     Cn'tot =   0.00025

  CLtot =   0.24231
  CDtot =   0.01423
  CDvis =   0.00908     CDind =   0.00515
  CLff  =   0.22839     CDff  =   0.00430    | Trefftz
  CYff  =  -0.00046       e   =     0.9356   | Plane

   camber      =   0.00000
   elevon      =  -6.56207
   aileron     =   0.00000
   rudder      =   0.00000

 ---------------------------------------------------------------

 Derivatives...
                        alpha             beta
                  ----------------  ----------------
 z force    |   CLa =   4.908901   CLb =   0.000033
 y force    |   CYa =   0.000492   CYb =  -0.407387
 roll  x mom.|   Cla =   0.000063   Clb =  -0.052118
 pitch y mom.|   Cma =  -0.213549   Cmb =  -0.000155
 yaw   z mom.|   Cna =  -0.000281   Cnb =   0.052306

                   roll rate  p      pitch rate  q        yaw rate  r
                  ---------------  ---------------  ---------------
 z force    |   CLp =   0.000019   CLq =   6.873032   CLr =  -0.000045
 y force    |   CYp =   0.102075   CYq =   0.003789   CYr =   0.133055
 roll  x mom.|   Clp =  -0.376740   Clq =   0.000476   Clr =   0.094162
 pitch y mom.|   Cmp =  -0.000062   Cmq =  -3.856785   Cmr =   0.000194
 yaw   z mom.|   Cnp =  -0.034768   Cnq =  -0.002164   Cnr =  -0.181769

                camber      d1     elevon      d2     aileron      d3     rudder      d4
                ---------------  ---------------  ---------------  ---------------
 z force    |  CLd1 =   0.059518  CLd2 =   0.046535  CLd3 =   0.000000  CLd4 =   0.000000
 y force    |  CYd1 =  -0.000001  CYd2 =  -0.000001  CYd3 =   0.000000  CYd4 =  -0.003658
 roll  x mom.|  Cld1 =   0.000000  Cld2 =   0.000000  Cld3 =   0.000000  Cld4 =  -0.000381
 pitch y mom.|  Cmd1 =  -0.028536  Cmd2 =  -0.020143  Cmd3 =   0.000000  Cmd4 =   0.000000
 yaw   z mom.|  Cnd1 =   0.000001  Cnd2 =   0.000001  Cnd3 =   0.000000  Cnd4 =   0.001845
 Trefftz drag| CDffd1 =   0.001951 CDffd2 =   0.001326 CDffd3 =   0.000000 CDffd4 =   0.000006
 span eff.  |  ed1 =   0.061142   ed2 =   0.091255   ed3 =   0.000000   ed4 =  -0.001400

 Neutral point  Xnp =  27.666876

 Clb Cnr / Clr Cnb  =   1.923438    ( > 1 if spirally stable )
```

H.2.2.3 CRUISE SURFACE BODY RESULTS

```
---------------------------------------------------------------
 Vortex Lattice Output -- Total Forces

 Configuration: AVPlanform
    # Surfaces =   7
```

```
   # Strips   = 76
   # Vortices = 608

 Sref =  509.02       Cref =  11.100       Bref =  45.850
 Xref =  27.184       Yref =  0.0000       Zref = -1.2880

Standard axis orientation,  X fwd, Z down

Run case: - Mach 0.8 Cruise @ 38000ft -

 Alpha =   4.18922     pb/2V =   0.00000     p'b/2V =   0.00000
 Beta  =   0.00000     qc/2V =   0.00000
 Mach  =     0.802     rb/2V =   0.00000     r'b/2V =   0.00000

 CXtot =   0.00351     Cltot =  -0.00005     Cl'tot =  -0.00003
 CYtot =  -0.00045     Cmtot =   0.00000
 CZtot =  -0.24271     Cntot =   0.00025     Cn'tot =   0.00025

 CLtot =   0.24231
 CDtot =   0.01423
 CDvis =   0.00908     CDind =   0.00515
 CLff  =   0.22839     CDff  =   0.00430    | Trefftz
 CYff  =  -0.00046       e   =     0.9356   | Plane

  camber      =   0.00000
  elevon      =  -6.56207
  aileron     =   0.00000
  rudder      =   0.00000

------------------------------------------------------------------

Geometry-axis derivatives...

               axial   vel. u     sideslip vel. v      normal  vel. w
              ---------------    ---------------    ---------------
x force    |   CXu =  -0.010348    CXv =   0.000090    CXw =   0.438664
y force    |   CYu =  -0.000944    CYv =  -0.408478    CYw =   0.000425
z force    |   CZu =  -0.424386    CZv =  -0.000026    CZw =  -4.947588
roll  x mom.|   Clu =  -0.000100    Clv =  -0.052258    Clw =   0.000056
pitch y mom.|   Cmu =  -0.097635    Cmv =  -0.000155    Cmw =  -0.221272
yaw   z mom.|   Cnu =   0.000527    Cnv =   0.052446    Cnw =  -0.000243

               roll rate  p       pitch rate  q         yaw rate  r
              ---------------    ---------------    ---------------
x force    |   CXp =   0.000012    CXq =   0.243366    CXr =  -0.000088
y force    |   CYp =   0.092083    CYq =   0.003789    CYr =   0.140156
z force    |   CZp =  -0.000021    CZq =  -6.873619    CZr =   0.000037
roll  x mom.|   Clp =  -0.382612    Clq =   0.000476    Clr =   0.066389
pitch y mom.|   Cmp =  -0.000076    Cmq =  -3.856785    Cmr =   0.000188
yaw   z mom.|   Cnp =  -0.021397    Cnq =  -0.002164    Cnr =  -0.183823

              camber      d1     elevon      d2     aileron      d3     rudder      d4
              ---------------    ---------------    ---------------    ---------------
x force    |  CXd1 =   0.002134   CXd2 =   0.001739   CXd3 =   0.000000   CXd4 =   0.000000
y force    |  CYd1 =  -0.000001   CYd2 =  -0.000001   CYd3 =   0.000000   CYd4 =  -0.003658
z force    |  CZd1 =  -0.059521   CZd2 =  -0.046532   CZd3 =   0.000000   CZd4 =   0.000000
roll  x mom.|  Cld1 =   0.000000   Cld2 =   0.000000   Cld3 =   0.000000   Cld4 =  -0.000381
pitch y mom.|  Cmd1 =  -0.028536   Cmd2 =  -0.020143   Cmd3 =   0.000000   Cmd4 =   0.000000
yaw   z mom.|  Cnd1 =   0.000001   Cnd2 =   0.000001   Cnd3 =   0.000000   Cnd4 =   0.001845
```

H.2.2.4 CRUISE TOTAL STRIP FORCES RESULTS

```
------------------------------------------------------------------
 Vortex Lattice Output -- Total Forces

 Configuration: AVPlanform
   # Surfaces =   7
   # Strips   = 76
   # Vortices = 608

 Sref =  509.02       Cref =  11.100       Bref =  45.850
 Xref =  27.184       Yref =  0.0000       Zref = -1.2880

Standard axis orientation,  X fwd, Z down

Run case: - Mach 0.8 Cruise @ 38000ft -
```

```
 Alpha =  4.18922     pb/2V =   0.00000     p'b/2V =   0.00000
 Beta  =  0.00000     qc/2V =   0.00000
 Mach  =    0.802     rb/2V =   0.00000     r'b/2V =   0.00000

 CXtot =  0.00351     Cltot =  -0.00005     Cl'tot =  -0.00003
 CYtot =  -0.00045    Cmtot =   0.00000
 CZtot =  -0.24271    Cntot =   0.00025     Cn'tot =   0.00025

 CLtot =  0.24231
 CDtot =  0.01423
 CDvis =  0.00908     CDind =   0.00515
 CLff  =  0.22839     CDff  =   0.00430    | Trefftz
 CYff  =  -0.00046    e     =   0.9356     | Plane

  camber      =  0.00000
  elevon      =  -6.56207
  aileron     =  0.00000
  rudder      =  0.00000

 ---------------------------------------------------------------
 ---------------------------------------------------------------
 Surface Forces (referred to Sref,Cref,Bref about Xref,Yref,Zref)
 Standard axis orientation,  X fwd, Z down

    Sref =  509.0       Cref =  11.1000   Bref =  45.8500
    Xref =    27.1840   Yref =    0.0000  Zref =   -1.2880

 n     Area     CL      CD      Cm      CY      Cn      Cl     CDi     CDv
 1   293.990  0.1131  0.0022  0.0066  0.0046 -0.0001 -0.0276  0.0022  0.0000   Wing
 2   293.990  0.1131  0.0022  0.0066 -0.0046  0.0001  0.0276  0.0022  0.0000   Wing (YDUP)
 3    59.797  0.0000  0.0000  0.0000 -0.0004  0.0002  0.0000  0.0000  0.0000   Vertical Stabilisor
 4     6.685  0.0005 -0.0001 -0.0005 -0.0018  0.0004 -0.0002 -0.0001  0.0000   Upper Winglet
 5     6.685  0.0005 -0.0001 -0.0005  0.0018 -0.0004  0.0002 -0.0001  0.0000   Upper Winglet (YDUP)
 6     1.249  0.0000  0.0000  0.0000  0.0000  0.0000  0.0000  0.0000  0.0000   lower Winglet
 7     1.249  0.0000  0.0000  0.0000  0.0000  0.0000  0.0000  0.0000  0.0000   lower Winglet (YDUP)

 Surface Forces (referred to Ssurf, Cave about root LE on hinge axis)

  n     Ssurf      Cave       cl       cd      cdv    cm_LE
  1   293.990    12.799   0.1959   0.0038   0.0000   0.0000  Wing
  2   293.990    12.799   0.1959   0.0038   0.0000   0.0000  Wing (YDUP)
  3    59.797     6.536   0.0038   0.0000   0.0000   0.0000  Vertical Stabilisor
  4     6.685     1.720   0.1436  -0.0053   0.0000   0.0000  Upper Winglet
  5     6.685     1.720   0.1436  -0.0053   0.0000   0.0000  Upper Winglet (YDUP)
  6     1.249     1.120  -0.0049  -0.0001   0.0000   0.0000  lower Winglet
  7     1.249     1.120  -0.0049  -0.0001   0.0000   0.0000  lower Winglet (YDUP)
 ---------------------------------------------------------------
 ---------------------------------------------------------------
 Surface and Strip Forces by surface

  Forces referred to Sref, Cref, Bref about Xref, Yref, Zref
 Standard axis orientation,  X fwd, Z down

  Surface # 1     Wing
    # Chordwise = 10   # Spanwise = 22     First strip =  1
    Surface area =  293.990051       Ave. chord =   12.798667
    CLsurf  =   0.11307     Clsurf  =  -0.02759
    CYsurf  =   0.00456     Cmsurf  =   0.00664
    CDsurf  =   0.00222     Cnsurf  =  -0.00007
    CDisurf =   0.00222     CDvsurf =   0.00000

  Forces referred to Ssurf, Cave about hinge axis thru LE
    CLsurf  =   0.19587     CDsurf  =   0.00384
    Deflect =

 Strip Forces referred to Strip Area, Chord
   j     Yle    Chord     Area     c cl      ai      cl       cd      cdv    cm_c/4    cm_LE  C.P.x/c
   1  0.0298  27.1644   3.2397   2.0333   0.0133   0.0665   0.1187   0.0000   0.0149  -0.0014    0.060
   2  0.2669  26.7694   9.5127   2.4900   0.0138   0.0918   0.0207   0.0000   0.0145  -0.0039    0.094
   3  0.7362  25.9875  15.1824   2.5323   0.0171   0.0972   0.0073   0.0000   0.0162  -0.0036    0.084
   4  1.4283  24.8344  19.8971   2.5470   0.0232   0.1024   0.0063   0.0000   0.0196  -0.0025    0.059
   5  2.3291  23.3339  23.3770   2.5794   0.0270   0.1104   0.0062   0.0000   0.0241  -0.0011    0.032
   6  3.4201  21.5163  25.4346   2.6037   0.0260   0.1210   0.0053   0.0000   0.0290   0.0001    0.011
   7  4.6792  19.4186  25.9881   2.6001   0.0222   0.1339   0.0042   0.0000   0.0339   0.0011   -0.003
   8  6.0808  17.0837  25.0663   2.5735   0.0174   0.1509   0.0022   0.0000   0.0391   0.0016   -0.010
   9  7.5963  14.5589  22.8044   2.5443   0.0118   0.1753  -0.0011   0.0000   0.0457   0.0021   -0.012
  10  9.1871  12.7109  20.5187   2.5692   0.0135   0.2028  -0.0018   0.0000   0.0485  -0.0011    0.010
  11 10.8202  11.6280  19.1606   2.6350   0.0236   0.2273  -0.0017   0.0000   0.0400  -0.0128    0.074
  12 12.4702  10.5339  17.3577   2.7027   0.0332   0.2574  -0.0014   0.0000   0.0288  -0.0279    0.138
  13 14.1033   9.4509  15.2562   2.7475   0.0420   0.2916  -0.0009   0.0000   0.0156  -0.0454    0.196
  14 15.6864   8.4012  13.0038   2.7537   0.0500   0.3287  -0.0004   0.0000   0.0011  -0.0646    0.247
  15 17.1873   7.4059  10.7381   2.7178   0.0570   0.3680  -0.0001   0.0000  -0.0140  -0.0847    0.288
```

```
  16  18.5393   6.5605   8.2095   2.6900   0.0924   0.4109   0.0026   0.0000  -0.0319  -0.1136    0.328
  17  19.7200   5.8715   6.4897   2.4548   0.0882   0.4190   0.0029   0.0000  -0.0365  -0.1193    0.337
  18  20.7431   5.2745   4.9408   2.1262   0.0848   0.4041   0.0015   0.0000  -0.0347  -0.1148    0.336
  19  21.5878   4.7816   3.5820   1.7327   0.0813   0.3634  -0.0011   0.0000  -0.0292  -0.1017    0.331
  20  22.2368   4.4029   2.4051   1.2835   0.0742   0.2926  -0.0046   0.0000  -0.0215  -0.0802    0.324
  21  22.6770   4.1460   1.3776   0.7838   0.0508   0.1903  -0.0103   0.0000  -0.0121  -0.0505    0.314
  22  22.8993   4.0163   0.4479   0.2613  -0.1426   0.0669  -0.0227   0.0000  -0.0036  -0.0169    0.304

 Surface # 2     Wing (YDUP)
   # Chordwise = 10   # Spanwise = 22     First strip = 23
   Surface area =  293.990051       Ave. chord =   12.798667
   CLsurf  =   0.11308     Clsurf  =   0.02759
   CYsurf  =  -0.00456     Cmsurf  =   0.00664
   CDsurf  =   0.00222     Cnsurf  =   0.00007
   CDisurf =   0.00222     CDvsurf =   0.00000

 Forces referred to Ssurf, Cave about hinge axis thru LE
   CLsurf  =   0.19587     CDsurf  =   0.00384
   Deflect =

Strip Forces referred to Strip Area, Chord
   j     Yle    Chord     Area     c cl      ai      cl       cd      cdv    cm_c/4    cm_LE  C.P.x/c
  23  -0.0298  27.1644   3.2397   2.0333   0.0132   0.0665   0.1187   0.0000   0.0149   0.0014    0.060
  24  -0.2669  26.7694   9.5127   2.4900   0.0136   0.0918   0.0207   0.0000   0.0145   0.0039    0.094
  25  -0.7362  25.9875  15.1824   2.5323   0.0168   0.0972   0.0073   0.0000   0.0162   0.0036    0.084
  26  -1.4283  24.8344  19.8971   2.5470   0.0227   0.1024   0.0063   0.0000   0.0196   0.0025    0.059
  27  -2.3291  23.3339  23.3770   2.5794   0.0265   0.1104   0.0062   0.0000   0.0241   0.0011    0.032
  28  -3.4201  21.5163  25.4346   2.6038   0.0255   0.1210   0.0053   0.0000   0.0290  -0.0001    0.011
  29  -4.6792  19.4186  25.9881   2.6001   0.0217   0.1340   0.0042   0.0000   0.0339  -0.0011   -0.003
  30  -6.0808  17.0837  25.0663   2.5735   0.0170   0.1509   0.0022   0.0000   0.0391  -0.0016   -0.010
  31  -7.5963  14.5589  22.8044   2.5443   0.0115   0.1753  -0.0011   0.0000   0.0457  -0.0021   -0.012
  32  -9.1871  12.7109  20.5187   2.5693   0.0133   0.2028  -0.0018   0.0000   0.0485   0.0011    0.010
  33 -10.8202  11.6280  19.1606   2.6351   0.0234   0.2273  -0.0017   0.0000   0.0400   0.0129    0.074
  34 -12.4702  10.5339  17.3577   2.7028   0.0331   0.2574  -0.0014   0.0000   0.0288   0.0279    0.138
  35 -14.1033   9.4509  15.2562   2.7476   0.0419   0.2916  -0.0009   0.0000   0.0156   0.0454    0.196
  36 -15.6864   8.4012  13.0038   2.7539   0.0499   0.3287  -0.0004   0.0000   0.0011   0.0646    0.247
  37 -17.1873   7.4059  10.7381   2.7179   0.0570   0.3680  -0.0001   0.0000  -0.0140   0.0847    0.288
  38 -18.5393   6.5605   8.2095   2.6901   0.0923   0.4110   0.0026   0.0000  -0.0319   0.1136    0.328
  39 -19.7200   5.8715   6.4897   2.4549   0.0882   0.4190   0.0029   0.0000  -0.0365   0.1193    0.337
  40 -20.7431   5.2745   4.9408   2.1263   0.0848   0.4041   0.0015   0.0000  -0.0347   0.1148    0.336
  41 -21.5878   4.7816   3.5820   1.7328   0.0813   0.3634  -0.0011   0.0000  -0.0292   0.1017    0.331
  42 -22.2368   4.4029   2.4051   1.2836   0.0741   0.2927  -0.0046   0.0000  -0.0215   0.0803    0.324
  43 -22.6770   4.1460   1.3776   0.7838   0.0508   0.1903  -0.0103   0.0000  -0.0121   0.0505    0.314
  44 -22.8993   4.0163   0.4479   0.2613  -0.1427   0.0669  -0.0227   0.0000  -0.0036   0.0169    0.304

 Surface # 3     Vertical Stabilisor
   # Chordwise =  8   # Spanwise = 14     First strip = 45
   Surface area =   59.797329       Ave. chord =    6.535571
   CLsurf  =   0.00000     Clsurf  =  -0.00005
   CYsurf  =  -0.00045     Cmsurf  =   0.00000
   CDsurf  =   0.00000     Cnsurf  =   0.00025
   CDisurf =   0.00000     CDvsurf =   0.00000

 Forces referred to Ssurf, Cave about hinge axis thru LE
   CLsurf  =   0.00379     CDsurf  =   0.00000
   Deflect =

Strip Forces referred to Strip Area, Chord
   j     Yle    Chord     Area     c cl      ai      cl       cd      cdv    cm_c/4    cm_LE  C.P.x/c
  45   0.0000   8.6649   2.1611   0.0077   0.0020   0.0009   0.0000   0.0000  -0.0006  -0.0005
  46   0.0000   8.5057   3.5481   0.0158   0.0021   0.0019   0.0000   0.0000  -0.0012  -0.0011
  47   0.0000   8.2691   4.7312   0.0229   0.0025   0.0028   0.0000   0.0000  -0.0017  -0.0017
  48   0.0000   7.9632   5.6273   0.0247   0.0018   0.0031   0.0000   0.0000  -0.0018  -0.0018
  49   0.0000   7.5994   6.1854   0.0265   0.0016   0.0035   0.0000   0.0000  -0.0020  -0.0020
  50   0.0000   7.1919   6.3906   0.0279   0.0015   0.0039   0.0000   0.0000  -0.0021  -0.0021
  51   0.0000   6.7574   6.2632   0.0288   0.0015   0.0043   0.0000   0.0000  -0.0021  -0.0023
  52   0.0000   6.3137   5.8520   0.0291   0.0015   0.0046   0.0000   0.0000  -0.0022  -0.0024
  53   0.0000   5.8792   5.2242   0.0285   0.0016   0.0048   0.0000   0.0000  -0.0022  -0.0024
  54   0.0000   5.4718   4.4537   0.0270   0.0015   0.0049   0.0000   0.0000  -0.0021  -0.0024
  55   0.0000   5.1079   3.6096   0.0250   0.0019   0.0049   0.0000   0.0000  -0.0020  -0.0023
  56   0.0000   4.8020   2.7475   0.0219   0.0024   0.0046   0.0000   0.0000  -0.0019  -0.0022
  57   0.0000   4.5654   1.9044   0.0177   0.0032   0.0039   0.0000   0.0000  -0.0016  -0.0019
  58   0.0000   4.4062   1.0990   0.0114   0.0049   0.0026   0.0000   0.0000  -0.0012  -0.0013

 Surface # 4     Upper Winglet
   # Chordwise =  4   # Spanwise =  5     First strip = 59
   Surface area =    6.685101       Ave. chord =    1.720000
   CLsurf  =   0.00047     Clsurf  =  -0.00020
   CYsurf  =  -0.00183     Cmsurf  =  -0.00050
   CDsurf  =  -0.00007     Cnsurf  =   0.00044
   CDisurf =  -0.00007     CDvsurf =   0.00000
```

```
 Forces referred to Ssurf, Cave about hinge axis thru LE
   CLsurf  =   0.14356     CDsurf  =  -0.00526
   Deflect =

Strip Forces referred to Strip Area, Chord
   j     Yle    Chord     Area     c cl      ai      cl       cd       cdv     cm_c/4    cm_LE  C.P.x/c
  59  22.9477   2.5569   0.9490   0.0742  -0.4450   0.0290  -0.0005   0.0000  -0.0225  -0.0227
  60  23.1016   2.2373   2.1739   0.2723  -0.0950   0.1218  -0.0038   0.0000  -0.0499  -0.0631    1.947
  61  23.3506   1.7200   2.0658   0.3272  -0.0357   0.1904  -0.0067   0.0000  -0.0541  -0.0837    1.399
  62  23.5996   1.2027   1.1687   0.2447  -0.0200   0.2036  -0.0083   0.0000  -0.0461  -0.0865    1.150
  63  23.7535   0.8831   0.3277   0.0973  -0.0046   0.1103  -0.0084   0.0000  -0.0197  -0.0467    0.904

 Surface # 5     Upper Winglet (YDUP)
   # Chordwise =  4   # Spanwise =  5     First strip = 64
   Surface area =    6.685101       Ave. chord =    1.720000
   CLsurf  =   0.00047     Clsurf  =   0.00020
   CYsurf  =   0.00183     Cmsurf  =  -0.00050
   CDsurf  =  -0.00007     Cnsurf  =  -0.00044
   CDisurf =  -0.00007     CDvsurf =   0.00000

 Forces referred to Ssurf, Cave about hinge axis thru LE
   CLsurf  =   0.14356     CDsurf  =  -0.00526
   Deflect =

Strip Forces referred to Strip Area, Chord
   j     Yle    Chord     Area     c cl      ai      cl       cd       cdv     cm_c/4    cm_LE  C.P.x/c
  64 -22.9477   2.5569   0.9490   0.0742  -0.4451   0.0290  -0.0005   0.0000  -0.0225   0.0227
  65 -23.1016   2.2373   2.1739   0.2723  -0.0950   0.1218  -0.0038   0.0000  -0.0499   0.0631    1.947
  66 -23.3506   1.7200   2.0658   0.3272  -0.0358   0.1904  -0.0067   0.0000  -0.0541   0.0837    1.399
  67 -23.5996   1.2027   1.1687   0.2447  -0.0201   0.2036  -0.0083   0.0000  -0.0461   0.0865    1.150
  68 -23.7535   0.8831   0.3277   0.0973  -0.0047   0.1104  -0.0084   0.0000  -0.0197   0.0467    0.904

 Surface # 6     lower Winglet
   # Chordwise =  2   # Spanwise =  4     First strip = 69
   Surface area =    1.249446       Ave. chord =    1.120000
   CLsurf  =   0.00000     Clsurf  =   0.00000
   CYsurf  =  -0.00001     Cmsurf  =  -0.00001
   CDsurf  =   0.00000     Cnsurf  =   0.00000
   CDisurf =   0.00000     CDvsurf =   0.00000

 Forces referred to Ssurf, Cave about hinge axis thru LE
   CLsurf  =  -0.00493     CDsurf  =  -0.00010
   Deflect =

Strip Forces referred to Strip Area, Chord
   j     Yle    Chord     Area     c cl      ai      cl       cd       cdv     cm_c/4    cm_LE  C.P.x/c
  69  22.9521   1.5635   0.2554  -0.0010  -0.6486  -0.0007   0.0024   0.0000  -0.0179  -0.0133
  70  23.1305   1.3037   0.5142   0.0020  -0.2027   0.0015   0.0014   0.0000  -0.0510  -0.0385
  71  23.3827   0.9363   0.3693  -0.0110  -0.1332  -0.0117  -0.0020   0.0000  -0.0726  -0.0525
  72  23.5611   0.6765   0.1105  -0.0151  -0.1353  -0.0221  -0.0064   0.0000  -0.0488  -0.0324

 Surface # 7     lower Winglet (YDUP)
   # Chordwise =  2   # Spanwise =  4     First strip = 73
   Surface area =    1.249446       Ave. chord =    1.120000
   CLsurf  =   0.00000     Clsurf  =   0.00000
   CYsurf  =   0.00001     Cmsurf  =  -0.00001
   CDsurf  =   0.00000     Cnsurf  =   0.00000
   CDisurf =   0.00000     CDvsurf =   0.00000

 Forces referred to Ssurf, Cave about hinge axis thru LE
   CLsurf  =  -0.00492     CDsurf  =  -0.00010
   Deflect =

Strip Forces referred to Strip Area, Chord
   j     Yle    Chord     Area     c cl      ai      cl       cd       cdv     cm_c/4    cm_LE  C.P.x/c
  73 -22.9521   1.5635   0.2554  -0.0010  -0.6487  -0.0007   0.0024   0.0000  -0.0179   0.0133
  74 -23.1305   1.3037   0.5142   0.0020  -0.2027   0.0015   0.0014   0.0000  -0.0510   0.0385
  75 -23.3827   0.9363   0.3693  -0.0110  -0.1332  -0.0117  -0.0020   0.0000  -0.0726   0.0526
  76 -23.5611   0.6765   0.1105  -0.0151  -0.1353  -0.0221  -0.0064   0.0000  -0.0488   0.0324
---------------------------------------------------------------------
```

H.2.3 BDSF Second Run Case and Results for Low Speed/Approach

```
---------------------------------------------
 Run case  2:  -SL approach @ 57.5m/s -

 alpha        ->  CL          =  1.128345
 beta         ->  beta        =  0.00000
 pb/2V        ->  pb/2V       =  0.00000
 qc/2V        ->  qc/2V       =  0.00000
 rb/2V        ->  rb/2V       =  0.00000
 camber       ->  camber      =  0.00000
 elevon       ->  Cm pitchmom =  0.00000
 aileron      ->  aileron     =  0.00000
 rudder       ->  rudder      =  0.00000

 alpha     =  0.00000
 beta      =  0.00000
 pb/2V     =  0.00000
 qc/2V     = -0.737769E-16
 rb/2V     =  0.00000
 CL        =  0.00000
 CDo       =  0.010008
 bank      =  0.00000
 elevation =  0.00000
 heading   =  0.00000
 Mach      =  0.168954
 velocity  =  57.49351
 density   =  1.22300
 grav.acc. =  9.81000
 turn_rad. =  0.00000
 load_fac. =  0.00000
 X_cg      =  27.163
 Y_cg      =  0.00000
 Z_cg      = -1.206
 mass      =  123390.73
 Ixx       =  2.09000E+02
 Iyy       =  2.09000E+02
 Izz       =  1.81000E-01
 Ixy       = -6.1400E+00
 Iyz       =  3.51000E-15
 Izx       =  3.51000E-15
 visc CL_a =  0.00000
 visc CL_u =  0.00000
 visc CM_a =  0.00000
 visc CM_u =  0.00000
```

H.2.3.1 BD Initial Results for second low speed / approach case

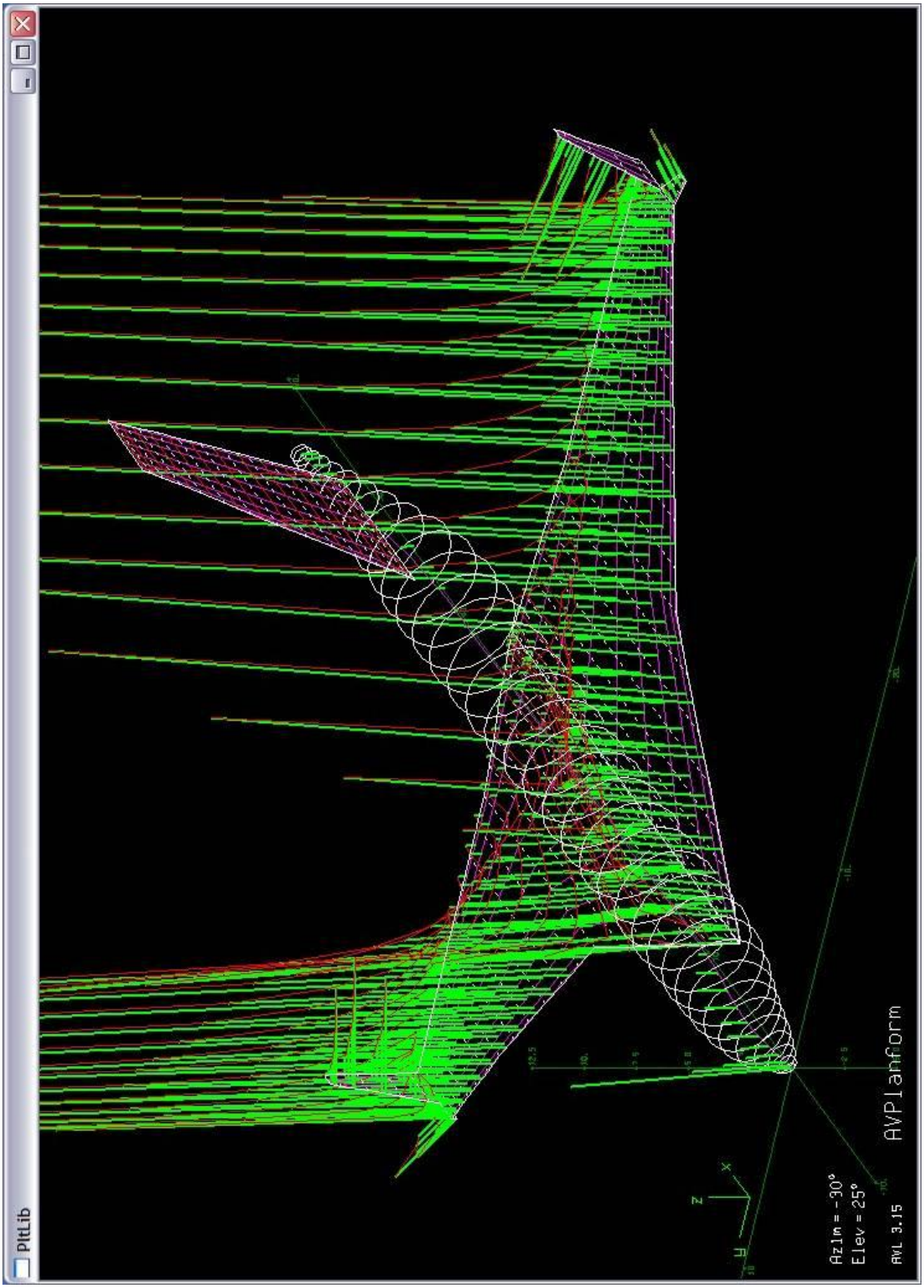

Fig H-3: BDSF Geometry for a low speed flight case of 57.5 m/s at SL

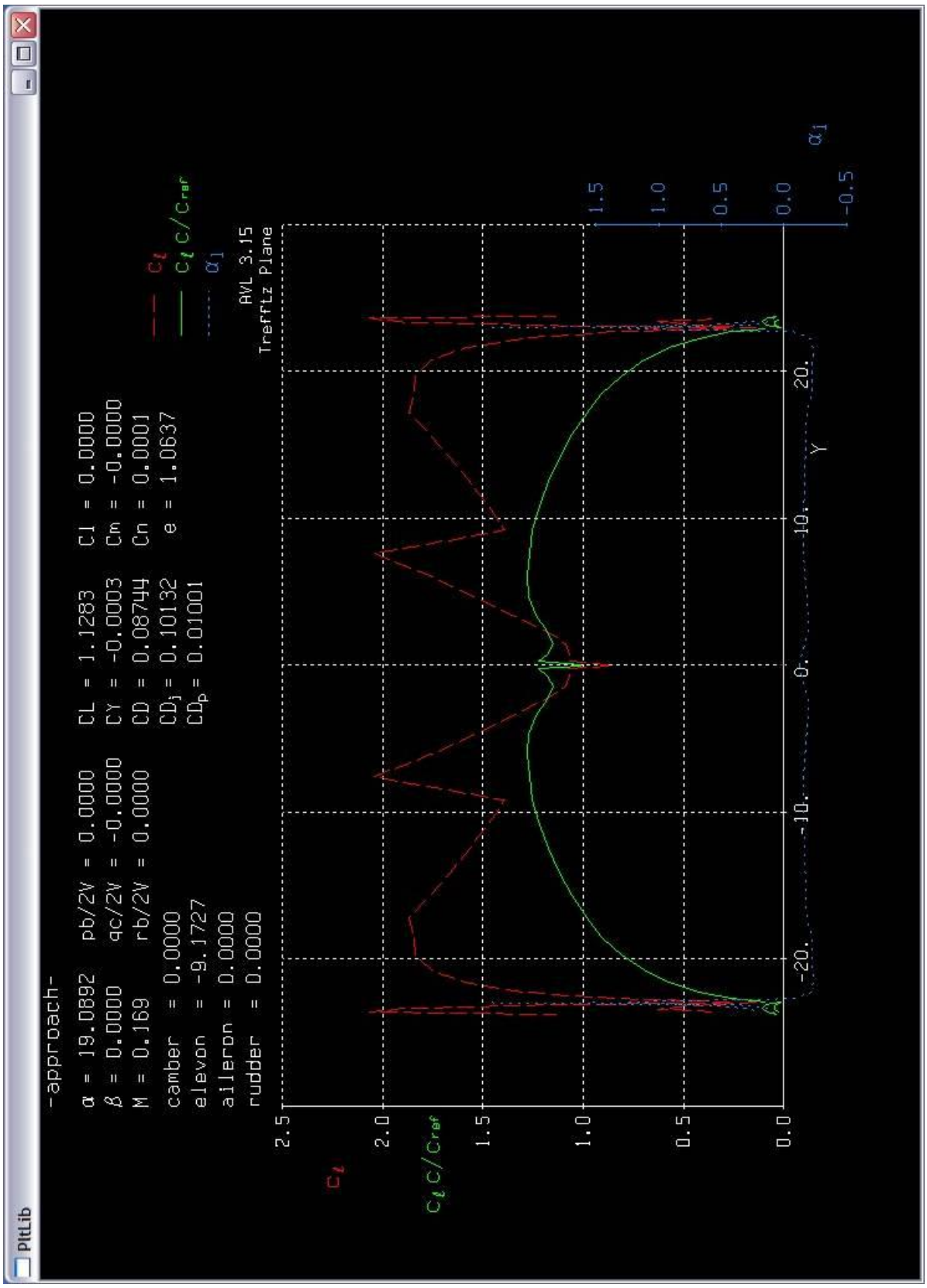

Fig H-4: BDSF Trefftz plane plot for a low speed flight case of 57.5 m/s at SL

H.2.3.2 LOW SPEED STABILITY RESULTS

```
---------------------------------------------------------------
 Vortex Lattice Output -- Total Forces

 Configuration: AVPlanform
    # Surfaces =   7
    # Strips   =  76
    # Vortices = 608

  Sref =  509.02       Cref =  11.100       Bref =  45.850
  Xref =  27.184       Yref =  0.0000       Zref = -1.2880

 Standard axis orientation,  X fwd, Z down

 Run case: -SL approach @ 57.5m/s -

  Alpha =   3.97405     pb/2V =   0.00000     p'b/2V =   0.00000
  Beta  =   0.00000     qc/2V =   0.00000
  Mach  =     0.802     rb/2V =   0.00000     r'b/2V =   0.00000

  CXtot =   0.00183     Cltot =  -0.00005     Cl'tot =  -0.00003
  CYtot =  -0.00045     Cmtot =   0.00000
  CZtot =  -0.24277     Cntot =   0.00025     Cn'tot =   0.00025

  CLtot =   0.24231
  CDtot =   0.01500
  CDvis =   0.00908     CDind =   0.00592
  CLff  =   0.22831     CDff  =   0.00502   | Trefftz
  CYff  =  -0.00046       e   =     0.8002  | Plane

   camber      =   0.00000
   elevon      =  -7.45227
   aileron     =   0.00000
   rudder      =   0.00000

 ---------------------------------------------------------------

 Derivatives...
                      alpha              beta
             ----------------   ----------------
 z force     |   CLa =   4.912133    CLb =   0.000032
 y force     |   CYa =   0.000489    CYb =  -0.407144
 roll  x mom.|   Cla =   0.000064    Clb =  -0.056696
 pitch y mom.|   Cma =  -0.216134    Cmb =  -0.000155
 yaw   z mom.|   Cna =  -0.000279    Cnb =   0.051869

                  roll rate  p       pitch rate  q        yaw rate  r
             ----------------   ----------------   ----------------
 z force     |   CLp =   0.000019    CLq =   6.899244    CLr =  -0.000044
 y force     |   CYp =   0.098903    CYq =   0.003791    CYr =   0.132729
 roll  x mom.|   Clp =  -0.376272    Clq =   0.000484    Clr =   0.106405
 pitch y mom.|   Cmp =  -0.000063    Cmq =  -3.874367    Cmr =   0.000193
 yaw   z mom.|   Cnp =  -0.034655    Cnq =  -0.002163    Cnr =  -0.182060

              camber      d1     elevon      d2     aileron      d3     rudder      d4
             ----------------   ----------------   ----------------   ----------------
 z force     |  CLd1 =   0.059535   CLd2 =   0.046560   CLd3 =   0.000000   CLd4 =   0.000000
 y force     |  CYd1 =  -0.000001   CYd2 =  -0.000001   CYd3 =   0.000000   CYd4 =  -0.003658
 roll  x mom.|  Cld1 =   0.000000   Cld2 =   0.000000   Cld3 =   0.000000   Cld4 =  -0.000388
 pitch y mom.|  Cmd1 =  -0.028617   Cmd2 =  -0.020193   Cmd3 =   0.000000   Cmd4 =   0.000000
 yaw   z mom.|  Cnd1 =   0.000001   Cnd2 =   0.000001   Cnd3 =   0.000000   Cnd4 =   0.001844
 Trefftz drag| CDffd1 =   0.001925 CDffd2 =   0.001183 CDffd3 =   0.000000 CDffd4 =   0.000006
 span eff.   |   ed1 =   0.108834    ed2 =   0.136505    ed3 =   0.000000    ed4 =  -0.001026

 Neutral point  Xnp =  27.672400

 Clb Cnr / Clr Cnb  =   1.870266    ( > 1 if spirally stable )
```

H.2.4 LOW SPEED SURFACE BODY RESULTS

```
---------------------------------------------------------------
 Vortex Lattice Output -- Total Forces

 Configuration: AVPlanform
    # Surfaces =   7
```

```
   # Strips   = 76
   # Vortices = 608

 Sref =  509.02       Cref =  11.100       Bref =  45.850
 Xref =  27.184       Yref =  0.0000       Zref = -1.2880

Standard axis orientation,  X fwd, Z down

Run case: -SL approach @ 57.5m/s -

 Alpha =   3.97405     pb/2V =   0.00000     p'b/2V =   0.00000
 Beta  =   0.00000     qc/2V =   0.00000
 Mach  =     0.802     rb/2V =   0.00000     r'b/2V =   0.00000

 CXtot =   0.00183     Cltot =  -0.00005     Cl'tot =  -0.00003
 CYtot =  -0.00045     Cmtot =   0.00000
 CZtot =  -0.24277     Cntot =   0.00025     Cn'tot =   0.00025

 CLtot =   0.24231
 CDtot =   0.01500
 CDvis =   0.00908     CDind =   0.00592
 CLff  =   0.22831     CDff  =   0.00502    | Trefftz
 CYff  =  -0.00046       e   =     0.8002   | Plane

  camber      =   0.00000
  elevon      =  -7.45227
  aileron     =   0.00000
  rudder      =   0.00000

------------------------------------------------------------------

Geometry-axis derivatives...

               axial   vel. u     sideslip vel. v      normal  vel. w
              ---------------    ---------------    ---------------
x force    |   CXu =  -0.008906   CXv =   0.000090   CXw =   0.421081
y force    |   CYu =  -0.000946   CYv =  -0.408125   CYw =   0.000425
z force    |   CZu =  -0.484316   CZv =  -0.000026   CZw =  -4.954509
roll  x mom.|   Clu =  -0.000102   Clv =  -0.056833   Clw =   0.000057
pitch y mom.|   Cmu =  -0.116356   Cmv =  -0.000155   Cmw =  -0.224738
yaw   z mom.|   Cnu =   0.000527   Cnv =   0.051994   Cnw =  -0.000243

               roll rate  p       pitch rate  q         yaw rate  r
              ---------------    ---------------    ---------------
x force    |   CXp =   0.000012   CXq =   0.210363   CXr =  -0.000088
y force    |   CYp =   0.089467   CYq =   0.003791   CYr =   0.139265
z force    |   CZp =  -0.000021   CZq =  -6.901258   CZr =   0.000037
roll  x mom.|   Clp =  -0.382741   Clq =   0.000484   Clr =   0.080072
pitch y mom.|   Cmp =  -0.000076   Cmq =  -3.874367   Cmr =   0.000188
yaw   z mom.|   Cnp =  -0.021954   Cnq =  -0.002163   Cnr =  -0.184024

              camber      d1     elevon      d2     aileron      d3     rudder      d4
              ---------------    ---------------    ---------------    ---------------
x force    |  CXd1 =   0.001716   CXd2 =   0.001511   CXd3 =   0.000000   CXd4 =   0.000000
y force    |  CYd1 =  -0.000001   CYd2 =  -0.000001   CYd3 =   0.000000   CYd4 =  -0.003658
z force    |  CZd1 =  -0.059559   CZd2 =  -0.046567   CZd3 =   0.000000   CZd4 =   0.000000
roll  x mom.|  Cld1 =   0.000000   Cld2 =   0.000000   Cld3 =   0.000000   Cld4 =  -0.000388
pitch y mom.|  Cmd1 =  -0.028617   Cmd2 =  -0.020193   Cmd3 =   0.000000   Cmd4 =   0.000000
yaw   z mom.|  Cnd1 =   0.000001   Cnd2 =   0.000001   Cnd3 =   0.000000   Cnd4 =   0.001844
```

H.2.4.1 LOW SPEED TOTAL STRIP FORCES RESULTS

```
------------------------------------------------------------------
 Vortex Lattice Output -- Total Forces

 Configuration: AVPlanform
   # Surfaces =   7
   # Strips   =  76
   # Vortices = 608

 Sref =  509.02       Cref =  11.100       Bref =  45.850
 Xref =  27.163       Yref =  0.0000       Zref = -1.2060

Standard axis orientation,  X fwd, Z down

Run case: -SL approach @ 57.5m/s -

 Alpha =  18.98729     pb/2V =   0.00000     p'b/2V =   0.00000
```

```
 Beta =   0.00000     qc/2V =   0.00000
 Mach =     0.169     rb/2V =   0.00000     r'b/2V =   0.00000

 CXtot =   0.28445     Cltot =   0.00001     Cl'tot =   0.00006
 CYtot =  -0.00026     Cmtot =   0.00000
 CZtot =  -1.09540     Cntot =   0.00014     Cn'tot =   0.00013

 CLtot =   1.12835
 CDtot =   0.08743
 CDvis =   0.01001     CDind =   0.07742
 CLff  =   1.18045     CDff  =   0.10097    | Trefftz
 CYff  =  -0.00032         e =    1.0637    | Plane

  camber      =   0.00000
  elevon      =  -9.02673
  aileron     =   0.00000
  rudder      =   0.00000

 ---------------------------------------------------------------
 ---------------------------------------------------------------
 Surface Forces (referred to Sref,Cref,Bref about Xref,Yref,Zref)
 Standard axis orientation,  X fwd, Z down

    Sref =   509.0       Cref =   11.1000   Bref =   45.8500
    Xref =    27.1630    Yref =    0.0000   Zref =   -1.2060

 n     Area      CL      CD      Cm      CY      Cn      Cl     CDi     CDv
 1   293.990  0.5572  0.0373 -0.0274  0.0071 -0.0032 -0.1322  0.0373  0.0000   Wing
 2   293.990  0.5572  0.0373 -0.0274 -0.0071  0.0032  0.1322  0.0373  0.0000   Wing (YDUP)
 3    59.797  0.0000  0.0000  0.0000 -0.0003  0.0001  0.0000  0.0000  0.0000   Vertical Stabilisor
 4     6.685  0.0028 -0.0008 -0.0025 -0.0064  0.0011 -0.0008 -0.0008  0.0000   Upper Winglet
 5     6.685  0.0028 -0.0008 -0.0025  0.0064 -0.0011  0.0008 -0.0008  0.0000   Upper Winglet (YDUP)
 6     1.249  0.0005 -0.0001 -0.0003  0.0008 -0.0002 -0.0004 -0.0001  0.0000   lower Winglet
 7     1.249  0.0005 -0.0001 -0.0003 -0.0008  0.0002  0.0004 -0.0001  0.0000   lower Winglet (YDUP)

 Surface Forces (referred to Ssurf, Cave about root LE on hinge axis)

  n     Ssurf      Cave       cl       cd      cdv    cm_LE
  1   293.990    12.799   0.9636   0.0645   0.0000   0.0000  Wing
  2   293.990    12.799   0.9636   0.0645   0.0000   0.0000  Wing (YDUP)
  3    59.797     6.536   0.0022   0.0000   0.0000   0.0000  Vertical Stabilisor
  4     6.685     1.720   0.5259  -0.0572   0.0000   0.0000  Upper Winglet
  5     6.685     1.720   0.5260  -0.0572   0.0000   0.0000  Upper Winglet (YDUP)
  6     1.249     1.120   0.3795  -0.0329   0.0000   0.0000  lower Winglet
  7     1.249     1.120   0.3795  -0.0330   0.0000   0.0000  lower Winglet (YDUP)
 ---------------------------------------------------------------
 ---------------------------------------------------------------
 Surface and Strip Forces by surface

  Forces referred to Sref, Cref, Bref about Xref, Yref, Zref
 Standard axis orientation,  X fwd, Z down

  Surface # 1     Wing
    # Chordwise = 10   # Spanwise = 22     First strip =  1
    Surface area =  293.990051       Ave. chord =   12.798667
    CLsurf  =   0.55718     Clsurf  =  -0.13221
    CYsurf  =   0.00712     Cmsurf  =  -0.02736
    CDsurf  =   0.03727     Cnsurf  =  -0.00323
    CDisurf =   0.03727     CDvsurf =   0.00000

  Forces referred to Ssurf, Cave about hinge axis thru LE
    CLsurf  =   0.96355     CDsurf  =   0.06453
    Deflect =

 Strip Forces referred to Strip Area, Chord
   j     Yle    Chord     Area     c cl      ai      cl       cd      cdv    cm_c/4    cm_LE  C.P.x/c
   1  0.0298  27.1644   3.2397  10.6617   0.1217   0.1267   0.8706   0.0000  -0.0321  -0.0568    0.401
   2  0.2669  26.7694   9.5127  13.5029   0.1250   0.4659   0.2031   0.0000  -0.0345  -0.0720    0.321
   3  0.7362  25.9875  15.1824  13.1147   0.1417   0.4915   0.1272   0.0000  -0.0313  -0.0699    0.312
   4  1.4283  24.8344  19.8971  12.7668   0.1719   0.5043   0.1189   0.0000  -0.0252  -0.0673    0.299
   5  2.3291  23.3339  23.3770  13.1226   0.1931   0.5572   0.1130   0.0000  -0.0170  -0.0683    0.280
   6  3.4201  21.5163  25.4346  13.7480   0.1933   0.6409   0.1042   0.0000  -0.0076  -0.0719    0.262
   7  4.6792  19.4186  25.9881  14.1411   0.1820   0.7386   0.0936   0.0000   0.0020  -0.0770    0.247
   8  6.0808  17.0837  25.0663  14.2092   0.1685   0.8550   0.0721   0.0000   0.0125  -0.0829    0.235
   9  7.5963  14.5589  22.8044  14.0291   0.1553   1.0106   0.0227   0.0000   0.0301  -0.0881    0.220
  10  9.1871  12.7109  20.5187  13.9222   0.1524   1.1488   0.0265   0.0000   0.0513  -0.1693    0.205
  11 10.8202  11.6280  19.1606  13.5271   0.1588   1.2198   0.0293   0.0000   0.0438  -0.1887    0.214
  12 12.4702  10.5339  17.3577  13.0284   0.1645   1.2990   0.0247   0.0000   0.0340  -0.2112    0.224
  13 14.1033   9.4509  15.2562  12.4248   0.1699   1.3842   0.0162   0.0000   0.0236  -0.2351    0.233
  14 15.6864   8.4012  13.0038  11.7155   0.1757   1.4729   0.0033   0.0000   0.0138  -0.2590    0.241
  15 17.1873   7.4059  10.7381  10.9106   0.1827   1.5633  -0.0179   0.0000   0.0064  -0.2808    0.246
  16 18.5393   6.5605   8.2095  10.0780   0.2277   1.6318  -0.0224   0.0000  -0.0027  -0.3215    0.252
```

```
  17  19.7200   5.8715   6.4897   8.9727   0.2255   1.6283  -0.0367   0.0000  -0.0004  -0.3185    0.250
  18  20.7431   5.2745   4.9408   7.7172   0.2284   1.5676  -0.0605   0.0000   0.0095  -0.2973    0.244
  19  21.5878   4.7816   3.5820   6.3124   0.2315   1.4266  -0.0901   0.0000   0.0228  -0.2568    0.234
  20  22.2368   4.4029   2.4051   4.7223   0.2135   1.1778  -0.1281   0.0000   0.0345  -0.1955    0.221
  21  22.6770   4.1460   1.3776   2.9085   0.0782   0.8061  -0.1881   0.0000   0.0372  -0.1157    0.204
  22  22.8993   4.0163   0.4479   0.9694  -1.2566   0.3691  -0.3329   0.0000   0.0173  -0.0361    0.203

 Surface # 2     Wing (YDUP)
   # Chordwise = 10   # Spanwise = 22     First strip = 23
   Surface area =  293.990051       Ave. chord =   12.798667
   CLsurf  =   0.55719     Clsurf  =   0.13221
   CYsurf  =  -0.00712     Cmsurf  =  -0.02736
   CDsurf  =   0.03727     Cnsurf  =   0.00323
   CDisurf =   0.03727     CDvsurf =   0.00000

 Forces referred to Ssurf, Cave about hinge axis thru LE
   CLsurf  =   0.96357     CDsurf  =   0.06453
   Deflect =

 Strip Forces referred to Strip Area, Chord
   j     Yle    Chord     Area     c cl      ai      cl       cd      cdv    cm_c/4    cm_LE  C.P.x/c
  23  -0.0298  27.1644   3.2397  10.6617   0.1217   0.1267   0.8706   0.0000  -0.0321   0.0568    0.401
  24  -0.2669  26.7694   9.5127  13.5029   0.1249   0.4659   0.2031   0.0000  -0.0345   0.0720    0.321
  25  -0.7362  25.9875  15.1824  13.1147   0.1414   0.4915   0.1272   0.0000  -0.0313   0.0699    0.312
  26  -1.4283  24.8344  19.8971  12.7668   0.1716   0.5043   0.1189   0.0000  -0.0252   0.0673    0.299
  27  -2.3291  23.3339  23.3770  13.1226   0.1927   0.5572   0.1130   0.0000  -0.0170   0.0683    0.280
  28  -3.4201  21.5163  25.4346  13.7480   0.1929   0.6409   0.1042   0.0000  -0.0076   0.0719    0.262
  29  -4.6792  19.4186  25.9881  14.1412   0.1817   0.7386   0.0936   0.0000   0.0020   0.0770    0.247
  30  -6.0808  17.0837  25.0663  14.2093   0.1682   0.8550   0.0721   0.0000   0.0125   0.0829    0.235
  31  -7.5963  14.5589  22.8044  14.0292   0.1551   1.0106   0.0227   0.0000   0.0301   0.0881    0.220
  32  -9.1871  12.7109  20.5187  13.9224   0.1522   1.1488   0.0265   0.0000   0.0513   0.1693    0.205
  33 -10.8202  11.6280  19.1606  13.5273   0.1586   1.2198   0.0293   0.0000   0.0438   0.1887    0.214
  34 -12.4702  10.5339  17.3577  13.0286   0.1644   1.2990   0.0247   0.0000   0.0340   0.2112    0.224
  35 -14.1033   9.4509  15.2562  12.4251   0.1698   1.3842   0.0162   0.0000   0.0236   0.2351    0.233
  36 -15.6864   8.4012  13.0038  11.7157   0.1756   1.4730   0.0033   0.0000   0.0138   0.2590    0.241
  37 -17.1873   7.4059  10.7381  10.9108   0.1827   1.5634  -0.0179   0.0000   0.0064   0.2808    0.246
  38 -18.5393   6.5605   8.2095  10.0783   0.2276   1.6319  -0.0224   0.0000  -0.0027   0.3215    0.252
  39 -19.7200   5.8715   6.4897   8.9729   0.2255   1.6283  -0.0367   0.0000  -0.0004   0.3185    0.250
  40 -20.7431   5.2745   4.9408   7.7174   0.2284   1.5677  -0.0604   0.0000   0.0095   0.2973    0.244
  41 -21.5878   4.7816   3.5820   6.3126   0.2315   1.4266  -0.0901   0.0000   0.0228   0.2568    0.234
  42 -22.2368   4.4029   2.4051   4.7224   0.2135   1.1778  -0.1281   0.0000   0.0345   0.1955    0.221
  43 -22.6770   4.1460   1.3776   2.9086   0.0781   0.8061  -0.1882   0.0000   0.0372   0.1157    0.204
  44 -22.8993   4.0163   0.4479   0.9694  -1.2566   0.3691  -0.3329   0.0000   0.0173   0.0361    0.203

 Surface # 3     Vertical Stabilisor
   # Chordwise =  8   # Spanwise = 14     First strip = 45
   Surface area =  59.797329       Ave. chord =    6.535571
   CLsurf  =   0.00000     Clsurf  =   0.00001
   CYsurf  =  -0.00026     Cmsurf  =   0.00000
   CDsurf  =   0.00000     Cnsurf  =   0.00014
   CDisurf =   0.00000     CDvsurf =   0.00000

 Forces referred to Ssurf, Cave about hinge axis thru LE
   CLsurf  =   0.00221     CDsurf  =   0.00000
   Deflect =

 Strip Forces referred to Strip Area, Chord
   j     Yle    Chord     Area     c cl      ai      cl       cd      cdv    cm_c/4    cm_LE  C.P.x/c
  45   0.0000   8.6649   2.1611   0.0036   0.0020   0.0004   0.0000   0.0000  -0.0002  -0.0003
  46   0.0000   8.5057   3.5481   0.0055   0.0009   0.0006   0.0000   0.0000  -0.0003  -0.0004
  47   0.0000   8.2691   4.7312   0.0097   0.0010   0.0012   0.0000   0.0000  -0.0006  -0.0007
  48   0.0000   7.9632   5.6273   0.0148   0.0015   0.0019   0.0000   0.0000  -0.0009  -0.0011
  49   0.0000   7.5994   6.1854   0.0161   0.0012   0.0021   0.0000   0.0000  -0.0010  -0.0012
  50   0.0000   7.1919   6.3906   0.0169   0.0011   0.0023   0.0000   0.0000  -0.0010  -0.0013
  51   0.0000   6.7574   6.2632   0.0174   0.0011   0.0026   0.0000   0.0000  -0.0010  -0.0013
  52   0.0000   6.3137   5.8520   0.0175   0.0011   0.0028   0.0000   0.0000  -0.0010  -0.0014
  53   0.0000   5.8792   5.2242   0.0171   0.0011   0.0029   0.0000   0.0000  -0.0010  -0.0014
  54   0.0000   5.4718   4.4537   0.0164   0.0011   0.0030   0.0000   0.0000  -0.0009  -0.0015
  55   0.0000   5.1079   3.6096   0.0149   0.0013   0.0029   0.0000   0.0000  -0.0009  -0.0014
  56   0.0000   4.8020   2.7475   0.0130   0.0016   0.0027   0.0000   0.0000  -0.0008  -0.0013
  57   0.0000   4.5654   1.9044   0.0104   0.0021   0.0023   0.0000   0.0000  -0.0007  -0.0011
  58   0.0000   4.4062   1.0990   0.0067   0.0034   0.0015   0.0000   0.0000  -0.0006  -0.0008

 Surface # 4     Upper Winglet
   # Chordwise =  4   # Spanwise =  5     First strip = 59
   Surface area =   6.685101       Ave. chord =    1.720000
   CLsurf  =   0.00281     Clsurf  =  -0.00083
   CYsurf  =  -0.00643     Cmsurf  =  -0.00252
   CDsurf  =  -0.00075     Cnsurf  =   0.00111
   CDisurf =  -0.00075     CDvsurf =   0.00000
```

```
 Forces referred to Ssurf, Cave about hinge axis thru LE
   CLsurf  =   0.52594     CDsurf  =  -0.05721
   Deflect =

Strip Forces referred to Strip Area, Chord
   j     Yle    Chord     Area     c cl      ai      cl       cd       cdv     cm_c/4    cm_LE  C.P.x/c
  59  22.9477   2.5569   0.9490   0.2559  -1.5195   0.1017  -0.0130   0.0000  -0.0085  -0.0392   0.462
  60  23.1016   2.2373   2.1739   0.9525  -0.3426   0.4304  -0.0303   0.0000   0.0079  -0.1413   0.198
  61  23.3506   1.7200   2.0658   1.1912  -0.1314   0.7027  -0.0731   0.0000   0.0369  -0.2223   0.120
  62  23.5996   1.2027   1.1687   0.9033  -0.0801   0.7644  -0.1024   0.0000   0.0726  -0.2401   0.036
  63  23.7535   0.8831   0.3277   0.3633  -0.0165   0.4235  -0.1025   0.0000   0.0883  -0.1158  -0.108

 Surface # 5     Upper Winglet (YDUP)
   # Chordwise =  4   # Spanwise =  5     First strip = 64
   Surface area =    6.685101       Ave. chord =    1.720000
   CLsurf  =   0.00281     Clsurf  =   0.00083
   CYsurf  =   0.00643     Cmsurf  =  -0.00253
   CDsurf  =  -0.00075     Cnsurf  =  -0.00111
   CDisurf =  -0.00075     CDvsurf =   0.00000

 Forces referred to Ssurf, Cave about hinge axis thru LE
   CLsurf  =   0.52596     CDsurf  =  -0.05721
   Deflect =

Strip Forces referred to Strip Area, Chord
   j     Yle    Chord     Area     c cl      ai      cl       cd       cdv     cm_c/4    cm_LE  C.P.x/c
  64 -22.9477   2.5569   0.9490   0.2559  -1.5196   0.1017  -0.0130   0.0000  -0.0085   0.0392   0.462
  65 -23.1016   2.2373   2.1739   0.9526  -0.3426   0.4304  -0.0303   0.0000   0.0079   0.1413   0.198
  66 -23.3506   1.7200   2.0658   1.1913  -0.1315   0.7027  -0.0731   0.0000   0.0369   0.2223   0.120
  67 -23.5996   1.2027   1.1687   0.9033  -0.0801   0.7644  -0.1024   0.0000   0.0726   0.2401   0.036
  68 -23.7535   0.8831   0.3277   0.3633  -0.0165   0.4235  -0.1025   0.0000   0.0883   0.1158  -0.108

 Surface # 6     lower Winglet
   # Chordwise =  2   # Spanwise =  4     First strip = 69
   Surface area =    1.249446       Ave. chord =    1.120000
   CLsurf  =   0.00052     Clsurf  =  -0.00036
   CYsurf  =   0.00078     Cmsurf  =  -0.00032
   CDsurf  =  -0.00008     Cnsurf  =  -0.00017
   CDisurf =  -0.00008     CDvsurf =   0.00000

 Forces referred to Ssurf, Cave about hinge axis thru LE
   CLsurf  =   0.37951     CDsurf  =  -0.03295
   Deflect =

Strip Forces referred to Strip Area, Chord
   j     Yle    Chord     Area     c cl      ai      cl       cd       cdv     cm_c/4    cm_LE  C.P.x/c
  69  22.9521   1.5635   0.2554   0.1880  -2.3161   0.1238  -0.0074   0.0000  -0.0199  -0.0205   0.529
  70  23.1305   1.3037   0.5142   0.4943  -0.5930   0.3878  -0.0097   0.0000  -0.0511  -0.0564   0.479
  71  23.3827   0.9363   0.3693   0.5053  -0.2651   0.5600  -0.0598   0.0000  -0.0450  -0.0654   0.397
  72  23.5611   0.6765   0.1105   0.2054  -0.1813   0.3287  -0.1105   0.0000  -0.0085  -0.0301   0.304

 Surface # 7     lower Winglet (YDUP)
   # Chordwise =  2   # Spanwise =  4     First strip = 73
   Surface area =    1.249446       Ave. chord =    1.120000
   CLsurf  =   0.00052     Clsurf  =   0.00036
   CYsurf  =  -0.00078     Cmsurf  =  -0.00032
   CDsurf  =  -0.00008     Cnsurf  =   0.00017
   CDisurf =  -0.00008     CDvsurf =   0.00000

 Forces referred to Ssurf, Cave about hinge axis thru LE
   CLsurf  =   0.37952     CDsurf  =  -0.03295
   Deflect =

Strip Forces referred to Strip Area, Chord
   j     Yle    Chord     Area     c cl      ai      cl       cd       cdv     cm_c/4    cm_LE  C.P.x/c
  73 -22.9521   1.5635   0.2554   0.1880  -2.3162   0.1238  -0.0074   0.0000  -0.0199   0.0205   0.529
  74 -23.1305   1.3037   0.5142   0.4943  -0.5930   0.3878  -0.0097   0.0000  -0.0511   0.0564   0.479
  75 -23.3827   0.9363   0.3693   0.5053  -0.2651   0.5600  -0.0598   0.0000  -0.0450   0.0654   0.397
  76 -23.5611   0.6765   0.1105   0.2054  -0.1813   0.3287  -0.1105   0.0000  -0.0085   0.0301   0.304
 ---------------------------------------------------------------
```

H.3 BDVT AVL Anlaysis

H.3.1 BDVT Input AVL file

```
AVPlanform
0.800                 !  Mach
0     0     0.0       !  iYsym  iZsym  Zsym
397.0545   12.2   46.40716966      !  Sref   Cref   Bref   reference area, chord, span
26.367    0.0   -0.481      !  Xref   Yref   Zref   moment reference location (arb.)
0.008659              !  CDp
#
#==============================================================
#
SURFACE
Wing
10  1.0  22  1.0   ! Nchord   Cspace   Nspan  Sspace
#
# reflect image wing about y=0 plane
YDUPLICATE
    0.00000
#
# twist angle bias for whole surface
ANGLE
    0.00000
#
SCALE
  1.0   1.0   1.0
#
# x,y,z bias for whole surface
TRANSLATE
   10.87482     0.00000     -1.88
#
#------------------------------------------------------------
#   Xle         Yle         Zle         chord       angle   Nspan  Sspace
SECTION
    0.0         0.0         0.0         23.372      0.000   9     -0.75

AFIL
BD1-63A-0(10.5)A-Mod34.dat

#Cname   Cgain  Xhinge  HingeVec      SgnDup
CONTROL
camber   1.0    0.70    0.0 1.0 0.0     1.0

CONTROL
VCF     1.0   0.70     0.0 1.0 0.0     1.0
#------------------------------
SECTION
   13.327587     8.489116     -0.694269       10.489309       -0.500   7     -1.25

AFIL
BD2-63A-0(10.5)A-Mod34.dat

CONTROL
camber   1.0    0.70    0.0 1.0 0.0     1.0

CONTROL
VCF     1.0    0.7     0.0 1.0 0.0     1.0
#------------------------------
SECTION
   20.176318    18.109116       -1.170379     4.767868      -1.2500   5     -1.25

AFIL
BD3-63A-009A.dat

CONTROL
camber   1.0    0.70    0.0 1.0 0.11    1.0

CONTROL
aileron     0.3   0.70     0.0 1.0 0.0   -1.0
#------------------------------
SECTION
   23.040642    23.199116      -1.330143      2.500      -2.000   5     -1.25

AFIL
BD4-63A-010A.dat

CONTROL
camber   1.0    0.70    0.0 1.0 0.11    1.0
```

```
CONTROL
aileron  -1.0   0.70    0.0 1.0 0.11   -1.0
#
#============================================================
#
SURFACE
V-tail
8  1.0  5  -1.5  !  Nchord   Cspace
#
# reflect image wing about y=0 plane
YDUPLICATE
    0.00000
#
# twist angle bias for whole surface
ANGLE
    3.50000
#
# x,y,z bias for whole surface
TRANSLATE
  43.55485     1.050     1.50000
#------------------------------------------------------------
#    Xle         Yle         Zle         chord       angle   Nspan  Sspace
SECTION
  0.00          0.0         0.0         9.500        0.000   5     -1.50

AFIL
SC2-0010hs.dat

CONTROL
Ruddervator  1.0    0.35    0.0 1.0 0.0     1.0
#-----------------------------
SECTION
  8.392195        5.436686        4.247604         5.000        0.000   0      0

AFIL
SC2-0010hs.dat

CONTROL
Ruddervator  1.0    0.35    0.0 1.0 0.0     1.0
#
#============================================================
#
SURFACE
Upper Winglet
4  1.0  5  1.0   ! Nchord   Cspace   Nspan  Sspace
#
# reflect image wing about y=0 plane
YDUPLICATE
    0.00000
#
# twist angle bias for whole surface
ANGLE
    -4.00000
#
SCALE
  1.0   1.0   1.0
#
# x,y,z bias for whole surface
TRANSLATE
    34.760    23.199116         -3.210143
#
#------------------------------------------------------------
#    Xle         Yle         Zle         chord       angle   Nspan  Sspace
SECTION
    0             0         0         1.625      0.000   9     -0.75

AFIL
BD4-63A-010A.dat

#-----------------------------
SECTION
  3.063331    0.847232         2.5         0.525      0.000   9     -0.75

AFIL
BD4-63A-010A.dat
#
#============================================================
#
SURFACE
lower Winglet
2  1.0  4  1.0   ! Nchord   Cspace   Nspan  Sspace
#
```

```
# reflect image wing about y=0 plane
YDUPLICATE
    0.00000
#
# twist angle bias for whole surface
ANGLE
    0.00000
#
SCALE
 1.0   1.0   1.0
#
# x,y,z bias for whole surface
TRANSLATE
   33.915462     23.199116     -3.210143
#
#------------------------------------------------------------
#   Xle         Yle         Zle         chord       angle   Nspan  Sspace
SECTION
    0      0         0         1.0      -7.000   9     -0.75

AFIL
BD4-63A-010A.dat

#-----------------------------
SECTION
  1.110467    0.659175         -0.575         0.4      -11.000   9     -0.75

AFIL
BD4-63A-010A.dat
#
#============================================================
#

BODY
fuselage
37  1
#
TRANSLATE
   0.00000     0.00000     0.00000
#
BFIL
fusemodAVPB767.dat

#============================================================
```

H.3.2 BDVT Primary Run Case and Results for Cruise

```
-------------------------------------------------
 Run case  1:  - Mach 0.8 Cruise @ 39500ft -

 alpha        ->  CL          =  0.337999
 beta         ->  beta        =   0.00000
 pb/2V        ->  pb/2V       =   0.00000
 qc/2V        ->  qc/2V       =   0.00000
 rb/2V        ->  rb/2V       =   0.00000
 camber       ->  camber      =   0.00000
 VCF          ->  VCF         =   0.00000
 aileron      ->  aileron     =   0.00000
 Ruddervator  ->  Ruddervator =   0.00000

 alpha     =   0.00000
 beta      =   0.00000
 pb/2V     =   0.00000
 qc/2V     =   0.00000
 rb/2V     =   0.00000
 CL        =   0.00000
 CDo       =  0.865900E-02
 bank      =   0.00000
 elevation =   0.00000
 heading   =   0.00000
 Mach      =  0.802000
 velocity  =   236.644
 density   =  0.311000
 grav.acc. =   9.81000
 turn_rad. =   0.00000
 load_fac. =   0.00000
 X_cg      =   26.3050
 Y_cg      =   0.00000
 Z_cg      = -0.561000
 mass      =   117795.
 Ixx       =   740.000
 Iyy       =   1190.00
 Izz       =   453.000
 Ixy       =   579.000
 Iyz       =  0.194000E-12
 Izx       =  0.194000E-12
 visc CL_a =   0.00000
 visc CL_u =   0.00000
 visc CM_a =   0.00000
 visc CM_u =   0.00000
```

BD Initial Results for primary cruise case

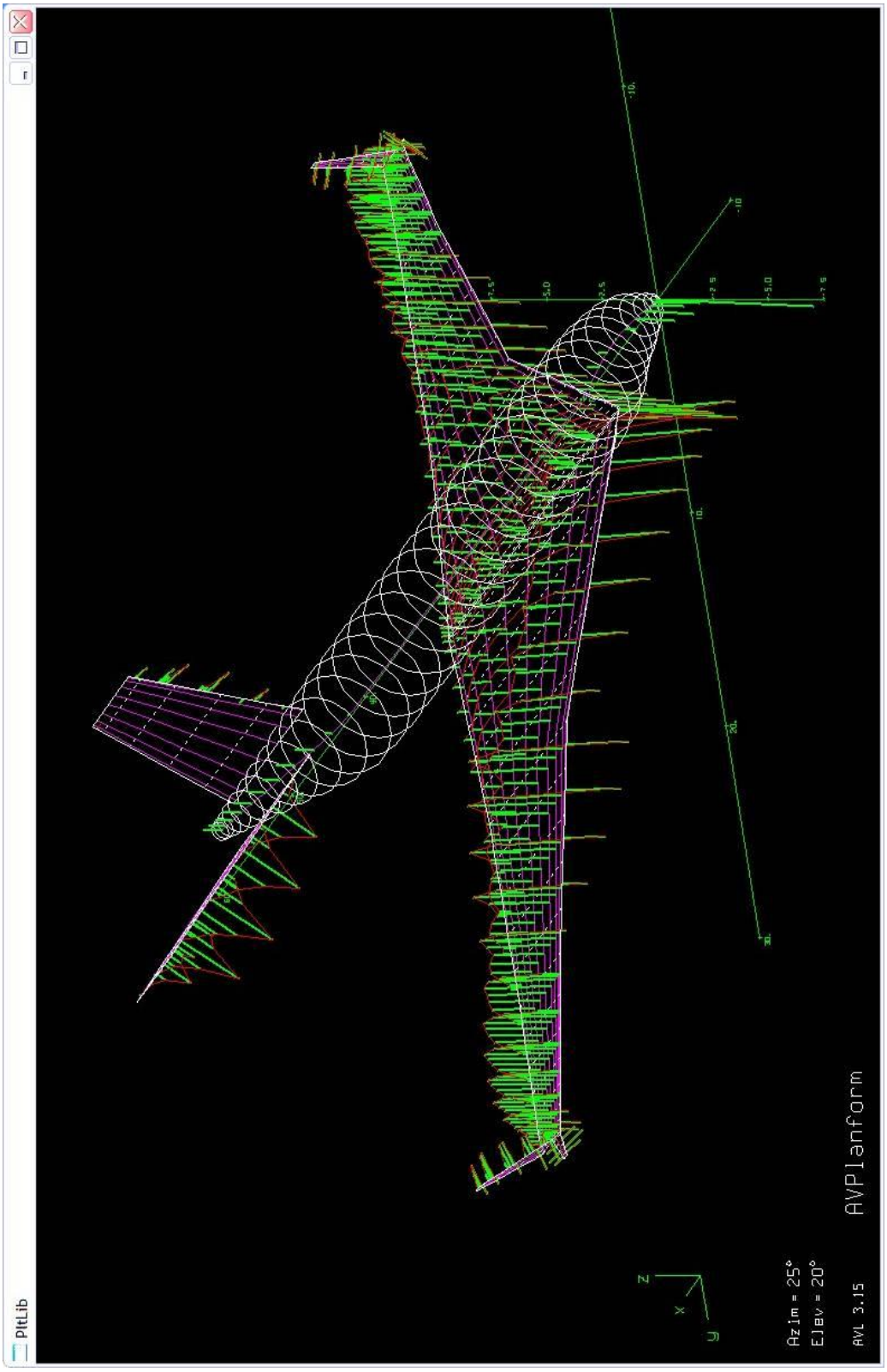

Fig H-5: BDVT Geometry for flight case of Mach 0.8 with cruise @ 39,500 ft

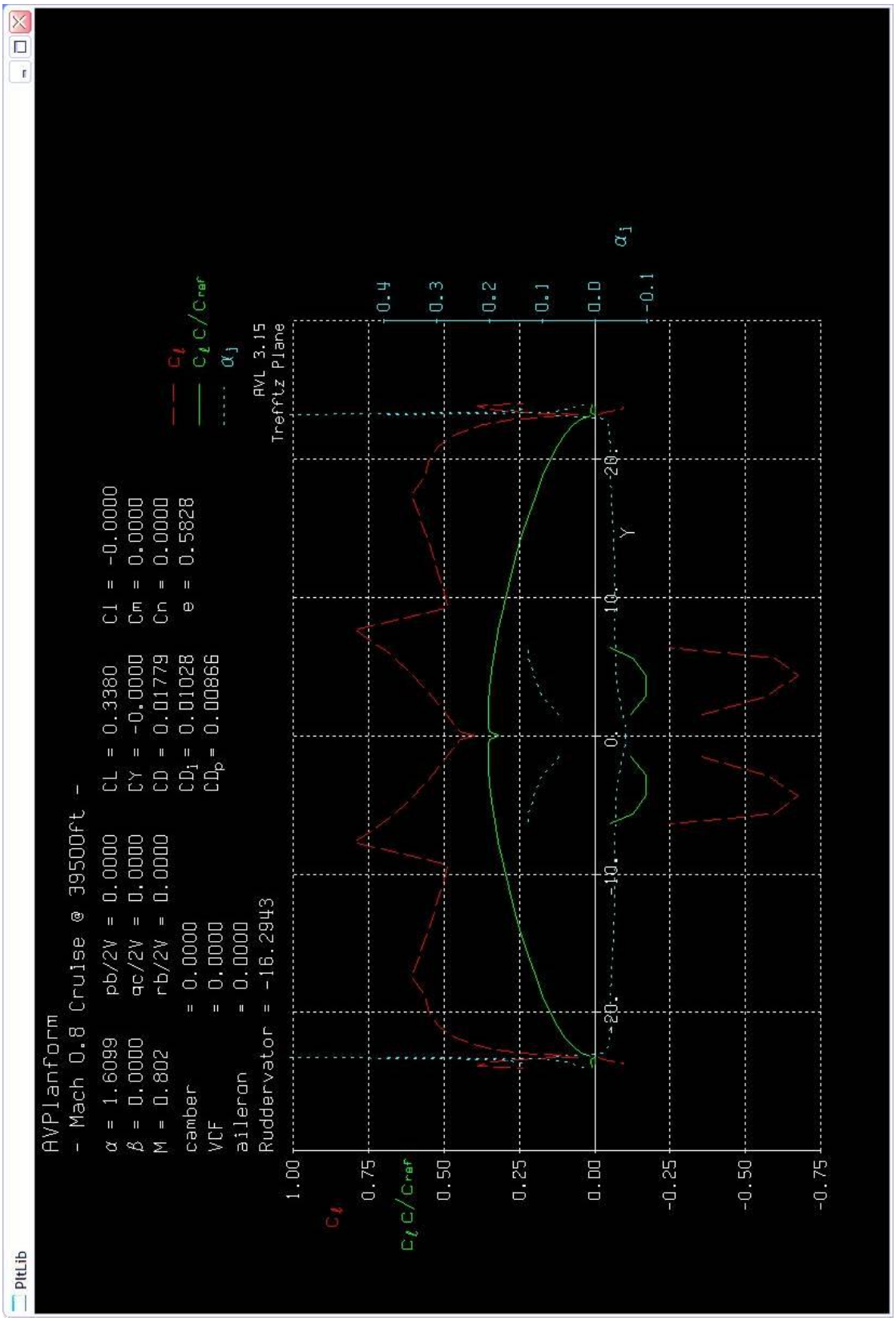

Fig H-6: BDVT Trefftz plane plot for flight case of Mach 0.8 with cruise @ 39,500 ft

CRUISE STABILITY RESULTS

```
---------------------------------------------------------------
---------------------------------------------------------------
 Vortex Lattice Output -- Total Forces

 Configuration: AVPlanform
    # Surfaces =   8
    # Strips   =  72
    # Vortices = 576

  Sref =  397.05       Cref =  12.200       Bref =  46.407
  Xref =  26.305       Yref =  0.0000       Zref =-0.56100

 Standard axis orientation,  X fwd, Z down

 Run case: - Mach 0.8 Cruise @ 39500ft -

  Alpha =   0.88837     pb/2V =   0.00000     p'b/2V =   0.00000
  Beta  =   0.00000     qc/2V =   0.00000
  Mach  =     0.802     rb/2V =   0.00000     r'b/2V =   0.00000

  CXtot =  -0.00967     Cltot =   0.00000     Cl'tot =   0.00000
  CYtot =   0.00000     Cmtot =  -0.13972
  CZtot =  -0.33819     Cntot =   0.00000     Cn'tot =   0.00000

  CLtot =   0.33800
  CDtot =   0.01491
  CDvis =   0.00866     CDind =   0.00625
  CLff  =   0.31748     CDff  =   0.00638    | Trefftz
  CYff  =   0.00000       e   =     0.9271   | Plane

  camber      =   0.00000
  VCF         =   0.00000
  aileron     =   0.00000
  Ruddervator =   0.00000

 ---------------------------------------------------------------

 Derivatives...
                      alpha              beta
                ---------------    ---------------
 z force    |    CLa =   5.854410    CLb =   0.000000
 y force    |    CYa =   0.000000    CYb =  -0.243322
 roll  x mom.|   Cla =   0.000000    Clb =  -0.023507
 pitch y mom.|   Cma =  -0.114650    Cmb =   0.000000
 yaw   z mom.|   Cna =   0.000000    Cnb =  -0.048090

                   roll rate  p       pitch rate  q         yaw rate  r
                ---------------    ---------------    ---------------
 z force    |    CLp =   0.000000    CLq =   6.150762    CLr =   0.000000
 y force    |    CYp =   0.116111    CYq =   0.000000    CYr =  -0.072684
 roll  x mom.|   Clp =  -0.440621    Clq =   0.000000    Clr =   0.077447
 pitch y mom.|   Cmp =   0.000000    Cmq =  -4.345937    Cmr =   0.000000
 yaw   z mom.|   Cnp =  -0.033188    Cnq =   0.000000    Cnr =  -0.111646

                camber      d1     VCF         d2     aileron      d3     Ruddervator  d4
                ---------------    ---------------    ---------------    ---------------
 z force    |  CLd1 =   0.065577   CLd2 =   0.034882   CLd3 =   0.000000   CLd4 =   0.004385
 y force    |  CYd1 =   0.000000   CYd2 =   0.000000   CYd3 =  -0.000003   CYd4 =   0.000000
 roll  x mom.|  Cld1 =   0.000000   Cld2 =   0.000000   Cld3 =   0.000513   Cld4 =   0.000000
 pitch y mom.|  Cmd1 =  -0.017840   Cmd2 =  -0.005477   Cmd3 =   0.000000   Cmd4 =  -0.008283
 yaw   z mom.|  Cnd1 =   0.000000   Cnd2 =   0.000000   Cnd3 =   0.000001   Cnd4 =   0.000000
 Trefftz drag| CDffd1 =   0.002264 CDffd2 =   0.001371 CDffd3 =   0.000000 CDffd4 =   0.000390
 span eff.  |   ed1 =   0.052145    ed2 =   0.003710    ed3 =   0.000000    ed4 =  -0.030935

Neutral point  Xnp =  26.543919

 Clb Cnr / Clr Cnb  =  -0.704678    ( > 1 if spirally stable )
```

CRUISE SURFACE BODY RESULTS

```
---------------------------------------------------------------
 Vortex Lattice Output -- Total Forces

 Configuration: AVPlanform
    # Surfaces =   8
    # Strips   =  72
```

```
   # Vortices = 576

 Sref =  397.05       Cref =  12.200       Bref =  46.407
 Xref =  26.305       Yref =  0.0000       Zref =-0.56100

Standard axis orientation,  X fwd, Z down

Run case: - Mach 0.8 Cruise @ 39500ft -

 Alpha =   0.88837     pb/2V =   0.00000     p'b/2V =   0.00000
 Beta  =   0.00000     qc/2V =   0.00000
 Mach  =     0.802     rb/2V =   0.00000     r'b/2V =   0.00000

 CXtot =  -0.00967     Cltot =   0.00000     Cl'tot =   0.00000
 CYtot =   0.00000     Cmtot =  -0.13972
 CZtot =  -0.33819     Cntot =   0.00000     Cn'tot =   0.00000

 CLtot =   0.33800
 CDtot =   0.01491
 CDvis =   0.00866     CDind =   0.00625
 CLff  =   0.31748     CDff  =   0.00638    | Trefftz
 CYff  =   0.00000       e   =     0.9271   | Plane

  camber      =   0.00000
  VCF         =   0.00000
  aileron     =   0.00000
  Ruddervator =   0.00000

---------------------------------------------------------------

Geometry-axis derivatives...

               axial   vel. u     sideslip vel. v      normal  vel. w
             ----------------    ----------------    ----------------
x force    |   CXu =  -0.022782    CXv =   0.000000    CXw =   0.191262
y force    |   CYu =   0.000000    CYv =  -0.243351    CYw =   0.000000
z force    |   CZu =  -0.577578    CZv =   0.000000    CZw =  -5.877422
roll  x mom.|   Clu =   0.000000    Clv =  -0.023510    Clw =   0.000000
pitch y mom.|   Cmu =  -0.255712    Cmv =   0.000000    Cmw =  -0.118628
yaw   z mom.|   Cnu =   0.000000    Cnv =  -0.048096    Cnw =   0.000000

               roll rate  p       pitch rate  q         yaw rate  r
             ----------------    ----------------    ----------------
x force    |   CXp =   0.000000    CXq =  -0.083750    CXr =   0.000000
y force    |   CYp =   0.117224    CYq =   0.000000    CYr =  -0.070875
z force    |   CZp =   0.000000    CZq =  -6.152799    CZr =   0.000000
roll  x mom.|   Clp =  -0.441769    Clq =   0.000000    Clr =   0.070606
pitch y mom.|   Cmp =   0.000000    Cmq =  -4.345937    Cmr =   0.000000
yaw   z mom.|   Cnp =  -0.031453    Cnq =   0.000000    Cnr =  -0.112147

             camber      d1     VCF         d2     aileron      d3     Ruddervator  d4
             ----------------    ----------------    ----------------    ----------------
x force    |   CXd1 =  -0.000149   CXd2 =  -0.000208   CXd3 =   0.000000   CXd4 =  -0.000262
y force    |   CYd1 =   0.000000   CYd2 =   0.000000   CYd3 =  -0.000003   CYd4 =   0.000000
z force    |   CZd1 =  -0.065587   CZd2 =  -0.034889   CZd3 =   0.000000   CZd4 =  -0.004390
roll  x mom.|   Cld1 =   0.000000   Cld2 =   0.000000   Cld3 =   0.000513   Cld4 =   0.000000
pitch y mom.|   Cmd1 =  -0.017840   Cmd2 =  -0.005477   Cmd3 =   0.000000   Cmd4 =  -0.008283
yaw   z mom.|   Cnd1 =   0.000000   Cnd2 =   0.000000   Cnd3 =   0.000001   Cnd4 =   0.000000
```

CRUISE TOTAL STRIP FORCES RESULTS

```
---------------------------------------------------------------
 Vortex Lattice Output -- Total Forces

 Configuration: AVPlanform
   # Surfaces =   8
   # Strips   =  72
   # Vortices = 576

 Sref =  397.05       Cref =  12.200       Bref =  46.407
 Xref =  26.305       Yref =  0.0000       Zref =-0.56100

Standard axis orientation,  X fwd, Z down

Run case: - Mach 0.8 Cruise @ 39500ft -

 Alpha =   1.60987     pb/2V =   0.00000     p'b/2V =   0.00000
 Beta  =   0.00000     qc/2V =   0.00000
 Mach  =     0.802     rb/2V =   0.00000     r'b/2V =   0.00000
```

```
 CXtot =  -0.00829     Cltot =   0.00000     Cl'tot =   0.00000
 CYtot =   0.00000     Cmtot =   0.00000
 CZtot =  -0.33837     Cntot =   0.00000     Cn'tot =   0.00000

 CLtot =   0.33800
 CDtot =   0.01779
 CDvis =   0.00866     CDind =   0.00913
 CLff  =   0.31958     CDff  =   0.01028    | Trefftz
 CYff  =   0.00000         e =   0.5828     | Plane

  camber      =   0.00000
  VCF         =   0.00000
  aileron     =   0.00000
  Ruddervator =  -16.29429

------------------------------------------------------------------
------------------------------------------------------------------
Surface Forces (referred to Sref,Cref,Bref about Xref,Yref,Zref)
Standard axis orientation,  X fwd, Z down

    Sref =   397.1       Cref =   12.2000   Bref =   46.4072
    Xref =    26.3050    Yref =    0.0000   Zref =   -0.5610

n     Area     CL      CD      Cm      CY      Cn      Cl     CDi     CDv
1   236.367  0.1834  0.0041 -0.0292  0.0099 -0.0004 -0.0378  0.0041  0.0000   Wing
2   236.367  0.1834  0.0041 -0.0292 -0.0099  0.0004  0.0378  0.0041  0.0000   Wing (YDUP)
3    49.970 -0.0244  0.0006  0.0493  0.0181 -0.0095  0.0032  0.0006  0.0000   V-tail
4    49.970 -0.0244  0.0006  0.0493 -0.0181  0.0095 -0.0032  0.0006  0.0000   V-tail (YDUP)
5     2.838  0.0003  0.0000 -0.0003 -0.0008  0.0002 -0.0001  0.0000  0.0000   Upper Winglet
6     2.838  0.0003  0.0000 -0.0003  0.0008 -0.0002  0.0001  0.0000  0.0000   Upper Winglet (YDUP)
7     0.612  0.0000  0.0000  0.0000  0.0000  0.0000  0.0000  0.0000  0.0000   lower Winglet
8     0.612  0.0000  0.0000  0.0000  0.0000  0.0000  0.0000  0.0000  0.0000   lower Winglet (YDUP)

Surface Forces (referred to Ssurf, Cave about root LE on hinge axis)

 n     Ssurf     Cave      cl       cd      cdv    cm_LE
 1   236.367    10.170   0.3085   0.0070   0.0000   0.0000  Wing
 2   236.367    10.170   0.3085   0.0070   0.0000   0.0000  Wing (YDUP)
 3    49.970     7.243  -0.2413   0.0050   0.0000   0.0000  V-tail
 4    49.970     7.243  -0.2413   0.0050   0.0000   0.0000  V-tail (YDUP)
 5     2.838     1.075   0.1219  -0.0056   0.0000   0.0000  Upper Winglet
 6     2.838     1.075   0.1219  -0.0056   0.0000   0.0000  Upper Winglet (YDUP)
 7     0.612     0.700  -0.0245   0.0010   0.0000   0.0000  lower Winglet
 8     0.612     0.700  -0.0245   0.0010   0.0000   0.0000  lower Winglet (YDUP)
------------------------------------------------------------------
------------------------------------------------------------------
Surface and Strip Forces by surface

 Forces referred to Sref, Cref, Bref about Xref, Yref, Zref
Standard axis orientation,  X fwd, Z down

 Surface # 1     Wing
   # Chordwise = 10   # Spanwise = 22     First strip =  1
   Surface area =  236.367264       Ave. chord =   10.169948
   CLsurf  =   0.18342     Clsurf  =  -0.03779
   CYsurf  =   0.00987     Cmsurf  =  -0.02925
   CDsurf  =   0.00414     Cnsurf  =  -0.00035
   CDisurf =   0.00414     CDvsurf =   0.00000

 Forces referred to Ssurf, Cave about hinge axis thru LE
   CLsurf  =   0.30853     CDsurf  =   0.00695
   Deflect =

Strip Forces referred to Strip Area, Chord
  j      Yle    Chord      Area     c cl      ai      cl       cd      cdv    cm_c/4    cm_LE  C.P.x/c
  1   0.0301  23.3263   2.8155   3.9291   0.0586   0.1657   0.1001   0.0000  -0.0520  -0.0503    0.550
  2   0.2701  22.9621   8.2582   4.2569   0.0584   0.1849   0.0213   0.0000  -0.0540  -0.0536    0.541
  3   0.7452  22.2411  13.1505   4.3012   0.0572   0.1932   0.0104   0.0000  -0.0542  -0.0548    0.531
  4   1.4457  21.1781  17.1723   4.3100   0.0540   0.2033   0.0092   0.0000  -0.0533  -0.0557    0.512
  5   2.3574  19.7945  20.0704   4.3021   0.0482   0.2172   0.0094   0.0000  -0.0520  -0.0568    0.490
  6   3.4617  18.1187  21.6768   4.2630   0.0426   0.2351   0.0094   0.0000  -0.0509  -0.0586    0.467
  7   4.7361  16.1847  21.9215   4.1837   0.0397   0.2583   0.0091   0.0000  -0.0501  -0.0613    0.444
  8   6.1547  14.0319  20.8370   4.0616   0.0390   0.2893   0.0088   0.0000  -0.0494  -0.0650    0.421
  9   7.6886  11.7041  18.5540   3.8954   0.0382   0.3328   0.0067   0.0000  -0.0475  -0.0697    0.393
 10   9.2982  10.0081  16.3421   3.7014   0.0377   0.3698   0.0052   0.0000  -0.0450  -0.1117    0.372
 11  10.9503   9.0256  15.0439   3.4871   0.0384   0.3864   0.0040   0.0000  -0.0469  -0.1167    0.372
 12  12.6193   8.0329  13.3894   3.2463   0.0376   0.4042   0.0026   0.0000  -0.0497  -0.1227    0.373
 13  14.2713   7.0504  11.5124   2.9812   0.0358   0.4230   0.0008   0.0000  -0.0535  -0.1298    0.377
 14  15.8728   6.0979   9.5476   2.6968   0.0334   0.4425  -0.0014   0.0000  -0.0582  -0.1377    0.382
 15  17.3910   5.1950   7.6193   2.3997   0.0312   0.4622  -0.0045   0.0000  -0.0629  -0.1459    0.386
 16  18.7589   4.4784   5.6708   2.1000   0.0296   0.4693  -0.0065   0.0000  -0.0650  -0.1596    0.389
```

17	19.9537	3.9460	4.4135	1.8018	0.0288	0.4570	-0.0070	0.0000	-0.0634	-0.1557	0.389
18	20.9890	3.4847	3.3032	1.4998	0.0286	0.4308	-0.0081	0.0000	-0.0582	-0.1458	0.385
19	21.8437	3.1039	2.3529	1.1905	0.0282	0.3840	-0.0092	0.0000	-0.0496	-0.1282	0.379
20	22.5005	2.8113	1.5540	0.8691	0.0260	0.3096	-0.0102	0.0000	-0.0380	-0.1018	0.373
21	22.9459	2.6128	0.8785	0.5296	0.0149	0.2031	-0.0118	0.0000	-0.0238	-0.0659	0.367
22	23.1709	2.5126	0.2835	0.1760	-0.0742	0.0706	-0.0181	0.0000	-0.0077	-0.0224	0.360

Surface # 2 Wing (YDUP)
Chordwise = 10 # Spanwise = 22 First strip = 23
Surface area = 236.367264 Ave. chord = 10.169948
CLsurf = 0.18342 Clsurf = 0.03779
CYsurf = -0.00987 Cmsurf = -0.02925
CDsurf = 0.00414 Cnsurf = 0.00035
CDisurf = 0.00414 CDvsurf = 0.00000

Forces referred to Ssurf, Cave about hinge axis thru LE
CLsurf = 0.30853 CDsurf = 0.00695
Deflect =

Strip Forces referred to Strip Area, Chord

j	Yle	Chord	Area	c cl	ai	cl	cd	cdv	cm_c/4	cm_LE	C.P.x/c
23	-0.0301	23.3263	2.8155	3.9291	0.0586	0.1657	0.1001	0.0000	-0.0520	0.0503	0.550
24	-0.2701	22.9621	8.2582	4.2569	0.0584	0.1849	0.0213	0.0000	-0.0540	0.0536	0.541
25	-0.7452	22.2411	13.1505	4.3012	0.0572	0.1932	0.0104	0.0000	-0.0542	0.0548	0.531
26	-1.4457	21.1781	17.1723	4.3100	0.0540	0.2033	0.0092	0.0000	-0.0533	0.0557	0.512
27	-2.3574	19.7945	20.0704	4.3021	0.0482	0.2172	0.0094	0.0000	-0.0520	0.0568	0.490
28	-3.4617	18.1187	21.6768	4.2630	0.0426	0.2351	0.0094	0.0000	-0.0509	0.0586	0.467
29	-4.7361	16.1847	21.9215	4.1837	0.0397	0.2583	0.0091	0.0000	-0.0501	0.0613	0.444
30	-6.1547	14.0319	20.8370	4.0616	0.0390	0.2893	0.0088	0.0000	-0.0494	0.0650	0.421
31	-7.6886	11.7041	18.5540	3.8954	0.0382	0.3328	0.0067	0.0000	-0.0475	0.0697	0.393
32	-9.2982	10.0081	16.3421	3.7014	0.0377	0.3698	0.0052	0.0000	-0.0450	0.1117	0.372
33	-10.9503	9.0256	15.0439	3.4871	0.0384	0.3864	0.0040	0.0000	-0.0469	0.1167	0.372
34	-12.6193	8.0329	13.3894	3.2463	0.0376	0.4042	0.0026	0.0000	-0.0497	0.1227	0.373
35	-14.2713	7.0504	11.5124	2.9812	0.0358	0.4230	0.0008	0.0000	-0.0535	0.1298	0.377
36	-15.8728	6.0979	9.5476	2.6968	0.0334	0.4425	-0.0014	0.0000	-0.0582	0.1377	0.382
37	-17.3910	5.1950	7.6193	2.3997	0.0312	0.4622	-0.0045	0.0000	-0.0629	0.1459	0.386
38	-18.7589	4.4784	5.6708	2.1000	0.0296	0.4693	-0.0065	0.0000	-0.0650	0.1596	0.389
39	-19.9537	3.9460	4.4135	1.8018	0.0288	0.4570	-0.0070	0.0000	-0.0634	0.1557	0.389
40	-20.9890	3.4847	3.3032	1.4998	0.0286	0.4308	-0.0081	0.0000	-0.0582	0.1458	0.385
41	-21.8437	3.1039	2.3529	1.1905	0.0282	0.3840	-0.0092	0.0000	-0.0496	0.1282	0.379
42	-22.5005	2.8113	1.5540	0.8691	0.0260	0.3096	-0.0102	0.0000	-0.0380	0.1018	0.373
43	-22.9459	2.6128	0.8785	0.5296	0.0149	0.2031	-0.0118	0.0000	-0.0238	0.0659	0.367
44	-23.1709	2.5126	0.2835	0.1760	-0.0742	0.0706	-0.0181	0.0000	-0.0077	0.0224	0.360

Surface # 3 V-tail
Chordwise = 8 # Spanwise = 5 First strip = 45
Surface area = 49.970009 Ave. chord = 7.242814
CLsurf = -0.02442 Clsurf = 0.00321
CYsurf = 0.01808 Cmsurf = 0.04929
CDsurf = 0.00062 Cnsurf = -0.00946
CDisurf = 0.00062 CDvsurf = 0.00000

Forces referred to Ssurf, Cave about hinge axis thru LE
CLsurf = -0.24134 CDsurf = 0.00496
Deflect =

Strip Forces referred to Strip Area, Chord

j	Yle	Chord	Area	c cl	ai	cl	cd	cdv	cm_c/4	cm_LE	C.P.x/c
45	1.5418	9.0930	12.6883	-1.4739	-0.0677	-0.1622	0.0038	0.0000	0.0317	0.0459	0.492
46	2.8444	8.0148	14.6194	-2.0732	-0.0993	-0.2590	0.0095	0.0000	0.0536	0.0762	0.505
47	4.3313	6.7840	12.4090	-2.0923	-0.1148	-0.3087	0.0086	0.0000	0.0494	0.0838	0.448
48	5.6301	5.7090	7.7208	-1.5539	-0.1252	-0.2723	-0.0002	0.0000	0.0248	0.0645	0.365
49	6.3867	5.0828	2.5325	-0.5708	-0.1269	-0.1119	-0.0171	0.0000	0.0039	0.0234	0.300

Surface # 4 V-tail (YDUP)
Chordwise = 8 # Spanwise = 5 First strip = 50
Surface area = 49.970009 Ave. chord = 7.242814
CLsurf = -0.02442 Clsurf = -0.00321
CYsurf = -0.01808 Cmsurf = 0.04929
CDsurf = 0.00062 Cnsurf = 0.00946
CDisurf = 0.00062 CDvsurf = 0.00000

Forces referred to Ssurf, Cave about hinge axis thru LE
CLsurf = -0.24134 CDsurf = 0.00496
Deflect =

Strip Forces referred to Strip Area, Chord

j	Yle	Chord	Area	c cl	ai	cl	cd	cdv	cm_c/4	cm_LE	C.P.x/c
50	-1.5418	9.0930	12.6883	-1.4739	-0.0677	-0.1622	0.0038	0.0000	0.0317	-0.0459	0.492
51	-2.8444	8.0148	14.6194	-2.0732	-0.0993	-0.2590	0.0095	0.0000	0.0536	-0.0762	0.505
52	-4.3313	6.7840	12.4090	-2.0923	-0.1148	-0.3087	0.0086	0.0000	0.0494	-0.0838	0.448
53	-5.6301	5.7090	7.7208	-1.5539	-0.1252	-0.2723	-0.0002	0.0000	0.0248	-0.0645	0.365

```
  54  -6.3867   5.0828   2.5325  -0.5708  -0.1269  -0.1119  -0.0171   0.0000   0.0039  -0.0234    0.300

 Surface # 5     Upper Winglet
   # Chordwise =  4   # Spanwise =  5     First strip = 55
   Surface area =    2.837634       Ave. chord =    1.075000
   CLsurf  =   0.00032     Clsurf  =  -0.00013
   CYsurf  =  -0.00081     Cmsurf  =  -0.00028
   CDsurf  =  -0.00004     Cnsurf  =   0.00016
   CDisurf =  -0.00004     CDvsurf =   0.00000

 Forces referred to Ssurf, Cave about hinge axis thru LE
   CLsurf  =   0.12195     CDsurf  =  -0.00563
   Deflect =

Strip Forces referred to Strip Area, Chord
   j     Yle    Chord     Area     c cl      ai      cl       cd       cdv    cm_c/4    cm_LE  C.P.x/c
  55  23.2198   1.5981   0.4028   0.0385  -0.3921   0.0241  -0.0007   0.0000  -0.0215  -0.0172
  56  23.3737   1.3983   0.9227   0.1464  -0.0932   0.1048  -0.0042   0.0000  -0.0429  -0.0437    1.378
  57  23.6227   1.0750   0.8769   0.1705  -0.0479   0.1587  -0.0072   0.0000  -0.0424  -0.0551    0.969
  58  23.8717   0.7517   0.4961   0.1302  -0.0337   0.1733  -0.0087   0.0000  -0.0331  -0.0583    0.756
  59  24.0256   0.5519   0.1391   0.0577  -0.0108   0.1046  -0.0082   0.0000  -0.0094  -0.0332    0.472

 Surface # 6     Upper Winglet (YDUP)
   # Chordwise =  4   # Spanwise =  5     First strip = 60
   Surface area =    2.837634       Ave. chord =    1.075000
   CLsurf  =   0.00032     Clsurf  =   0.00013
   CYsurf  =   0.00081     Cmsurf  =  -0.00028
   CDsurf  =  -0.00004     Cnsurf  =  -0.00016
   CDisurf =  -0.00004     CDvsurf =   0.00000

 Forces referred to Ssurf, Cave about hinge axis thru LE
   CLsurf  =   0.12195     CDsurf  =  -0.00563
   Deflect =

Strip Forces referred to Strip Area, Chord
   j     Yle    Chord     Area     c cl      ai      cl       cd       cdv    cm_c/4    cm_LE  C.P.x/c
  60 -23.2198   1.5981   0.4028   0.0385  -0.3921   0.0241  -0.0007   0.0000  -0.0215   0.0172
  61 -23.3737   1.3983   0.9227   0.1464  -0.0932   0.1048  -0.0042   0.0000  -0.0429   0.0437    1.378
  62 -23.6227   1.0750   0.8769   0.1705  -0.0479   0.1587  -0.0072   0.0000  -0.0424   0.0551    0.969
  63 -23.8717   0.7517   0.4961   0.1302  -0.0337   0.1733  -0.0087   0.0000  -0.0331   0.0583    0.756
  64 -24.0256   0.5519   0.1391   0.0577  -0.0108   0.1046  -0.0082   0.0000  -0.0094   0.0332    0.472

 Surface # 7     lower Winglet
   # Chordwise =  2   # Spanwise =  4     First strip = 65
   Surface area =    0.612305       Ave. chord =    0.700000
   CLsurf  =  -0.00002     Clsurf  =   0.00001
   CYsurf  =  -0.00003     Cmsurf  =   0.00001
   CDsurf  =   0.00000     Cnsurf  =   0.00001
   CDisurf =   0.00000     CDvsurf =   0.00000

 Forces referred to Ssurf, Cave about hinge axis thru LE
   CLsurf  =  -0.02450     CDsurf  =   0.00095
   Deflect =

Strip Forces referred to Strip Area, Chord
   j     Yle    Chord     Area     c cl      ai      cl       cd       cdv    cm_c/4    cm_LE  C.P.x/c
  65  23.2242   0.9772   0.1252  -0.0056  -0.5785  -0.0058   0.0023   0.0000  -0.0174  -0.0103
  66  23.4026   0.8148   0.2520  -0.0120  -0.1820  -0.0148   0.0012   0.0000  -0.0473  -0.0280
  67  23.6548   0.5852   0.1810  -0.0262  -0.1328  -0.0448   0.0008   0.0000  -0.0611  -0.0315
  68  23.8332   0.4228   0.0542  -0.0190  -0.1377  -0.0448  -0.0029   0.0000  -0.0512  -0.0234

 Surface # 8     lower Winglet (YDUP)
   # Chordwise =  2   # Spanwise =  4     First strip = 69
   Surface area =    0.612305       Ave. chord =    0.700000
   CLsurf  =  -0.00002     Clsurf  =  -0.00001
   CYsurf  =   0.00003     Cmsurf  =   0.00001
   CDsurf  =   0.00000     Cnsurf  =  -0.00001
   CDisurf =   0.00000     CDvsurf =   0.00000

 Forces referred to Ssurf, Cave about hinge axis thru LE
   CLsurf  =  -0.02450     CDsurf  =   0.00095
   Deflect =

Strip Forces referred to Strip Area, Chord
   j     Yle    Chord     Area     c cl      ai      cl       cd       cdv    cm_c/4    cm_LE  C.P.x/c
  69 -23.2242   0.9772   0.1252  -0.0056  -0.5785  -0.0058   0.0023   0.0000  -0.0174   0.0103
  70 -23.4026   0.8148   0.2520  -0.0120  -0.1820  -0.0148   0.0012   0.0000  -0.0473   0.0280
  71 -23.6548   0.5852   0.1810  -0.0262  -0.1328  -0.0448   0.0008   0.0000  -0.0611   0.0315
  72 -23.8332   0.4228   0.0542  -0.0190  -0.1377  -0.0448  -0.0029   0.0000  -0.0512   0.0234
---------------------------------------------------------------
```

H.3.3 BDVT Second Run Case and Results for Low speed/Approach

```
-------------------------------------------------
 Run case  2:  - SL approach @ 58.4m/s -

 alpha       ->  CL         =   1.44877
 beta        ->  beta       =   0.00000
 pb/2V       ->  pb/2V      =   0.00000
 qc/2V       ->  qc/2V      =   0.00000
 rb/2V       ->  rb/2V      =   0.00000
 camber      ->  camber     =   0.00000
 VCF         ->  VCF        =   0.00000
 aileron     ->  aileron    =   0.00000
 Ruddervator ->  Ruddervator =   0.00000

 alpha     =   0.00000
 beta      =   0.00000
 pb/2V     =   0.00000
 qc/2V     = -0.737769E-16
 rb/2V     =   0.00000
 CL        =   0.00000
 CDo       =  0.241220E-01
 bank      =   0.00000
 elevation =   0.00000
 heading   =   0.00000
 Mach      =  0.171609
 velocity  =   58.3969
 density   =   1.22300
 grav.acc. =   9.81000
 turn_rad. =   0.00000
 load_fac. =   0.00000
 X_cg      =   27.1630
 Y_cg      =   0.00000
 Z_cg      =  -1.20600
 mass      =   122134.
 Ixx       =   2260.00
 Iyy       =   3000.00
 Izz       =   747.000
 Ixy       =   1300.00
 Iyz       = -0.336000E-12
 Izx       = -0.336000E-12
 visc CL_a =   0.00000
 visc CL_u =   0.00000
 visc CM_a =   0.00000
 visc CM_u =   0.00000
```

BD Initial Results for second low speed / approach case

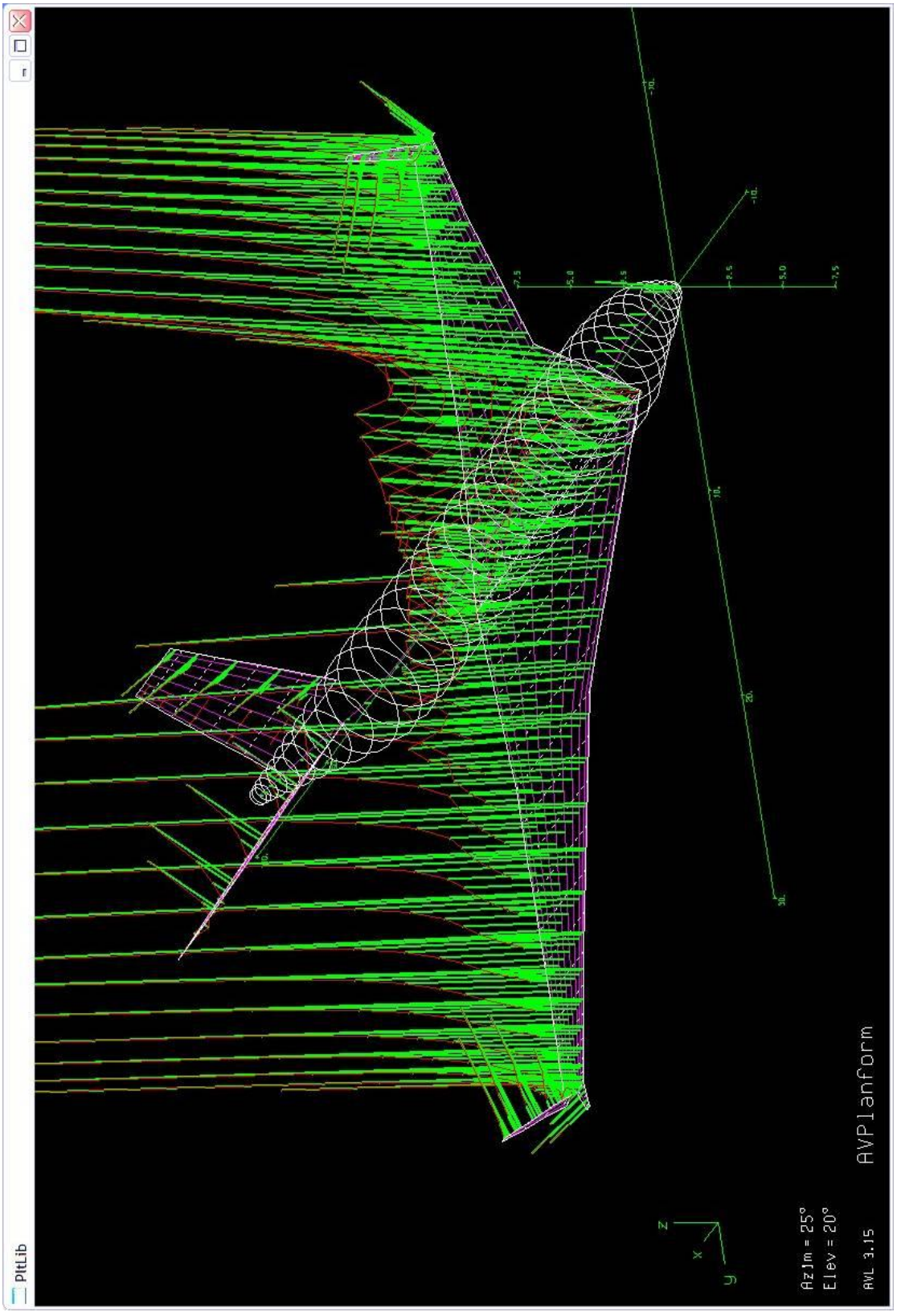

Fig H-7: BDVT Geometry for a low speed flight case of 58.4 m/s at SL

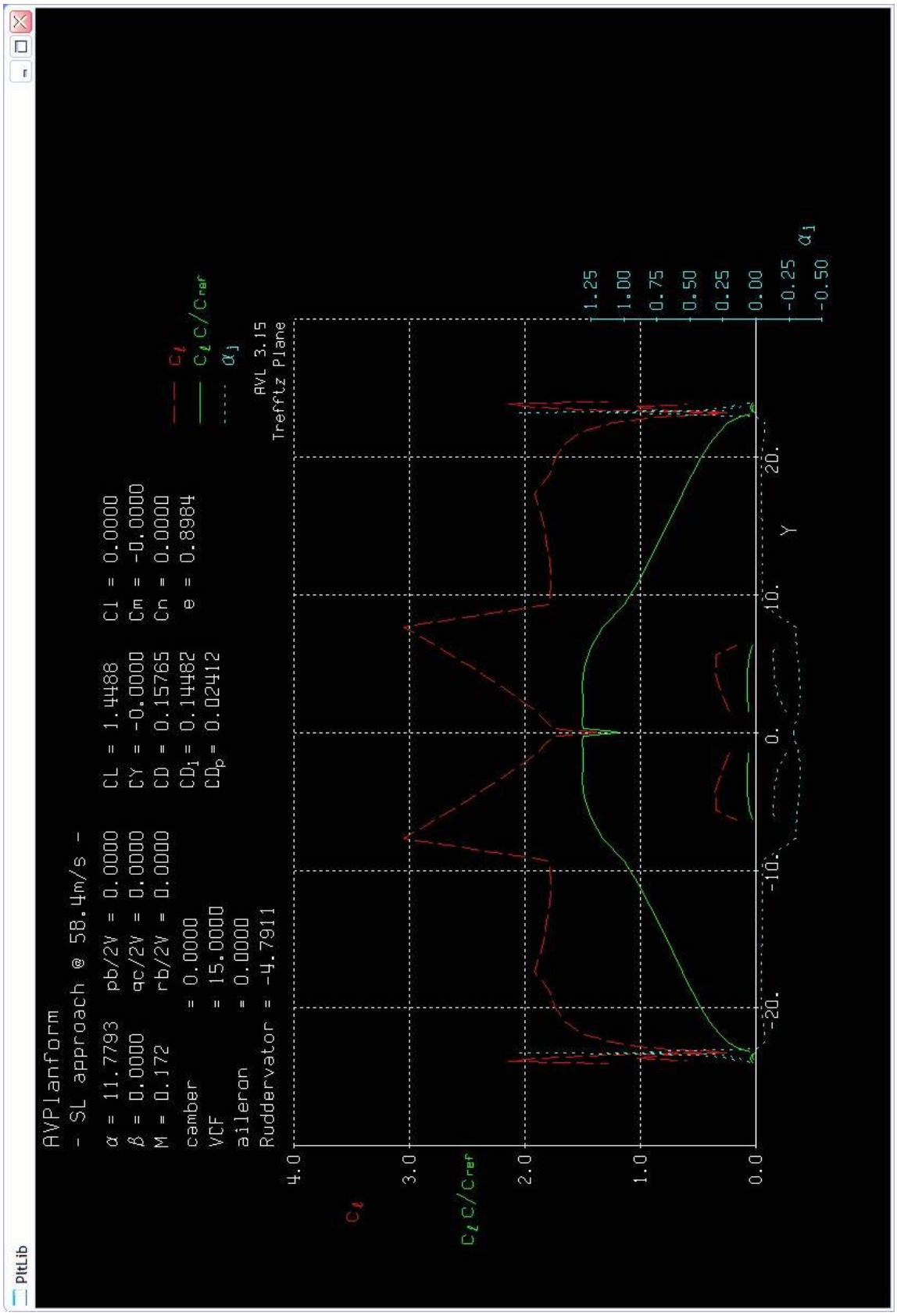

Fig H-8: BDVT Trefftz plane plot for a low speed flight case of 58.4 m/s at SL

LOW SPEED STABILITY RESULTS

```
---------------------------------------------------------------
 Vortex Lattice Output -- Total Forces

 Configuration: AVPlanform
    # Surfaces =   8
    # Strips   =  72
    # Vortices = 576

  Sref =  397.05       Cref =  12.200       Bref =  46.407
  Xref =  27.163       Yref =  0.0000       Zref = -1.2060

 Standard axis orientation,  X fwd, Z down

 Run case: - SL approach @ 58.4m/s -

  Alpha =  11.77934     pb/2V =   0.00000     p'b/2V =   0.00000
  Beta  =   0.00000     qc/2V =   0.00000
  Mach  =     0.172     rb/2V =   0.00000     r'b/2V =   0.00000

  CXtot =   0.14143     Cltot =   0.00000     Cl'tot =   0.00000
  CYtot =   0.00000     Cmtot =   0.00000
  CZtot =  -1.45044     Cntot =   0.00000     Cn'tot =   0.00000

  CLtot =   1.44877
  CDtot =   0.15765
  CDvis =   0.02412     CDind =   0.13353
  CLff  =   1.48897     CDff  =   0.14482    | Trefftz
  CYff  =   0.00000         e =     0.8984   | Plane

  camber      =   0.00000
  VCF         =  15.00000
  aileron     =   0.00000
  Ruddervator =  -4.79114

 ---------------------------------------------------------------

 Derivatives...
                        alpha              beta
              ----------------   ----------------
 z force    |   CLa =   4.050539    CLb =   0.000000
 y force    |   CYa =   0.000000    CYb =  -0.245644
 roll  x mom.|   Cla =   0.000000    Clb =  -0.224566
 pitch y mom.|   Cma =   0.298447    Cmb =   0.000000
 yaw   z mom.|   Cna =   0.000000    Cnb =   0.059190

                   roll rate  p       pitch rate  q        yaw rate  r
              ----------------   ----------------   ----------------
 z force    |   CLp =   0.000000    CLq =   4.396367    CLr =   0.000000
 y force    |   CYp =   0.486067    CYq =   0.000000    CYr =  -0.112661
 roll  x mom.|   Clp =  -0.352760    Clq =   0.000000    Clr =   0.266494
 pitch y mom.|   Cmp =   0.000000    Cmq =  -3.098462    Cmr =   0.000000
 yaw   z mom.|   Cnp =  -0.177488    Cnq =   0.000000    Cnr =  -0.101566

              camber      d1     VCF         d2     aileron      d3     Ruddervator  d4
              ----------------   ----------------   ----------------   ----------------
 z force    |  CLd1 =   0.045675   CLd2 =   0.024005   CLd3 =   0.000000   CLd4 =   0.003853
 y force    |  CYd1 =   0.000000   CYd2 =   0.000000   CYd3 =  -0.000040   CYd4 =   0.000000
 roll  x mom.|  Cld1 =   0.000000   Cld2 =   0.000000   Cld3 =   0.000409   Cld4 =   0.000000
 pitch y mom.|  Cmd1 =  -0.006504   Cmd2 =  -0.000421   Cmd3 =   0.000000   Cmd4 =  -0.007007
 yaw   z mom.|  Cnd1 =   0.000000   Cnd2 =   0.000000   Cnd3 =   0.000002   Cnd4 =   0.000000
 Trefftz drag| CDffd1 =   0.008405 CDffd2 =   0.006162 CDffd3 =   0.000000 CDffd4 =   0.000804
 span eff.  |   ed1 =   0.005122    ed2 =  -0.007561    ed3 =   0.000000    ed4 =  -0.000145

 Neutral point  Xnp =  26.264093

 Clb Cnr / Clr Cnb  =   1.445949    ( > 1 if spirally stable )
```

LOW SPEED SURFACE BODY RESULTS

```
---------------------------------------------------------------
 Vortex Lattice Output -- Total Forces

 Configuration: AVPlanform
    # Surfaces =   8
    # Strips   =  72
    # Vortices = 576
```

```
 Sref =  397.05       Cref =  12.200       Bref =  46.407
 Xref =  27.163       Yref =  0.0000       Zref = -1.2060

Standard axis orientation,  X fwd, Z down

Run case: - SL approach @ 58.4m/s -

 Alpha =  11.77934     pb/2V =   0.00000     p'b/2V =   0.00000
 Beta  =   0.00000     qc/2V =   0.00000
 Mach  =     0.172     rb/2V =   0.00000     r'b/2V =   0.00000

 CXtot =   0.14143     Cltot =   0.00000     Cl'tot =   0.00000
 CYtot =   0.00000     Cmtot =   0.00000
 CZtot =  -1.45044     Cntot =   0.00000     Cn'tot =   0.00000

 CLtot =   1.44877
 CDtot =   0.15765
 CDvis =   0.02412     CDind =   0.13353
 CLff  =   1.48897     CDff  =   0.14482    | Trefftz
 CYff  =   0.00000         e =     0.8984   | Plane

  camber          =   0.00000
  VCF             =  15.00000
  aileron         =   0.00000
  Ruddervator     =  -4.79114

---------------------------------------------------------------

Geometry-axis derivatives...

                 axial   vel. u     sideslip vel. v      normal  vel. w
               ----------------    ----------------    ----------------
x force     |    CXu =  -0.046114    CXv =   0.000000    CXw =   1.696228
y force     |    CYu =   0.000000    CYv =  -0.250928    CYw =   0.000000
z force     |    CZu =  -1.698060    CZv =   0.000000    CZw =  -4.385938
roll  x mom.|    Clu =   0.000000    Clv =  -0.229397    Clw =   0.000000
pitch y mom.|    Cmu =  -0.086520    Cmv =   0.000000    Cmw =   0.286825
yaw   z mom.|    Cnu =   0.000000    Cnv =   0.060464    Cnw =   0.000000

                 roll rate  p       pitch rate  q         yaw rate  r
               ----------------    ----------------    ----------------
x force     |    CXp =   0.000000    CXq =   0.229807    CXr =   0.000000
y force     |    CYp =   0.498830    CYq =   0.000000    CYr =  -0.011061
z force     |    CZp =   0.000000    CZq =  -4.443018    CZr =   0.000000
roll  x mom.|    Clp =  -0.399734    Clq =   0.000000    Clr =   0.188869
pitch y mom.|    Cmp =   0.000000    Cmq =  -3.098462    Cmr =   0.000000
yaw   z mom.|    Cnp =  -0.153016    Cnq =   0.000000    Cnr =  -0.135660

               camber       d1     VCF          d2     aileron      d3     Ruddervator  d4
               ----------------    ----------------    ----------------    ----------------
x force     |   CXd1 =   0.003340   CXd2 =   0.000555   CXd3 =   0.000000   CXd4 =   0.000076
y force     |   CYd1 =   0.000000   CYd2 =   0.000000   CYd3 =  -0.000040   CYd4 =   0.000000
z force     |   CZd1 =  -0.045961   CZd2 =  -0.024406   CZd3 =   0.000000   CZd4 =  -0.003920
roll  x mom.|   Cld1 =   0.000000   Cld2 =   0.000000   Cld3 =   0.000409   Cld4 =   0.000000
pitch y mom.|   Cmd1 =  -0.006504   Cmd2 =  -0.000421   Cmd3 =   0.000000   Cmd4 =  -0.007007
yaw   z mom.|   Cnd1 =   0.000000   Cnd2 =   0.000000   Cnd3 =   0.000002   Cnd4 =   0.000000
```

LOW SPEED TOTAL STRIP FORCES RESULTS

```
---------------------------------------------------------------
Vortex Lattice Output -- Total Forces

Configuration: AVPlanform
   # Surfaces =   8
   # Strips   =  72
   # Vortices = 576

 Sref =  397.05       Cref =  12.200       Bref =  46.407
 Xref =  27.163       Yref =  0.0000       Zref = -1.2060

Standard axis orientation,  X fwd, Z down

Run case: - SL approach @ 58.4m/s -

 Alpha =  11.77934     pb/2V =   0.00000     p'b/2V =   0.00000
 Beta  =   0.00000     qc/2V =   0.00000
 Mach  =     0.172     rb/2V =   0.00000     r'b/2V =   0.00000

 CXtot =   0.14143     Cltot =   0.00000     Cl'tot =   0.00000
 CYtot =   0.00000     Cmtot =   0.00000
 CZtot =  -1.45044     Cntot =   0.00000     Cn'tot =   0.00000

 CLtot =   1.44877
```

```
 CDtot =   0.15765
 CDvis =   0.02412     CDind =   0.13353
 CLff  =   1.48897     CDff  =   0.14482    | Trefftz
 CYff  =   0.00000         e =    0.8984    | Plane

  camber         =   0.00000
  VCF            =  15.00000
  aileron        =   0.00000
  Ruddervator    =  -4.79114

------------------------------------------------------------------
------------------------------------------------------------------
Surface Forces (referred to Sref,Cref,Bref about Xref,Yref,Zref)
Standard axis orientation,  X fwd, Z down

    Sref =   397.1       Cref =   12.2000   Bref =   46.4072
    Xref =    27.1630    Yref =    0.0000   Zref =   -1.2060

n     Area      CL      CD      Cm      CY      Cn      Cl     CDi     CDv
1   236.367  0.7065  0.0638  0.0028  0.0226 -0.0032 -0.1394  0.0638  0.0000   Wing
2   236.367  0.7065  0.0638  0.0028 -0.0226  0.0032  0.1394  0.0638  0.0000   Wing (YDUP)
3    49.970  0.0102  0.0017 -0.0179 -0.0089  0.0040 -0.0007  0.0017  0.0000   V-tail
4    49.970  0.0102  0.0017 -0.0179  0.0089 -0.0040  0.0007  0.0017  0.0000   V-tail (YDUP)
5     2.838  0.0018 -0.0004 -0.0012 -0.0026  0.0003 -0.0007 -0.0004  0.0000   Upper Winglet
6     2.838  0.0018 -0.0004 -0.0012  0.0026 -0.0003  0.0007 -0.0004  0.0000   Upper Winglet (YDUP)
7     0.612  0.0004 -0.0001 -0.0002  0.0005 -0.0001 -0.0003 -0.0001  0.0000   lower Winglet
8     0.612  0.0004 -0.0001 -0.0002 -0.0005  0.0001  0.0003 -0.0001  0.0000   lower Winglet (YDUP)

Surface Forces (referred to Ssurf, Cave about root LE on hinge axis)

 n     Ssurf      Cave       cl       cd      cdv    cm_LE
 1   236.367    10.170   1.1866   0.1072   0.0000   0.0000  Wing
 2   236.367    10.170   1.1866   0.1072   0.0000   0.0000  Wing (YDUP)
 3    49.970     7.243   0.1070   0.0131   0.0000   0.0000  V-tail
 4    49.970     7.243   0.1070   0.0131   0.0000   0.0000  V-tail (YDUP)
 5     2.838     1.075   0.4212  -0.0550   0.0000   0.0000  Upper Winglet
 6     2.838     1.075   0.4212  -0.0550   0.0000   0.0000  Upper Winglet (YDUP)
 7     0.612     0.700   0.4437  -0.0501   0.0000   0.0000  lower Winglet
 8     0.612     0.700   0.4437  -0.0501   0.0000   0.0000  lower Winglet (YDUP)
------------------------------------------------------------------
------------------------------------------------------------------
Surface and Strip Forces by surface

 Forces referred to Sref, Cref, Bref about Xref, Yref, Zref
Standard axis orientation,  X fwd, Z down

 Surface # 1     Wing
   # Chordwise = 10   # Spanwise = 22     First strip =  1
   Surface area =  236.367264       Ave. chord =   10.169948
   CLsurf  =   0.70646     Clsurf  =  -0.13939
   CYsurf  =   0.02258     Cmsurf  =   0.00279
   CDsurf  =   0.06385     Cnsurf  =  -0.00323
   CDisurf =   0.06385     CDvsurf =   0.00000

 Forces referred to Ssurf, Cave about hinge axis thru LE
   CLsurf  =   1.18663     CDsurf  =   0.10725
   Deflect =

Strip Forces referred to Strip Area, Chord
   j     Yle    Chord     Area     c cl      ai      cl       cd      cdv    cm_c/4    cm_LE  C.P.x/c
   1  0.0301  23.3263   2.8155  14.6625   0.2842   0.4041   1.1610   0.0000  -0.1516  -0.1595    0.566
   2  0.2701  22.9621   8.2582  18.2932   0.2879   0.7499   0.3106   0.0000  -0.1938  -0.2045    0.503
   3  0.7452  22.2411  13.1505  18.3677   0.3003   0.7992   0.2154   0.0000  -0.1972  -0.2099    0.494
   4  1.4457  21.1781  17.1723  18.2116   0.3215   0.8352   0.2101   0.0000  -0.1950  -0.2128    0.481
   5  2.3574  19.7945  20.0704  18.3088   0.3359   0.9018   0.2091   0.0000  -0.1929  -0.2197    0.462
   6  3.4617  18.1187  21.6768  18.3795   0.3346   0.9941   0.2042   0.0000  -0.1908  -0.2297    0.441
   7  4.7361  16.1847  21.9215  18.1293   0.3234   1.1044   0.1926   0.0000  -0.1878  -0.2412    0.419
   8  6.1547  14.0319  20.8370  17.4667   0.3100   1.2358   0.1726   0.0000  -0.1805  -0.2527    0.396
   9  7.6886  11.7041  18.5540  16.2335   0.2994   1.3947   0.1051   0.0000  -0.1565  -0.2571    0.363
  10  9.2982  10.0081  16.3421  13.9564   0.0472   1.4219   0.0118   0.0000  -0.0738  -0.3379    0.302
  11 10.9503   9.0256  15.0439  12.4643   0.0525   1.4132  -0.0129   0.0000  -0.0529  -0.3184    0.288
  12 12.6193   8.0329  13.3894  11.1752   0.0524   1.4287  -0.0376   0.0000  -0.0450  -0.3143    0.282
  13 14.2713   7.0504  11.5124   9.9754   0.0490   1.4577  -0.0608   0.0000  -0.0426  -0.3177    0.279
  14 15.8728   6.0979   9.5476   8.8326   0.0440   1.4969  -0.0845   0.0000  -0.0428  -0.3253    0.279
  15 17.3910   5.1950   7.6193   7.7461   0.0396   1.5467  -0.1148   0.0000  -0.0421  -0.3340    0.277
  16 18.7589   4.4784   5.6708   6.7298   0.0393   1.5614  -0.1272   0.0000  -0.0366  -0.3587    0.274
  17 19.9537   3.9460   4.4135   5.7803   0.0434   1.5226  -0.1269   0.0000  -0.0325  -0.3478    0.271
  18 20.9890   3.4847   3.3032   4.8599   0.0519   1.4517  -0.1308   0.0000  -0.0234  -0.3255    0.266
  19 21.8437   3.1039   2.3529   3.9336   0.0626   1.3223  -0.1340   0.0000  -0.0094  -0.2863    0.257
  20 22.5005   2.8113   1.5540   2.9547   0.0672   1.1018  -0.1361   0.0000   0.0065  -0.2257    0.244
  21 22.9459   2.6128   0.8785   1.8564   0.0081   0.7564  -0.1475   0.0000   0.0179  -0.1411    0.226
  22 23.1709   2.5126   0.2835   0.6209  -0.8158   0.2969  -0.2139   0.0000   0.0119  -0.0442    0.210
```

Surface # 2 Wing (YDUP)
Chordwise = 10 # Spanwise = 22 First strip = 23
Surface area = 236.367264 Ave. chord = 10.169948
CLsurf = 0.70646 Clsurf = 0.13939
CYsurf = -0.02258 Cmsurf = 0.00279
CDsurf = 0.06385 Cnsurf = 0.00323
CDisurf = 0.06385 CDvsurf = 0.00000

Forces referred to Ssurf, Cave about hinge axis thru LE
CLsurf = 1.18663 CDsurf = 0.10725
Deflect =

Strip Forces referred to Strip Area, Chord

j	Yle	Chord	Area	c cl	ai	cl	cd	cdv	cm_c/4	cm_LE	C.P.x/c
23	-0.0301	23.3263	2.8155	14.6625	0.2842	0.4041	1.1610	0.0000	-0.1516	0.1595	0.566
24	-0.2701	22.9621	8.2582	18.2932	0.2879	0.7499	0.3106	0.0000	-0.1938	0.2045	0.503
25	-0.7452	22.2411	13.1505	18.3677	0.3003	0.7992	0.2154	0.0000	-0.1972	0.2099	0.494
26	-1.4457	21.1781	17.1723	18.2116	0.3215	0.8352	0.2101	0.0000	-0.1950	0.2128	0.481
27	-2.3574	19.7945	20.0704	18.3088	0.3359	0.9018	0.2091	0.0000	-0.1929	0.2197	0.462
28	-3.4617	18.1187	21.6768	18.3795	0.3346	0.9941	0.2042	0.0000	-0.1908	0.2297	0.441
29	-4.7361	16.1847	21.9215	18.1293	0.3234	1.1044	0.1926	0.0000	-0.1878	0.2412	0.419
30	-6.1547	14.0319	20.8370	17.4667	0.3100	1.2358	0.1726	0.0000	-0.1805	0.2527	0.396
31	-7.6886	11.7041	18.5540	16.2335	0.2994	1.3947	0.1051	0.0000	-0.1565	0.2571	0.363
32	-9.2982	10.0081	16.3421	13.9564	0.0472	1.4219	0.0118	0.0000	-0.0738	0.3379	0.302
33	-10.9503	9.0256	15.0439	12.4643	0.0525	1.4132	-0.0129	0.0000	-0.0529	0.3184	0.288
34	-12.6193	8.0329	13.3894	11.1752	0.0524	1.4287	-0.0376	0.0000	-0.0450	0.3143	0.282
35	-14.2713	7.0504	11.5124	9.9754	0.0490	1.4577	-0.0608	0.0000	-0.0426	0.3177	0.279
36	-15.8728	6.0979	9.5476	8.8326	0.0440	1.4969	-0.0845	0.0000	-0.0428	0.3253	0.279
37	-17.3910	5.1950	7.6193	7.7461	0.0396	1.5467	-0.1148	0.0000	-0.0421	0.3340	0.277
38	-18.7589	4.4784	5.6708	6.7298	0.0393	1.5614	-0.1272	0.0000	-0.0366	0.3587	0.274
39	-19.9537	3.9460	4.4135	5.7803	0.0434	1.5226	-0.1269	0.0000	-0.0325	0.3478	0.271
40	-20.9890	3.4847	3.3032	4.8599	0.0519	1.4517	-0.1308	0.0000	-0.0234	0.3255	0.266
41	-21.8437	3.1039	2.3529	3.9336	0.0626	1.3223	-0.1340	0.0000	-0.0094	0.2863	0.257
42	-22.5005	2.8113	1.5540	2.9547	0.0672	1.1018	-0.1361	0.0000	0.0065	0.2257	0.244
43	-22.9459	2.6128	0.8785	1.8564	0.0081	0.7564	-0.1475	0.0000	0.0179	0.1411	0.226
44	-23.1709	2.5126	0.2835	0.6209	-0.8158	0.2969	-0.2139	0.0000	0.0119	0.0442	0.210

Surface # 3 V-tail
Chordwise = 8 # Spanwise = 5 First strip = 45
Surface area = 49.970009 Ave. chord = 7.242814
CLsurf = 0.01017 Clsurf = -0.00068
CYsurf = -0.00887 Cmsurf = -0.01791
CDsurf = 0.00165 Cnsurf = 0.00396
CDisurf = 0.00165 CDvsurf = 0.00000

Forces referred to Ssurf, Cave about hinge axis thru LE
CLsurf = 0.10697 CDsurf = 0.01312
Deflect =

Strip Forces referred to Strip Area, Chord

j	Yle	Chord	Area	c cl	ai	cl	cd	cdv	cm_c/4	cm_LE	C.P.x/c
45	1.5418	9.0930	12.6883	0.7778	0.2255	0.0845	0.0126	0.0000	0.0180	-0.0083	-0.041
46	2.8444	8.0148	14.6194	0.8712	0.1604	0.1076	0.0146	0.0000	0.0234	-0.0109	-0.043
47	4.3313	6.7840	12.4090	0.8749	0.1369	0.1280	0.0153	0.0000	0.0290	-0.0133	-0.049
48	5.6301	5.7090	7.7208	0.7168	0.1335	0.1253	0.0117	0.0000	0.0358	-0.0098	-0.117
49	6.3867	5.0828	2.5325	0.2866	0.1363	0.0571	0.0009	0.0000	0.0213	-0.0019	-0.189

Surface # 4 V-tail (YDUP)
Chordwise = 8 # Spanwise = 5 First strip = 50
Surface area = 49.970009 Ave. chord = 7.242814
CLsurf = 0.01017 Clsurf = 0.00068
CYsurf = 0.00887 Cmsurf = -0.01791
CDsurf = 0.00165 Cnsurf = -0.00396
CDisurf = 0.00165 CDvsurf = 0.00000

Forces referred to Ssurf, Cave about hinge axis thru LE
CLsurf = 0.10697 CDsurf = 0.01312
Deflect =

Strip Forces referred to Strip Area, Chord

j	Yle	Chord	Area	c cl	ai	cl	cd	cdv	cm_c/4	cm_LE	C.P.x/c
50	-1.5418	9.0930	12.6883	0.7778	0.2255	0.0845	0.0126	0.0000	0.0180	0.0083	-0.041
51	-2.8444	8.0148	14.6194	0.8712	0.1604	0.1076	0.0146	0.0000	0.0234	0.0109	-0.043
52	-4.3313	6.7840	12.4090	0.8749	0.1369	0.1280	0.0153	0.0000	0.0290	0.0133	-0.049
53	-5.6301	5.7090	7.7208	0.7168	0.1335	0.1253	0.0117	0.0000	0.0358	0.0098	-0.117
54	-6.3867	5.0828	2.5325	0.2866	0.1363	0.0571	0.0009	0.0000	0.0213	0.0019	-0.189

Surface # 5 Upper Winglet
Chordwise = 4 # Spanwise = 5 First strip = 55
Surface area = 2.837634 Ave. chord = 1.075000
CLsurf = 0.00176 Clsurf = -0.00074
CYsurf = -0.00258 Cmsurf = -0.00124
CDsurf = -0.00039 Cnsurf = 0.00029

```
   CDisurf =  -0.00039     CDvsurf =   0.00000

 Forces referred to Ssurf, Cave about hinge axis thru LE
   CLsurf  =   0.42123     CDsurf  =  -0.05497
   Deflect =

Strip Forces referred to Strip Area, Chord
   j     Yle    Chord     Area     c cl      ai      cl       cd      cdv    cm_c/4    cm_LE  C.P.x/c
  55  23.2198   1.5981   0.4028   0.1260  -1.1311   0.0800  -0.0104   0.0000  -0.0072  -0.0248    0.414
  56  23.3737   1.3983   0.9227   0.4732  -0.2650   0.3420  -0.0301   0.0000   0.0121  -0.0853    0.182
  57  23.6227   1.0750   0.8769   0.5869  -0.1248   0.5537  -0.0703   0.0000   0.0462  -0.1315    0.107
  58  23.8717   0.7517   0.4961   0.4616  -0.0829   0.6245  -0.0977   0.0000   0.0910  -0.1469    0.018
  59  24.0256   0.5519   0.1391   0.2014  -0.0033   0.3748  -0.1000   0.0000   0.1138  -0.0715   -0.131

 Surface # 6     Upper Winglet (YDUP)
   # Chordwise =  4   # Spanwise =  5     First strip = 60
   Surface area =    2.837634       Ave. chord =    1.075000
   CLsurf  =   0.00176     Clsurf  =   0.00074
   CYsurf  =   0.00258     Cmsurf  =  -0.00124
   CDsurf  =  -0.00039     Cnsurf  =  -0.00029
   CDisurf =  -0.00039     CDvsurf =   0.00000

 Forces referred to Ssurf, Cave about hinge axis thru LE
   CLsurf  =   0.42123     CDsurf  =  -0.05497
   Deflect =

Strip Forces referred to Strip Area, Chord
   j     Yle    Chord     Area     c cl      ai      cl       cd      cdv    cm_c/4    cm_LE  C.P.x/c
  60 -23.2198   1.5981   0.4028   0.1260  -1.1311   0.0800  -0.0104   0.0000  -0.0072   0.0248    0.414
  61 -23.3737   1.3983   0.9227   0.4732  -0.2650   0.3420  -0.0301   0.0000   0.0121   0.0853    0.182
  62 -23.6227   1.0750   0.8769   0.5869  -0.1248   0.5537  -0.0703   0.0000   0.0462   0.1315    0.107
  63 -23.8717   0.7517   0.4961   0.4616  -0.0829   0.6245  -0.0977   0.0000   0.0910   0.1469    0.018
  64 -24.0256   0.5519   0.1391   0.2014  -0.0033   0.3748  -0.1000   0.0000   0.1138   0.0715   -0.131

 Surface # 7     lower Winglet
   # Chordwise =  2   # Spanwise =  4     First strip = 65
   Surface area =    0.612305       Ave. chord =    0.700000
   CLsurf  =   0.00044     Clsurf  =  -0.00027
   CYsurf  =   0.00054     Cmsurf  =  -0.00022
   CDsurf  =  -0.00008     Cnsurf  =  -0.00012
   CDisurf =  -0.00008     CDvsurf =   0.00000

 Forces referred to Ssurf, Cave about hinge axis thru LE
   CLsurf  =   0.44370     CDsurf  =  -0.05008
   Deflect =

Strip Forces referred to Strip Area, Chord
   j     Yle    Chord     Area     c cl      ai      cl       cd      cdv    cm_c/4    cm_LE  C.P.x/c
  65  23.2242   0.9772   0.1252   0.1446  -1.7914   0.1513  -0.0122   0.0000  -0.0312  -0.0305    0.560
  66  23.4026   0.8148   0.2520   0.3702  -0.4227   0.4630  -0.0294   0.0000  -0.0778  -0.0862    0.502
  67  23.6548   0.5852   0.1810   0.3641  -0.2022   0.6405  -0.0860   0.0000  -0.0621  -0.1048    0.404
  68  23.8332   0.4228   0.0542   0.1491  -0.1382   0.3720  -0.1138   0.0000  -0.0005  -0.0492    0.252

 Surface # 8     lower Winglet (YDUP)
   # Chordwise =  2   # Spanwise =  4     First strip = 69
   Surface area =    0.612305       Ave. chord =    0.700000
   CLsurf  =   0.00044     Clsurf  =   0.00027
   CYsurf  =  -0.00054     Cmsurf  =  -0.00022
   CDsurf  =  -0.00008     Cnsurf  =   0.00012
   CDisurf =  -0.00008     CDvsurf =   0.00000

 Forces referred to Ssurf, Cave about hinge axis thru LE
   CLsurf  =   0.44370     CDsurf  =  -0.05008
   Deflect =

Strip Forces referred to Strip Area, Chord
   j     Yle    Chord     Area     c cl      ai      cl       cd      cdv    cm_c/4    cm_LE  C.P.x/c
  69 -23.2242   0.9772   0.1252   0.1446  -1.7914   0.1513  -0.0122   0.0000  -0.0312   0.0305    0.560
  70 -23.4026   0.8148   0.2520   0.3702  -0.4227   0.4630  -0.0294   0.0000  -0.0778   0.0862    0.502
  71 -23.6548   0.5852   0.1810   0.3641  -0.2022   0.6405  -0.0860   0.0000  -0.0621   0.1048    0.404
  72 -23.8332   0.4228   0.0542   0.1491  -0.1382   0.3720  -0.1138   0.0000  -0.0005   0.0492    0.252
 ------------------------------------------------------------
```

Appendix I Broad Delta Cost Analysis

I.1 Background

This Appendix focuses on a basic cost analysis methodology developed by [Burns, 1994] for application to aircraft at the preliminary design development stage. The results obtained reflect the current stage of the conceptual design, where the author is aware that mass, c.g., and performance will change if the design is taken to the next phase 'preliminary' design stage. Never-the-less an overview of the predicted life-cycle, acquisition, operating and disposal costs were estimated for the BDSF and BDVT configurations.

I.2 Cost Analysis

The cost analysis is directly derived using [Burns, 1994] for calculating the aircraft life-cycle costs, acquisition costs, and the fuel operations costs. The operating cost of the aircraft is separated into direct (*DOC*) and indirect (*IOC*) operating costs, where the fuel costs calculated from [Burns, 1994] is combined with guidelines from [Raymer, 1992] to provide an estimate for the total operating cost. An investigation into the cost of aircraft disposals was undertaken, where a relationship between the cost of acquisition and cost of disposal was established.

I.2.1 Design, Development, Test, and Evaluation Costs

The design, development, test, and evaluation (*DDTE*, *D*) cost considers the labour, time, materials, manufacturing of tooling and parts, and testing of the airframe components. Development of five airframe structures (Q_D = 5) is considered for the *DDTE* phase, where each of the five designs will be manufactured and tested for alternate load cases and pre-flight checks prior to the production of the commercial product.

The total number of airframe engineering hours (E_{HD}) required for development is:

$$E_{HD} = 0.066 \cdot A_{UW}^{\ 0.796} \cdot V_D^{\ 1.538} \cdot Q_D^{\ 0.183} \cdot A_{TF} \cdot C_{AMC}$$

Equation I-1

Where the airframe unit weight (A_{UW}) is defined as the total airframe empty weight and does not include any systems, undercarriage, or avionics, and is simply the fuselage, wing, and empennage and attaching structures. The maximum cruise flight speed (V_D) is also required along-with a judgement factor for advanced technologies (A_{TF} = 0.9), and an advanced materials factor (C_{AMC} = 1.0). Engineering development phase cost (C_{AED}) is calculated by:

$$C_{AED} = E_{HD} \cdot E_{RATE} \cdot C_S$$

Equation I-2

An engineering labour rate (E_{RATE}) of $150 (£77) per hour is estimated for 2015 prices and a cost factor (C_S) is introduced for security concerns associated with the production of a commercial civil aircraft. The development and support costs (C_{DSC}) are calculated by:

$$C_{DSC} = 0.0356 \cdot A_{UW}^{0.903} \cdot V_D^{1.93} \cdot Q_D^{0.346} \cdot C_{PI} \cdot A_{TF} \cdot C_S$$

Equation I-3

The consumer price index cost escalation factor (C_{PI} = 1.6) is used to estimate the rise in *DDTE* costs over the years. The flight test operations costs (C_{FTAR}) cover all the flight testing costs, other than that of the test aircraft itself, and is calculated using:

$$C_{FTAR} = 0.00558 \cdot A_{UW}^{1.19} \cdot V_D^{1.401} \cdot Q_D^{1.281} \cdot C_{PI} \cdot A_{TT} \cdot C_S$$

Equation I-4

Introducing an advanced technology testing factor (A_{TT} = 0.85) allows military concepts that utilise low observability (stealth) to be tested. The tooling hours required for development (T_{HD}) includes all programming, tool planning, fabrication, and production for the *DDTE* phase, where:

$$T_{HD} = 5.083 \cdot A_{UW}^{0.768} \cdot V_D^{0.899} \cdot Q_D^{0.18} \cdot R_P^{0.066} \cdot C_{AMC}$$

Equation I-5

Where an aircraft production rate factor (R_P) is estimated for the production of 15 aircraft per month, primarily used in section I-2.2; which is similar to the *B787* production rate.

The DDTE manufacturing and development cost for tooling (C_{TD}) is calculated by:

$$C_{TD} = T_{HD} \cdot T_R \cdot C_S$$

Equation I-6

Where (T_R) is the tooling and quality labour rates, which are approximately $93 (£47) per hour. The manufacturing labour hours (M_{HD}) include time for machining, fabrication, and assembly of the major structure, where:

$$M_{HD} = 43.61 \cdot A_{UW}^{0.76} \cdot V_D^{0.549} \cdot Q_D^{0.554} \cdot C_{AMC}$$

Equation I-7

The cost associated with labour hours (C_{MD}) is:

$$C_{MD} = M_{HD} \cdot M_R \cdot C_S$$

Equation I-8

Where the manufacturing rate (M_R) associated with machining and assembly is estimated as \$80 per hour (£41). The manufacturing of items requires a quality control procedure (Q_{HD}), where a number of quality control man-hours is required in addition to the manufacture of the components, where:

$$Q_{HD} = 0.13 \cdot M_{HD}$$

Equation I-9

The cost of quality control labour (C_{QD}) is given by:

$$C_{QD} = Q_R \cdot Q_{HD}$$

Equation I-10

Where the average hourly rate for quality control (Q_R) is the same as for tooling labour, where Q_R = T_R = \$93 (£47). The manufacturing materials and equipment (C_{MMD}) includes raw materials, hardware, and purchased components for the assembly of the airframe, where:

$$C_{MMD} = 96.677 \cdot A_{UW}^{0.692} \cdot V_D^{0.639} \cdot Q_D^{0.803} \cdot C_{PI} \cdot C_{AMC}$$

Equation I-11

Development cost for the engine (C_E) requires the use of maximum sea level static thrust (T_{SL}) and the number of installed engines (N_e). The BD configurations both have four (4) engines, with varied static thrust requirements as per **Appendix B**.

$$C_E = 121.5 \cdot T_{SL}^{1.00161} \cdot N_e \cdot C_{PI}$$

Equation I-12

The cost of avionics (C_{AV}) is a factored result based on the weight of the avionics components defined within the BD aircraft mass breakdown in **Appendix G**:

$$C_{AV} = 1.5 \cdot \left(3950 \cdot W_{AV} \cdot C_{PI}\right)$$

Equation I-13

The total development cost (C_{DDTE}) is the sum of all major cost components, where:

$$C_{DDTE} = C_{AED} + C_{DSC} + C_{FTAR} + C_{TD} + C_{MD} + C_{QD} + C_{MMD} + C_{E} + C_{AV}$$

Equation I-14

Table I-1 below provides a summary of the total calculated design, development, test, and evaluation results for the BDSF and BDVT.

Cost Description	***symbol***	***BDSF***	***BDVT***
Engineering	C_{AED}	1,836	1,574
Development & support	C_{DSC}	531	456
Flight test operations	C_{FTAR}	345	315
Tooling	C_{TD}	6,547	6,849
Manufacture/labour	C_{MD}	1,533	1,603
Quality control	C_{QD}	3,461	3,618
Materials & equipment	C_{MMD}	82	85
Engines	C_{E}	784	796
Avionics	C_{AV}	79	79
Total DDTE costs	C_{DDTE}	15,198	15,376

Table I-1: BDSF and BDVT development, test, and evaluation (DDTE) cost summary [Million $US]

I.2.2 Production Costs

The production cost (P) considers the labour, time, materials, manufacturing of tooling and parts, and testing of the airframe components that will be made for customers and not subjected to rigorous testing phases as with the *DDTE* airframes. The total production of 400 airframe structures (Q_P = 400) is considered for this phase, and the preceding calculations are almost identical as the *DDTE* equations. The total number of airframe engineering hours (E_{HP}) required for production is:

$$E_{HP} = \left(0.066 \cdot A_{UW}{}^{0.796} \cdot V_{D}{}^{1.538} \cdot \left(Q_D + Q_P\right)^{0.183} \cdot A_{TF} \cdot C_{AMC}\right) - E_{HD} \text{ [hr]}$$

Equation I-15

The engineering production phase cost (C_{AEP}) is calculated by:

$$C_{AEP} = E_{HP} \cdot E_{RATE} \cdot C_{S} \text{ [\$]}$$

Equation I-16

The tooling hours required for production (T_{HP}) includes all programming, tool planning, fabrication, and production, where:

$$T_{HP} = \left(5.083 \cdot A_{UW}{}^{0.768} \cdot V_D{}^{0.899} \cdot \left(Q_D + Q_P\right)^{0.18} \cdot R_P{}^{0.066} \cdot C_{AMC}\right) - T_{HD} \text{ [hr]}$$

Equation I-17

Where a production rate factor (R_P) is estimated for the production of 15 aircraft per month. The production cost for tooling (C_{TP}) is calculated by:

$$C_{TP} = T_{HP} \cdot T_R \cdot C_S \text{ [\$]}$$

Equation I-18

The manufacturing labour hours (M_{HP}) include time for machining, fabrication, and assembly of the major structure, where:

$$M_{HP} = \left(43.61 \cdot A_{UW}{}^{0.76} \cdot V_D{}^{0.549} \cdot \left(Q_D + Q_P\right)^{0.554} \cdot C_{AMC}\right) - M_{HD} \text{ [hr]}$$

Equation I-19

The cost associated with labour hours (C_{MP}) is:

$$C_{MP} = M_{HP} \cdot M_R \cdot C_S \text{ [\$]}$$

Equation I-20

The quality control (Q_{HP}) man-hours required for productions is:

$$Q_{HP} = 0.13 \cdot M_{HP} \text{ [hr]}$$

Equation I-21

The cost of quality control labour (C_{QP}) is given by:

$$C_{QP} = Q_D \cdot Q_{HP} \text{ [\$]}$$

Equation I-22

The production phase of manufacturing, materials, and equipment (C_{MMP}) includes raw materials, hardware, and purchased components for the assembly of the airframe, where:

$$C_{MMP} = \left(96.677 \cdot A_{UW}{}^{0.692} \cdot V_D{}^{0.639} \cdot \left(Q_D + Q_P\right)^{0.803} \cdot C_{PI} \cdot C_{AMC} \cdot C_{LO}\right) - C_{MMD} \text{ [\$]}$$

Equation I-23

The cost of the passenger cabin is determined by the number of passengers (N_{PAX}), number of production aircraft (Q_D + Q_P), and an interior cost factor per passenger (F_{INT}). The ratio of consumer price index reflects an increase in costs using current technologies compared with that of the 90's.

$$C_{INT} = F_{INT} \cdot N_{PAX} \cdot N_{PAC} \cdot \left(\frac{C_{PI}}{(C_{PI})_{1990}} \right) \quad \textbf{[\$]}$$

Equation I-24

Cost Description	*symbol*	*BDSF*	*BDVT*
Engineering	C_{AEP}	2,062	1,944
Tooling	C_{TP}	7,894	8,257
Manufacture/labour	C_{MP}	15,957	16,683
Quality control	C_{QP}	36,028	37,667
Materials & equipment	C_{MMP}	2,716	2,828
Internal Cabin	C_{INT}	557	557
Total production costs	C_P	66,075	68,810

Table I-2: BDSF and BDVT Production cost summary [Million $US]

The total production cost (C_{PROD}) is therefore given by:

$$C_{PROD} = C_{AEP} + C_{TP} + C_{MP} + C_{QP} + C_{MMP} + C_E + C_{AV} + C_{INT} \quad [\$]$$

Equation I-25

Table I-2 above provides a summary of the total calculated production cost results for the BDSF and BDVT, which includes the previous results for engine and avionics costs.

I.2.3 Life Cycle Cost

The life-cycle cost (LCC) is the total of *DDTE*, acquisition, operating, and disposal cost of a single aircraft. The previous analyses above provide a result for the first term in Equation I-26 below, where the *DDTE* is divided by the number of aircraft productions to provide a unit cost for the design, development, test, and evaluation.

$$LCC = C_{UDDTE} + C_{UA} + C_{OPER} + C_{DISP} \quad [\$]$$

Equation I-26

The unit acquisition cost (C_{UA}) is calculated using the C_{DDTE} and C_{PROD} values previously determined where the recurring fly-away cost can also be calculated.

$$C_{UA} = \left[\frac{C_{DDTE} + C_{PROD}}{Q_D + Q_P} \right] \quad [\$]$$

Equation I-27

The recurring fly-away cost is:

$$C_{RF} = \left[\frac{C_{PROD}}{Q_P} \right] \quad [\$]$$

Equation I-28

At a later stage of the preliminary design stage, it may be useful to understand the impact of cost variation due to the change in aircraft mass, and the AMPR provides this cost per pound increase. For every pound that the aircraft mass increases, the recurring cost, engine cost per aircraft, and avionics cost per aircraft increases, and is expressed as a fraction of the airframe unit weight.

$$C_{AMPR} = \left[\frac{C_{RF} - C_{EQ} - C_{AVQ}}{A_{UW}} \right] \quad [\$]$$

Equation I-29

The operational fuel cost includes items such as the fuel, oil, maintenance, depreciation, and crew salaries. [Burns, 1994] only addresses the fuel component of the operating costs, where assumptions using mass ratios from [Raymer, 1992] were applied to this fuel ratio to predict the overall operating cost for a first estimation. The total amount of fuel used during the aircraft life, is calculated below, where:

$$T_{FUEL} = 1.1 \cdot \left[\left(\frac{K_{FF} \cdot M_0}{L/D} \right) \cdot c_{cruise} \right] \cdot FH_{YR} \cdot Y_S \quad [\text{lb}]$$

Equation I-30

The mass of fuel used in a single aircraft life is calculated using the lift-to-drag ratio (L/D), specific fuel consumption (c_{cruise}), the aircraft fuel fraction factor (K_{FF} = 0.88), and the take-off gross weight (M_0). In addition it is assumed that the total number of flying hours per year (HH_{YR}) reflects 18hours of flying per day for 365.25 days in the year and a 20 year service life (Y_S), where HH_{YR} = 6575 hours.

The total life cycle fuel cost per aircraft is calculated by using the density of fuel *(ρ_{fuel})*, where for this analysis JP-8 is estimated to have ρ_{fuel} = 6.8 lb/gallon, and the cost of fuel at present is around $4.00 per US gallon, providing:

$$TC_{FUEL} = \left(\frac{T_{FUEL}}{F_{DEN}} \right) \cdot C_{FUEL} \quad [\$]$$

Equation I-31

Using the same equations, the aircraft mass can be replaced by a savings weight ratio, where the increase in fuel cost per additional aircraft pound mass increase can be determined, but is not useful for the purpose of this investigation.

To provide a summary of the operating cost description provided within [Raymer, 1992], the total operating costs are broken down into fuel (38%), crew (24%), maintenance (25%), depreciation (12%), and finally insurance (1%). Calculated above is the total fuel life cycle mass for the aircraft, where this is manipulated to determine the aircraft operating cost assuming that the ratio of fuel to operating cost remains at 38%. By calculating the total operating cost we can quantify the direct (*DOC*) and indirect operating costs (*IOC*), for which we can determine the cost per passenger seat mile for each BD aircraft configuration.

In addition to calculating the operating costs (C_{OPER}), the final unknown to quantify the *LCC* is the disposal cost (C_{DISP}) of the aircraft. The disposal cost was found to be 20% of the aircraft acquisition cost with the final results shown in Table I-3 and Table I-4 below. Table I-5 contains results for DOC per seat nautical mile, with a comparison shown in Fig I-1 of current short-medium range operator actual costs per seat mile.

Cost Description	***symbol***	***BDSF***	***BDVT***
Recurring fly-away	C_{RF}	164	180
Total life cycle fuel	TC_{FUEL}	1,229	1,139
Total Crew	TC_{CREW}	776	719
Total maintenance	TC_{MAIN}	808	749
Total depreciation	TC_{DEPR}	388	360
Total insurance	TC_{INS}	32	30
Total DOC	TC_{DOC}	2,441	2,263
Total IOC	TC_{IOC}	792	734

Table I-3: BDSF and BDVT development and production cost summary [$US Million]

Cost Description	***symbol***	***BDSF***	***BDVT***
DDTE per unit	C_{UDDTE}	38	38
Acquisition *per unit*	C_{UA}	201	208
Operating *per unit*	C_{UOPER}	3,233	2,997
Disposal *per unit*	C_{UDISP}	40	42
Life Cycle Cost *per unit*	C_P	3,512	3,285

Table I-4: BDSF and BDVT Summary of Life Cycle Cost (*LCC*) per aircraft [*$US Million*]

Cost Description	***symbol***	***BDSF***	***BDVT***
DOC *per unit* [*$US*]	C_{UDOC}	64,187	59,507
mission block fuel [*lb*]	F_{BLOCK}	21,490	19,923
block fuel/seat [*lb*]	F_{BPS}	99	92
DOC/block hour [*$US/hr*]	C_{UDPH}	10,661	9,884
DOC/seat [*$US*]	C_{DPS}	297	275
DOC/seat n.mile [*$US/n.mile*]	C_{DPSM}	0.0739	0.0685

Table I-5: BDSF and BDVT Summary of DOC and mission fuel per seat nautical mile; with a block time of 6.02hours and mission range of 4,020 nautical miles (*B767-300 fuel/pax/n.mile = 0.0936 lb/n.mile*)

Cost per Available Seat Mile

Company	2004	2005	2006	2007
Air France ADS (AKH)	Add	$0.0631	$0.064	$0.0656
AirTran Holdings (AAI)	$0.0845	$0.0928	$0.0974	$0.0957
Alaska Air Group (ALK)	$0.101	$0.102	$0.12	$0.105
Allegiant Travel Company (ALGT)	$0.0692	$0.0741	$0.0769	$0.0819
American Airlines (AMR)	$0.0973	$0.105	$0.109	$0.114
China Eastern Airlines (CEA)	$0.49	$0.52	$0.58	Add
China Southern Airlines Company (ZNH)	$0.43	$0.45	$0.47	Add
Continental Airlines (CAL)	$0.0984	$0.102	$0.106	$0.108
Copa Holdings, S.A. (CPA)	$0.0872	$0.0932	$0.0998	Add
Delta Air Lines Inc. (DAL)	$0.122	$0.116	$0.116	$0.119
EXPRESSJET HOLDINGS (XJT)	$0.125	$0.117	$0.116	$0.132
Frontier Airlines Holdings (FRNT)	$0.0848	$0.0873	$0.0936	Add
Gol Linhas Aereas Inteligentes S.A. (GOL)	$0.157	$0.155	$0.153	Add
Hawaiian Airlines (HA)	$0.097	$0.106	$0.109	$0.106
JetBlue Airways (JBLU)	$0.061	$0.0698	$0.0782	$0.0838
Lan Chile S.A. (LFL)	$0.091	$0.00099	$0.00103	Add
MAIR Holdings (MAIR)	Add	$0.337	$0.363	$0.344
Mesa Air Group (MESA)	Add	$0.116	$0.135	$0.147
Midwest Air Group (MEH)	$0.104	$0.112	$0.113	Add
Northwest Airlines (NWA)	$0.106	$0.115	$0.11	$0.108
Pinnacle Airlines (PNCL)	$0.134	$0.142	$0.123	$0.111
Republic Airways Holdings (RJET)	$0.126	$0.124	$0.112	$0.102
Ryanair Holdings (RYAAY)	Add	$0.0628	$0.0686	$0.0722
SkyWest (SKYW)	$0.136	$0.141	$0.143	$0.137
Southwest Airlines Company (LUV)	$0.0797	$0.0805	$0.088	$0.091
TAM S.A. (TAM)	$0.192	$0.179	$0.175	Add
United Airlines (UAUA)	$0.102	$0.106	$0.112	$0.139
US Airways Group (LCC)	$0.11	$0.108	$0.114	$0.113

Fig I-1**:** Comparison of operators cost per available seat mile for short-medium range operations

Appendix J Airframe Configurations 3-Views

The following section includes all three view diagrams of the airframe concepts described within the text above. The following vehicle representations are the authors' perception of how each airframe configuration should be visualised based upon the analysis performed for each conceptual design.

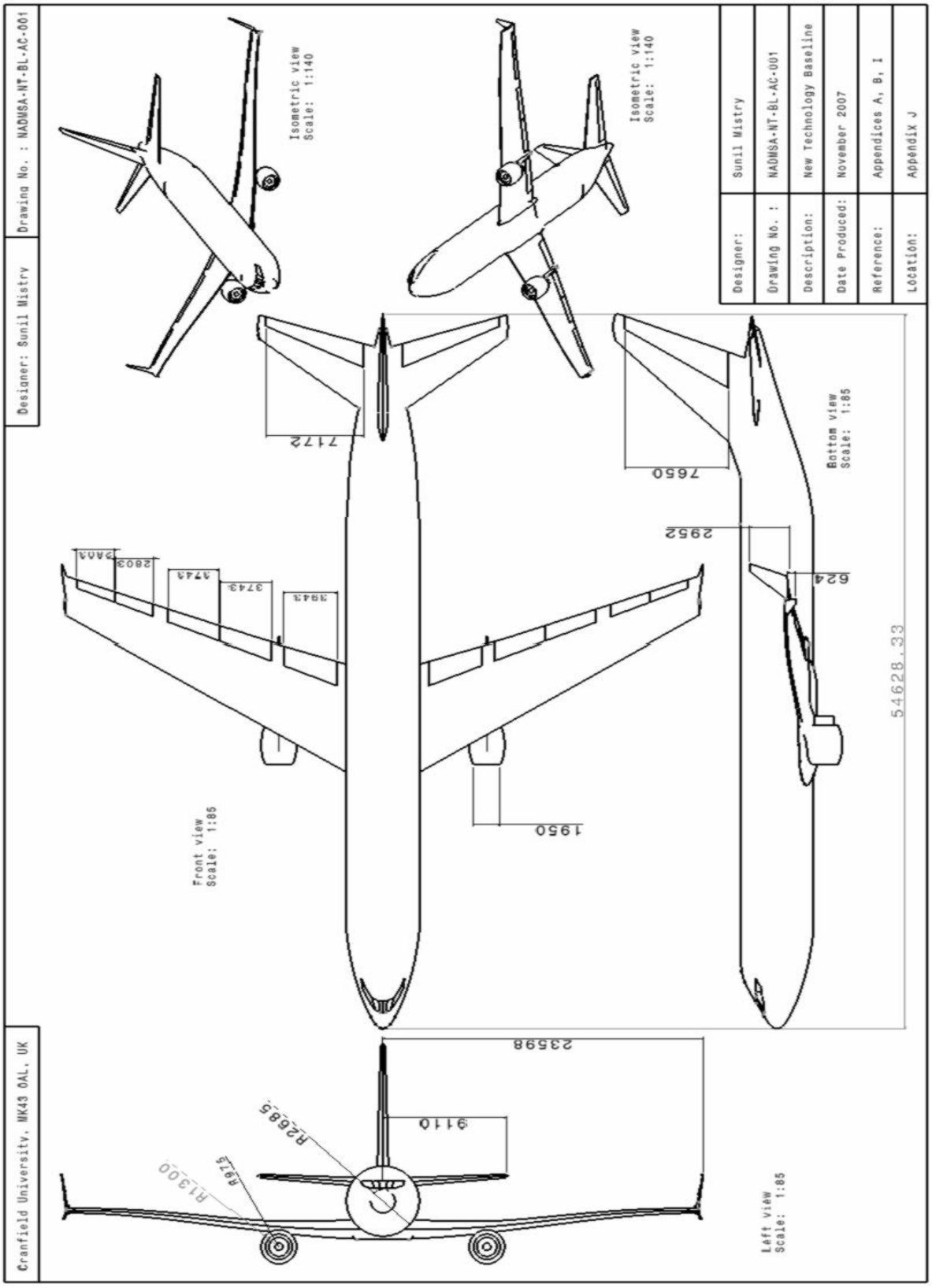
Cranfield University, MK43 0AL, UK
Designer: Sunil Mistry
Drawing No. : NADWSA-NT-BL-AC-001
Designer: Sunil Mistry
Drawing No. : NADWSA-NT-BL-AC-001
Description: New Technology Baseline
Date Produced: November 2007
Reference: Appendices A, B, I
Location: Appendix J
Isometric view
Scale: 1:140
Isometric view
Scale: 1:140
Front view
Scale: 1:85
Bottom view
Scale: 1:85
Left view
Scale: 1:85
54628.33
23598
7650
2952
624
1950
9110
R2685
R1300
7172

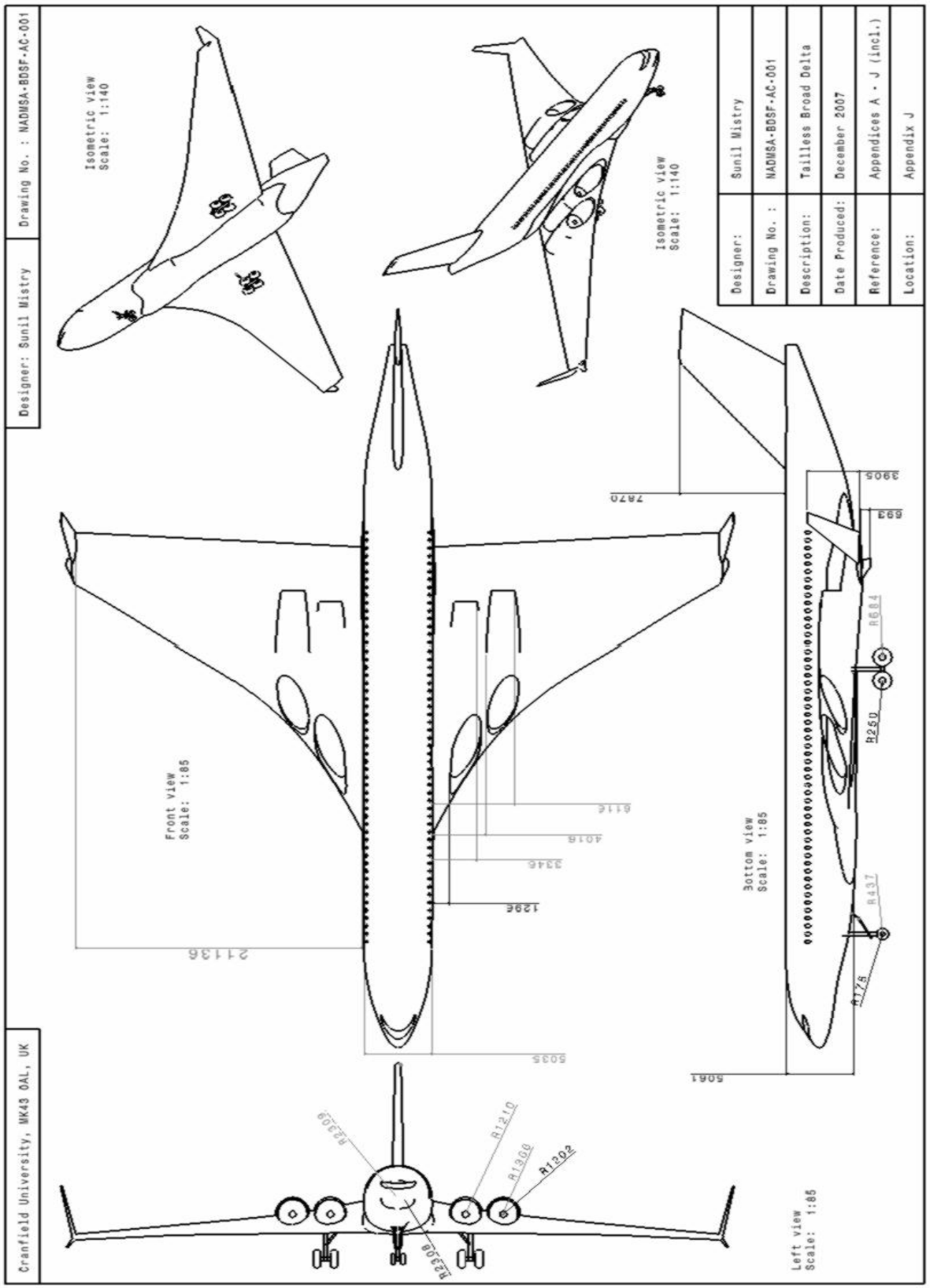
Cranfield University, MK43 0AL, UK
Designer: Sunil Mistry
Drawing No. : NADMSA-BDSF-AC-001
Designer: Sunil Mistry
Drawing No. : NADMSA-BDSF-AC-001
Description: Tailless Broad Delta
Date Produced: December 2007
Reference: Appendices A - J (incl.)
Location: Appendix J
Isometric view
Scale: 1:140
Isometric view
Scale: 1:140
Front view
Scale: 1:85
Bottom view
Scale: 1:85
Left view
Scale: 1:85
21136
5035
5061
7870
3905
683
R684
R280
R437
R178
R2309
R1210
R1300
R1202
R2308

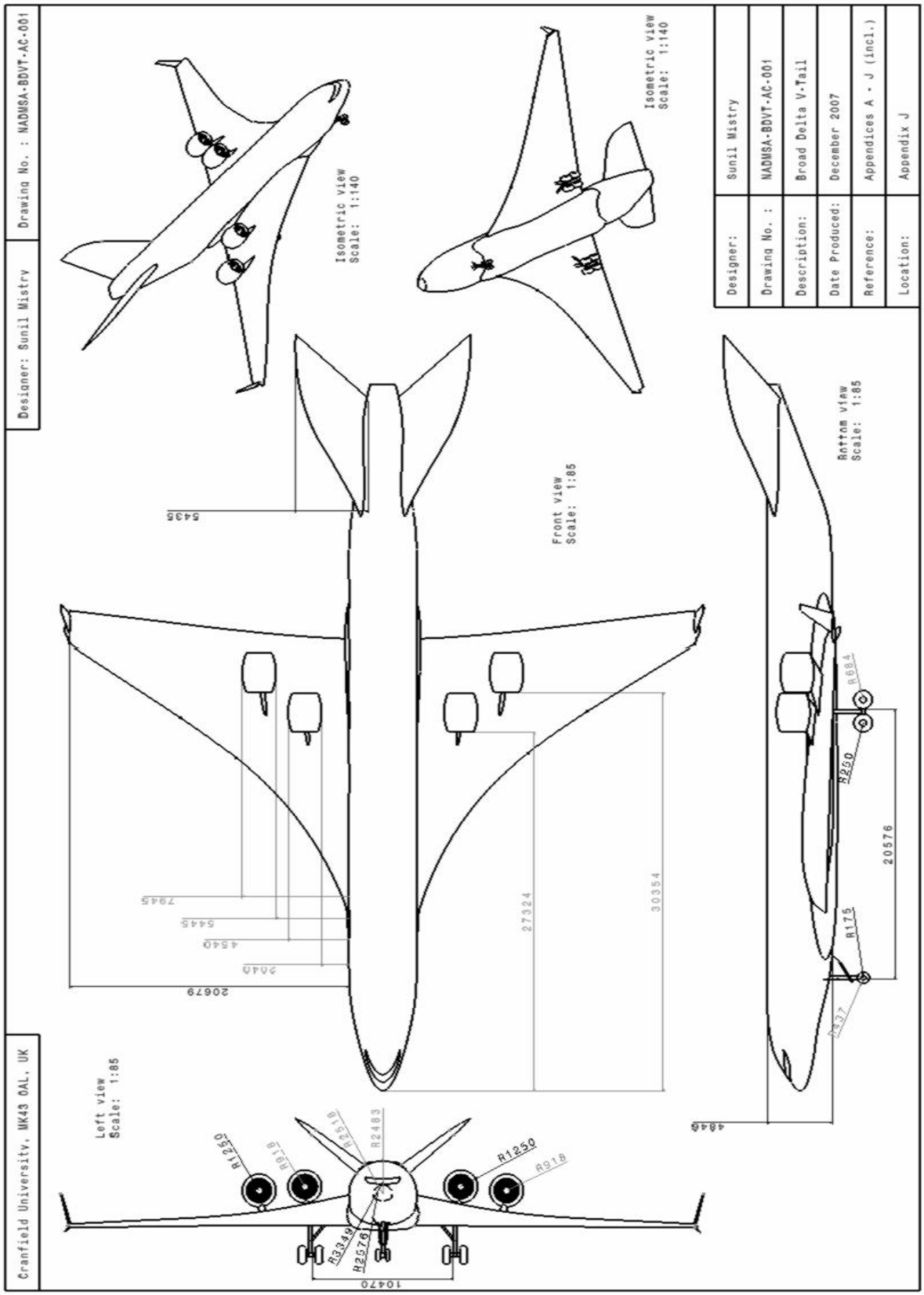
Designer: Sunil Mistry
Drawing No. : NADMSA-BDVT-AC-001
Cranfield University, MK43 0AL, UK
Designer: Sunil Mistry
Drawing No. : NADMSA-BDVT-AC-001
Description: Broad Delta V-Tail
Date Produced: December 2007
Reference: Appendices A - J (incl.)
Location: Appendix J
Isometric view
Scale: 1:140
Isometric view
Scale: 1:140
Front view
Scale: 1:85
Bottom view
Scale: 1:85
Left view
Scale: 1:85
20679
30354
27324
20576
10470

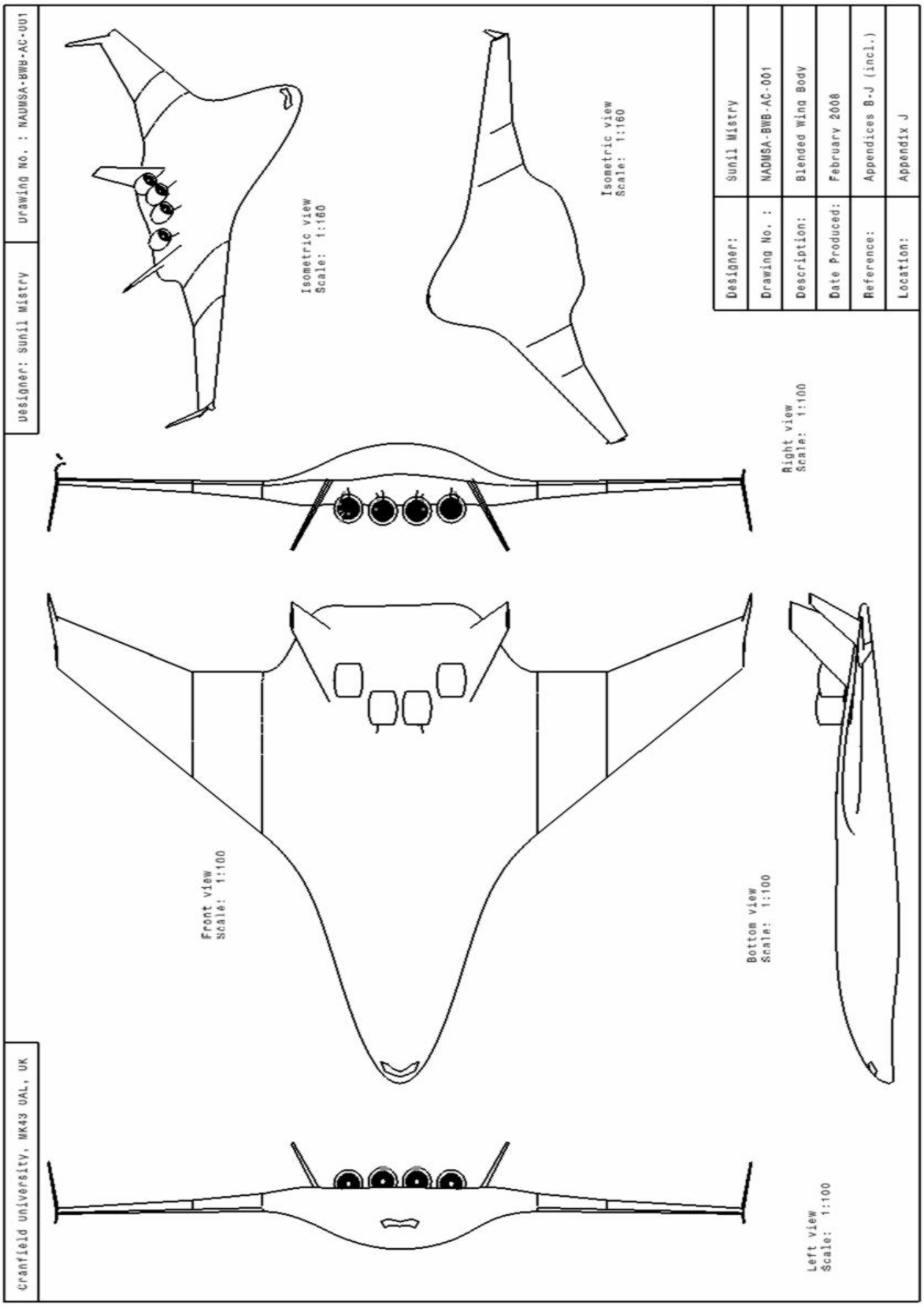
Designer: Sunil Mistry
Drawing No. : NADMSA-BWB-AC-001
Description: Blended Wing Body
Date Produced: February 2008
Reference: Appendices B-J (incl.)
Location: Appendix J
Designer: Sunil Mistry
Drawing No. : NADMSA-BWB-AC-001
Cranfield University, MK43 0AL, UK
Isometric view
Scale: 1:160
Isometric view
Scale: 1:160
Front view
Scale: 1:100
Right view
Scale: 1:100
Bottom view
Scale: 1:100
Left view
Scale: 1:100

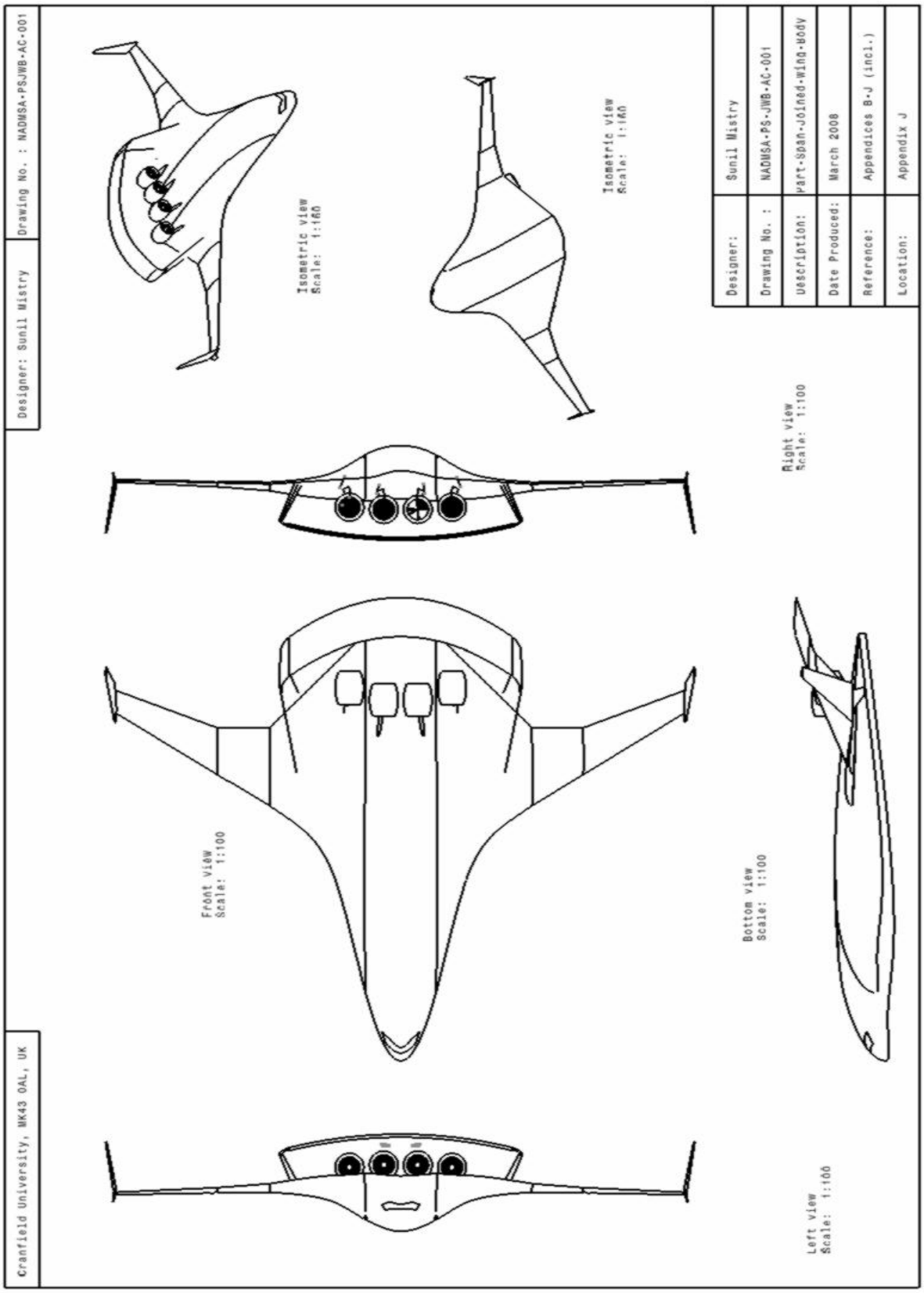
Designer: Sunil Mistry
Drawing No. : NADWSA-PSJWB-AC-001
Isometric view
Scale: 1:160
Isometric view
Scale: 1:160
Designer: Sunil Mistry
Drawing No. : NADWSA-PS-JWB-AC-001
Description: Part-Span-Joined-Wing-Body
Date Produced: March 2008
Reference: Appendices B-J (incl.)
Location: Appendix J
Right view
Scale: 1:100
Front view
Scale: 1:100
Bottom view
Scale: 1:100
Left view
Scale: 1:100
Cranfield University, MK43 0AL, UK

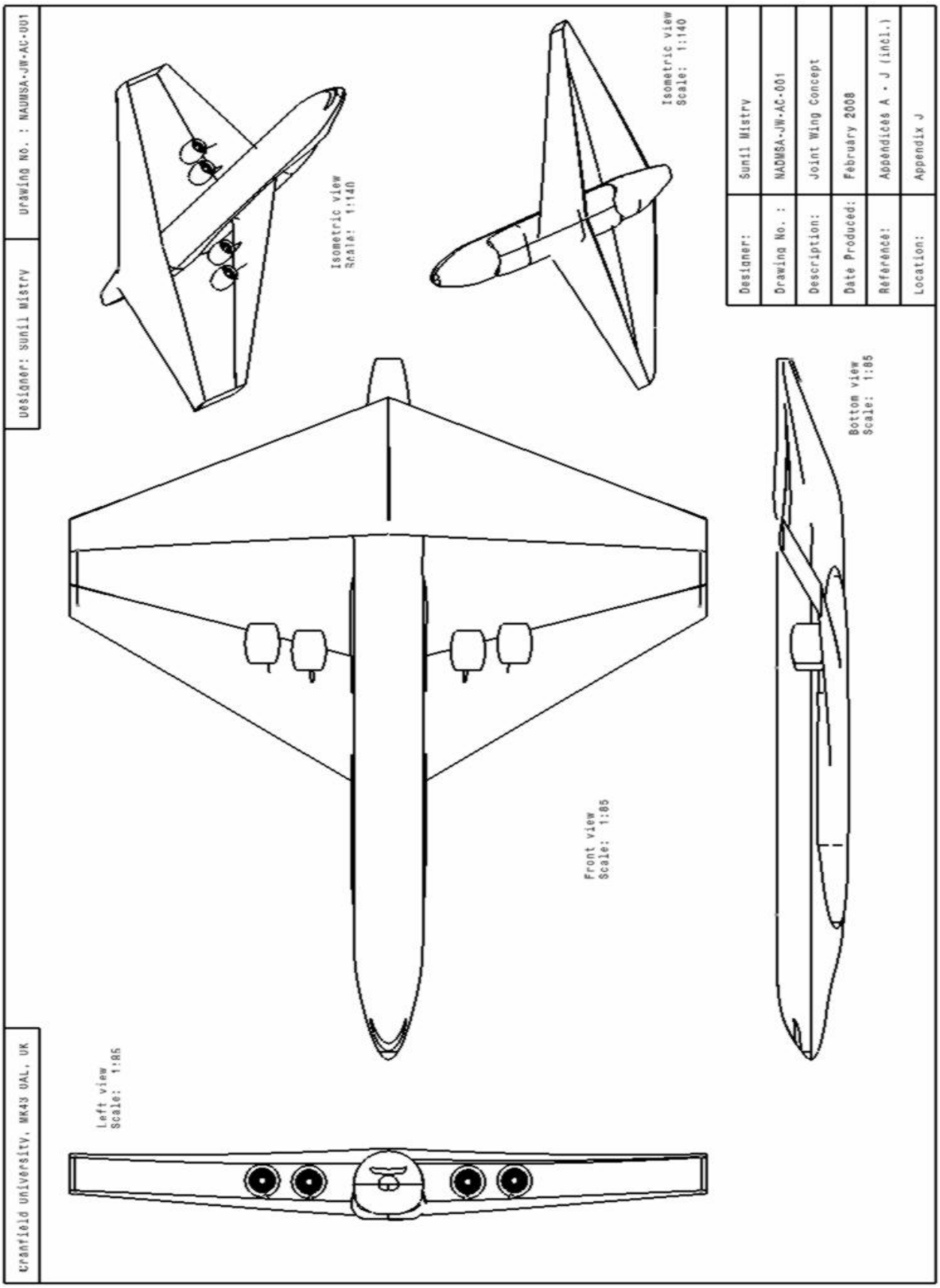
Cranfield University, MK43 0AL, UK
Designer: Sunil Mistry
Drawing No. : NADWSA-JW-AC-001
Isometric view
Scale: 1:140
Isometric view
Scale: 1:140
Designer: Sunil Mistry
Drawing No. : NADWSA-JW-AC-001
Description: Joint Wing Concept
Date Produced: February 2008
Reference: Appendices A - J (incl.)
Location: Appendix J
Bottom view
Scale: 1:85
Front view
Scale: 1:85
Left view
Scale: 1:85

END